

GL61503

ZUNIL 1
INDE, GUATEMALA, C.A.
Geology y Geophysics

Earth Science Laboratory

University of Utah Research Institute
420 Chipeta Way, Suite 120
Salt Lake City, Utah 84108
(801) 581-5283



3.1.6.2 Other potential areas and exploratory holes

As discussed earlier the area within the triangle made by the villages of Almolonga-Cantel-Zunil has potential. Another fault zone, related to the extension of the Zunil graben is believed to be here. The basin is expected to be deeper and faulted more than in the Zunil field. Here the graben is intersected by two sets of faults: the northeast faults of the Zunil fault system and the northerly to northwesterly faults from the caldera formation and related ring fractures. The best spot to locate an exploration well is in the alluvial flood plain north of Los Baños Almolonga perhaps a kilometer SSE of Almolonga.

Another area which requires serious consideration in future plans is on the eastern flanks of Santa María above the projected extension of the Zunil fault zone. Because this area is heavily forested and the slopes are relatively steep, drilling may be difficult. In view of this, another area with relatively easy access with flat terrain will be Las Majadas within the crater of Cerro El Galápago. The floor of this crater is covered with basaltic andesite lava flows from Santa María. Cerro El Galápago may be a small dacitic pyroclastic cone or a phreatomagmatic explosion crater. The crater may be filled with pyroclastic material some of which may be coarsely brecciated. This provides an ideal permeable unit capped by the impermeable basaltic andesite lava flows from Santa María. The granodiorite basement may be highly fractured below and may even be deeper here. A deep hole (2000 m.) would be ideal. If direction on the hole is possible, it would be best to direct it to the NW to explore the extension of the Zunil fault zone further.

3.2 Geochemistry

3.2.1 Introduction

Data is available for each kind of geothermal feature, but not all features are fully described and sampled. The available well data is summarized in Tables 3.2-1 and 3.2-2. For this report, geochemical assessment for liquids is based on those data and for the thermal springs described by the Japan International Cooperation Agency (JICA), 1977, and INDE, Informe Geoquímico, April, 1978.

TABLE 3.2-1

SUMMARY OF DATA ON LIQUIDS FROM WELLS NEAR ZUNIL

WELL	OPEN ELEVATION (MASL)	TDS	CHLORIDE	NA/LI.	NA/(CL.+HCO ₃)	CL/B SO ₄ /(CL+HCO ₃ +SO ₄)
Z-2						
Z-4						
Z-6						
Z-11	1436-1938	3791		197	0.62	24. 0.054
ZCQ-1	705-1505					
ZCQ-2	1255-1550	2000	787	51	1.06	33. 0.126
ZCQ-3	1030-1435	3100	1550	32	0.85	42. 0.70
ZCQ-4	1090-1610	3487	1658	30	0.87	34. 0.033
ZCQ-5	1095-1390		718			
ZCQ-6	1030-1570	3350	1623	37	0.88	40.

TABLE 3.2-2

GAS COMPOSITIONS

WELL	WT. % GAS IN STEAM	WT% IN DRY GAS				R	N O T E S
		CO ₂	H ₂ S	H ₂			
Z-11	0.4 TO 0.85	87.5	7.0	0.5		5.0	One analysis
ZCQ-2	0.14 TO 0.41	82-86	7-8	1.1-1.4		2-5	Increases with time
ZCQ-3	0.3 TO 0.8						2 tests have dif. patterns
ZCQ-4	0.6 TO 0.94	70	2.2				Pattern is complex
ZCQ-5							
ZCQ-6	0.85 TO 1.0						

3.2.2 Objectives

There exist several objectives in the geochemical analysis. These include:

1. Correlation of deep water compositions with surface springs in terms of
 - a) Structural relationships of faults and rock units with the developed reservoir and recharge mechanism.
 - b) Chemical evolution of the hot waters, and steam from them, that mixes with shallow ground water to form the surface features.

be compared with other deep well compositions and before clear conclusions can be made in regard to water rock reactions that affect compositions of the reservoir fluid.

Geothermometers based on sodium and potassium are not affected by steam loss, because the ratio of concentrations is the key factor. However, the accuracy of the Na/K geothermometer depends on the water being in equilibrium with certain feldspar minerals.

The sodium-potassium-calcium geothermometer is affected by steam loss because mathematically it involves the square root of calcium concentration with the first power of other concentrations. Also, its applicability depends on the presence of certain minerals and the absence of others. These details will be addressed when more data for the deep wells become available.

Of the 21 thermal spring compositions given in (JICA, 1977), only one is NaCl - type and six are acid-sulfate - type waters. The data (INDE, April 1978) for 71 features, includes compositions for 67 waters. Three of those are NaCl -type and ten are acid-sulfate. Most of the remainders in both lists are bicarbonate waters and for all but two of the listing (INDE, April 1978), bicarbonate concentration exceeds the sum of chloride plus sulfate. Elevations of the NaCl -type springs are 1905, 1985, 2030 and 2099 m. These could possibly indicate the top of the deep geothermal resource, and the highest, (Z-37) is in the area developed by the ZCQ wells.

Most springs near the Samalá River are bicarbonate type. If these are related to the deep resource, then such relationship would involve steam heating of cool groundwater, combined with local water-rock reaction due to carbon dioxide (CO₂) that accompanies the steam.

The acid-sulfate springs are clearly related to steam heating. Most occur above 2100 m. elevation, and the sulfate acidity is a typical result from atmospheric oxidation of hydrogen sulfide (H₂S) that accompanies the steam and CO₂

It is reasonable to consider the acid-sulfate and the bicarbonate springs as due to exhalations from the deep resource at elevations above its hydro-potential (gravity) surface. The presence of relatively low sulfate found in some of the bicarbonate waters may be due to formation of sulfide mineral, such as pyrite, along the vapor flow pathways below depths that atmosphere can penetrate.

Warm springs which contain the least dissolved solids occur near Los Baños and south of Cantel. These are east of the Cerro Quemado summit and it is worth considering whether they belong to the same geochemical source as the warm springs along the Samalá River and the deep waters of the ZCQ wells. The two springs near Cantel are each dilute bicarbonate type. The Los Baños springs may be considered as chloride-bicarbonate type. It does not seem unreasonable from a chemical evolutionary point of view that

these relatively dilute springs represent the upper-most reaches of steam movement. That evolution, due to passage through fractures, could involve nearly complete extraction of CO₂ and H₂S from the steam before the local groundwaters at these higher elevations were contacted and warmed. The springs south of Cantel and at Los Baños are from 6 to 4 km from the area of deep wells. Thus, if they are due to the same thermal source, the geothermal resource would seem to be much more extensive than the area explored so far by deep drilling (Z and ZCQ wells).

Two other acid-sulfate springs (Z-35 and Z-36) are along the Pachamiya River at elevations near 2030 m. These locations are about one-half kilometer east of the Samalá River. Of potentially large significance, are springs of the Balneario Fuentes Georginas (Z-31,34), about 4 kms. southeast of the deep wells, because they could suggest an extension of the resource explored so far. They are of acid-sulfate type and occur at elevations above 2400 m. This is substantially above the levels of all other warm springs and may indicate a separate structural fault that penetrates to a major geothermal resource.

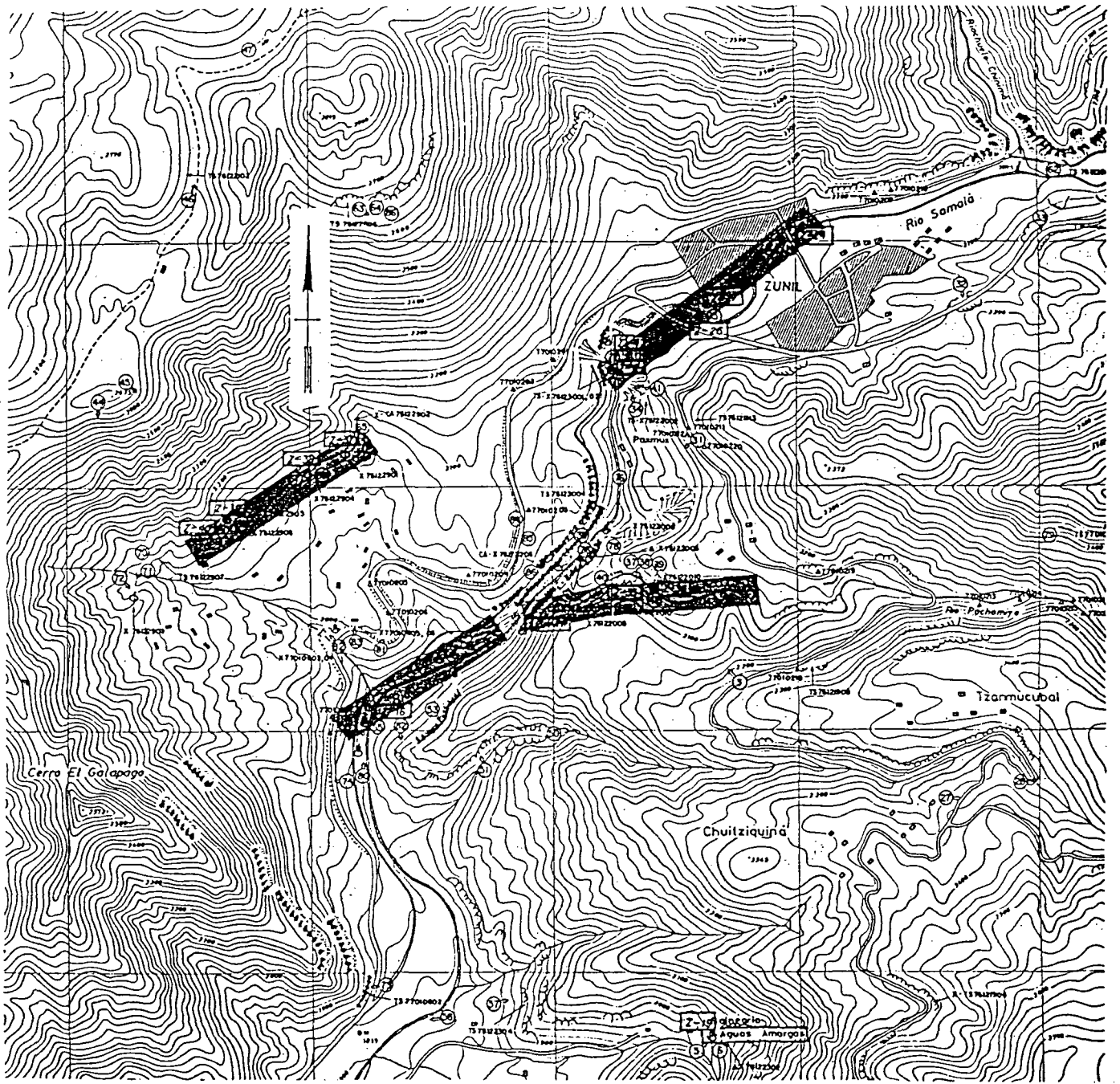
The acid-sulfate spring at Balneario Aguas Amargas is at an elevation of 1980 m., in a tributary canyon more than 1 Km east of the Samalá River. They are 2 Km south of Z-35 and Z-36. In conjunction with Z-31 and 34 they may indicate structures away from the Samalá River and from the area of deep drilling.

3.2.4 Connection to Local Structures

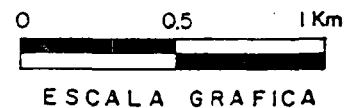
All the warm springs within two kilometers of the ZCQ wells can be considered as surface expressions of three faults defined by geophysics and geology, (see Figure 3.2-1). An interpreted graben is bounded on the northwest by a fault dipping to the southeast. In sequence from SW to NE that fault provides fluid conduit for springs Z-40, 39, 38, and 37 near the drilled area and for Z-4, 6, 26, 27, and 24 along the Samalá River into the community of Zunil. This fault is called "D" in JICA, 1977.

Several thermal springs occur along the Samalá River between the elevations of 1940 and 1860 m. They are the surface expression of a fault trending NE - SW, dipping NW (Figure 3.2-1). This fault possibly bounds the southeastern part of the graben.

An east-west fault marked by the Río Pachamiya on the east side of the Samalá River is aligned with springs Z-36 and Z-35. It intersects the NE -SW fault of the Samalá River at spring Z-20. This is significant, because Z-20 is an NaCl - type spring, as are the waters of the deep wells. This east-west fault apparently crosses the Samalá River fault to feed an unnamed thermal spring on the western side. Additional surface expression is the small canyon south of ZCQ-3. This is a suspected E-W fault that dips steeply to the south and could be considered as a major feeding route to the area of the deep wells. Its location is appropriate for the temperatures contours (increasing to the southwest) in the area defined by deep drilling.



 MANIFESTACIONES TERMALES ASOCIADAS A FALLAS PROBABLES.



NOTA:
MAPA BASE: LOCALIZACION DE MANANTIALES DEL AREA DE ZUNIL, INDE 1977.

INSTITUTO NACIONAL DE ELECTRIFICACION .. INDE GUATEMALA C.A.	
PROYECTO GEOTERMICO ZUNIL I	
ALINEACION DE MANIFESTACIONES TERMALES	
CyM/MKF.	FIGURA: 3.2-1

3.2.5 Suggestions for Future Work

The pattern of faults which support the present site of deep drilling extends more broadly. Certain of these areas deserve more study because they may support additional geothermal power plants.

3.2.5.1 When existing data for brine compositions of the ZCQ wells are made available, along with data on non-condensable gases, steam and liquid flow rates, the interpretation can proceed. This review will aim to characterize the liquid resource, checking for mixed waters and compositional gradients through the drilled area. Structural features suggest a fluid source south of ZCQ-3 and moving up and northward. A relationship to the cooler waters flowing through the high ground on the west and northwest would be explored. Also, the relationship of ZCQ-6 to this proposed fluid source is required. These existing data would also help make preliminary plans for a power plant design. Such a design should not be made firm on the basis of these data however. Waters from new drill sites may be hotter and their actual results must be considered before finalizing a power plant design.

3.2.5.2 Additional sampling of several kinds of waters should be done. Some of these support the current assessment of the ZCQ area, others support assessment of prospect areas described later.

- a) No data are available for surface waters and cool springs. These are needed in order to complete mixing models for the hot spring samples. Ten to twenty samples should be obtained from small streams and springs in the area within about 4 to 6 km of Zunil.
- b) The Samalá River south of Zunil receives a large amount of thermal water. That heat input constitutes a drain on the geothermal development area. The size of that thermal input to the river is an index for the heat available for development. That thermal input can be estimated from the increase of geothermal components (boron, chloride, etc.) that can be measured in liquid samples. Thus, a small project should be designed to sample the Samalá River and its tributaries from above the town of Zunil to about the location of the tunnel. The main objective is to interpret the results in terms of heat input to the river. This review would also provide a base line for hazardous constituents such as boron and fluoride, that might be introduced in to the river by discharge from geothermal power plants.

- c) New samples of liquid and steam should be taken when ZCQ wells 1 through 6 and any new wells are tested. If possible, the flow tests should use steam separators. This would enable separation and accurate monitoring of the two phases, as desired for purposes of reservoir and geochemical assessment and power plant design. Samples of the separated phases should be obtained at each stable flow rate. Analyses should aim partly to confirm earlier data, but mainly to establish the character of the individual wells that will provide a mixture to the power plant. Gas samples should be analyzed for a full spectrum of components (CO₂, H₂S, CH₄, N₂, Ar., H₂, and O₂). Brine samples should be obtained and preserved to assure accurate results for components that are susceptible to change before analysis (SiO₂, NH₃, HCO₃, Fe, etc.). Samples should be collected so changes of composition in early stages of production can be identified. Results from the samples of new and old wells should be reviewed in terms of what happens for the power plant as the waters are mixed.

3.2.5.3 The NE - SW fault which bounds the NW side of the present area projects through Zunil. It progresses at least as far as Cantel, as indicated by the thermal springs there. It may be a major structural feature of the Quetzaltenango valley and deserves assessment as an exploratory prospect along its entire projected length NE from Volcán Santa María.

3.2.5.4 The E - W fault through the Pachamiyá canyon is suspected to dip to the south. This makes it accessible by drilling from sites located on gentle terrain east of the Samalá River. This location may be similar to the structure of the ZCQ-well sites.

3.2.5.5 The thermal springs at Aguas Amargas are in an east-west drainage that is tributary to the Samalá River in the same way as Río Pachamiyá. The presence of springs suggests connection with a deep structure. Significantly these springs are on the extension of fault A (JICA, 1977) which was selected as the southeast boundary to a major graben. Aerial surveys for thermal features should look specially at this area to confirm other thermal features. Ground reconnaissance for altered rock could also be useful. If thermal features are found, the area would appear similar to the ZCQ area and drilling would be warranted. Drilling targets would also be fault zones in the granodiorite.

3.3 Geophysics

3.3.1. Introduction

Geophysical investigations were carried out in the Zunil geothermal area in 1977 by personnel from the Japan International Cooperation Agency (JICA) and in 1977 and 1978 by the Instituto Nacional de Electrificación (INDE). A total of six geophysical methods were used, including: electrical resistivity (ER) surveys, seismic reflection, seismic refraction, gravimetry, magnetics and temperature gradient studies. An analysis describing the validity and results of each of these methods is presented in Section 3.3.3; in addition gravity data required both interpretation and analysis. Results from all techniques assisted in providing additional information on the area's subsurface characteristics, though some methods were more valuable than others. Although a regional investigative study was performed using ER, gravity, and magnetics, the geophysical program within the local framework of the Zunil geothermal complex appears to have been oriented as a detailed phase; it is possible that a prior reconnaissance phase would have increased the areal coverage and selected specific areas for subsequent detailing. The southwestern portion of the Zunil geothermal area has less detailed geophysical coverage than the eastern side, and it is in this southwestern area where deep drilling encountered favorable and exploitable geothermal conditions. Constraints due to the rugged topography, however, limit the areal coverage by some geophysical methods in this and other areas around Zunil. ER surveys are especially restricted since lines greater than 2 km. are required along fairly constant elevation.

The most useful data obtained were from gravity, ER, seismic reflection and temperature gradient geophysical methods; secondary exploratory techniques such as seismic refraction and magnetics tend to support previous findings. It should be noted that even though geophysical results rely greatly on interpretation, the analytical procedures and data reduction processes of each method were performed with considerable accuracy by both JICA and INDE.

3.3.2. Document Summary

A number of documents were reviewed at this stage of the project in order to formulate analyses and evaluations of geophysical studies in addition to gaining an overall perspective of the geothermal field. Those reports reviewed are included in the Appendix 1.

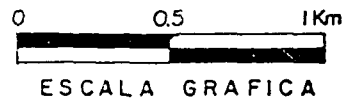
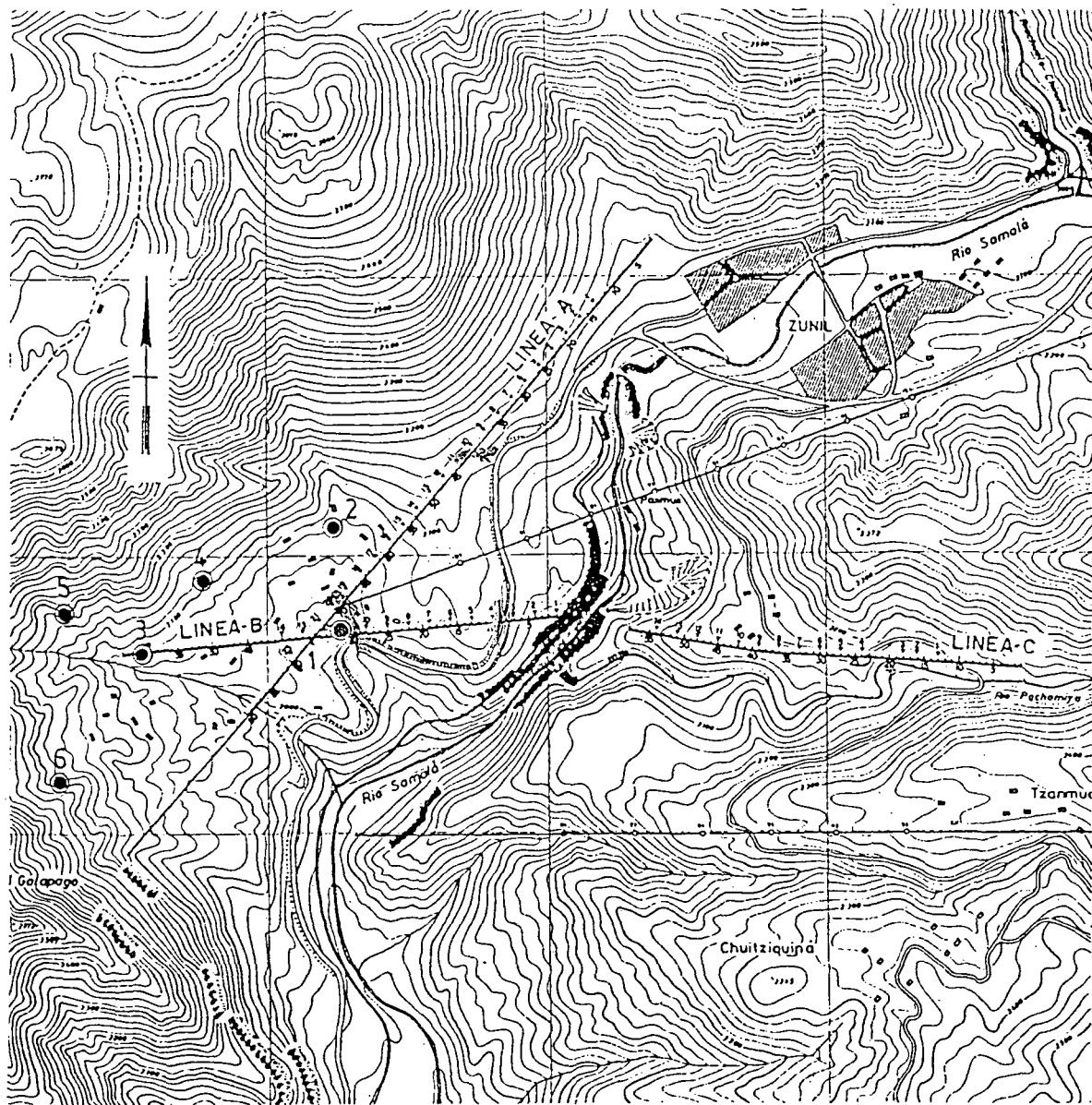
3.3.3 Analyses

3.3.3.1 Seismics

3.3.3.1.1 Seismic Reflection Studies

Both seismic reflection and refraction studies were performed within the Zunil geothermal complex at locations shown in Figure 3.3-1. Line C, however, is the only line where refraction studies were performed. It should also be noted that the locations of the lines are the same ones for the ER surveys so that information on both the structure and subsurface conditions are known.

Seismic reflection studies were conducted along lines A, B and C using 25 m. geophone spacings and 75 m. intervals for shot points, to follow the common depth point (CDP) method in four fold. This technique appears adequate to investigate the structure down to approximately 1000 m. depth. CDP methods not only enhance weak reflections in relation to background noise but also reduce signals from multiple reflections (signal-generated noise). This may be quite pronounced in geothermal areas where mineralization and/or alteration of subsurface materials cause density and velocity variations within a single formation. Lateral variations especially pose a problem for processing CDP data as stacking "out of phase" occurs and signals are lost. As reflection (and refraction) depend on velocity contrasts among various rocks, the presence of numerous reflections is to be expected, as evidenced in the depth sections presented in Figures 3.3-2 and 3.3-3. Comparing the various continuous reflectors with borehole data shows that the top of the granodiorite basement was in most cases detected, although it was at times unclear which reflector defined this boundary. This situation is demonstrated in Figure 3.3-2 where the top of the granodiorite is shown by non-continuous reflectors. The continuous reflectors, denoted by L2, may actually define the top boundary of a less altered and fractured (massive) basement where seismic waves would reflect a pronounced variation or increase in velocity. The presence of faults may have been accurately plotted, especially when correlated with other geophysical methods, although their dip is possibly obscured by multiple reflections and dispersion along steeply inclined boundaries. The various low signal to noise (S/N) zones detected correspond to discontinuous reflection waves related to the Tertiary volcanics and the basal conglomerate overlying the granodioritic basement as well as to some alteration, fracturing and faulting. The presence of this low velocity layer would create a masking effect along its upper contact with the dacite so that its actual thickness would have to be inferred. This is demonstrated in Figure 3.3-2 where the S/N layer is over 350 m thick, whereas data from hole ZCQ-1 and ZCQ-2 show it is less than 150 m thick; a similar effect occurs in line B (Figure 3.3-3).



INSTITUTO NACIONAL DE ELECTRIFICACION
INDE GUATEMALA C.A.

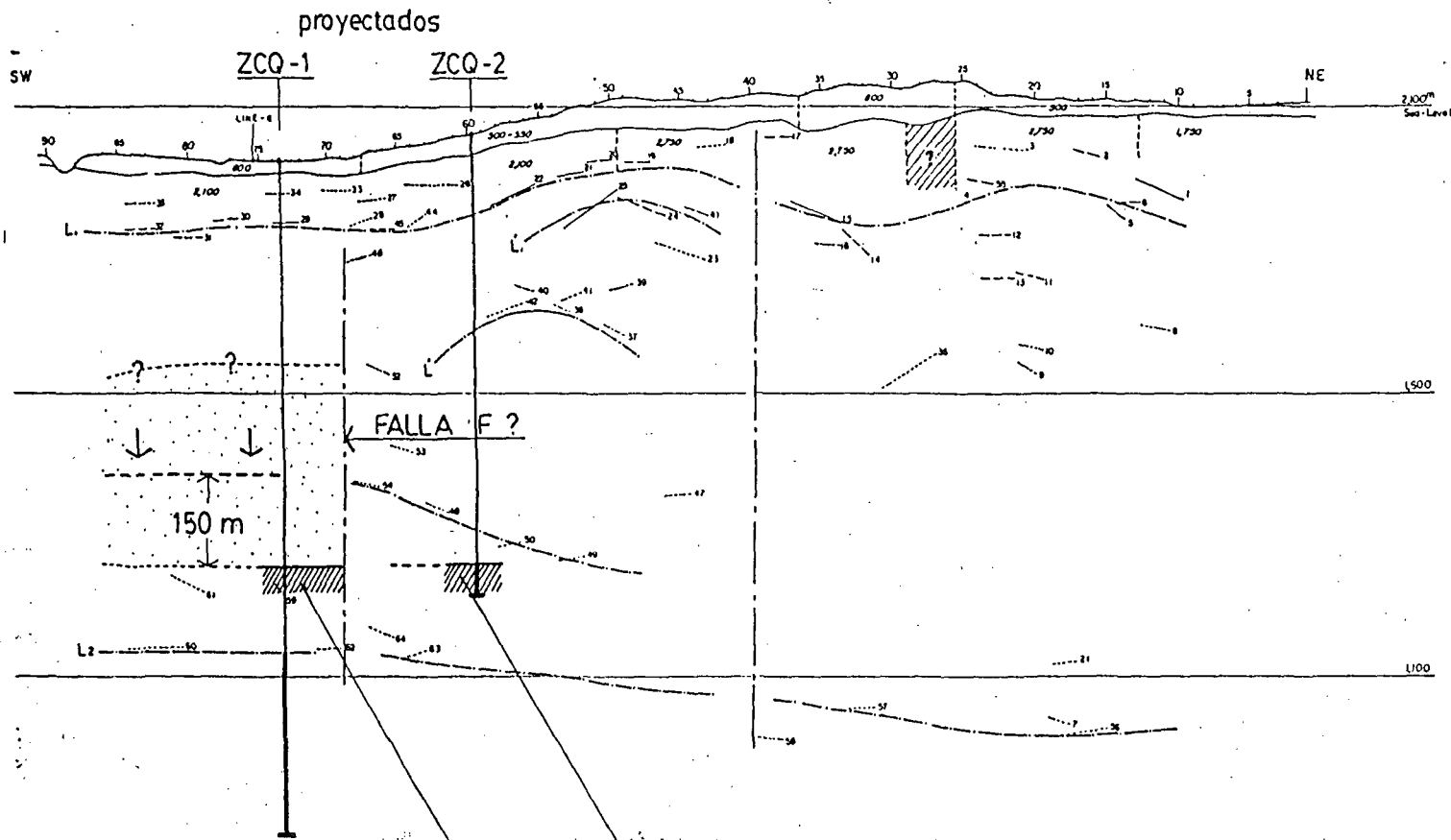
PROYECTO GEOTERMICO ZUNIL I.

LOCALIZACION
DE LINEAS SISMICAS

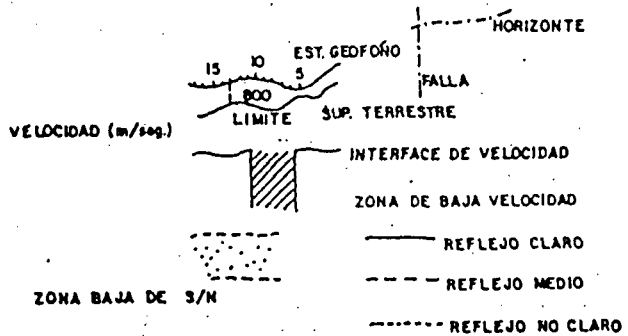
CyM/MKF.

FIGURA: 3.3-1

INFORMACION BASE: AGENCIA INTERNACIONAL DE
COOPERACION DEL JAPON.
(JICA).

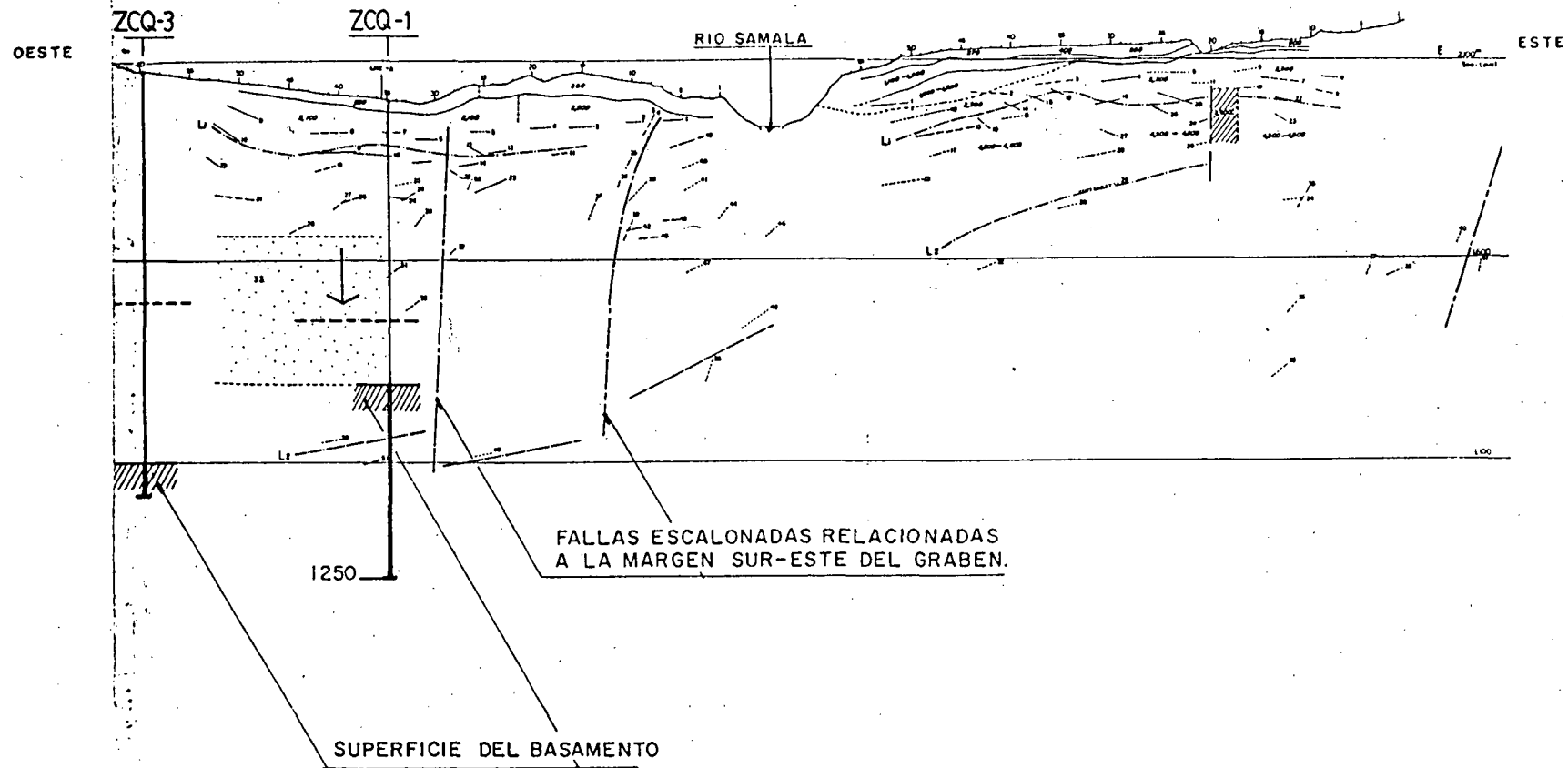


LOCALIZACION DE LA SUPERFICIE DEL BASAMENTO. (SEGUN DATOS DE POZOS PROFUNDOS).

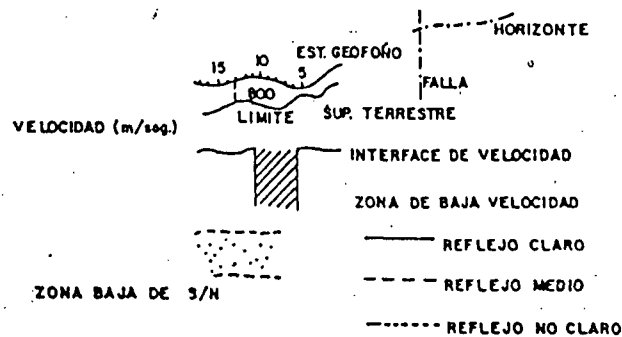


INFORMACION BASE: AGENCIA INTERNACIONAL DE COOPERACION DEL JAPON (JICA).

INSTITUTO NACIONAL DE ELECTRIFICACION INDE GUATEMALA C.A.
PROYECTO GEOTERMICO ZUNIL I
SECCION DE REFLEXION A PROFUNDIDAD LINEA A
CyM/MKF. FIGURA: 3.3-2



INFORMACION BASE : AGENCIA INTERNACIONAL DE COOPERACION DEL JAPON (JICA).



INSTITUTO NACIONAL DE ELECTRIFICACION INDE GUATEMALA C.A.

PROYECTO GEOTERMICO ZUNIL I

SECCION DE REFLEXION A PROFUNDIDAD LINEA B-C

CyM/MKF.

FIGURA: 3.3-3

Overall, the seismic reflection technique was useful in outlining probable fault zones and, in some cases, rock boundaries such as the top of the basement. The study needs to be supported by drillhole data, especially in volcanic areas where continuity is rather poor. Seismic reflection is generally more accurate in geothermal reservoirs of sedimentary settings where horizons are more pronounced and vast information exists from the oil field industry. In general, reflection studies in geothermal areas is limited, basically still in research, and only few studies in Japan (Matsukawa, Onikobe, Kakkonda, Ohdake, Hachimantai); Cerro Prieto, Mexico; and Leach Hot Springs, U.S.A. have been performed with limited success. In Cerro Prieto, for example, the basement is actually located 1000 m. deeper than was shown by reflection studies.

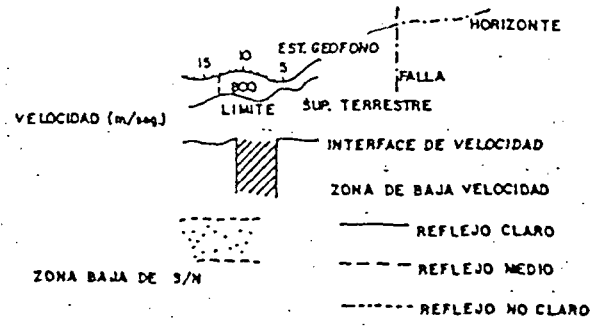
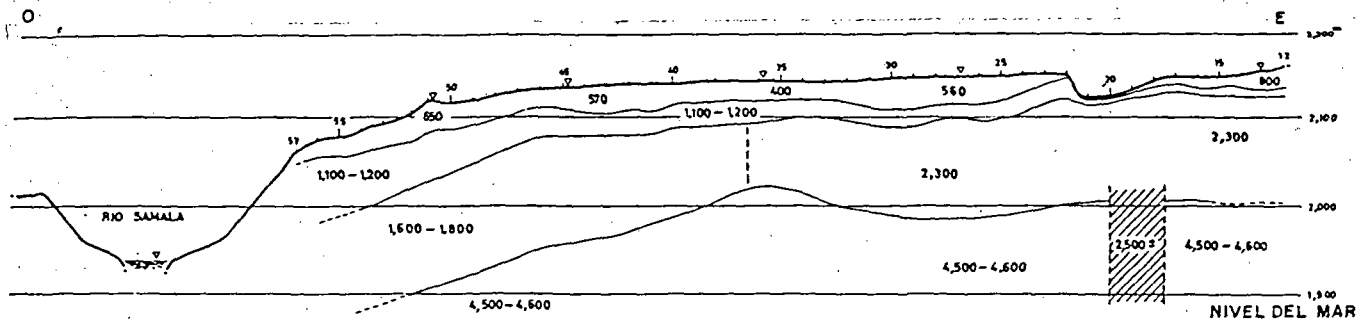
3.3.3.1.2 Seismic Refraction Studies

Seismic refraction surveys were conducted only along line C south of the town of Zunil and east of the known geothermal field. Geophones were spaced at 25 m intervals with shot point intervals every 150 to 350 m. Considering the entire length of the line (1,125 m) as the seismic spread, the refraction survey would have been accurate only to a depth of approximately 400m. The objectives would therefore be confined to the overburden layers and the overburden-bedrock contact. Results are presented in Figure 3.3.-4. Four velocity layers were detected with the bottom layer (4,500-4,600 m/sec.) representing the dacitic bedrock (Almolonga complex). The transition from layer 2 to layer 3 may reflect saturation, as the compressional velocity of water is close to 1500 m/sec., as well as a more compact material or a combination of both.

The refraction survey delineated only the upper 300 m of line C and its usefulness is therefore somewhat limited since we are interested in greater depths.

3.3.3.2 Magnetics

Three magnetic anomaly maps were produced from previous studies and reviewed. These are: a regional magnetic anomaly map, a magnetic anomaly map, and a residual magnetic anomaly map. (Refer to Figures 3.3-5, 3.3-6 and 3.3-7) All three encompass an area of approximately 130 km² within the vicinity of Zunil. Groundmagnetic measurements over prospects in volcanic settings such as Zunil are always disturbed by near surface inhomogeneities, as well as the weak magnetic susceptibility contrast between the volcanics and the underlying granitic rocks. These areas are usually investigated with airborne magnetic surveys as was done in the Theistareykir prospect in Iceland with considerable success. In addition, rough terrain, as in the Zunil area, gives rise to anomalies related to the topography and not subsurface conditions. A station situated in a depression such as the Zunil valley will result in false negative anomalies



INFORMACION BASE: AGENCIA INTERNACIONAL DE COOPERACION DEL JAPON (JICA)

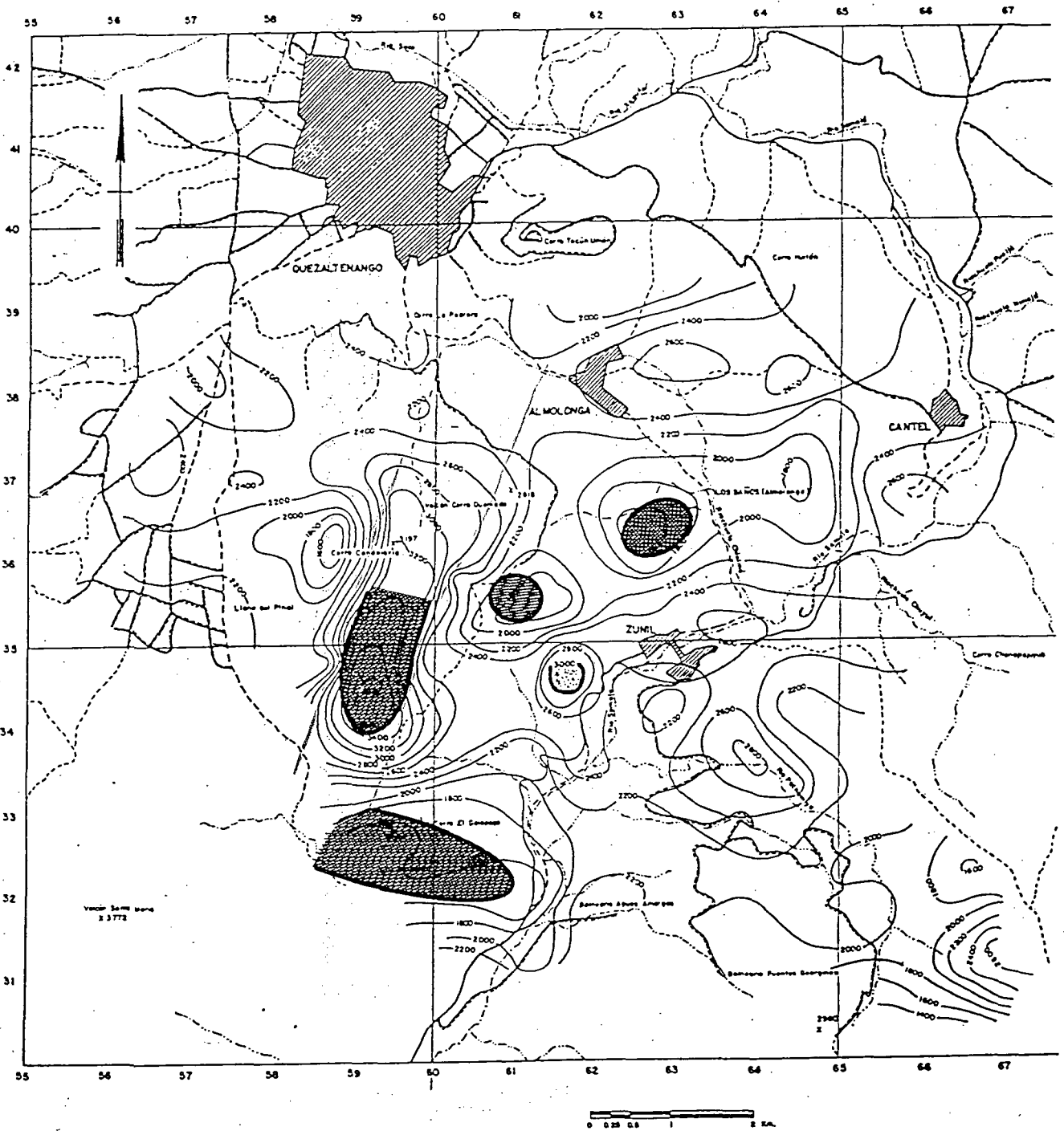
INSTITUTO NACIONAL DE ELECTRIFICACION INDE GUATEMALA C.A.

PROYECTO GEOTERMICO ZUNIL I

SECCION DE VELOCIDADES DE REFRACCION

CyM/MKF.

FIGURA: 3.3-4



ZONA DE POSIBLE INTERES



ZONAS ALTAS TOPOGRAFICAS

INFORMACION BASE: PLANO INDE POR ING. J. PALMA

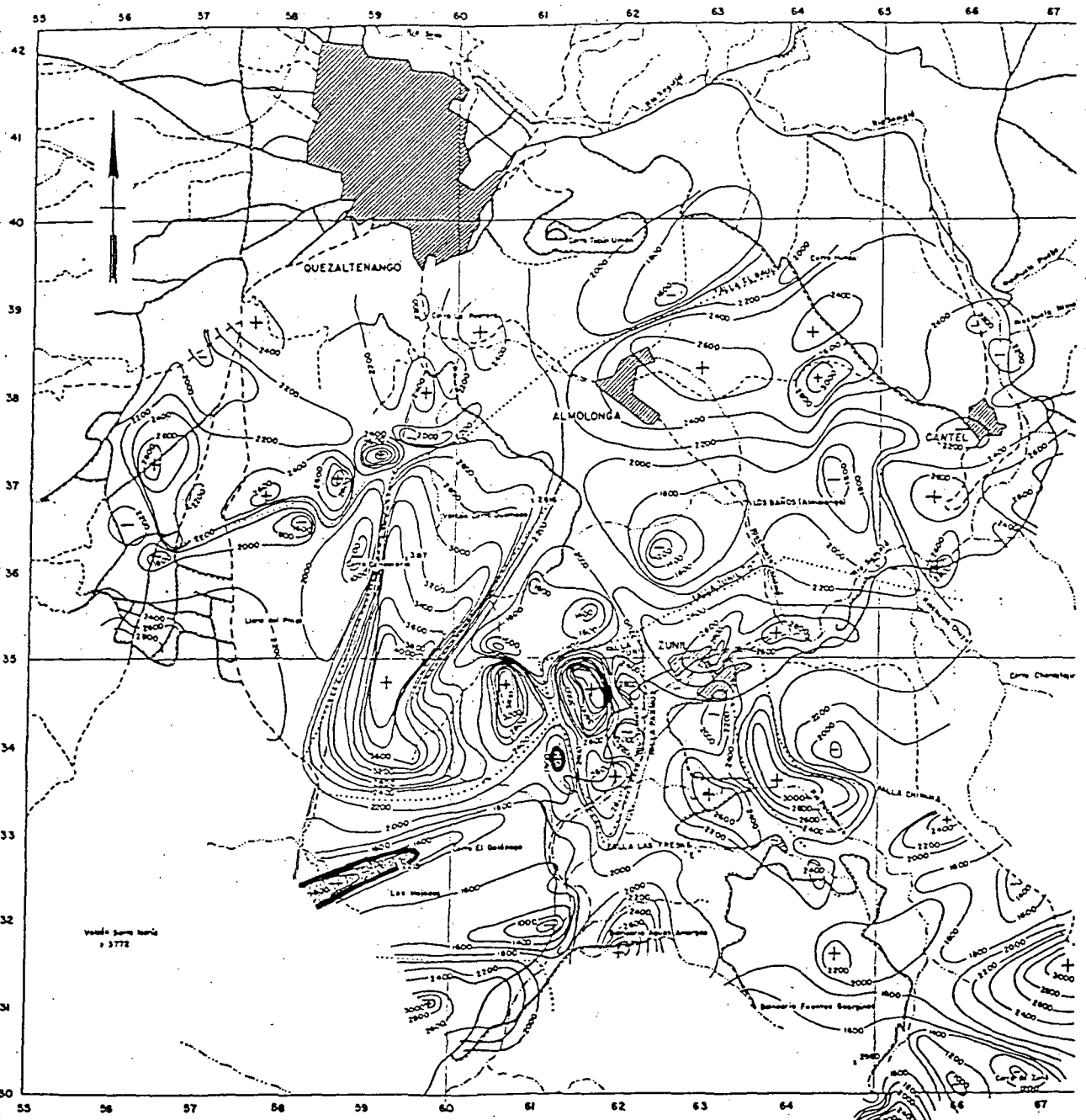
INSTITUTO NACIONAL DE ELECTRIFICACION
INDE GUATEMALA C.A.

PROYECTO GEOTERMICO ZUNIL I

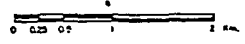
MAPA REGIONAL DE ANOMALIA
MAGNETICA

CyM/MKF.

FIGURA: 3.3-5



..... PROBABLE CORRELACION CON FALLAS O CONTACTOS GEOLÓGICOS



ZONAS DE INTERES

INFORMACION, BASE: PLANO INDE POR ING. J. PALMA

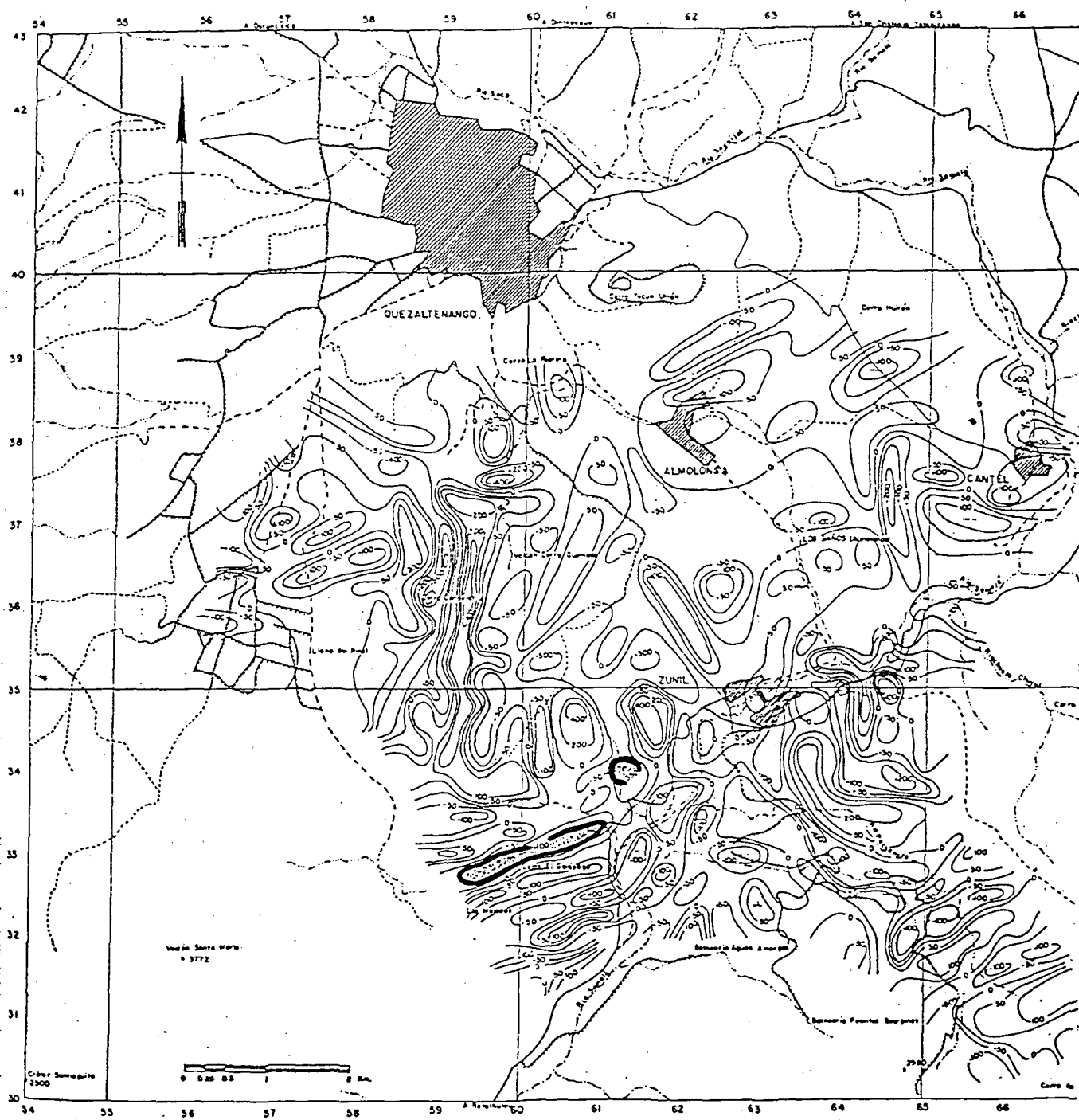
INSTITUTO NACIONAL DE ELECTRIFICACION
INDE GUATEMALA C.A.

PROYECTO GEOTERMICO ZUNIL I

MAPA DE ANOMALIAS
MAGNETICAS

CyM/MKF.

FIGURA 3.3-6



ZONA DE INTERES

INFORMACION BASE: PLANO INDE POR
ING. J. PALMA

INSTITUTO NACIONAL DE ELECTRIFICACION
INDE GUATEMALA C.A.

PROYECTO GEOTERMICO ZUNIL I

MAPA DE ANOMALIAS
MAGNETICAS RESIDUALES

Cym/MKF

FIGURA: 3.3-7

due to the effect of magnetic rocks above the station. Magnetic anomalies showing a strong correlation with the terrain are therefore regarded as less significant than others and the overall interpretation considered qualitative. This was the case in the magnetic anomaly maps such as the regional map shown in Figure 3.3-5. Magnetic highs and lows are associated with known topographic features lying north and west of Zunil. Inferences regarding faulting or thermoremanent magnetization (TRM) of deep seated rocks related to geothermal systems may be quite misleading if only magnetic maps such as Figure 3.3-5 are used.

The effect of the topography also influences the results depicted in Figures 3.3-6 and 3.3-7. An anomaly of interest in Figure 3.3-5 lies approximately 1 km. west of the town of Zunil. Though the effect of the surrounding hills may influence this anomaly, the high may be the result of increased magnetization, such as larger amounts of magnetite and/or titanomagnetite in the fresh volcanics. This area is also demonstrated on Figures 3.3-6 and 3.3-7 as a positive magnetic anomaly. In geothermal areas where magnetite is stable (such as Olkaria in Kenya) or where magnetic pyrrhotite forms as a replacement mineral or directly from solution (as in various fields in New Zealand) the "de-magnetization" of rocks does not occur and negative anomalies related to geothermal processes are not exhibited. The negative anomalies in this case may correlate with the contact with the Almolonga lavas, as described by INDE.

Two other interesting negative anomalies occur in the western part of Zunil; these are depicted in figures 3.3-6 and 3.3-7 as zones of interest. The zone closest to Zunil corresponds with an area of low resistivity detected by both JICA and INDE in 1977-1978. In Zunil, these anomalies are caused by lithologic contacts (as proposed by INDE) and fault zones. The groundmagnetic survey serves only to support other geophysical data obtained by more reliable primary methods. The two zones of interest are noted as supporting evidence.

3.3.3.3 Gravity

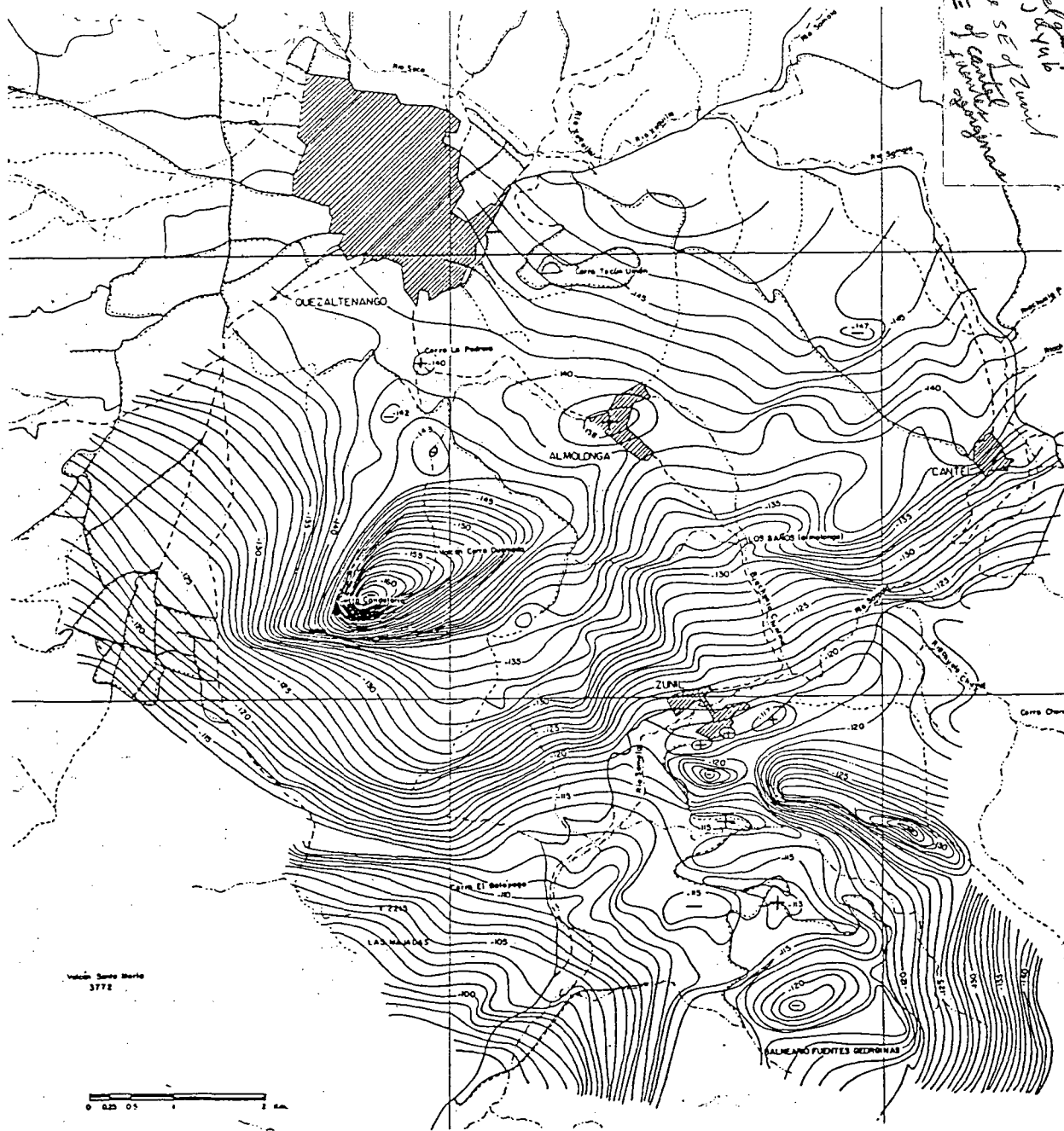
Gravity studies were performed by INDE both in a regional context extending from Quetzaltenango to south of Cerro El Galápago (approximately 90 km²) and in a local framework around Zunil, covering approximately 30 km². Two Bouguer anomaly maps were produced and only the regional map was discussed with some detail. This report will therefore include interpretations and analyses of gravity investigations for the local Bouguer anomalies. Since station density was not shown, the accuracy of contouring could not be verified and interpretations will be based solely on the maps presented. Basement density was taken as 2.67 gm./cm³. Some anomalies may be obscured by either an altered upper basement which decreases the density and subsequently increases the negative anomalies or by a denser mass over the basement which would produce the opposite effect.

Figure 3.3-8 depicts the regional Bouguer anomaly map which principally demonstrates the general dip of the basement structure toward the northeast within the Quetzaltenango-Zunil region. Immediately north and west of Zunil, however, the basement appears to have a gradient toward the northwest. This is to be expected as the basement steepens as it underlies the Quetzaltenango basin to the north. No appreciable information is obtained within the geothermal area west of Zunil; small gravity highs and lows south of Zunil are probably related to basement highs/lows, block faulting, and hydrothermally altered areas. Some faulting such as the Zunil fault zone may be inferred from Figure 3.3-8 but the local gravity map depicts this more clearly.

Figure 3.3-9 depicts a local Bouguer anomaly map within the geothermal zone and presents an interesting view into the basement structure. It is from Figure 3.3-9 that subsequent interpretations are based. By drawing a series of sections across the geothermal area and correlating these with probable density contrasts within the basement, a NE-SW graben structure approximately 1 km. wide was detected under the Zunil geothermal field. This is possibly part of a larger graben structure described by INDE (Reports and discussions with Ing. E. Tobias and Ing. J. Palma). Its location is outlined in the figure. The gravity graben may be defined by actual basement structure or by thermally altered zones, however, when correlated with other studies the structural interpretation appears more reasonable. This down-dropped structure is bounded on the NW by a horst or ridge like structure which correlates with the Zunil fault zone, on the SE by step faults and a higher basement and to the NE by a probable fault which defines the boundary of a higher basement block under the town of Zunil. This fault was detected by seismic reflection studies (refer to Figure 3.3-2). It should also be noted that another graben structure exists immediately NE of the Zunil area, as shown on Figure 3.3-9, and extending in a northeasterly direction toward the town of Cantel. The interpreted graben within the geothermal field is depicted in the cross-section shown in Figure 3.3-10. Both the NW and SE sides are step faulted and numerous faults and fractures may be encountered. Some of these fractures probably extend into the Tertiary volcanics. A reasonable interpretation contends that the fractures within the upper granodioritic basement control the exploitable geothermal system. It follows that fractures that extend close to the surface give rise to the surface thermal manifestations. Other probable faults inferred from gravity data are also shown in Figure 3.3-9.

It is the faulting on the NW side of this graben, depicted as the horst in Figure 3.3-10, that gives rise to the Zunil Fault Zone. The trace of this fault closely follows the NW boundary of the graben. Faulting on the SE boundary may be less pronounced but it is nevertheless existent, as demonstrated by seismic reflection studies (Figure 3.3-3). A major fault in this area projects to the surface at an angle close to 60° and its trace is expressed by the Samalá River and the numerous thermal springs which follow a linear pattern. This fault was also detected by

P = Volc. Cerro Guatemalco
 SH = Cerro con anomalía
 + en 1946
 E = N 118° 49' S E de Zunil
 S E de Cerro Guatemalco



$\frac{22}{11.7}$

INSTITUTO NACIONAL DE ELECTRIFICACION
 INDE GUATEMALA C.A.

PROYECTO GEOTERMICO ZUNIL I

MAPA REGIONAL DE ANOMALIAS
 BOUGUER

INFORMACION BASE: PLANO INDE POR ING. J. PALMA

CyM/MKF.

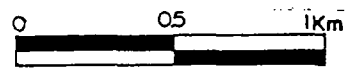
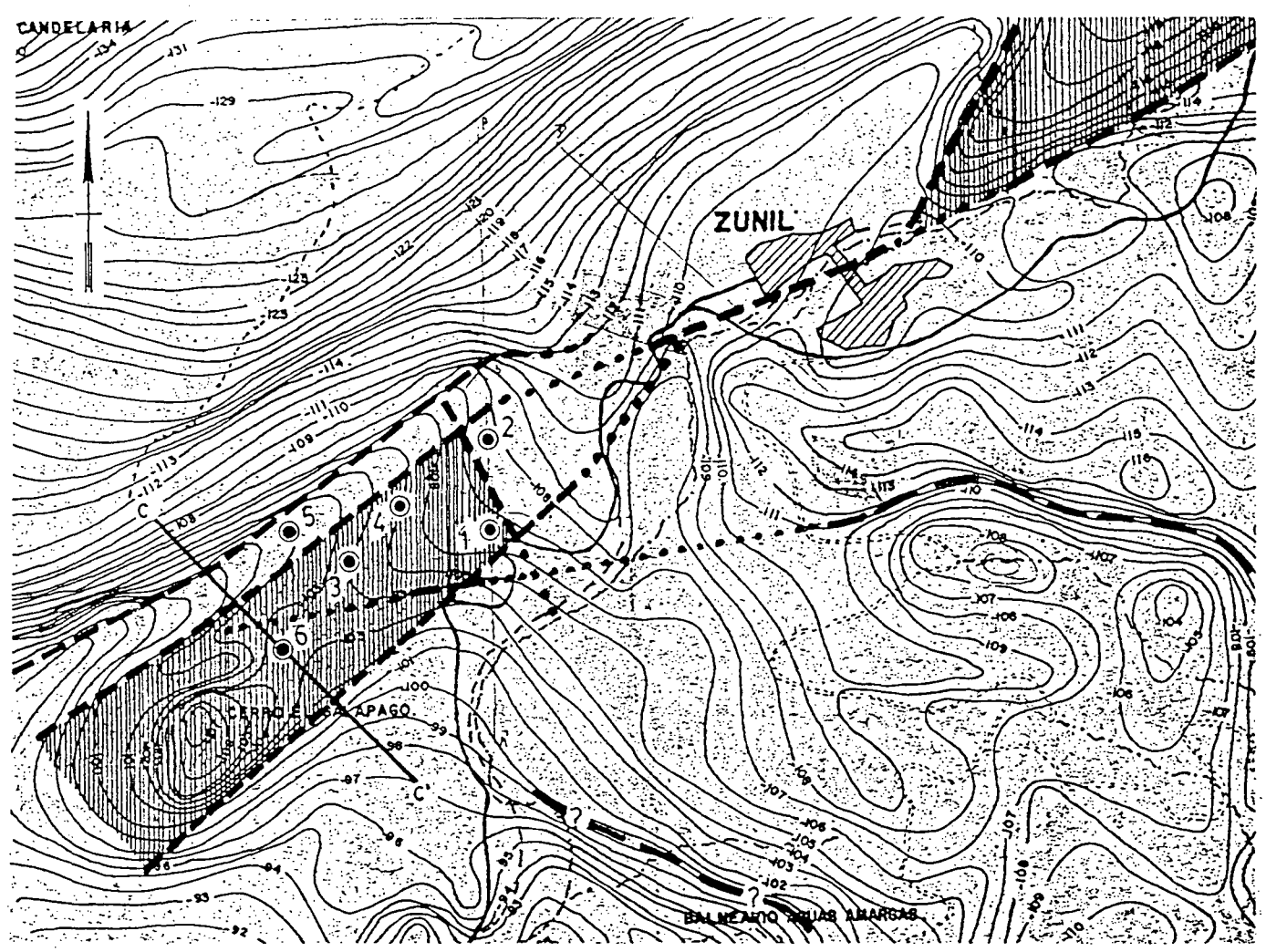
FIGURA: 3.3-8

9.2

$$\frac{13}{18} = 1.35$$


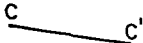


$$\frac{17}{32} = 1.29$$

$$\frac{35}{46} = 1.28$$



ESCALA GRAFICA
wrong scale

SIMBOLOGIA

-  AREA CON DEPLAZAMIENTO HACIA ABAJO DEL BASAMENTO ASI COMO UN GRABEN.
-  SECCION
-  PROBABLE FALLA RELACIONADA A FALLAMIENTO EN EL BASAMENTO. PUNTOS DENOTAN SOSPECHA.
-  POZO

INFORMACION BASE: PLANO INDE POR ING. J. PALMA

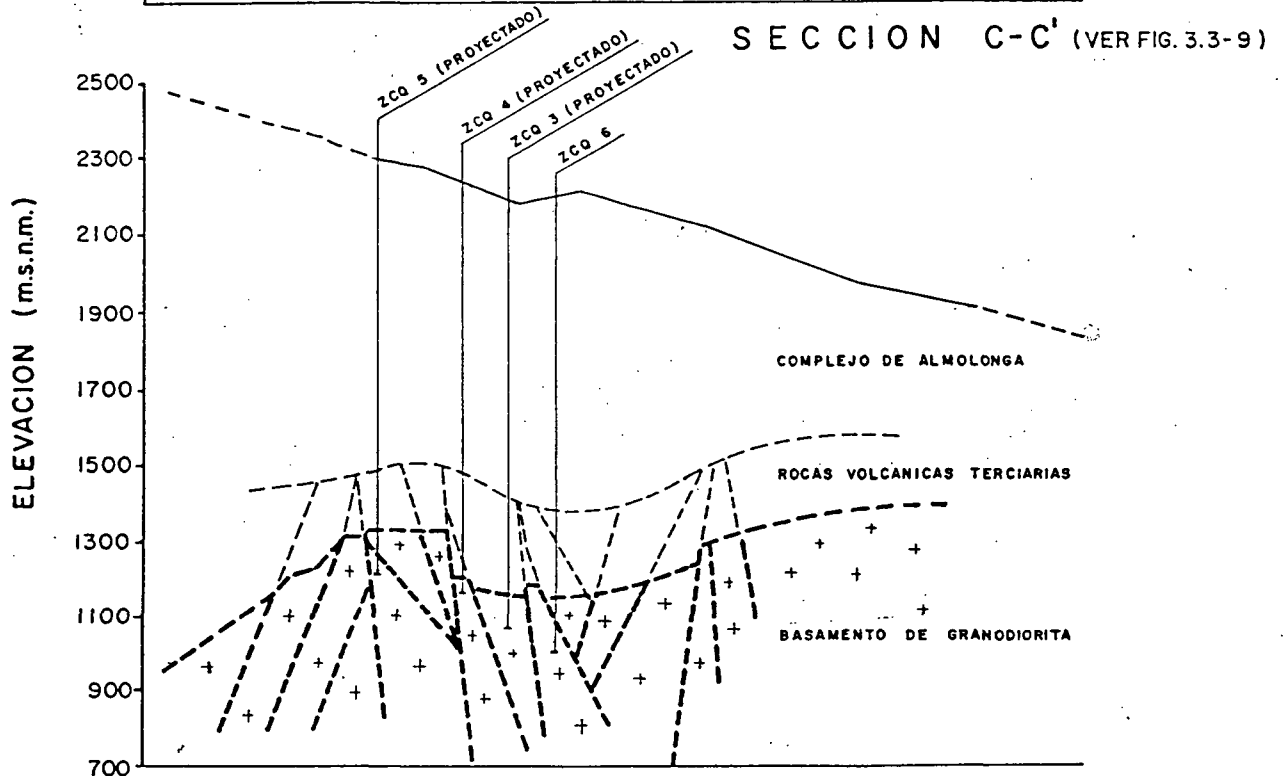
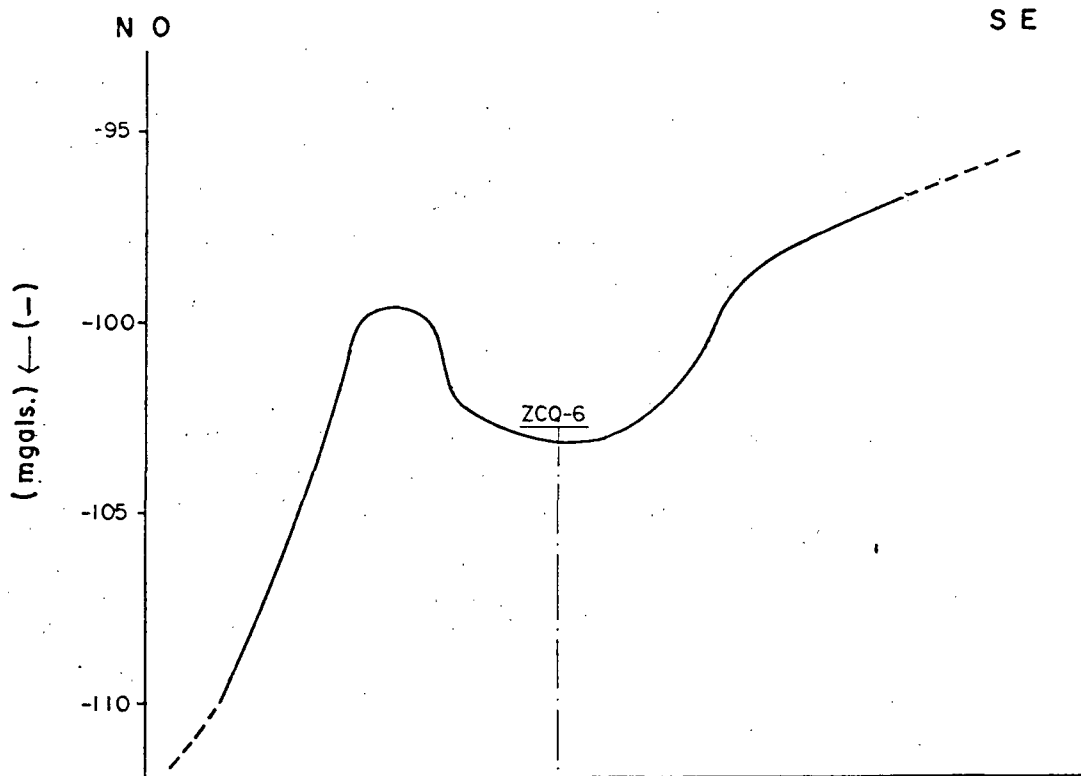
INSTITUTO NACIONAL DE ELECTRIFICACION
INDE GUATEMALA C.A.

PROYECTO GEOTERMICO ZUNIL I

MAPA DE ANOMALIAS BOUGUER

CyM/MKF.

FIGURA: 3.3-9



PREPARADO POR: ING. U. CORDON CYM/ MKF

INSTITUTO NACIONAL DE ELECTRIFICACION
INDE GUATEMALA C.A.

PROYECTO GEOTERMICO ZUNIL I.

ESQUEMA REPRESENTATIVO DE
ANOMALIAS DE LA GRAVEDAD.
INTERPRETATIVA

Cym/ MKF.

FIGURA: 3.3-10

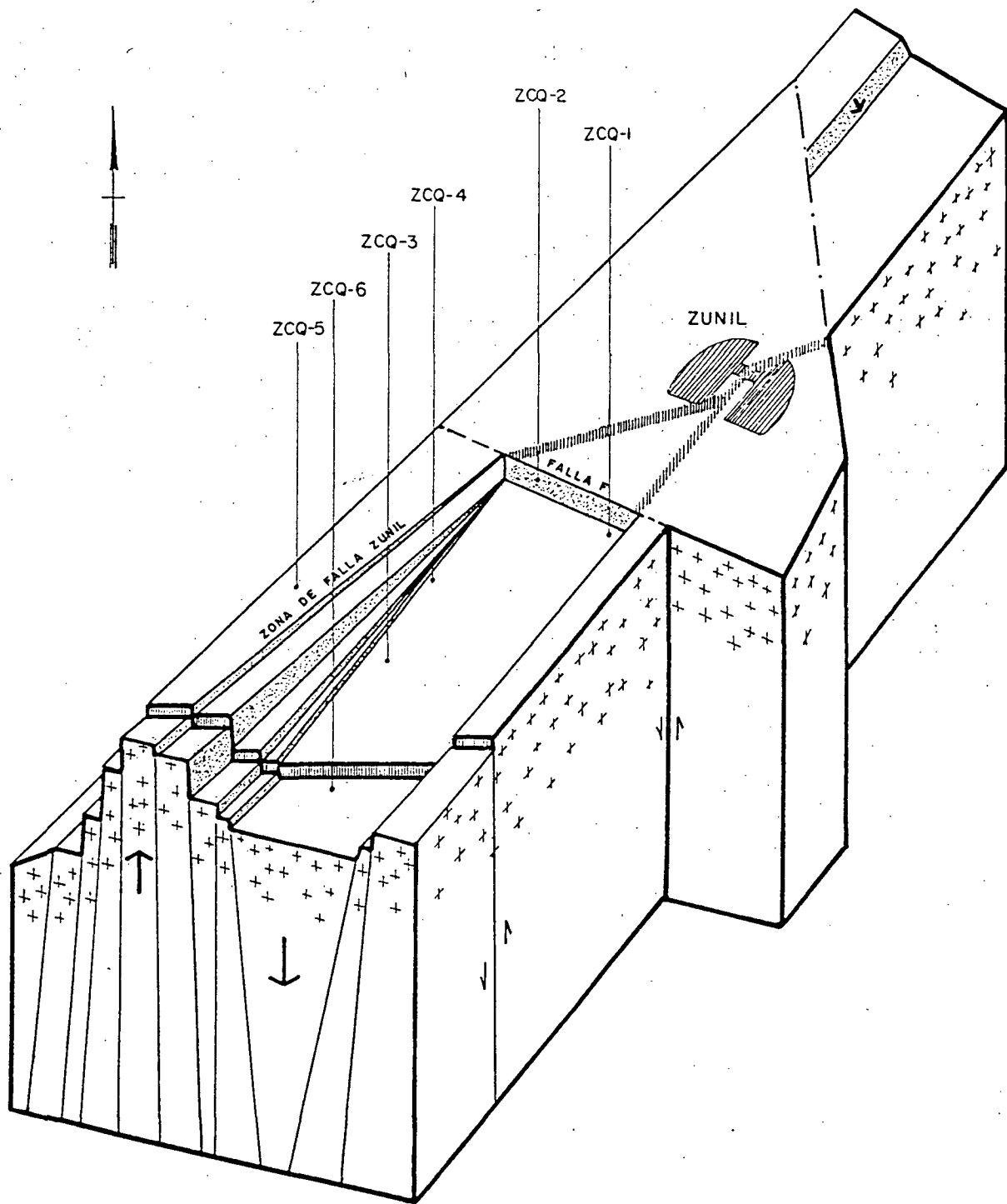
ER surveys. It should also be noted that the fault which crosses between boreholes ZCQ-1 and ZCQ-2 and outlined in Figure 3.3-9 as the NE graben boundary was also identified by the reflection studies (refer to Figure 3.3-2). This fault may be Fault F in some reports, though its orientation is possibly toward the NW. The gravity and seismic reflection studies are therefore corroborating each other's data as well as linear patterns from thermal manifestations. It should also be noted that many of these faults were previously plotted by INDE.

The wells plotted on Figures 3.3-9 and 3.3-10 are located within the graben and horst structures of the Zunil field. A projection of wells ZCQ-3, 4 and 5 into the cross-section of Figure 3.3-10 shows that their productivity is dependent on both their location within this structural depression and their interception of faults and fractures. It is evident that the deeper the wells penetrate into the fractured upper basement, the greater the likelihood of crossing fractures associated with step faults and the geothermal system.

The SW area of the graben shows a decrease in negative Bouguer anomalies probably related to a denser mass overlying the basement and not necessarily due to a shallower basement. This may be corroborated by mineralogical evidence (discussions with Dr. A. Kudo) which shows that basaltic andesites (denser rocks) extend from Volcán Santa María toward this area. This would cause the negative anomalies to decrease toward the southwest. A conceptual model of the aforementioned interpretation is depicted in Figure 3.3-11.

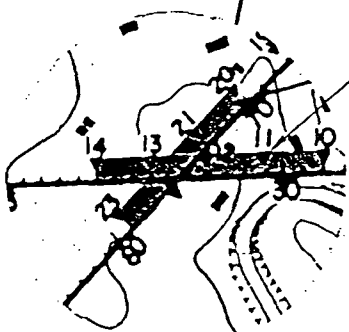
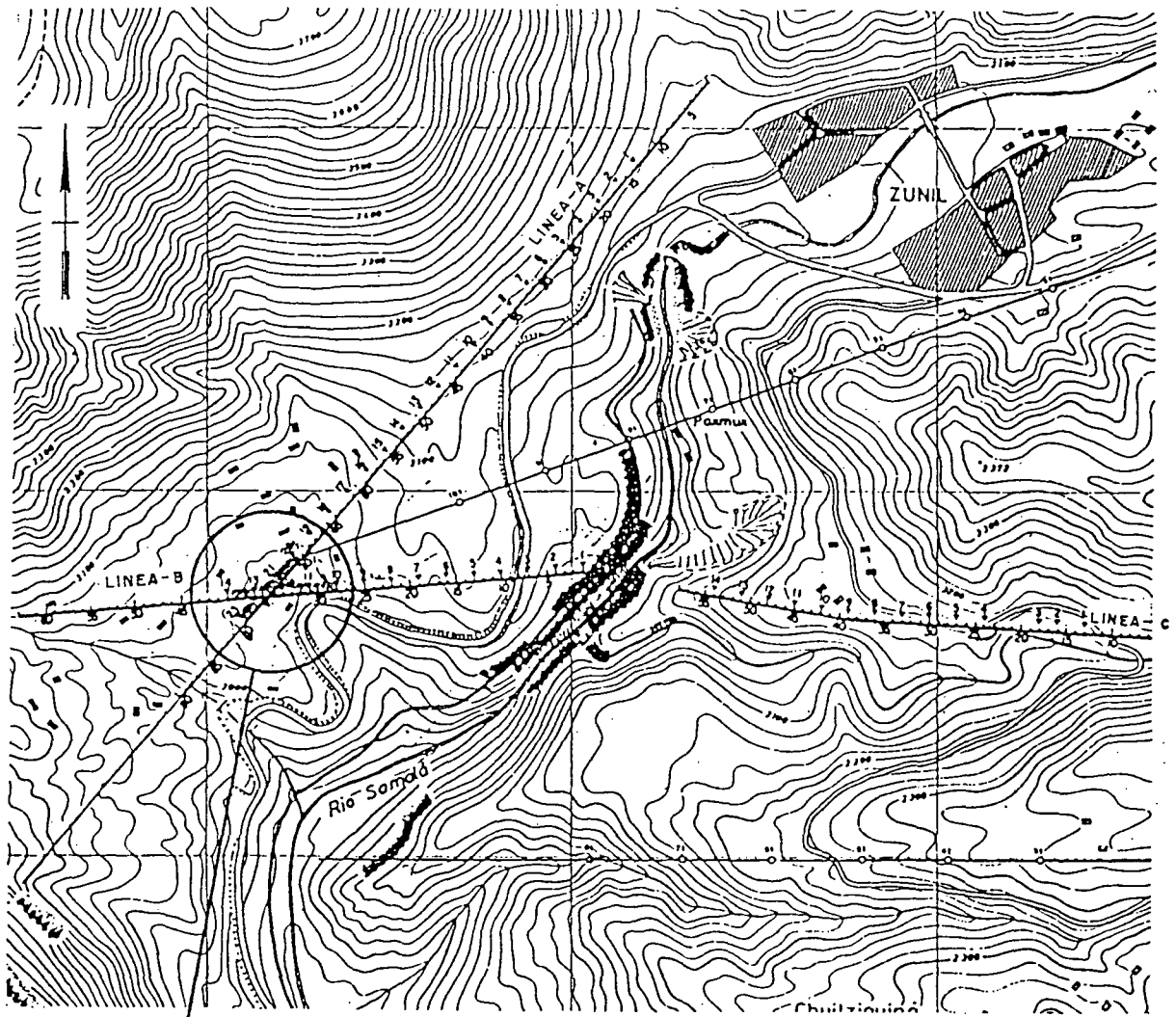
3.3.3.4 Temperature Gradient Studies

Temperature measurements in boreholes were taken by JICA in 1977 and by INDE 1978 and in years following the drilling of the deep production wells. The temperature gradient study by JICA was conducted during the seismic reflection work; shot holes varying in depth from 3 m. to 18 m. (avg. 15 m.) were utilized for temperature measurements prior to blasting. Their locations are shown on Figure 3.3-12. Results of this study are presented in Figure 3.3-13. The isotherms should have been drawn closer to the surface in this figure since holes 37 and 31 reach depths of 12.5 m. and 15.9 m. respectively while the figure depicts depths close to 30 m. Isothermal contours lie nearly parallel the ground surface, with the highest temperature encountered (70 °C) along the intersection of lines A and B. Considering a ground surface temperature of 20 °C, this represents an increase of 50 °C/16m. or a gradient of approximately 3 °C/m. for the upper 16 m.; this eventually decreases with depth. Its lateral extension remains unknown in this study. Results of this investigation therefore outline this zone as favorable due to anomalous heat flow. Other areas outlined in Figure 3.3-13 show temperatures only as high as 30°C. Temperature gradient studies by INDE in 1978 were conducted in holes Z-1 to Z-5. Refer to Figure 3.3-14 for their locations. The temperature profiles corresponding to

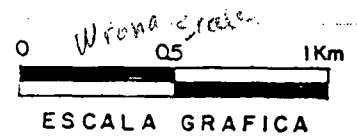


PREPARADO POR: ING. U. CORDON CYM/MKF

INSTITUTO NACIONAL DE ELECTRIFICACION INDE GUATEMALA C.A.	
PROYECTO GEOTERMICO ZUNIL I	
MODELO CONCEPTUAL DEL BASAMENTO BASADO EN ANALISIS GRAVIMETRICO	
CyM/MKF.	FIGURA: 3. 3-II



ZONA DE ALTA TEMPERATURA



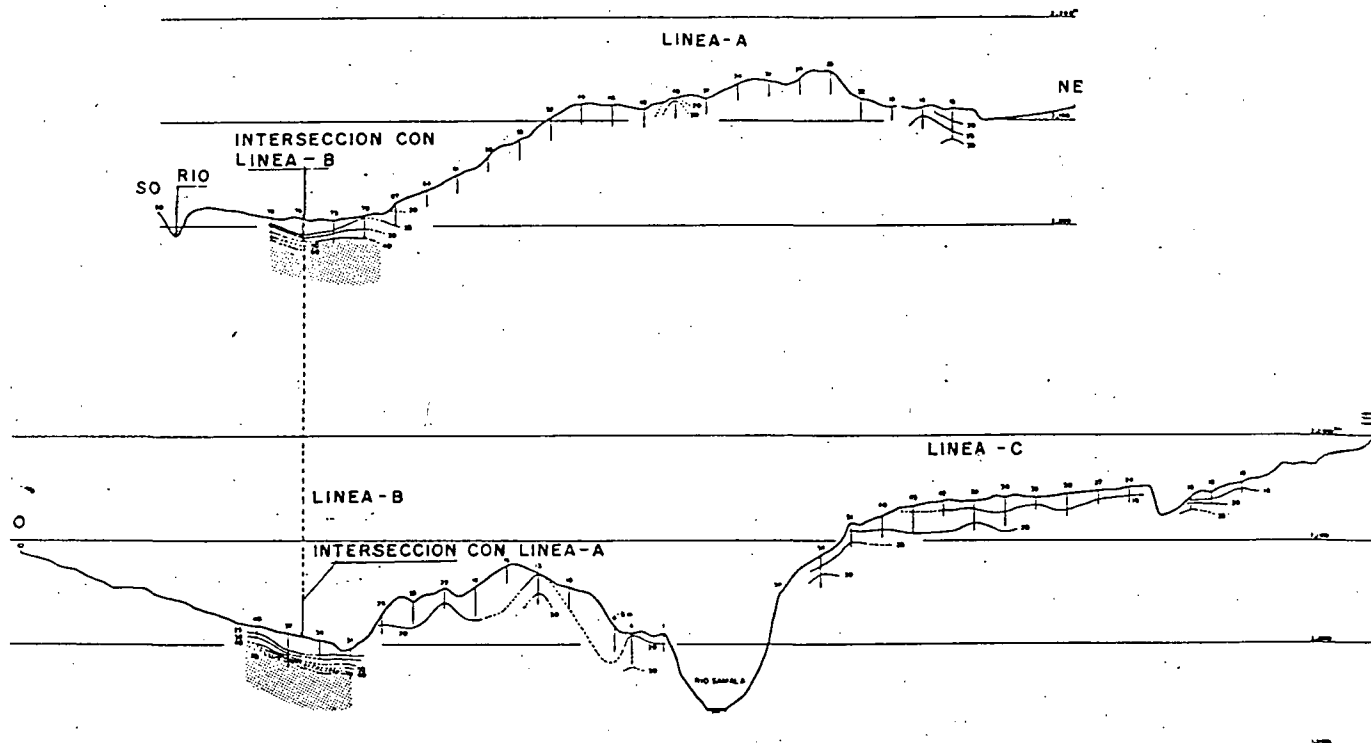
ESCALA GRAFICA

POZO = ▽

INFORMACION BASE: AGENCIA INTERNACIONAL DE COOPERACION DEL JAPON. (JICA).

INSTITUTO NACIONAL DE ELECTRIFICACION INDE GUATEMALA C.A.
PROYECTO GEOTERMICO ZUNIL I
UBICACION DE POZOS
CyM / MKF

FIGURA: 3.3-12.



INFORMACION BASE : AGENCIA INTERNACIONAL DE
COOPERACION DEL JAPON.
(JICA).

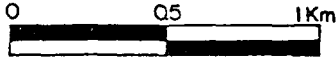
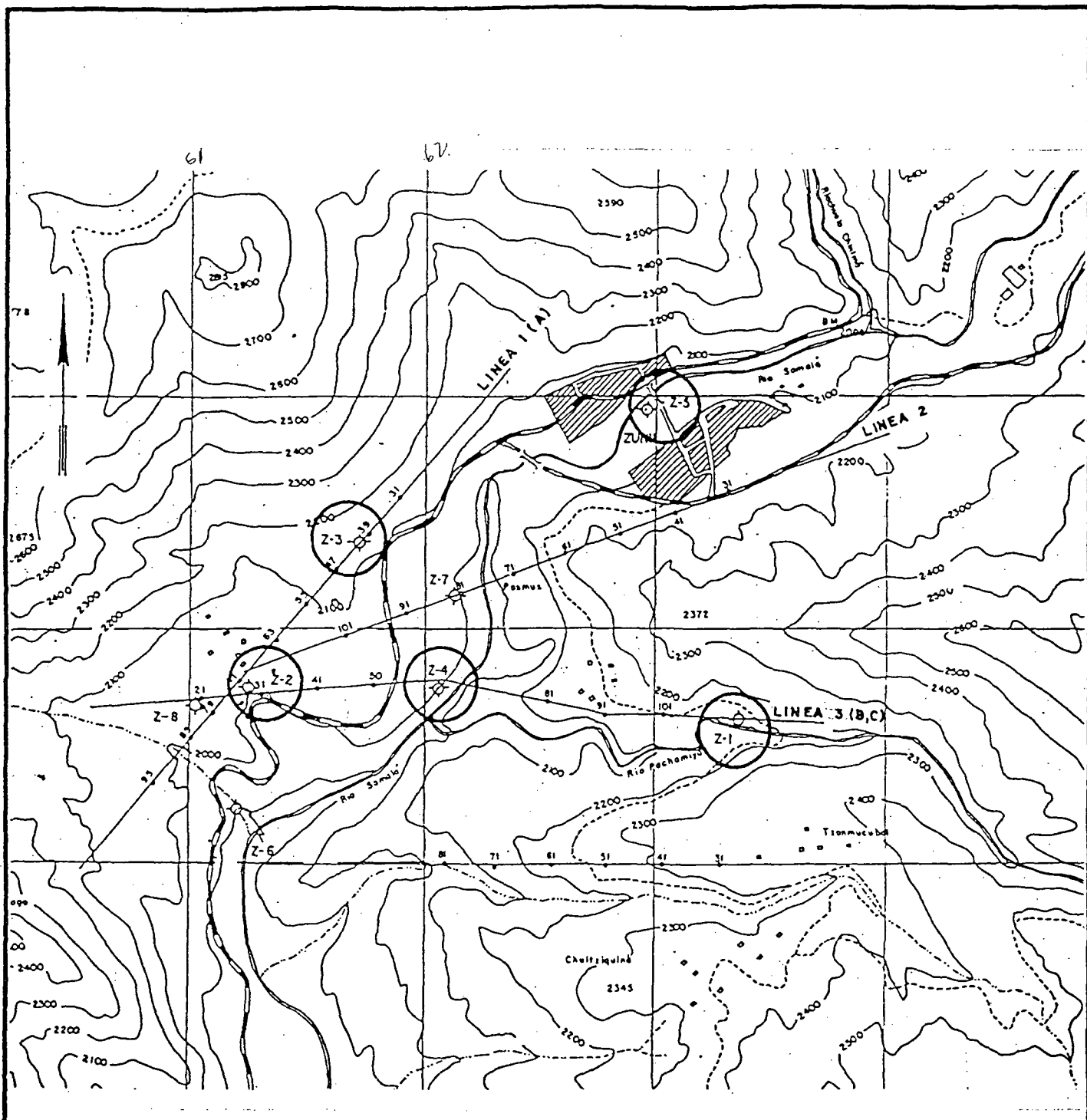
INSTITUTO NACIONAL DE ELECTRIFICACION
INDE GUATEMALA C.A.

PROYECTO GEOTERMICO ZUNIL I

DISTRIBUCION DE
TEMPERATURAS
EN LINEAS A-B-C

CyM/MKF.

FIGURA: 3.3-13



ESCALA GRAFICA

INSTITUTO NACIONAL DE ELECTRIFICACION
INDE GUATEMALA C.A.

PROYECTO GEOTERMICO ZUNIL I

UBICACION DE POZOS DE GRADIENTE
DE TEMPERATURA Z-1 AL Z-5

Cym/MKF.

FIGURA: 3.3-14

INFORMACION BASE: PLANO INDE POR ING.
J. PALMA

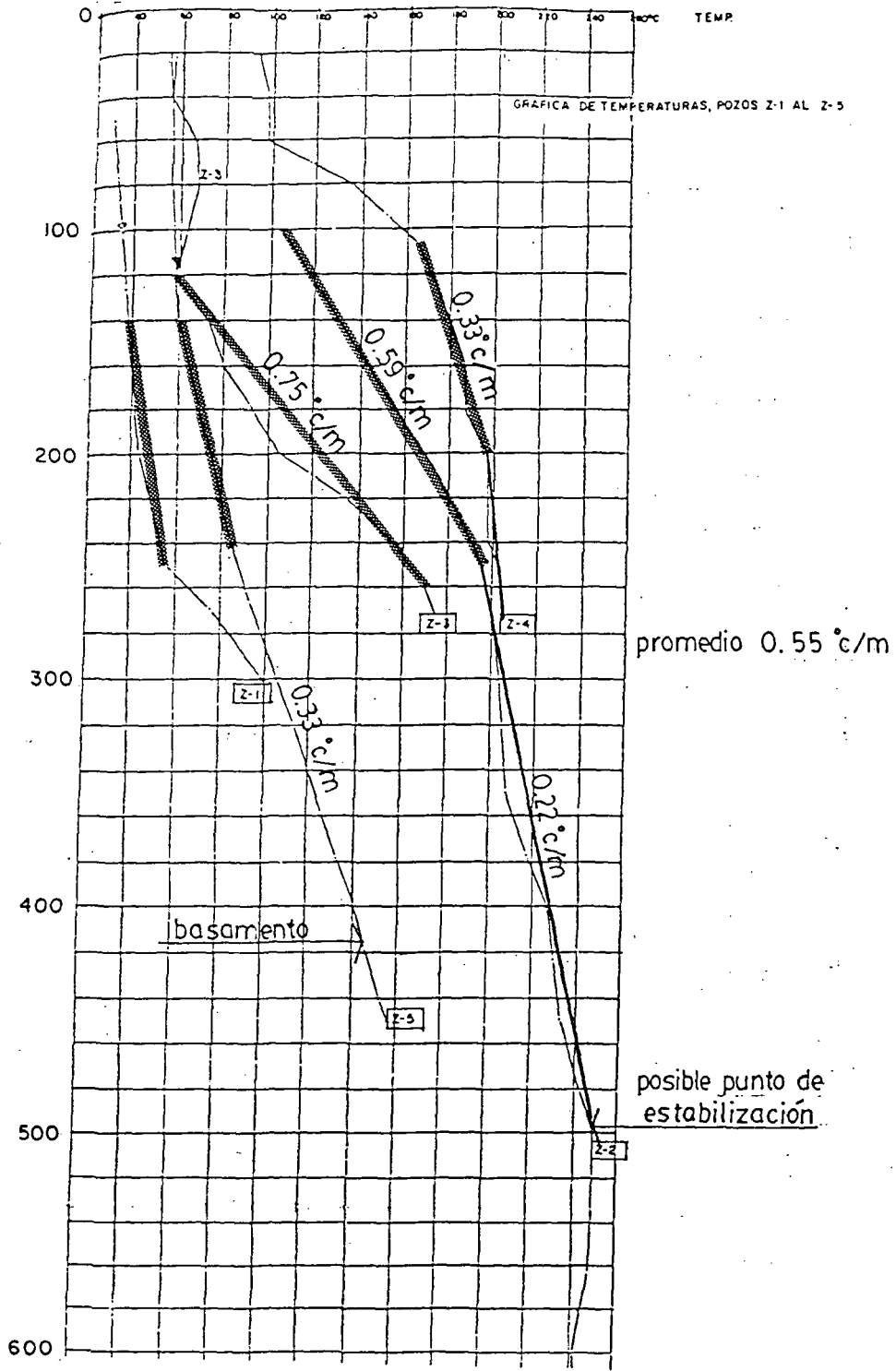
these holes are presented in Figure 3.3-15. Holes Z-1 and Z-5 are located outside the known geothermal field in an area where the basement is shallow. The profiles are therefore representative of the graben structure west of Zunil. Z-1 intercepted the basement at a depth of only 417 m. but the gradient remained constant at 0.33 °C/m. from 140 m. to 450 m. Wells Z-3 and Z-4 also lie within the shallow bedrock block inferred from gravity data (see Figures 3.3-9 and 3.3-14) but they are located in the vicinity of probable fault zones. It may be that the proximity of Z-3 to the Zunil Fault Zone which bounds the geothermal field gives the rise to its gradient of 0.75 °C /m. between 120 m. and 270 m. depth. Well Z-2 and Z-4 exhibit gradients of only 0.57 °C/m and 0.33°C/m. respectively in this interval. Well Z-2 lies within the upper reaches of the graben and also close to faults associated with the graben formation (Figure 3.3-9). It also lies in an area outlined by low resistivity (< 10 ohm-m). This well shows a gradient change from 0.59 °C/m. to 0.22 °C/m. at a depth of 270 m. and maintains this gradient to a depth of 500 m. where it appears to stabilize. The highest temperature of 247 °C was therefore obtained in well Z-2 at 500 m. depth. By extrapolating the gradient in the other wells it is conceivable that wells Z-3 and Z-4 may have attained this temperature if they had been drilled deeper. Data from these wells demonstrate that favorable temperatures lie in an area southwest of Zunil.

Temperatures in production wells ZCQ-1 through ZCQ-6 were also reviewed; the isotherms are presented in Figure 3.3-16. It is clearly noticeable that the highest temperatures are encountered in a southwesterly direction, following the graben outlined by gravity data. This is again demonstrated in Figures 3.3-17 and 3.3-18 where cross-sections through the wells depict the area of highest heat flow originating southwest of well ZCQ-6. In view that the geothermal field is a fracture dominated system, the presence of faults and fractures acting as conduits for thermal fluids would give rise to zones of high heat flow; this is exhibited by the isotherms in Figures 3.3-17 and 3.3-18.

3.3.3.5 Electrical Resistivity Surveys

Vertical electrical soundings (VES) with the Schlumberger array were performed in the Zunil geothermal area by both the Japanese (JICA) in 1976-1977 and INDE in 1977. The selection of Schlumberger arrays was adequate since the soundings are less affected by near-surface disturbances than those made with other 4-point arrays such as Wenner or dipole-dipole. The arrays were extended along 4 lines of approximately 3,000 m. lengths south and southwest of the town of Zunil (Figure 3.3-19). Variable separations from $AB/2 = 250$ m. to $AB/2 = 1000$ m. were used. The rugged topography is a limiting factor for areal coverage, nevertheless, an excellent program was implemented by both parties. Data reduction and subsequent interpretations are based on accurate procedures and sound judgement.





INSTITUTO NACIONAL DE ELECTRIFICACION
INDE GUATEMALA C.A.

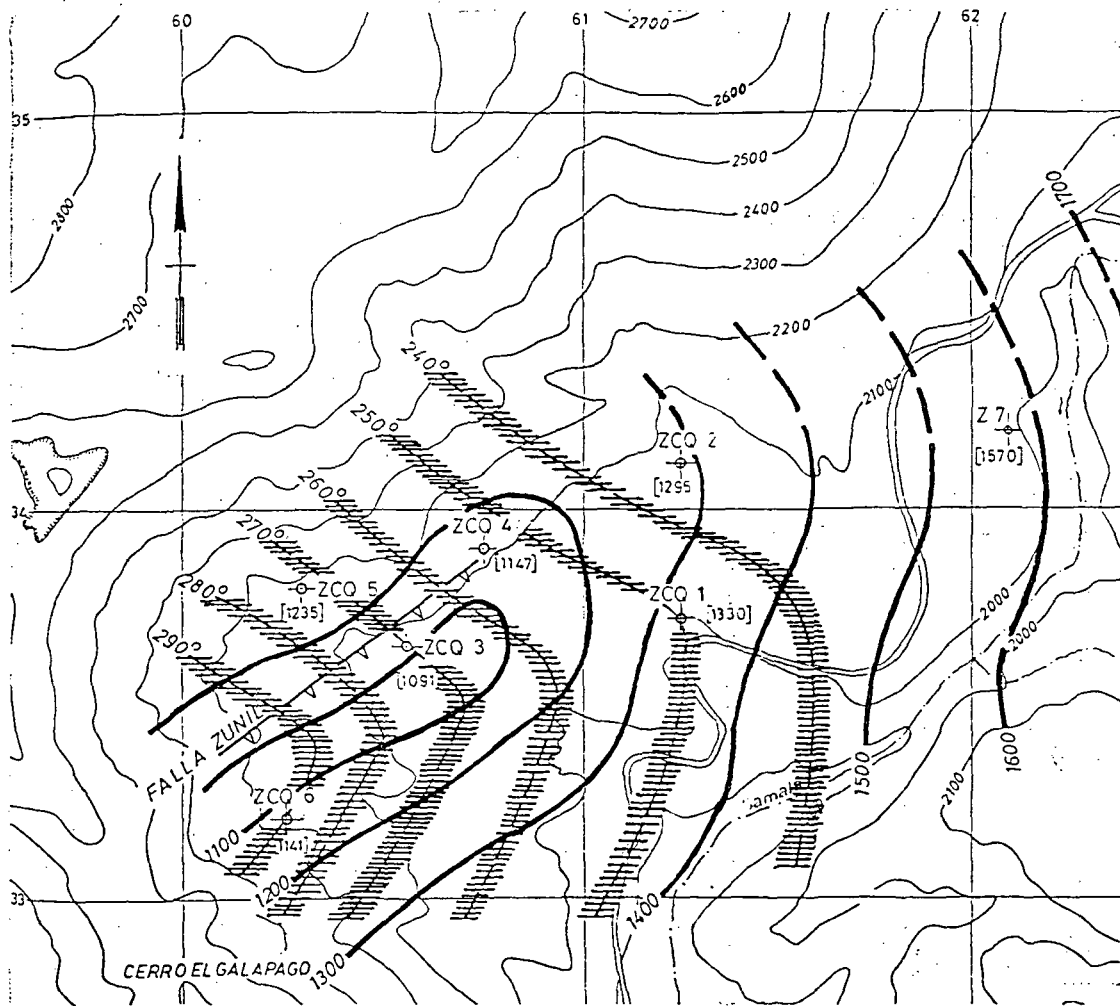
PROYECTO GEOTERMICO ZUNIL I.

GRAFICA DE TEMPERATURAS
POZOS Z-1 AL Z-5

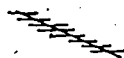
CyM/MKF.

FIGURA: 3.3-15

INFORMACION BASE: PLANO INDE POR ING. J. PALMA



SIMBOLOGIA

 COTAS DE TEMPERATURA

INFORMACION BASE: INFORME FINAL, ELECTRO-CONSULT, 1982.

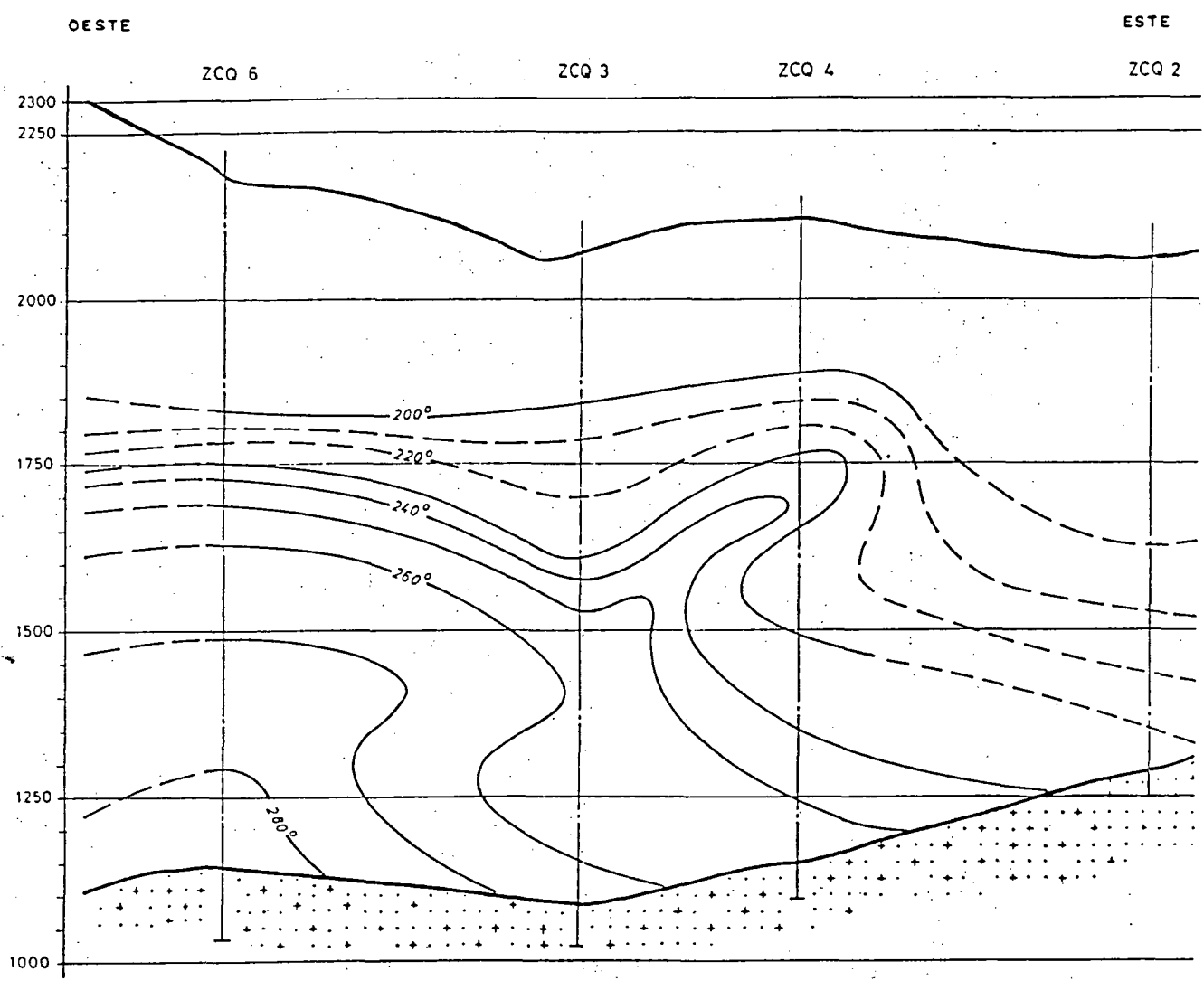
**INSTITUTO NACIONAL DE ELECTRIFICACION
INDE GUATEMALA C.A.**

PROYECTO GEOTERMICO ZUNIL I

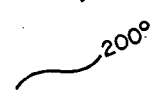
**COTAS Y TEMPERATURAS
AL TECHO DEL SUBSTRATO**

CYM/MKF.

FIGURA: 3.3-16

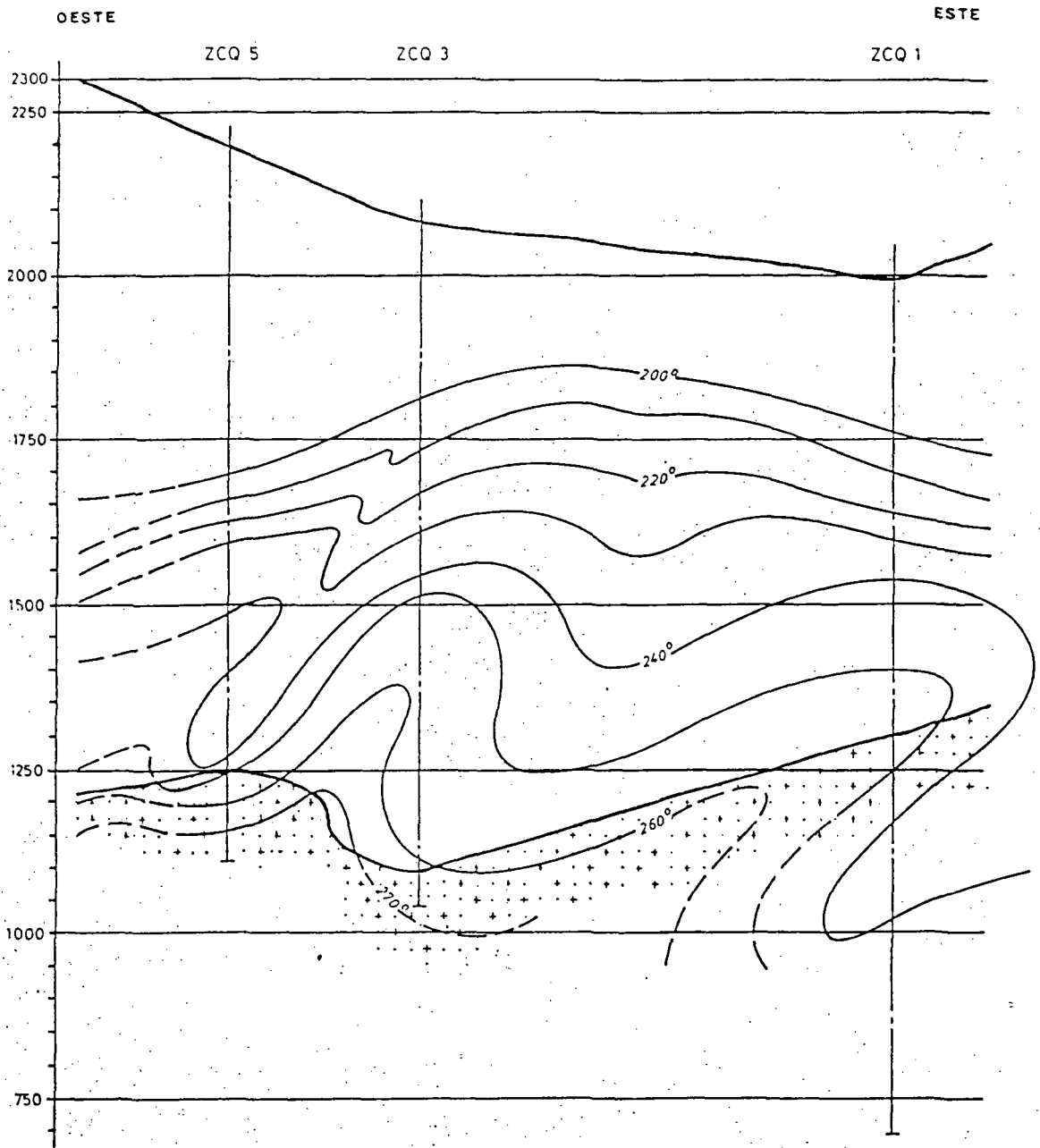


SIMBOLOGIA

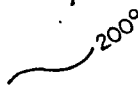

 ISOTERMA

INFORMACION BASE: INFORME FINAL, ELECTRO-CONSULT, 1982.

INSTITUTO NACIONAL DE ELECTRIFICACION INDE GUATEMALA C.A.	
PROYECTO GEOTERMICO ZUNIL I.	
ISOTERMAS EN LOS POZOS SECCION A-A	
Cym/MKF.	FIGURA: 3.3-17



SIMBOLOGIA


 ISOTERMA

INFORMACION BASE: INFORME FINAL ELECTRO-CONSULT, 1982.

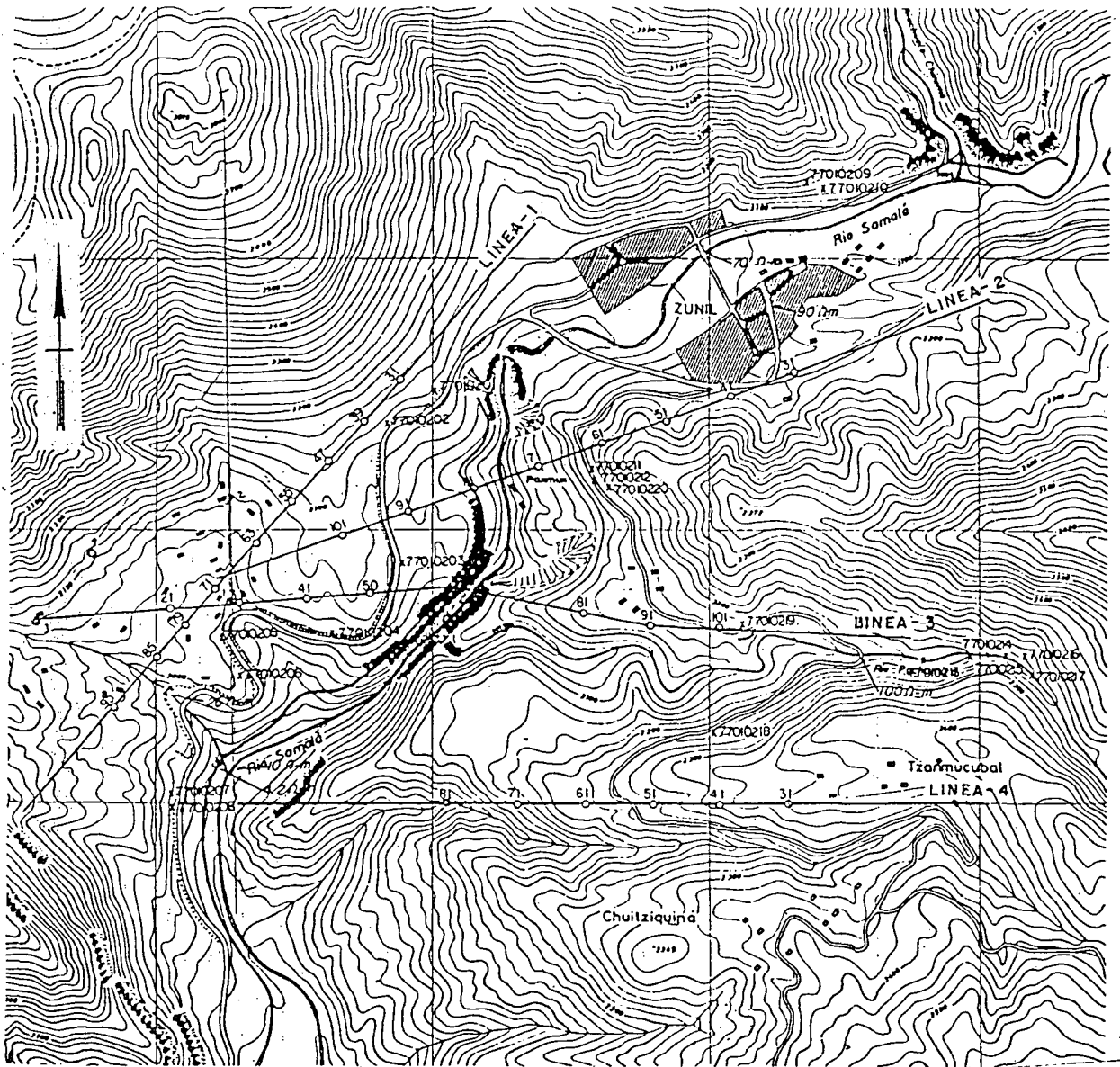
INSTITUTO NACIONAL DE ELECTRIFICACION
INDE GUATEMALA C.A.

PROYECTO GEOTERMICO ZUNIL I

ISOTERMAS EN LOS POZOS
SECCION B-B

CyM/MKF.

FIGURA: 3.3-18



0 0.5 1 Km.



ESCALA GRAFICA
 a 1:25,000

SIMBOLOGIA

○—○—○—○ PUNTOS CENTRALES

INFORMACION BASE: PLANO INDE POR ING.
 J. PALMA

INSTITUTO NACIONAL DE ELECTRIFICACION
 INDE GUATEMALA C.A.

PROYECTO GEOTERMICO ZUNIL I

**UBICACION DE LINEAS
 DE SONDEOS ELECTRICOS**

CyM/MKF

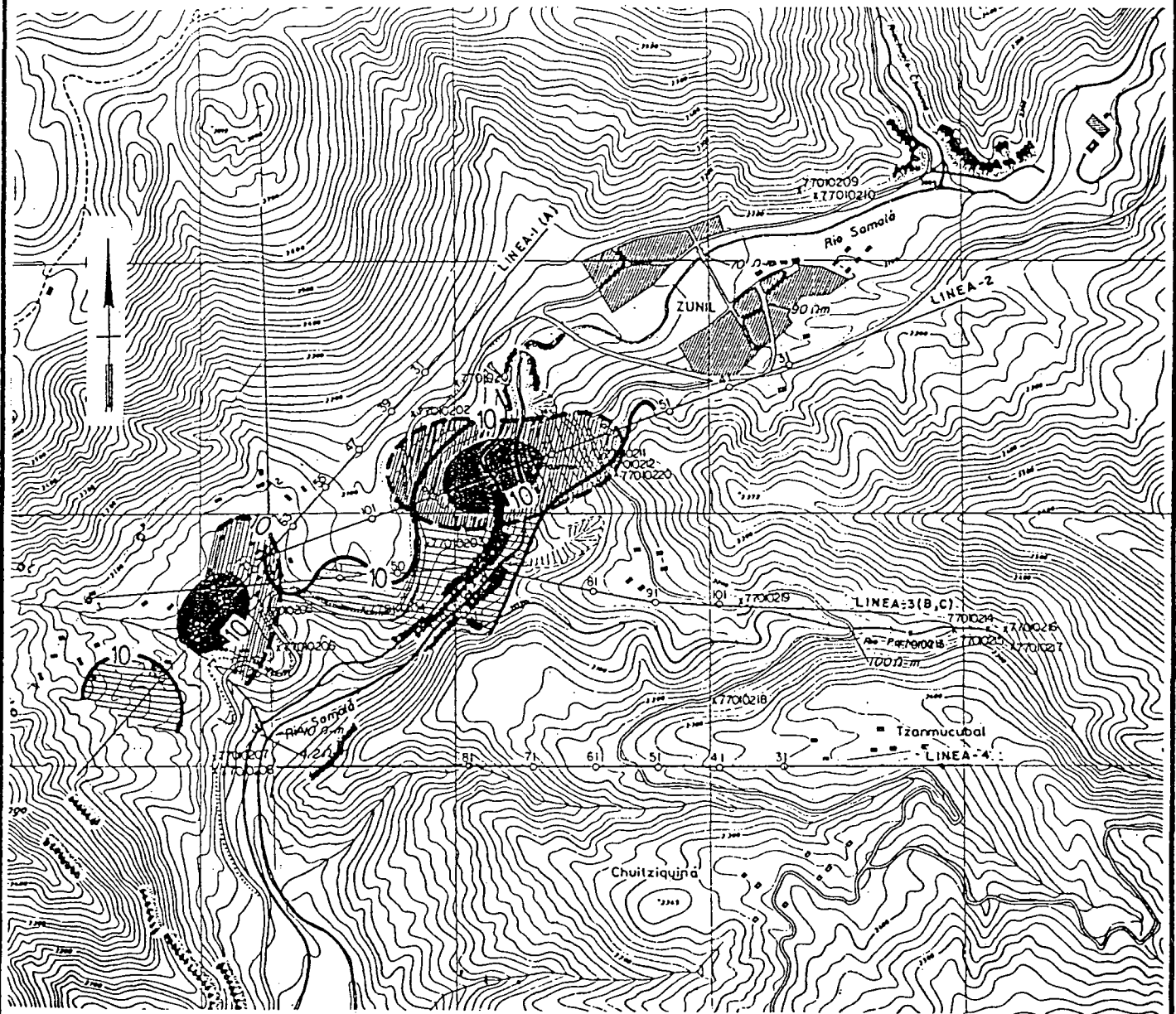
FIGURA: 3.3-19

3.3.3.5.1 Studies by JICA




A total of 12,000 lineal meters were covered by JICA using VES. Results of their investigation are presented in Figure 3.3-20. The low resistivity areas (<10 ohm-m) are outlined for the three spacings ($AB/2 = 250$ m., 500 m., and 750 m.) and two areas are observed as most favorable. One should note that the anomalous area closest to Zunil would include the influence of a fractured higher basement, as inferred from the gravity model, since the maximum probed depth was close to 750 m. A fault associated with the SE graben structure crosses this area (see Figure 3.3-11) and possibly gives rise to the low resistivity. The extension of the 10 ohm-m contour is probably smaller than shown in Figure 3.3-20, and is better represented by the INDE study (Figure 3.3-22). The larger and more interesting area lies toward the southwest, approximately 1,800 m. from Zunil. The low resistivity zones at depths close to 500 m. and 750 m. extend toward the west and southwest. The basement was not probed, as it lies deeper, but the influence of thermal fluids in faults and fractures within the Tertiary volcanics in the graben as well as thermal alteration would produce these anomalies. The iso-resistivity contours in this area correlate well with those from the INDE study which also depict the open contours of possibly lower resistivities toward the southwest. The 10 ohm-m contour of $AB/2 = 750$ m. in Figure 3.3-20 is located in the area forming the NE boundary of the graben where a fault is inferred. Terrain limitations possibly prevented this study from extending SW along Line 1 which may have shown lower resistivity areas where the current production wells are located. It is also unfortunate that the study did not include spacings greater than $AB/2 = 750$ m. as that the influence of the basement structure would have been noted. The resistivity block diagram shown in Figure 3.3-21 summarizes the aforementioned discussion.

3.3.3.5.2 Studies by INDE

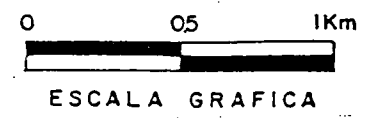
ER surveys by INDE were performed along the same traverses used by JICA but with electrode spacings of 1,000 m., 1,600 m., and 2,000 m. This permitted investigating to depths of approximately 1,000 m., close to the top of the granodioritic basement. Results are presented in Figure 3.3-22. One prominent area was outlined by the 10 ohm-m contour for the three spacings ($AB/2 = 500$ m., 800 m., 1,000 m.). The area lies between wells ZCQ-1 and ZCQ-2 and extends to the southwest. Both gravity data and seismic reflection studies indicate the presence of a fault in this zone which may correlate with Fault F in the geologic map; the low resistivity is therefore partly caused by thermal fluids and hydrothermal alteration associated with this fault. The extension of the low resistivity zone at depths close to 1,000 m. is best depicted by the cross-section in Figure 3.3-23. It is conceivable this zone extends deeper than as indicated, especially because it is a fracture/fault controlled anomaly originating in the basement rocks. Cross-sections through lines 2,3 and 4 presented



SIMBOLOGIA

-  $AB/2 = 250$
-  $AB/2 = 500$
-  $AB/2 = 750$

JICA



INFORMACION BASE: AGENCIA INTERNACIONAL DE COOPERACION DEL JAPON. (JICA).

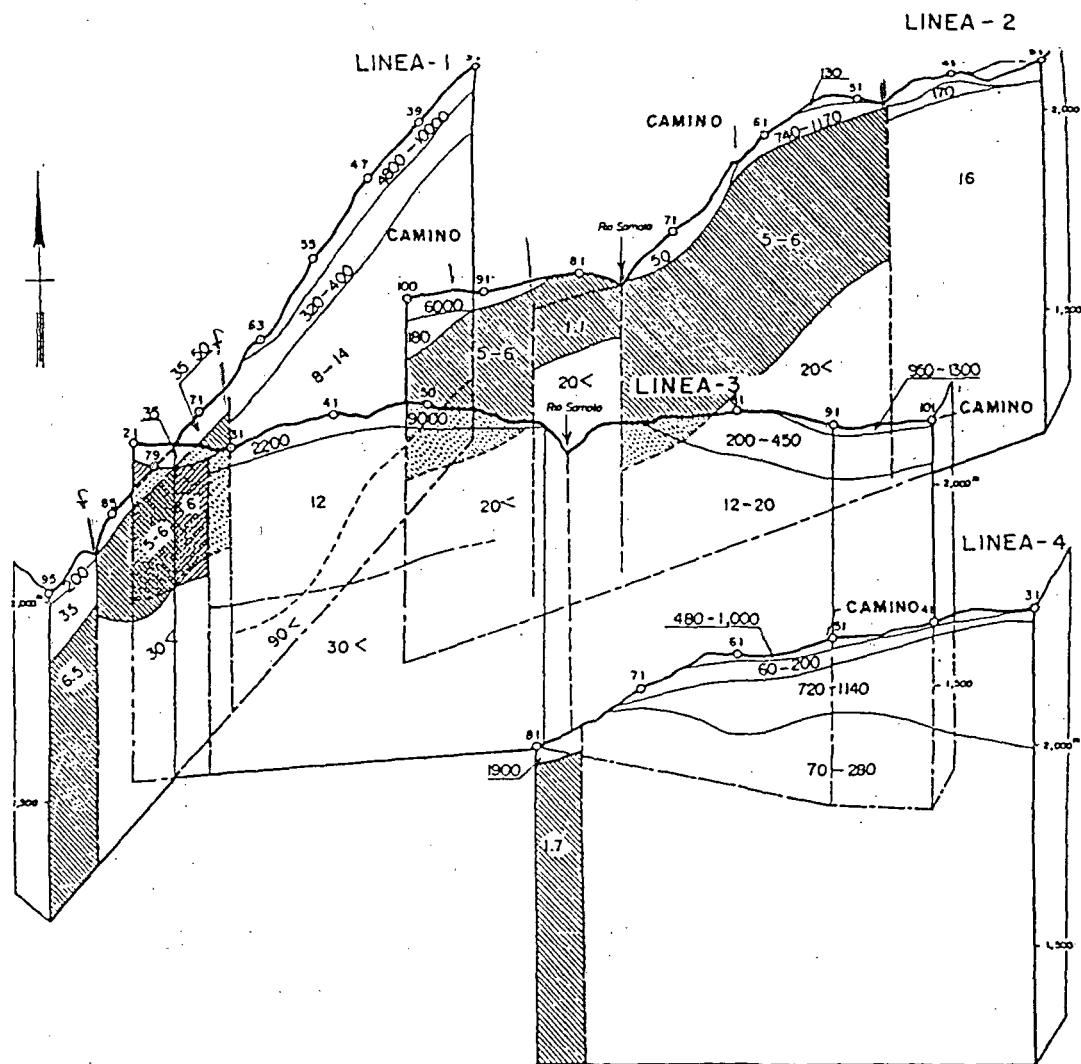
**INSTITUTO NACIONAL DE ELECTRIFICACION
INDE GUATEMALA C.A.**

PROYECTO GEOTERMICO ZUNIL I

**MAPA DE RESISTIVIDAD
APARENTE**

CyM / MKF

FIGURA: 3.3-20



- LINEA DE CONTRASTE DE CAPA DE RESISTIVIDAD.
- FALLA.
- PUNTO CENTRAL Y LINEA.



JICA

INSTITUTO NACIONAL DE ELECTRIFICACION
INDE GUATEMALA C.A.

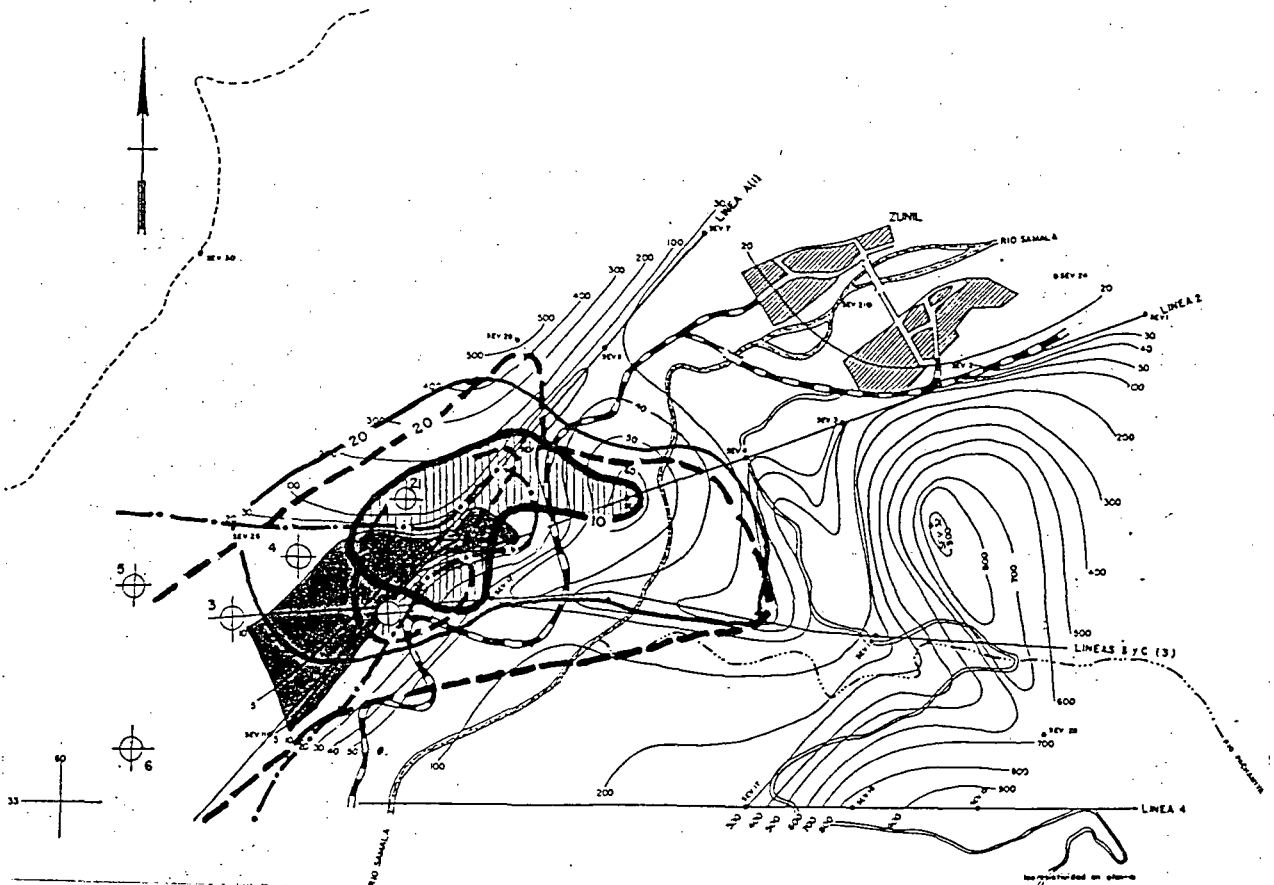
PROYECTO GEOTERMICO ZUNIL I

DIAGRAMA DE BLOQUE DE
RESISTIVIDAD

CYM/MKF

FIGURA 3.3-21




INFORMACION BASE: AGENCIA INTERNACIONAL DE
COOPERACION DEL JAPON.
(JICA).



● SEV 10
 SONDEO ELECTRICO VERTICAL
 ARREGLO SCHLUMBERGER
 AB/2 = 2000 m

33 ———
 10 ———
 1 ———
 COORDENADAS

100 ———
 CURVAS DE ISORESISTIVIDAD

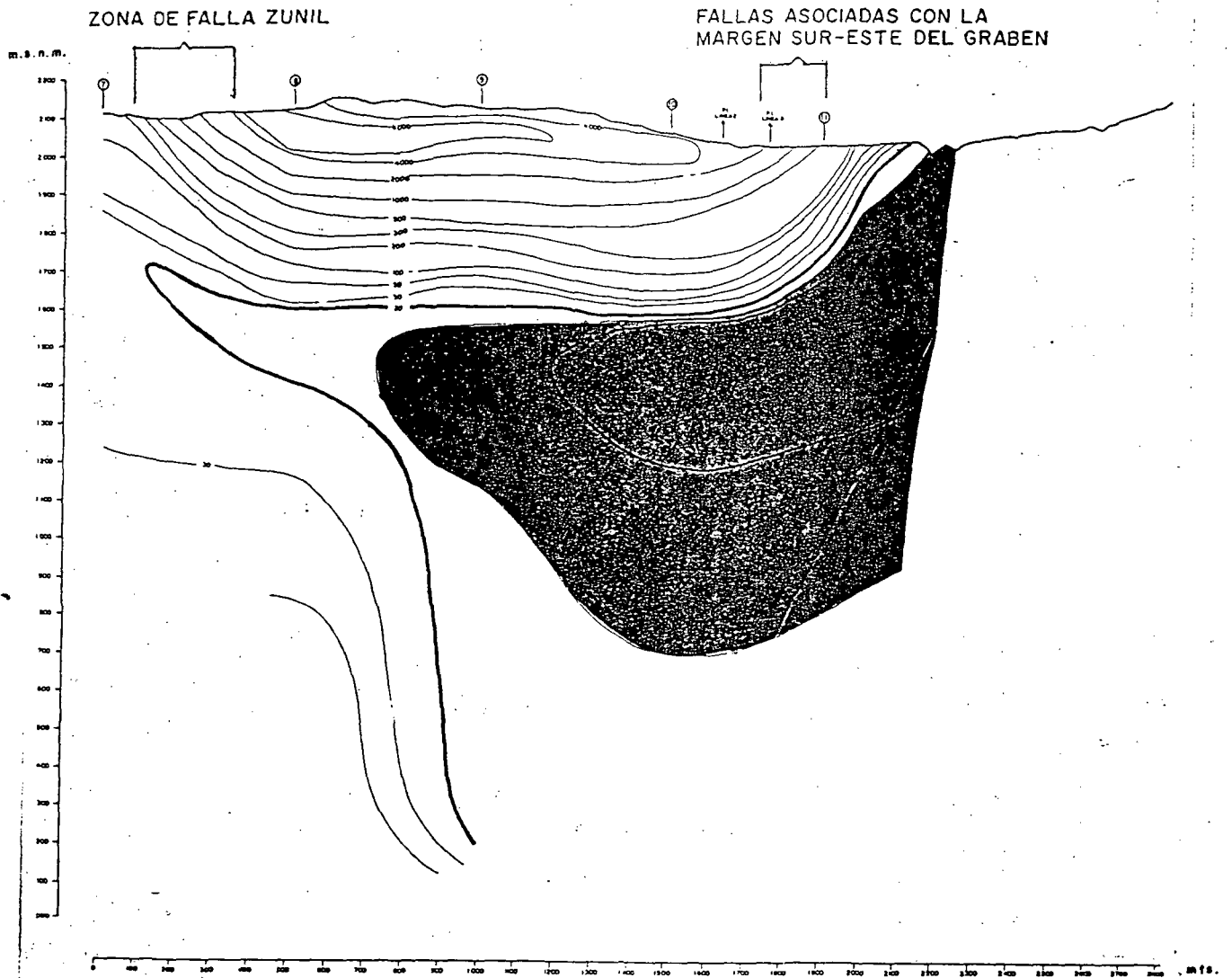
SIMBOLOGIA	INDE
	AB/2 = 500 m. — — — — —
	AB/2 = 800 m. — — — — —
	AB/2 = 1000 m. — — — — —

INFORMACION BASE: PLANO INDE POR ING. J. PALMA

INSTITUTO NACIONAL DE ELECTRIFICACION ..INDE GUATEMALA C.A.
PROYECTO GEOTERMICO ZUNIL I
CURVAS DE ISORESISTIVIDAD COMPILADA
CyM/MKF
FIGURA 3.3-22

NORESTE

SUROESTE



INSTITUTO NACIONAL DE ELECTRIFICACION
INDE GUATEMALA C.A.

PROYECTO GEOTERMICO ZUNIL I

LINEA I

INFORMACION BASE: PLANO INDE POR ING. J. PALMA

CyM/MKF.

FIGURA: 3.3-23

in Figures 3.3-24, 3.3-25 and 3.3-26 also support the decrease in resistivity with depth toward the southwest, on the western side of the Samalá River. A geoelectric discontinuity along the Samalá River detected by lines 2 and 3 is probably the trace of a fault along the southeastern boundary of the graben. The projection of the basement fault zone shown on Figure 3.3-9 through 700 m. of upper volcanics and surfacing along the Samalá River would suggest a fault dipping approximately 60° to the northwest. The presence of a fault trace in this area is further supported by the alignment of thermal manifestations along this section of the river. A resistivity block diagram presented by INDE as Figure 6.1.28 in the "Informe Geoelectrico" (not reproduced here because of color restrictions) clearly summarizes the ER results with considerable accuracy.

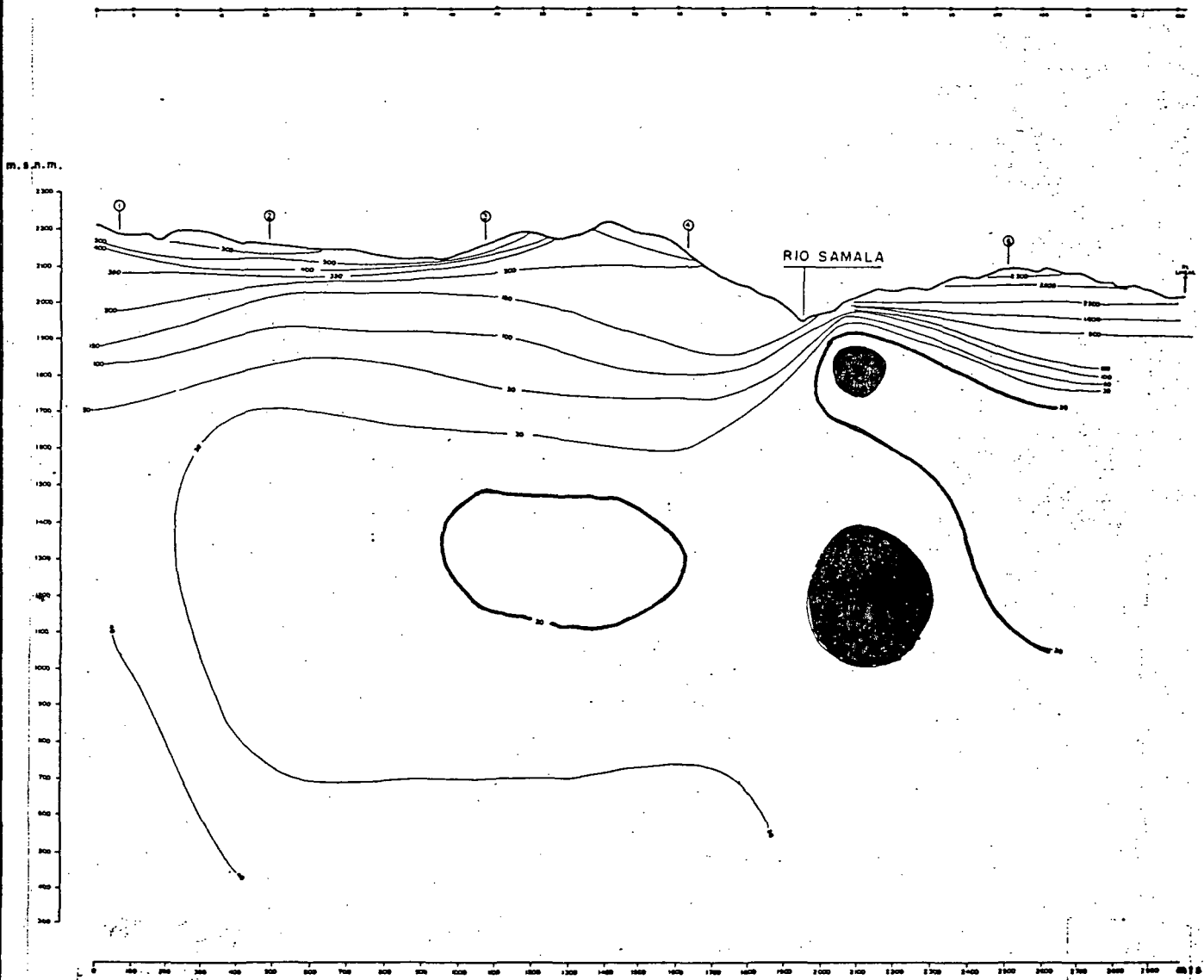
The longitudinal conductance map shown in Figure 3.3-27 clearly demonstrates the NE-SW orientation of a high conductance area related to the interpreted graben and the geothermal zone. The suspected faults in the basement are also plotted in this figure to show their correlation with the ER study. Two discontinuities noted on ER line 1 correspond to two suspected fault zones as shown on Figure 3.3-23. The geoelectric investigations are in general agreement with the suspected structure of the subsurface as well as with other geophysical techniques.

Regional ER survey results were also examined. The three maps available included an areal coverage of approximately 170 km² extending from north of Quetzaltenango to 4 km. south of Zunil. Isoresistivity curves were plotted for AB/2 = 500 m., 1000 m. and 1500 m. The low resistivity area within Zunil site is located in the same general vicinity as shown on Figure 3.3-22 (< 10 ohm-m) for the maps with AB/2 = 500m. and 1000m.

This location correlates with the results from detailed studies which indicate the presence of a high conductance zone at that depth (Figures 3.3-20, 3.3-22, 3.3-27). The map with AB/2 = 1500m. encloses the entire Zunil geothermal site with the 50 ohm-m contour, with the lowest resistivity encountered approximately 1 km. west of Zunil. The penetration is within the granodiorite basement and the conductive areas are basically expressions of fault/fracture related geothermal processes. Results from this regional study are in general agreement with the detailed investigations described previously and which present a more accurate study of subsurface conditions.

3.3.4. Summary of Conclusions

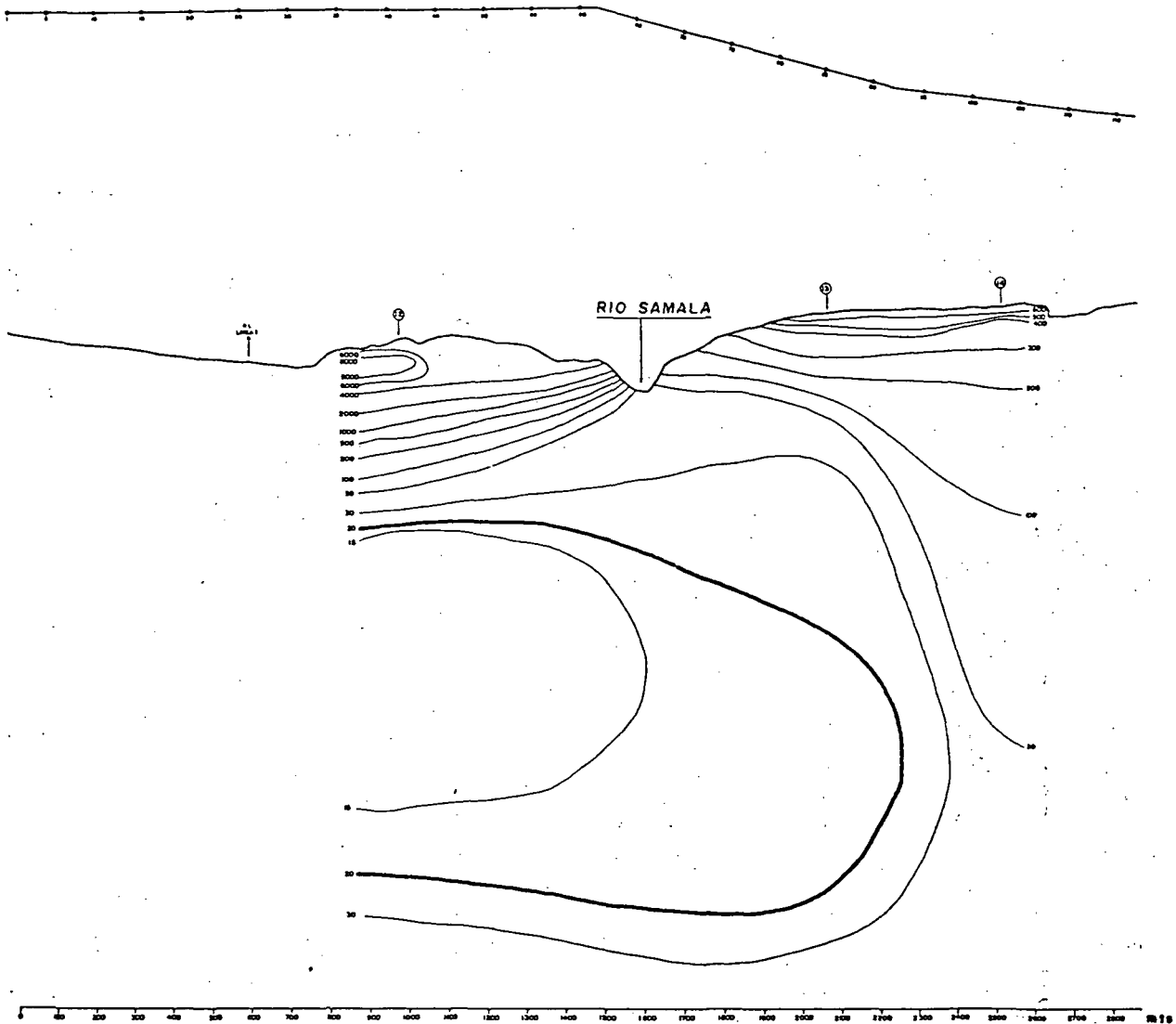
Geophysical investigations carried out in the Zunil area produced invaluable results from which the subsurface structure and processes were interpreted. The combination of various geophysical techniques served not only to gain additional information on the area but also corroborated results obtained by other methods; a strategy of particular importance in the Zunil study due to the difficulties that volcanic terrains (and in this case also topography) generally engender on geophysical



INSTITUTO NACIONAL DE ELECTRIFICACION INDE GUATEMALA C.A.	
PROYECTO GEOTERMICO ZUNIL I	
LINEA 2	
CyM/MKF.	FIGURA: 3.3-24

INFORMACION BASE : PLANO INDE POR ING. J. PALMA

M. S. N. M.



INSTITUTO NACIONAL DE ELECTRIFICACION
INDE GUATEMALA C.A.

PROYECTO GEOTERMICO ZUNIL I

LINEA 3

INFORMACION BASE: PLANO INDE POR ING. J. PALMA

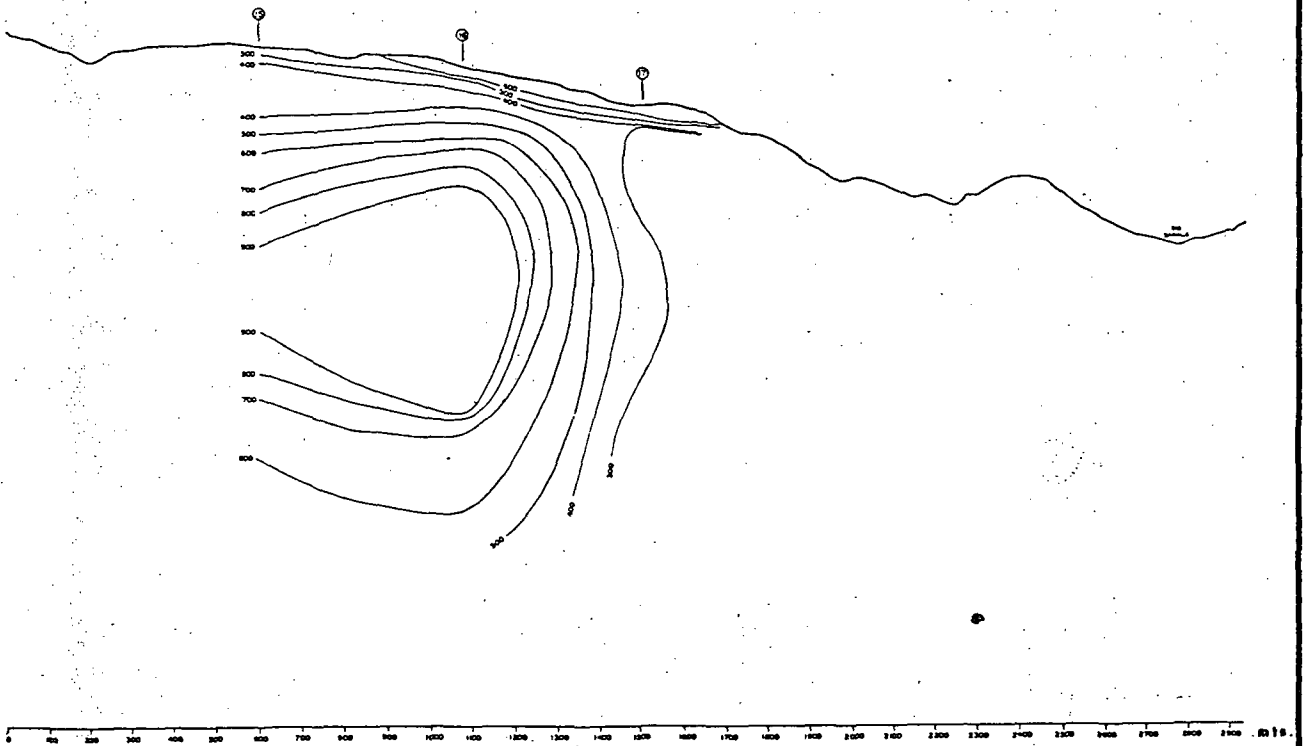
CyM/MKF.

FIGURA: 3.3-25

ESTE

OESTE

m.s.n.m.



INSTITUTO NACIONAL DE ELECTRIFICACION
INDE GUATEMALA C.A.

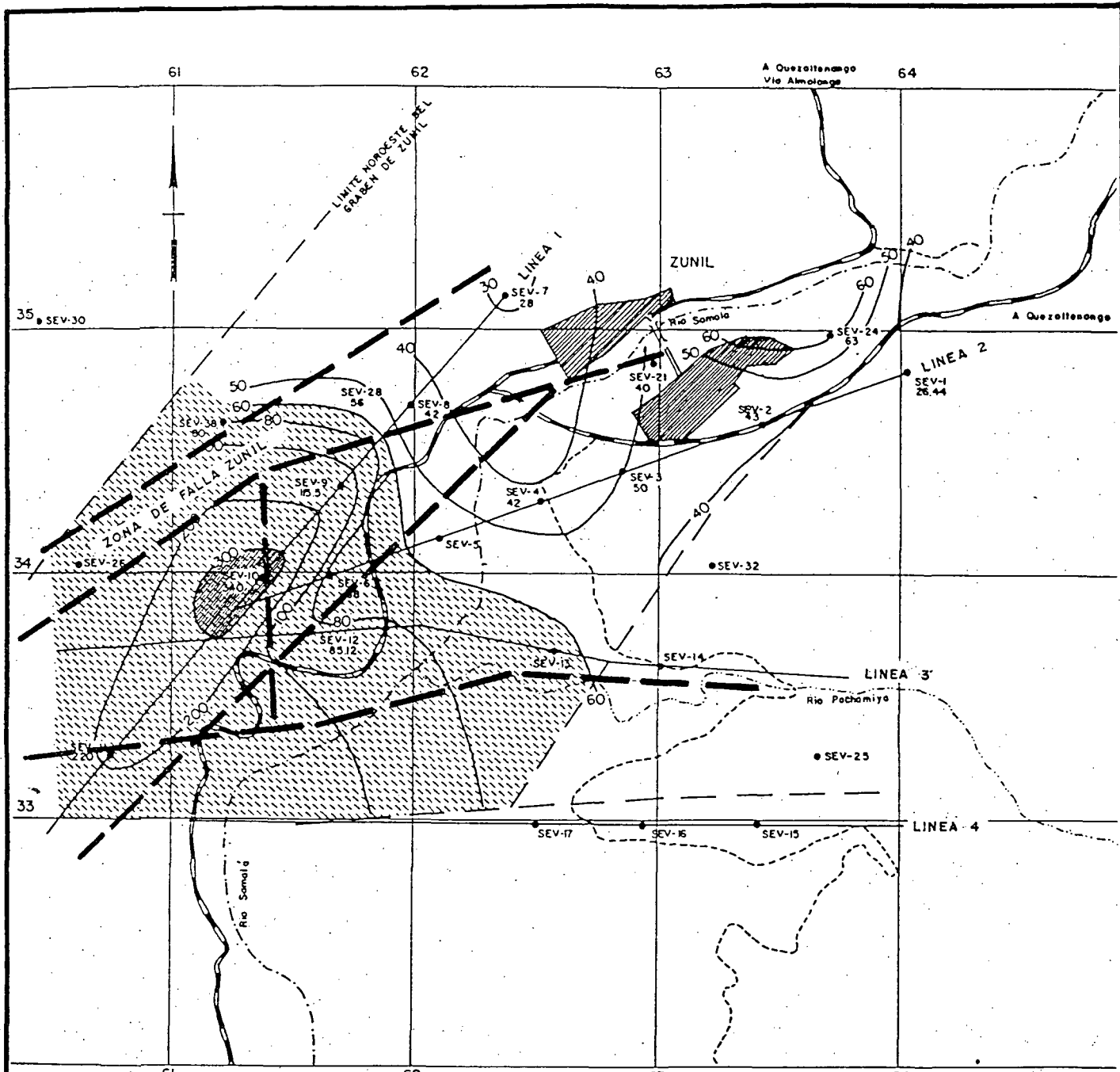
PROYECTO GEOTERMICO ZUNIL I.

LINEA 4

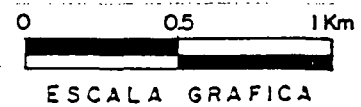
INFORMACION BASE: PLANO INDE POR ING. J. PALMA

CyM/MKF.

FIGURA: 3.3-26

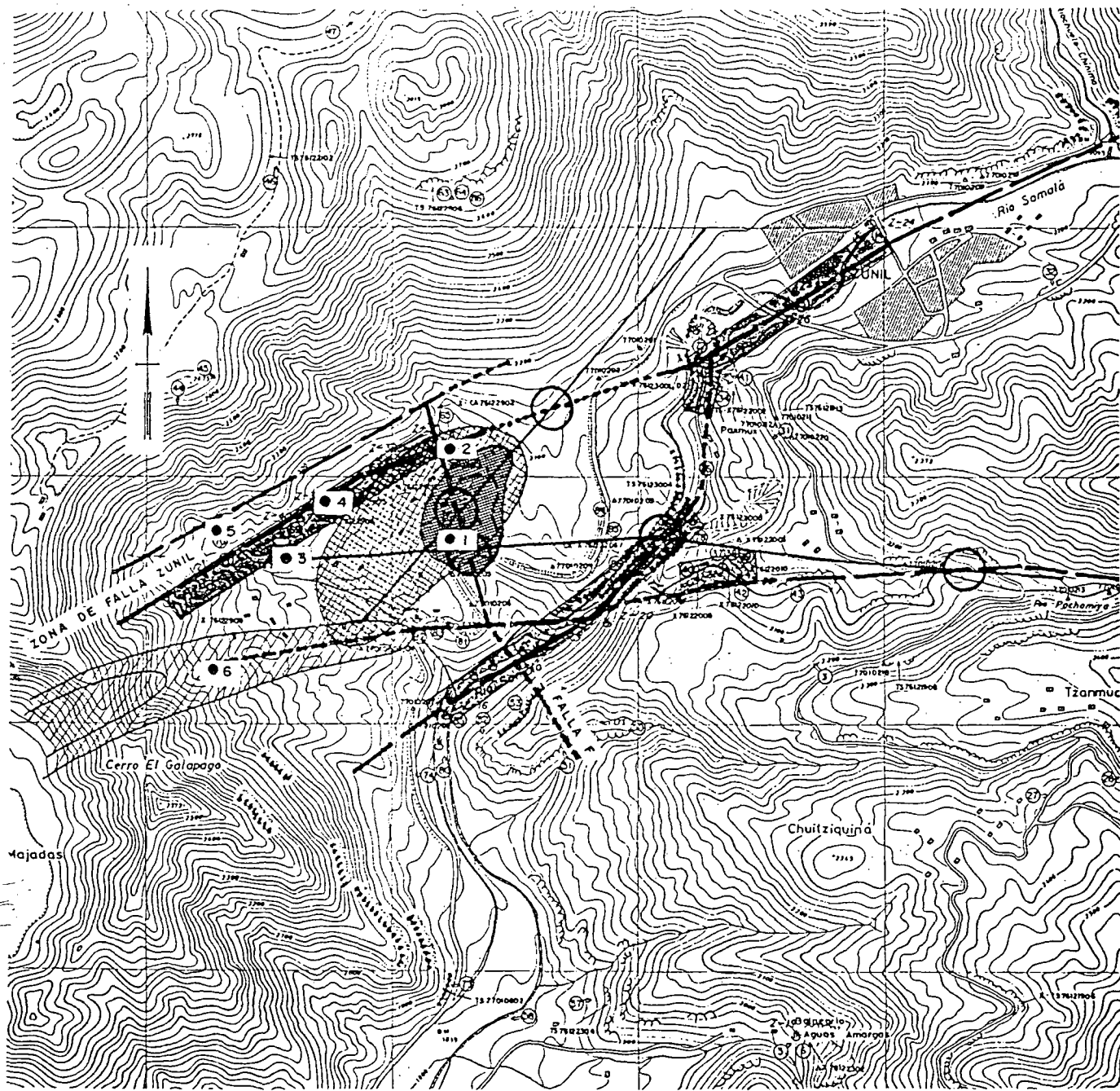


- SONIDO ELECTRICO VERTICAL (S E V)
- PERFORACION TIPO WELPHER 40/2 x 1000 m
- CURVAS DE CONDUCTANCIA LONGITUDINAL (---)
- RIO SAMALÁ
- DISCONTINUIDAD SEDELECTRICA
- ▨ DELIMITACION DEL AREA DE MAYOR CONDUCTANCIA
- - - - - POSIBLE FALLA EN EL BASAMENTO




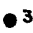





INSTITUTO NACIONAL DE ELECTRIFICACION
 INDE GUATEMALA C.A.
 PROYECTO GEOTERMICO ZUNIL I
CONDUCTANCIA LONGITUDINAL
 Cym/MKF. FIGURA: 3.3-27

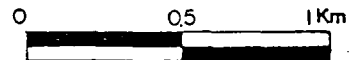
INFORMACION BASE: PLANO INDE POR ING. J. PALMA



SIMBOLOGIA

- 
 UBICACION DE FALLAS POR INTERPRETACION GRAVIMETRICA.
- 
 CONFIRMACION DE FALLA POR LINEA SISMICA REFLEXION SISMICA.
- 
 TENDENCIA LINEAL DE MANIFESTACIONES TERMALES RELACIONADA A FALLAS.
- 
 POZO ZCQ-3.
- 
 ZONA DE ANOMALIA MAGNETICA
- 
 ZONA DE BAJA RESISTIVIDAD.
- 
 ZONA DE ALTA CONDUCTANCIA LONGITUDINAL

INFORMACION BASE: PLANO INDE POR ING. J. PALMA



ESCALA GRAFICA

**INSTITUTO NACIONAL DE ELECTRIFICACION
INDE GUATEMALA C.A.**

PROYECTO GEOTERMICO ZUNIL I

**RESUMEN DE RESULTADOS
GEOFISICOS**

CyM / MKF.

FIGURA: 3.3-28

-geological investigations. It was through the cross-referencing of results as well as corroboration by geological data that confident interpretations were formulated. The summary of results is presented in Figure 3.3-28. Because of topographic constraints many geophysical surveys were not extended to the southwest toward Las Majadas. The absence of data in this area, however, does not imply that unfavorable geothermal conditions exist in this zone; on the contrary, indications from geology, gravimetry, magnetometry, and temperature gradient analyses suggest the extension of a geothermal complex toward this area.

Figure 3.3-28 presents the surface trace of basement faults inferred from gravimetric interpretations. Of particular importance is the location of a down-dropped structure southwest of Fault F (refer to Figures 3.3-9 and 3.3-11). This graben is possibly part of a larger graben within the Zunil Valley, as suggested by geologic reports. The Zunil Fault Zone bounds this structure to the northwest. This fault zone was previously outlined in geologic reports and is now supported by gravimetric interpretation and the alignment of thermal manifestations. In view of a basement drop on both sides of this fault zone, the basement structure would resemble a horst with step faults along both sides. The faulted zone extends as a single fault toward the northeast, through the town of Zunil, again giving rise to a linear pattern of thermal manifestations along the surface, and further NE toward the town of Cantel. Surface manifestations are noted along this trace. Seismic line A intercepts the Zunil Fault approximately 1 km. SW of Zunil, as shown on Figure 3.3-28. The presence of productive wells ZCQ-3, 4 and 5 along the fault zone attest to the importance of the fault structure in the basement and within this graben.

The fault along the Samalá River is the trace of a basement fault along the SE boundary of the graben, as previously described in Section 3.3.3.3. Again the alignment of thermal manifestations along the river supports this interpretation; furthermore the fault was detected by seismic line B at the location shown in Figure 3.3-28. This fault possibly extends toward the north and intersects the Zunil Fault approximately 400 m. SW of Zunil where thermal manifestations are again present.

The fault between wells ZCQ-1 and ZCQ-2 forms the NE boundary of the graben. This fault may be correlated with a previously mapped Fault F though the orientations are slightly different. The location of this fault is corroborated by magnetics, electrical resistivity, and seismic lines A and B as shown on Figure 3.3-28. The NW extension of this fault may be bounded by the Zunil Fault Zone; the SE extension remains unknown. It is conceivable that since this fault is a transverse fault related to block faulting and therefore orthogonal to the step faults associated with the graben, it is less active and possibly tighter, thus precluding thermal fluids from reaching the surface and restricting their flow in the subsurface. A low resistivity layer is present at depth along the area outlined in Figure 3.3-28 and all geophysical indications support the locations of

wells ZCQ-1 and ZCQ-2. It may be that the tightness of the fault or its lack of associated fractures in view of its transverse character are confined; the creation of fractures in well ZCQ-1 by proven techniques could create the necessary conditions for some exploitability from this well.

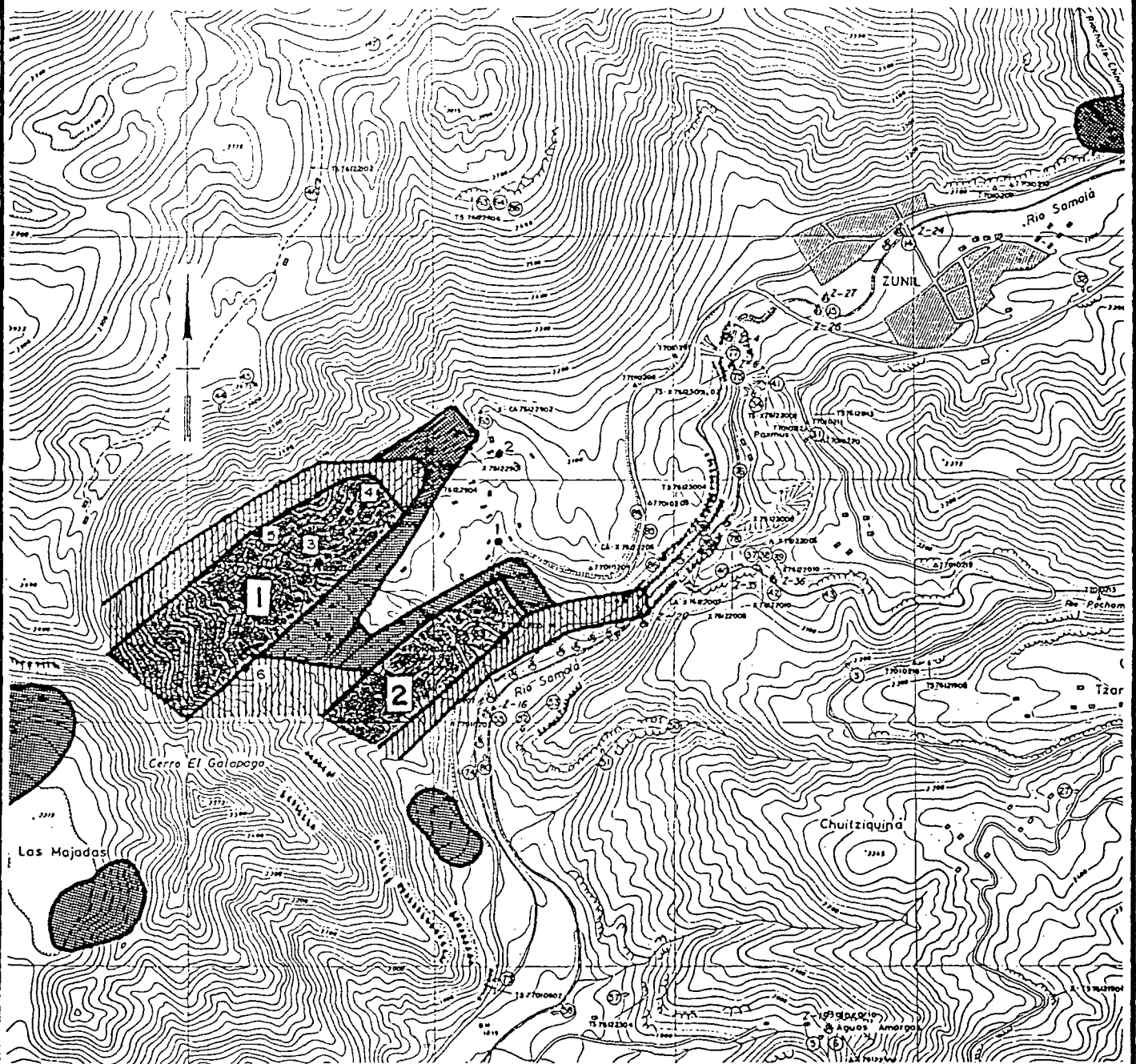
An E-W fault along the Pachamiya River and across the graben is also depicted in Figure 3.3-28. This fault was also previously outlined in geologic reports by INDE. Its location is supported by gravity studies and seismic reflection which detected the fault at the location shown. Some thermal manifestations also support its orientation but of particular importance is that the only spring with NaCl-rich water (and over saturated with SiO₂) in the Zunil area occurs at the intersection of this fault and the Samalá River fault, as shown in Figure 3.3-28. This is possibly caused by the intersection of the faults; other waters in the area are of carbonate (neutral HCO₃) or sulfate (acidic SO₄) character which are associated with shallow groundwater being heated by steam or high temperatures. It should be noted that the chemical composition of thermal fluids in the production wells are NaCl type. The extension of this fault to the west is partly supported by an elongated magnetic anomaly and gravity studies. Well ZCQ-6 is located close to its trace and the high temperature measured in this well may be associated with the fault.

The thermal occurrences, fault locations, geophysical results, geologic information, and geochemistry data have been combined to develop a reasonable and logical interpretation of the Zunil area and the geothermal complex. The correlation of data enabled the understanding of an overall general picture of the field from individual components.

3.3.5. Recommendations

3.3.5.1 Drilling Sites

Based on an analysis of geophysical investigations coupled with geology, geochemistry and information from the six deep wells, the most promising areas for future drilling are outlined on Figure 3.3-29. Information from the summary of results (Section 4) and Figure 3.3-28 were used to outline the areas shown in Figure 3.3-29. The most promising area forms the northwest boundary of the graben and is defined by the Zunil Fault Zone. The location of wells ZCQ-3, 4 and 5 are favorably located in this faulted zone and any other wells located SW of ZCQ-3 and 5 would also intersect this structure if drilled deeper into the granodiorite. Well ZCQ-6 lies close to the center of the graben, possibly the deepest and hottest area but with less faulting than the margins. Deeper penetration and/or induced fracturing could make this well more productive.



ZONA MAS FAVORABLE PARA UBICAR SITIOS DE PERFORACION (PRODUCTIVA).



SEGUNDA ZONA FAVORABLE.

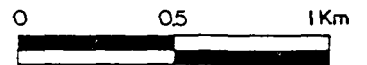


TERCERA ZONA FAVORABLE.



ZONA FAVORABLE PARA UBICAR POZOS DE EXPLORACION.

INFORMACION BASE:
PLANO INDE ING. J.
PALMA.



ESCALA GRAFICA

INSTITUTO NACIONAL DE ELECTRIFICACION
INDE GUATEMALA C.A.

PROYECTO GEOTERMICO ZUNIL I

MAPA DE ZONAS FAVORABLES
PARA PERFORACIONES PRODUCTIVAS
Y EXPLORATORIAS

The second most promising area forms the SE boundary of the graben where step faults are also prominent. The intersection of the E-W fault and the Rio Samalá fault at depth would be a prime target; the terrain is also not steep in this area. This area has the potential of being just as important as its NW counterpart and should not be discarded.

Additional favorable zones (labeled as third most favorable in Figure 3.3-29) are also outlined. These areas are also related to faults in the basement structure.

In view of the fracture dominated complex, step and block faults, and the importance of these in providing for the migration of thermal fluids, target areas for exploration drilling were also outlined in Figure 3.3-29. These include zones within the graben structure as well as sites crossed by fault zones and aided by favorable topography. This is especially the case of the area in Las Majadas and northeast of Zunil.

3.3.5.2 Geophysical Studies

Results from previous geophysical investigations appear to be sufficiently adequate for the current work program. Since the geothermal field extends to the southwest, it is advisable that additional information be obtained on this area at some future date. Based on past survey results and topographic limitations, the detailed gravity studies could easily be extended along this area. This would provide valuable information on the continuation of the structure to the SW. Some seismic reflection and ER surveys could also be extended along the ridge of Cerro El Galápago and within Las Majadas. A survey would have to be conducted to estimate if sufficiently long lines could be extended in these areas, though for the reflection survey the detection of faults could be achieved with lines less than 2,000 m. in length.

Additional studies to consider are microseismics, to detect small seismic events related to fault movement and regional stresses in the crust as well as monitoring the seismicity. Also to consider are dipole-dipole surveys and time-domain electromagnetic (TDEM) but these are also limited by the rugged topography.



**EARTH SCIENCE LABORATORY
420 CHIPETA WAY, SUITE 120
SALT LAKE CITY, UTAH 84108
TELEPHONE 801-581-5283**

ZUNIL 1
INDE, GUATEMALA, C.A.
Resistivity Data

Earth Science Laboratory

University of Utah Research Institute
420 Chipeta Way, Suite 120
Salt Lake City, Utah 84108
(801) 581-5283



6772
1/11/89

Instituto Nacional de Electrificación
INDE, Guatemala, C.A.



PROYECTO ZUNIL

estudio de factibilidad preliminar

Estudios Geotérmicos

Instituto Nacional de Electrificación
INDE, Guatemala, C.A.



PROYECTO ZUNIL

estudio de factibilidad preliminar

informe geoeléctrico.

ESTUDIOS GEOTERMICOS.
Septiembre de 1977.

PERSONAL TECNICO DE ESTUDIOS GEOTERMICOS

. Ingeniero Hugo Rolando Bethancourt
DELEGADO RESIDENTE

. Ingeniero Oscar Sequeira Hidalgo
SUPERVISOR GENERAL

. Ingeniero Emilio Soto Meneses
INGENIERO SUPERVISOR

. Ingeniero Jorge Silva Guillén
INGENIERO INSPECTOR DE PERFORACIONES

. Ingeniero Edgar Tobías Gutiérrez
GEOLOGO

. Ingeniero Julio César Palma Ayala *GEOFISICO

. Licenciada Delia Paniagua de Gudiel
GEOQUIMICA

* Autor del Informe

CONTENIDO

	Pag.
1. CONCLUSIONES	1
2. INTRODUCCION	4
3. PROSPECCION GEOELECTRICA APLICADA A ESTUDIOS GOTERMICOS	5
3.1 El Método de Resistividad Eléctrica	6
3.2 Ventajas del Arreglo Schlumberger de S.E.V.	9
4. LOCALIZACION DEL AREA DE ESTUDIO	11
4.1 Trabajos de Prospección Geoeléctrica Efec- tuados por el INDE a la fecha	11
4.2 Trabajo de Campo	13
EVALUACION E INTERPRETACION DE LOS RESULTADOS	
5. INTERPRETACION CUALITATIVA DE LOS S.E.V.	15
5.1 Análisis de acuerdo a las características de las curvas	15
5.2 Mapa de Resistividad Aparente o Isoresis- tivas	21
5.3 Perfiles de Resistividad Aparente	23
5.4 Mapa de Conductancia Longitudinal	26

	Pag.
6. INTERPRETACION CUANTITATIVA	30
6.1 Análisis Cuantitativo de los S.E.V.	30
6.2 Mapa del Isonivel del Sustrato Resistivo ..	34
6.3 Mapa de Isopacas del Estrato Conductivo ...	35
7. PERFORACIONES REALIZADAS	36

FIGURAS

- 4.1 MAPA DE LOCALIZACION DE SONDEOS ELECTRICOS VERTICALES
- 5.1.1 DELIMITACION DE AREAS DE ACUERDO A LAS CARACTERISTICAS DE LAS CURVAS Y NUMERO DE CAPAS
- 5.2.1 CURVAS DE ISORESISTIVIDAD $AB/2 = 500$ m.
- 5.2.2 CURVAS DE ISORESISTIVIDAD $AB/2 = 800$ m.
- 5.2.3 CURVAS DE ISORESISTIVIDAD $AB/2 = 1,000$ m.
- 5.3.1 PERFIL DE RESISTIVIDAD APARENTE LINEA 1
- 5.3.2 PERFIL DE RESISTIVIDAD APARENTE LINEA 2
- 5.3.3 PERFIL DE RESISTIVIDAD APARENTE LINEA 3
- 5.3.4 PERFIL DE RESISTIVIDAD APARENTE LINEA 4
- 5.4.2 CONDUCTANCIA LONGITUDINAL
- 6.1.1 a 6.1.23 INTERPRETACION DE SONDEOS ELECTRICOS Y CONDUCTANCIA LONGITUDINAL
- 6.1.24 PERFIL GEOELECTRICO LINEA 1
- 6.1.25 PERFIL GEOELECTRICO LINEA 2
- 6.1.26 PERFIL GEOELECTRICO LINEA 3
- 6.1.27 PERFIL GEOELECTRICO LINEA 4
- 6.1.28 MODELO DEL BLOQUE DIAGRAMATICO ESTRUCTURAL-GEOELECTRICO PRELIMINAR
- 6.2.1 CURVAS DE ISONIVEL DEL SUSTRATO RESISTIVO
- 6.3.1 ISOPACAS DEL CONDUCTIVO

1. CONCLUSIONES

La interpretación de los resultados de los sondeos eléctricos verticales (S.E.V.) con dispositivo Schlumberger, efectuados en Zunil, han permitido construir un bloque diagramático (fig. 6.1.28) con el cual se ha obtenido el modelo estructural preliminar del área estudiada.

De acuerdo al bloque diagramático, la zona anómala de baja resistividad (<10 ohm-m) que puede correlacionar con la existencia de un reservorio geotérmico, se distribuye hacia el lado ^{west} oeste del río Samalá a través de la línea No. 1 y flanco oeste de las líneas Nos. 2 y 3, además del área del poblado de Zunil, ^{has} siendo limitada hacia el ^{west} noroeste por una discontinuidad geoelectrica que parece coincidir con la falla que limita hacia este mismo lado el graben de Zunil. El fondo del sustrato resistivo se levanta hacia el norte en el poblado de Zunil y hacia el suroeste cerca del S.E.V. No. 11, ^{infer} infiriéndose dos discontinuidades que pueden correlacionar con contactos o fallas geológicas (línea No. 1, fig. 6.1.28).

El ^{Thickness} espesor del estrato conductor parece ser modelado por el fondo del sustrato resistivo, ^{bottom} disminuyendo donde este se levanta y aumentando donde se profundiza. ^{raising} ^{deeper}

A través del río Samalá se ha inferido una discontinuidad geoelectrica, debido a que la resistividad de las ^{layer} capas ^{due paper fit}

fondo = bottom back background

depth to

malaga room right here

bottom

layers?

raised

vicinity

Across

superficiales en el lado oeste del mismo, son mucho más altas que en su lado este, donde también el espesor conductivo aumenta su resistividad a ^{more} más de 10 ohm-m.

Entre la línea Nos. 3 y 4 existe una clara discontinuidad, debido a que la resistividad y el espesor de las capas ^{due} superficiales a través del perfil de la línea No. 4 aumentan considerablemente comparados con los de la línea No. 3, excepto a partir del S.E.V. No. 14 y hacia el lado este del mismo, sobre los S.E.V. Nos. 25 y 32 donde ^{over} también la resistividad y el espesor de las capas superficiales aumentan, tendiendo la última capa a bajar muy bruscamente de resistividad, no pudiendo determinarse su espesor y resistividad verdadera, por no haberse detectado el fondo del sustrato resistivo en ninguno de los S.E.V. mencionados, pero que por la tendencia de las curvas ^{not able to} podría ser menor de 10 ohm-m, lo que indicaría la existencia de un espesor conductivo más profundo dentro de esta área, que la del lado oeste del río Samalá que puede manifestarse también a través de los S.E.V. Nos. 15, 16 y 17 localizados sobre el perfil de la línea No. 4, ya que las características de la configuración inicial de sus curvas coinciden con las de los S.E.V. Nos. 25 y 32. Esta situación tendrá que ser aclarada, ejecutando dentro de esta área nuevos S.E.V., alargando los electrodos de corriente AB/2 hasta detectar el fondo del sustrato resistivo, delimitándose la dirección de la discontinuidad geoelectrica por medio de S.E.V. con arreglo Dipolo-Dipolo.

De ser confirmada la hipótesis ^{we have} expuesta con anterioridad, ^{hypothesis exposed} esta zona sería también de interés geotérmico, coincidiendo su límite hacia el lado este probablemente con la falla que ^{previously}

limita hacia este mismo flanco el graben de Zunil.

En base a los resultados geoelectricos obtenidos, se sugie-
on the basis *obtained* *suggest*

re que sean efectuadas como mínimo tres perforaciones pro-
3 wells

fundas, con el fin de confirmar la existencia de vapor en
deep with the purpose *steam*

cantidades comerciales, dichas perforaciones deben ser lo-
quantities *which* *wells* *are to be*

calizadas dentro de la zona de baja resistividad situada
within

en el lado oeste del río Samalá, principiando por el área
place west of *for*

de más alta conductancia longitudinal situada alrededor de
higher *around*

los S.E.V. Nos. 10 y 11 (fig. 5.4.2), sin olvidarse que
oblivion?

hacia el lado este del río Samalá, también podría existir
place east *not*

una zona de alto potencial geotérmico, que está sujeta ac-
is the subject

tualmente a mayor investigación geofísica.
of a major

2. INTRODUCCION

El presente informe contiene la evaluación e interpretación de los resultados geoelectricos obtenidos por el INSTITUTO NACIONAL DE ELECTRIFICACION "INDE" en los estudios del campo geotermico de Zunil.

Su objetivo, es la localización de las áreas donde los espesores de las rocas son de baja resistividad (< 10 ohm-m) que pueden indicar la existencia de un reservorio geotermico. Para correlacionar sus resultados se han efectuado perforaciones de mediana profundidad que han permitido investigar el gradiente geotermico y la sección geológica estratigráfica.

Como métodos complementarios a la prospección geoelectrica serán utilizados el magnético y el gravimétrico, con los cuales se podrán establecer nuevas estructuras geológicas situadas bajo la superficie terrestre y confirmar las establecidas en el mapeo geológico superficial, lo que permitirá una mejor información así como formarse un mejor criterio para la localización de pozos exploratorios profundos que confirmen la existencia de vapor en cantidades comerciales; además de estos otros dos métodos, se tendrá también los resultados del método sísmico aplicado por la Misión Japonesa, en los meses de diciembre de 1976 y enero del presente año.

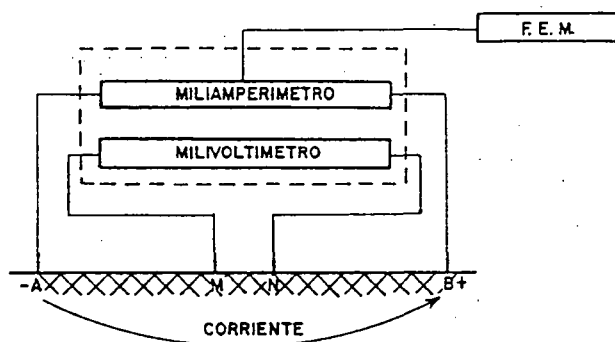
3. PROSPECCION GEOELECTRICA APLICADA A ESTUDIOS GEOTERMICOS

La prospección geoelectrica por el método de resistividad y el método electromagnético magnetotelúrico, son métodos aplicables en forma directa a la exploración geotérmica, debido a que la resistividad de las rocas decrece con el aumento de temperatura y contenido de fluidos dentro de sus poros o fracturas, debiéndose tener cuidado con la interpretación de los resultados, ya que la baja resistividad encontrada dentro de una zona puede ser debido también a otros fenómenos, tales como alto contenido de Na Cl de las aguas contenidas en las rocas, capas arcillosas, capas arcillosas derivadas de la alteración hidrotermal, fracturamiento secundario del espesor de rocas considerado como probable reservorio sellado por la precipitación de algunos elementos químicos por acción hidrotermal, como por ejemplo la precipitación de carbonato de calcio (Ca CO_3) con alto contenido de pirita diseminada, etc.

Otro método de prospección geoelectrica que ha sido aplicado a geotermia es el de potencial natural (S.P), en el campo geotérmico de Otake, Japón, para mapear zonas de alteración hidrotermal.

3.1 El Método de Resistividad Eléctrica

La aplicación del método de resistividad eléctrica consiste en introducir en el terreno corriente eléctrica (conmutada o alterna de baja frecuencia) a través de dos electrodos (barras de hierro, cobre, planchas de cobre, etc.) A y B (fig. 3.1.1) conectados a las terminales de una fuente de fuerza electromotriz (f.e.m.). Al introducir la corriente se establece en el terreno una distribución de potencial que se lee por medio de un milivoltímetro conectado a otros dos electrodos (preferiblemente impolarizables) M y N (fig. 3.1.1) y de cuyo conocimiento puede deducirse la distribución de la resistividad eléctrica en el subsuelo.



(fig. 3.1.1)

En exploración geotérmica se aplica la resistividad eléctrica efectuando sondeos eléctricos verticales S.E.V. los cuales pueden hacerse utilizando diferentes configuraciones. Aunque son posibles dispositivos electródicos muy variados para ejecutar S.E.V. como por ejemplo sondeo Dipolar Equatorial El Azimutal etc. se limitará a describir las tres

configuraciones lineales más comunes, como son el Arreglo Wenner, Schlumberger y Dipolo-Dipolo.

Arreglo Electrónico Wenner

En el S.E.V. con el dispositivo Wenner la distancia "a" entre los electrodos de corriente y potencial (fig. 3.1.2), se va aumentando escalonadamente manteniendo fijo el punto central de la configuración.

Entre más grande sea la distancia "a", mayor será la profundidad de investigación del subsuelo.

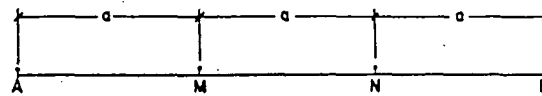
Arreglo Electrónico Schlumberger

En el S.E.V. con dispositivo Schlumberger (fig. 3.1.2) se mueven los electrodos de corriente AB, simétricamente y hacia fuera, quedando fijos en el centro los electrodos MN de potencial, abriéndose MN, únicamente hasta que el campo potencial creado por la corriente eléctrica introducida en AB no pueda ser leído; al abrir MN debe cumplirse con la condición $AB \geq 5 MN$; entre mayor sea la separación AB con respecto a MN, mayor la profundidad de investigación del subsuelo.

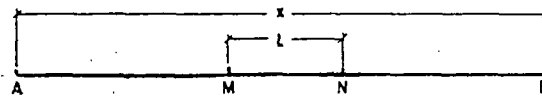
Arreglo Dipolo-Dipolo Lineal o Axial

En el dispositivo Dipolo-Dipolo lineal, los electrodos de corriente AB están muy próximos entre sí comparado con la distancia a que se mide la distribución de potencial creado por dicha corriente con los electrodos receptores MN, que también están muy próximos entre sí y con una sepa-

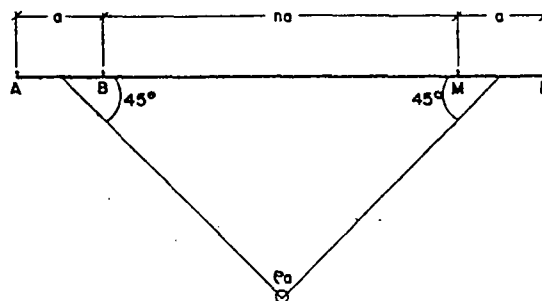
ración igual a AB, considerándoseles como dos dipolos. En este dispositivo los electrodos de corriente AB permanecen constantes, mientras que los electrodos receptores MN se van moviendo lateralmente una distancia "n" veces "a" (fig. 3.1.2), la resistividad del terreno medida será la proyección a 45° del punto medio entre los electrodos AB y MN, pudiéndose desplazar nuevamente los electrodos de corriente AB hacia ambos lados de la primera posición para poder cartografiar las resistividades lateralmente, obteniéndose en esta forma un panorama bidimensional de la distribución de resistividades a través de un perfil geoelectrico.



CONFIGURACION WENNER



CONFIGURACION SCHLUMBERGER



CONFIGURACION DIPOLO-DIPOLO O AXIAL

(fig. 3.1.2)

La ecuación general que rige cualquiera de los arreglos lineales expuestos aplicados sobre una superficie plana y un medio homogéneo es:

$$\Delta V = \frac{\rho I}{2\pi} \left(\frac{1}{AM} - \frac{1}{BM} - \frac{1}{AN} + \frac{1}{BN} \right) \quad (3.1.1)$$

ΔV = Diferencia de potencial medida entre electrodos MN

I = Intensidad de corriente transmitida a través del terreno por los electrodos AB

ρ = Resistividad verdadera del medio

de donde despejando de (3.1.1) se obtendrá que

$$\rho_a = 2\pi \left(\frac{1}{AM} - \frac{1}{BM} - \frac{1}{AN} + \frac{1}{BN} \right)^{-1} \frac{\Delta V}{I} \quad (3.1.2)$$

donde

ρ_a = Resistividad aparente

La resistividad será aparente y no la real ya que la superficie terrestre nunca es completamente plana y las rocas situadas bajo esta superficie nunca son homogéneas debido a sus diferentes características físicas, dando lugar a contrastes de resistividades entre ellas, lo que hace aplicable el método de Prospección Eléctrica.

3.2 Ventajas del Arreglo Schlumberger en la Aplicación de S.E.V.

La ventaja del dispositivo Schlumberger está en la calidad de las curvas de campo, las cuales son superiores a las Wenner debido a que en aquel dispositivo, los electrodos MN perma-

necen fijos, de tal forma que el efecto de la zona superficial donde están colocados es el mismo en todas las medidas realizadas, hasta que se efectúa un nuevo traslape o empalme, mientras que en el dispositivo Wenner la distancia "a" entre los electrodos de potencia MN, se desplaza cada vez que se aumenta escalonadamente la distancia "a", o sea que en cada lectura que se efectúa hay un traslape o empalme, reflejándose en la curva por medio de saltos.

Otra de las desventajas del dispositivo Wenner es de que en cada medida hay que desplazar los cuatro electrodos y no solo los dos de corriente como en el dispositivo Schlumberger, que implica mayor personal de campo y más tiempo, aumentando así el costo de exploración.

El dispositivo Dipolo-Dipolo es aplicado muy frecuentemente en la exploración geotérmica, pues por medio de él, se puede obtener en forma bidimensional la distribución de resistividades de las rocas bajo el subsuelo, teniendo la ventaja de poder visualizar discontinuidades laterales a través de un perfil geoelectrico.

En resumen la exploración geotérmica puede ser efectuada aplicando el método de S.E.V. por medio de arreglo Schlumberger, pudiendo ser complementado por Dipolo-Dipolo en las zonas donde se tenga duda que existan discontinuidades laterales de resistividad que puedan afectar la interpretación realizada.

4. LOCALIZACION DEL AREA DE ESTUDIO

El área geotérmica de Zunil fué delimitada para los estudios iniciales por el cuadrángulo dado por las coordenadas siguientes:

X = 59.00	Y = 36.00
X = 66.00	Y = 36.00
X = 59.00	Y = 31.5
X = 66.00	Y = 31.5

Hojas escala 1:50,000 (I.G.N.) No. 1860 II Colomba y No. 1960 III Santa Catarina Ixtahuacán.

Cubriendo un área aproximada de 31.5 Kms².

A sugerencia de la 1a. Misión Japonesa, se trazaron sobre esta área, 4 líneas principales que servirían para efectuar estudios geofísicos preliminares (fig. 4.1).

4.1 Trabajos de Prospección Geoeléctrica Efectuados por el INDE a la fecha

En el mes de octubre y principios de noviembre de 1976, el INDE inició los estudios a través de las 4 líneas principales, aplicando el método geoelectrico de resistividad por

medio de sondeos eléctricos verticales (S.E.V.) con arreglo tipo Schlumberger, con un $AB/2$ entre electrodos de corriente hasta 2,000 m. considerado suficiente para alcanzar a detectar el sustrato resistivo dentro de la zona estudiada. El INDE efectuó durante este período un total de 17 S.E.V. con una separación entre cada uno de ellos de más o menos 500 m. estando localizados de la siguiente manera: (fig. 4.1).

LINEA No. 1	S.E.V. No. 7, 8, 9, 10, 11
LINEA No. 2	S.E.V. No. 1, 2, 3, 4, 5, 6
LINEA No. 3	S.E.V. No. 12, 13, 14
LINEA No. 4	S.E.V. No. 15, 16, 17

Posteriormente en base a los resultados obtenidos y con el objeto de complementar y ampliar el área en estudio se efectuaron en el mes de marzo y agosto del presente año un total de 19 S.E.V. más, del No. 20 al No. 38 localizados como sigue: (fig. 4.1).

S.E.V. No. 20, 22	Carretera a Almolonga
S.E.V. No. 21, 24	Pueblo de Zunil
S.E.V. No. 23	Los Vahos
S.E.V. No. 25	Entre línea No. 4 y línea No. 3
S.E.V. No. 27, 30	Cerro Quemado
S.E.V. No. 26, 28, 38	Al noreste de línea No. 1
S.E.V. No. 29	Carretera Aguas Amargas
S.E.V. No. 31	Cementerio Cantel
S.E.V. No. 32	Entre línea No. 2 y línea No. 3

S.E.V. No. 34	Al sureste línea No. 4 y carretera a Aguas Georginas
S.E.V. No. 35, 36, 37	Llanos del Pinal, suroeste de ciudad Quetzaltenango

4.2 Trabajo de Campo

Para efectuar los S.E.V. se utilizó un equipo de fabricación Italiana con las siguientes características:

- a) Geo-Resistivity Meter D/39
- b) Fuente de alimentación (f.e.m.) con un voltaje máximo hasta 550 voltios
- c) Intensidad máxima entre electrodos de corriente AB de 3 amperios
- d) Precisión de lectura entre electrodos de potencial MN hasta de una centésima de milivoltio (0.01 milivoltio)
- e) Compensador manual para anular ruidos debidos a corrientes telúricas, S.P. etc.

Topográficamente el área presenta características muy abruptas, seleccionándose las 4 líneas para realizar los estudios geoelectricos (fig. 4.1) sobre el relieve del terreno más plano para evitar en la mejor forma posible que las curvas deducidas de los S.E.V. estuvieran influenciadas al mínimo, por efectos topográficos del terreno.

Así, de esta manera, las líneas no presentan orientación en retícula sino que siguiendo la superficie más plana del terreno, adecuándolas respecto al área de investigación requerida.

El arreglo electródico utilizado para efectuar los S.E.V. fué el sistema Schlumberger, hasta una distancia máxima entre electrodos de corriente AB de 4,000 metros, considerados su-

ficientes para detectar el fondo del sustrato resistivo, aunque en algunos sondeos fué insuficiente y en otros se tuvo que limitar a causa de dificultades de acceso debido a la morfología escabrosa del terreno.

Las curvas fueron ploteadas en la forma usual AB/2 contra resistividad aparente (ρ_a) en papel Log-Log, chequeándose el cálculo de ρ_a , cambiando de posición los electrodos de corriente AB, comprobándose la relación entre intensidad de corriente y diferencia de potencial entre los electrodos MN. En general no se tuvo mayor dificultad para ejecutar los S.E.V.

EVALUACION E INTERPRETACION DE LOS RESULTADOS

5. INTERPRETACION CUALITATIVA DE LOS S.E.V.

La interpretación cualitativa tiene como objeto obtener una primera visualización de los diferentes contrastes de resistividades, espesores aproximados y discontinuidades laterales de las formaciones que existen en el subsuelo, valiéndose para ello del análisis de las características de las curvas de cada S.E.V., trazado de mapas y perfiles de iso-resistivas etc.

Si el estudio cualitativo se lleva simultáneamente con la prospección eléctrica de campo, dará opción a ubicar nuevos S.E.V. claves, de cuyos resultados se obtendrá una mejor definición del área estudiada.

5.1 Análisis de Acuerdo a las Características de las Curvas

Como primer paso para evaluar el trabajo de prospección de campo, se hizo un análisis cualitativo de los S.E.V. ejecutados, clasificándolos de acuerdo a los cortes geoelectricos y número de capas, con el objeto de correlacionarlos y delimitar las zonas de S.E.V. de características semejantes que pudieran estar relacionadas con condiciones geológicas homogéneas.

Los cuatro tipos de curvas para cortes geoelectricos de tres

capas se clasifican como sigue:

1. Tipo H: $\rho_1 > \rho_2 < \rho_3$
2. Tipo K: $\rho_1 < \rho_2 > \rho_3$
3. Tipo Q: $\rho_1 > \rho_2 > \rho_3$
4. Tipo A: $\rho_1 < \rho_2 < \rho_3$

Las curvas de mayor número de capas se designan con una combinación de las anteriores.

En base a lo expuesto, en el área estudiada se clasificaron 4 diferentes tipos de curvas (KH, QH, HK, QQ), delimitándose 5 áreas con diferentes características (fig. 5.1.1).

AREA I (fig. 5.1.1)

Está localizada en el lado oeste del área principal estudiada, limitada al este por el río Samalá, al noreste por la población de Zunil, al suroeste entre el S.E.V. Nos. 10 y 11 de la línea No. 1 y al oeste el límite real no ha sido comprobado con los S.E.V. efectuados, pero seguramente se encuentra entre los sondeos No. 38 y No. 30, correlacionando con una falla geológica con rumbo noreste-suroeste, que los Geólogos en el mapeo de campo superficial, han estimado como el límite noroeste de una estructura en forma de graben de aproximadamente 3 Kms. de ancho.

Las curvas de los S.E.V. fueron clasificadas del tipo KH e incluyen los S.E.V. siguientes:

LINEA No. 1	8, 9, 10
LINEA No. 2	5 y 6
LINEA No. 3	12

AL NORESTE
LINEA No. 1

28, 38

Las primeras capas son de alta resistividad mientras que la tercera capa en todos los sondeos es de baja resistividad (<10 ohm-m) con espesores aproximados de 300 a 500 m., seguida de otra capa de alta resistividad que probablemente corresponde al basamento de la zona (granodiorita); considerándosele como una de las áreas mas atractivas dentro de los estudios realizados.

AREA II y II A (fig. 5.1.1)

Estan localizadas al suroeste del área I y en el área que cubre el poblado de Zunil, respectivamente.

Las curvas de los S.E.V. ejecutados en ambas áreas tienen las mismas características y fueron clasificadas del tipo QH incluyendo los S.E.V. siguientes:

AREA II

LINEA No. 1	11
AL NOROESTE LINEA No. 1	26

AREA II A

LINEA No. 1	7
POBLADO ZUNIL	21, 24

Las capas superficiales son de baja resistividad variando de 300 a 20 ohm-m, seguidos de una capa muy conductiva con una resistividad menor de 10 ohm-m y de un espesor que varía

de más o menos 150 a 200 m. en el área del poblado de Zunil (AREA II A) y aproximadamente 400 m. en el AREA II.

Abajo del espesor conductivo se encuentra la capa resistiva que podría coincidir con el basamento (granodiorita), dando la impresión de que en ambas áreas el fondo del sustrato resistivo se levanta.

AREA III (fig. 5.1.1)

Está localizada al lado este del río Samalá y comprende los S.E.V. siguientes:

LINEA No. 2	1, 2
LINEA No. 3	13

Las curvas fueron clasificadas del tipo KH.

La primera capa es de mediana resistividad que varía de 200 a 340 ohm-m teniendo un espesor muy pequeño, la segunda capa aumenta de resistividad, siendo la tercera una capa conductiva de baja resistividad que varía entre 10 y 20 ohm-m con un espesor aproximado de 500 a 600 m. seguidas también de la capa resistiva.

Las características de estas curvas son iguales a las del área I pero la resistividad del espesor conductivo no es menor de 10 ohm-m, siendo de tendencia más suave.

AREA IV (fig. 5.1.1)

Está localizada al este del AREA III y al noreste del AREA V.

Para determinar esta área se tomaron en cuenta dos tipos de

de curvas, QQ y HK.

LINEA No. 3	S.E.V. No. 14	(QQ)
ENTRE LINEA No. 2 y 3	S.E.V. No. 32	(HK)
ENTRE LINEA No. 3 y 4	S.E.V. No. 25	(HK)

En el S.E.V. No. 14 de tipo QQ, las capas superiores descienden desde una resistividad de más o menos 2,200 hasta 90 ohm-m en un espesor de aproximadamente 340 m. tendiendo la curva a seguir descendiendo muy rápidamente, no pudiendo estimarse la resistividad ni el espesor aproximado de la siguiente capa por no detectarse otra capa inferior más resistiva, pero que por la tendencia de la curva podría llegar a ser menor de 10 ohm-m.

En los S.E.V. No. 25 y No. 32 de tipo HK la resistividad de las primeras capas varía de altas a medias (1,300-400 ohm-m) ascendiendo la resistividad de la tercera capa (2,000 ohm-m) hasta un espesor de más o menos 400 m., no pudiendo también ser estimada la resistividad ni el espesor de la siguiente capa, pero que por la tendencia de ambas curvas podría también ser menor de 10 ohm-m.

Esta área podría ser de interés geotérmico por lo que tendrá que explorarse más a detalle alargando la distancia de los electrodos AB/2 para tratar de encontrar el fondo resistivo.

AREA V (fig. 5.1.1)

Está localizada al sur de las áreas III y IV, e incluye los S.E.V. siguientes:

LINEA No. 4	15, 16 y 17
-------------	-------------

Las curvas fueron clasificadas del tipo HK.

La resistividad de las primeras 2 capas varía en su orden, de más de 700 a menos de 170 ohm-m, aumentando nuevamente la resistividad de la tercera capa más o menos alrededor de 1,000 ohm-m, tendiendo la última capa a bajar de resistividad.

Si se comparan las configuraciones de las curvas de los S.E.V. Nos. 32, 25, 15, 16, 17, se puede apreciar que la primera parte de todas las curvas correlacionan, tendiendo los S.E.V. Nos. 32 y 25 a bajar muy bruscamente de resistividad, lo que podría suceder igualmente en los S.E.V. Nos. 15, 16, 17, si se alargan los electrodos de corriente AB/2, pues por las condiciones topográficas del terreno, los electrodos de corriente AB/2, se extendieron unicamente hasta 1,000, 1,200 y 800 m. respectivamente, teniéndose que comprobar su tendencia final efectuados nuevos sondeos con un AB/2 mayor.

La confirmación de lo expuesto anteriormente tendría como consecuencia que el área IV y V tuvieran las mismas características y fueran una sola, siendo su límite hacia el este una discontinuidad geoelectrica (fig. 5.1.1) que probablemente correlacione con una falla geológica.

Se debe tomar en cuenta que la delimitación de las áreas se efectuó solamente en forma cualitativa, atendiendo solamente a las características de las curvas de campo de acuerdo a los valores absolutos de resistividad aparente (ρ_a), máximos, mínimos, asíntotas y puntos de inflexión, con el fin de obtener una primera idea de las estructuras del subsuelo estudiado, pues al hacerse la interpretación cuantitativa

puede aumentar o disminuir el número de capas estimadas visualmente, determinándose los espesores y resistividades verdaderas de los diferentes estratos.

5.2 Mapas de Resistividad Aparente o Isoresistivas

Los mapas de Isoresistivas se obtienen interpolando los puntos de igual resistividad aparente, anotando a la par de cada S.E.V. los valores de resistividad correspondientes a cierta distancia determinada $AB/2$, trazando posteriormente las líneas isoresistivas.

En el área de Zunil se hicieron mapas de líneas isoresistivas con $AB/2$ de 500, 800 y 1,000 m. (fig. 5.2.1., 5.2.2., 5.2.3.) tomando en cuenta los valores más significativos de ρ_a , visualizando en las curvas de campo los valores de resistividad aparente a la distancia $AB/2$ que tuvieron mayor influencia en las capas de baja resistividad (<10 ohm-m), que como ya se mencionó son las que interesan en los estudios de exploración geotérmica.

Debe tomarse en cuenta que la distribución vertical de resistividades aparentes (ρ_a) vistas en planta, no corresponden a una profundidad determinada, sino que a una distancia específica $AB/2$ entre electrodos de corriente.

Mapa de $AB/2 = 500$ m. (fig. 5.2.1)

Las zonas de baja resistividad (<10 a 20 ohm-m) se encuentran localizadas en el lado suroeste del área estudiada hacia el flanco oeste del río Samalá alrededor de los S.E.V. Nos. 10 y 11 de la línea No. 1, y hacia el noreste sobre el po-

blado de Zunil, alrededor de los S.E.V. Nos. 21 y 24, demostrando el mapa que la distribución vertical de la conductividad de las capas es más superficial en ambas zonas, coincidiendo con la delimitación de las áreas II y II A, mencionadas en el inciso 5.1.

Mapa AB/2 = 800 m. (fig. 5.2.2)

La zona de baja resistividad (<10 ohm-m) se observa en la parte oeste del río Samalá, alrededor de los S.E.V. Nos. 5, 9 y 10 situados sobre las líneas Nos. 1 y 2, aumentando muy suavemente la resistividad de 10 a 20 ohm-m hacia el poblado de Zunil y al este del río Samalá, siendo la influencia de las capas conductivas más profunda en esta zona, comenzando a desaparecer las áreas de baja resistividad determinados con la distancia AB/2 = 500 m. probablemente debido al incremento de resistividad de las capas a la distancia AB/2 = 800 m.

La resistividad aparente (ρ_a) aumenta muy rápidamente de 20 a >100 ohm-m hacia el noroeste entre los S.E.V. Nos. 28 y 30 y hacia el lado este del río Samalá a partir del S.E.V. No. 14, lo que hace suponer nuevamente la existencia de las dos discontinuidades geoelectricas con rumbo noreste-sureste mencionados en el inciso 5.1., coincidiendo el área de baja resistividad con la delimitación del área I (fig. 5.1.1).

Mapa AB/2 = 1,000 m. (fig. 5.2.3)

La zona de baja resistividad (<10 ohm-m), se encuentra localizada en las mismas coordenadas del Mapa AB/2 = 800 m. alrededor del S.E.V. No. 10 sobre la línea No. 1, aprecián-

dose que dicha área disminuye de extensión debido al aumento de resistividad aparente (ρ_a) de las capas más profundas, actuando la influencia de la baja resistividad solamente sobre el S.E.V. No. 10, demostrando que las capas conductoras se profundizan en esta zona.

Al efectuar la evaluación cualitativa de los resultados obtenidos con la configuración de los mapas de Isoresistivas se puede apreciar que son similares a los obtenidos en el análisis de los S.E.V. de acuerdo a las características de las curvas (inciso 5.1), ya que nuevamente se manifiesta que aparentemente el fondo del sustrato resistivo se levanta en las áreas del poblado de Zunil y en el suroeste del área, alrededor de los S.E.V. Nos. 10 y 11, siendo la influencia de las capas conductoras más superficiales en ambas zonas, profundizándose alrededor de los S.E.V. Nos. 5, 9 y 10.

También se manifiestan, por medio de un cambio brusco de resistividad, las dos discontinuidades Geoeléctricas de rumbo noreste-suroeste mencionados en el inciso 5.1, una hacia el noroeste entre los sondeos Nos. 28 y 30 que correlaciona con el límite noroeste de la estructura en forma de graben alrededor de 3 Kms. de ancho y la otra hacia el oeste del río Samalá a partir del S.E.V. No. 14 (fig. 5.2.2. y 5.2.3).

5.3 Perfiles de Resistividad Aparente

Los perfiles de resistividad aparente representan la variación lateral de la resistividad a lo largo de un perfil determinado.

Para construir los perfiles, se tomó ^{volumen} el valor de la resis-

tividad aparente calculado para las distancias de separación $AB/2$ entre electrodos de corriente tomados en cada uno de los sondeos, la cual se ploteo sobre un eje de ordenadas dirigido hacia abajo en la ubicación de cada uno de los S.E.V., interpolándose posteriormente los valores de igual resistividad aparente a la distancia $AB/2$.

Su interpretación debe ser cuidadosa ya que un aumento de la distancia $AB/2$ para una misma resistividad, puede significar un aumento de profundidad de la capa o una disminución de la resistividad verdadera de las capas superiores.

LINEA No. 1 (fig. 5.3.1)

La distribución de resistividades a través del perfil No. 1 parece indicar que las capas superficiales a través de los S.E.V. Nos. 8, 9 y 10 son de alta resistividad, no siendo así en los sondeos Nos. 7 y 11 localizados en los extremos noreste y suroeste de la línea, donde dichas capas disminuyen de resistividad.

Por otro lado, las resistividades de los espesores inferiores a través de los S.E.V. Nos. 9, 10 y 11 disminuyen considerablemente a 10 y 15 ohm-m, siendo de mayor profundidad en los S.E.V. Nos. 9 y 10 y levantándose hacia el sondeo No. 11. Hacia el extremo noreste de la línea en los S.E.V. Nos. 7 y 8 la resistividad de los espesores conductivos inferiores disminuye a 20 ohm-m, siendo de menor profundidad hacia el sondeo No. 7.

De lo expuesto con anterioridad se puede inferir que existen dos discontinuidades laterales a través de este perfil, una entre los S.E.V. Nos. 7 y 8 donde la inclinación aproxi-

mada de 45° de las curvas iso-resistivas podrían dar la pauta de la existencia de la discontinuidad y la otra entre los sondeos Nos. 10 y 11.

LINEA No. 2 (fig. 5.3.2)

En el perfil de resistividad aparente de la línea No. 2, se puede observar claramente que las curvas iso-resistivas superficiales hacia el lado este del río Samalá son de menor valor que hacia su lado oeste, lo que podría indicar que el tipo de rocas superficiales situadas a ambos lados del río tienen diferentes características físicas, pudiendo inferirse que a través del río Samalá existe una discontinuidad geoelectrica que correlaciona con un contacto o falla geológica.

Por otro lado, la resistividad aparente de las capas inferiores hacia el lado oeste del río Samalá desciende a 20 y 10 ohm-m, mientras que en su lado este disminuye a 20 ohm-m. También hacia el sondeo No. 1 la resistividad de las capas inferiores tiende a aumentar, existiendo probablemente entre el S.E.V. No. 1 y No. 2 otra discontinuidad.

LINEA No. 3 (fig. 5.3.3)

En este perfil se vuelve a reflejar que las capas superficiales hacia el lado oeste del río Samalá son de mucho mayor resistividad que los del lado este, pudiendo inferirse nuevamente que a través del río Samalá existe una discontinuidad eléctrica.

El valor de resistividad aparente en profundidad vuelve a ser menor en el lado oeste del río (<15 ohm-m).

LINEA No. 4 (5.3.4)

El perfil de resistividad aparente de la línea No. 4 demuestra que la distribución de resistividades a través del perfil es alta, tendiendo a disminuir en profundidad y hacia el río Samalá debiéndose efectuar mayor investigación geofísica para obtener mayor detalle del perfil.

5.4 Mapa de Conductancia Longitudinal

A la relación

$$C.L_j = \frac{E_j}{\rho_j} \quad (5.4.1)$$

Se le da el nombre de Conductancia Longitudinal Unitaria.

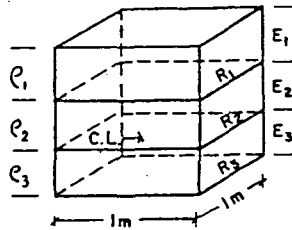
donde

$C.L_j$ = Conductancia Longitudinal Unitaria

E_j = ^{thick layer} Espesor de la capa

ρ_j = ^{average} Resistividad verdadera de la capa

El principio se basa en suponer un medio estratificado por medio de un prisma de sección cuadrada y de lado igual a la unidad (fig. 5.4.1).



(fig. 5.4.1)

Si se hace fluir una corriente paralela a la estratificación, la resistencia de cada una de las capas al paso de dicha corriente estará dada por:

$$R_i = \rho_i \frac{L}{S} = \frac{\rho_i \times 1}{E_i \times 1} = \frac{\rho_i}{E_i} \quad (5.4.2)$$

R_i = Resistividad de ^{each layer} cada capa

Como las resistencias de las capas están en paralelo no se pueden sumar como las resistencias en serie, como sucedería si la corriente se supone perpendicular a las capas; utilizándose el parámetro de conductancia longitudinal ($\frac{1}{R_i}$), que si tiene la propiedad de adición, para resolver esta circunstancia.

De donde:

$$R_i = \frac{1}{C.L_i} \quad (5.4.3)$$

$$C.L_i = \frac{1}{R_i} = \frac{E_i}{\rho_i}$$

La suma de "N" capas tendrá una Conductancia Longitudinal de

$$C.L = \sum_i \frac{E_i}{\rho_i} \quad (5.4.4)$$

El mapa de Conductancia Longitudinal es de suma importancia en Prospección Geotérmica, pues en él se delimitan las zonas de mayor conductividad eléctrica que pueden estar en correspondencia con la presencia de fluidos geotérmicos: así mismo, se pueden estimar discontinuidades laterales que pueden correlacionar con fallas geológicas al presentarse un cambio brusco de la conductancia en un espacio relativamente corto.

Para encontrar la Conductancia Longitudinal se utilizó el método gráfico creado por Ernesto Orellana, con el cual no se necesita saber previamente los espesores y resistividades de las capas del subsuelo, siendo de solución única y necesitándose solamente que la parte derecha de la curva sea ascendente.

El valor gráfico de Conductancia Longitudinal encontrado en cada sondeo puede ser observado en las curvas correspondientes (Fig. 6.1.1 a 6.1.23) no pudiendo ser calculada para los S.E.V. Nos. 14, 15, 16, 17, 25, 32, por no haberse encontrado el fondo del sustrato resistivo y por lo tanto la parte derecha de la curva no es ascendente.

El mapa de Conductancia Longitudinal (Fig. 5.4.2) demuestra que el área anómala de mayor conductancia (200 a >300 mho), se encuentra localizada en el lado suroeste del río Samalá alrededor de los S.E.V. Nos. 10 y 11, disminuyendo gradualmente hacia el poblado de Zunil, y hacia el lado este del río Samalá, donde es limitada por una discontinuidad eléctrica inferida debido a que en los S.E.V. (Nos. 14, 15, 16, 17, 25, 32) situados al lado este de ella, aumenta considerablemente el espesor de las capas resistivas superficiales, no pudiendo ser determinada la resistividad de la última capa por no haberse detectado el fondo del sustrato resistivo, pero que por la tendencia de las curvas podría ser menor de 10 ohm-m.

Si al investigar con nuevos S.E.V. se encuentra el fondo del sustrato resistivo y se determina la capa de baja resistividad con una alta conductancia longitudinal, esta área se reflejaría también como anómala, siendo el proba-

ble reservorio más profundo hacia este lado que en el área delimitada en la Fig. 5.4.2.

El límite del área de alta conductancia longitudinal hacia el noroeste del río Samalá se ha correlacionado con la falla que limita hacia el noroeste el Graben de Zunil. En el poblado de Zunil en donde conforme a las características de los S.E.V. Nos. 7, 21 y 24 existe una capa de baja resistividad (< 10 ohm-m), la conductancia longitudinal es baja, debido probablemente a que esta capa es de poco espesor en esta zona, siendo el fondo del sustrato resistivo relativamente superficial.

6. INTERPRETACION CUANTITATIVA

La interpretación cuantitativa tiene como finalidad ^{how} encontrar los espesores ^{depth} y las resistividades ^{true} verdaderas correspondientes a las formaciones situadas ^{is situated} bajo la superficie terrestre, partiendo de los datos de resistividad aparente calculados de acuerdo a las medidas efectuadas en superficie en cada uno de los S.E.V. ejecutados.

El objetivo principal en prospección geotérmica es definir el espesor de las capas de baja resistividad (<10 ohm-m) que podrían estar relacionadas con la presencia de fluidos geotérmicos, además de determinarse el fondo del sustrato resistivo que serviría de límite en profundidad del probable reservorio geotérmico, excepto si existiera vapor seco.

6.1 Análisis Cuantitativo de los S.E.V.

La interpretación cuantitativa de los S.E.V. se efectuó ^{by} por el método del punto auxiliar, ^{the method of auxiliary points} empleando para ello las curvas teóricas para tres estratos horizontales editadas por "FONDAZIONE ING. C.M. LERICI DEL POLITECNICO DE MILANO".

La interpretación cuantitativa de los S.E.V., puede ser observada en las fig. 6.1.1 a la 6.1.23., en donde aparecen los espesores y resistividades calculadas para cada uno de los S.E.V. ejecutados dentro del área principal estudiada.

Basándose en los resultados anteriores se trazaron los perfiles geoelectricos correspondientes a cada una de las 4 líneas, ubicando cada uno de los S.E.V. en su respectivo perfil (fig. 6.1.24., 6.1.25., 6.1.26., 6.1.27).

Perfil Geoelectrico de la Línea No. 1 (fig. 6.1.24)

La línea No. 1 se encuentra localizada en el lado oeste del río Samalá siguiendo un rumbo noreste-suroeste, en ella están localizados los S.E.V. Nos. 7, 8, 9, 10 y 11 (fig. 4.1). La capa de baja resistividad (10 ohm-m) se distribuye a través de todos los S.E.V. mencionados, siendo de mayor espesor en el sondeo No. 10 (510 m.), disminuyendo hacia el noreste y suroeste de la línea, hacia los sondeos Nos. 7 y 11, donde el espesor conductivo disminuye a 210 y 400 m. respectivamente.

El fondo del sustrato resistivo se profundiza en el sondeo No. 10 (690 m.) levantándose gradualmente hacia el noreste de la línea hasta el S.E.V. No. 8 (520 m.).

En el perfil se han inferido dos discontinuidades geoelectricas, que podrían correlacionar con alguna falla o contacto geológico; la primera se encuentra localizada entre los S.E.V. Nos. 7 y 8 inferida debido a que el sustrato resistivo en el sondeo No. 7 se levanta considerablemente hasta una profundidad de 280 m. además de que las capas superficiales son de baja resistividad comparadas con las del S.E.V. No. 8; la segunda se encuentra localizada entre los S.E.V. Nos. 10 y 11 y se ha inferido de acuerdo a que las capas superficiales en el sondeo No. 11 son de baja resistividad y de menor espesor que en el S.E.V. No. 10, levantan-

tándose el fondo resistivo a 500 m. de profundidad. El espesor de las capas resistivas superficiales varía de más o menos 70 a 180 m. a través de todo el perfil.

Perfil Geoeléctrico de la Línea No. 2 (fig. 6.1.25)

La línea No. 2 se encuentra localizada en la parte norte del área estudiada, siguiendo un rumbo noreste-suroeste y atravesando el río Samalá; en ella se encuentran ubicados los S.E.V. Nos. 1, 2, 3, 4, 5 y 6 (fig. 4.1).

La capa de baja resistividad (<10 ohm-m) se distribuye a través de los S.E.V. Nos. 5 y 6, situados en el lado oeste del río, aumentando a más de 10 ohm-m hacia el lado este del mismo.

El espesor del estrato conductor y la profundidad del sustrato resistivo tienen un promedio de 530 y 640 metros respectivamente a través de todo el perfil.

En este perfil también se han inferido dos discontinuidades geoeléctricas; la primera en el río Samalá pues las capas superficiales hacia el lado oeste del río, son de mucho más alta resistividad que en el lado este, y por otra parte la resistividad del estrato conductor aumenta a más de 10 ohm-m en el lado este del mismo; la segunda discontinuidad se localiza entre los S.E.V. Nos. 1 y 2, infiriéndose de acuerdo a que la capa conductiva aumenta considerablemente de resistividad de 12 a 22 ohm-m.

Perfil Geoeléctrico de la Línea No. 3 (fig. 6.1.26)

La línea No. 3 se encuentra localizada más o menos con un

rumbo este-oeste, cruzando también su sección el río Samalá; en ella se encuentran ubicados los S.E.V. Nos. 12, 13 y 14 (fig. 4.1).

El comportamiento electroestratigráfico de este perfil es similar al perfil geoelectrico No. 2, exceptuando una discontinuidad que probablemente exista entre los S.E.V. Nos. 13 y 14, que tendrá que ser investigada más a fondo, ya que la profundidad de investigación para el S.E.V. No. 14 por medio de las curvas teóricas pudo ser determinada hasta 280 m. siendo la tendencia del último espesor a ser menor de 10 ohm-m; por otra parte, el espesor de las capas resistivas superficiales, aumenta de 99 m. en el sondeo No. 13 a 280 m. en el sondeo No. 14.

Perfil Geoelectrico de Línea No. 4 (fig. 6.1.27)

Esta línea se encuentra localizada al sur del área estudiada, siguiendo un rumbo este-oeste; en ella se encuentran ubicados los S.E.V. Nos. 15, 16 y 17 (fig. 4.1).

Las resistividades encontradas para los diferentes estratos relativamente altas, existiendo una clara discontinuidad entre este perfil y el No. 3.

Para tener una visión clara de la distribución de los espesores de baja resistividad (<10 ohm-m), que pueden estar relacionados con la existencia de un reservorio geotérmico en el área de Zunil, se hizo un bloque diagramático del área estudiada (fig. 6.1.28), en donde se han incluido además de los perfiles geoelectricos de las líneas Nos. 1, 2, 3 y 4 descritas anteriormente, otros cortes que toman en cuenta los últimos S.E.V. ejecutados, que han servido para

complementar en parte el estudio realizado.

En el bloque diagramático se puede observar que el espesor de las capas de baja resistividad (<10 ohm-m), se encuentran ubicadas hacia el lado oeste del río Samalá y en el poblado de Zunil donde su espesor se reduce, aumentando gradualmente a más de 10 ohm-m hacia el flanco este del río, excepto en el corte representado por los S.E.V. Nos. 25 y 32 donde en profundidad pudiera existir una capa con una resistividad de menos de 10 ohm-m que también se manifiesta en el S.E.V. No. 14, dicha circunstancia tendrá que investigarse, ya que esta zona podría ser también de interés geotérmico.

6.2 Mapa del Isonivel del Sustrato Resistivo (fig. 6.2.1)

El objetivo de encontrar el Isonivel del sustrato resistivo, es de que dicho isonivel, podría correlacionar con el límite inferior del probable reservorio geotérmico, coincidiendo quizás también, con el nivel del basamento dentro del área. El mapa de isonivel del sustrato resistivo se obtuvo anotando a la par de cada S.E.V., los valores correspondientes a la profundidad del fondo resistivo tomados del análisis cuantitativo de los S.E.V., estos valores se refirieron a la altura sobre el nivel del mar, interpolándose posteriormente los puntos de igual nivel.

Al analizar el mapa del isonivel, puede ser observado que el fondo resistivo se encuentra levantado en el poblado de Zunil profudizándose hacia el sur, considerándose que existe una discontinuidad geoelectrica con rumbo este-oeste entre la población de Zunil y la línea No. 2 que podría corre-

lacionar con una falla o contacto geológico; por otro lado, el fondo resistivo se levanta también gradualmente hacia el S.E.V. No. 11.

En el lado este del río Samalá, fueron inferidas otras dos discontinuidades, debido a que la profundidad del fondo resistivo no fué detectado en esta área.

6.3 Mapa de Isopacas del Estrato Conductivo (fig. 6.3.1)

La importancia de este mapa, radica en que dentro de este espesor puede existir el probable reservorio geotérmico. En el mapa de isopacas del conductivo se consideraron solamente estratos con resistividades menores de 15 ohm-m, tomando para ello los espesores de las capas determinadas en el análisis cuantitativo de los S.E.V. (fig. 6.1.1. a 6.1.23). La configuración de las curvas de isopacas es similar a las obtenidas en el mapa del sustrato resistivo, indicando con esto, que el espesor de las capas conductivas depende de la profundidad del fondo resistivo.

7. PERFORACIONES REALIZADAS

En base a la interpretación se programaron 5 perforaciones para correlacionar los resultados obtenidos.

Perforación No. 1 (Z-1)

Está localizada en la línea No. 3 en la parte este del río Samalá y aproximadamente a 200 m. del S.E.V. No. 14. Su objetivo inicial fué encontrar el tipo de roca de alta velocidad situada a una profundidad de aproximadamente 150 m., refractada por la prospección sísmica ejecutada por la Misión Japonesa en los meses de diciembre de 1976 y enero del presente año; sospechándose que podría correlacionar con el basamento granodiorítico de la zona; sin embargo la interpretación del S.E.V. No. 14, más próximo a la ubicación del pozo Z-1, indicaba que las resistividades de las capas superficiales hasta una profundidad de aproximadamente 280 m., descendían de 2,100 a 80 ohm-m, tendiendo las curvas a seguir bajando muy bruscamente de resistividad, probablemente menos de 10 ohm-m (fig. 6.1.13).

En base a lo expuesto se perforó el pozo Z-1 hasta una profundidad de 310 m., encontrándose que la capa de alta velocidad correspondía a una roca de tipo basáltico localizada a una profundidad de 122 m. y con un espesor de 85 m. habiéndose

dose determinado que el promedio del gradiente geotérmico de 0 a 250 m. fué de $1.8^{\circ}\text{C}/10\text{ m.}$ aumentando este gradiente a $8.4^{\circ}\text{C}/10\text{ m.}$ a partir de 250 a 300 m. obteniéndose una temperatura de fondo de 100°C.

Pozo No. 2 (Z-2)

Este pozo fué ubicado en el lugar denominado las Fresas, en el lado oeste del río Samalá aproximadamente 40 m. al este de la línea No. 1 entre los S.E.V. Nos. 10 y 11. Su objetivo fué el de investigar los resultados de la investigación geoelectrica interpretación en el S.E.V. No. 11 (fig. 6.1.10) más próximo a la ubicación de este pozo; su interpretación indica que las resistividades de las capas superficiales hasta una profundidad de 90 m. descienden de 140 a 18.5 ohm-m. siguiendo una capa de baja resistividad de 2 ohm-m. hasta una profundidad de 500 m. donde conforme a la interpretación se detecta el fondo del sustrato resistivo.

En base a lo expuesto se perforó el pozo Z-2 hasta una profundidad de 192 m. habiéndose determinado que el promedio de gradiente de 20 a 120 m. fué de $3.36^{\circ}\text{C}/10\text{ m.}$, aumentando este gradiente a $12.3^{\circ}\text{C}/10\text{ m.}$ a partir de 120 a 190 m., obteniéndose una temperatura del fondo de 173°C.

Pozo No. 3 (Z-3)

Este pozo está ubicado en el lado oeste del río Samalá sobre la línea No. 1, coincidiendo con la localización del S.E.V. No. 9

El objetivo del pozo fué el de correlacionar los resultados de la interpretación eléctrica del S.E.V. No. 9, donde las capas superficiales hasta una profundidad de 170 m. descienden de 7,500 a 140 ohm-m, siguiendo una capa de baja resistividad de aproximadamente 4 ohm-m hasta una profundidad de 600 m. donde de acuerdo a la interpretación se detecta el fondo del sustrato resistivo.

El pozo se encuentra actualmente en proceso de perforación, esperando obtenerse resultados positivos de gradiente a partir de 170 m.; por otra parte la resistividad de las capas superficiales en esta área son de mucho mayor resistividad que en el área donde está localizado el S.E.V. No. 11, existiendo una discontinuidad eléctrica entre éste sondeo y el No. 10, cuyo comportamiento es similar al No. 9.

Pozo No. 4 (Z-4)

El pozo No. 4 se encuentra localizado en el lado oeste del río Samalá, aproximadamente 30 m. hacia el sur de la línea No. 3 y al este de la carretera asfaltada que conduce a la ciudad de Quetzaltenango.

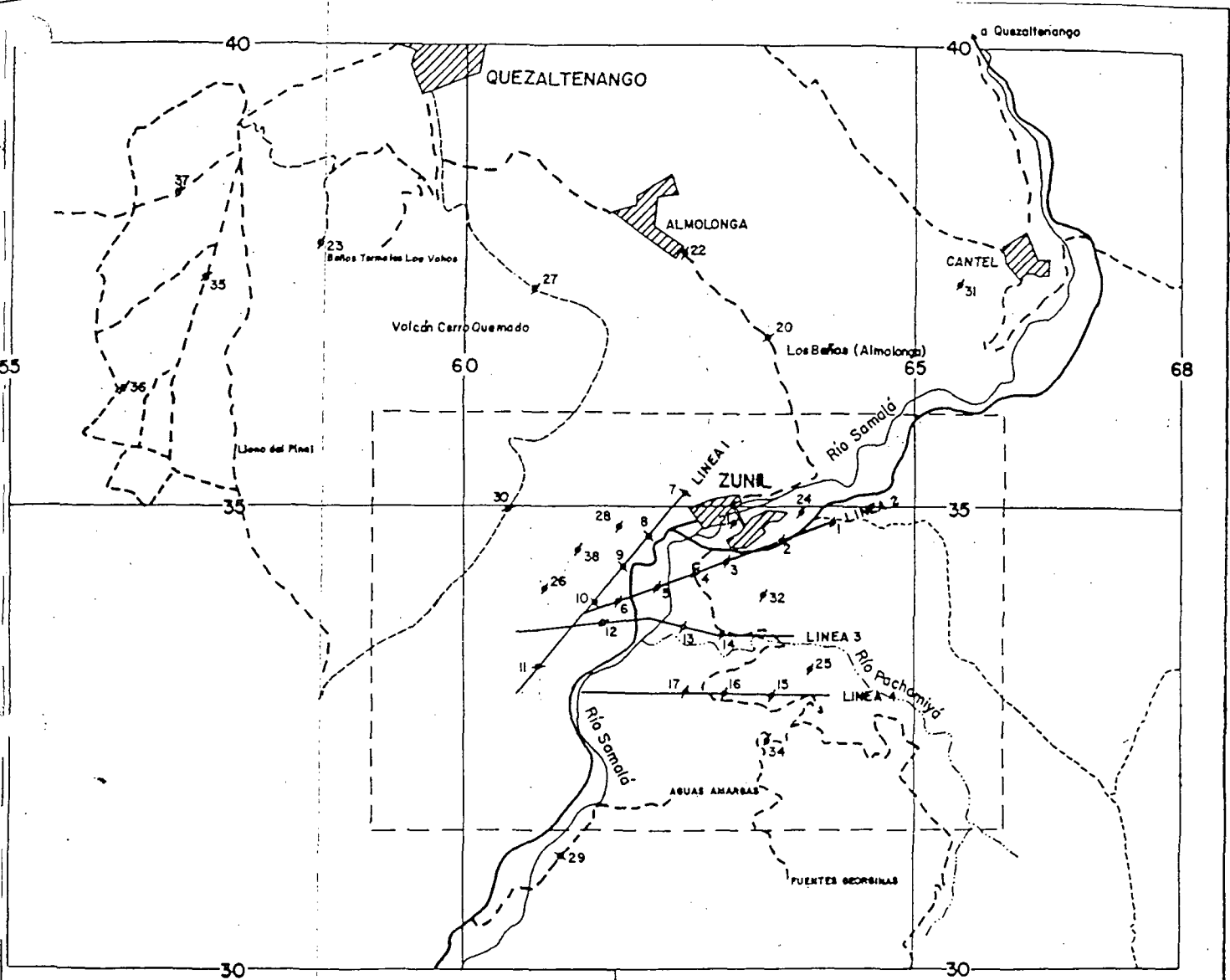
Su objetivo es la investigación tanto estratigráfica como de gradiente, ubicándose dentro de la zona considerada como anómala, encontrándose actualmente en proceso de perforación.

Pozo No. 5 (Z-5)

Se ha ubicado en el poblado de Zunil aproximadamente 40 m. hacia el norte del S.E.V. No. 21, el cual indica que la resistividad de las capas superficiales hasta una profundidad

de 65 m., desciende de 750 a 18 ohm-m seguida de una capa de aproximadamente 4 ohm-m hasta una profundidad de 240 m.; el objetivo principal de esta perforación, además de investigar el gradiente, es el de llegar a detectar el fondo del sustrato resistivo que según la interpretación se encuentra aproximadamente a 240 m. de profundidad, encontrándose actualmente en proceso de perforación.

FIGURAS



● SONDEO ELECTRICO VERTICAL (S.E.V.)
 AB/2 = 2000. ARREGLO SCHLUMBERGER.
 --- DELIMITACION DEL AREA ORIGINAL DE ESTUDIO.

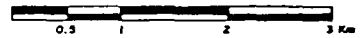
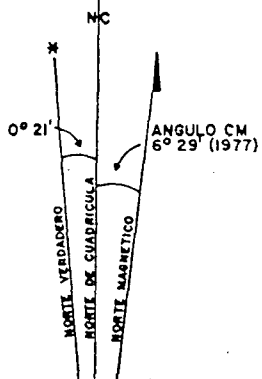


FIG. 4.1

INSTITUTO NACIONAL DE ELECTRIFICACION	
ESTUDIOS GEOTERMICOS DE ZUNIL	
MAPA DE LOCALIZACION DE SONDEOS ELECTRICOS VERTICALES	
GUATEMALA, AGOSTO/1977	ESCALA 1:50 000
Dibujó: L. BRADLEY	Realizó: ING. JULIO PALMA BETHANCOURT
	VoBo: ING. M. R.

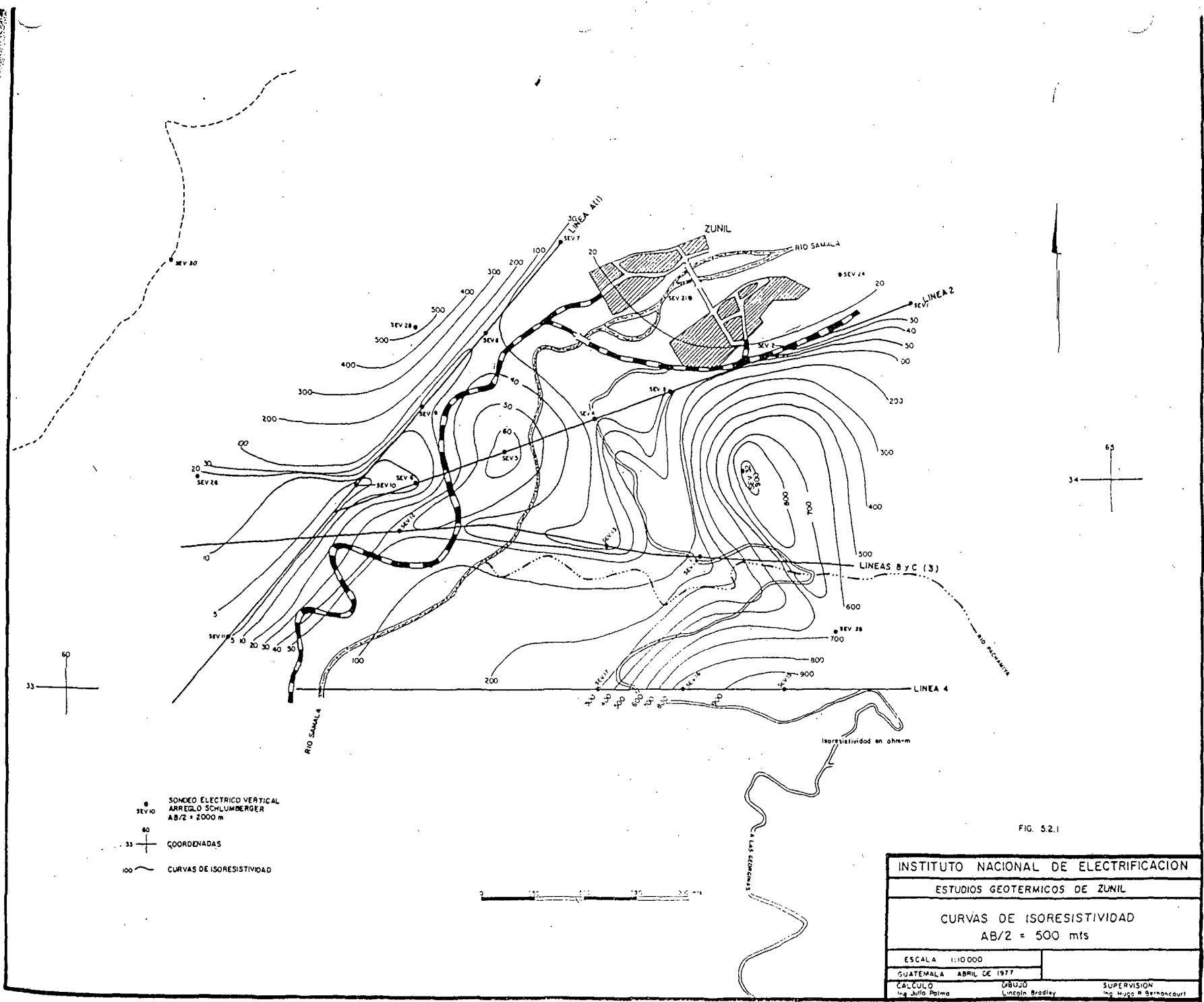


FIG. 5.2.1

INSTITUTO NACIONAL DE ELECTRIFICACION	
ESTUDIOS GEOTERMICOS DE ZUNIL	
CURVAS DE ISORESISTIVIDAD AB/2 = 500 mts	
ESCALA 1:10,000	
GUATEMALA ABRIL DE 1977	
CALCULO Ing. Julio Palma	SUPERVISION Ing. Lincoln Bradley Ing. Hugo R. Benincourt

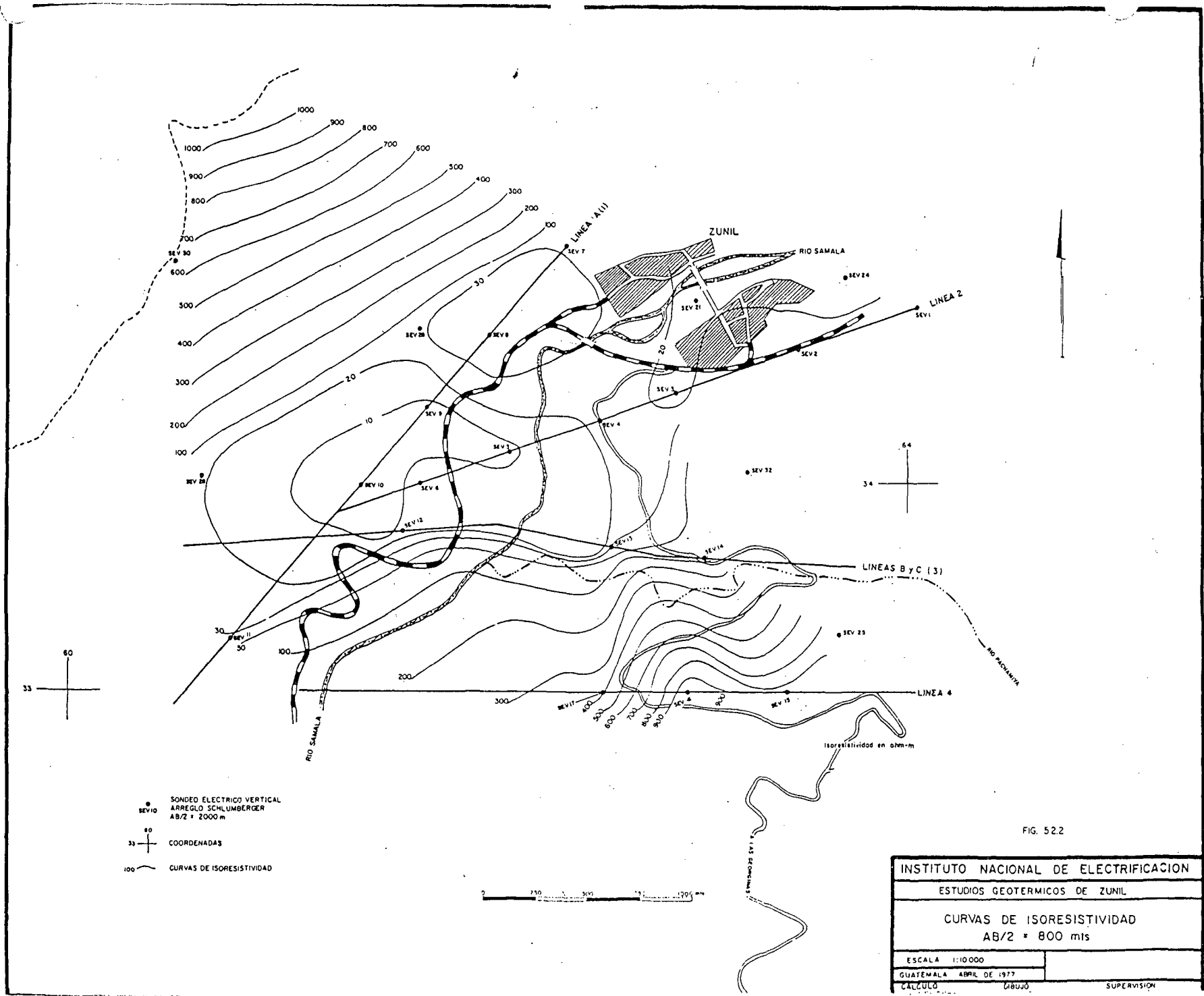
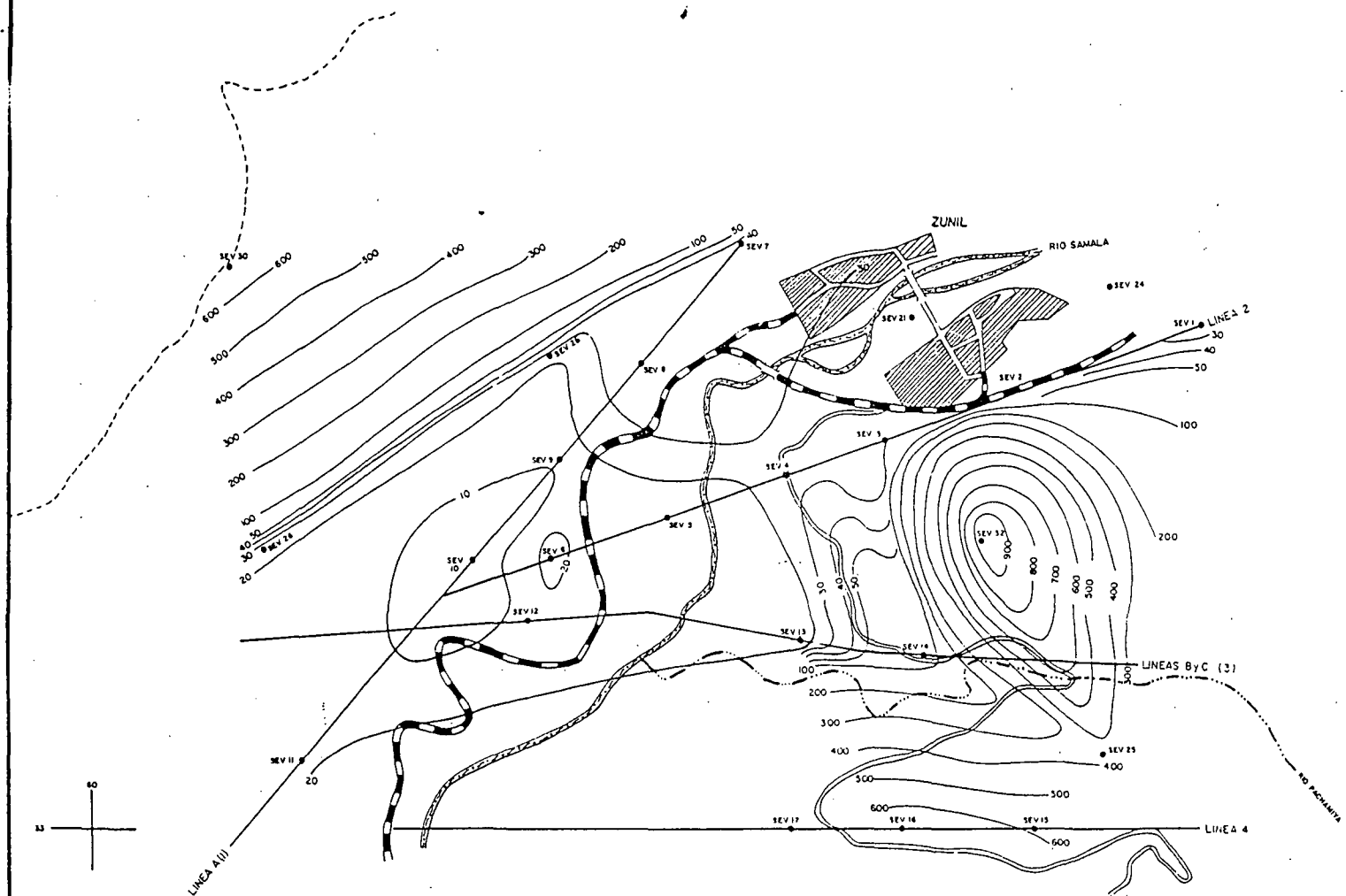


FIG. 522

INSTITUTO NACIONAL DE ELECTRIFICACION	
ESTUDIOS GEOTERMICOS DE ZUNIL	
CURVAS DE ISORESISTIVIDAD	
AB/2 * 800 mts	
ESCALA 1:10.000	
GUATEMALA ABRIL DE 1977	
CALCULO	SUPERVISION



● SONDED ELECTRICO VERTICAL
 ARREGLO SCHLUMBERGER
 AB/2 = 2000 m
 ● SEV 10
 40
 33 + COORDENADAS
 100 ~ CURVAS DE ISORESISTIVIDAD

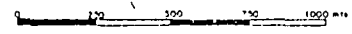
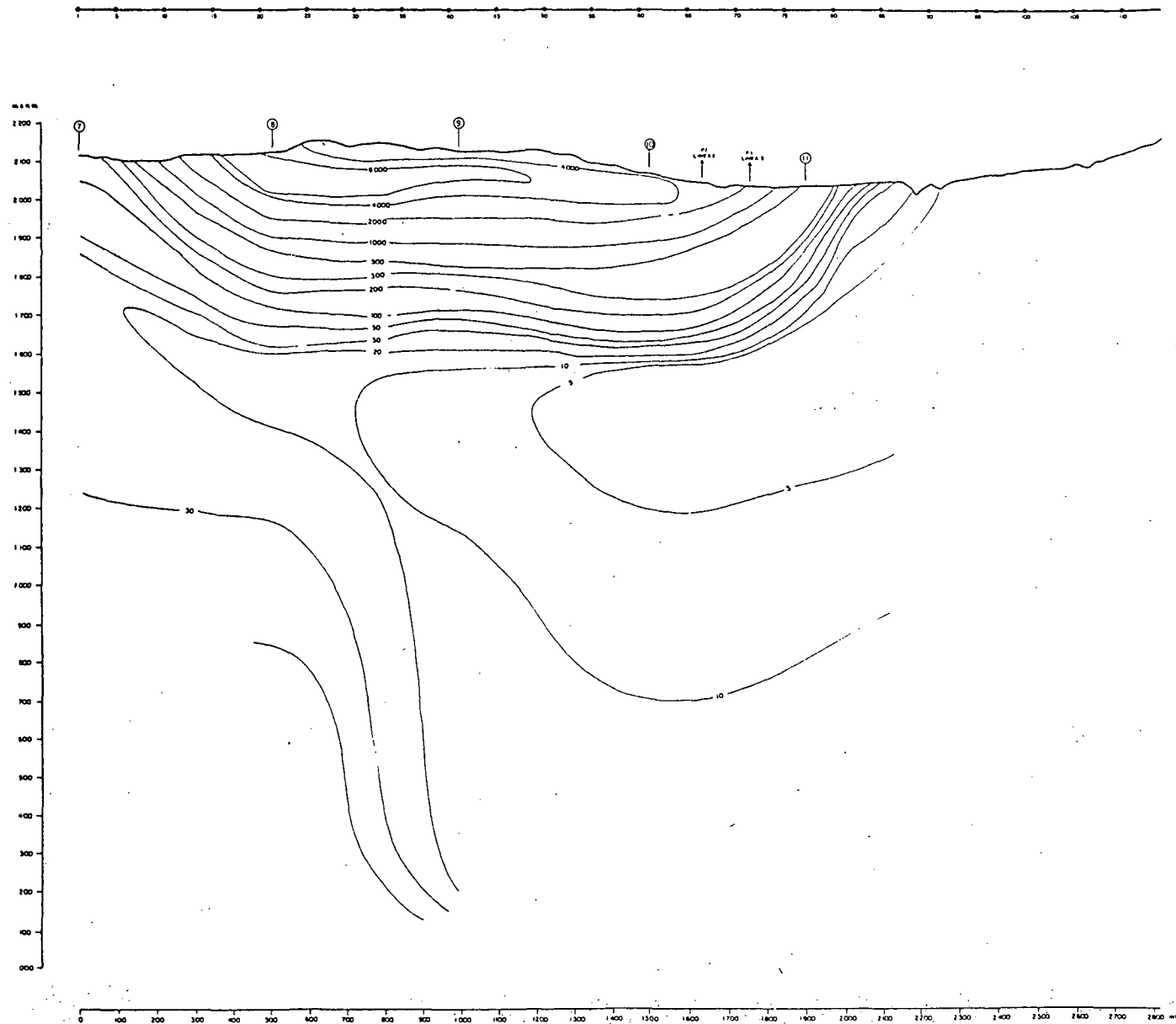


FIG. 5.2.3

INSTITUTO NACIONAL DE ELECTRIFICACION	
ESTUDIOS GEOTERMICOS DE ZUNIL	
CURVAS DE ISORESISTIVIDAD AB/2 = 1000 ms	
ESCALA 1:10 000	
GUATEMALA ABRIL DE 1977	
CALCULO	DIBUJO SUPERVISION



- SONDEO ELECTRICO VERTICAL (S.E.V.)
- CURVA DE RESISTIVIDAD APARENTE.
- P1 PUNTO DE INTERSECCION ENTRE LINEAS.

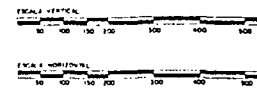
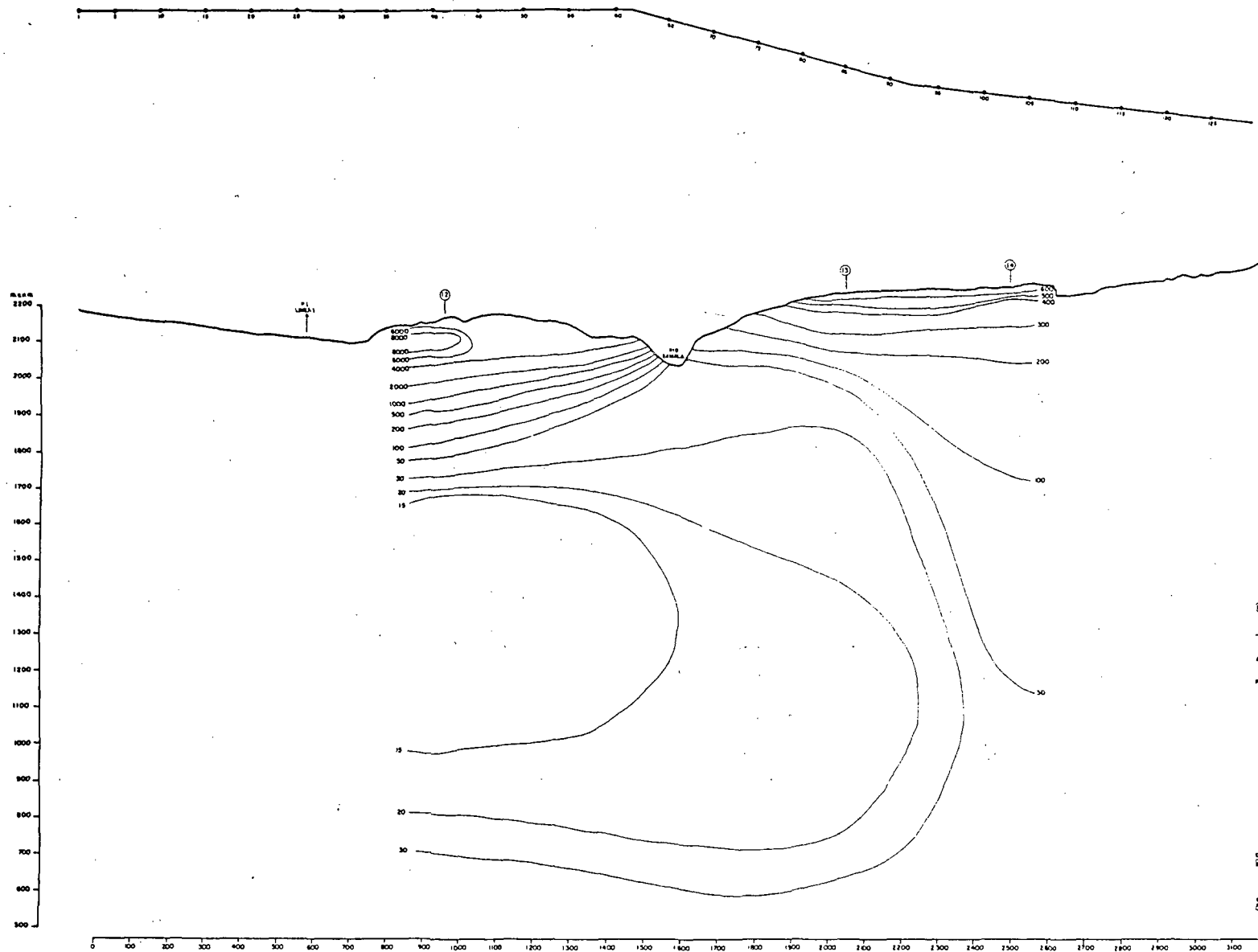


FIG 531

INSTITUTO NACIONAL DE ELECTRICIDAD	
ESTUDIOS GEOTERMICOS DE ZUNIL	
PERFIL DE RESISTIVIDAD APARENTE LINEA 1	
ESCALA VERTICAL 1:5000	GUATEMALA AGOSTO
ESCALA HORIZONTAL 1:5000	
Diseño: L. BRADLEY	Calculo: ING. JULIO PALMA
	ING. H. R. B.

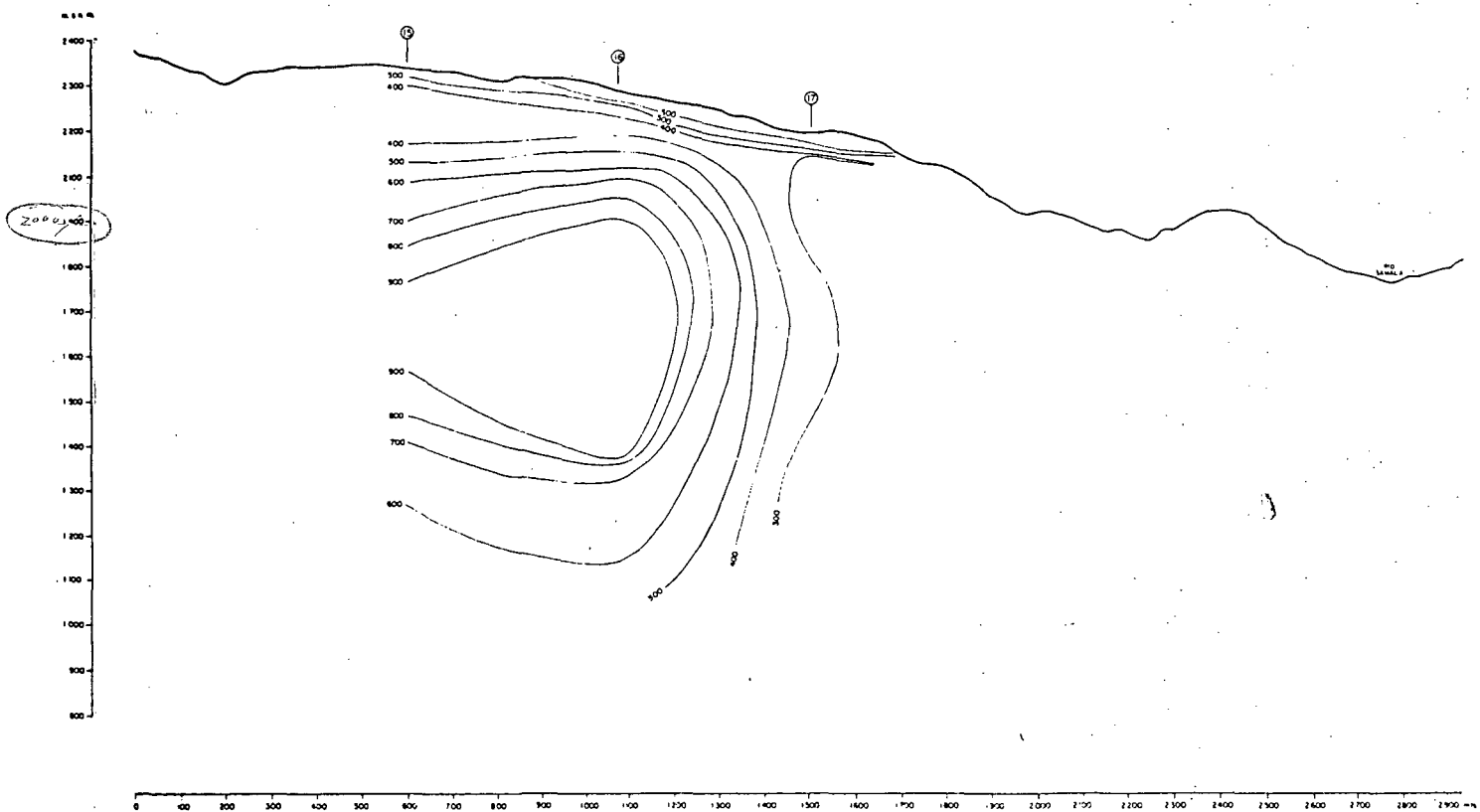
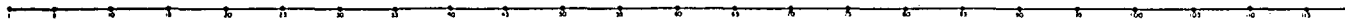




(P) SONDEO ELECTRICO VERTICAL (S.E.V.)
 — CURVA DE RESISTIVIDAD APARENTE
 1:2000
 P1 PUNTO DE INTERSECCION ENTRE LINEAS

INSTITUTO NACIONAL DE ELECTRIFICACION
 ESTUDIOS GEOTERMICOS DE ZUMIL
 PERFIL DE RESISTIVIDAD APARENTE
 LINEA 3

ESCALA VERTICAL 1:3000
 ESCALA HORIZONTAL 1:5000
 DIBUJÓ: RANOLFO DEL C. M. | CORRIÓ: ING. JULIO PALMA | V. B. S. ING. H. A. BETHAM

GUATEMALA AGOSTO DE 19...



 SONDEO ELECTRICO VERTICAL (S.E.V.)
 CURVA DE RESISTIVIDAD APARENTE.
 4872 • 2000 - m.m.

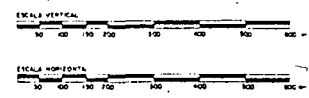
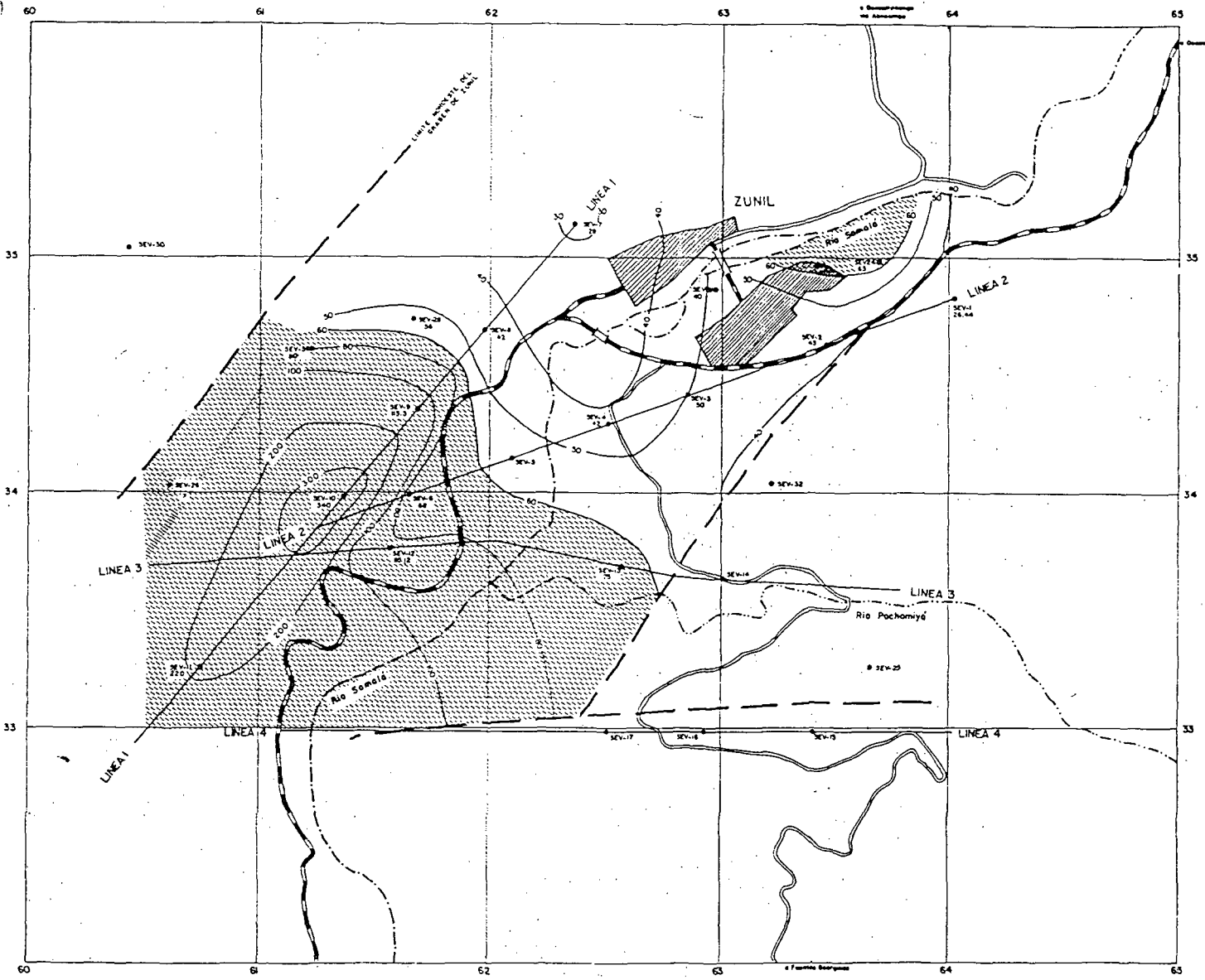


FIG 514

INSTITUTO NACIONAL DE ELECTRIFICACION	
ESTUDIOS GEOTERMICOS DE ZUNIL	
PERFIL DE RESISTIVIDAD APARENTE LINEA 4	
ESCALA VERTICAL 1:5 000	GUATEMALA AGOSTO DE 197
ESCALA HORIZONTAL 1:5 000	
DISEÑO: L. BRADLEY	CELEBRAR: ING. JULIO PALMA
	VERBO: ING. RA. BETHANCO



- SONDEO ELECTRICO VERTICAL (S.E.V.)
ARREGLO SCHLUMBERGER, AB/2 + 2000 m.
- 100 — CURVAS DE CONDUCTANCIA LONGITUDINAL (mho)
- RIO SAMALA
- - - DISCONTINUIDAD GEOELECTRICA
- ▨ DELIMITACION DEL AREA DE MAXIMA CONDUCTIVIDAD

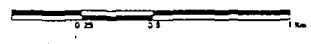
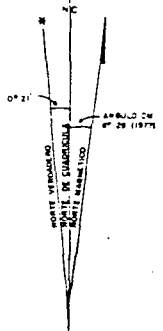


FIG. 5.4.2

INSTITUTO NACIONAL DE ELECTRIFICACION		
ESTUDIOS GEOTERMICOS DE ZUNIL		
CONDUCTANCIA LONGITUDINAL		
ESCALA 1:10 000	GUATEMALA, SEPTIEMBRE 1977	
Dibujó: L. BRADLEY	Calculó: ING. JULIO PALMA	Verificó: ING. M. R. BETHANCOURT

INDE

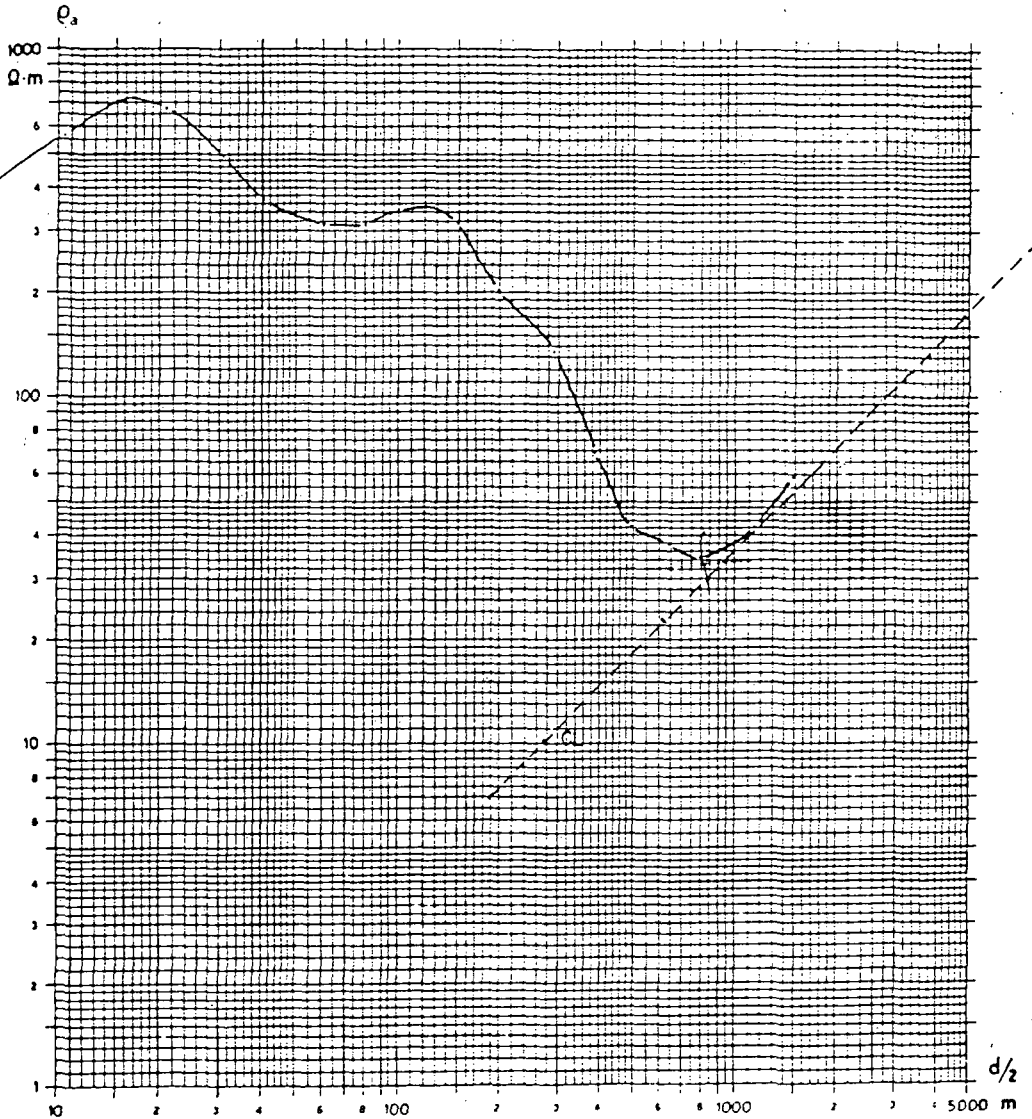
REGISTRO Z.2.1 FECHA 8/XI/76 UBICACION ZUNIL LINEA 2

SONDEO ELECTRICO No 1

COORDENADAS x 64.04 COTA 2177.00 m

CENTRO y 34.85 AZIMUT 61° 24'

OBSERVACIONES EST. 0+075 Hoja No 1960-III, Sta. Catarina Ixtahuacan, esc. 1:50,000



1300	245	1000	22	R	ohm-m
11.5		69	115	690	mts

INVESTIGACION ELECTROESTRATIGRAFICA

FIG. 6.1.1

CL = Conductancia Longitudinal Gráfica 28 mho
 Cl = Conductancia Longitudinal Teórica 0.01 + 0.01 + 0.23 + 0.05 + 26.14 = 26.44 mho

INDE

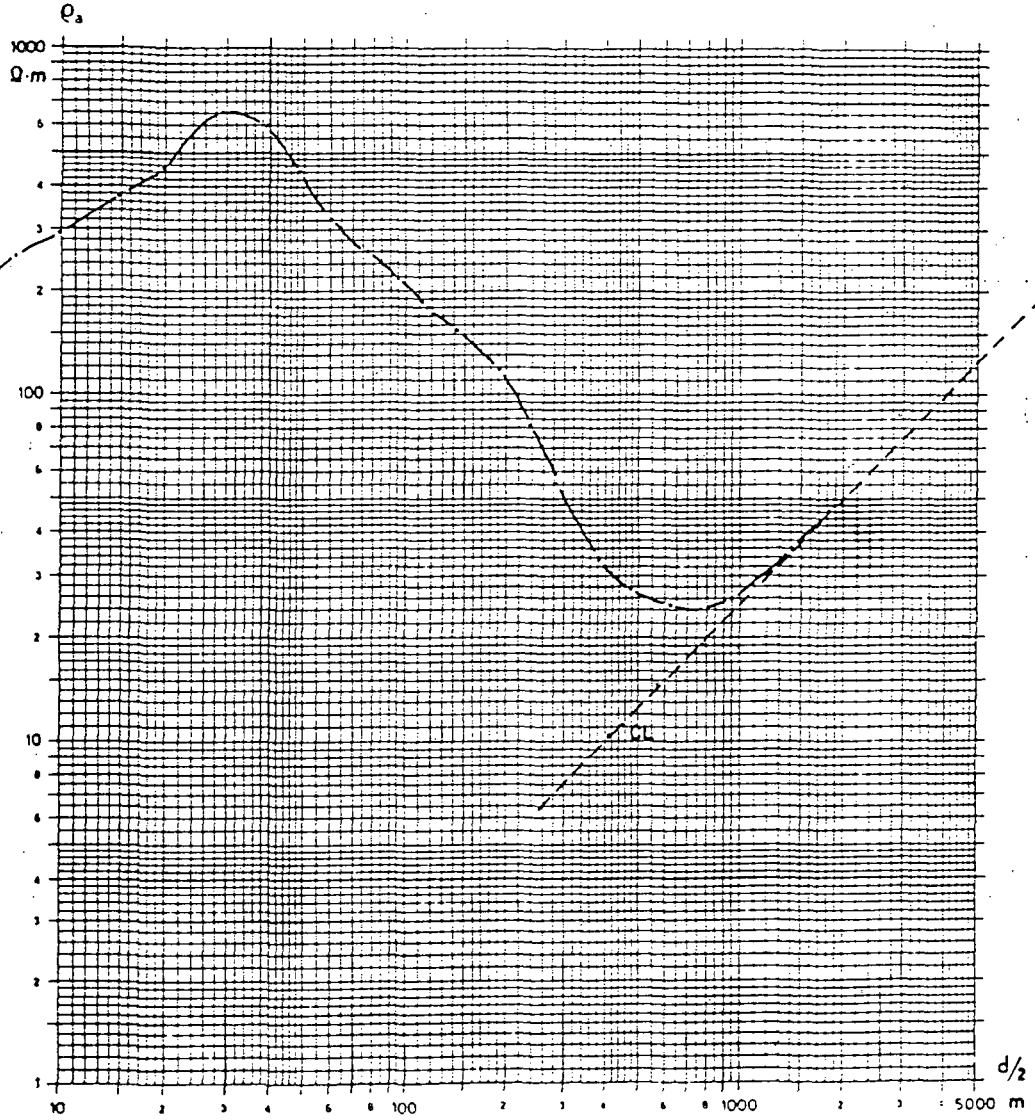
REGISTRO Z.2.2 FECHA 3/XI/76 UBICACION ZUNIL LINEA 2

SONDEO ELECTRICO No 2

COORDENADAS x 63.43 COTA _____

CENTRO y 34.63 AZIMUT 61° 24'

OBSERVACIONES EST. 0+481.55 Hoja No 1960-III, Sta. Catarina Ixtahuacan, esc. 1: 50 000



20	1180	220	12	R	ohm-m
5	17	100	610		mts

INVESTIGACION ELECTROESTRATIGRAFICA

FIG. 6.1.2

CL = Conductancia Longitudinal Gráfica 43 mho
 CL = Conductancia Longitudinal Teórica $0.03 + 0.01 + 0.38 + 42.5 = 42.92$ mho

INDE

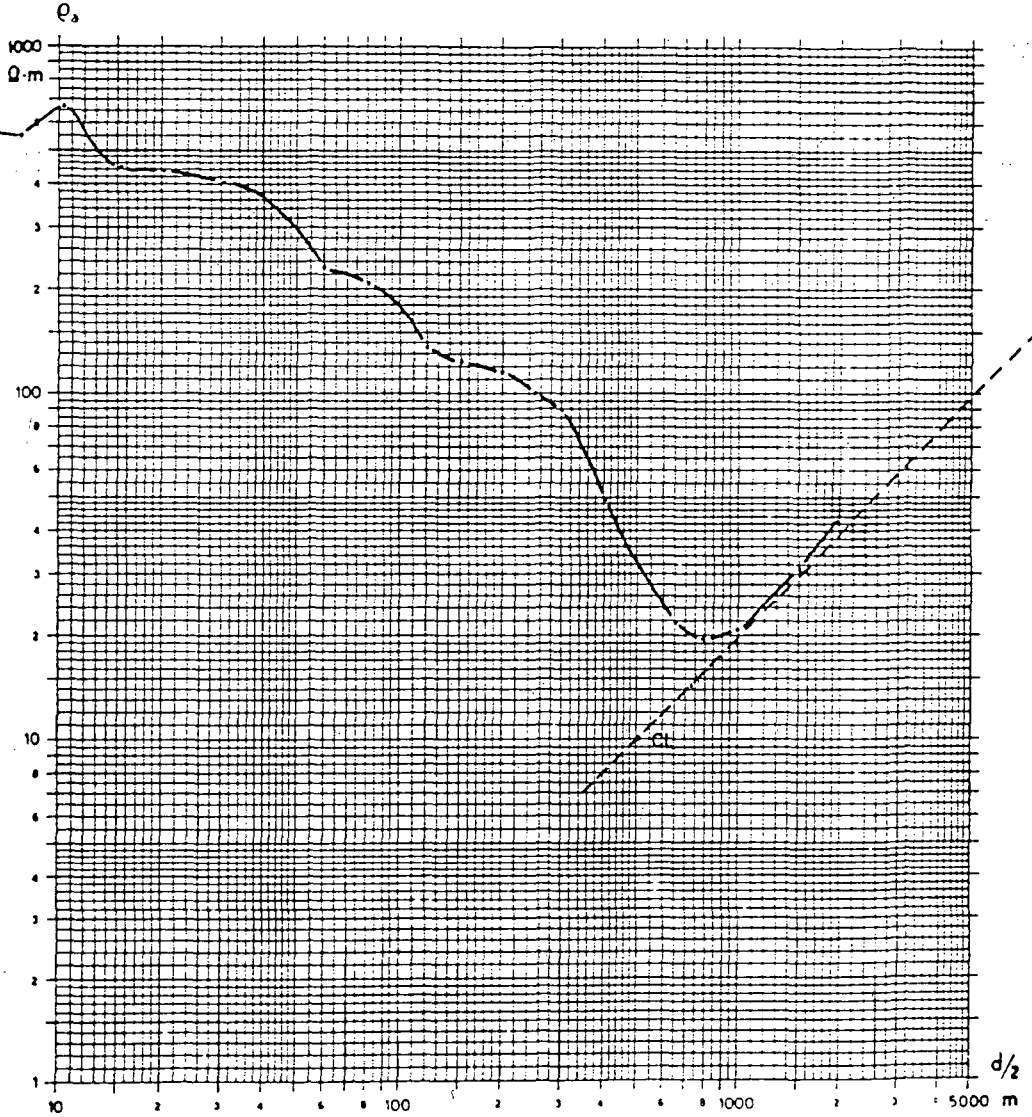
REGISTRO Z.23 FECHA 4/XI/76 UBICACION ZUNIL LINEA 2

SONDEO ELECTRICO No. 3

COORDENADAS x 62.90 COTA _____

CENTRO y 34.42 AZIMUT 61° 24'

OBSERVACIONES EST. I+061 Hoja No. 1960-III, Sta. Catarina Ixtahuacan, esc. 1: 50 000



1580	440	195	10.3	R	ohm-m
6.5	26	145	652		mts

INVESTIGACION ELECTROESTRATIGRAFICA

FIG. 6.1.3

CL = Conductancia Longitudinal Gráfica: 50 mho

INDE

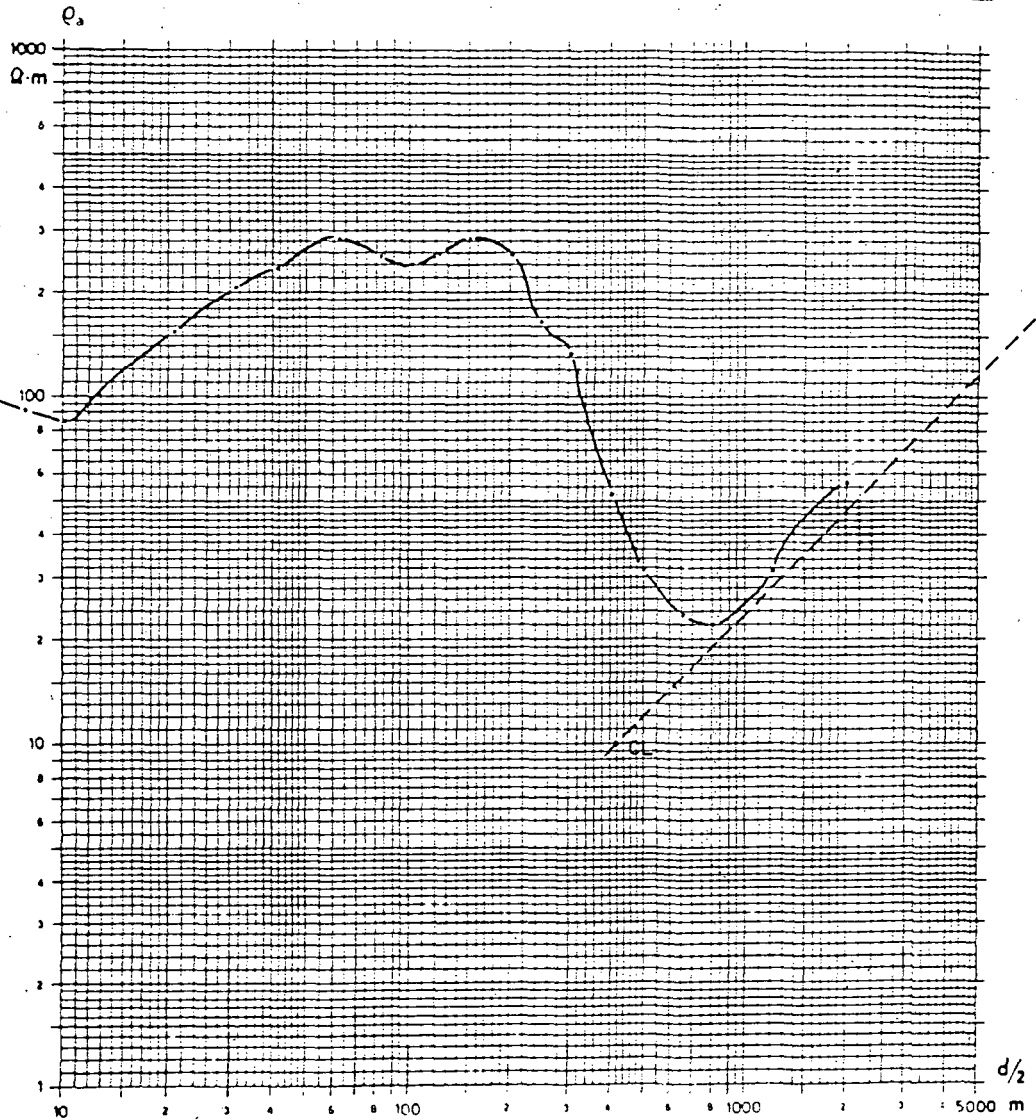
REGISTRO Z.2.4 FECHA 5/XI/76 UBICACION ZUNIL LINEA 2

SONDEO ELECTRICO No 4

COORDENADAS 62.53 COTA _____

CENTRO 34.29 AZIMUT 61° 241'

OBSERVACIONES EST. 1+620.55 Hoja No. 1960-III, Sta Catarina Ixtahuacan, esc. 1:50 000



4.4	460	110	13.4	660	R	ohm-m
						mts

INVESTIGACION ELECTROESTRATIGRAFICA

FIG 6.1.4

CL = Conductancia Longitudinal Gráfica 42 mho
 CL = Conductancia Longitudinal Teórica 0.18 + 0.23 + 4104 = 41.45 mho

INDE

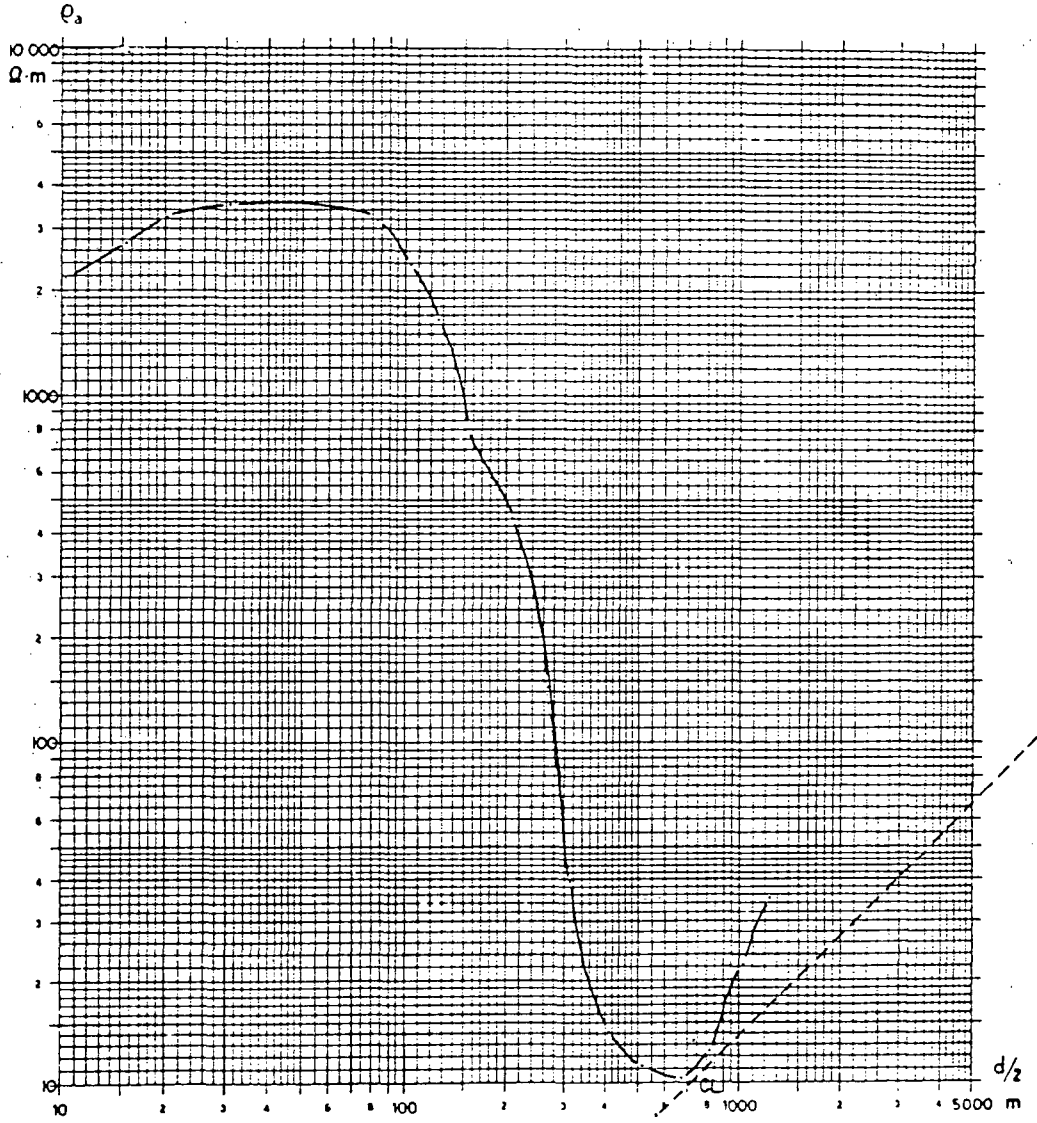
REGISTRO 2.2.6 FECHA 7/XI/76 UBICACION ZUNIL LINEA 2

SONDEO ELECTRICO No. 6

COORDENADAS x 61.70 COTA _____

CENTRO y 33.99 AZIMUT 61° 24'

OBSERVACIONES EST. 2+500 Hoja No. 1960-III, Sta. Catarina Ixtahuacan, esc. 1: 50 000.



5 500	290	7.4	R	ohm-m
	48	96	600	mts.

INVESTIGACION ELECTROSTRATIGRAFICA

FIG. 6.15

CL Conductancia Longitudinal Grafica 68 mho
 CL Conductancia Longitudinal Teorica $0.01 + 0.16 + 68.1 = 68.27$ mho

INDE

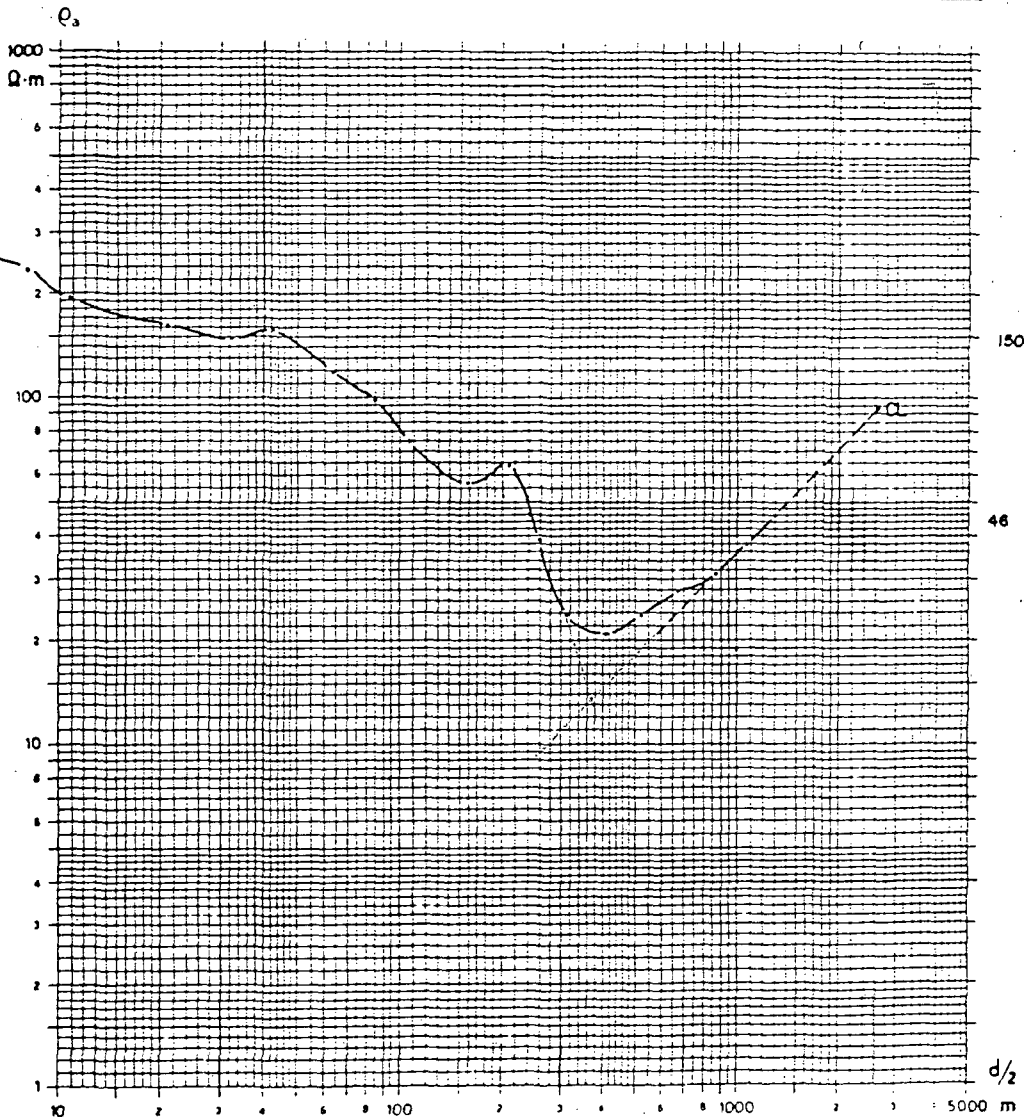
REGISTRO Z.17 FECHA 9/XI/76 UBICACION ZUNIL LINEA 1

SONDEO ELECTRICO No 7

COORDENADAS x 62.4 COTA _____

CENTRO y 35.2 AZIMUT 211° 11' 20"

OBSERVACIONES EST. 0+000 Hoja No. 1960-III, Sta. Catarina Ixtahuacan, esc. 1:50000



150	46	7.8	R	ohm-m
	30	70	280	mts

INVESTIGACION ELECTROESTRATIGRAFICA

FIG. 6.1.6

ρ_L = Conductancia Longitudinal Gráfica 28.00 mho

ρ_L = Conductancia Longitudinal Teórica $0.01 + 0.18 + 0.87 + 26.92 = 27.98$ mho

INDE

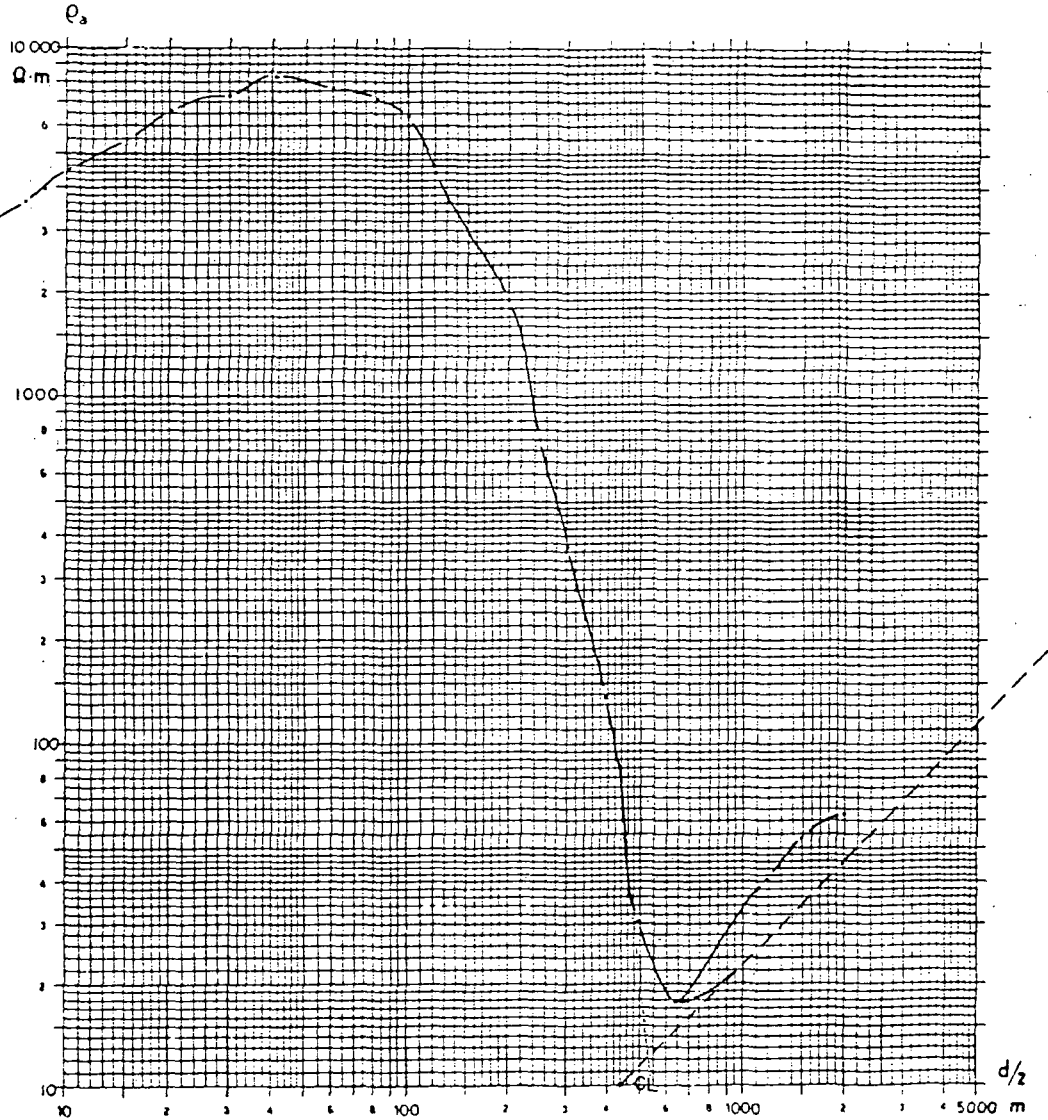
REGISTRO Z.I.8 FECHA 11/XI/76 UBICACION ZUNIL LINEA I

SONDEO ELECTRICO No. 8

COORDENADAS x 62.10 COTA _____

CENTRO y 34.69 AZIMUT _____

OBSERVACIONES EST. 0+500 Hoja No 1960-III, Sta. Catarina Ixtahuacan, esc. 1:50 000



8 500	1000	200	8	R	ohm-m
	43	75	190	520	m/s

INVESTIGACION ELECTROESTRATIGRAFICA

FIG. 6.17

ρ_s = Conductancia Longitudinal Gráfica 42 mho

INDE

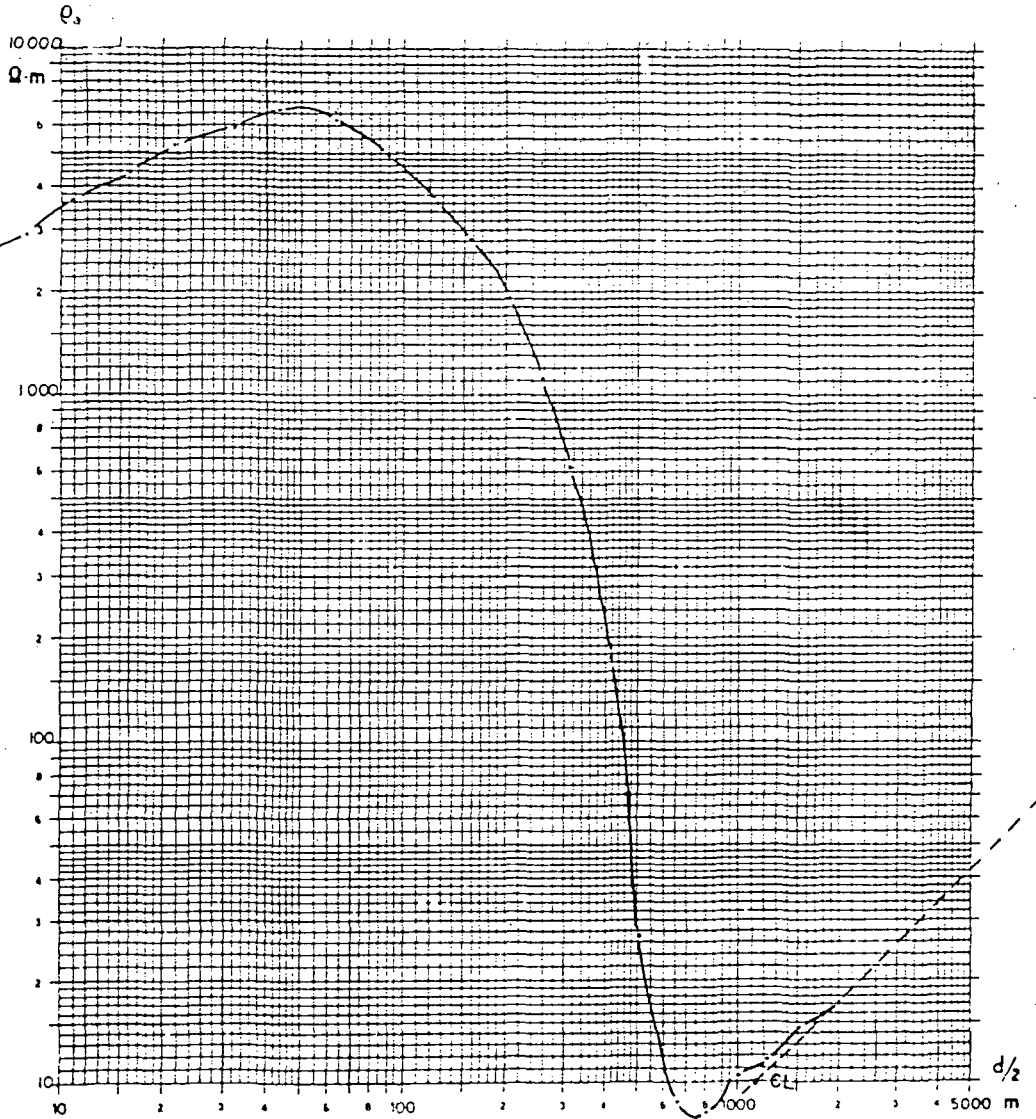
REGISTRO Z.I.9 FECHA 12/XI/76 UBICACION ZUNIL LINEA 1

SONDEO ELECTRICO No. 9

COORDENADAS x 61.72 COTA _____

CENTRO y 34.35 AZIMUT 211° 11' 20"

OBSERVACIONES EST. 0+989 Hoja No. 1960-III, Sta. Catarina Ixtahuacan, esc. 1:50 000



7500	1250	140	3.75	R	ohm-m
	55	85	170	600	mts

INVESTIGACION ELECTROESTRATIGRAFICA

FIG. 6.1.8

ρ_L = Conductancia Longitudinal Gráfica 115 mho
 ρ_L = Conductancia Longitudinal Teórica $0.002 + 0.001 + 0.024 + 0.8 + 114.66 = 115.5$ mho

INDE

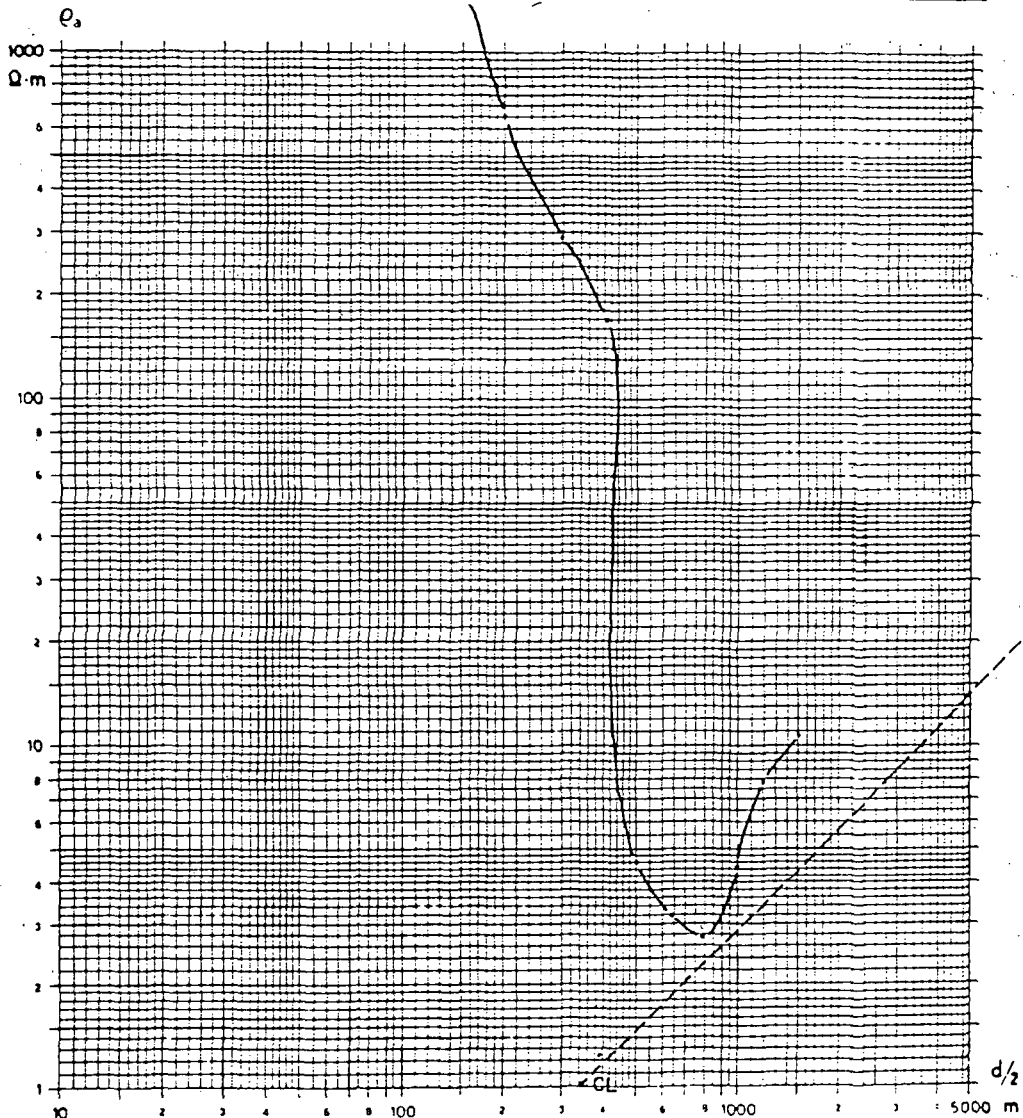
REGISTRO Z.1.10 FECHA 23/XI/76 UBICACION ZUNIL LINEA 1

SONDEO ELECTRICO No. 10

COORDENADAS x 61.40 COTA _____

CENTRO y 33.98 AZIMUT _____

OBSERVACIONES _____ Hoja No. 1860-II, Coloma, esc 1:50000



3200	7200	2100	110	1.5	R	ohm-m.
9	32	89	180	690		mts

INVESTIGACION ELECTROESTRATIGRAFICA

FIG. 6.1.9

$C_L = \text{Conductancia Longitudinal Gráfica } 340 \text{ mho}$
 $0.002 + 0.003 + 0.077 + 0.8 + 340 = 340.83 \text{ mho}$

INDE

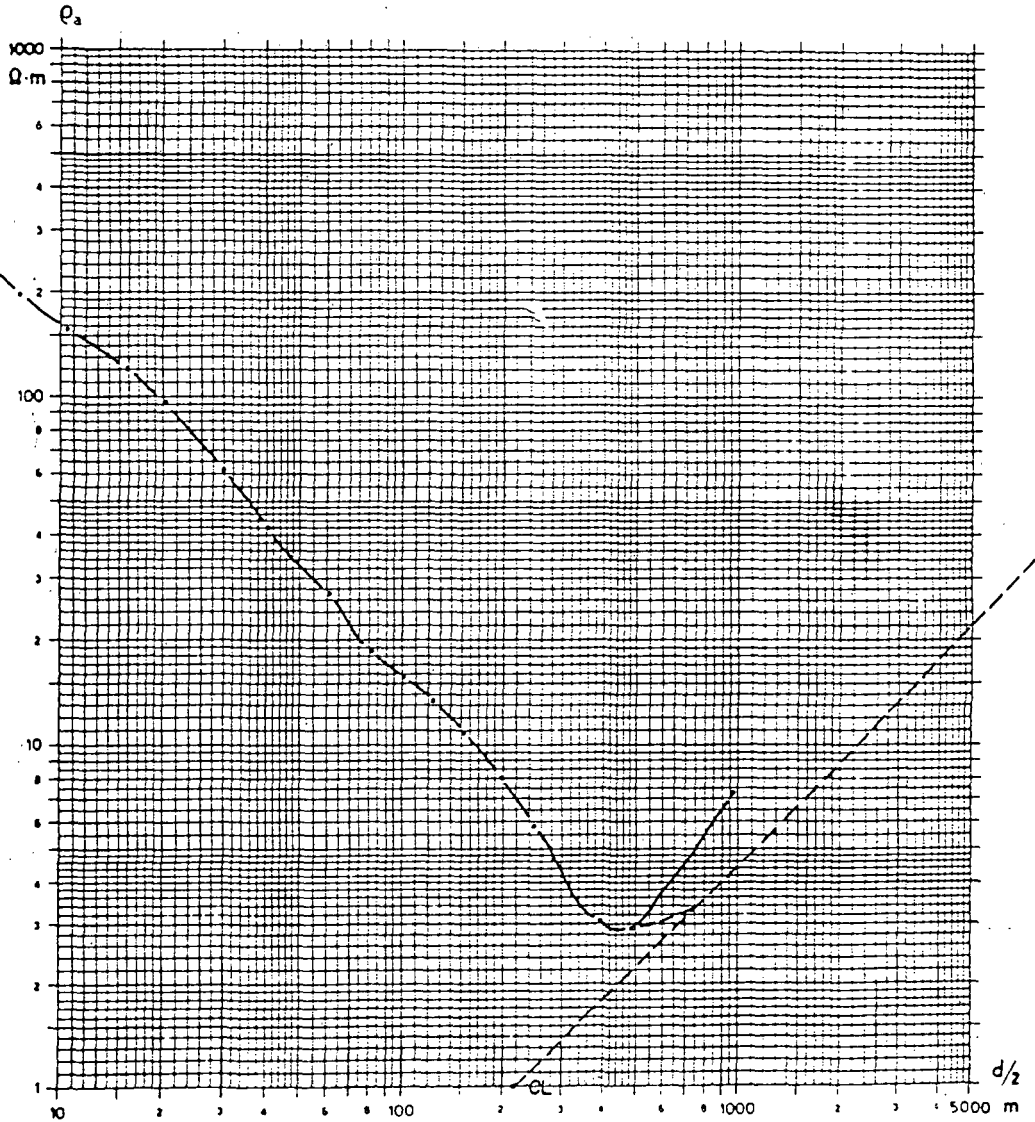
REGISTRO Z.I.II FECHA 24/II/76 UBICACION ZUNIL LINEA I

SONDEO ELECTRICO No 11

COORDENADAS x 60.75 COFA _____

CENTRO y 33.3 AZIMUT _____

OBSERVACIONES EST. 2 + 000 Hoja No. 1860-II, Colomba, esc. 1:50 000



140	18.5	2.1	R	ohm-m
12	90	500		mts.

INVESTIGACION ELECTROESTRATIGRAFICA

FIG. 6.110

CL = Conductancia Longitudinal Gráfica 220 mho
 CL = Conductancia Longitudinal Teórica $0.09 + 4.22 + 195.24 = 199.55$ mho

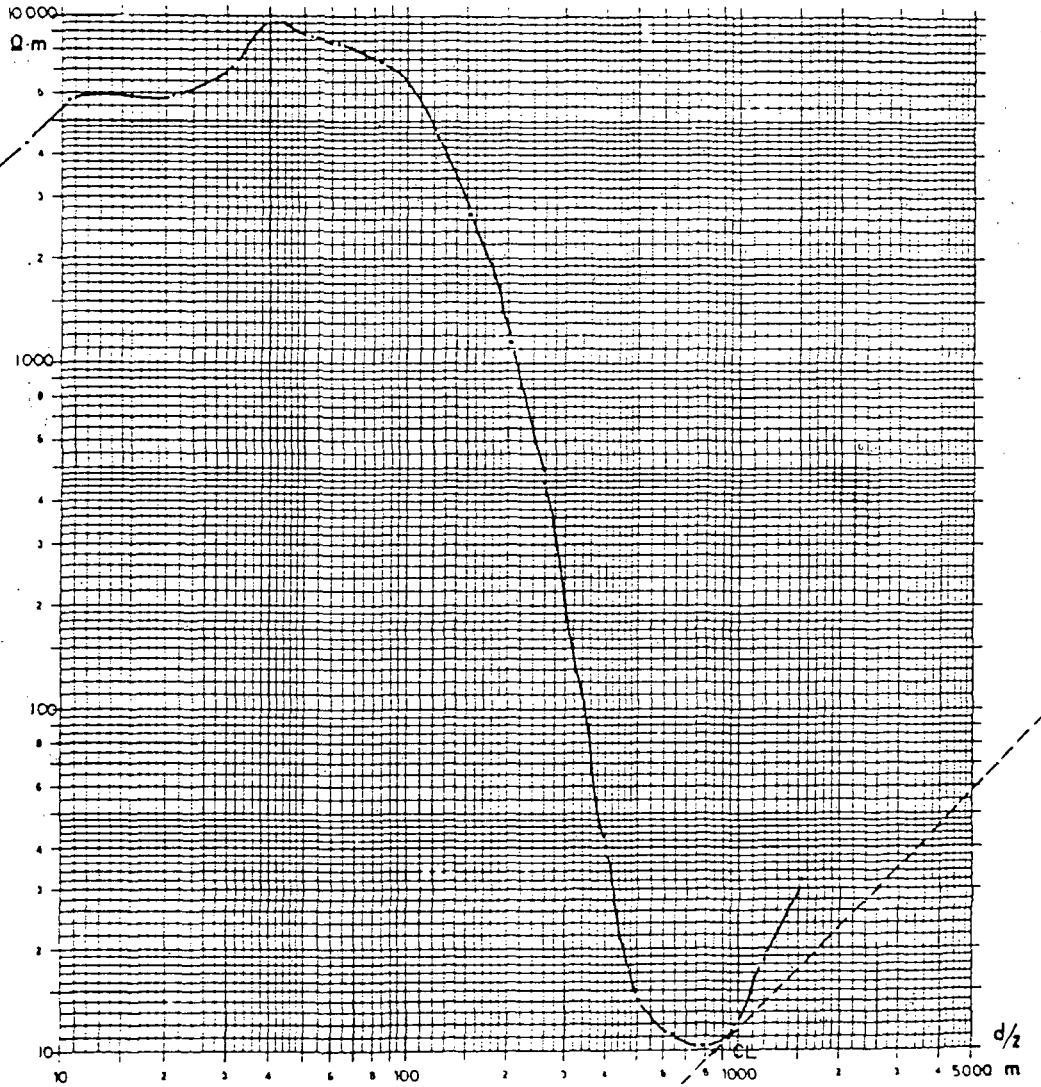
INDE

REGISTRO Z.3.12 FECHA 25/XI/76 UBICACION ZUNIL LINEA 3

SONDEO ELECTRICO No. 12

COORDENADAS x 61.60 COSTA _____
 CENTRO y 33.77 AZIMUT 76° 30' 50" - 256° 30' 50"

OBSERVACIONES EST 1+000 Hoja No 1960-III, Sta. Catarina Ixtahuacan, esc. 1:50 000
 ρ_s



11500	300	6	R	ohm-m
56.5	141	650		mts
INVESTIGACION ELECTROESTRATIGRAFICA				

FIG. 6.I.II

ρ_L = Conductancia Longitudinal Gráfica 86 mho
 ρ_L = Conductancia Longitudinal Teórica $0.005 + 0.28 + 84.83 = 85.12$ mho

INDE

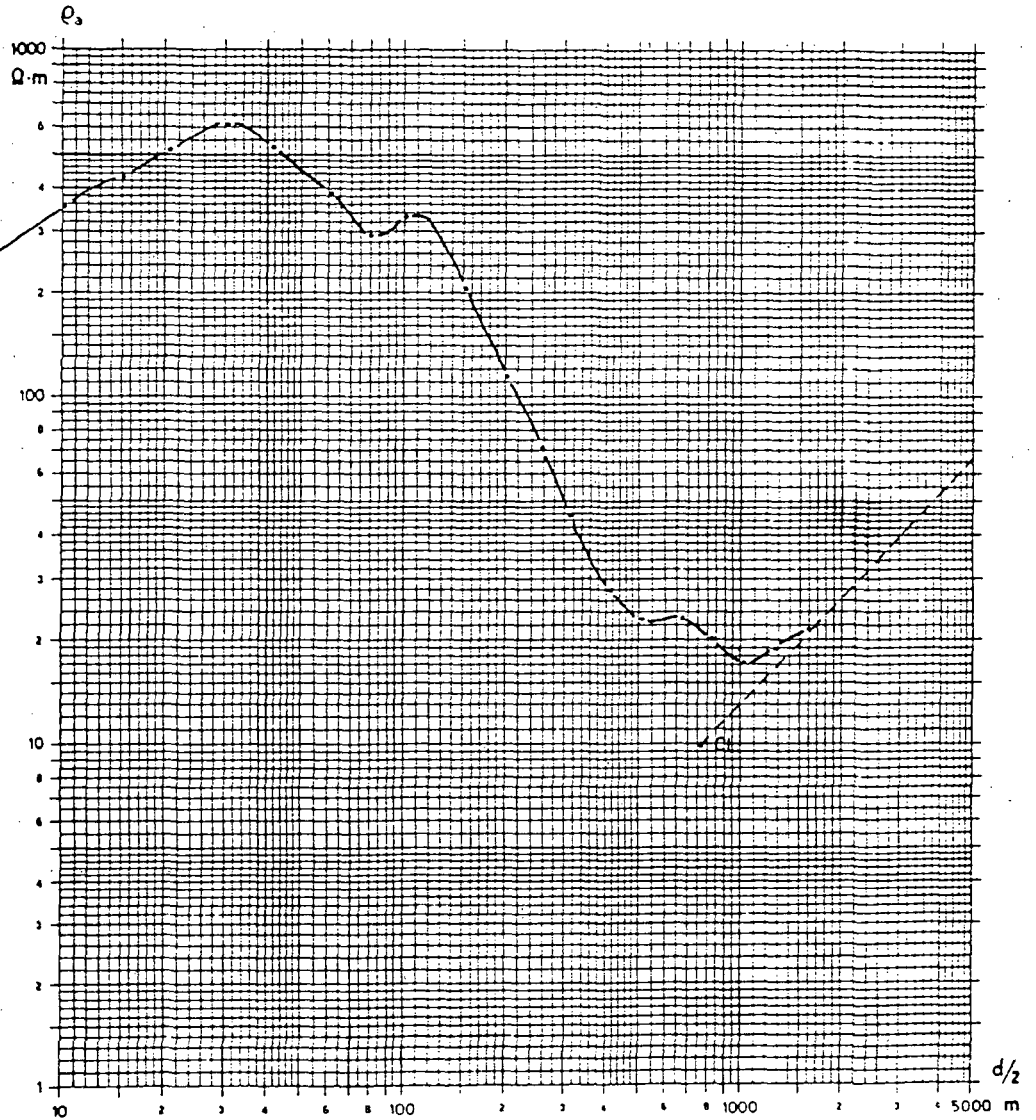
REGISTRO Z.3.13 FECHA 30/XI/76 UBICACION ZUNIL LINEA 3

SONDEO ELECTRICO No. 13

COORDENADAS x 62.59 COTA _____

CENTRO y 33.68 AZIMUT _____

OBSERVACIONES EST. 2+089 (Pozo No. 8) Hoja No. 1960-III, Sta. Catarina Ixtahuacan, esc. 1:50 000



850

200

10

R

ohm-m

23

98.9

650

mts

INVESTIGACION ELECTROESTRATIGRAFICA

FIG. S.112

CL = Conductancia Longitudinal Gráfica 75 mho

INDE

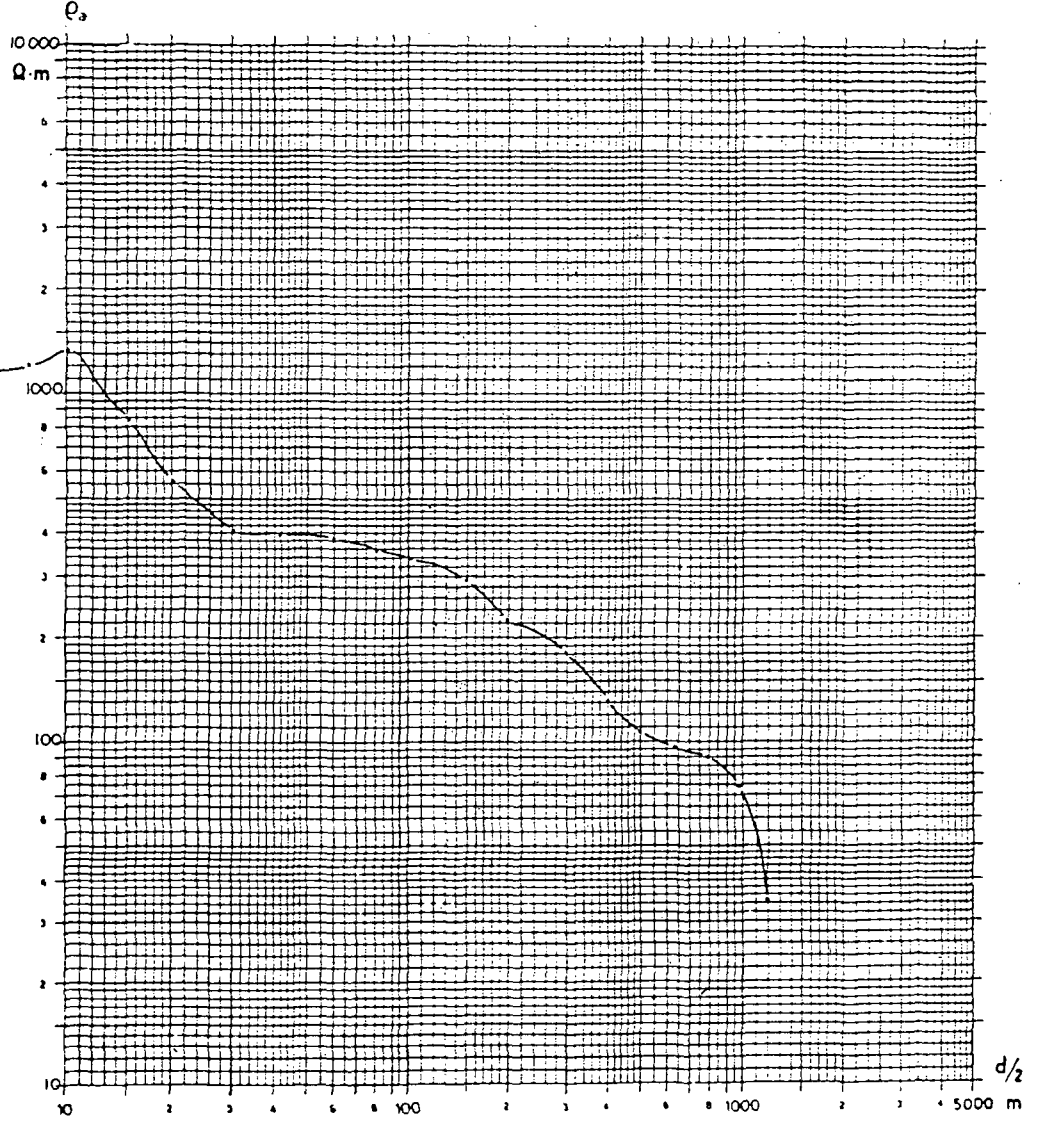
REGISTRO Z.3.14 FECHA 26/XI/76 UBICACION ZUNIL LINEA 3

SONDEO ELECTRICO No. 14

COORDENADAS x 63.10 COTA _____

CENTRO y 33.63 AZIMUT _____

OBSERVACIONES EST. 2+539 Hoja No. 1960-III, Sta. Catarina Ixtphuacon, esc. 1:50 000



2100	385	80	<10?	ohm-m
5.5	125	280		mts

INVESTIGACION ELECTROESTRATIGRAFICA

FIG. 6.1.13

INDE

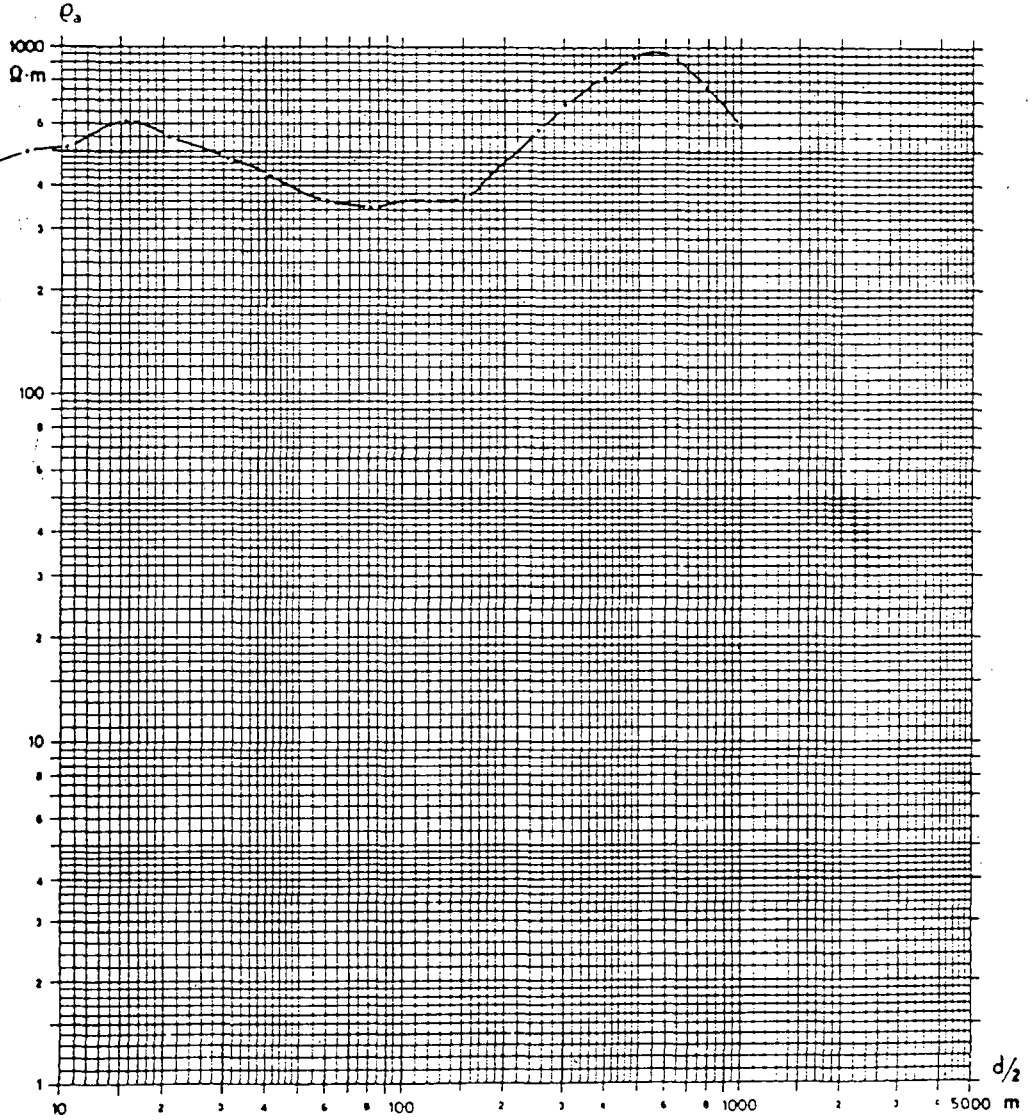
REGISTRO Z.4.15 FECHA 2/XII/76 UBICACION ZUNIL LINEA 4

SONDEO ELECTRICO No 15

COORDENADAS x 63.43 COTA _____

CENTRO y 32.99 AZIMUT _____

OBSERVACIONES EST. 0+600 Hoja No 1960-III, Sta Catarina Ixtchuacan, esc. 1:50 000



1150	290	6 000	?	ohm-m
5	21	95	510	mts

INVESTIGACION ELECTROESTRATIGRAFICA

FIG. 6.1.14

INDE

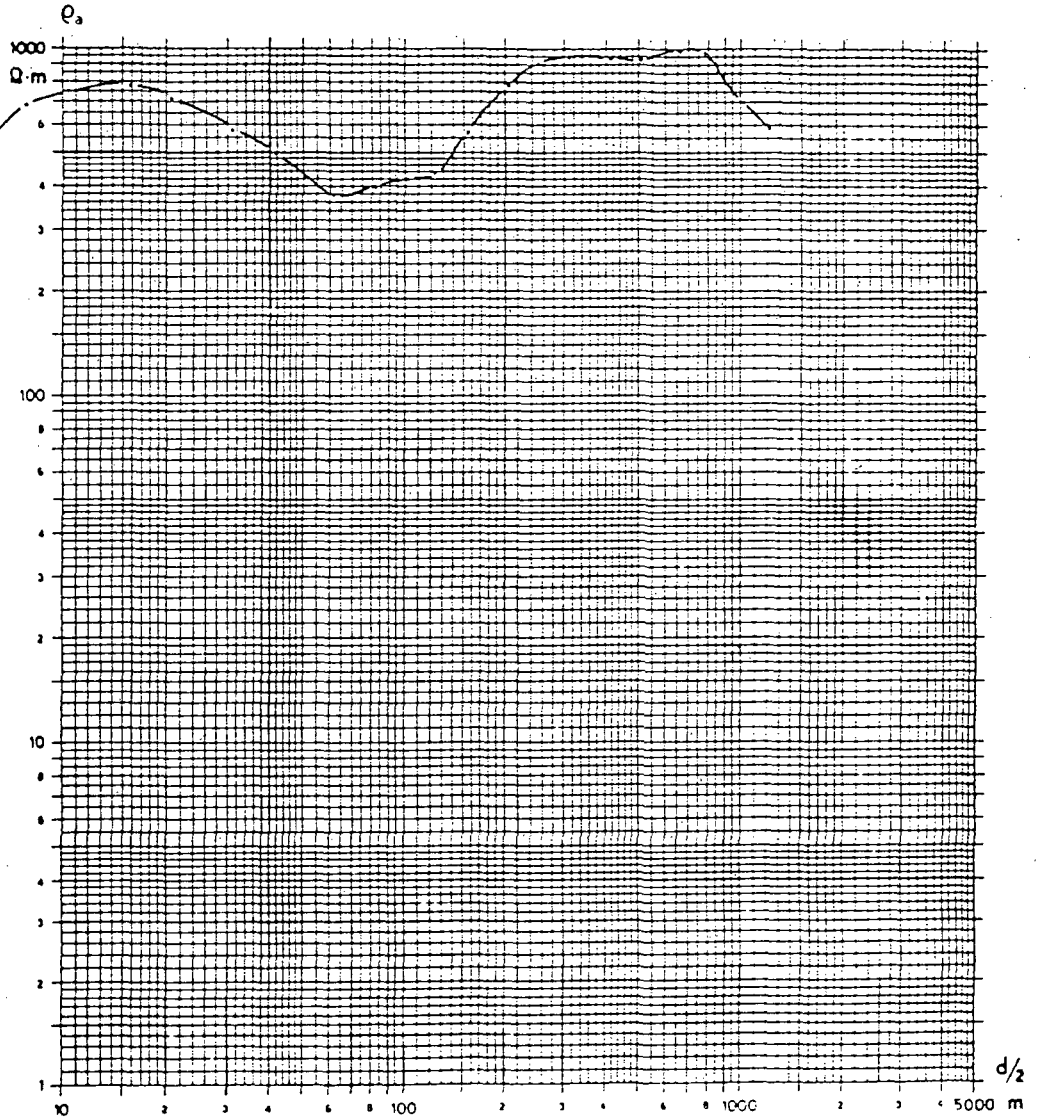
REGISTRO Z-4.16 FECHA 2/XII/76 UBICACION ZUNIL LINEA 4

SONDEO ELECTRICO No 16

COORDENADAS x 63.95 COTA _____

CENTRO y 32.99 AZIMUT _____

OBSERVACIONES EST. I+075 Hoja 1960-III, Sta. Catarina Ixtahuacan, esc. 1:50000



1150	290	6000	800	?	ohm-m
11.0	70	300	800		ms

INVESTIGACION ELECTROSTRATIGRAFICA

FIG. 6.1.15

INDE

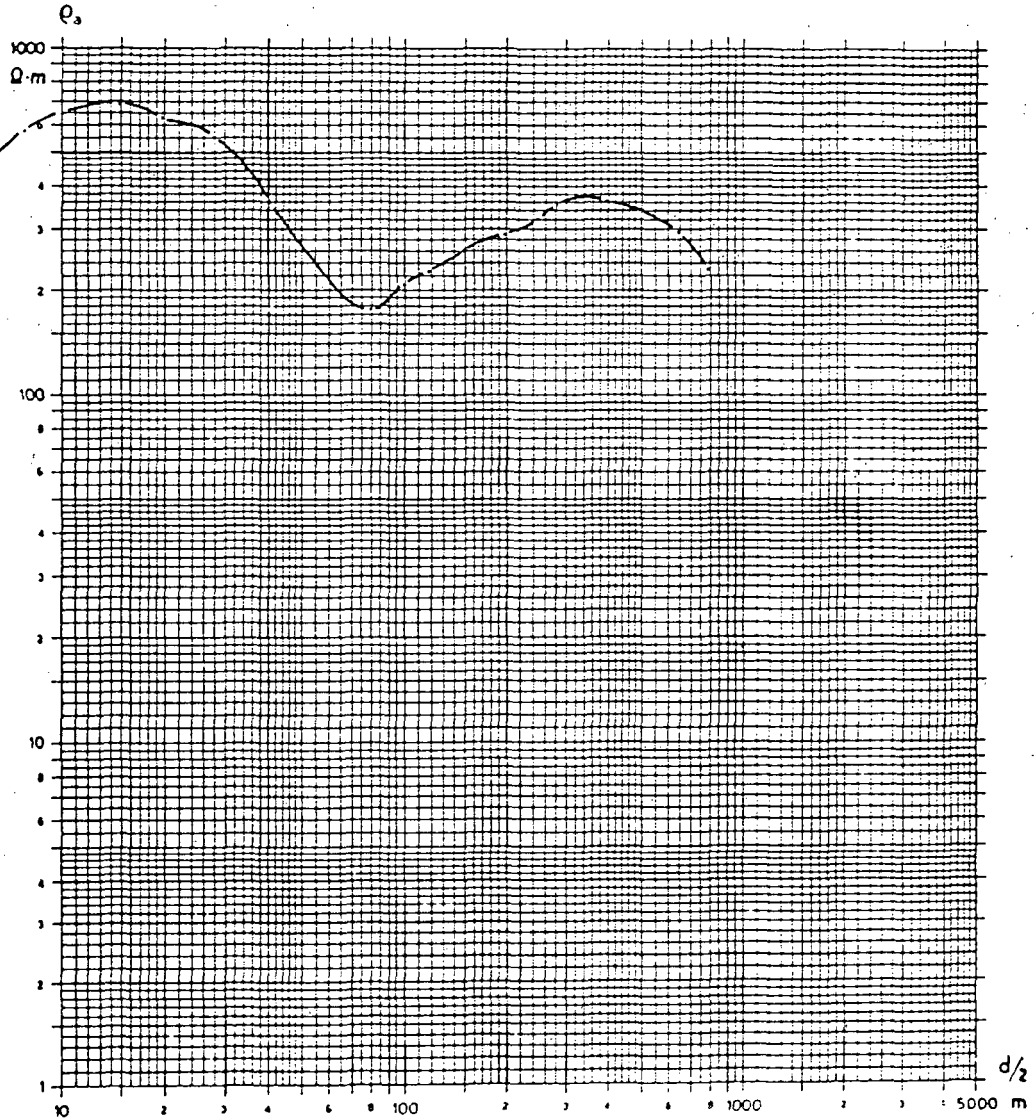
REGISTRO Z.4.17 FECHA 1/XII/76 UBICACION ZUNIL LINEA 4

SONDEO ELECTRICO No 17

COORDENADAS x 62.55 COTA _____

CENTRO y 32.99 AZIMUT _____

OBSERVACIONES Hoja No. 1960-III, Sta Catarina Ixtahuacan, esc. 1:50000



1150	125	500	?	ohm-m
15.5	58	330		mts

INVESTIGACION ELECTROESTRATIGRAFICA

FIG. 6.116

INDE

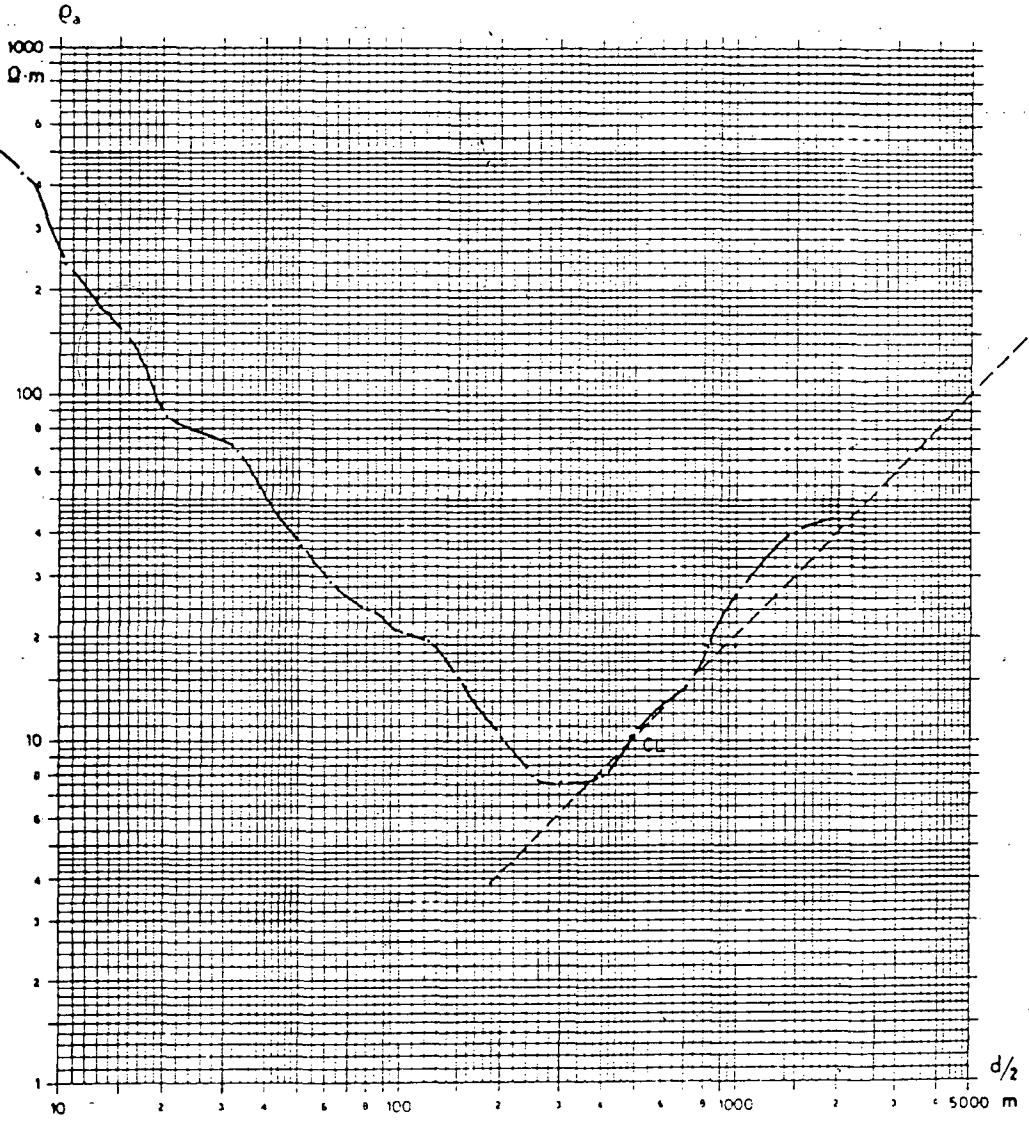
REGISTRO Z.21 FECHA 17/III/77 UBICACION ZUNIL LINEA _____

SONDEO ELECTRICO No 21

COORDENADAS x 62.99 COTA _____

CENTRO y 34.88 AZIMUT _____

OBSERVACIONES Campo Futbol de Zunil. Hoja No 1960-III, Sta. Catarina Ixtahuacan, esc. 1: 50 000



190	18	3.7	R	ohm-m
17	65	240		mts
INVESTIGACION ELECTROESTRATIGRAFICA				

FIG. 6.1.17

CL = Conductancia Longitudinal Gráfica 49 mho
 Cl = Conductancia Longitudinal Teórica $0.004 + 0.07 + 2.67 + 47.3 = 50.04$ mho

INDE

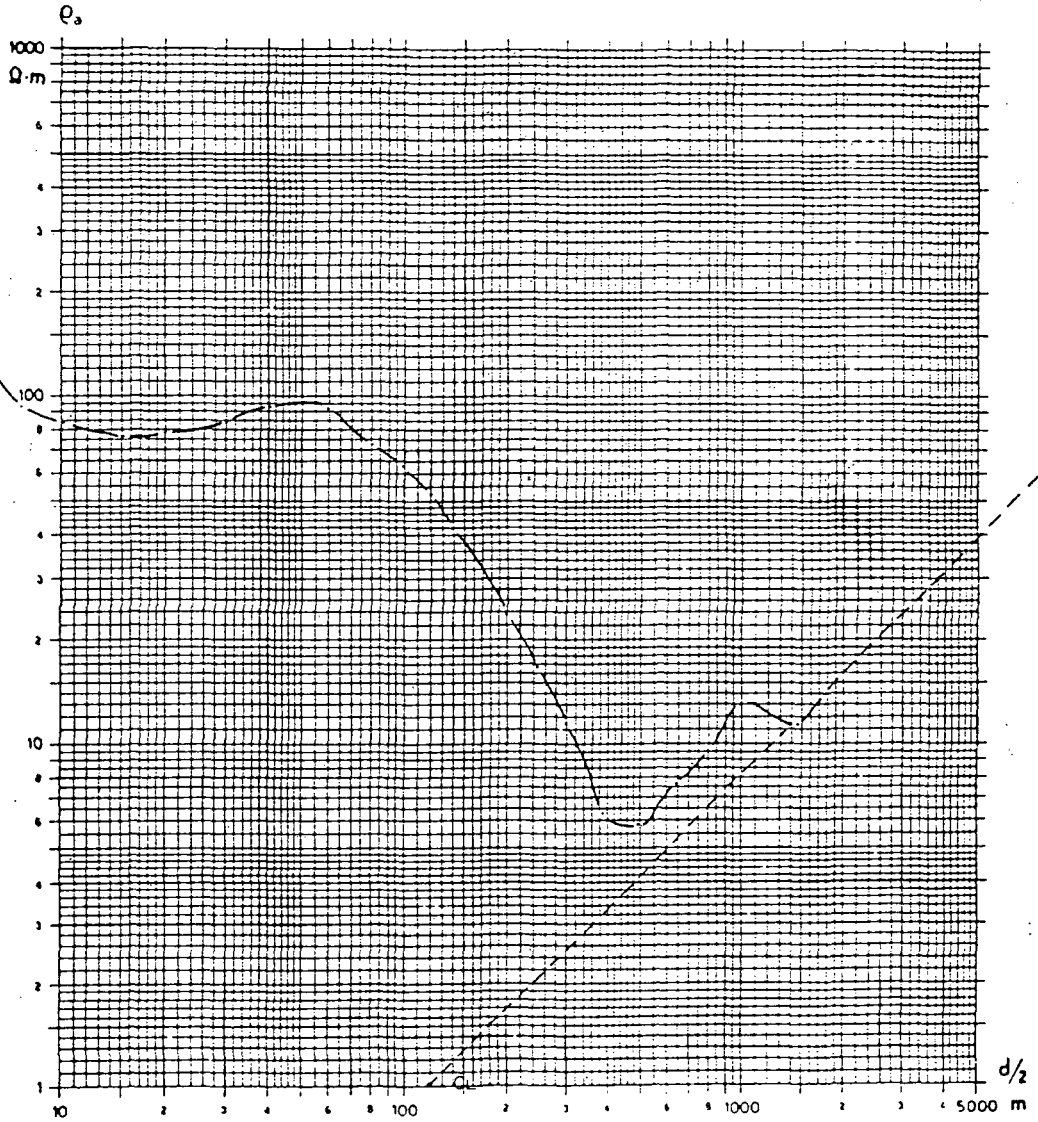
REGISTRO Z.22 FECHA 24/III/77 UBICACION ZUNIL LINEA _____

SONDEO ELECTRICO No. 22

COORDENADAS x 62.35 COTA _____

CENTRO y 37.75 AZIMUT _____

OBSERVACIONES _____ Hoja No 1960-III, Sta Catarina Ixtahuacn, esc. 1:50 000



70	163	3.5	R	ohm-m
17.5	85	510		mts
INVESTIGACION ELECTROSTRATIGRAFICA				

FIG. 6.1.18

CL = Conductancia Longitudinal Gráfica 121 mho
 CL = Conductancia Longitudinal Teórica 0.25 + 0.41 + 121.43 = 122.09 mho

INDE

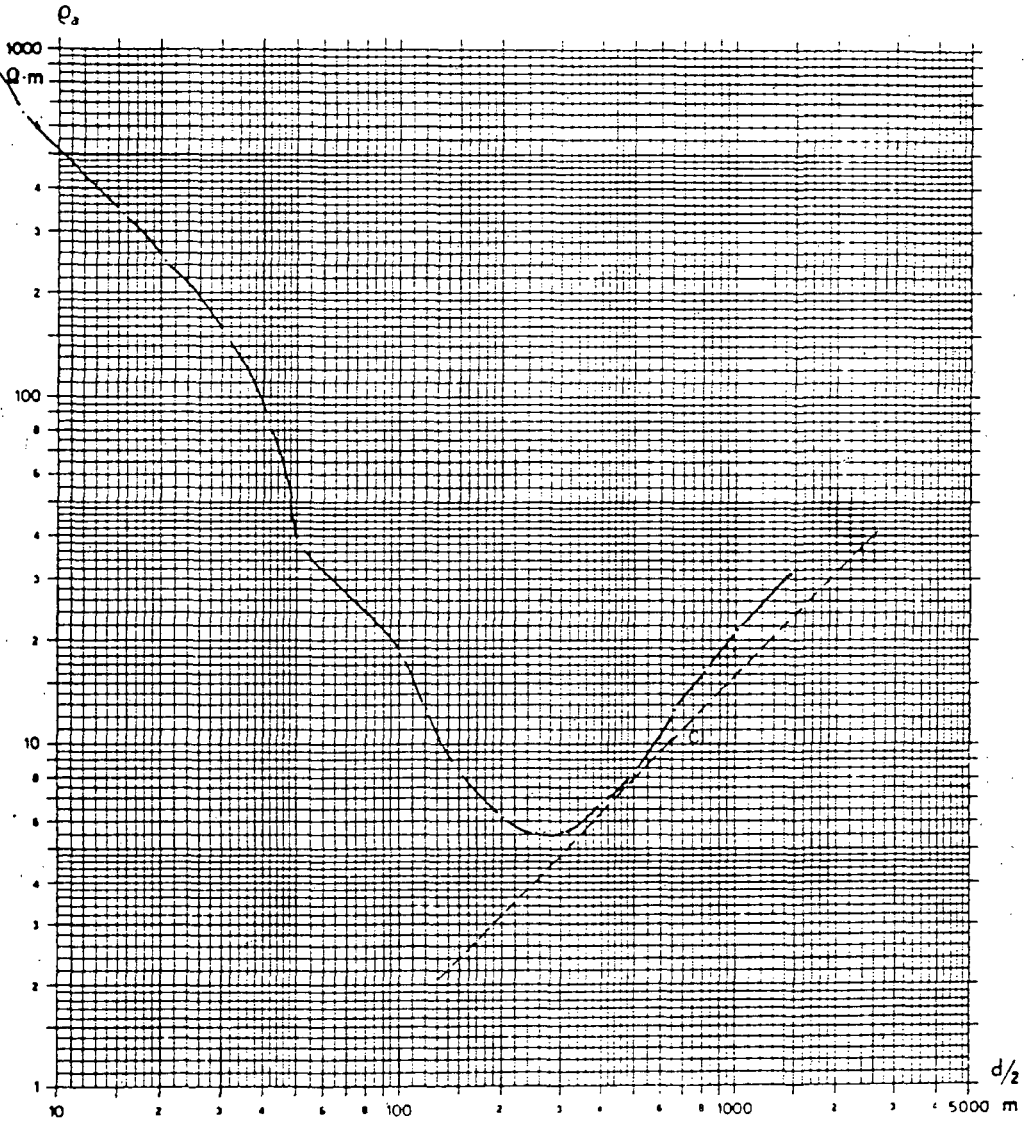
REGISTRO Z.24 FECHA 20/V/77 UBICACION ZUNIL LINEA _____

SONDEO ELECTRICO No 24

COORDENADAS x 63.65 COTA _____

CENTRO y 35.00 AZIMUT _____

OBSERVACIONES _____ Hoja No. 1960-III, Sta. Catarina Ixtahuacan, esc. 1:50000



310	17	2.3	R	ohm-m
	16	45	185	mts

INVESTIGACION ELECTROESTRATIGRAFICA

FIG. 6.119

CL = Conductancia Longitudinal Grdfico 62.5 mho
 CL = Conductancia Longitudinal Teorica $0.05 + 1.71 + 60.87 = 62.63$ mho

INDE

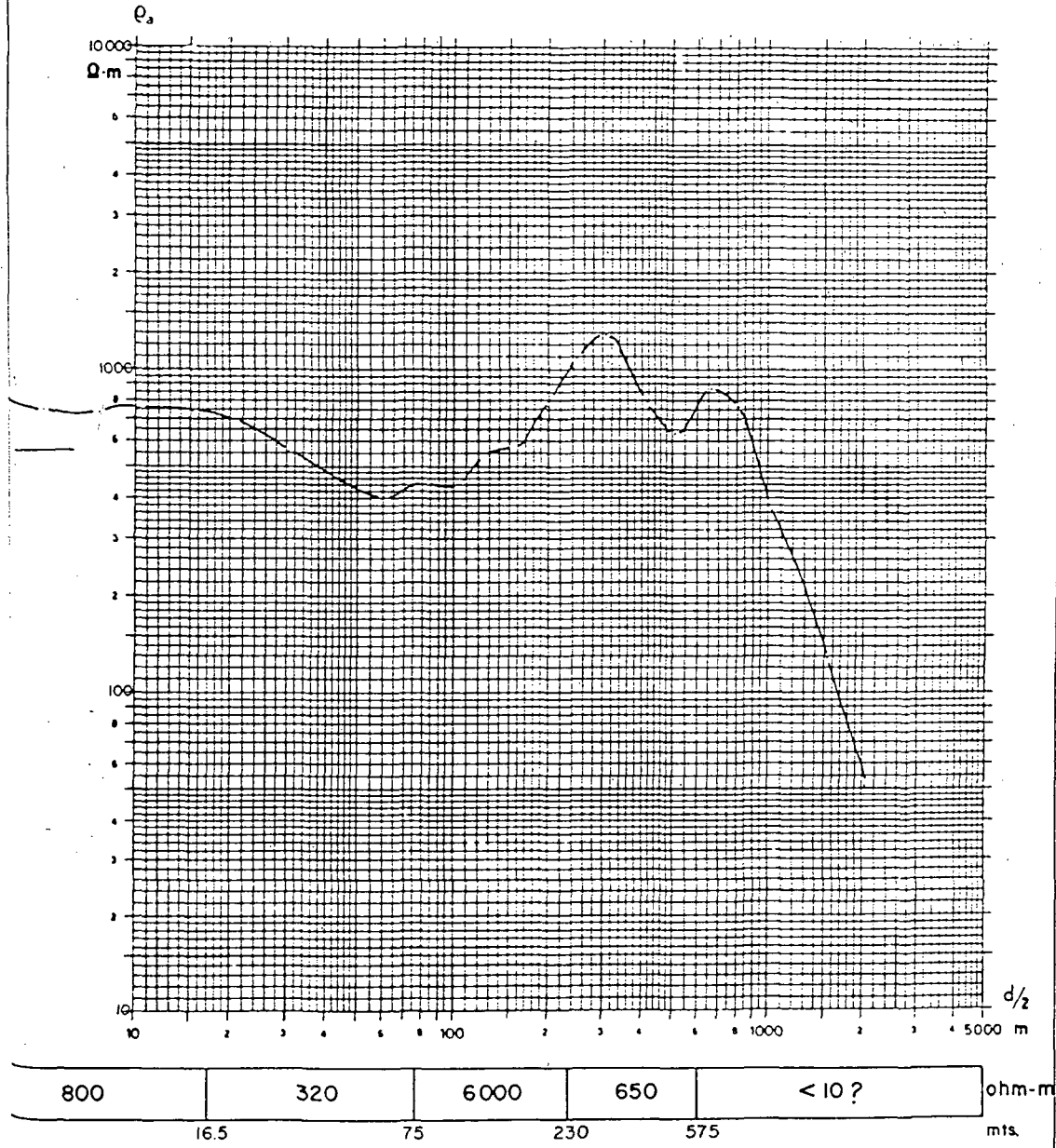
REGISTRO Z.25 FECHA 21/III./77 UBICACION ZUNIL LINEA _____

SONDEO ELECTRICO No. 25

COORDENADAS x 63.80 COTA _____

CENTRO y 33.30 AZIMUT _____

OBSERVACIONES _____ Hoja No 1960-III, Sta. Catarina Ixtahuacan, esc. 1:50 000



INVESTIGACION ELECTROESTRATIGRAFICA

FIG. 6.1.20

INDE

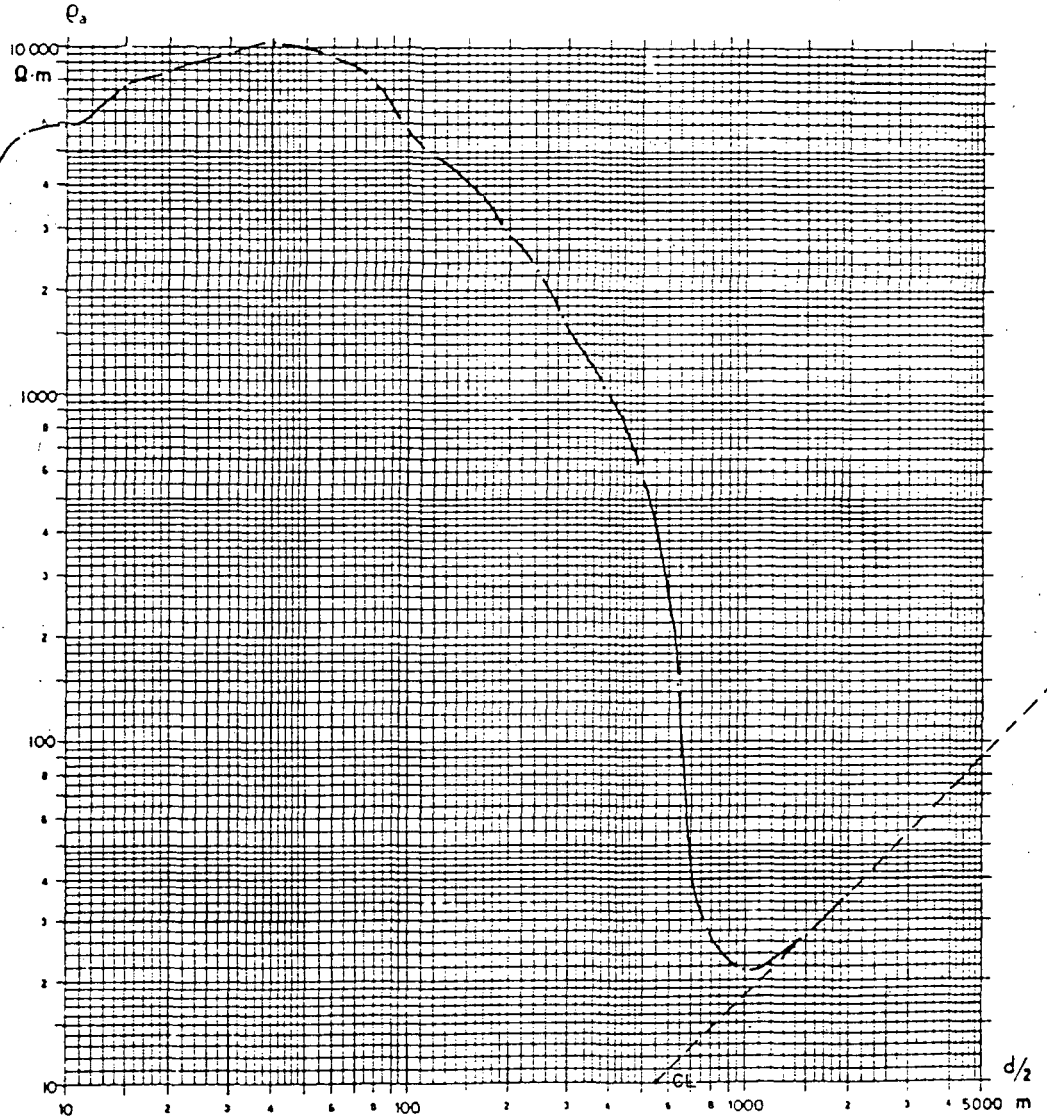
REGISTRO Z.28 FECHA 25/III/77 UBICACION ZUNIL LINEA _____

SONDEO ELECTRICO No. 28

COORDENADAS x 61.75 COTA _____

CENTRO y 34.70 AZIMUT _____

OBSERVACIONES _____ Hoja No. 1960-III, Sta. Catarina Ixtahuacan, esc. 1: 50 000



10 300	3 300	240	7.5	R	ohm-m
	36	132 198	620		mts

INVESTIGACION ELECTROESTRATIGRAFICA

FIG. 6.I.21

λ = Conductancia Longitudinal Gráfica 56 mho

λ = Conductancia Longitudinal Teórica $0.0034 + 0.03 + 0.28 + 56.27 = 56.58$ mho

INDE

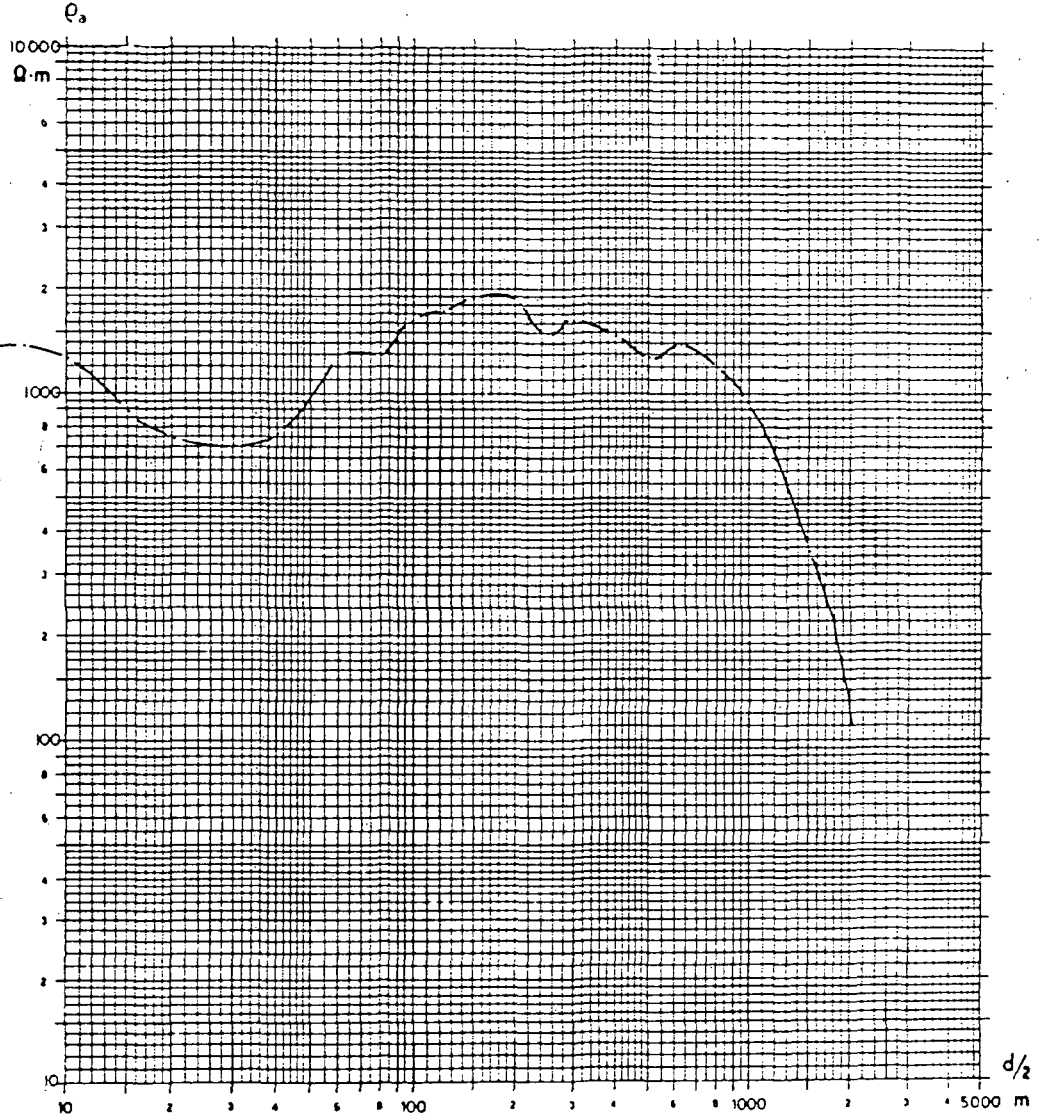
REGISTRO Z.32 FECHA 30/III/77 UBICACION ZUNIL LINEA _____

SONDEO ELECTRICO No. 32

COORDENADAS x 63.35 COTA _____

CENTRO y 34.10 AZIMUT _____

OBSERVACIONES _____ Hoja No 1960-III, Sta. Catarina Ixtahuacan, esc. 1:50 000



620	2500	< 10 ?	ohm-m
18	432		mts
INVESTIGACION ELECTROESTRATIGRAFICA			

FIG. 6.1.22

INDE

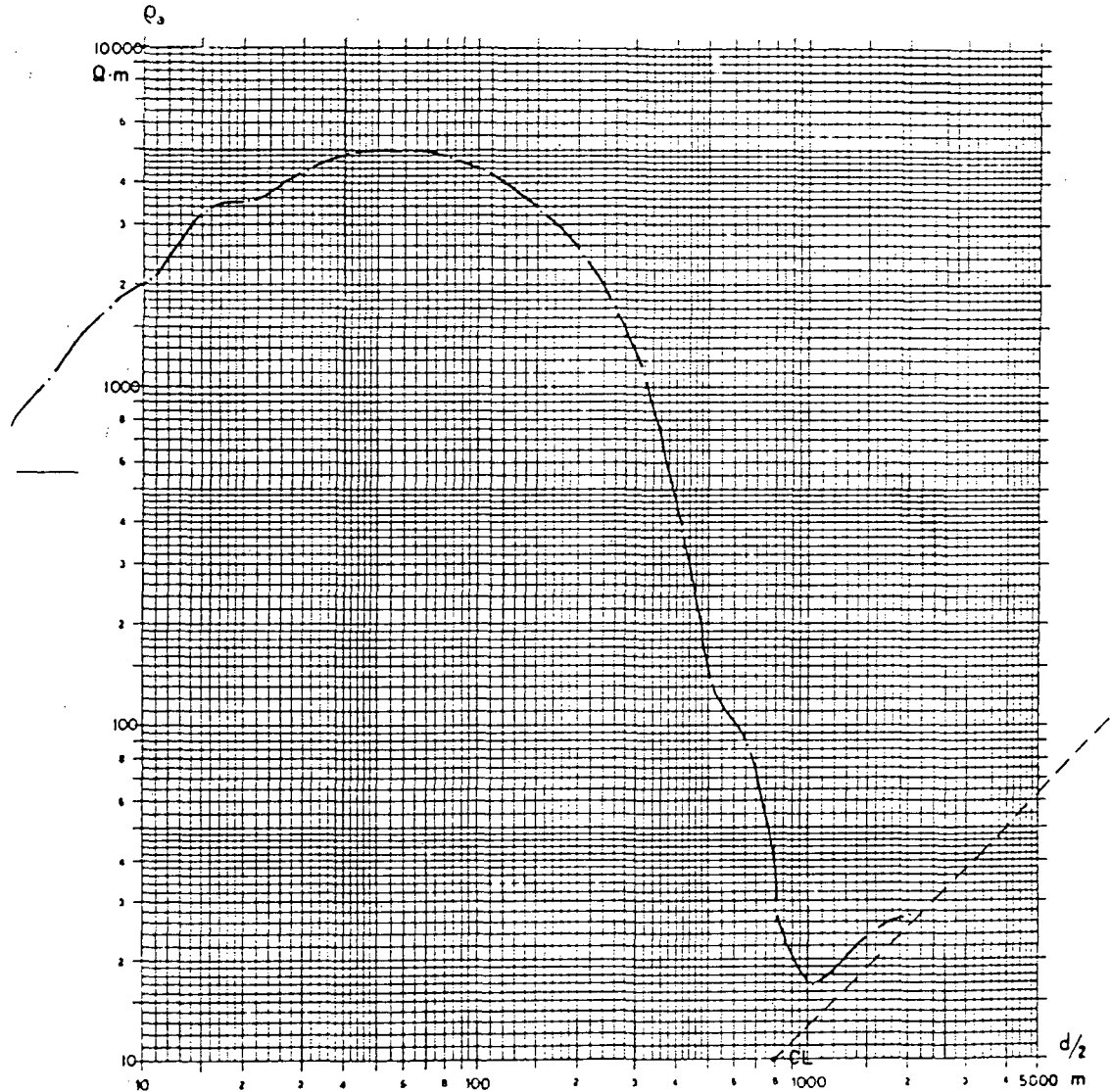
REGISTRO Z.38 FECHA 16/VIII/77 UBICACION ZUNIL LINEA _____

SONDEO ELECTRICO No. 38

COORDENADAS x 61.25 COTA _____

CENTRO y 34.6C AZIMUT _____

OBSERVACIONES _____ Hoja No. 1860-II, Colomba, esc. 1:50.000

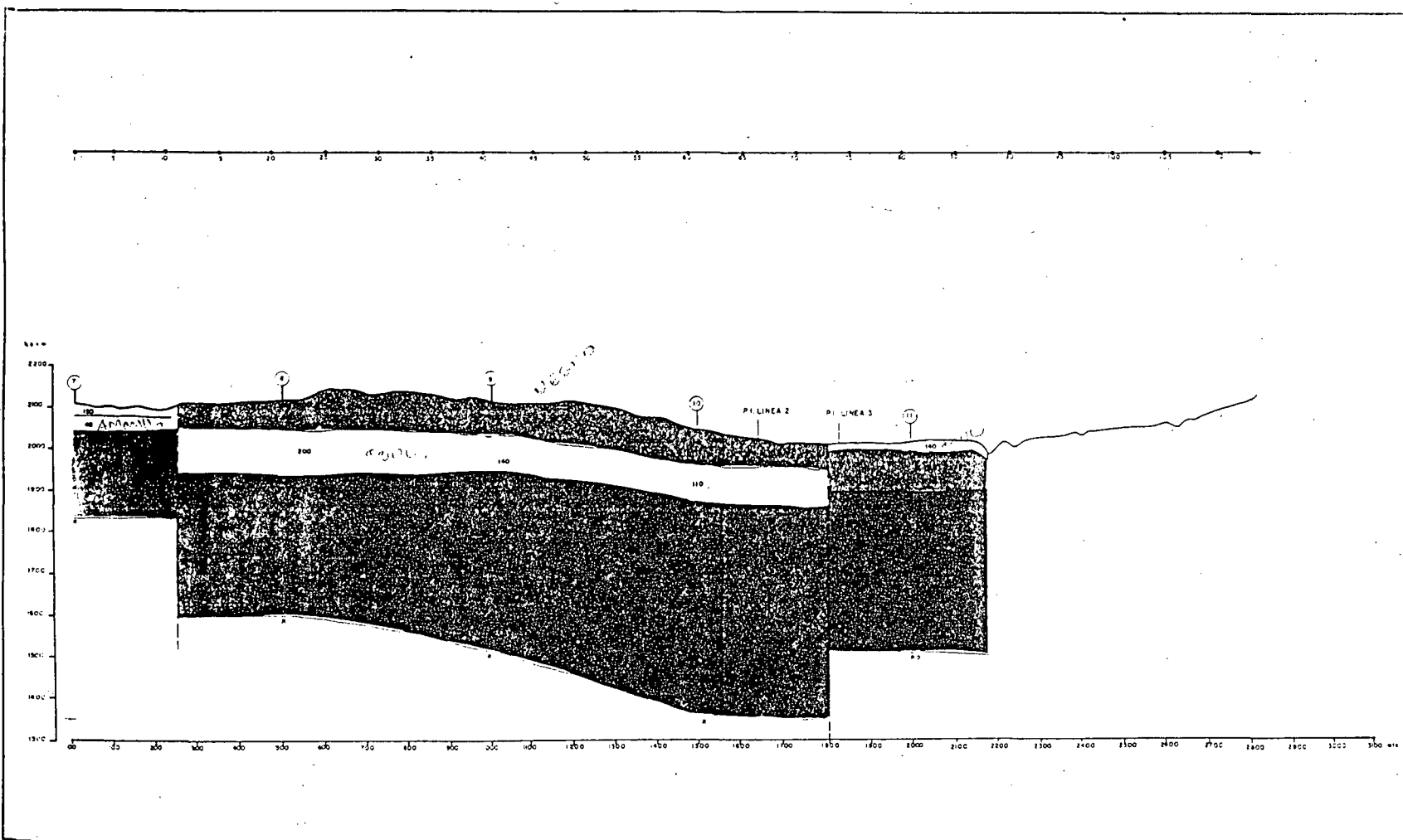


5800	135	6.4	R	ohm-m
	100	300	800	mts

INVESTIGACION ELECTROESTRATIGRAFICA

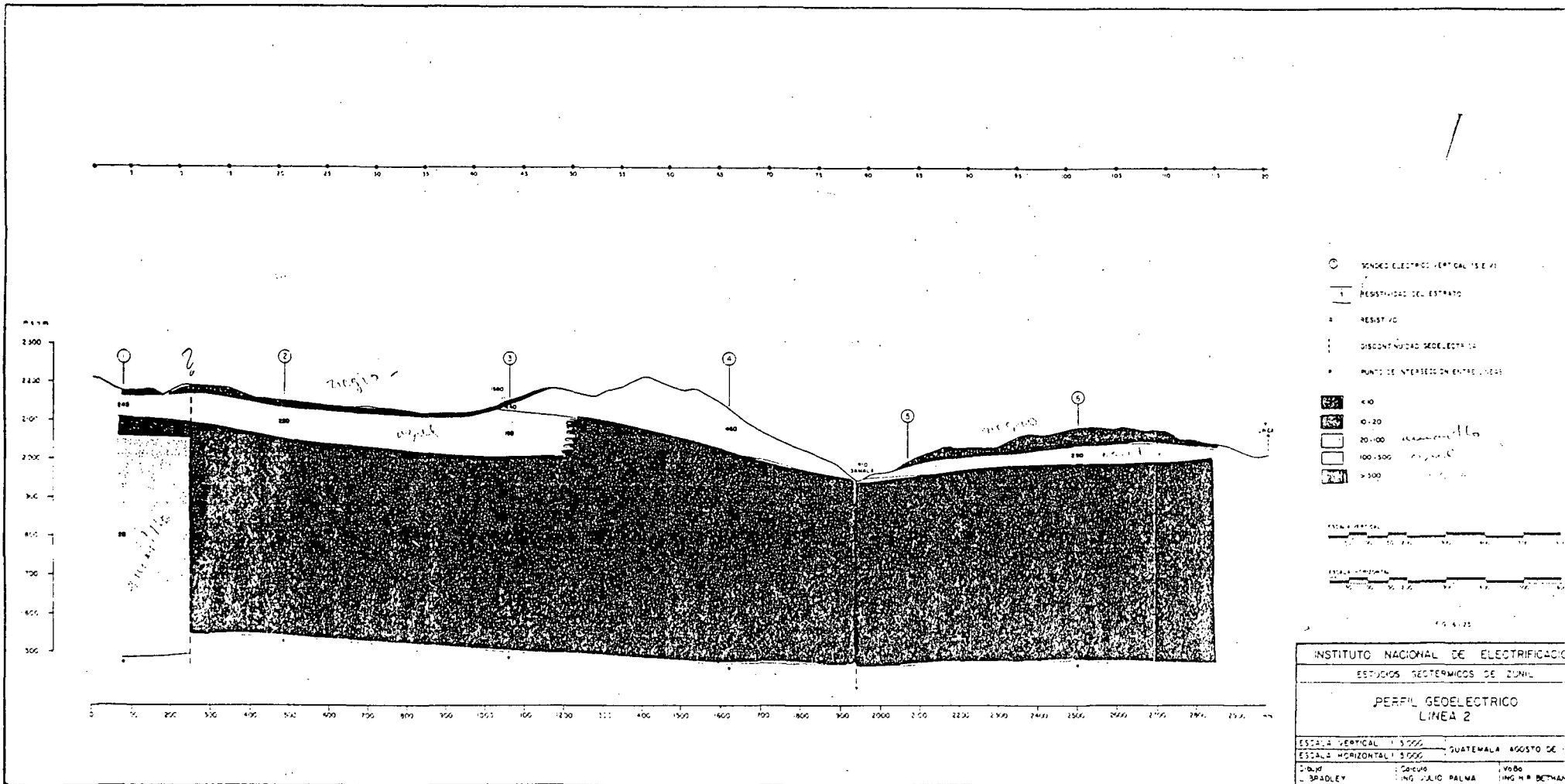
FIG. 6.1.23

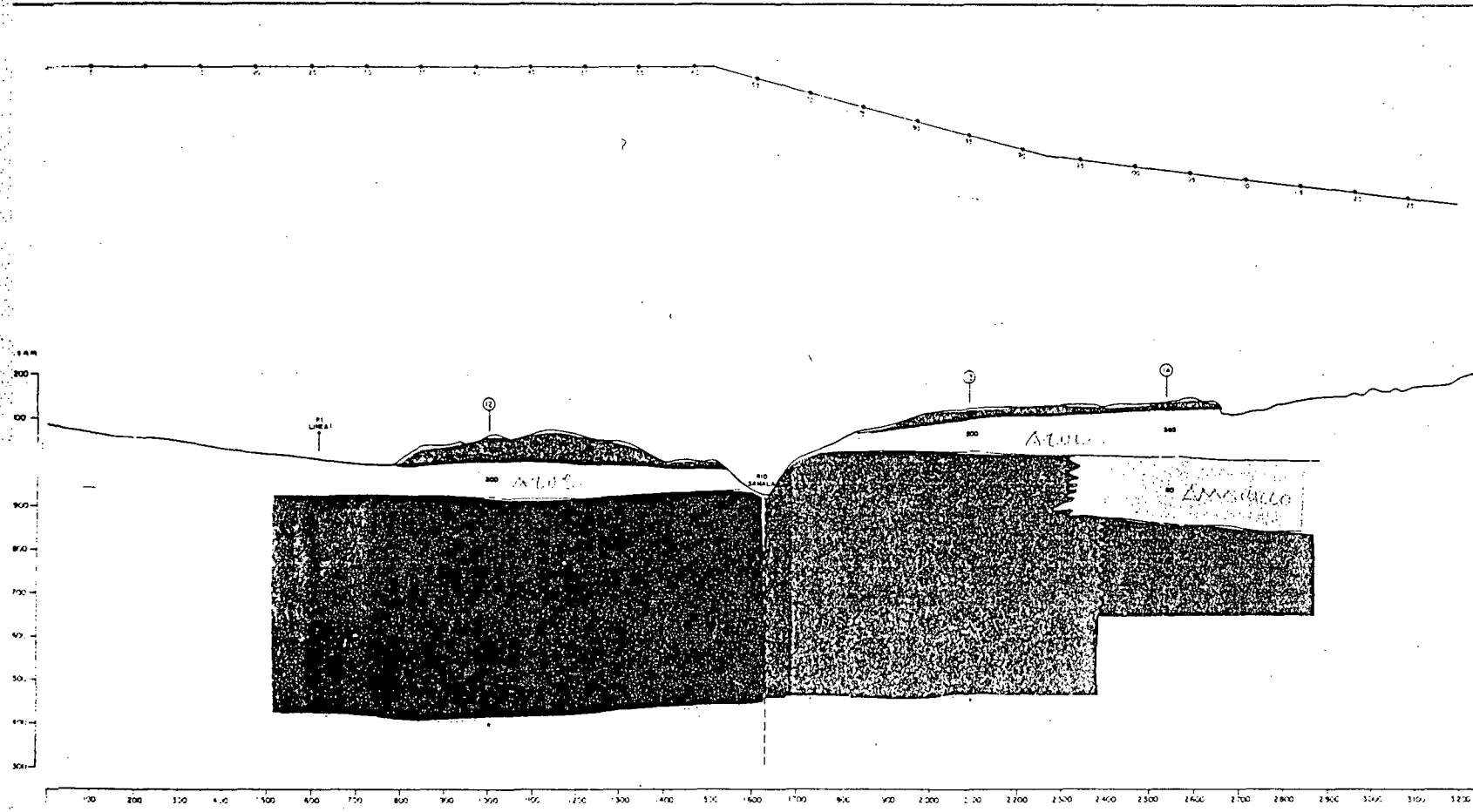
CL = Conductancia Longitudinal Gráfica = 80 mho
 CL = Conductancia Longitudinal Teórica = $0.02 + 1.48 + 78.13 = 79.63$ mho



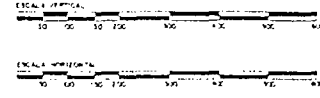
- SONDEO ELECTROGEOLOGICO (S.E.G.)
 - ⊕ RESISTIVIDAD DEL ESTRATO
 - ⊖ RESISTIVO
 - ⋮ DISCONTINUIDAD DE ELECTRICA
 - ⌋ LIMITE DE PROFUNDIDAD INVESTIGADA
 - ⋈ PUNTO DE INTERSECCION ENTRE LINEAS
 - 10
 - 10-20
 - 20-100
 - 100-500
 - >500
- ESCALA VERTICAL 1:1
- ESCALA HORIZONTAL 1:1000

INSTITUTO NACIONAL DE ELECTRICA		
ESTUDIOS GEOTERMICOS AREA ZUMIL		
PERFIL GEOELECTRICO LINEA		
ESCALAS	HORIZONTAL 1:1000	VERTICAL 1:1
GUATEMALA, SEPTIEMBRE DE 1972		
ELABORADO	CALCULO	REVISADO
OSCAR WARRINGTON	ING. JOSÉ C. SELVA	ING. JOSÉ C. SELVA



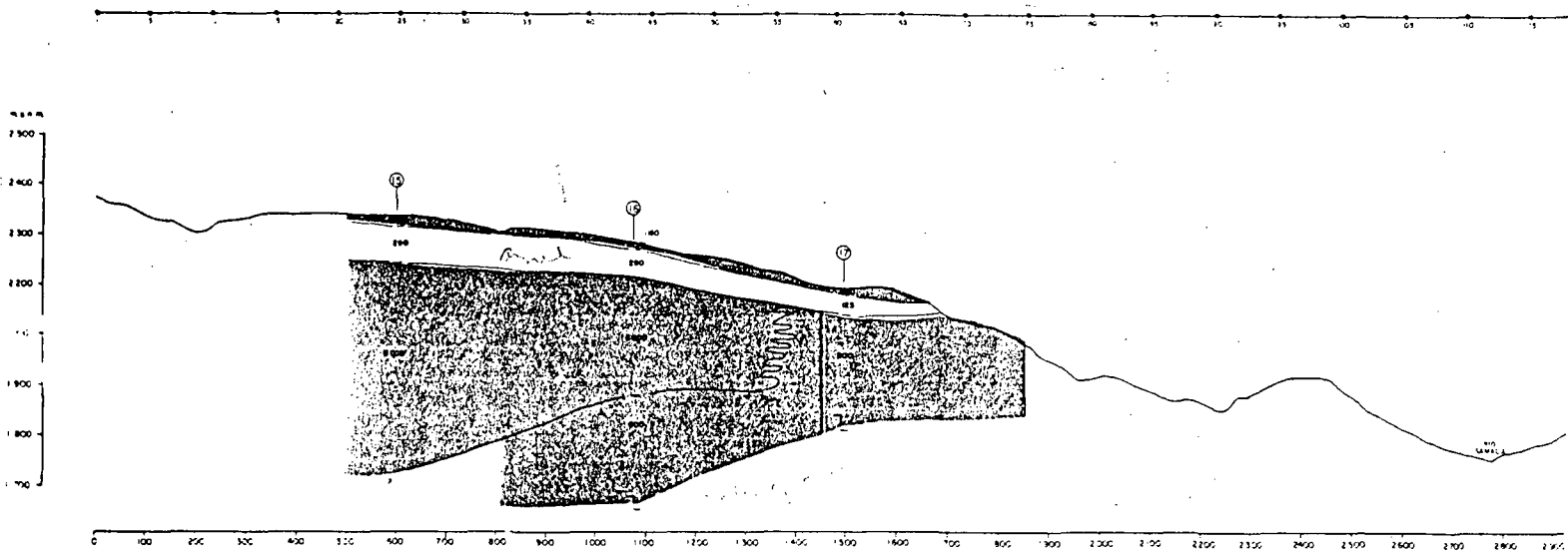


- ⊙ SONDEO ELECTRICO VERTICAL (S.E.V.)
- RESISTIVIDAD DEL ESTRATO
- R RESISTIVO
- ⋯ DISCONTINUIDAD GEOELECTRICA
- LIMITE DE PROFUNDIDAD INVESTIGADA
- P1 PUNTO DE INTERSECCION ENTRE LINEAS
- <10
- 10-20
- 20-100
- 100-500
- >500



13 13

INSTITUTO NACIONAL DE ELECTRIFICACION	
ESTUDIOS GEOTERMICOS DE ZUNIL	
PERFIL GEOELECTRICO LINEA 3	
ESCALA VERTICAL 1:5000	GUATEMALA AGOSTO DE 1980
ESCALA HORIZONTAL 1:5000	
Dibujó: L. BRADLEY	Geología: ING. JULIO PALMA
	Ing. Bº: ING. H. R. BETHMAN



- 7 SONDEO ELECTRICO VERTICAL 15 E.V.
- 1 RESISTIVIDAD DEL ESTRATO
- RESISTIVO
- DISCONTINUIDAD GEOELECTRICA
- LIMITE DE PROFUNDIDAD INVESTIGADA
- 100-300
- > 300

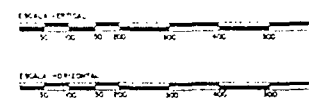
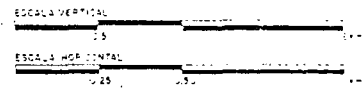
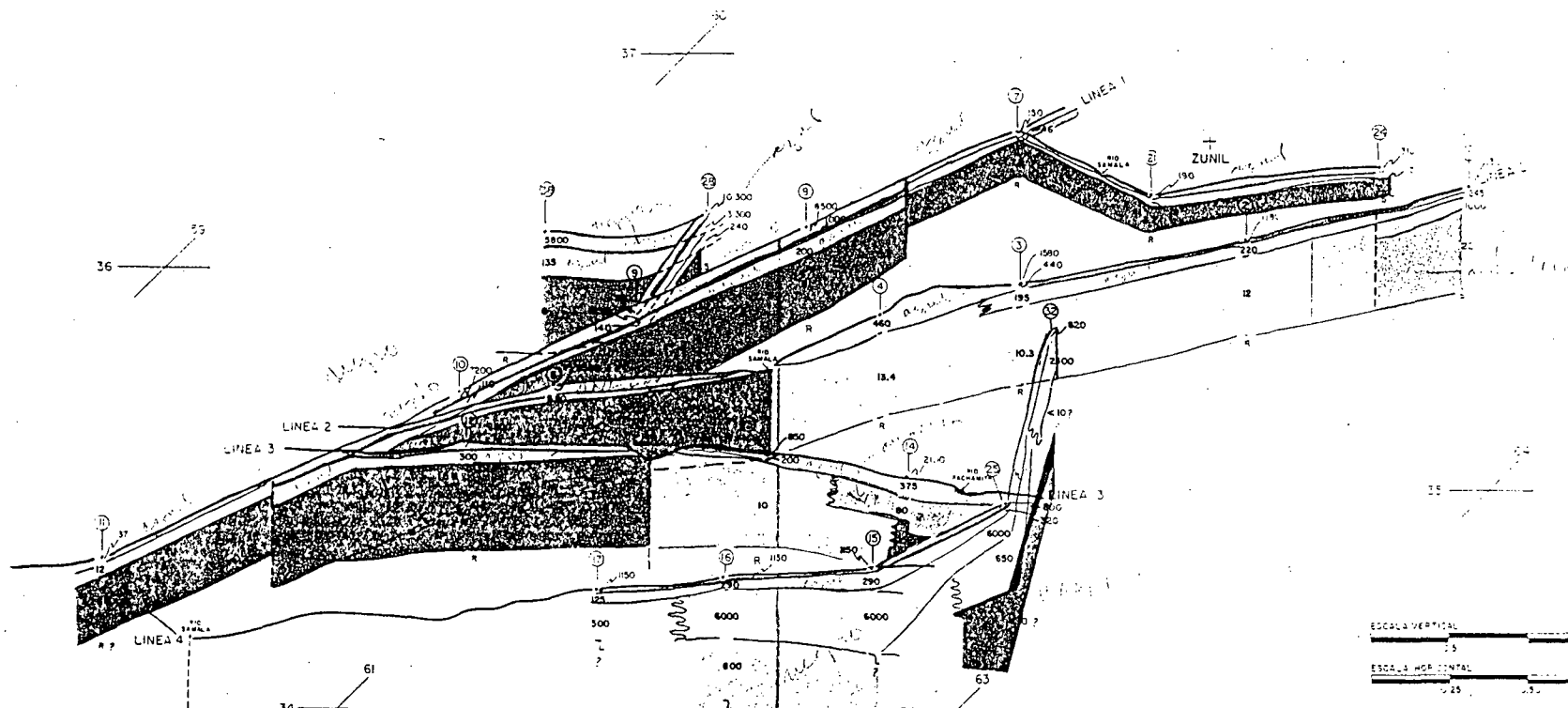


FIG. 6127

INSTITUTO NACIONAL DE ELECTRIFICACION	
ESTUDIOS GEOTERMICOS DE ZUNIL	
PERFIL GEOELECTRICO LINEA 4	
ESCALA VERTICAL: 1:5000	GUATEMALA AGOSTO DE 1968
ESCALA HORIZONTAL: 1:5000	
David L. BRADLEY	Geovid ING. JULIO PALMA
	JOSE ING. H.R. BETT

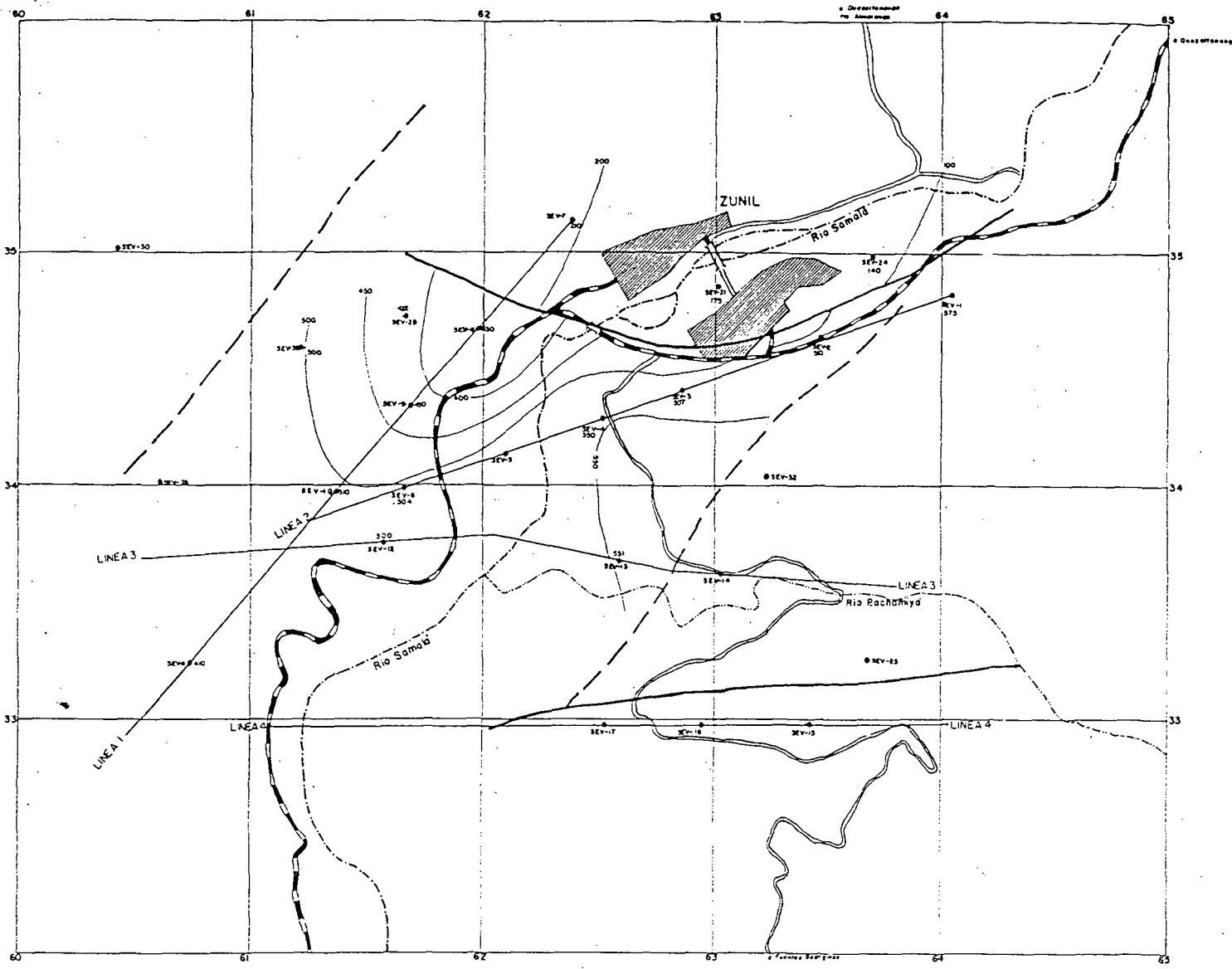


* Corresponde a Línea I, S.E.V. O
 () Numero de S.E.V.
 R Resistivo
 Q Resistividad del Estrato
 ~ Limite de Profundidad Investigado

	<10
	10-20
	20-50
	100-500
	>500

FIG. 2

INSTITUTO NACIONAL DE ELECTRICIDAD	
ESTUDIOS GEOTERMICOS DE ZUNIL	
MODELO DEL BLOQUE DIAGRAMATICO ESTRUCTURAL-GEOELECTRICO PRELIMINAR	
ESCALA VERTICAL	QUATEMALA, AGOSTO
ESCALA HORIZONTAL	
DIBUJO LINCOLN BRADLEY	CALCULO ING. JULIO H.



- SONDEO ELECTRICO VERTICAL (SEV)
ARREGLO SCHLUMBERGER AB/2 - 2000 m
- 500 — ISOPACAS DEL CONDUCTIVO
- RIO SAMALÁ
- DISCONTINUIDAD

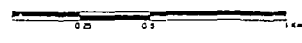
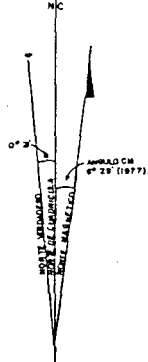
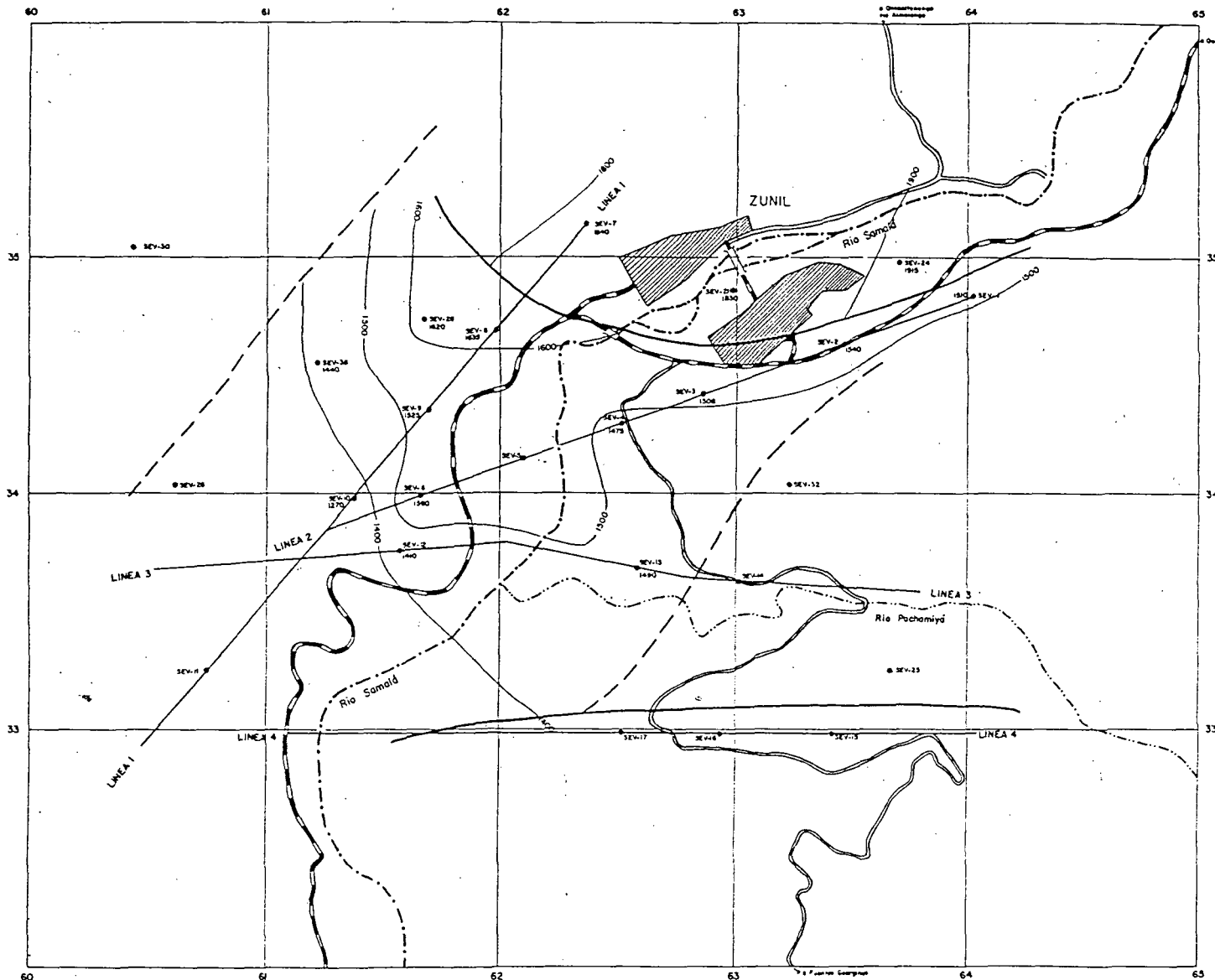


FIG. 6.3.1

INSTITUTO NACIONAL DE ELECTRIFICACION	
ESTUDIOS GEOTERMICOS DE ZUNIL	
ISOPACAS DEL CONDUCTIVO	
(Cg < 15 g/cm ³)	
ESCALA 1:10000	GUATEMALA, SEPT. / 1977
Dibujo - O. MARROQUIN P.	Calculó - ING. JULIO PALMA
	Vo Bo - ING. H.R. BETHANCOURT



- SONDEO ELECTRICO VERTICAL (S.E.V.)
ARREGLO SCHLUMBERGER, AB/2 = 2000 m
0.0210 m
- 1000 CURVAS DE ISONIVEL DEL FONDO RESISTIVO.
- 3700 ALTURA SOBRE EL NIVEL DEL MAR
DEL FONDO RESISTIVO.
- RIO SAMALÁ

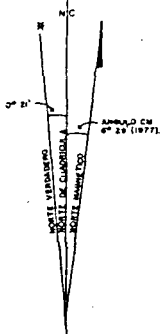


FIG. 6.2.1

INSTITUTO NACIONAL DE ELECTRIFICACION		
ESTUDIOS GEOTERMICOS DE ZUNIL		
CURVAS DE ISONIVEL DEL SUBSTRATO RESISTIVO		
ESCALA 1:10 000	GUATEMALA, AGOSTO/1977	
Dibujó L. BRADLEY	Calculó ING. JULIO PALMA	VoBo ING. H.R. BETHANCOURT
	x1.09	



**EARTH SCIENCE LABORATORY
420 CHIPETA WAY, SUITE 120
SALT LAKE CITY, UTAH 84108
TELEPHONE 801-581-5283**

INTERPRETATION OF SCHLUMBERGER DATA
IN THE VICINITY OF ZUNIL I

around ZCQ-3. The trends in the conductivity-thickness products are consistent with geochemical data which indicate that the reservoir fluids undergo progressive cooling and dilution as they move from the area near ZCQ-3 and 6 to the south and east. These changes to the fluid will promote an increase in the development of electrically conductive clay minerals.

INTRODUCTION

The Schlumberger method of electrical resistivity sounding measures the potential drop across a receiver wire between two electrodes M and N. The electric current is introduced into the earth by a transmitter through two electrodes which are collinear with the receiver wire and straddle it symmetrically. The distance between electrodes MN of the receiver is increased as needed to maintain the level of the received signal. The transmitted current has a waveform which has a repetition frequency low enough to minimize inductive effects but high enough to avoid geomagnetic noise, which is inversely proportional to frequency. The measured potential is transformed to an apparent resistivity, which is equivalent to the resistivity of a uniform earth which would yield the same value.

In a complete sounding, the apparent resistivity is determined for a large number of different transmitter electrode separations A - B. As the transmitter length AB is increased, the depth of investigation is also increased. By plotting the measured apparent resistivity against half the transmitter length (AB/2), information can be gained on the thickness and resistivities of the subsurface layers that the current penetrates. Since the Schlumberger array is primarily used to interpret the electrical resistivity variation with depth, the soundings are often referred to as Vertical Electric Soundings, or VES. A very low resistivity layer will prevent the current from extending any deeper, thus limiting the depth of exploration.

Approximately 30 Schlumberger soundings (VES) were taken in the vicinity of Zunil I. The soundings provided to us are located in the colored regions of Figure 1. These data were provided to UURI in the form of field

notes and Schlumberger apparent resistivity graphs. Layered earth inversion modeling was completed on VES 1, 3, 4, 6, 8, 10, 11, 12, 28, 38, 115 and 116. In general, the soundings were located in zones of radical lateral resistivity inhomogeneities and extreme topographic variations which dictate the electric current distribution and can be expected to complicate the interpretations. Because of the severity of the effects of these inhomogeneities in the data from the remaining soundings, it was not possible to interpret them with layered earth models. The sounding curves were oriented in only one direction and were widely spaced.

RESISTIVITY STRUCTURE

The soundings can be divided into two groups (A and B) as shown in Figure 1. The soundings in group A indicate high resistivity terrain, with little variation. For example, Figure 2 shows the observed apparent resistivity in VES 114, which is typical of group A. The data has been plotted for all potential electrode spacings (M-N), as is indicated by the multiple data points at single current electrode spacing, (A-B). We do this because we do not want to bias an interpretation by adjusting the curve up or down to make the curves for various potential electrode values coincident, as has been done traditionally. The apparent resistivity curves for the various potential electrode spacings should parallel one another if the data are accurate. When the curves are not parallel then data quality is suspect. Any offset in the apparent resistivity curves for different values of the potential electrode spacing reflects effects of lateral inhomogeneity on the potential electrodes.

The interpretation of data from group A is complicated by the jagged nature of the plotted data curves, which may be due to poor data quality and/or the effects of lateral inhomogeneities and by the lack of deep drillholes in the area. The influence of lateral inhomogeneities on the observed apparent resistivities cannot be evaluated because of the wide spacing between the soundings.

Most of the soundings in group B can be interpreted using a four layer model. The upper two layers are characterized by high resistivities. These layers are underlain by a thick intermediate layer with low resistivities, which is in turn underlain by a layer with high resistivities. The thickness of the deep resistive layer, however, cannot be resolved from the soundings. In a few cases, interpretation of the data required the presence of additional shallow high resistivity layers. In all cases, these layers are thin. The soundings in group B lie in the area where exploration has been most intense. Thus, the thicknesses of the layers can be compared with the distribution of lithologies and alteration assemblages encountered in the wells to determine the cause of the resistivity variations. Figure 3 shows a typical group B sounding (VES 115).

DISCUSSION OF RESULTS

Traditionally, Schlumberger soundings have been interpreted by fitting them to the calculated responses of layered earth resistivity distributions. The UURI interpretations were done using a ridge regression least-squares inversion computer program developed at UURI. The basic technique is discussed by Inman (1975). A complete set of all soundings that were interpreted are contained in Appendix I. Sensitivity analyses are shown in Appendix 2. Appendix 3 contains the percent parameter standard deviations and the parameter correlation matrix for interpreted soundings.

Twelve soundings were interpreted using a layered earth model. The nominal depth to the deep resistive layer of soundings in the vicinity of Zunil I is indicated on Figure 4. In general, the top of the deep resistive layer appears to be located at depths ranging from 200 to slightly over 400 m.

Comparison of the resistivity solutions with lithologies and alteration assemblages encountered in the wells indicates that the changes in the electrical properties of the rocks corresponds most closely to changes in

the conductivities of the clay minerals. At VES 115 (Figure 3), which is located near ZCQ-3 and Z-11, the top of the resistive layer is located at a depth of 335 m. At this depth, the rocks in ZCQ-3 consist of altered dacite lava flows of the Almolonga Volcanics. The granodiorite was intersected at a depth of 985 m in ZCQ-3.

Petrographic and X-ray studies of the production and gradient wells indicates that the alteration assemblages can generally be classed as either argillic or propylitic (CyM/MKE, this study). Argillic assemblages occur in the upper portions of the wells and are characterized by variable proportions of the clay minerals smectite, illite-smectite, and chlorite-smectite, quartz, and calcite. In contrast, propylitic assemblages are characterized by illite-rich clays (illite, illite-rich illite-smectite), chlorite, epidote, quartz, calcite, and wairakite. The clay assemblages in the argillic zone are more conductive than those in the deeper, higher temperature zone.

The top of the propylitic zone is marked by the first appearance of epidote. In ZCQ-3, the top of the propylitic zone is located at a depth between 250 and 450 m whereas in Z-11, it is found at a depth between 200 and 325 m. Generally similar relationships are found in ZCQ-4, which is located adjacent to sounding 116. This sounding yields a nominal depth of 243 m to the top of the deep resistive layer. The rocks at this depth in ZCQ-4 also consist of hydrothermally altered dacite (Tobias, 1980, unpublished lithologic log). Although the alteration assemblages in ZCQ-4 have not been studied in detail, the measured temperatures at 250 m are close to 240°C. The temperature is similar to that found near the top of the propylitic zone in ZCQ-3 (e.g. measured temperatures are about 200°C at 250 m and 235°C at 450 m; CyM/MKE, this study). Thus we would expect the mineralogies to be similar. In summary, the mineral relationships in these wells suggests that the transition from conductive to resistive rocks is due to a change in the clay minerals and not to the deep granodiorite.

In contrast to the soundings that showed the resistive layer to be at relatively shallow depths, sounding number 6 (Figure 5) indicates that the depth to the high resistive layer is 594 m. This depth is similar but slightly

shallower than the depth to the granitic basement in ZCQ-1 which is the closest well (680 m; Tobias, 1980, unpublished lithologic log; CyM/MKE, this study). Because of the uncertainties in the data, and the comparisons with the other wells described above, we cannot further test the possibility that the resistive layer at sounding 6 is indeed related to the top of the granodiorite.

Two approaches were used to determine the sensitivity of the interpretations. The parameter standard deviations give an estimate of the degree to which each model parameter can be perturbed and still give a model which will fit the data to within one estimated standard deviation. Since these statistics are based on a linearized approximation to the geoelectric response, they are accurate only in a local sense. In particular, standard deviations which are higher than 100% only indicate that the parameter is poorly resolved, not that there is a possibility that the parameter can assume a negative value. As can be seen from the percent parameter standard deviations calculated for each sounding, the individual resistivities and thicknesses of the conductive layers are poorly resolved. Thus, although we are certain that a conductive zone exists at depth, its thickness is largely unresolved from the soundings themselves. At most, a conductivity-thickness product can be determined for this conductive layer.

To further analyze the sensitivity of the interpretations, the conductive layer parameters were varied by a factor of two and the resulting model was compared with the interpreted model. This sensitivity analyses (Appendix 2) indicated that poor model parameter resolution can occur through unconstrained inversion of Schlumberger soundings. Figure 6 shows the perturbation done on sounding 3. The resistivity of the conductive layer (layer # 4) was increased from 4.15 ohm-m to 8.30 ohm-m. The thickness was increased from 216.85 m to 433.70 m (to maintain a constant conductivity-thickness product). The resulting calculated apparent resistivity curve changed an insignificant amount. This indicates that the layered earth model in this case is not sensitive to changes in the model parameters. Thus, the depth to the deep resistive layer is not well

constrained. However, even with the parameters varied by a factor of two, most of the soundings that are insensitive to parameter changes indicate that the depth to the deep resistive layer is still several hundred meters shallower than the granodiorite. Figure 7 illustrates this by showing the depth to the resistive zone with parameters increased two times. (Figure 7 only has a resistive layer depth listed for soundings that are insensitive to parameter changes.)

In contrast, soundings 1, 6, 11, 115, 116 are sensitive to the parameter changes. (Figure 8 illustrates the sensitivity analysis for sounding number 115.) For these soundings, the interpretations no longer fit the observed data when the model parameters were changed. This indicates that the initial interpretation is likely to be accurate.

Even though our analysis of the data has shown that the thicknesses and sensitivities of the of the conductive layer is poorly resolved, the conductivity-thickness product of the layer is well resolved. Figure 9 gives the values of conductivity-thickness products for the soundings. The conductivity-thickness product or conductance is proportional to the number of charge-carrying ions/anions available in the layer. Figure 9 shows that the conductivity-thickness product increases away from the area around ZCQ-3. An increase in the conductivity-thickness product could result from: an increase in the thickness of the clay-bearing alteration zones; an increase in the abundance of conductive clays; increased porosity; or increased conductivity of pore fluids. The latter is itself a function of both temperature and ion (TDS) content. Because of the lack of drill hole data from areas where the soundings were made, it is not possible to determine whether one of these factors or a combination has caused the observed changes.

The distribution of the conductivity-thickness products is consistent with the pattern of fluid movement inferred from chemical analyses of well and spring samples (Cym/MKE, this study). Chloride-enthalpy relationships indicate that the least diluted reservoir fluids are found in the vicinity of ZCQ-3 and 6 and that these fluids cool conductively and by dilution as they move to the east and south. Both cooling and dilution will promote

increased development of conductive clay minerals such as smectite, illite-smectite, and chlorite-smectite as the fluids move down their hydraulic gradients. The low conductance values at sounding sites 4, 12, 28, and 38 may reflect decreased exposure to the hydrothermal fluids.

Although we have interpreted the data using a layered earth model, many of the data sets show significant multidimensional effects. The steep 45° slopes in the ascending branches at large current electrode spacings for soundings 1, 3, 4, 5, 6, 8, 10, 11, 115, and 116 for example, cannot be produced by any layered earth. This behavior is consistent with the existence of lateral contacts, as shown in Figure 10 (Kunetz, 1966). The effects of topographic variations, both along the sounding line and lateral to it, also restrict the accuracy of our interpretations.

Sounding no. 4 (Figure 11) gives an example of a radical effect of lateral inhomogeneities on the apparent resistivities for two different potential electrode spacings for the receiver electrodes. On Figure 11, the effect occurs at an AB/2 value of 40 meters (AB/2 is half the distance between current electrodes). Two apparent resistivities that vary by almost one order of magnitude were recorded for the same current electrode spacing. Unfortunately, no data is available at the previous potential spacing for two consecutive current electrode spacings, and hence we cannot assess the possible role of data collection noise in producing such an offset. Another apparent discontinuity occurs between an AB/2 value of 60 and 100 meters, indicating poor data quality, lateral discontinuities, or extremely large resistivity contrasts between adjacent layers. The poor data fit achieved with the layered model is not surprising given the multi-dimensional or noisy character of the data. Clearly, no layered model would be able to achieve a statistically significant match of the data from this sounding. Unfortunately, the wide spacing of the soundings precludes the application of multi-dimensional models.

REFERENCES

Inman, J. R., 1975, Resistivity inversion with ridge regression: *Geophysics*, v. 40, p. 798-817.

Kunetz, G., 1966, *Principles of direct current resistivity prospecting*: Berlin, Gebruder Borntraeger.

CyM/MKE, 1988; Neotectonic study: Report submitted to INDE, 24 p.

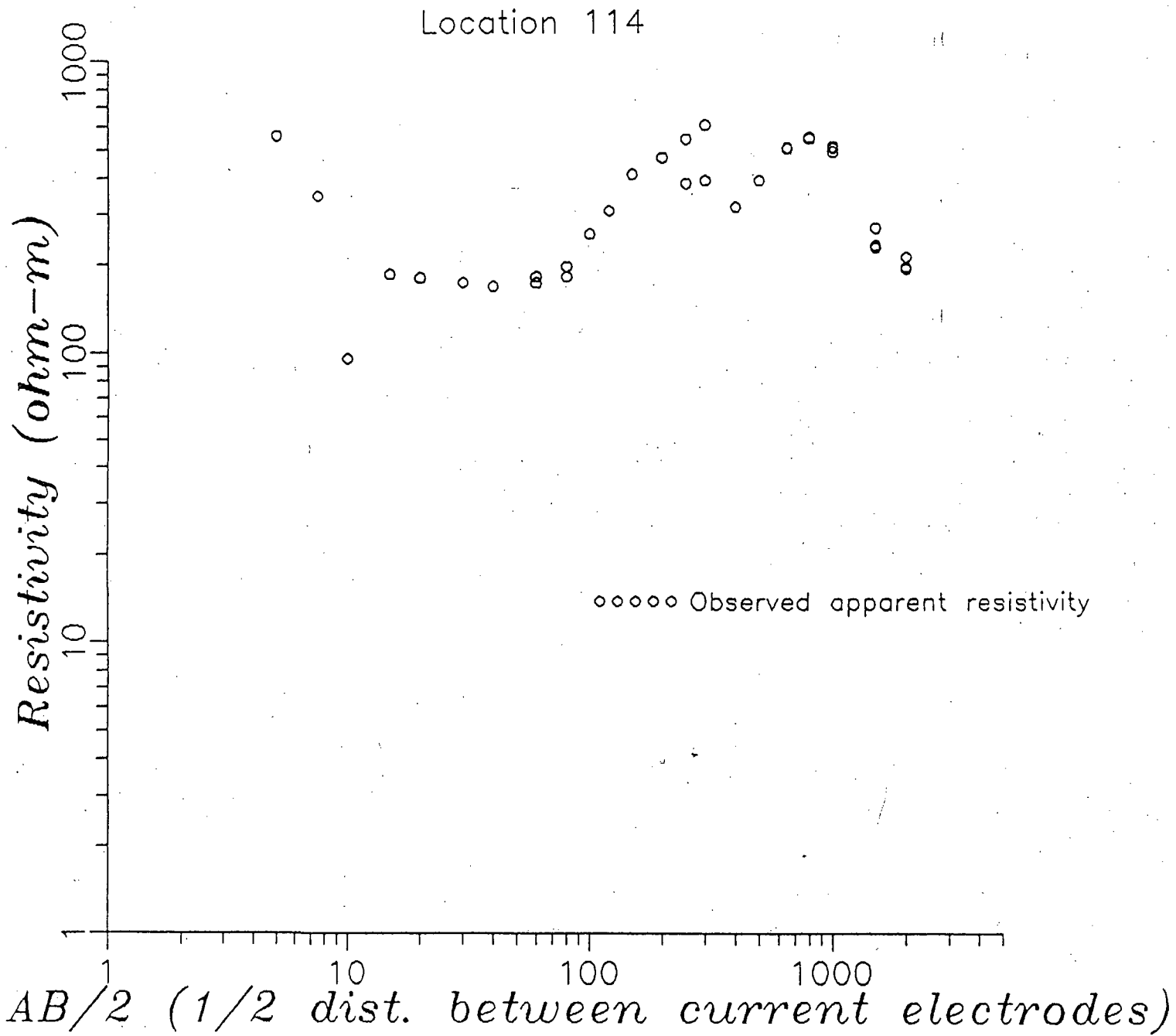


Figure 2. Observed apparent resistivity for VES 114, typical of group A soundings.

Figure 4

Location map for soundings in the vicinity of ZCQ-I. Map also gives best estimates to the resistive basement as given by layered earth modeling. VES 5 and 9 are not shown here due to inconsistencies in the observed data. Observed data for VES 10 and 11 were estimated graphically.

Figure 6

Illustration of the effect of a sensitivity analysis on a sounding that appears to be insensitive to parameter changes. Solid line indicates the optimum calculated apparent resistivity. Dashed lines indicate calculated apparent resistivities for layer 4 (conductive layer) with model parameters varied by a factor of 2. The interpretations based on the increased model parameters fits the observed data, therefore, the initial interpretation is not well constrained.

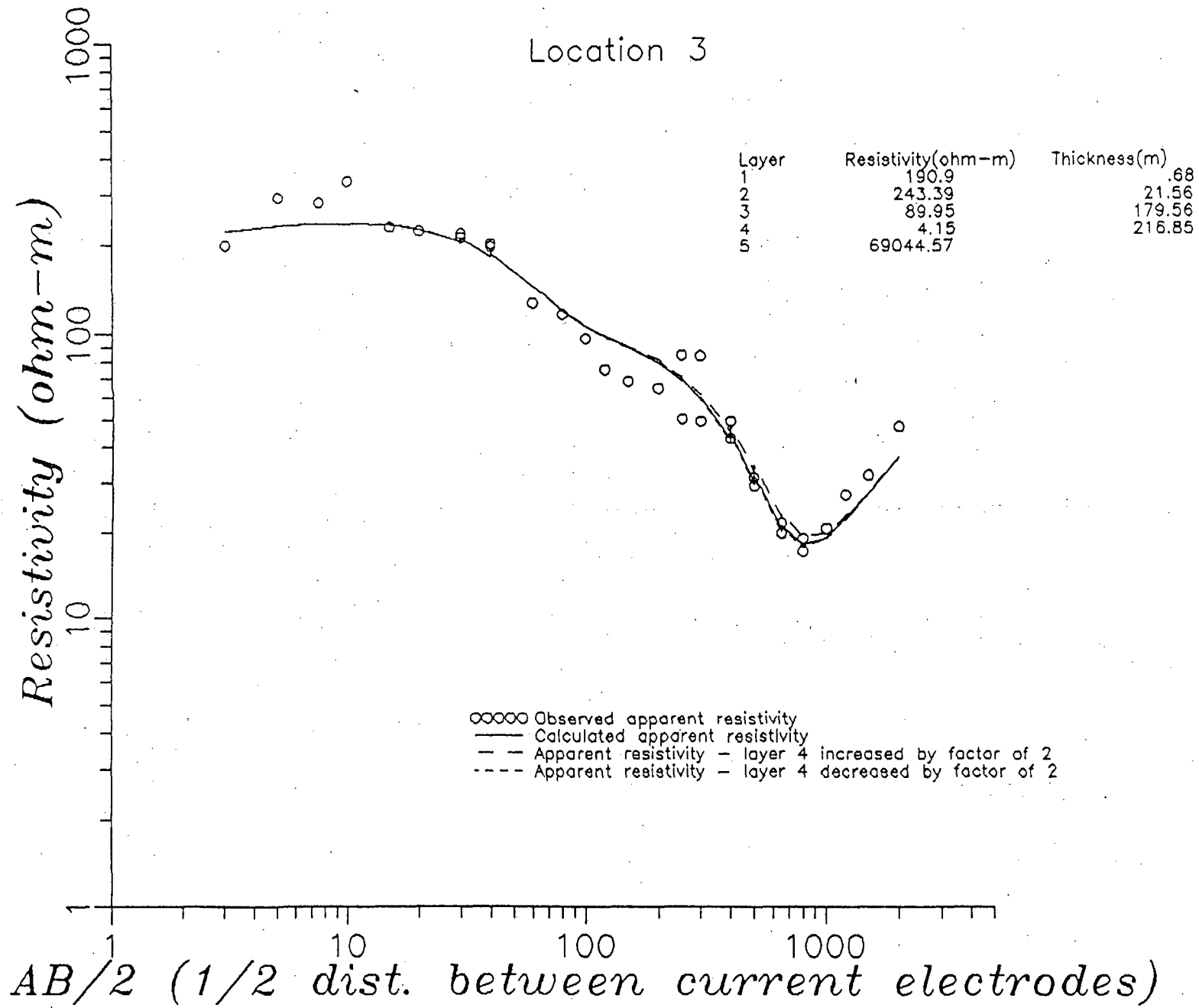
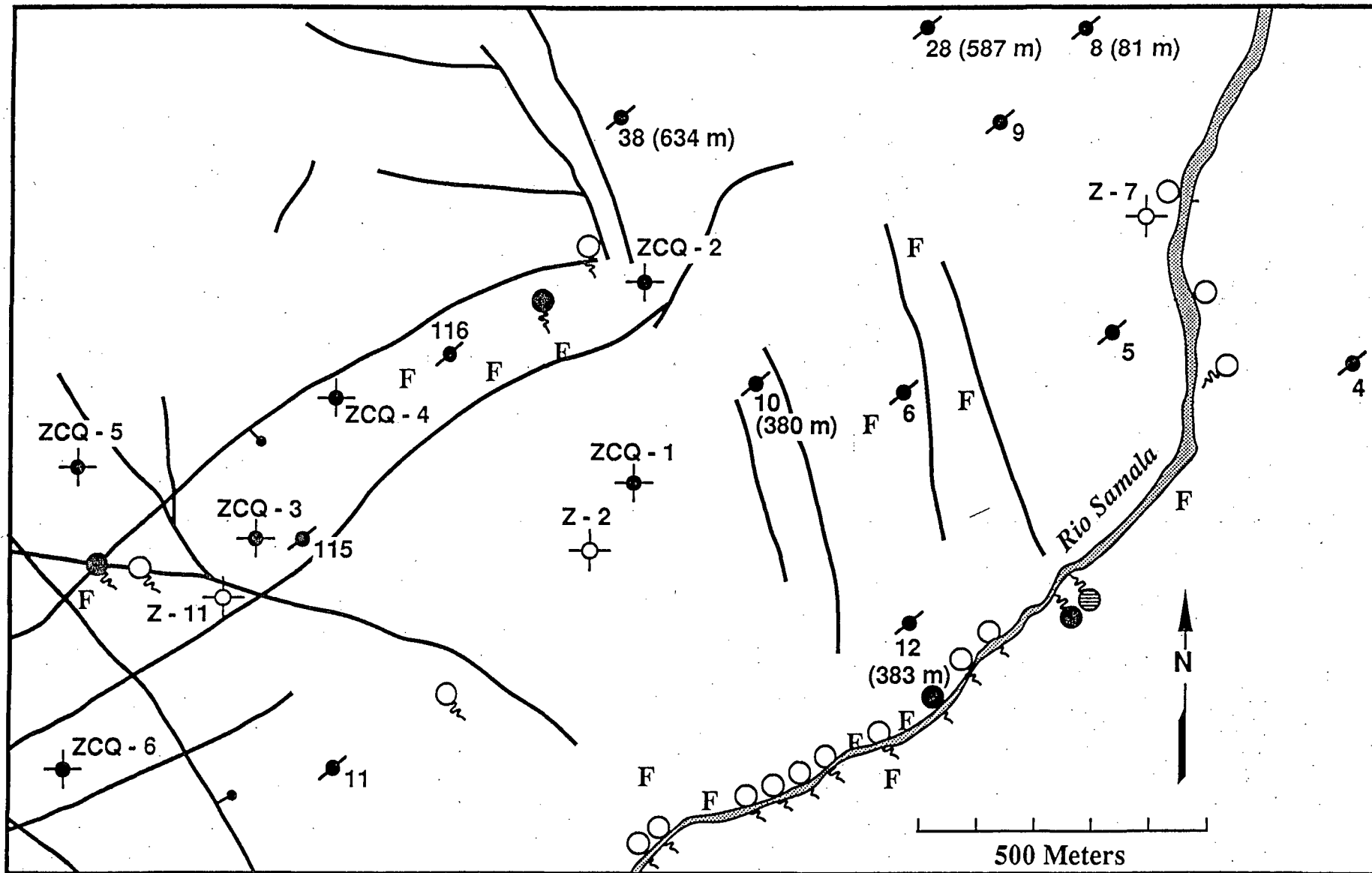


Figure 6

Figure 7

Illustration of the sensitivity analysis results on estimates to the depth to the high resistivity layer. New estimates of depth shown were calculated by increasing the conductive layer parameters by a factor of 2. Soundings without a new depth estimate were sensitive to changes in parameters. Thus, the initial depth estimate for these soundings (shown in Figure 4) is fairly well constrained.



- | | | | |
|---|-----------------|-----------------------|-------|
| Acid-sulfate spring | NaCl spring | F Fumarole | Fault |
| Bicarbonate spring | Production well | Thermal gradient well | |
| Sounding Location; Depth to resistive layer | | | |
- 10 (380 m)

Figure 7

Figure 8

Illustration of the effect of a sensitivity analysis on a sounding that appears to be sensitive to parameter changes. Solid line indicates the optimum calculated apparent resistivity. Dashed lines indicate calculated apparent resistivities for Layer 3 (conductive layer) with model parameters varied by a factor of 2. The interpretations based on the increased model parameters do not fit the observed data, therefore initial interpretation is well constrained.

Location No. 115

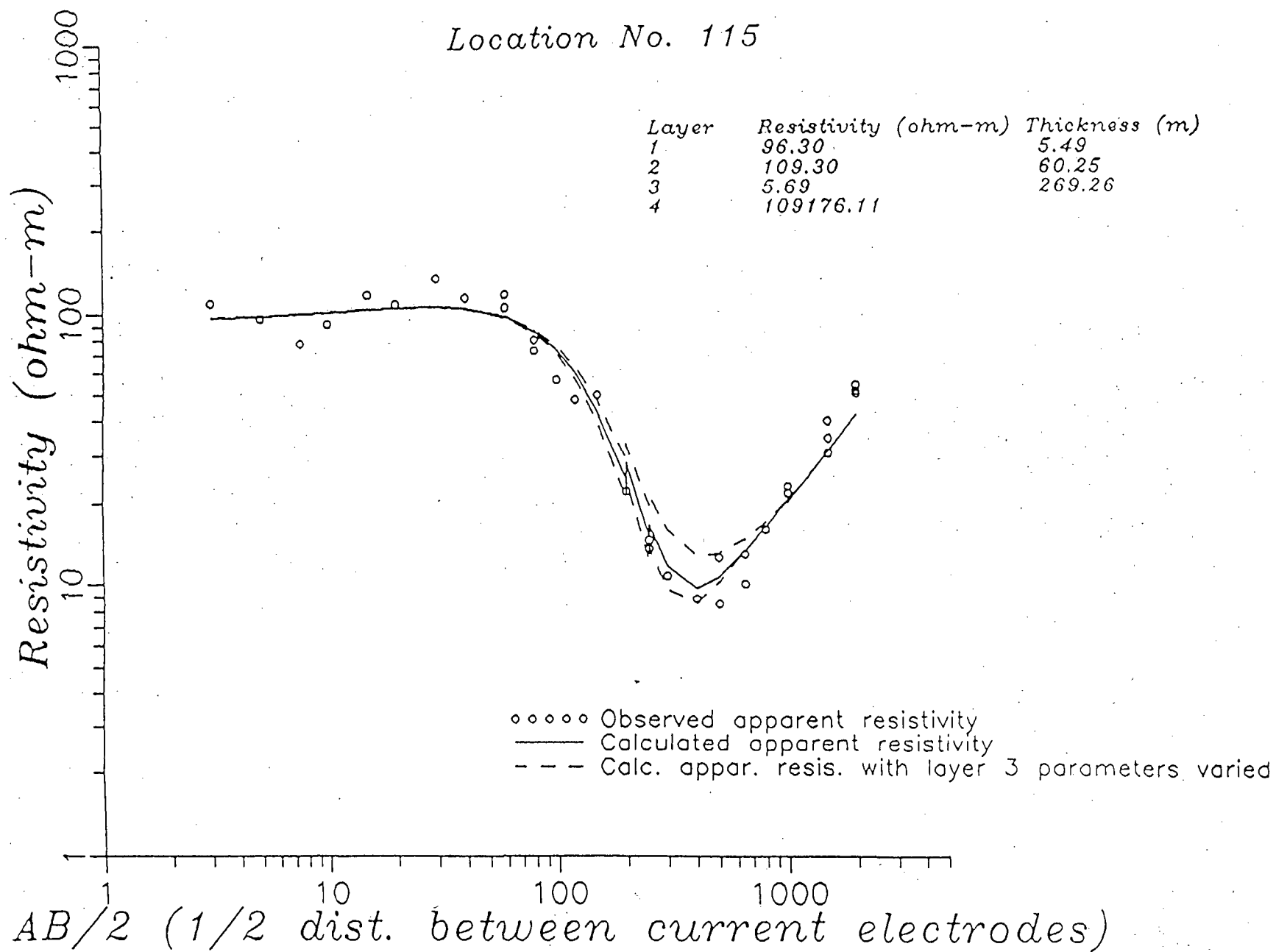
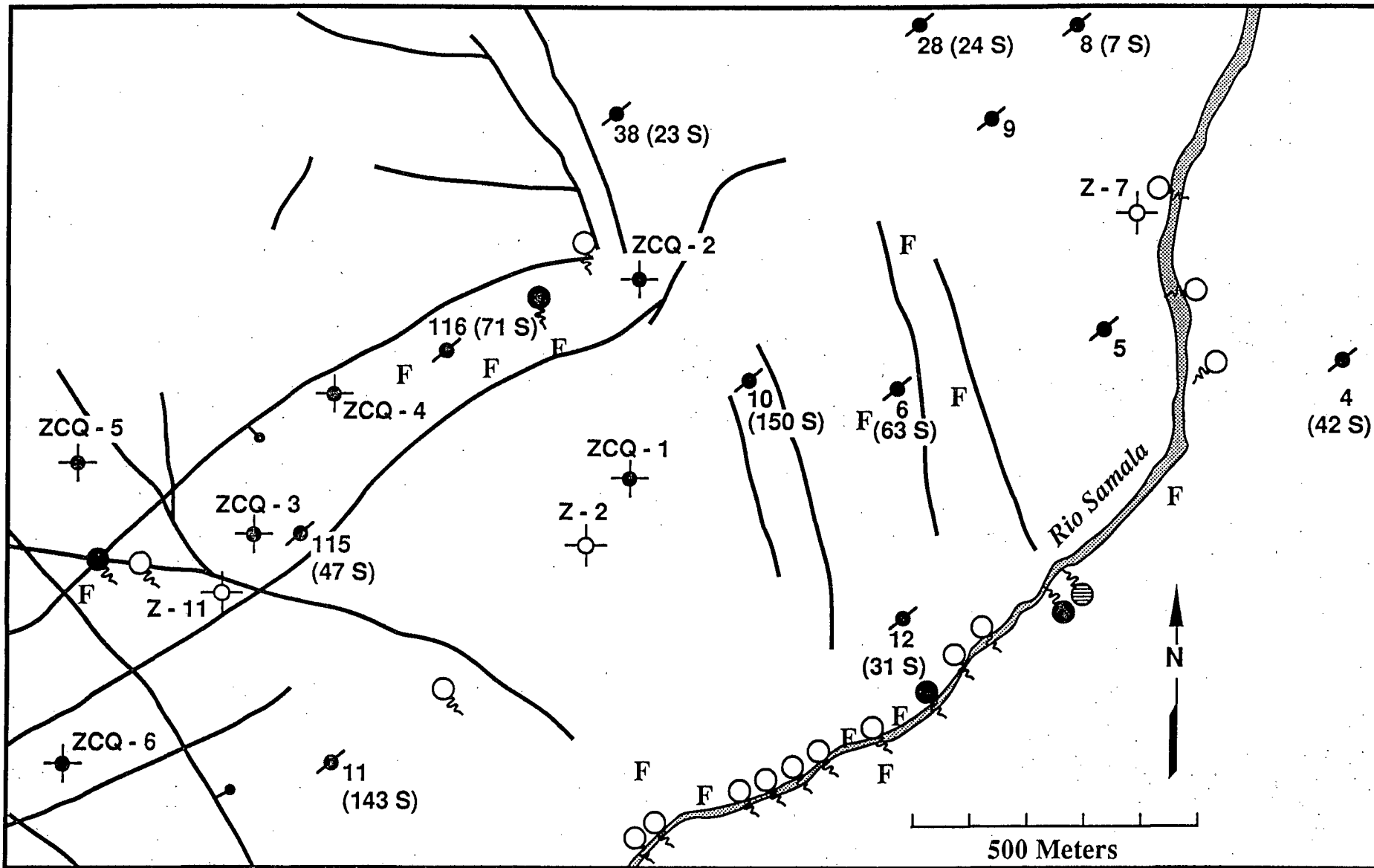


Figure 8



- Acid-sulfate spring
- Bicarbonate spring
- Sounding Location; conductive layer conductivity - thickness product in siemens (S)
- NaCl spring
- Production well
- 116 (71 S)
- F Fumarole
- Thermal gradient well
- Fault

Figure 9

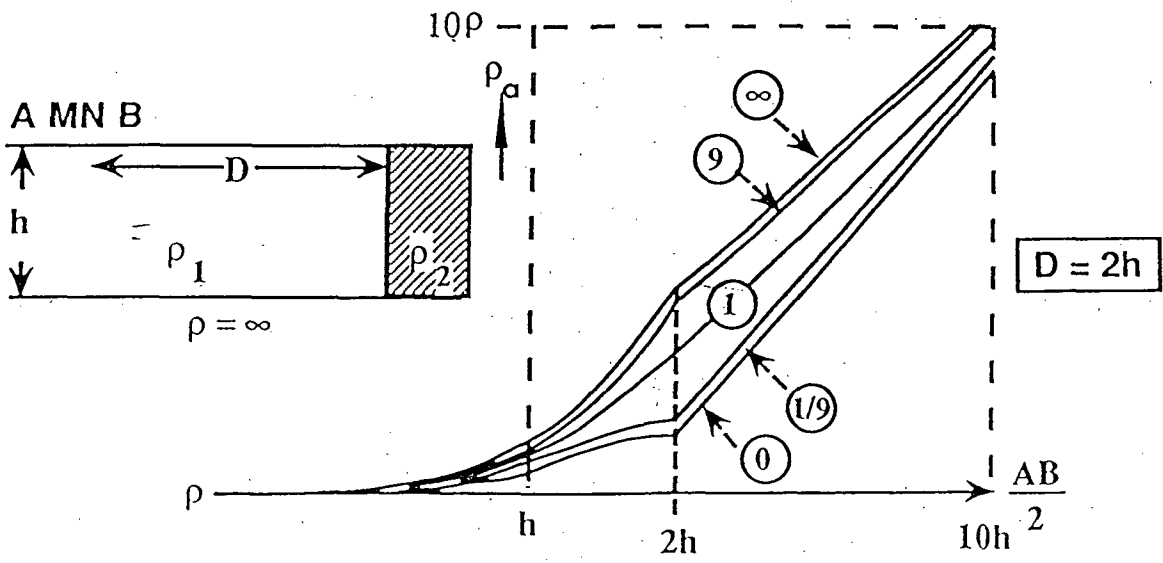
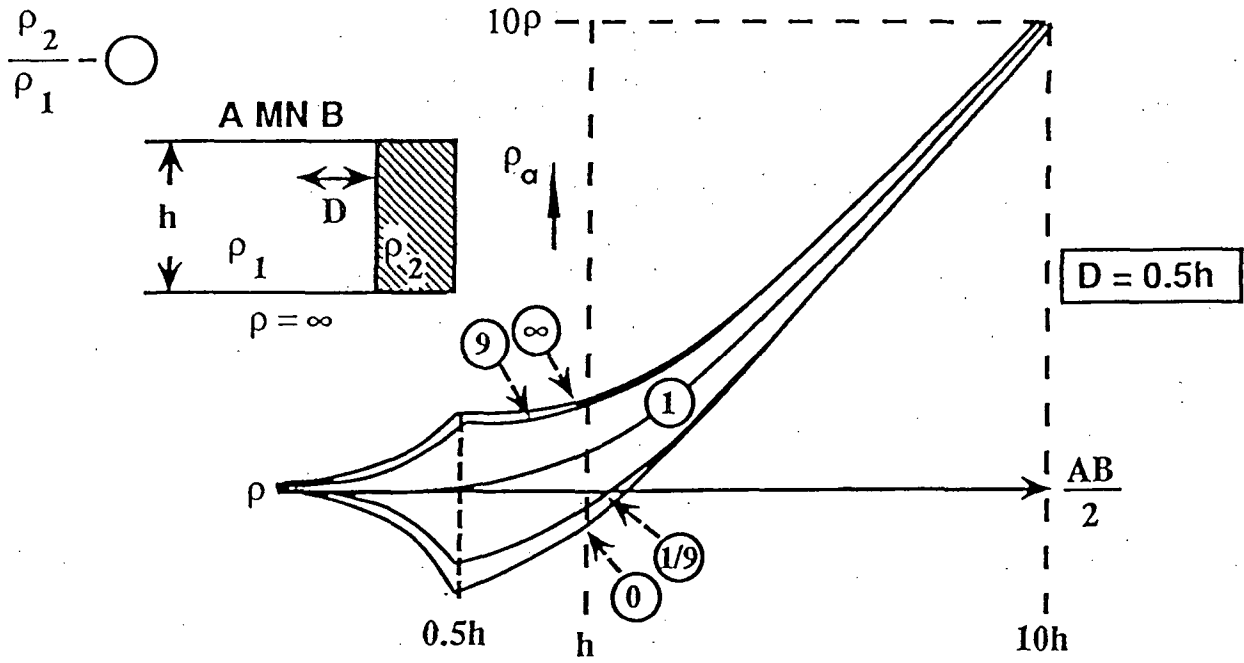


Figure 10. Illustration of the effect of a 2 dimensional structure on Schlumberger soundings (taken from Kunetz, 1966).

Figure 11

Observed and calculated apparent resistivity for sounding number 4. $AB/2$ value of 40 illustrates effects of lateral inhomogeneities (see text)

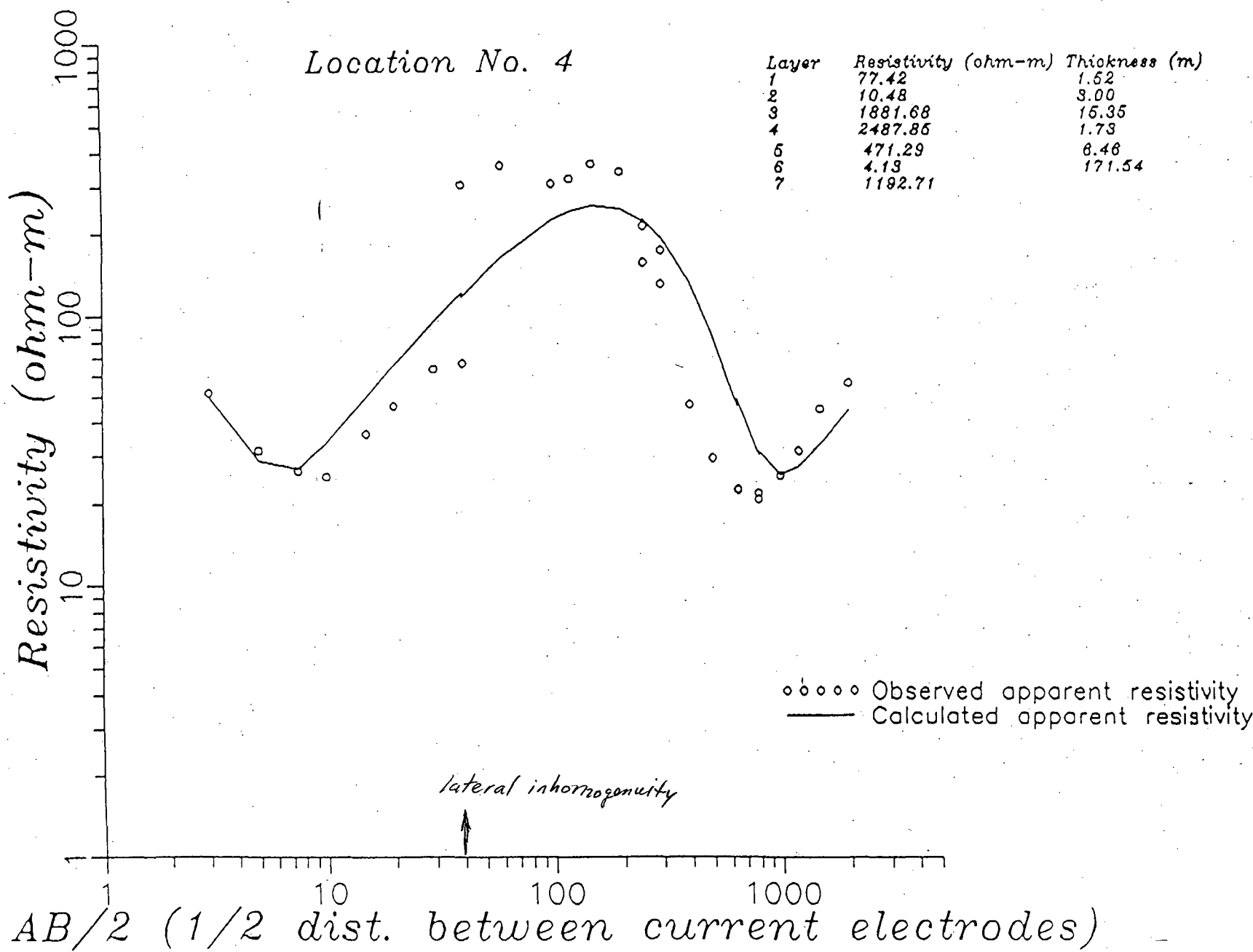
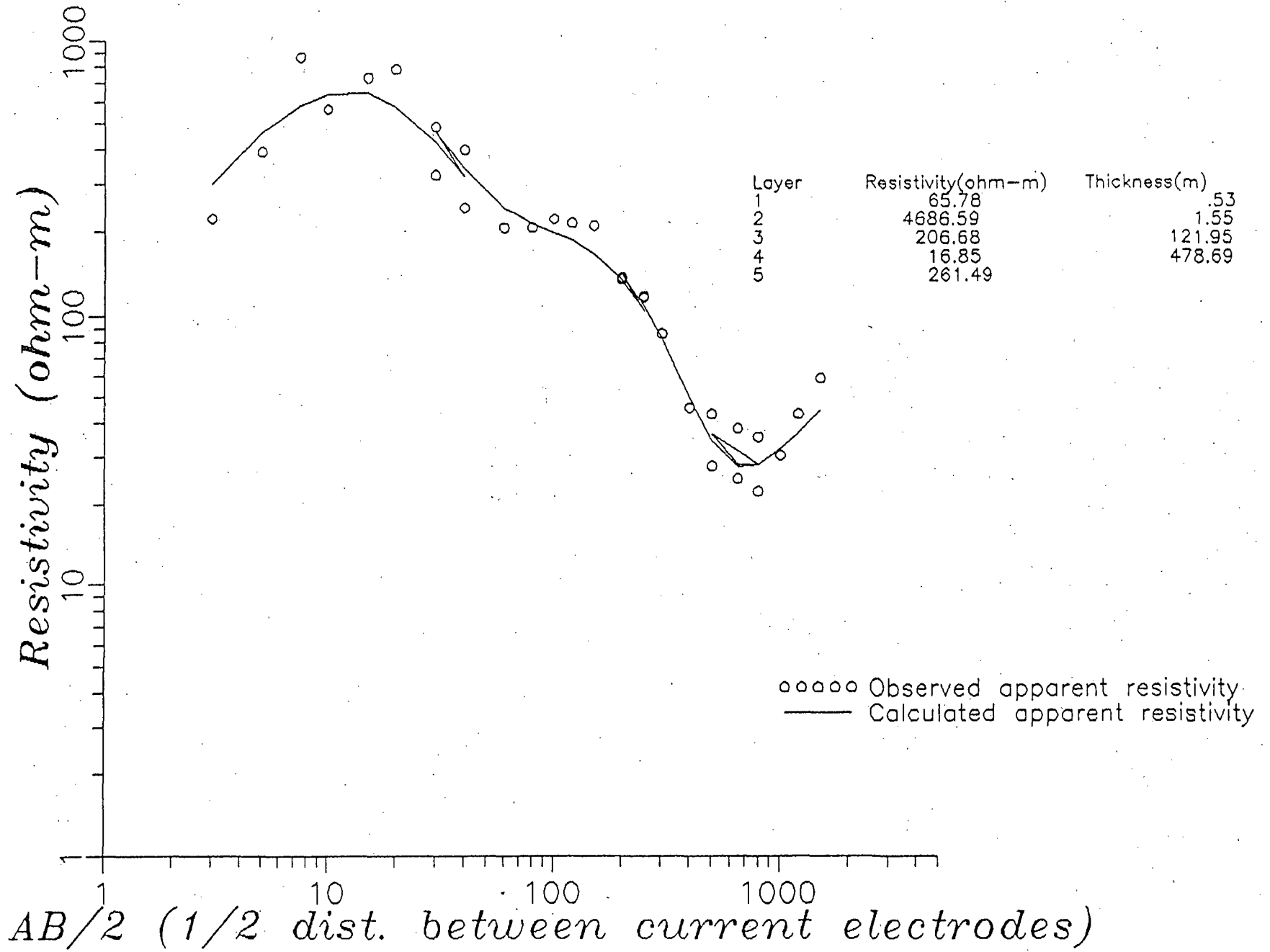


Figure 11

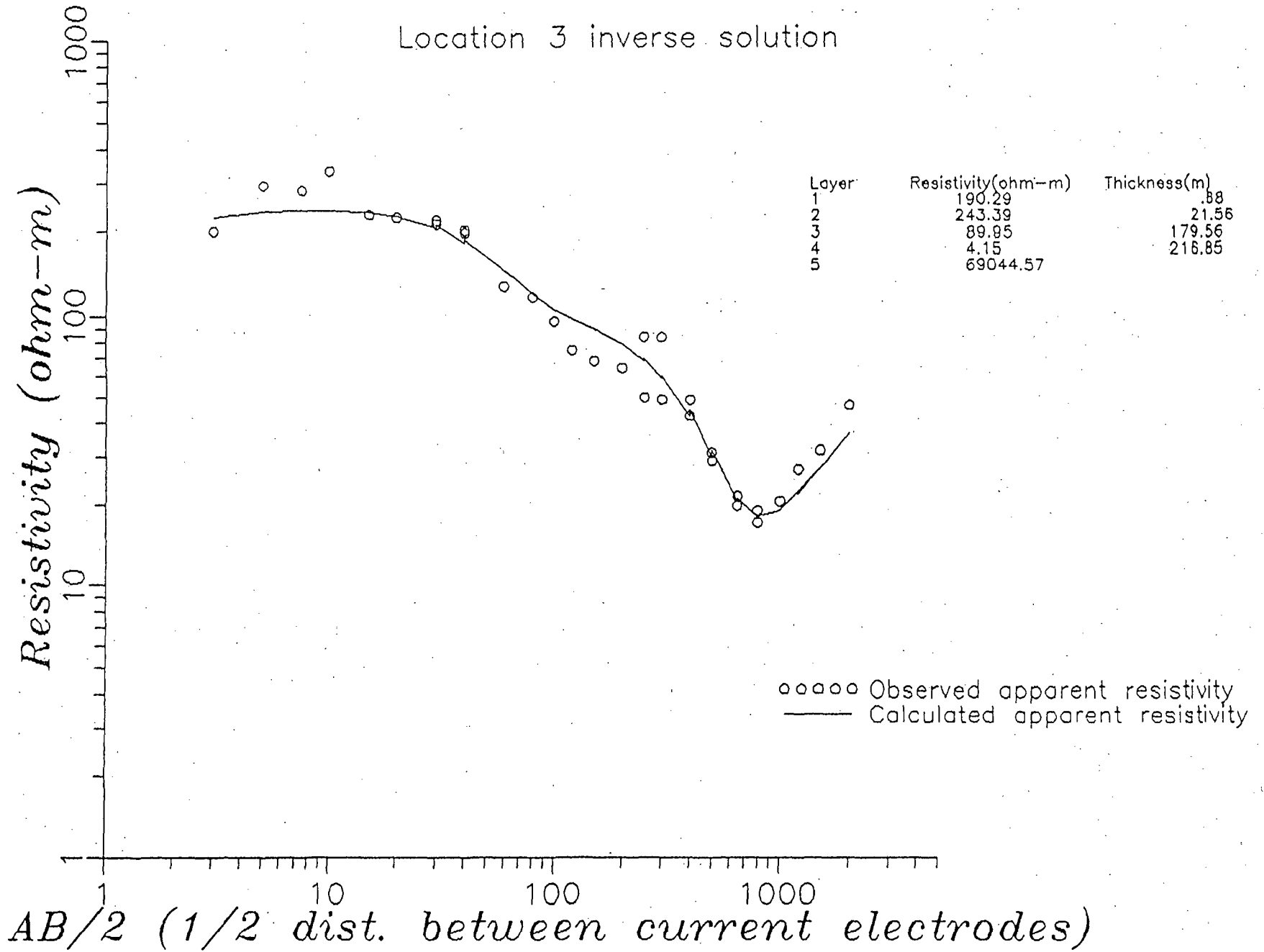
APPENDIX 1:

Selected Schlumberger soundings and interpretations.

Location 1 inverse solution

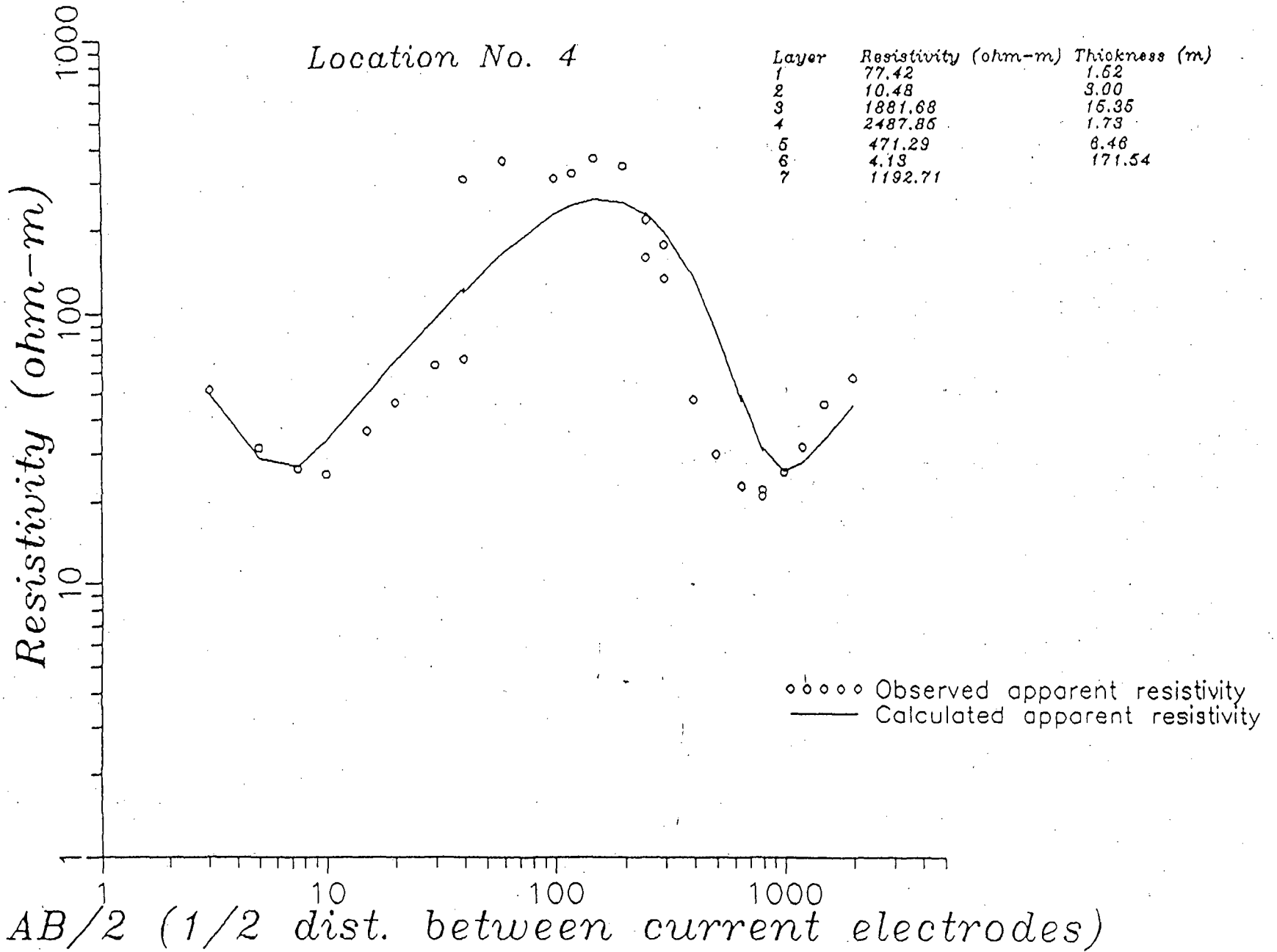


Location 3 inverse solution

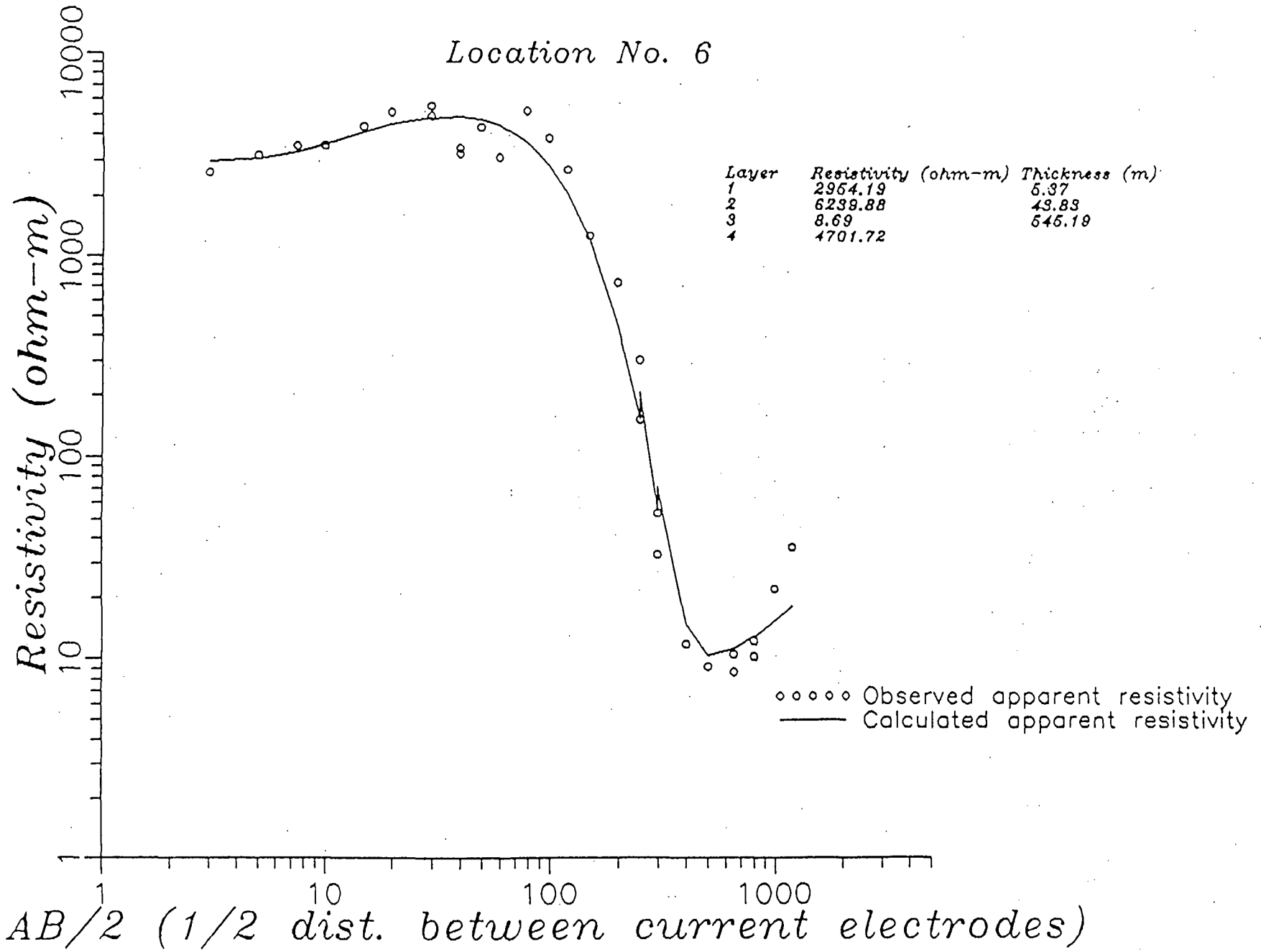


Location No. 4

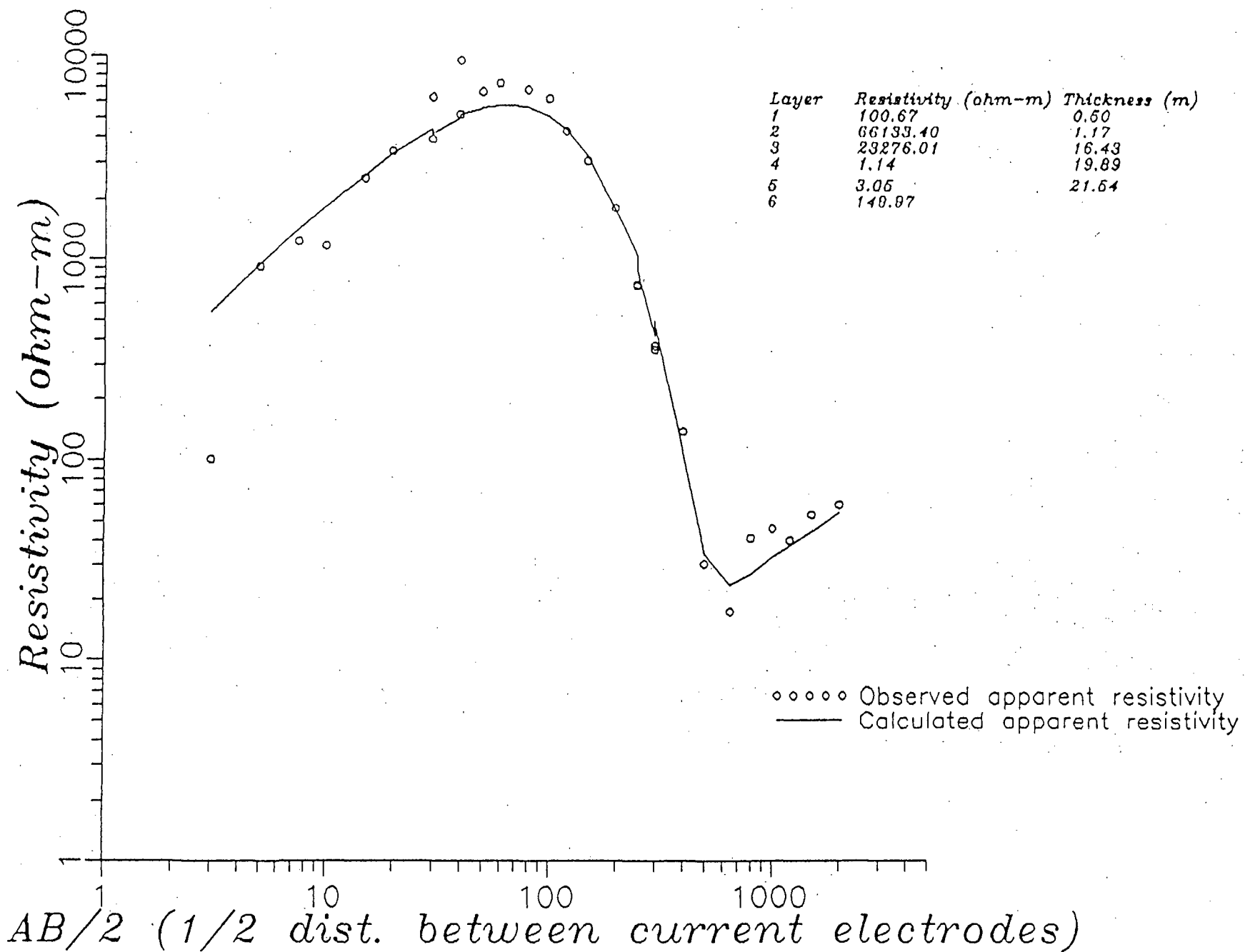
Layer	Resistivity (ohm-m)	Thickness (m)
1	77.42	1.52
2	10.48	3.00
3	1881.68	16.35
4	2487.85	1.73
5	471.29	8.46
6	4.13	171.54
7	1192.71	



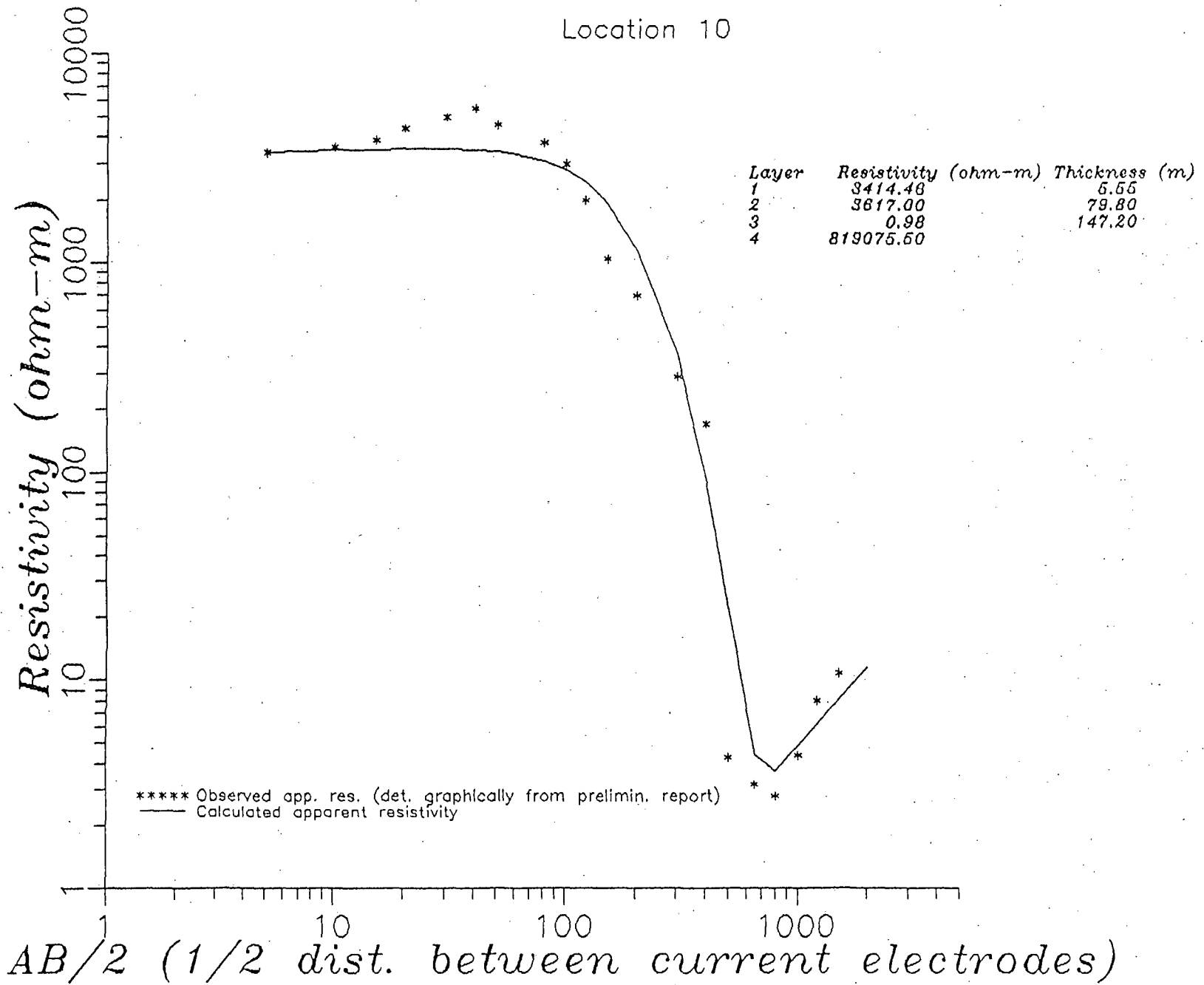
Location No. 6



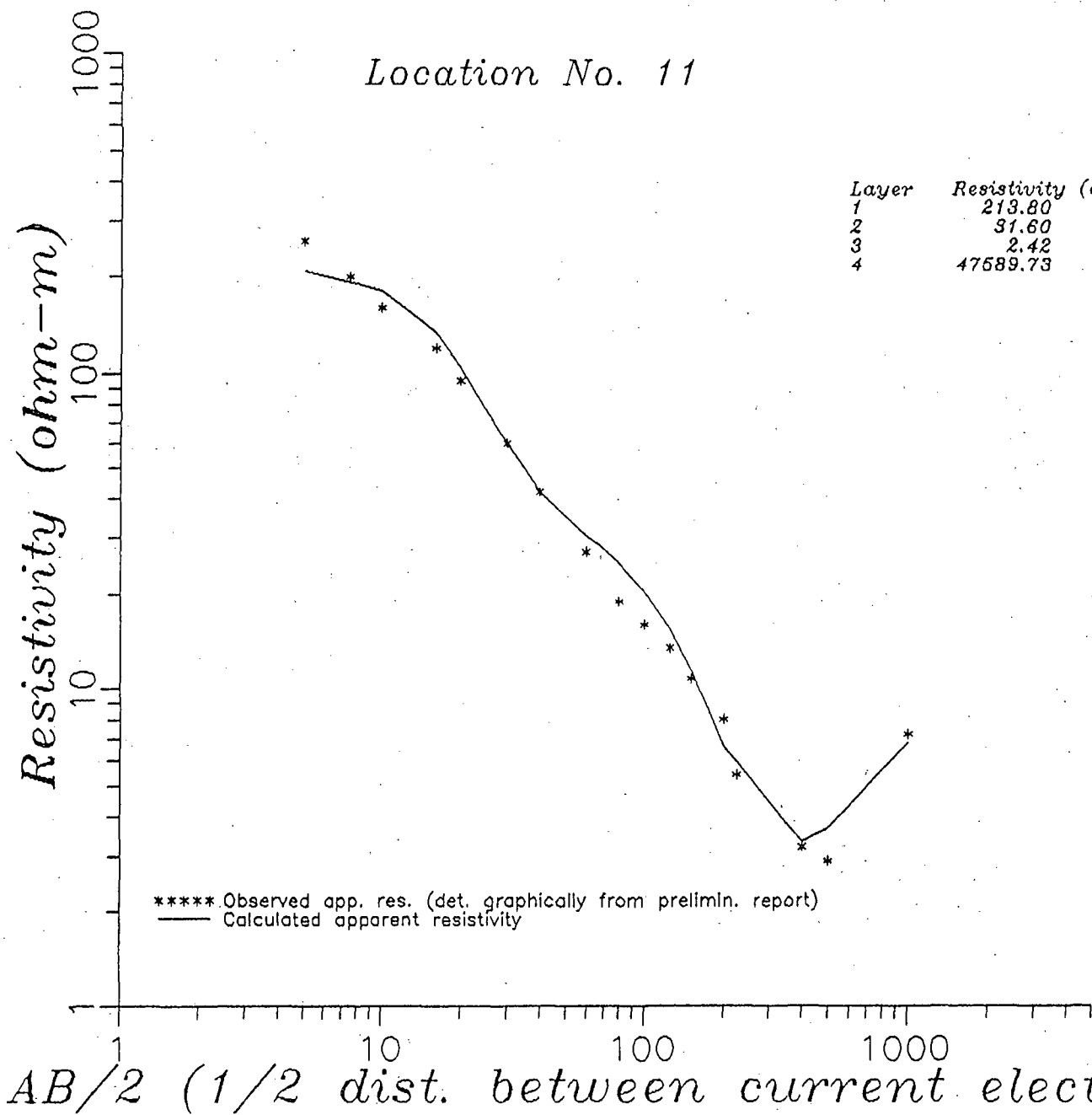
Location No. 8



Location 10

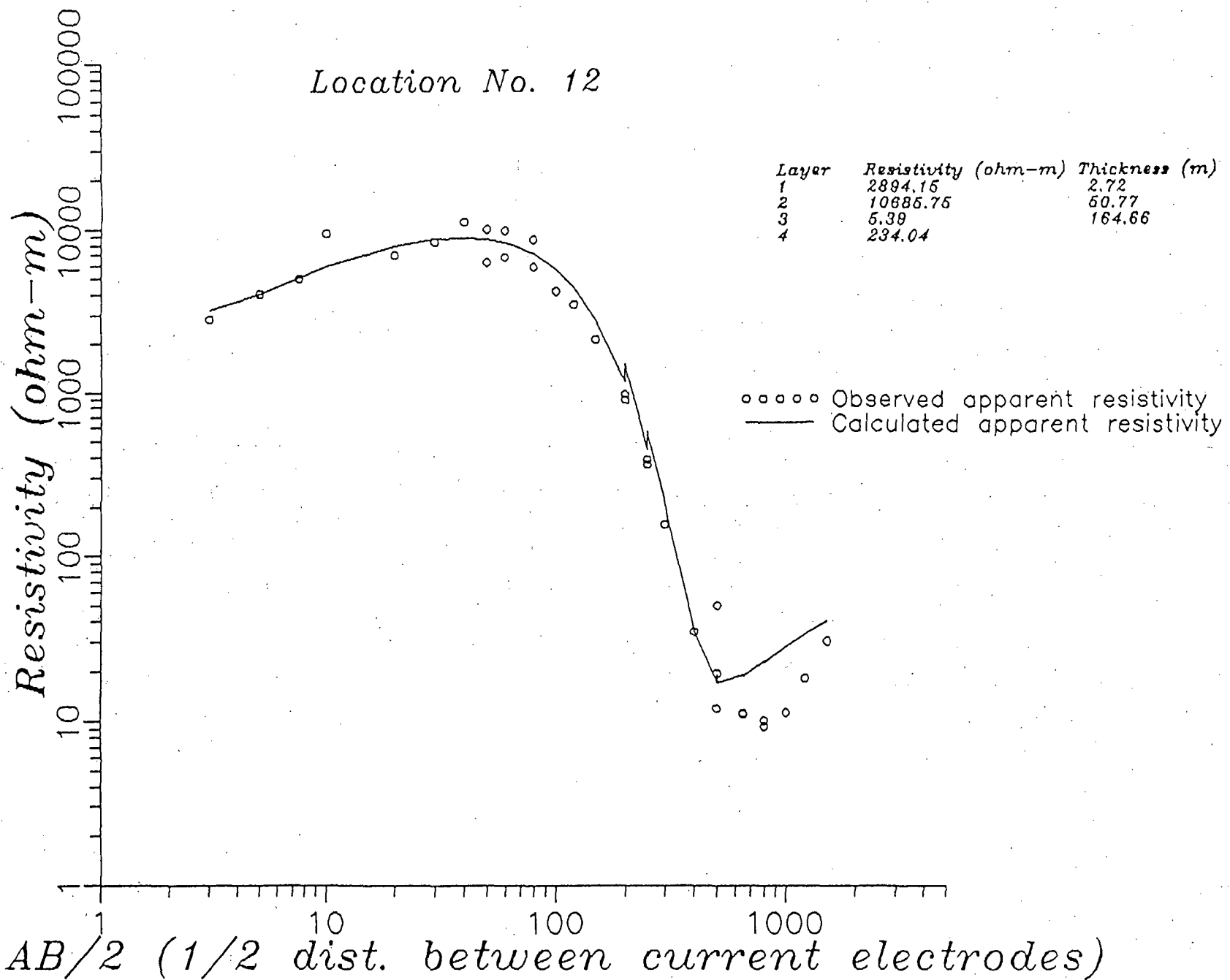


Location No. 11

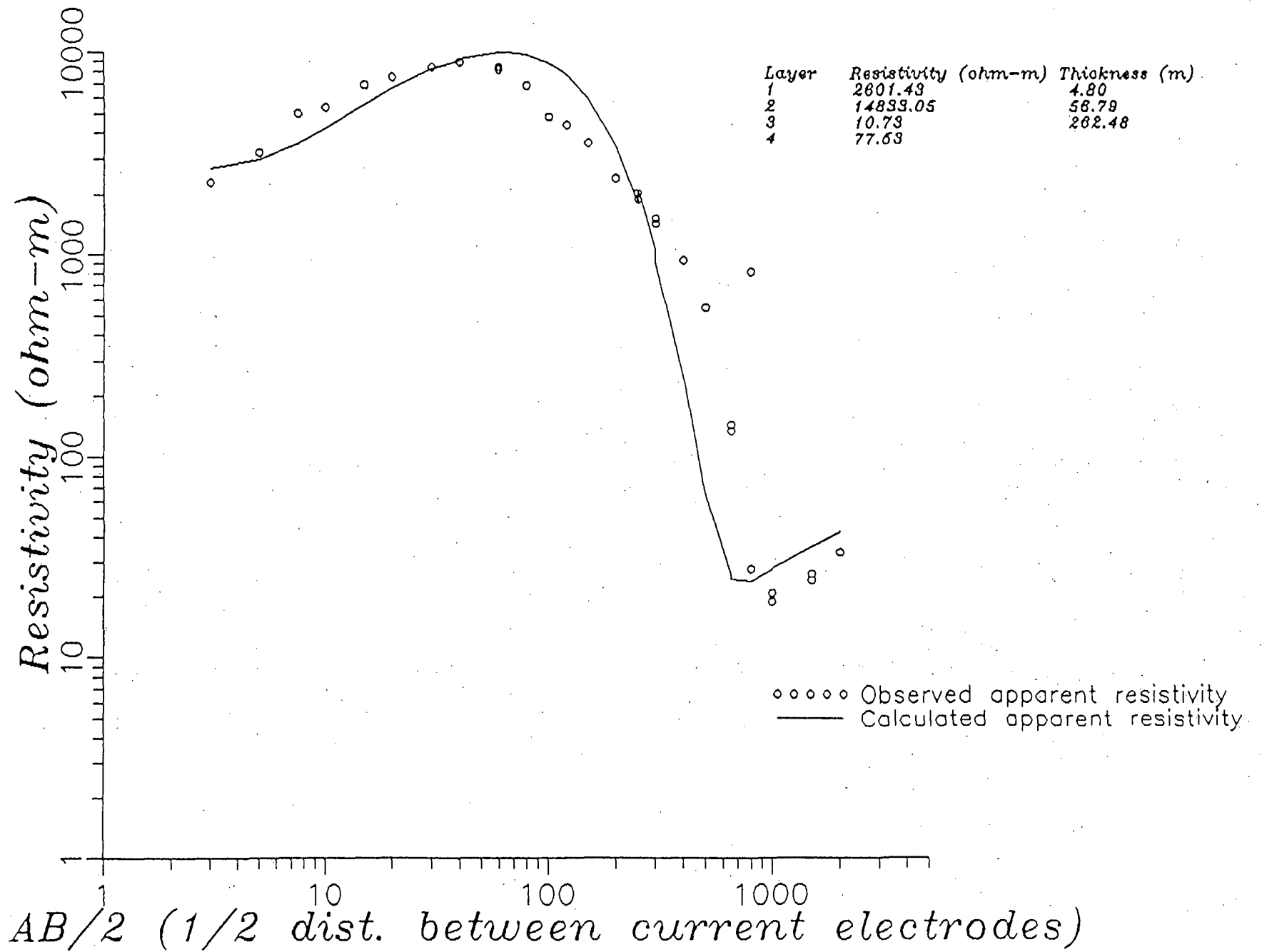


Layer	Resistivity (ohm-m)	Thickness (m)
1	213.80	9.01
2	31.60	58.41
3	2.42	346.33
4	47589.73	

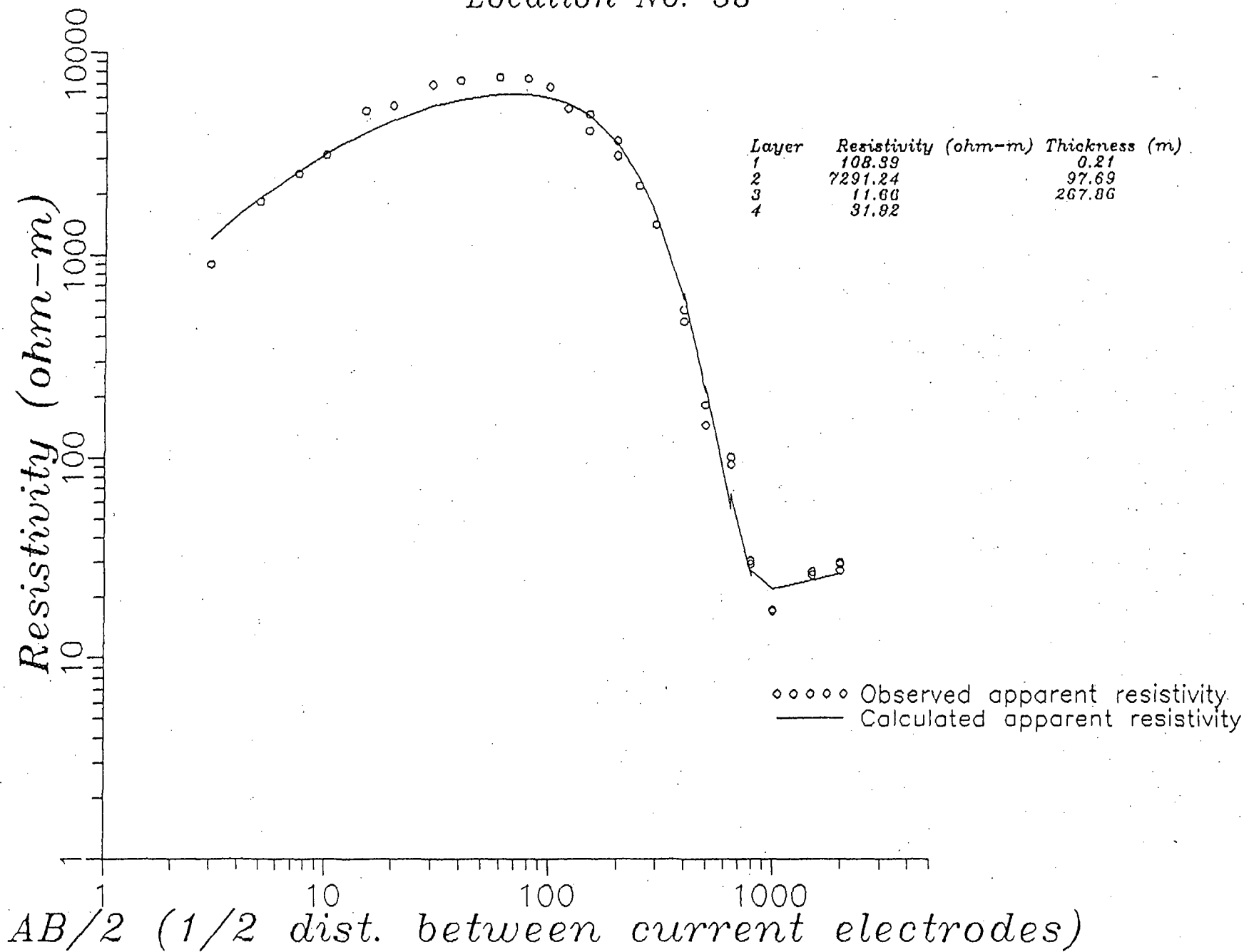
Location No. 12



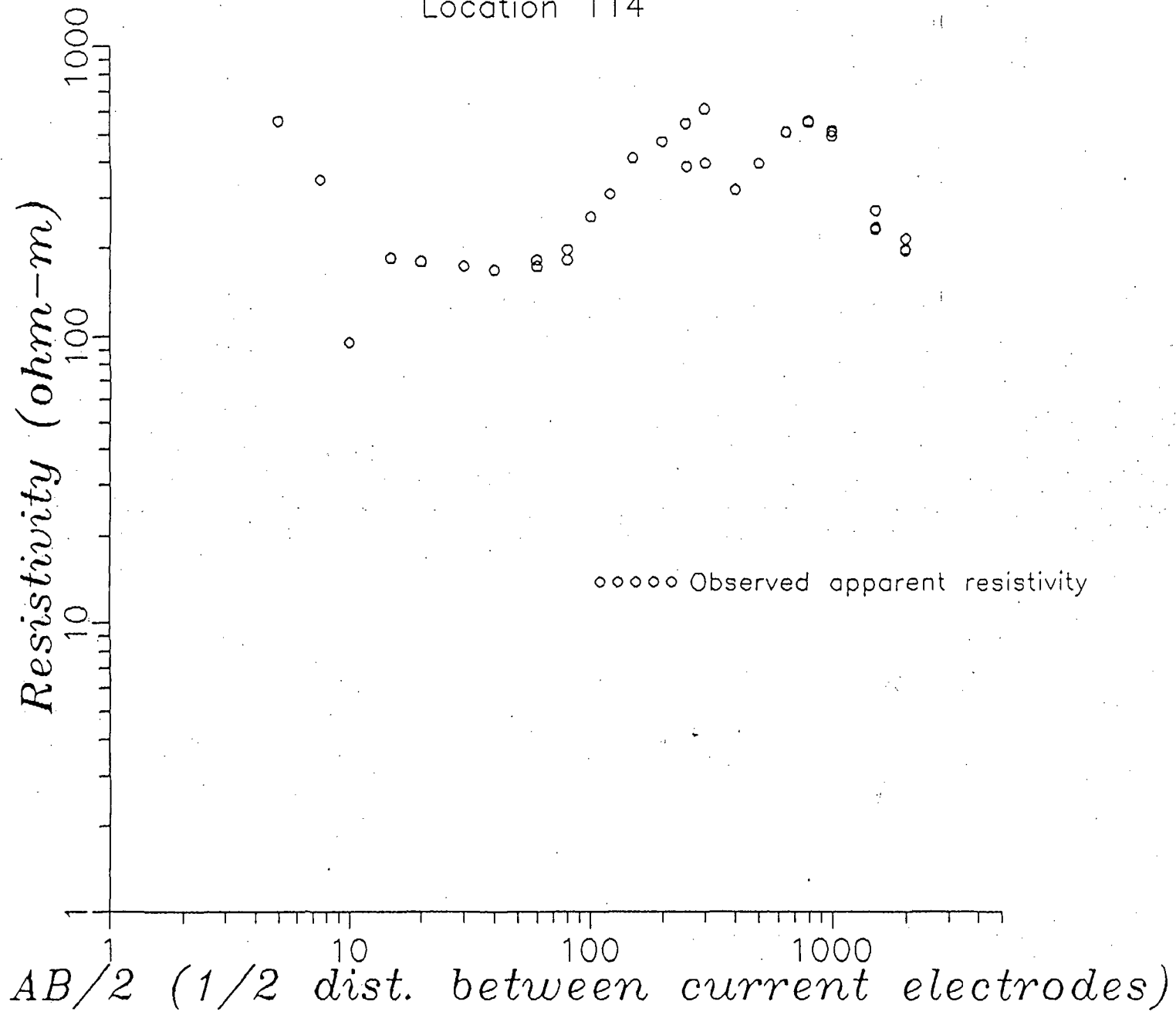
Location No. 28



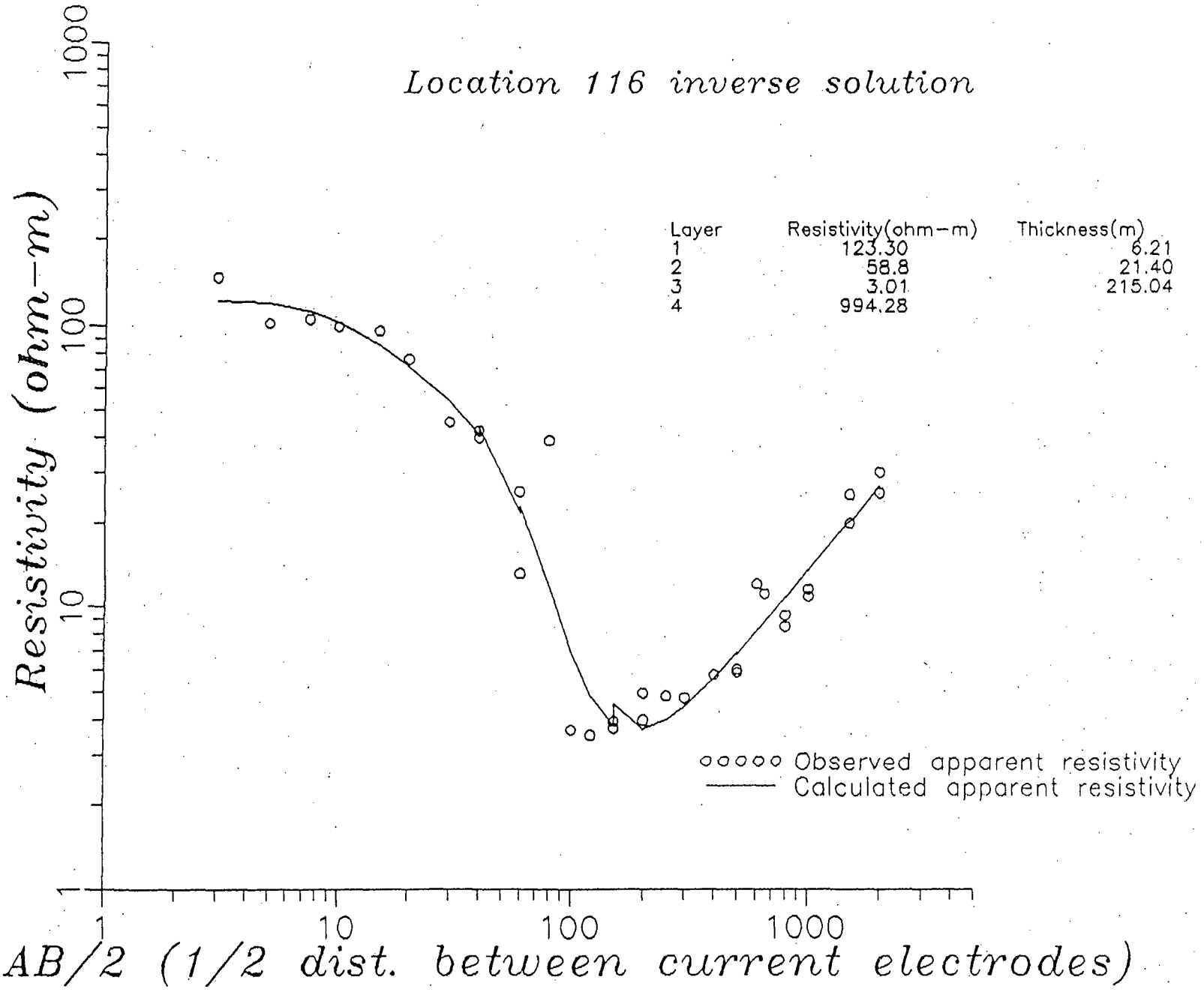
Location No. 38



Location 114

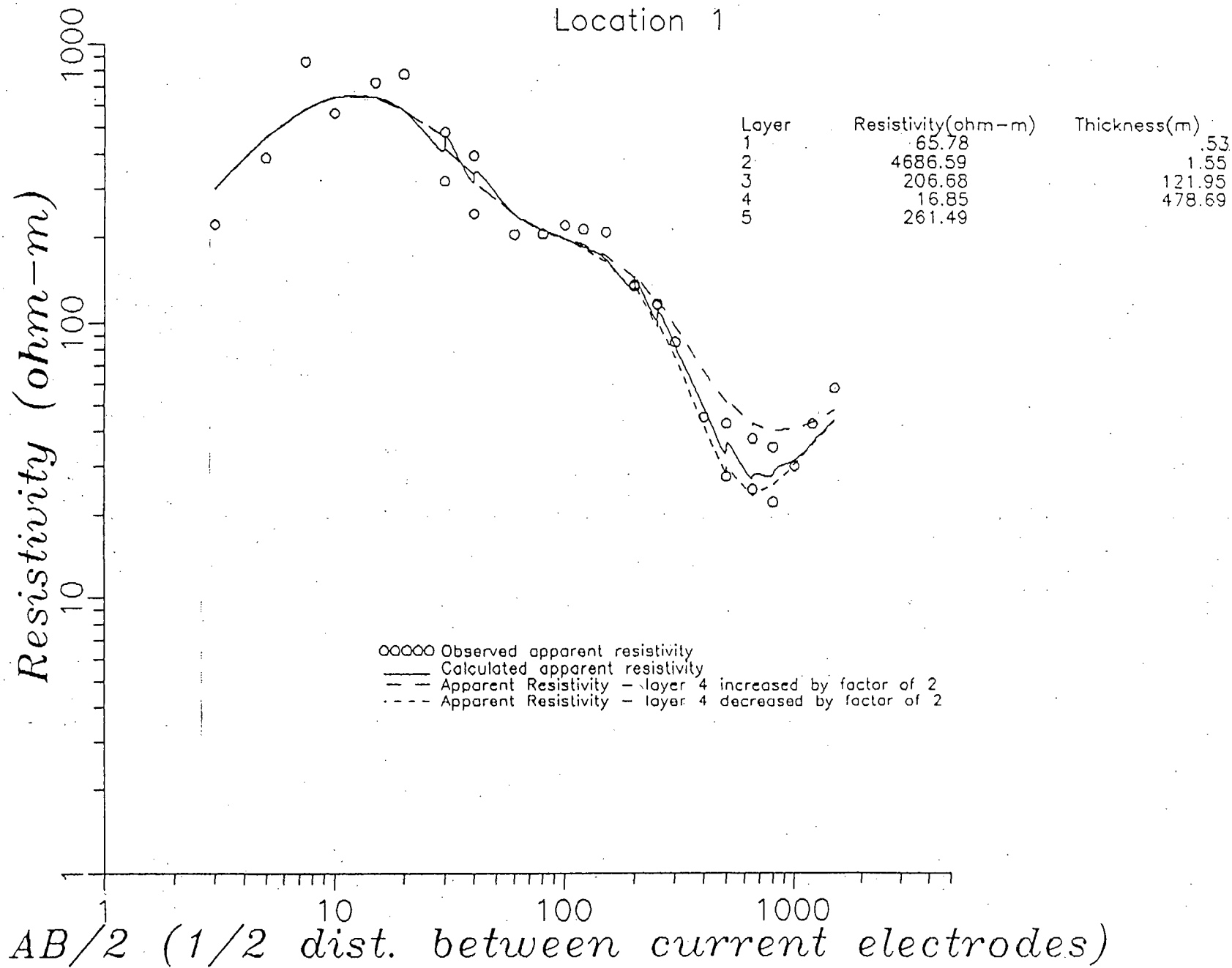


Location 116 inverse solution

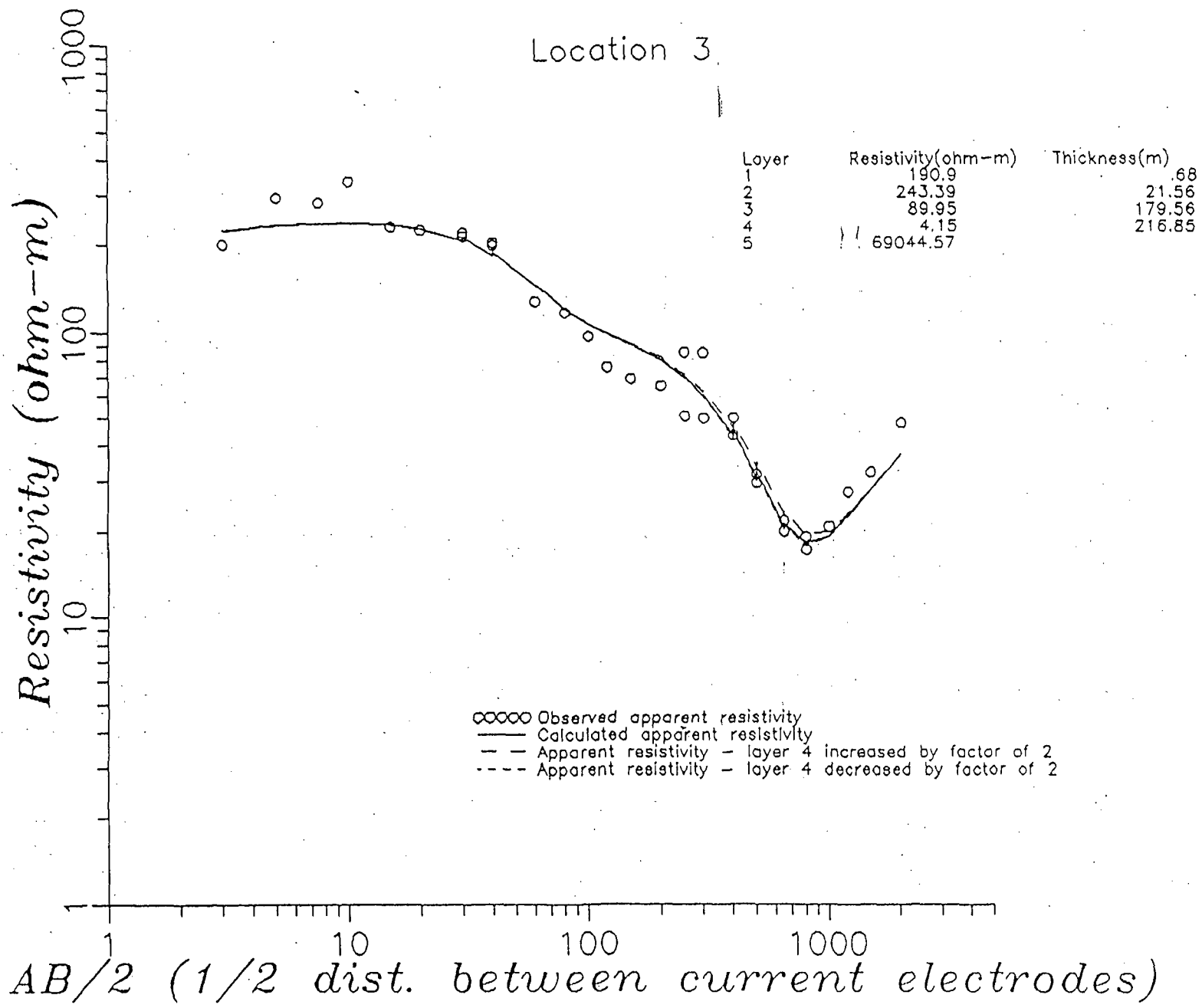


Appendix 2
Sensitivity Analysis

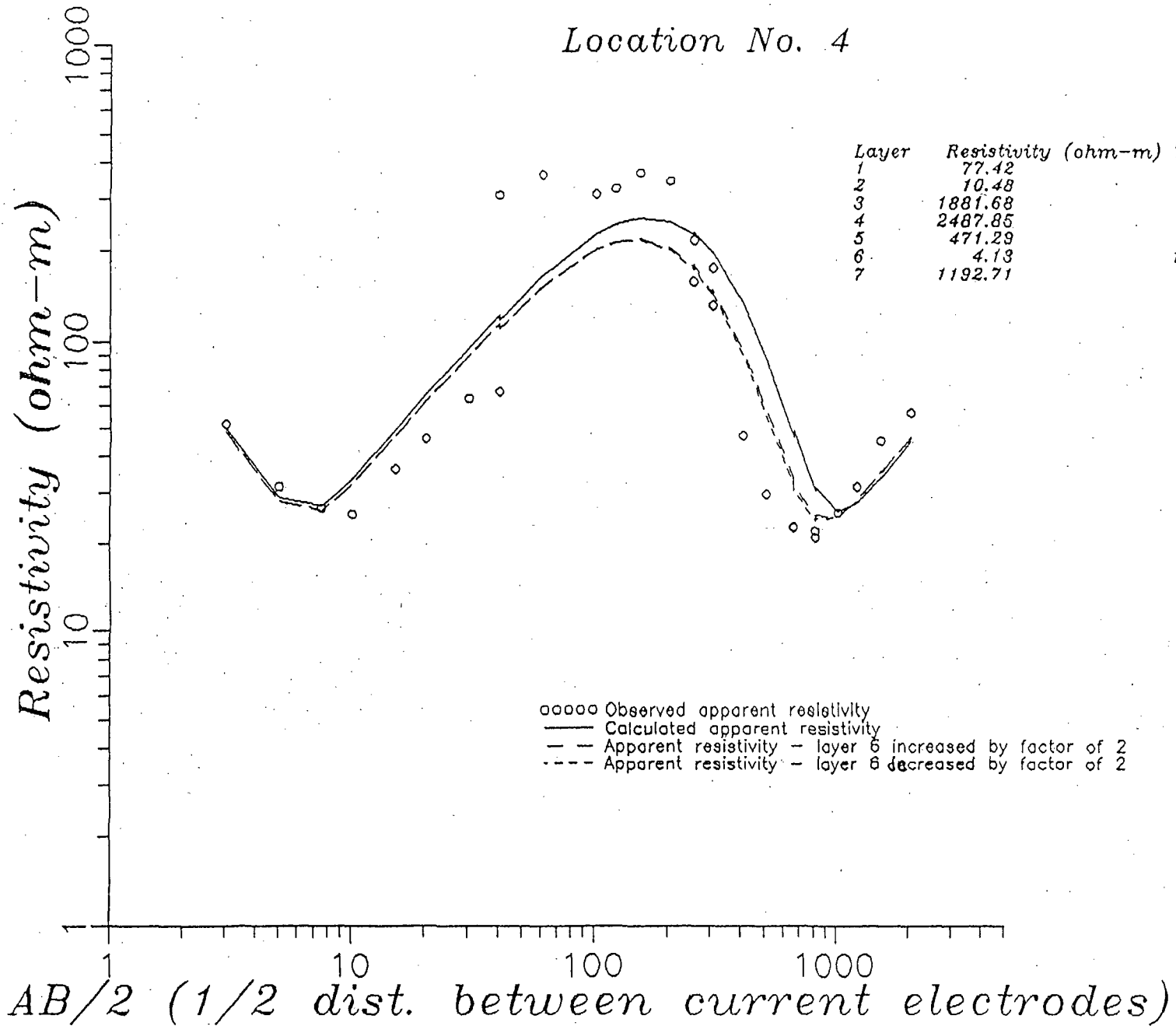
Location 1



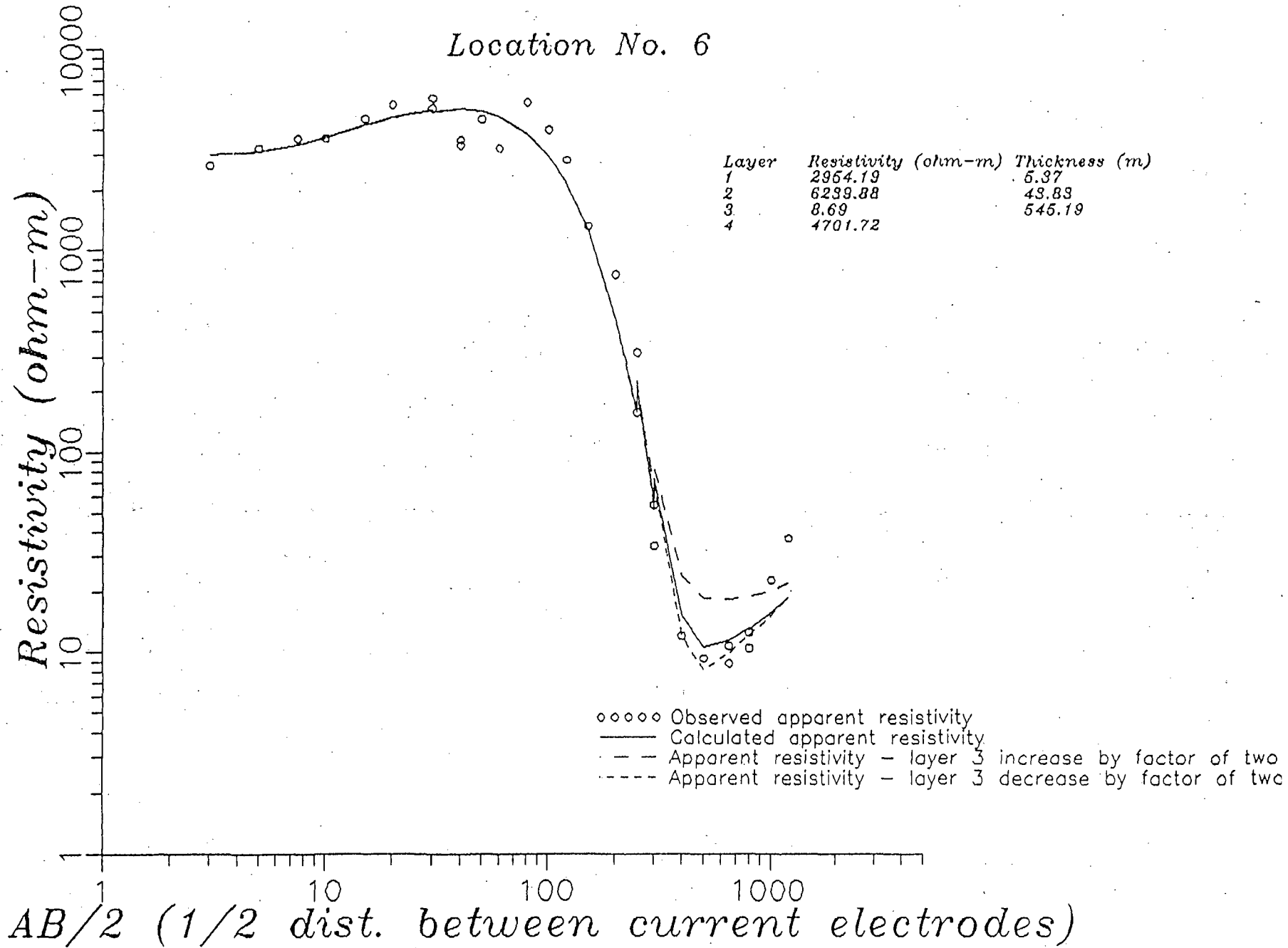
Location 3



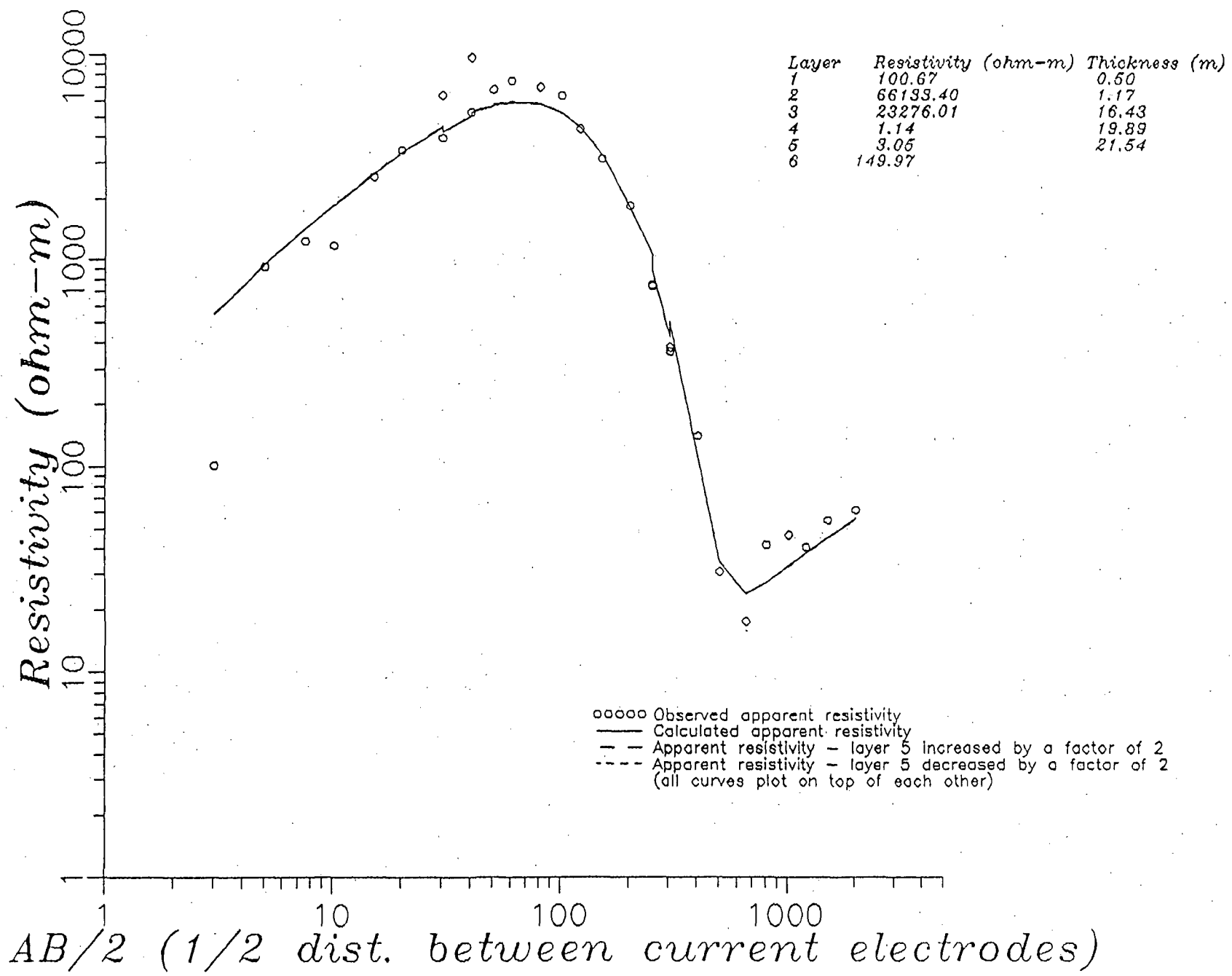
Location No. 4



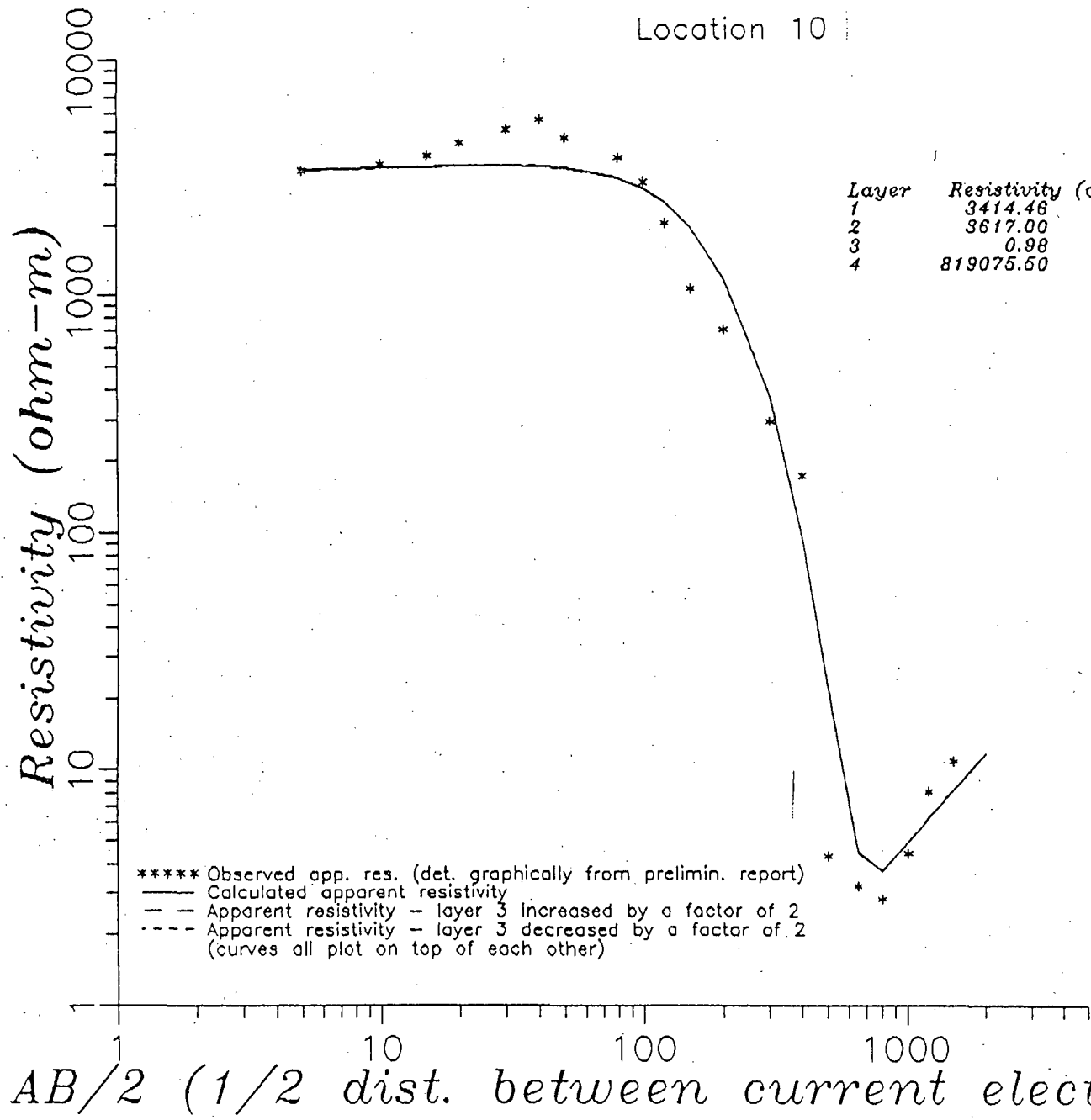
Location No. 6



Location No. 8

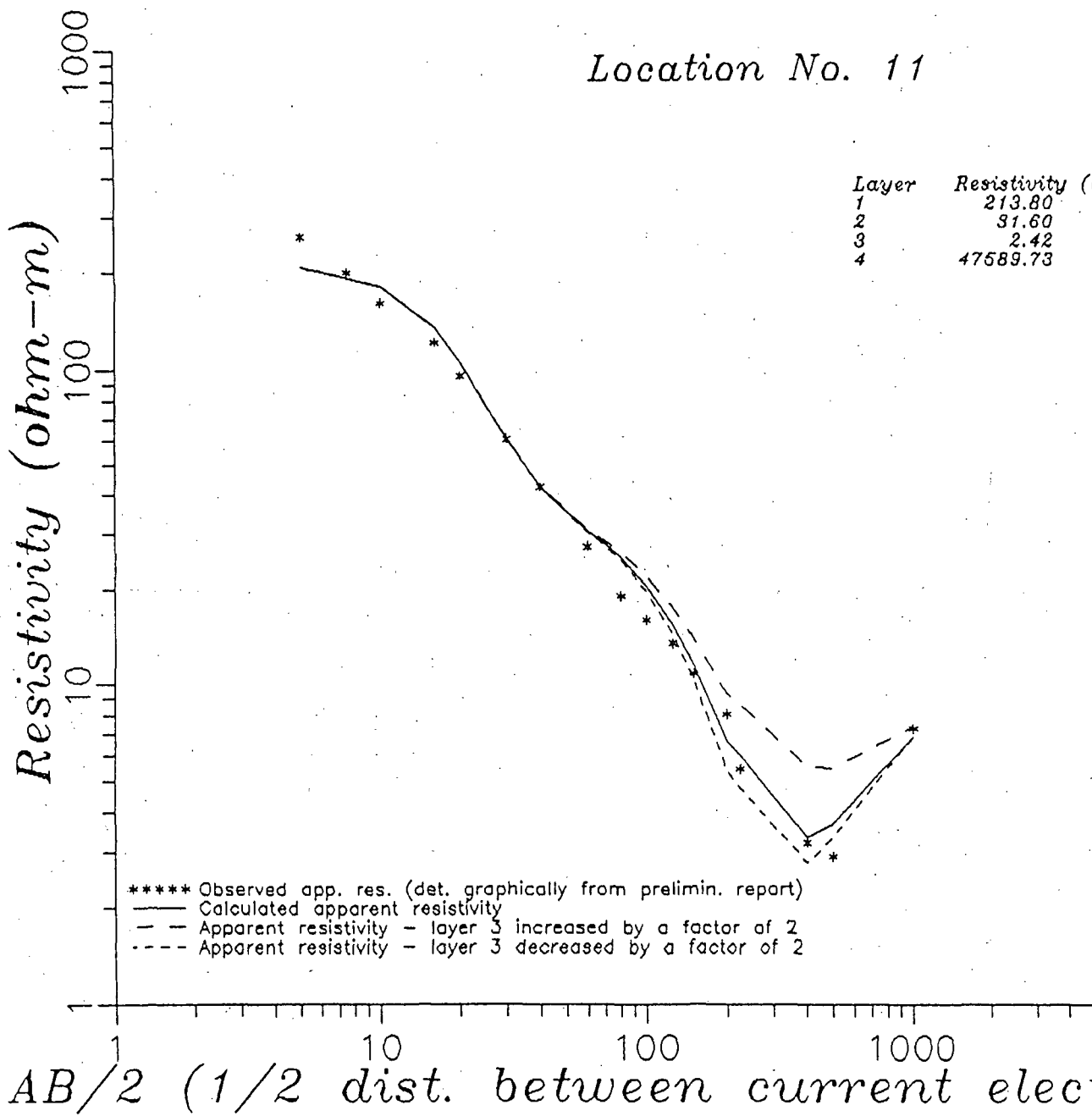


Location 10



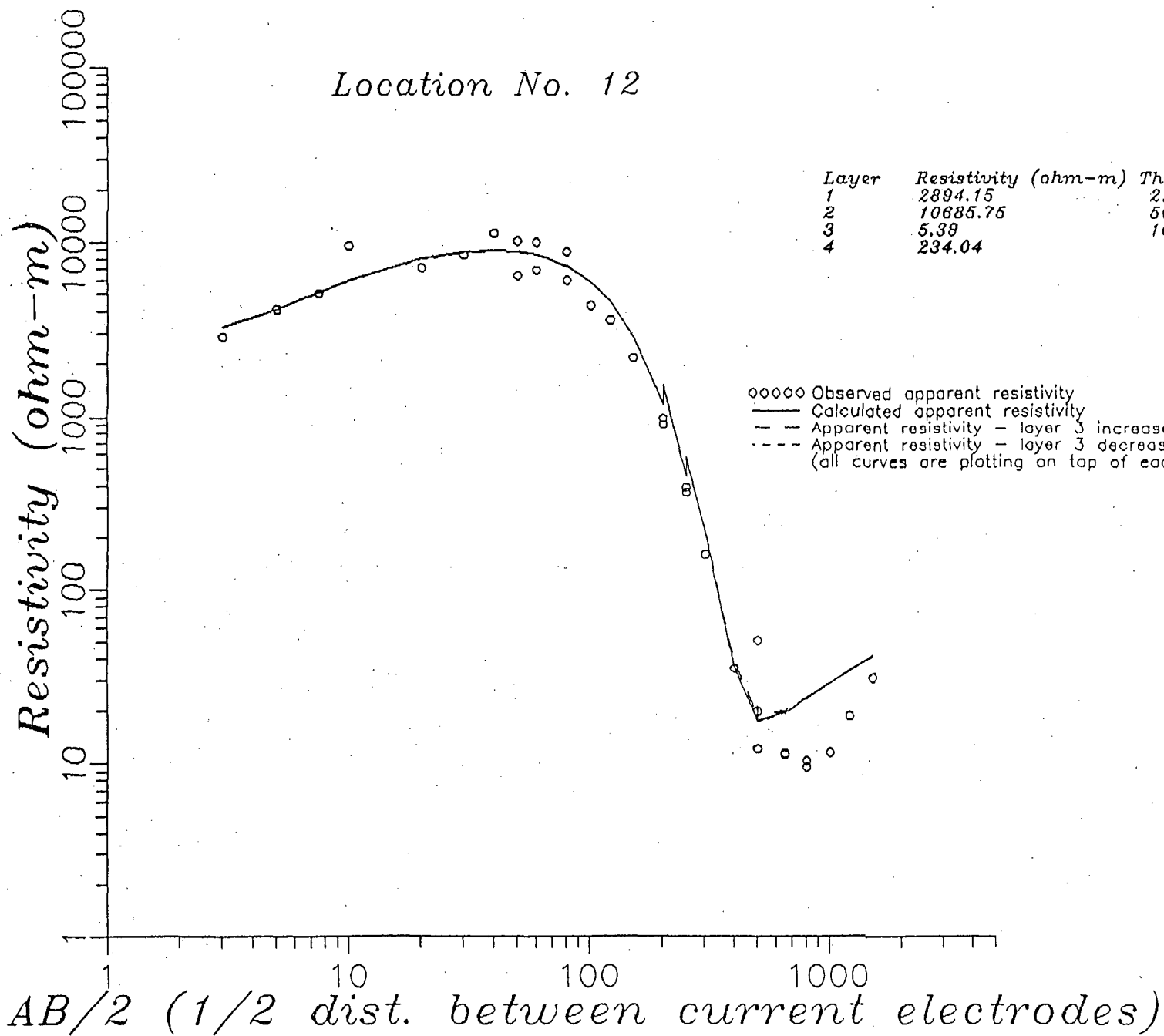
Layer	Resistivity (ohm-m)	Thickness (m)
1	3414.48	5.66
2	3617.00	79.80
3	0.98	147.20
4	819075.50	

Location No. 11

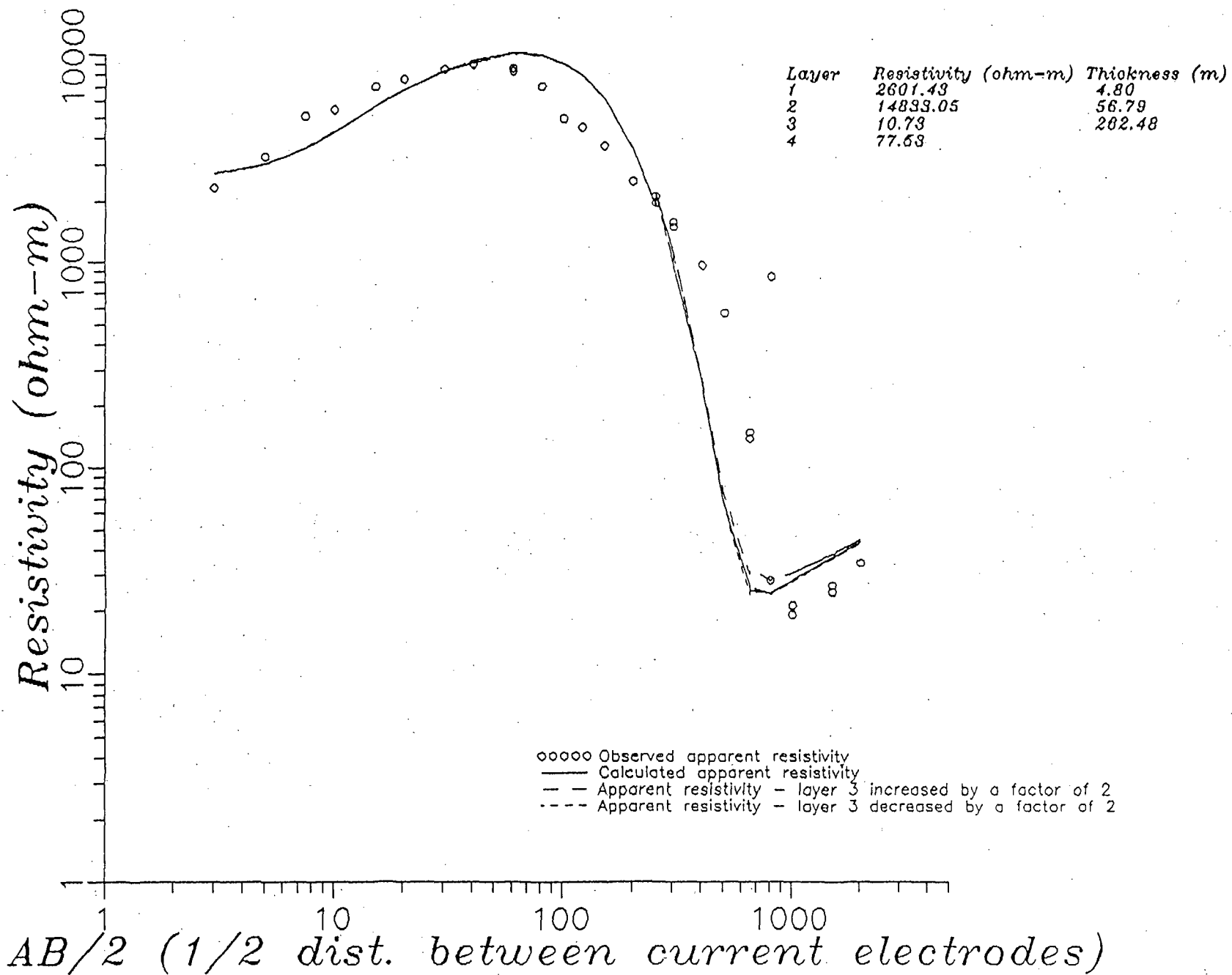


Layer	Resistivity (ohm-m)	Thickness (m)
1	213.80	9.01
2	31.60	58.41
3	2.42	346.33
4	47589.73	

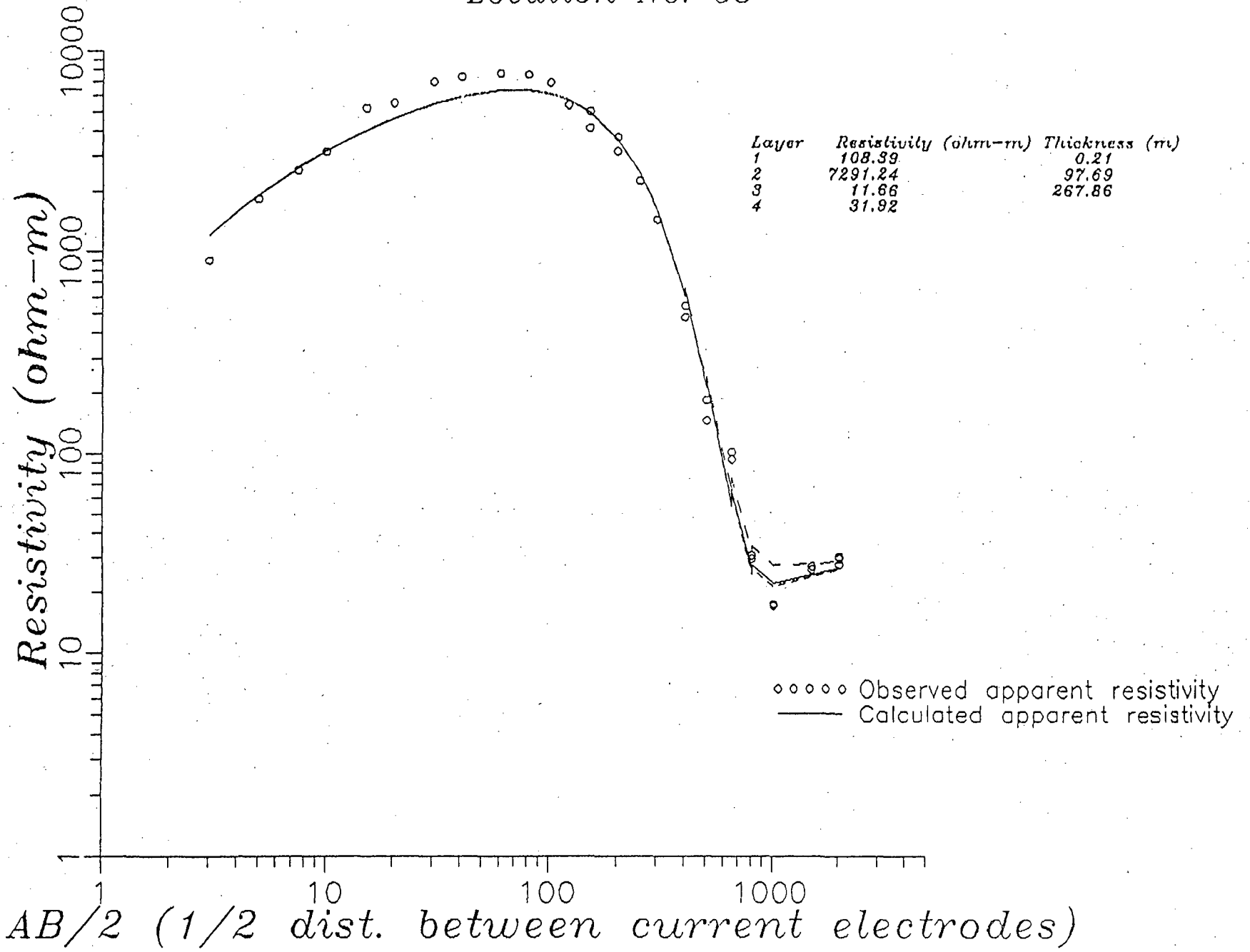
Location No. 12



Location No. 28

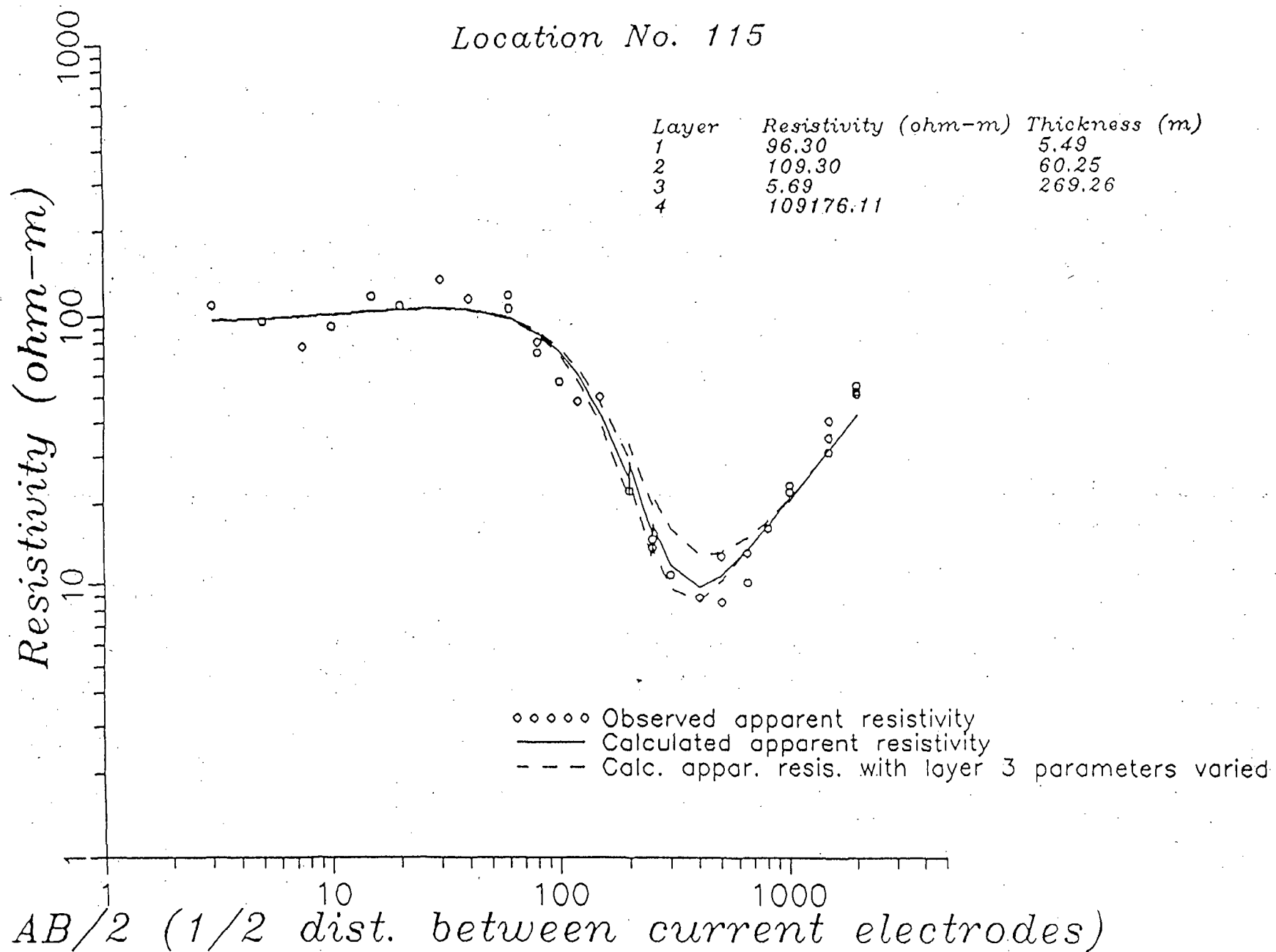


Location No. 38

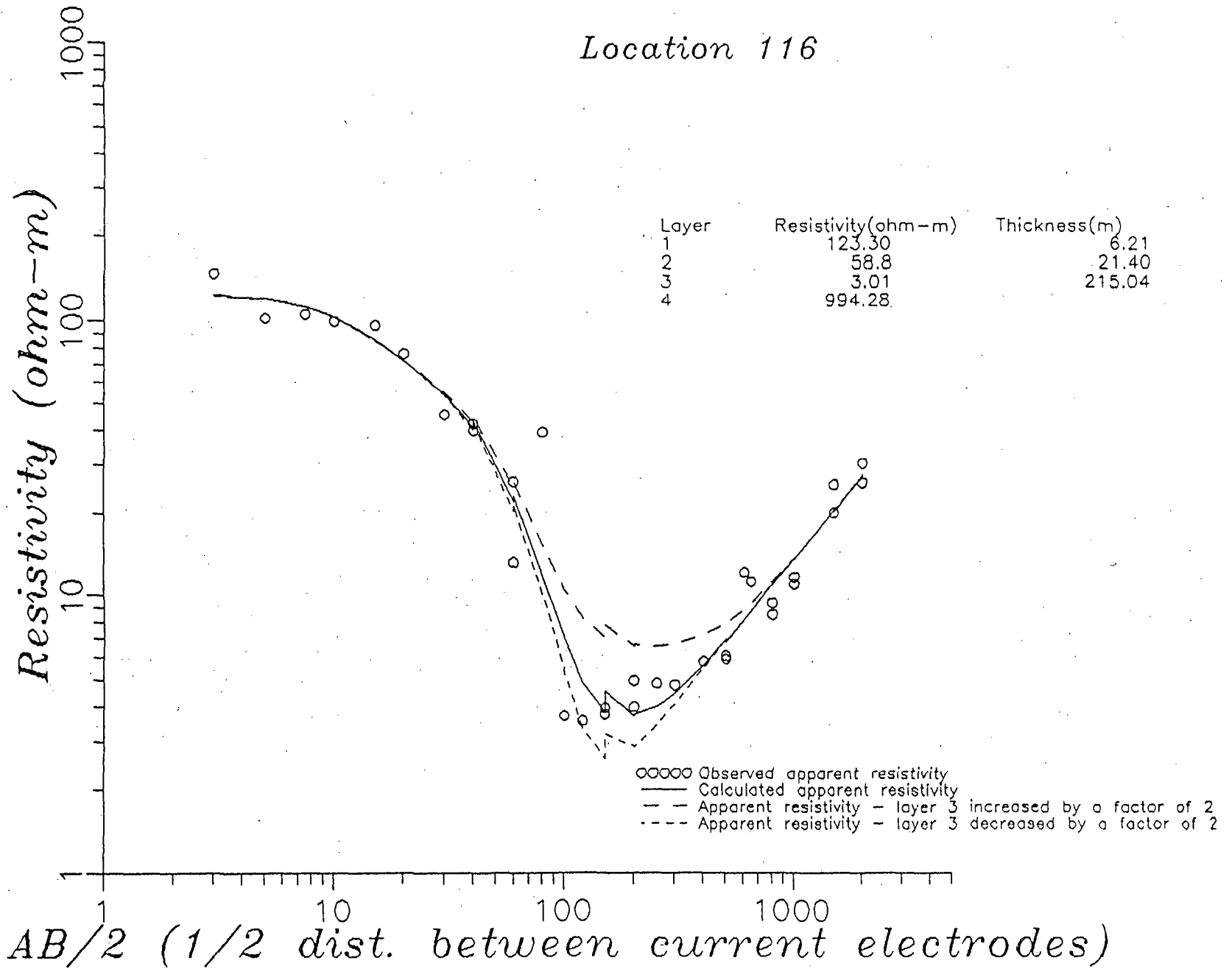


Location No. 115

Layer	Resistivity (ohm-m)	Thickness (m)
1	96.30	5.49
2	109.30	60.25
3	5.69	269.26
4	109176.11	



Location 116



APPENDIX 3

Percent Standard Deviations and Correlation Matrices

Location 1
Percent Standard Deviation

R1	10200
R2	5940
R3	60
R4	275
R5	161
T1	10200
T2	5940
T3	94
T4	374

Correlation Matrix

	R1	R2	R3	R4	R5	T1	T2	T3	T4
R1	1.000								
R2	0.230	1.000							
R3	-0.509	0.185	1.000						
R4	0.037	0.160	0.445	1.000					
R5	-0.093	0.032	0.293	0.759	1.000				
T1	1.000	0.251	-0.496	-0.053	-0.081	1.000			
T2	-0.230	-1.000	-0.216	-0.211	-0.073	-0.247	1.000		
T3	0.118	-0.093	-0.682	-0.892	-0.598	0.117	0.096	1.000	
T4	-0.013	0.105	0.395	0.956	-0.912	-0.012	-0.106	-0.812	1

Location 3
Percent Standard Deviation

R1	106
R2	44
R3	62
R4	2660
R5	28
T1	143
T2	107
T3	221
T4	2570

Correlation Matrix

	R1	R2	R3	R4	R5	T1	T2	T3	T4
R1	1.000								
R2	0.578	1.000							
R3	0.192	-0.423	1.000						
R4	0.037	0.195	0.700	1.000					
R5	-0.043	-0.009	-0.014	0.064	1.000				
T1	0.974	0.686	0.238	0.062	-0.050	1.000			
T2	0.851	-0.837	-0.513	-0.242	0.068	-0.912	1.000		
T3	0.047	-0.206	-0.776	-0.985	-0.005	-0.073	0.269	1.000	
T4	0.037	0.195	0.699	1.000	0.060	0.061	-0.242	-0.985	1.000

Location 6

Percent Standard Deviation

R1	82
R2	161
R3	137
R4	115
T1	241
T2	328
T3	198

Correletion Matrix

	R1	R2	R3	R4	T1	T2	T3
R1	1						
R2	0.308	1					
R3	0.388	0.365	1				
R4	-0.376	-0.383	-0.865	1			
T1	0.678	0.779	0.465	-0.452	1		
T2	-0.439	-0.935	-0.460	0.452	-0.926	1	
T3	0.402	0.359	0.956	-0.937	0.478	-0.459	1

Location 10
Percent Standard Deviation

R1	104
R2	104
R3	1370
R4	190
T1	1590
T2	1590
T3	1360

Correlation Matrix

	R1	R2	R3	R4	T1	T2	T3
R1	1						
R2	0.198	1					
R3	-0.376	-0.172	1				
R4	-0.185	-0.226	0.15	1			
T1	0.752	0.521	-0.463	-0.256	1		
T2	-0.729	-0.562	0.449	0.272	-0.998	1	
T3	-0.365	-0.15	0.991	0.0242	-0.443	0.427	1

Location 11
Percent Standard Deviation

R1	28.5
R2	44.1
R3	125
R4	53
T1	36.8
T2	54.4
T3	87.8

Correlation Matrix

	R1	R2	R3	R4	T1	T2	T3
R1	1						
R2	0.299	1					
R3	0.0462	0.338	1				
R4	-0.0228	0.0993	0.731	1			
T1	-0.682	-0.646	0.0869	0.0867	1		
T2	-0.135	-0.76	-0.703	-0.274	0.375	1	
T3	0.0616	0.365	0.931	0.486	-0.135	-0.74	1

Location 12

Percent Standard Deviation

R1 187
R2 142
R3 3920
R4 164
T1 275
T2 246
T3 3990

Correlation Matrix

	R1	R2	R3	R4	T1	T2	T3
R1	1.00						
R2	0.31	1.00					
R3	0.02	0.25	1.00				
R4	-0.03	-0.01	0.45	1.00			
T1	0.90	0.54	0.06	-0.03	1.00		
T2	-0.48	-0.90	-0.34	-0.02	-0.74	1.00	
T3	0.02	0.24	1.00	0.48	0.06	-0.33	1.00

Location 28

Percent Standard Deviation

R1	370
R2	721
R3	4510
R4	509
T1	613
T2	999
T3	4890

Correlation Matrix

	R1	R2	R3	R4	T1	T2	T3
R1	1.0000						
R2	0.3130	1.0000					
R3	-0.0230	0.0259	1.0000				
R4	-0.0334	-0.0621	0.7890	1.0000			
T1	0.8210	0.7030	-0.0121	-0.0506	1.0000		
T2	-0.3670	-0.9780	-0.0519	0.0475	-0.7810	1.0000	
T3	-0.0255	0.0151	0.9980	0.8250	-0.0178	-0.0402	1

Location 38
Percent Standard Deviation

R1	530
R2	50
R3	322
R4	70.9
T1	538
T2	63.9
T3	280

Correlation Matrix

	R1	R2	R3	R4	T1	T2	T3
R1	1						
R2	0.0893	1					
R3	-0.729	0.00002	1				
R4	0.424	-0.216	-0.585	1			
T1	0.998	0.118	-0.725	0.419	1		
T2	-0.057	-0.868	-0.979	0.247	-0.098	1	
T3	-0.7	-0.039	0.977	-0.412	-0.698	-0.0352	1

Location 115

Percent Standard Deviation

R1	28
R2	38
R3	186
R4	24
T1	122
T2	146
T3	176

Correlation Matrix

	R1	R2	R3	R4	T1	T2	T3
R1	1.00						
R2	0.27	1.00					
R3	-0.10	0.47	1.00				
R4	0.11	0.30	0.36	1.00			
T1	0.72	0.61	0.23	0.14	1.00		
T2	-0.62	-0.77	-0.49	-0.22	-0.94	1.00	
T3	0.10	0.45	0.99	0.29	0.23	-0.48	1.00

Location 116

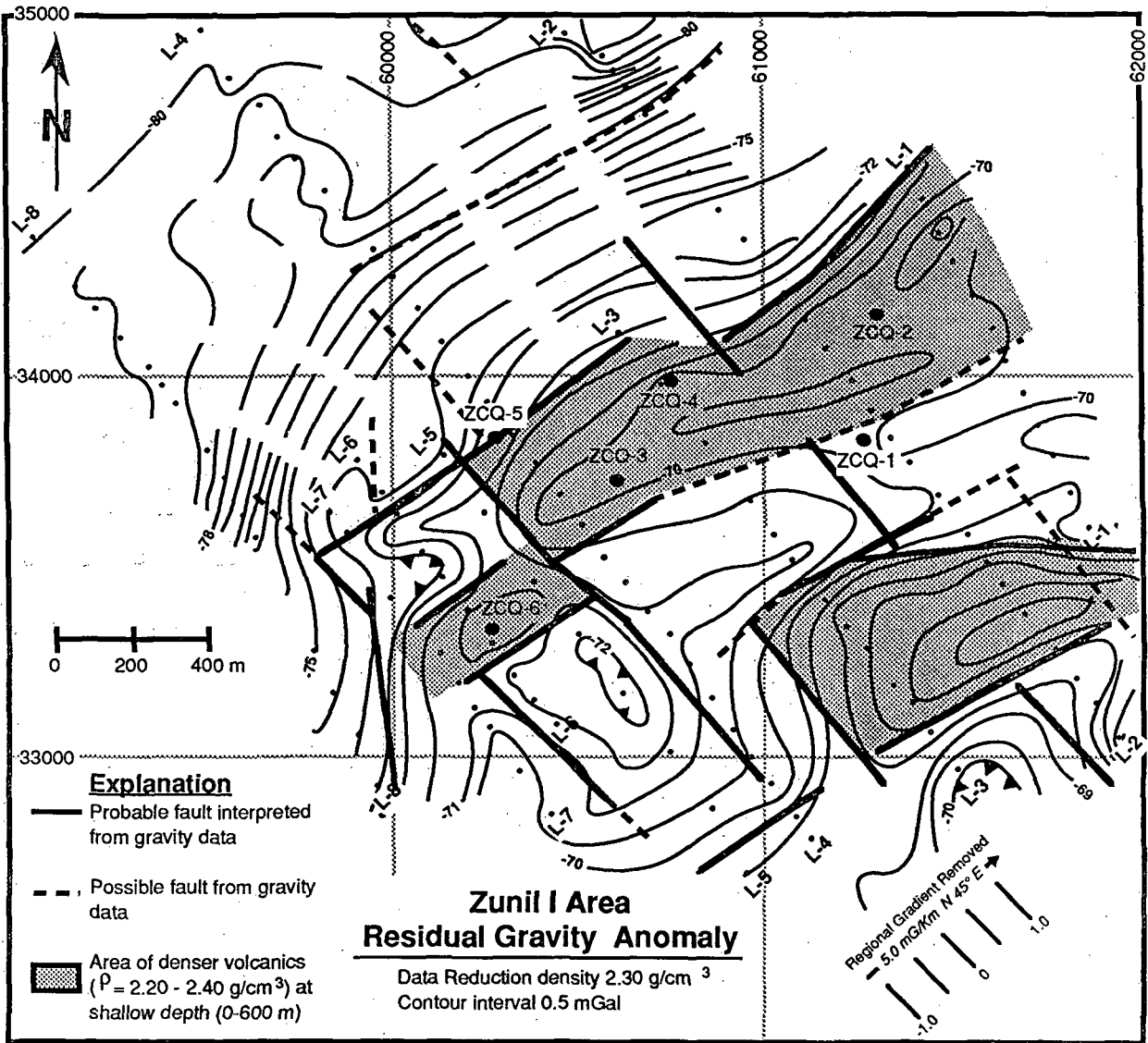
Percent Standard Deviation

R1	49
R2	139
R3	125
R4	70
T1	137
T2	86
T3	149

Correlation Matrix

	R1	R2	R3	R4	T1	T2	T3
R1	1.000						
R2	0.420	1.000					
R3	0.112	0.436	1.000				
R4	0.025	0.107	0.354	1.000			
T1	-0.066	-0.858	-0.289	-0.070	1.000		
T2	0.328	-0.391	-0.568	-0.155	-0.061	1.000	
T3	0.094	0.371	0.899	0.670	-0.246	-0.489	1.000

GRAVITY STUDIES OF THE ZUNIL I GEOTHERMAL AREA



35000

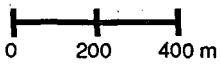
34000

33000

62000

61000

60000



Explanation

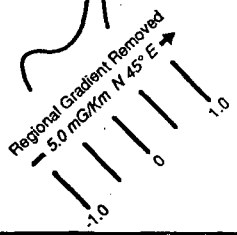
— Probable fault interpreted from gravity data

- - - Possible fault from gravity data

▨ Area of denser volcanics ($\rho = 2.20 - 2.40 \text{ g/cm}^3$) at shallow depth (0-600 m)

Zunil I Area Residual Gravity Anomaly

Data Reduction density 2.30 g/cm^3
Contour interval 0.5 mGal



SUMMARY

A detailed gravity survey covering approximately six sq km was completed in the Zunil I area by INDE between May and August of 1989, who reduced the data using densities of 2.00 and 2.67 g/cm³. UURI computed Bouguer gravity values for all stations using additional densities of 2.20 and 2.30 g/cm³, and prepared Bouguer gravity maps for four densities; 2.00, 2.20, 2.30, and 2.67 g/cm³.

We first completed a structural interpretation based on the locations of steep gravity gradients on the Bouguer anomaly maps for densities of 2.00, 2.20, and 2.30 g/cm³. A linear regional gradient was then removed from the Bouguer gravity maps for densities of 2.20 and 2.30 g/cm³, which we judged to be the most meaningful for further interpretation, and a qualitative interpretation was performed. The steep gradients observed on both Bouguer-gravity and residual-anomaly maps are generally only 50 to 300 m in breadth, indicating shallow density discontinuities or possible data errors. In view of the extreme topographic relief, and the large station to station differences in topographic corrections (up to 3 milligals (mGal)), we estimate the noise level for the survey to be 1 to 3 mGal.

We computed a series of three-dimensional numerical models to simulate the gravity anomalies produced by varying the depth to the dense (2.67 g/cm³) granodiorite and the effects of shallow (0-500 m deep) density differences in the overlying volcanics. The numerical model data clearly demonstrate that the observed gradients and contour patterns can only be explained by shallow density variations in the volcanics. These density variations define a series of northeast and northwest-trending discontinuities in the Zunil I area. In general, there is good agreement between the locations of these discontinuities and the locations of faults mapped in the field. Thus, the gravity data provide additional support for the presence and significance of structures mapped in the well field.

INTRODUCTION AND PREVIOUS WORK

Both regional and detailed gravity surveys were completed by INDE in the Zunil area. A regional survey extending from Quetzaltenango to approximately 3 km south of Cerro El Galapago covers an area of approximately 90 sq km. Two detailed gravity surveys centered on Zunil I were also completed. The earliest of these surveys covers approximately 30 sq km (CyM/MKE, 1988). The second detailed survey, which covers approximately 6 sq km, was completed in the Zunil I area between May and August of 1989. This latter survey is considered to be the more accurate of the two detailed surveys, and is the principal topic of this report.

The data provided to us by INDE from the regional gravity survey included Bouguer anomaly maps that were reduced using densities of 2.00, 2.50, and 2.67 g/cm³. A review of the 2.67 g/cm³ map shows large gravity minima corresponding to areas of high volcanic topography, such as at Vulcan Santa Maria. The correlation is much reduced for the Bouguer maps computed with lower rock densities. A strong northwest-trending regional gradient in the southwestern portion of the survey area near Vulcan Santa Maria is evident on the 2.67 g/cm³ density Bouguer map but not on the 2.00 g/cm³ density map. All three Bouguer maps indicate a complex regional gradient with a strong northeast component of approximately -5 mGal/km to the northeast. A simple linear regional gradient of -5 mGal/km in the N 45°E was judged to be the most certain and least biased regional gradient in the Zunil I area. We removed this regional gradient from the detailed gravity survey data as discussed below.

The initial detailed gravity survey completed by INDE was reduced using a density of 2.67 g/cm³ for both the Bouguer and the topographic corrections. This survey showed a northeast-trending elongate gravity high of about 4 mGal near ZCQ-5, and a small, circular low of approximately 8 mGal near Cerro El Galapago. The presence of these features was verified by the more recent detailed survey, although the representation of the northeast-trending gravity high is somewhat different. As discussed below,

interpretation of the new survey data yields a structural map that is very similar to the geologic maps prepared by CyM/MKE as part of this study.

1989 DETAILED GRAVITY SURVEY

The 1989 detailed gravity survey of the Zunil I area consisted of eight northwest-trending survey lines with station spacings of approximately 70 to 200 m (Plate 1). Lines 2, 4, and 8 were extended an additional 1 to 1.5 km in August to define regional gradients better and to determine if northeast trending faults, postulated on the basis of geologic relationships, could be located. INDE completed the data reduction, including terrain corrections, using densities of 2.00 and 2.67 g/cm³, and provided station elevation, Bouguer gravity, and topographic correction data to UURI for subsequent interpretation.

Density Studies for Bouguer Gravity Data Reduction

The accurate reduction of gravity survey data requires assigning the proper density value when making the Bouguer and terrain corrections. If an incorrect density is selected, the resulting gravity data will show a correlation with topographic elevation that is an artifact of the data reduction. False anomalies will be generated that do not represent subsurface geological variations. Determining the most appropriate density is particularly important in areas of high topographic relief such as Zunil, where elevations vary by more than 1000 m within the detailed survey area. Although a density of 2.67 g/cm³ was used in the interpretation of the gravity data from the earlier regional and local surveys, our studies and those of Cordon (1989) show that a lower value is required.

Cordon (1989) has reported density values determined by INDE for the volcanic rocks in Z-11. These values were determined on core samples from depths ranging from 0 to 620 m. Densities reported for the upper 500 m ranged from 2.21 to 2.32 g/cm³ with the higher densities being measured

on the deeper samples. We determined the densities of seven volcanic rock samples from wells Z-11, Z-2, and ZCQ-2 (Table 1.) These densities ranged from 2.07 to 2.43 g/cm³ for sample depths between 103 m and 590 m. The average density of these samples is 2.25 g/cm³.

To further investigate the proper density for use in the data reduction, we computed a series of Nettleton profiles (Telford et al., 1976) for Lines 2, 3, 7, and 8. Nettleton profiles are made by plotting reduced gravity values against elevation for a series of densities. Our profiles are shown as Figures A1-A4 in Appendix I. The profiles clearly demonstrate that the correct densities to use in reducing the data are in the range 1.9 and 2.3 g/cm³. Because of the complex topography, the relatively small number of stations on each profile, the fact that the survey lines are not perpendicular to the topographic contours, and the effects of geologic structure on topography, the Nettleton profiles do not uniquely define the proper density for the Bouguer and terrain corrections. They do however, demonstrate that densities greater than 2.40 g/cm³ are inappropriate.

While a density of 2.67 g/cm³ is commonly used for igneous, metamorphic and sedimentary terrains, it is almost always too high for young volcanic provinces. U. S. Geological Survey studies on Hawaii (Kinoshita et al, 1963) and those by Woollard (1951) on Oahu indicated that a density of 2.30 g/cm³ was appropriate even though the rocks consisted of basaltic lava flows. Williams and Finn (1982) concluded that the bulk densities of most volcanos in the Cascade range in the northwestern U.S. are in the range 2.15 to 2.35 g/cm³. Couch et al. (1982) used a Bouguer density of 2.43 for data reduction in their study of the Western and High Cascades of Oregon. The 2.30g/cm³ density reported by Cordon (1989) for the volcanic rocks in well Z-11 is in good agreement with both the Cascade and Hawaii studies. Thus, it appears that densities of 2.20 or 2.30 g/cm³ are most appropriate for reduction of the gravity data at Zunil. Lower densities (2.00 to 2.20 g/cm³) may be more appropriate for the high volcanoes south, west, and north of the Zunil I geothermal field.

Bouguer Gravity Data Reduction and Map Preparation

Station elevations, Bouguer gravity and terrain-correction data for densities of 2.00 and 2.67 g/cm³ were provided by INDE for the detailed survey. Using these data, we computed Bouguer gravity and terrain corrections for two additional densities -- 2.20 and 2.30 g/cm³. The reduced Bouguer gravity data for all densities are included as Appendix II.

Bouguer gravity maps reduced for densities of 2.00, 2.20, 2.30, and 2.67 g/cm³ were contoured and are included as Plates 2 to 5. The total gravity relief is less for the 2.00 and 2.20 g/cm³ density maps, and consequently a contour interval of 0.5 mGal has been used. The contour interval for the 2.30 and 2.67 g/cm³ maps, presented as Plates 4 and 5 respectively, is 1 mGal.

A review of principal facts provided by INDE reveals numerous topographic corrections exceeding 12 mGal, and a maximum topographic correction of 15.8 mGal for a density of 2.67 g/cm³. This corresponds to a maximum correction of 11.8 mGal for a density of 2.0 g/cm³ and 13.6 mGal for a density of 2.30 g/cm³. The difference in terrain corrections exceeds 3.0 mGal (at a density of 2.30 g/cm³) for adjacent stations at several locations. An error of 10 to 30 percent is common in estimating terrain corrections in cases of severe topography, suggesting a possible error of 1.4 to 4.1 mGal from inaccuracies in terrain corrections alone. The contoured Bouguer gravity maps suggest an error level somewhat less than this, indicating a diligent effort in terrain corrections by INDE. Nonetheless, it is apparent that the possible error range for topographic corrections alone exceeds the amplitude of anomalies of interest in the well field at Zunil I.

DATA INTERPRETATION

Qualitative Interpretations

We superimposed Bouguer anomaly maps for densities of 2.00, 2.20, and 2.30 g/cm³ (Plates 2 through 5) over the topographic map at a scale of

1:10,000 (Plate 1), and formed an estimate of the extent of topographic correlations. All three maps showed less correlation with topography than the 2.67 g/cm³ Bouguer anomaly map (Plate 5), while the 2.00 and 2.20 g/cm³ maps showed the weakest correlation.

We made a structural interpretation of the data by delineating discontinuities in the contoured maps prepared for densities of 2.00, 2.20, and 2.30 g/cm³ (Plates 2 through 4). Areas of steep gradients having continuity between survey lines, and the termination of anomaly patterns are believed to be the two best indications of faulting. The low relief in the gravity data compared to the estimated noise level due to terrain corrections and other survey errors will introduce some error in the interpretation. A simple, semi-quantitative estimate of the maximum depth to the source of a gravity anomaly is given by the breadth of the linear-gradient portion of gravity anomaly. For the anomalies of our maps, most of the linear-gradient distances are quite short, generally less than 300 m, which suggests that density differences occur at shallow depths or that there are errors in the data.

There is good correspondence in the location of most of the structures interpreted from the three Bouguer gravity maps (Plate 6), although not all of the observed discontinuities are present on each map. Furthermore, the locations of the structures shown on Plate 6 generally agree with the locations of the northeast-trending faults mapped near ZCQ-6, 5, and 3, and the northwest-trending faults mapped near ZCQ-6 (Fig. 1). Several other possible structures on Plate 6 are not shown on Figure 1.

The Bouguer gravity map for 2.67 g/cm³ is dominated by gradients that appear to be an artifact of the high density used to reduce the data. Therefore, this map was not interpreted in detail.

Quantitative Interpretations

The Bouguer gravity maps for densities of 2.20 and 2.30 g/cm³ appear to be most appropriate for numerical modeling. These densities represent

the midrange of volcanic densities reported by Cordon (1989) and are most consistent with studies cited above in similar volcanic terrains. These values are intermediate between the known low density (2.00 g/cm^3) of the recent volcanics and the higher densities of the granodiorite and more strongly silicified volcanic rocks in Zunil I. As discussed above, the regional gravity maps indicate a northeast-trending gradient of approximately -5 mGal/km across the area of the detailed survey. We subtracted this linear regional gradient from the 2.30 g/cm^3 Bouguer anomaly to produce a residual anomaly map shown as Plate 7. The same -5 mGal/km , $N 45^\circ E$ regional gradient was removed from the Bouguer gravity map based on a density of 2.20 g/cm^3 (Plate 3). This residual anomaly map (density = 2.20 g/cm^3) is shown as Plate 9 along with the locations of geologic structures based on this map. It is apparent that the maps for densities of 2.20 and 2.30 g/cm^3 are very similar.

The residual anomaly maps show a reduced correlation between the low gravity values and high topography west and north of the well field. Northeast- and northwest-trending maxima and minima that are not obvious in the Bouguer gravity maps, are much more clearly defined on the residual anomaly maps and are more suitable for interpretation.

Discontinuities in the gravity data which are represented by abrupt density changes are shown on Plate 8. Such discontinuities probably represent faults. Several interpreted faults are common to both the Bouguer gravity and residual anomaly maps, giving added credence to the interpretations and to the importance of removing the regional gradient.

Inspection of both residual anomaly maps (Plates 7 and 9) reveals a complex anomaly pattern with both northwest- and northeast-trending features throughout the ZCQ well area. In areas of such complex structure, two-dimensional numerical modeling is inappropriate. This is especially true in the western part of the well field where the highest temperatures wells are located. Accordingly, the three-dimensional (3-D) gravity modeling program GM3 (Maurer and Atwood, 1980) was used to help

quantify the density contrasts and geometries causing the residual gravity distribution.

The Advisory Panel suggested that the gravity interpretation might be constrained by the interpretation of the vertical electrical soundings (VES). While we agree that under certain circumstances electrical data can be used in such a manner, the limited number of soundings in the area of the Zunil I well field and the particular resistivity structure shown by the soundings preclude the use of the electrical data in this way. The basic problem is elaborated in a section below and is explained briefly here as follows.

Interpretation of the soundings shows a four-layer resistivity structure. The upper layer is a very thin resistive layer averaging 5 m in thickness. The second layer is somewhat more conductive, but is only about 50 m thick. Gravity effects produced within such thin layers, with any geologically probable density contrasts, would be negligible. The third layer is a good electrical conductor, and the fourth layer is a resistor. Our studies establish that the thickness of the conductive layer can not be uniquely determined from the electrical data -- only the conductivity-thickness product can be resolved. Thickness estimates could be in error by a factor of two or more, making it impossible to determine the depth to the top of the electrical basement from the resistivity soundings alone. Gravity analysis shows that the majority of the gravity variations of interest originate in the shallow subsurface, at depths shallower than about 700 m. Thus, these gravity variations probably originate in the electrically conducting layer. In view of all of this, there is no basis to use the non-uniquely determined top to electrical basement to constrain the gravity interpretation. To do so would be technically indefensible and would possibly lead to false conclusions.

Nevertheless, we agree with the panel that the two sets of data -- the gravity and the electrical data -- can provide useful and complimentary information. For this reason, we have interpreted the gravity data independently of the VES interpretation, using data from the production wells where possible to constrain our gravity models. The gravity models are then compared with the VES interpretations as an independent

evaluation of each method. We found the models produced by the gravity and electrical data to be in general agreement.

The three dimensional gravity models we developed for the Zunil area are shown in Figures 2 and 3. The computational center of the output grid used in developing these models corresponds to a point almost midway between ZCQ-3 and 6. The rectangular grid is oriented approximately N 40° E to minimize the number of prisms needed to model the observed data. We computed the model anomalies with a grid interval of 100 m on a 25 x 27 grid, yielding a total of 675 data points per computed map. This grid is substantially more detailed and uniform than the observed field data grid.

The model in Figure 2 contains 23 vertical right-rectangular prisms which are constrained by the interpreted structures and the depth to the granodiorite in the production wells. This model was used to determine the gravity anomaly pattern due to a varying depth to the granodiorite. The model assumes a density contrast of 0.47 g/cm³ with the volcanic rocks represented by a background density of 2.20 g/cm³. A density of 2.67 g/cm³ was used for the underlying granodiorite. Lower density volcanics (2.00 g/cm³) to the northwest are represented by a -0.20 g/cm³ density contrast. The computed anomaly map is far less complex than the residual anomaly map. A broad circular gravity maxima of 9.90 mGal occurs near the observed high 1.2 km SE of ZCQ-4. The computed relief between ZCQ-4 and this maxima is about 2.8 mGal versus 3 mGal observed, which is the right order of magnitude. The tops of the model blocks of denser granodiorite vary from 700 to 2000 m in depth, but this is not reflected significantly in the computed anomaly map. The observed steep gradients north of ZCQ-2 and 5 are simulated fairly well by the low density bodies (2.00 g/cm³) that extend from the surface to 600 m depth, and the absence of granodiorite at depth to the northwest.

Figure 3 shows the effects of varying the densities of the shallow volcanic rocks. The model is a better fit to the observed data. This figure, which shows a NE trending high of about 3 mGal along the residual gravity anomaly of about 2.3 mGal, includes the area where ZCQ-2, 3, and 4 are

located. A separate high of about 2.8 mGal corresponds to the residual high of about 3.0 mGal 1300 m southeast of ZCQ-4. Although this computed anomaly map provides a fair match to the gradients and shape of the observed map, the computed contours are smoother and the gradients are of longer wavelength. The model includes the granodiorite model of Figure 2, with six additional blocks (numbers 24-30) of low density volcanics (2.00 g/cm^3) extending from the surface to a depth of 500 m in the area between ZCQ-1 and ZCQ-5. Comparison between Figure 3 and Plates 7 and 9, the residual anomalies, demonstrates that density differences within the overlying volcanic units between the surface and depths of 700 m give rise to all of the valid steeper gradients and most of the character of the residual Bouguer gravity data. Thus, the gravity data does not appear to be effective in mapping pre-volcanic structures in the granodiorite. The gravity data do however appear to map post-volcanic faults which are likely to cut both the volcanic rocks and the granodiorite.

Figure 4 shows the anomaly computed for a variable depth to the top of a dense (2.67 g/cm^3) granodiorite. The depth to the top of this body varies from 500 m (block 3) to 3000 m (block 7). The computed data show a total anomaly of 8.08 mGal with a variation over the granodiorite itself of about 3.8 mGal. This is for a variation of 2500 m in depth which is much greater than that expected at Zunil from the known geology. The minimum distance between 0.5 mGal contour lines is 150 m. This distance is much greater than the contour separations shown on Plates 2 through 5, 7 and 9, for the observed and residual data. This relationship also indicates that structures which cause variations in the depth to top of the granodiorite are not being indicated in the observed data.

To further evaluate the gravity expression of small density variations in the volcanic rocks, which could correspond to the observed variations in the extent of hydrothermal alteration defined by petrologic investigations (Cym/MKE; this study), a simple three-dimensional density model was formed. Figure 5 shows the anomaly computed for a simple distribution of small density contrasts (-0.3 to $+0.1 \text{ g/cm}^3$) with respect to a background

density of 2.20 g/cm^3 . The range of gravity values (-3 to +1 mGal) and the wavelengths of the gradients are similar to the observed residual anomalies shown in Plates 7 and 9. Most of the steep gradients are only 100 to 200 m wide, which is comparable to those shown on the residual anomaly maps in Plates 7 and 8. These comparisons further support the conclusion that near-surface density variations cause most of the observed gravity features.

Figures 6 and 7 show the residual anomalies and computed gravity profiles of Figures 2 and 3, for Lines 3 and 4, respectively. The profiles computed for a varying depth to the granodiorite are far too smooth and show little of the observed gravity character -- only an increase in gravity values to the southeast is common to the computed and residual maps. The computed profiles for the granodiorite plus large bodies of shallow, low density (2.00 g/cm^3) volcanics have the correct amplitude variation as the residual anomalies, but are still unable to match the steeper gradients. This raises concern that observational or data reduction errors, or even greater contrasts in the overlying volcanics are present in the observed data.

COMPARISON WITH VES INTERPRETATIONS

Despite the structural complexity of the area, we were able to complete an optimum interpretation of the VES data in terms of an equivalent-layered resistivity structure, as discussed in detail in an accompanying report entitled "Interpretation of Schlumberger data in the vicinity of Zunil I". The upper two electrical layers consist of a thin zone of high resistivity rocks that includes deposits of ash, mudflows, and alluvium. Beneath this zone is a thick, low-resistivity layer corresponding to argillically altered volcanic rocks containing conductive clays (layer 3). Resistive basement underlays this layer. Well data indicate that the lower, resistive layer consists of compositionally similar volcanic rocks that contain non-conductive clays. These rocks are in places, strongly silicified. The vertical electrical soundings apparently did not sense the granodiorite.

Due to the thinness of the upper two layers, we did not explicitly consider them in the gravity modeling. The thickness of the low-resistivity layer defined by the VES data (layer 3) can not be uniquely determined from the electrical soundings. However, we are probably justified in saying that the top of the underlying resistive layer appears to be at a depth of several hundred meters, corresponding to the 500 m thickness of the low-density volcanic rocks modeled in Figure 3 and shown in the cross sections presented in Figures 6 and 7 below.

In summary, the gravity model defines a three-layer density distribution. The low density (2.00 g/cm³) volcanic layer is thin or absent along the northeast-trending gravity high, but is relatively thick to the northwest and southeast. The lack of low-density volcanic rocks in the well field may be due to the locally intense alteration and accompanying densification of the rocks.

The structural interpretation of the gravity data is summarized on Plate 10. These data provide additional support for the locations of the major structures that have been mapped within the Zunil I area. A prominent feature of the gravity data is the northeast-trending gravity high in the area of wells ZCQ-2, 3, and 4. This high corresponds with the observed hydrothermal alteration and densification of the rocks in these wells, and with the region of high conductivity-thickness values mapped by VES 115, 116, 38, and 28.

REFERENCES

Cordon, U. J., 1989, Gravity models of the Zunil I geothermal field, Quetzaltenango, Guatemala: M-K Engineers, Tech. rept., (draft), 17 p., February.

Maurer, J., and Atwood, J. W., 1980, GM3D -- Interactive 3-D gravity and magnetic modeling program (GM3DREV.1 User's Guide): University of Utah Research Institute, Earth Science Laboratory, rept. no. 44, DOE/ID/12079-16, 27 p.

Telford, W. M., Geldart, L. P., Sheriff, R. E., and Keys, D. A., 1976, Applied Geophysics, Cambridge Univ. Press., 860 p.

Table 1.

DENSITY MEASUREMENTS OF ZUNIL CORE SAMPLES

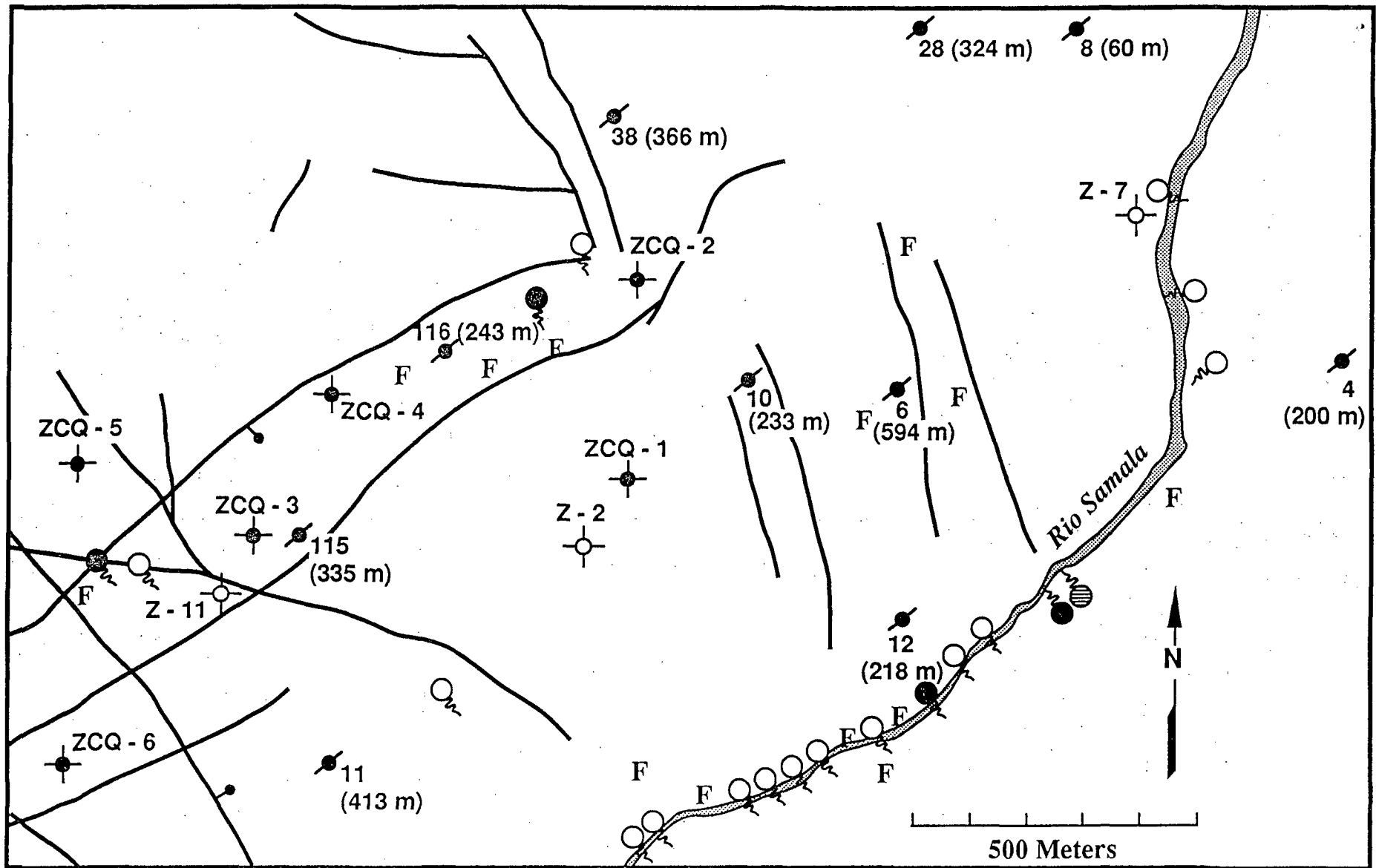
Sample #	Dry weight (g)	Suspended weight (g)	Saturated weight (g)	Vol (cu. cm)	Density (g/cu. cm)
Z-11 89m	283.61	167.95	297.30	129.35	2.19
Z-11 476m	211.00	130.30	222.65	92.35	2.28
Z-11 165m	305.30	173.05	312.60	139.55	2.19
Z-2 580m	295.05	175.65	308.00	132.35	2.23
Z-11 590m	148.50	89.21	152.10	62.89	2.36
ZCQ-2 103m	610.06	365.00	616.50	251.50	2.43
Z-2 624m	205.80	119.12	218.60	99.48	2.07
ZCQ-4 1015m (granodior.)	821.00	512.50	830.40	317.90	2.58
				Average:	2.29

LIST OF PLATES

- Plate 1. Topographic map showing location of detailed gravity survey, Zunil I Area. Scale = 1:10,000.
- Plate 2. Bouguer gravity map for a density of 2.00 g/cm³.
Scale = 1:10,000
- Plate 3. Bouguer gravity map for a density of 2.20 g/cm³.
Scale = 1:10,000
- Plate 4. Bouguer gravity map for a density of 2.30 g/cm³.
Scale = 1:10,000
- Plate 5. Bouguer gravity map for a density of 2.67 g/cm³.
Scale = 1:10,000
- Plate 6. Preliminary Structural Interpretation, Zunil I area,
from Bouguer gravity maps.
- Plate 7. Residual gravity anomaly map for a density of 2.30
g/cm³.
- Plate 8. Residual gravity anomaly map for a density of 2.20
g/cm³.
- Plate 9. Structural interpretation based on residual anomaly
maps.
- Plate 10. Summary of structural interpretations based on gravity
data.
- Plate 11. Computed gravity anomaly for the Zunil I Area based on a variable
depth to the granodiorite and varying densities of the near surface volcanics.
Scale = 1:10,000

Figure 1

Location map of the Zunil I geothermal area showing the major structural and thermal features, well locations, and the locations of the vertical electrical soundings (VES). The numbers in parentheses give the best estimate to the depth of the resistive basement determined from the soundings.

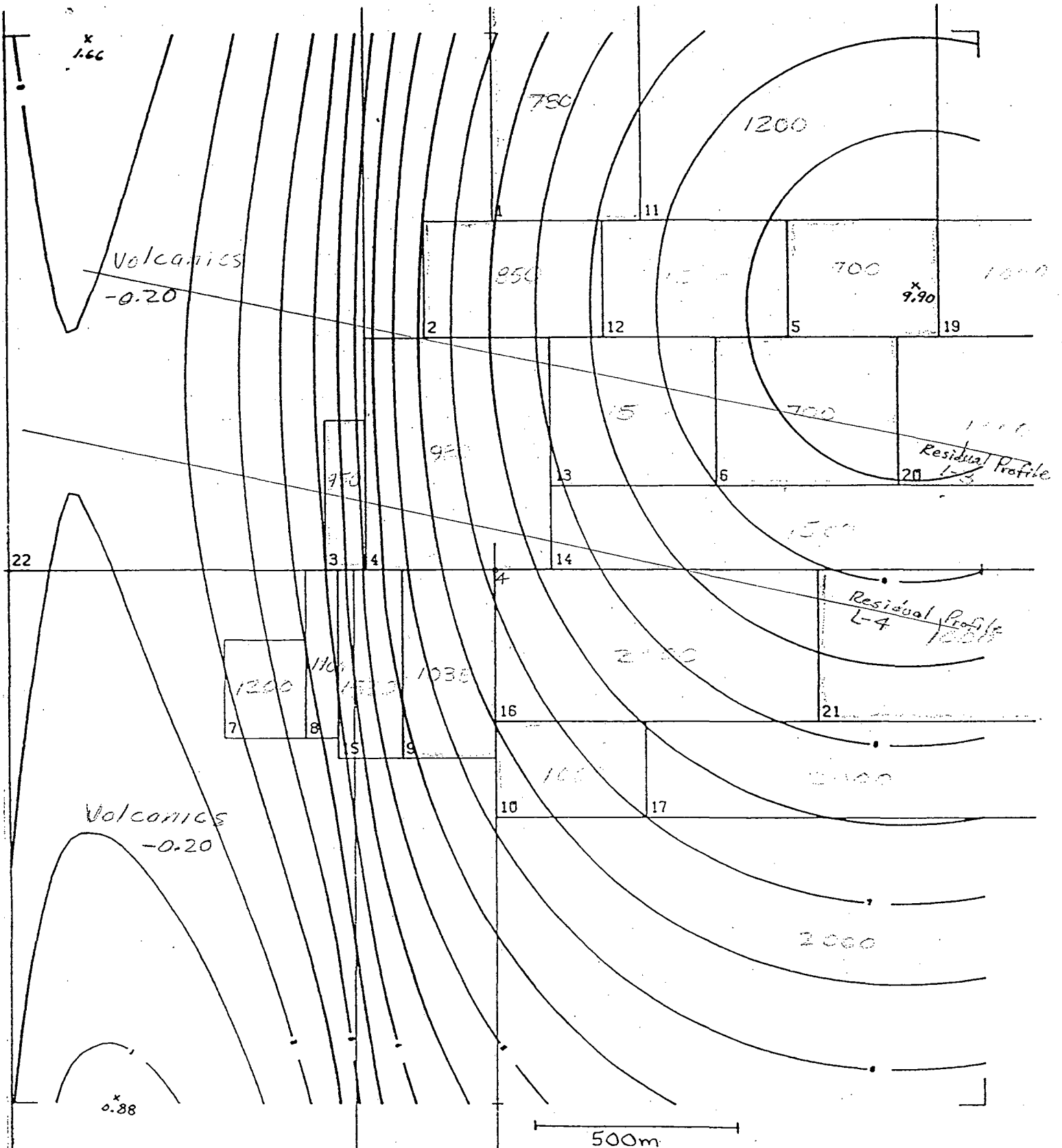


- | | | | |
|---------------------------------|-----------------|-----------------------|-------|
| Acid-sulfate spring | NaCl spring | F Fumarole | Fault |
| Bicarbonate spring | Production well | Thermal gradient well | |
| Sounding Location; Depth | | | |
| 116 (243 m) Best depth estimate | | | |

Figure 1

Figure 2

Computed gravity model for the Zunil area based on a variable depth to the granodiorite.



PROJECT NAME

TUNEL
MODEL 1

MODEL NAME

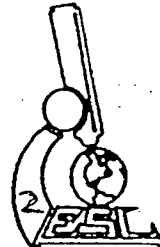
MODEL 1, iter 2

NUMBER OF PRISMS: 23.

GRAVITY MODEL (MILLIGALS)

GRID PARAMETERS

GRID POINTS X 25, Y 27.
 GRID SPACING = 100 METERS
 GRID DIMENSIONS X 2400, Y 2600 METERS
 GRID OFFSET X: 0, Y: 0 METERS
 SCALE 1: 10000. X 0.80
 DATA MAXIMUM: 18.
 DATA MINIMUM: 1.
 CONTOUR INTERVAL: 1.



FAULTED GRANODIOR
 $\rho = 2.67$

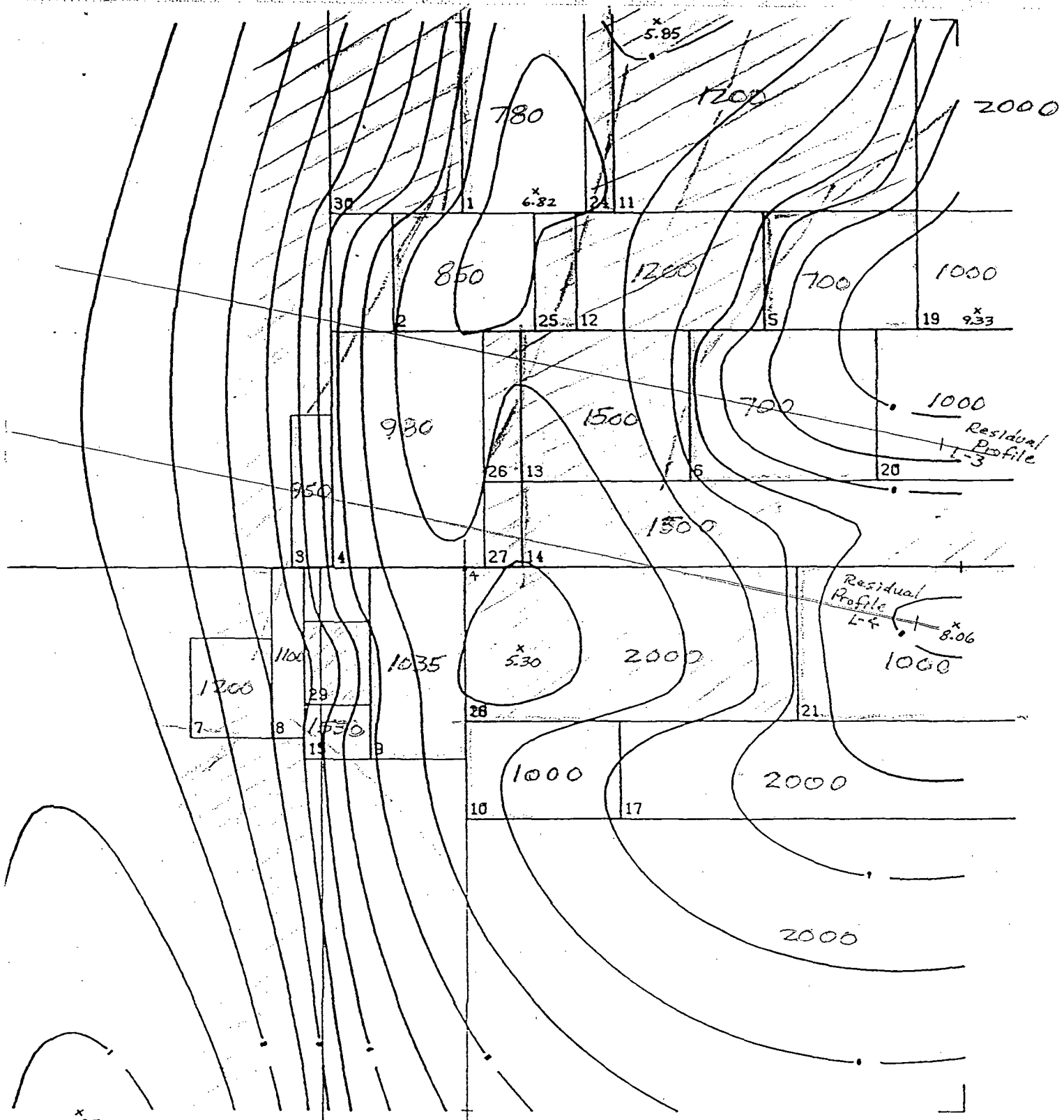
850 Depth (m) to top of block

□ Uplifted block

Figure 2

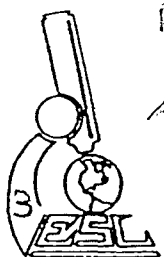
Figure 3

Computed gravity model for the Zunil area based on a variable depth to the granodiorite and varying densities of the overlying volcanics. Plate 11 shows the same information at a scale of 1:10,000 for comparison with the residual anomaly maps.



PROJECT NAME
 MODEL 1
 MODEL NAME
 MODEL 1, ITER 4
 NUMBER OF PRISMS: 30.
 GRAVITY MODEL (MILLIGALS)

GRID PARAMETERS
 GRID POINTS X 25. Y 27.
 GRID SPACING: 100 METERS
 GRID DIMENSIONS X 2400. Y 2600. METERS
 GRID OFFSET X: 0. Y: 0. METERS
 SCALE 1: 10000. X.80
 DATA MAXIMUM: 8.
 DATA MINIMUM: 1.
 CONTOUR INTERVAL: 1.

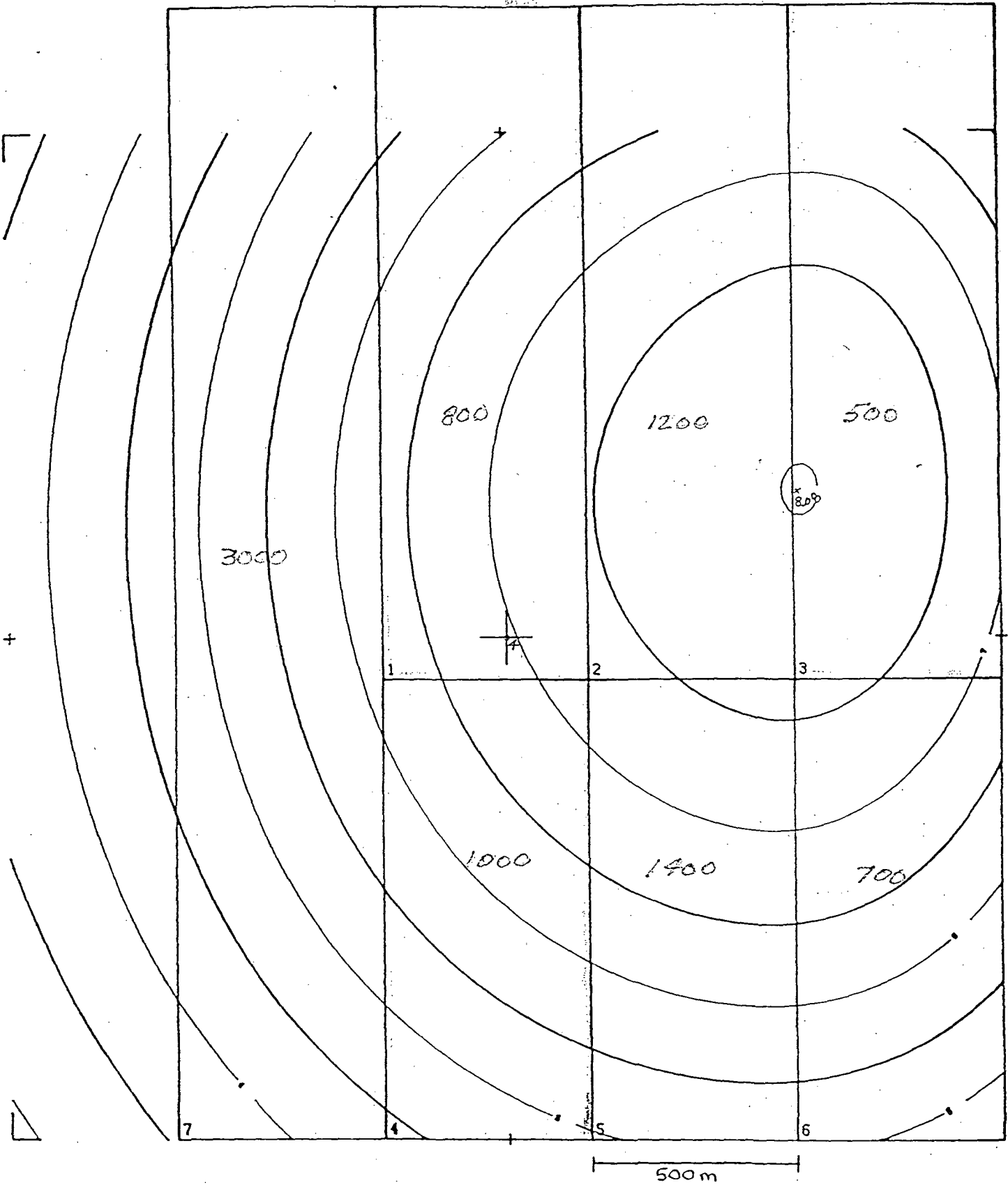


FAULTED GRANODIORITE AND VARIABLE VOLCANICS
 Shallow Granodiorite $\rho = 2.67$
 Volcanics, $\rho = 2.00$ depth 0-500m
 Background $\rho = 2.20$
 2000 Depth to top, m

Figure 3

Figure 4

Computed gravity model based on a variable depth to the granodiorite. The depth to the top of the granodiorite varies from 500 to 3000 m.



PROJECT NAME

UNCL.
DEEP GRANITE STRUCTURE

MODEL NAME

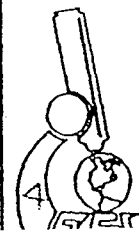
DEEP GRANITE STRUCTURE

NUMBER OF PRISMS: 7.

GRAVITY MODEL (MILLIGALS)

GRID PARAMETERS

GRID POINTS X 25. Y 25.
 GRID SPACING = 100. METERS
 GRID DIMENSIONS X 2400. Y 2400. METERS
 GRID OFFSET X: 0. Y: 0. METERS
 SCALE 1: 10000. X: 80
 DATA MAXIMUM: 8.
 DATA MINIMUM: 2.
 CONTOUR INTERVAL: 1.

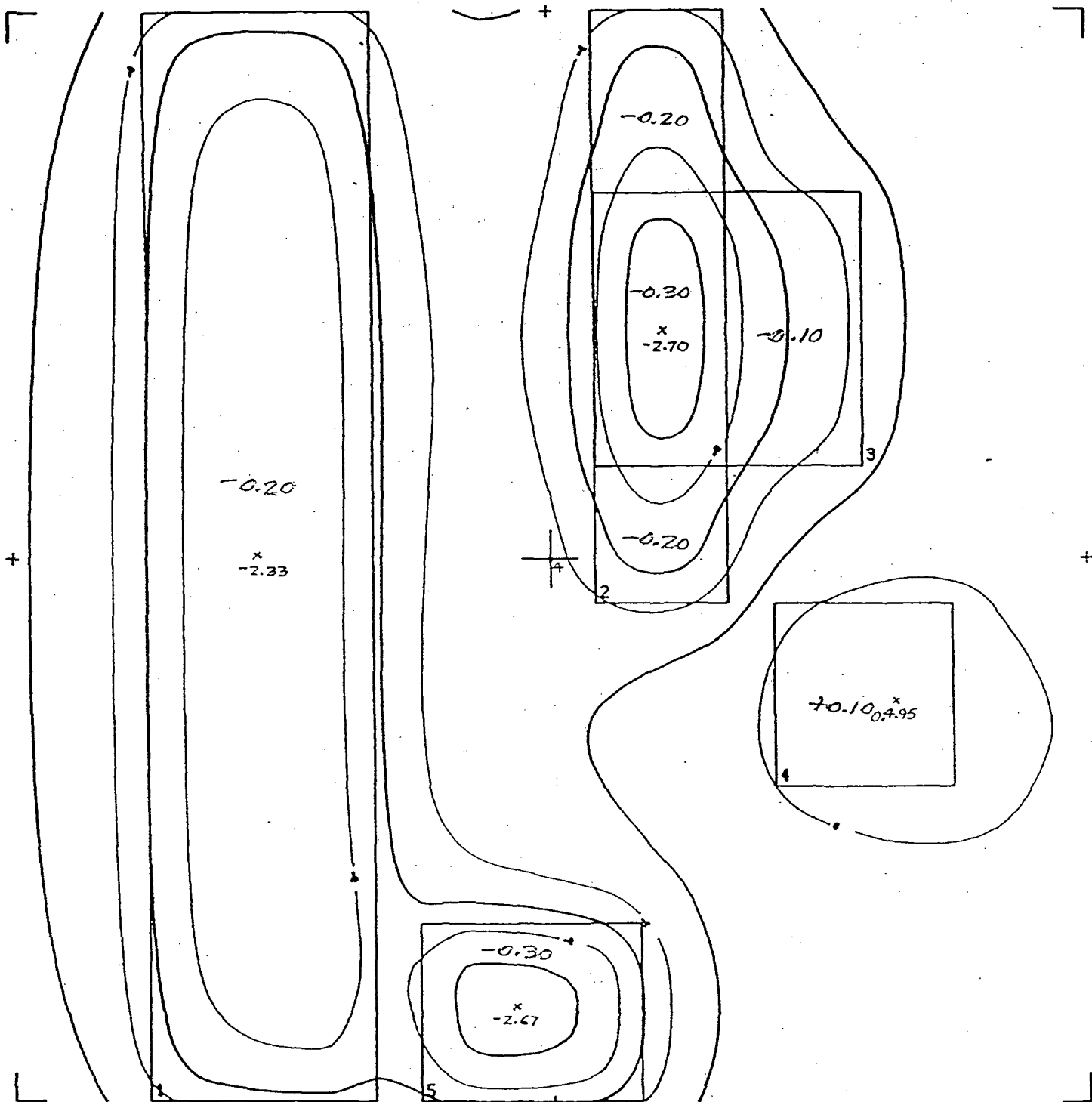


1000 Depth (m) to
granodiorite
 $\rho = 0.47$
← Uplifted block

Figure 4

Figure 5

Computed gravity model for density variations between -0.3 and $+0.1 \text{ g/cm}^3$ in the volcanic rocks between the surface and depths of 500 m.



PROJECT NAME	GRID PARAMETERS
EARTH	GRID POINTS X 25. Y 25.
SURFACE VOLCANICS	GRID SPACING = 100. METERS
MODEL NAME	GRID DIMENSIONS X 2400. Y 2400. METERS
SURFACE VOLCANICS	GRID OFFSET X = 0. Y = 0. METERS
NUMBER OF PRISMS: 5.	SCALE 1:10000. X-80
GRAVITY MODEL (MILLIGALS)	DATA MAXIMUM = 0.
	DATA MINIMUM = -8.
	CONTOUR INTERVAL 1.

Variable Volcanics
 -0.20 Density Contrast
 (g/cc)
 All blocks depth:
 0-500m

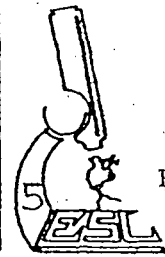


Figure 5

Figure 6

Model cross section along gravity line 3 comparing the computed and residual gravity anomalies.

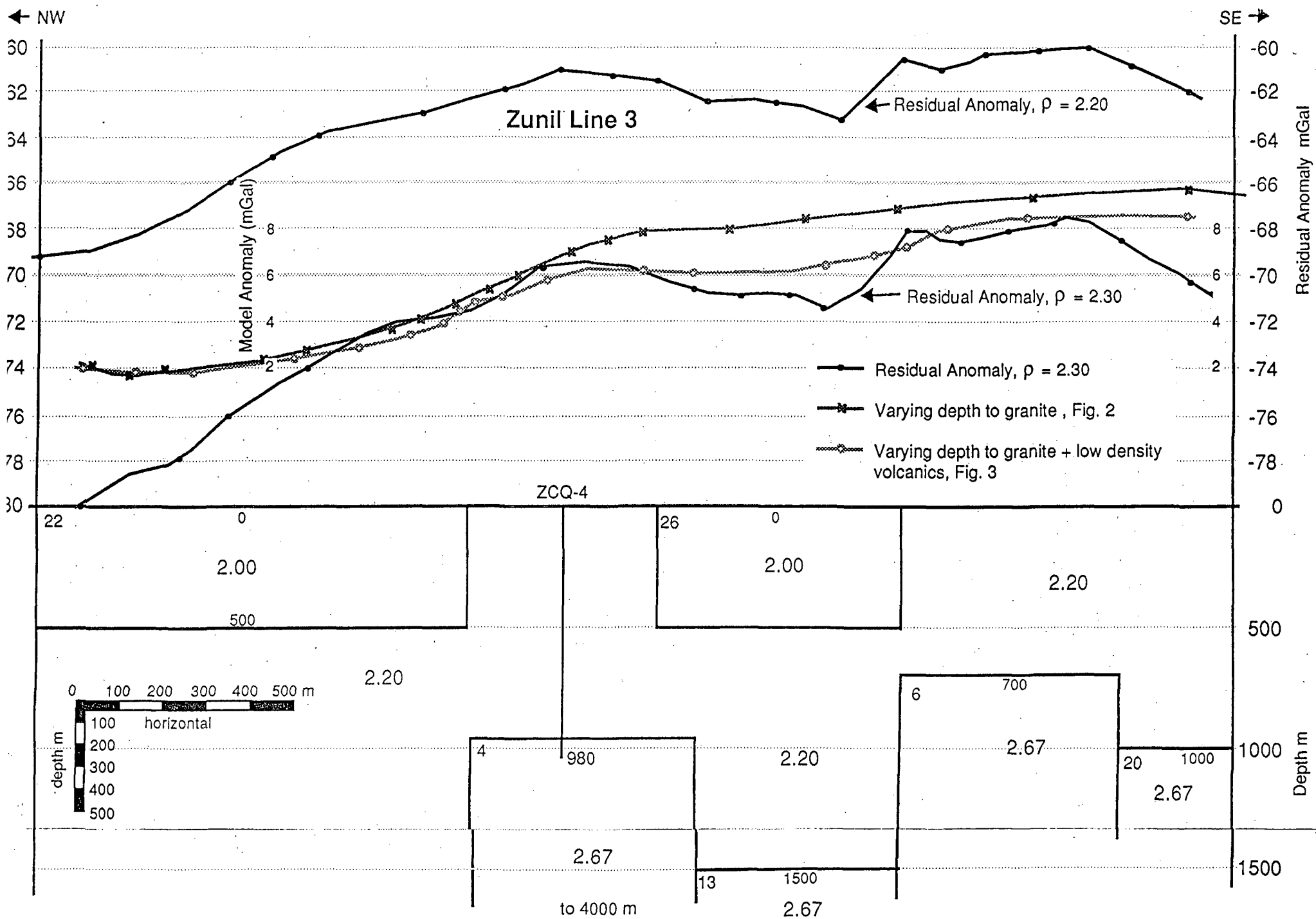


Figure 6

Figure 7

Model cross section along gravity line 4 comparing the computed and residual gravity anomalies.

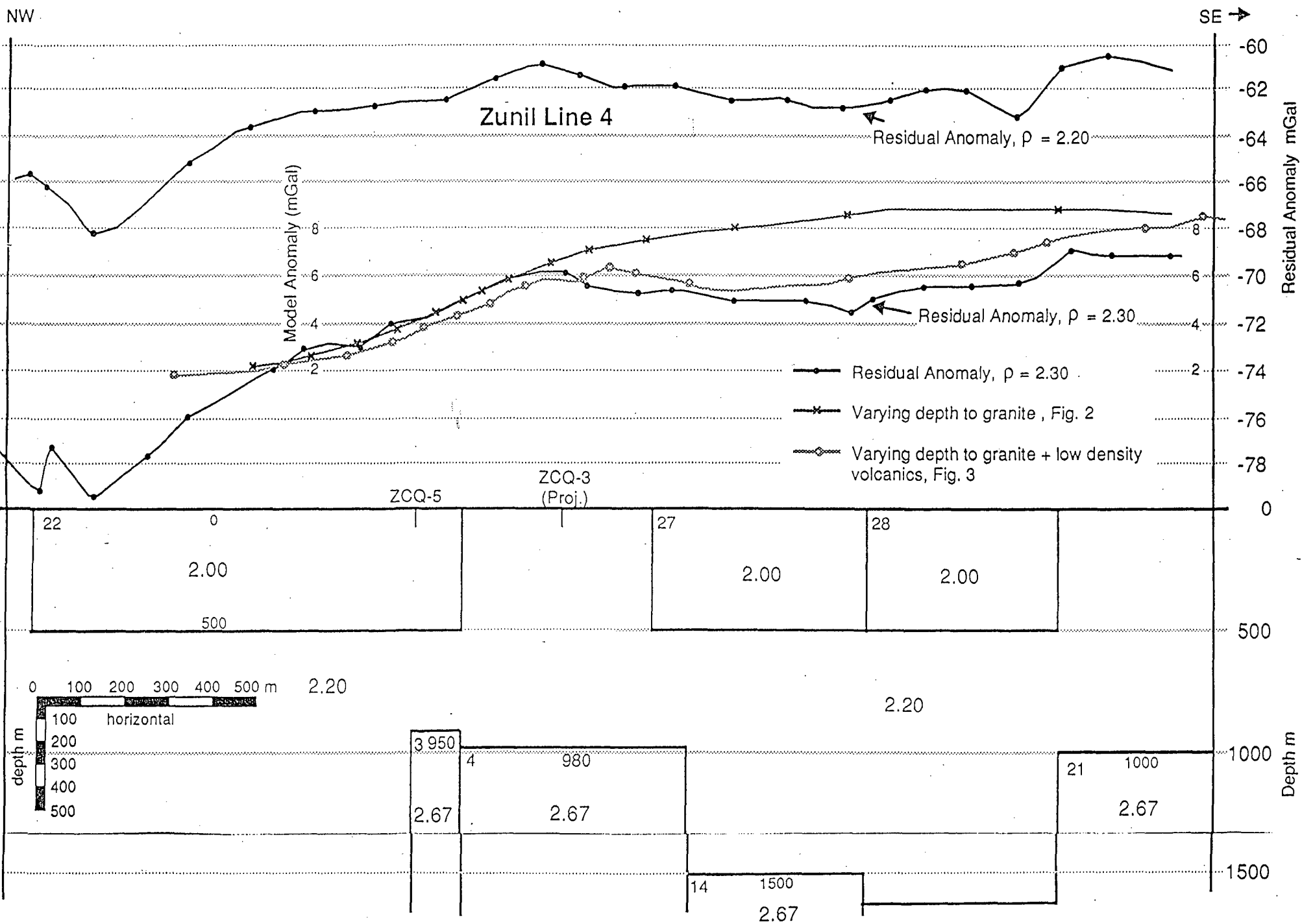


Figure 7

APPENDIX I

NETTLETON PROFILES

Nettleton profiles calculated for the evaluation of the proper density for the Bouguer and topographic corrections. The profiles were calculated for densities of 1.7, 1.9, 2.0, 2.1, 2.2, 2.3, 2.4, and 2.67 g/cm³).

Line 2

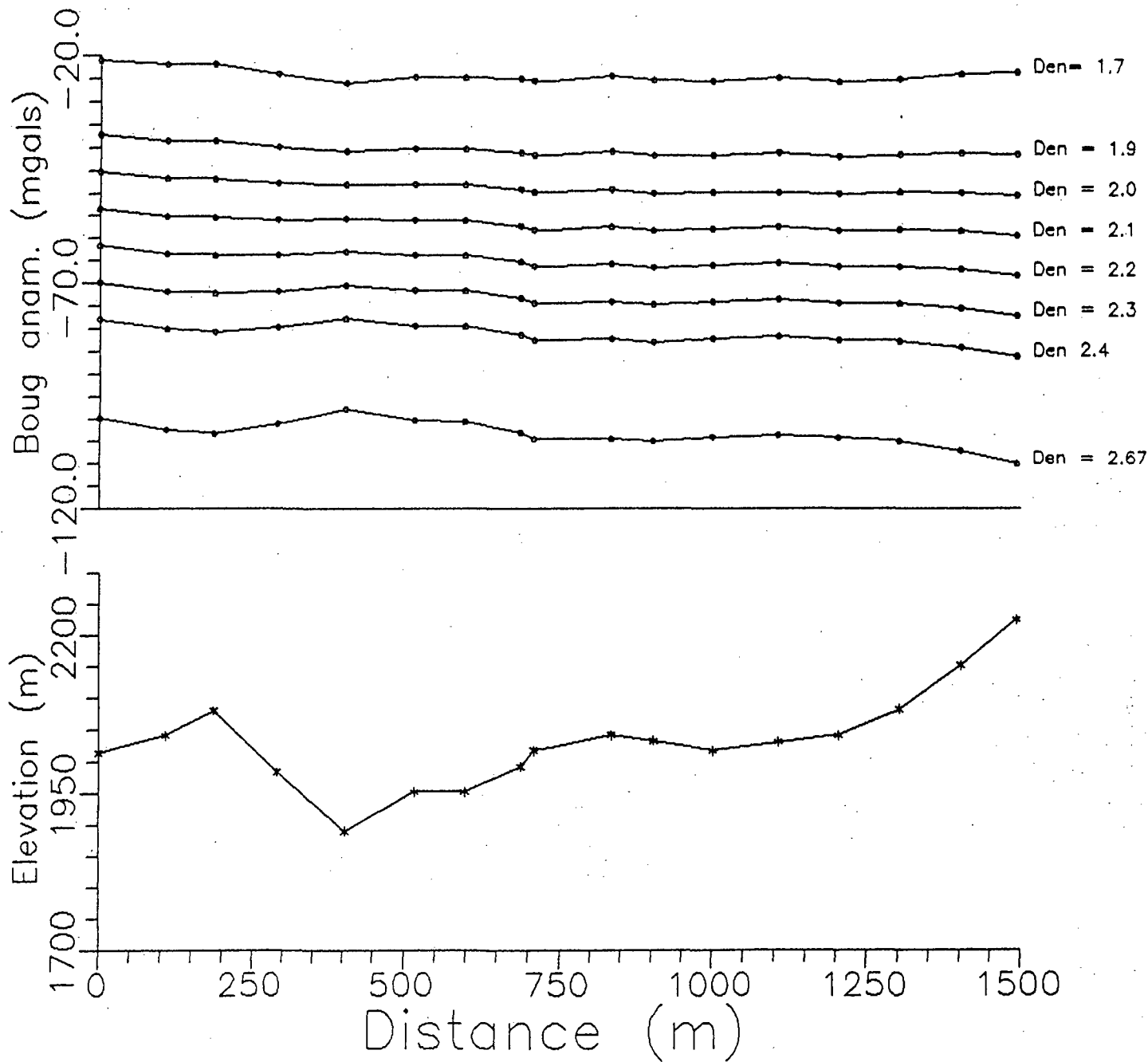


Figure A.1 - Nettleton profiles, line 2.

Line 3

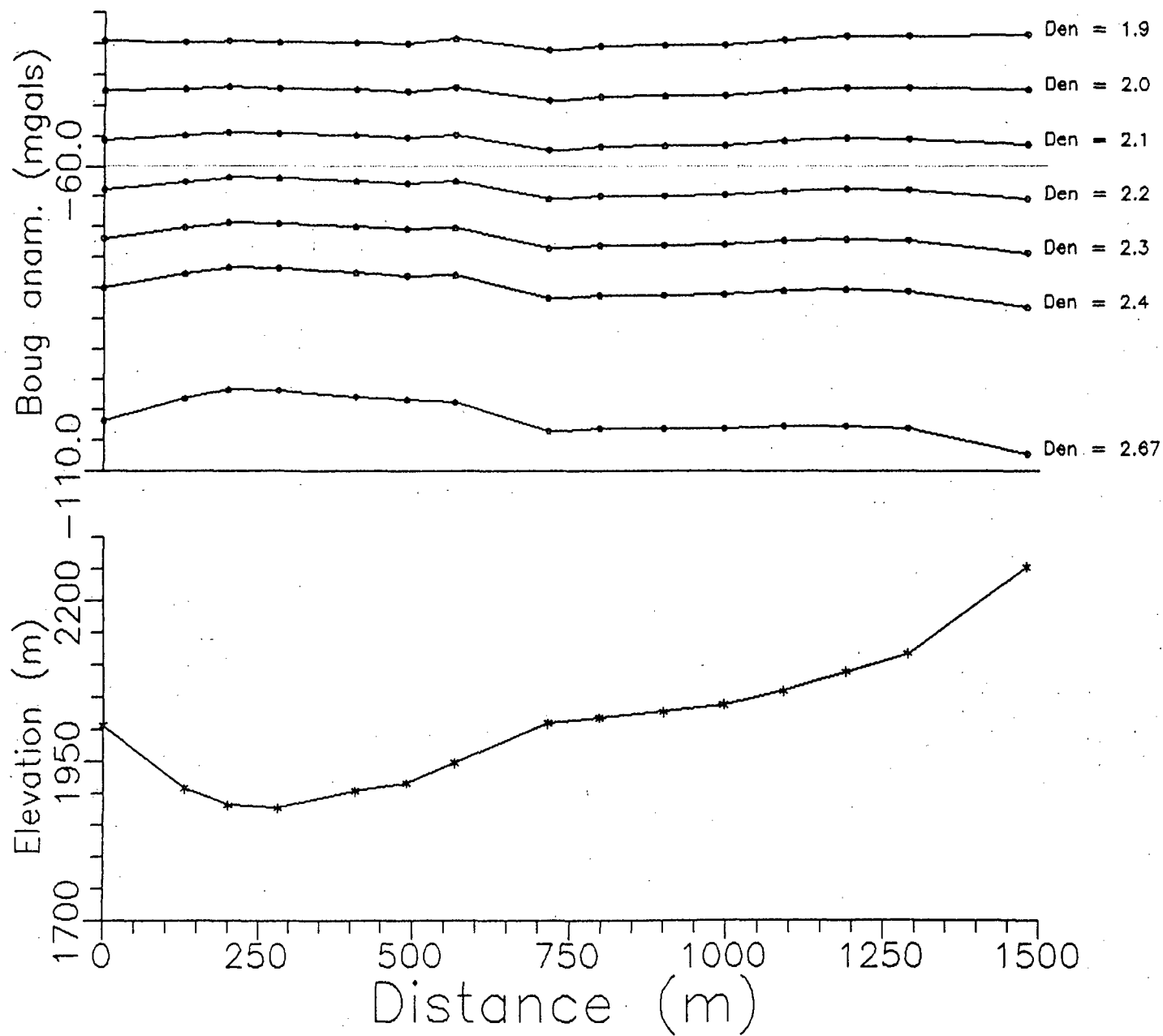


Figure A.2 - Nettleton profiles, line 3.

Line 7

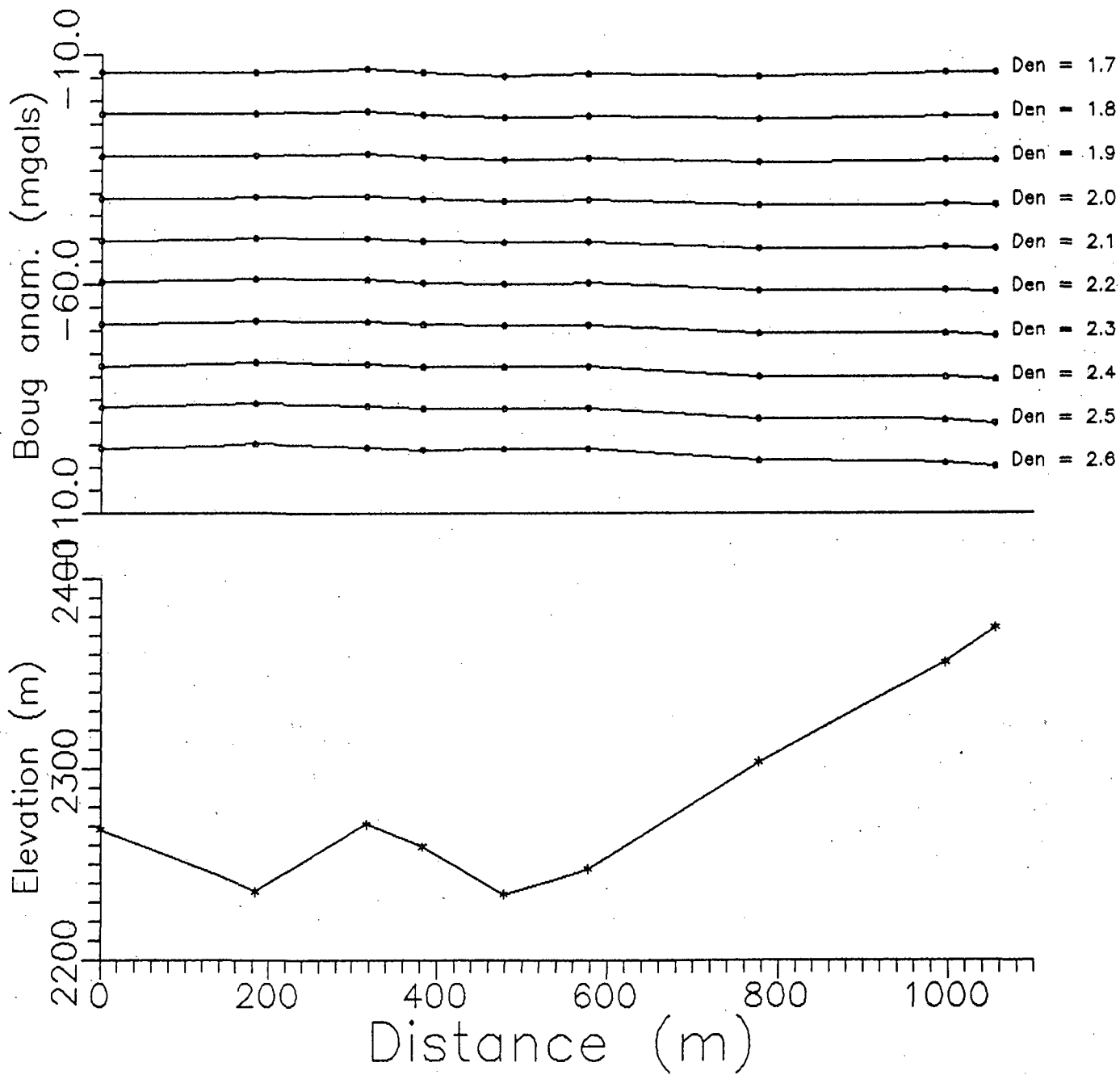


Figure A.3 - Nettleton profiles, line 7.

Line 8

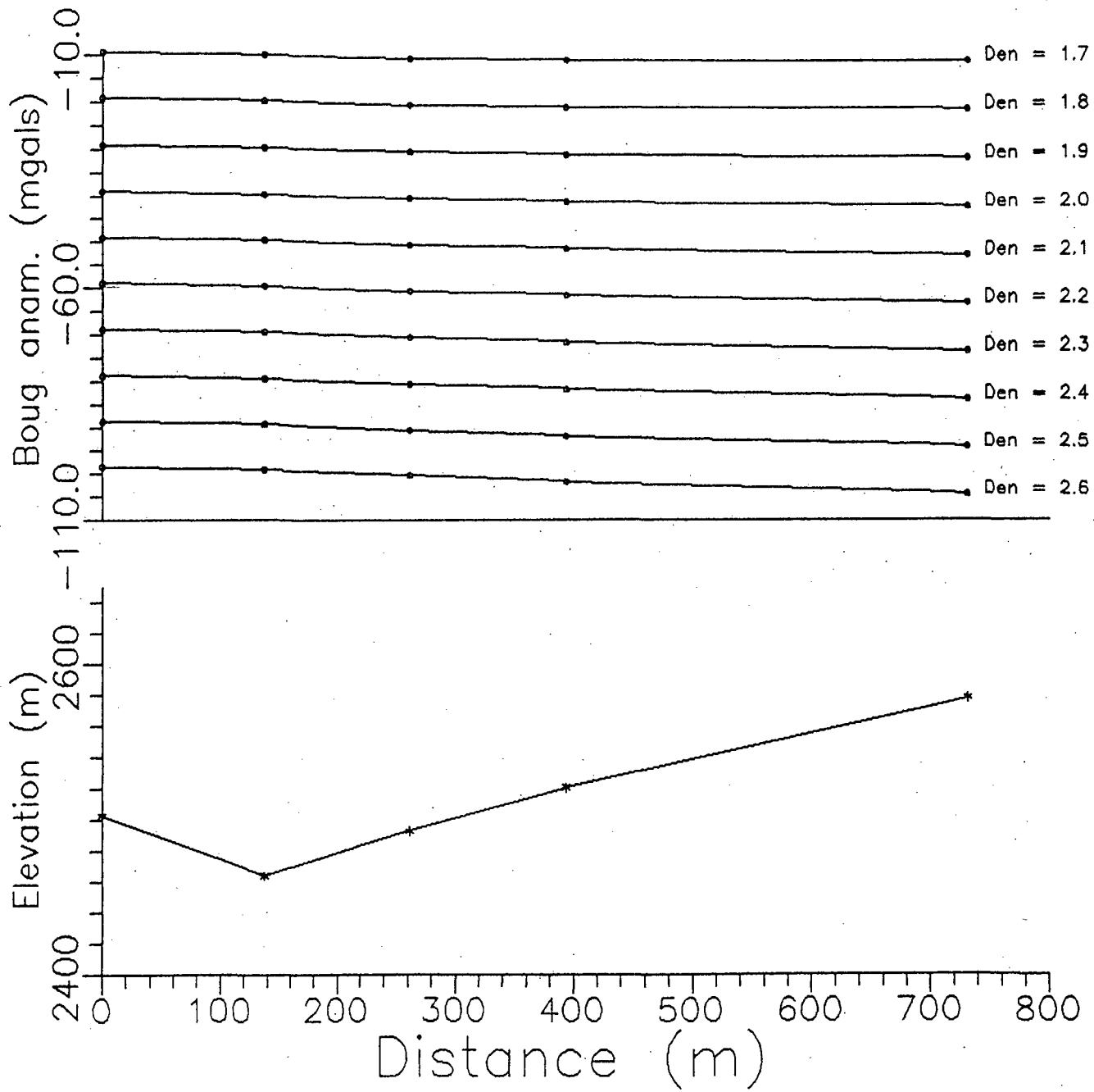


Figure A.4 - Nettleton profiles, line 8.

APPENDIX 2

BOUGUER GRAVITY DATA

check 1

LINE #	STATION #	ELEVATION #	G boug	G boug	TOPO CORR.	TOPO CORR.	G boug	**	G boug	G boug	TOPO CORR.	TOPO CORR.	G boug	**
			(dens. = 2.67) #gals	(new dens.) #gals	(orig.)	(new)	(with topo corr)	(dens. = 2.00) #gals	(new dens.) #gals	(orig.)	(new)	(with topo corr)	(dens. = 2.00) #gals	
1	1 + 297.70	2031.93	-112.297	-55.32	6.668	4.99	-50.33	**	-55.302	-55.30	4.986	4.986	-50.32	**
1	1 + 200.00	2036.75	-112.238	-55.13	6.836	5.12	-50.01	**	-55.106	-55.11	5.052	5.052	-50.05	**
1	1 + 211.91	2069.28	-112.642	-54.62	6.396	4.79	-49.83	**	-54.601	-54.60	4.791	4.791	-49.81	**
1	1 + 000.00	2084.36	-112.763	-54.32	6.432	4.82	-49.50	**	-54.296	-54.30	4.745	4.745	-49.55	**
1	0 + 900.00	2090.32	-113.772	-55.16	6.07	4.55	-50.61	**	-54.588	-54.59	4.546	4.546	-50.04	**
1	0 + 800.00	2086.59	-113.772	-55.27	6.342	4.75	-50.51	**	-55.243	-55.24	4.751	4.751	-50.49	**
1	0 + 706.80	2097.98	-114.693	-55.87	7.256	5.44	-50.43	**	-55.847	-55.85	5.435	5.435	-50.41	**
1	0 + 600.00	2111.87	-116.174	-56.96	8.376	6.27	-50.68	**	-56.935	-56.94	6.274	6.274	-50.66	**
1	0 + 493.00	2136.12	-117.200	-57.30	9.158	6.86	-50.44	**	-57.283	-57.29	6.87	6.870	-50.41	**
1	0 + 408.00	2146.18	-118.000	-57.82	10.362	7.76	-50.06	**	-57.802	-57.80	7.762	7.762	-50.04	**
1	0 + 302.00	2201.37	-120.309	-58.58	10.907	8.17	-50.41	**	-58.560	-58.56	8.17	8.170	-50.39	**
1	0 + 197.00	2249.83	-122.055	-58.97	10.672	7.99	-50.98	**	-58.945	-58.95	7.994	7.994	-50.95	**
2	0 + 928.67	2014.73	-108.622	-52.13	8.871	6.64	-45.49	**	-52.110	-52.11	6.645	6.645	-45.47	**
2	0 + 820.69	2041.99	-109.779	-52.52	7.460	5.59	-46.93	**	-52.504	-52.50	5.605	5.605	-46.90	**
2	0 + 741.68	2080.72	-112.292	-53.95	9.100	6.82	-47.13	**	-53.948	-53.95	6.817	6.817	-47.13	**
2	0 + 637.72	1984.49	-111.141	-55.50	10.074	7.55	-47.95	**	-55.476	-55.48	7.546	7.546	-47.93	**
2	0 + 525.00	1890.87	-112.058	-59.04	14.385	10.78	-48.26	**	-59.018	-59.02	10.776	10.776	-48.24	**
2	0 + 412.10	1953.69	-110.882	-56.10	10.655	7.98	-48.12	**	-56.081	-56.08	7.981	7.981	-48.10	**
2	0 + 330.31	1953.90	-110.844	-56.06	10.369	7.77	-48.29	**	-56.037	-56.04	7.768	7.768	-48.27	**
2	0 + 240.78	1992.83	-111.478	-55.60	8.519	6.38	-49.22	**	-55.581	-55.58	6.381	6.381	-49.20	**
2	0 + 130.02	2018.32	-112.739	-56.15	8.298	6.22	-49.93	**	-56.126	-56.13	6.216	6.216	-49.91	**
2	0 + 850.00	2042.36	-112.551	-55.28	8.079	6.05	-49.23	**	-55.262	-55.26	6.052	6.052	-49.21	**
2	0 + 071.51	2032.90	-113.394	-56.39	8.449	6.33	-50.06	**	-56.371	-56.37	6.329	6.329	-50.04	**
2	0 + 168.49	2017.82	-113.929	-57.35	9.956	7.46	-49.89	**	-57.330	-57.33	7.455	7.455	-49.88	**
2	0 + 274.86	2031.34	-114.128	-57.17	10.623	7.96	-49.21	**	-57.782	-57.78	7.952	7.952	-49.83	**
2	0 + 372.00	2042.06	-116.608	-59.35	12.448	9.32	-50.03	**	-59.330	-59.33	9.325	9.325	-50.01	**
2	0 + 470.47	2082.97	-117.840	-59.43	12.968	9.71	-49.72	**	-59.410	-59.41	9.714	9.714	-49.70	**
2	0 + 570.63	2152.43	-119.222	-58.87	12.144	9.10	-49.77	**	-58.847	-58.85	9.096	9.096	-49.75	**
2	0 + 661.85	2226.04	-121.260	-58.84	11.240	8.42	-50.42	**	-58.840	-58.84	8.445	8.445	-50.40	**
2	0 + 736.44	2195.00	-121.067	-59.52				**	-59.497	-59.50	10.414	10.414	-49.08	**
2	0 + 856.91	2311.17	-123.162	-58.36				**	-58.333	-58.33	8.985	8.985	-49.35	**
2	0 + 971.53	2404.37	-125.977	-58.56				**	-58.534	-58.53	8.836	8.836	-49.70	**
2	1 + 189.12	2544.88	-128.044	-56.69				**	-58.231	-58.23	7.893	7.893	-50.34	**
2	1 + 271.49	2591.70	-131.244	-58.57				**	-58.541	-58.54	7.152	7.152	-51.39	**
2	1 + 334.09	2639.12	-134.219	-60.22				**	-60.398	-60.40	7.246	7.246	-52.15	**
2	1 + 371.32	2644.36	-134.219	-60.07				**	-60.043	-60.04	6.586	6.586	-53.46	**
2	1 + 493.42	2625.38	-131.438	-57.82				**	-57.796	-57.80	4.857	4.857	-52.94	**
2	1 + 567.60	2625.47	-131.566	-57.95				**	-57.911	-57.91	4.644	4.644	-53.27	**
2	1 + 676.35	2644.44	-132.5	-58.35				**	-58.325	-58.33	4.507	4.507	-53.82	**
2	1 + 792.31	2672.99	-134.199	-59.25				**	-59.224	-59.22	4.607	4.607	-54.42	**
2	1 + 880.57	2676.17	-133.436	-58.40				**	-58.369	-58.37	4.673	4.673	-53.70	**
2	1 + 986.21	2707.54	-133.24	-57.32				**	-57.295	-57.30	4.729	4.729	-52.57	**
2	2 + 095.22	2745.62	-134.608	-57.62				**	-57.597	-57.60	4.927	4.927	-52.67	**
2	2 + 185.42	2799.47	-136.706	-58.21				**	-58.18	-58.18	5.185	5.185	-53.00	**

DENSITY = 2

check 1

LINE #	STATION #	ELEVATION	G boug (dens. = 2.67) egals	G boug (new dens.) egals	TOPO CORR. (orig.)	TOPO CORR. (new)	G boug (with topo corr) egals	** egals	G boug (dens. = 2.00) egals	** egals	G boug (new dens.) egals	TOPO CORR. (orig.)	TOPO CORR. (new)	G boug (with topo corr) egals	** egals
3	1 + 000.00	2006.50	-110.341	-54.08	8.549	6.40	-47.68	**	-54.058	**	-54.06	6.404	6.404	-47.65	**
3	0 + 871.00	1908.13	-109.093	-55.59	10.948	8.20	-47.39	**	-55.571	**	-55.57	8.2	8.200	-47.37	**
3	0 + 800.00	1881.82	-109.031	-56.27	12.340	9.24	-47.02	**	-56.247	**	-56.25	9.234	9.234	-47.01	**
3	0 + 718.20	1877.49	-109.455	-56.81	12.694	9.51	-47.30	**	-56.791	**	-56.79	9.48	9.480	-47.31	**
3	0 + 593.20	1904.29	-109.897	-56.50	12.102	9.07	-47.44	**	-56.484	**	-56.48	9.065	9.065	-47.42	**
3	0 + 510.20	1916.59	-110.605	-56.86	12.25	9.18	-47.69	**	-56.845	**	-56.85	9.176	9.176	-47.67	**
3	0 + 434.00	1948.15	-110.514	-55.89	11.764	8.81	-47.08	**	-55.867	**	-55.87	8.693	8.693	-47.17	**
3	0 + 285.00	2010.22	-111.651	-55.29	8.139	6.10	-49.19	**	-55.265	**	-55.27	6.097	6.097	-49.17	**
3	0 + 203.00	2018.54	-111.628	-55.03	8.532	6.39	-48.64	**	-55.010	**	-55.01	6.391	6.391	-48.62	**
3	0 + 100.00	2027.70	-112.067	-55.23	8.992	6.74	-48.50	**	-55.210	**	-55.21	6.737	6.737	-48.47	**
3	0 + 364.98	2038.92	-112.944	-55.77	9.869	7.39	-48.38	**	-55.747	**	-55.75	7.392	7.392	-48.36	**
3	0 + 101.70	2060.05	-113.700	-55.94	11.12	8.33	-47.61	**	-55.914	**	-55.91	8.364	8.364	-47.55	**
3	0 + 200.00	2089.17	-114.741	-56.16	12.136	9.09	-47.07	**	-56.139	**	-56.14	9.09	9.090	-47.05	**
3	0 + 300.00	2117.23	-116.884	-57.52	13.913	10.42	-47.10	**	-57.497	**	-57.50	10.42	10.420	-47.08	**
3	0 + 491.00	2253.21	-120.846	-57.67	13.635	10.21	-47.45	**	-57.644	**	-57.64	10.22	10.220	-47.42	**
4	1 + 221.70	1858.08	-108.227	-56.13	12.64	9.47	-46.66	**	-56.107	**	-56.11	9.498	9.498	-46.61	**
4	1 + 125.50	1878.11	-108.470	-55.81	12.517	9.38	-46.43	**	-55.789	**	-55.79	9.396	9.396	-46.39	**
4	1 + 034.70	1902.97	-108.775	-55.42	12.239	9.17	-46.25	**	-55.399	**	-55.40	9.167	9.167	-46.23	**
4	0 + 922.70	1977.20	-109.691	-54.25	10.24	7.67	-46.58	**	-54.231	**	-54.23	7.671	7.671	-46.56	**
4	0 + 825.00	1998.27	-109.355	-53.32	9.242	6.92	-46.40	**	-53.303	**	-53.30	6.949	6.949	-46.35	**
4	0 + 725.00	2010.85	-109.314	-52.93	8.963	6.71	-46.22	**	-52.909	**	-52.91	6.714	6.714	-46.20	**
4	0 + 625.00	2026.27	-107.78	-50.96	8.637	6.47	-44.49	**	-52.942	**	-52.94	6.53	6.530	-46.41	**
4	0 + 518.00	2035.44	-110.248	-53.18	8.503	6.37	-46.81	**	-53.156	**	-53.16	6.367	6.367	-46.79	**
4	0 + 425.00	2050.85	-110.305	-52.80	8.557	6.41	-46.39	**	-52.777	**	-52.78	6.409	6.409	-46.37	**
4	0 + 325.00	2057.29	-110.886	-53.20	8.989	6.73	-46.47	**	-53.179	**	-53.18	6.733	6.733	-46.45	**
4	0 + 225.00	2067.44	-111.467	-53.50	9.828	7.36	-46.14	**	-53.477	**	-53.48	7.362	7.362	-46.11	**
4	0 + 125.00	2072.36	-112.449	-54.34	10.779	8.07	-46.27	**	-54.318	**	-54.32	8.074	8.074	-46.24	**
4	0 + 100.30	2070.24	-113.833	-55.78	12.877	9.65	-46.14	**	-55.764	**	-55.76	9.646	9.646	-46.12	**
4	0 + 071.40	2089.03	-114.122	-55.55	13.327	9.98	-45.56	**	-55.626	**	-55.63	9.983	9.983	-45.64	**
4	0 + 175.00	2127.05	-115.567	-55.93	13.576	10.17	-45.76	**	-55.902	**	-55.90	10.17	10.170	-45.73	**
4	0 + 249.80	2182.34	-116.79	-55.60	12.589	9.43	-46.17	**	-55.577	**	-55.58	9.426	9.426	-46.15	**
4	0 + 375.00	2249.97	-118.668	-55.58	13.094	9.81	-45.77	**	-55.558	**	-55.56	9.81	9.810	-45.75	**
4	0 + 474.00	2328.34	-120.579	-55.29	13.051	9.78	-45.52	**	-55.27	**	-55.27	9.776	9.776	-45.49	**
4	0 + 575.80	2402.01	-121.989	-54.64	12.892	9.66	-44.98	**	-54.613	**	-54.61	9.657	9.657	-44.96	**
4	0 + 680.56	2496.02	-122.212	-52.22					-54.354	**	-54.35	9.582	9.582	-44.77	**
4	0 + 795.45	2596.56	-124.102	-51.30					-53.637	**	-53.64	8.382	8.382	-45.26	**
4	0 + 896.43	2633.69	-127.081	-53.23					-54.05	**	-54.05	7.374	7.374	-46.68	**
4	1 + 011.56	2697.38	-127.419	-51.79					-53.818	**	-53.82	6.424	6.424	-47.39	**
4	1 + 094.36	2721.44	-130.354	-54.05					-54.05	**	-54.05	8.501	8.501	-45.55	**
4	1 + 100.10	2720.89	-129.76	-53.47					-53.439	**	-53.44	8.392	8.392	-45.05	**
4	1 + 225.46	2731.6	-128.373	-51.78					-51.895	**	-51.90	6.639	6.639	-45.26	**
4	1 + 300.00	2785.83	-131.89	-53.78					-53.748	**	-53.75	7.459	7.459	-46.29	**
4	1 + 408.64	2836.87	-131.891	-53.19					-53.157	**	-53.16	7.65	7.650	-45.51	**
4	1 + 500.00	2841.41	-133.341	-53.67					-53.64	**	-53.64	6.708	6.708	-46.93	**

check 1

LINE #	STATION #	ELEVATION	6 boug (dens. = 2.67) # #gals	6 boug (new dens.) #gals	TOPO CORR. (orig.)	TOPO CORR. (new)	6 boug (with topo corr) #	** #	6 boug (dens. = 2.00) # #gals	6 boug (new dens.) #gals	TOPO CORR. (orig.)	TOPO CORR. (new)	6 boug (with topo corr) #	** #
4	1 + 600.62	2849.29	-133.199	-53.31					-53.277		6.547	6.547		-46.73
4	1 + 674.64	2835.67	-132.702	-53.19					-53.161		5.662	5.662		-47.50
5	1 + 400.09	1864.17	-106.235	-53.96	12.306	9.22	-44.75 **		-53.944		9.222	9.222		-44.72
5	1 + 200.07	1899.01	-107.573	-54.33	12.424	9.31	-45.02 **		-54.306		9.234	9.234		-45.07
5	1 + 000.23	1937.96	-108.573	-54.23	12.381	9.27	-44.96 **		-54.236		9.277	9.277		-44.96
5	1 + 797.32	1981.4	-110.109	-54.55	11.817	8.85	-45.70 **		-54.531		8.712	8.712		-45.82
5	0 + 600.02	2049.13	-109.91	-52.45	8.833	6.62	-45.84 **		-52.433		6.617	6.617		-45.82
5	0 + 399.81	2083.37	-110.741	-52.32	8.21	6.15	-46.17 **		-52.302		6.149	6.149		-46.15
5	0 + 200.22	2104.22	-111.303	-52.30	8.448	6.33	-45.97 **		-52.28		6.328	6.328		-45.95
5	0 + 290.04	2116.74	-112.465	-53.11	10.431	7.81	-45.30 **		-53.091		7.814	7.814		-45.28
5	0 + 199.99	2131.44	-114.332	-54.57	12.364	9.26	-45.31 **		-54.546		9.263	9.263		-45.28
5	0 + 399.84	2234.86	-117.537	-54.87	11.943	8.95	-45.93 **		-54.848		8.946	8.946		-45.90
6	0 + 311.58	2167.96	-111.145	-50.36	9.255	6.93	-43.42 **		-50.335		6.933	6.933		-43.40
6	0 + 200.30	2167.47	-111.218	-50.44	8.992	6.74	-43.71 **		-50.42		6.733	6.733		-43.69
6	0 + 117.63	2192.56	-111.37	-49.89	8.548	6.40	-43.49 **		-49.818		6.403	6.403		-43.42
6	0 + 510.00	2171.03	-111.059	-50.18	9.738	7.29	-42.89 **		-50.163		7.267	7.267		-42.90
6	0 + 105.69	2189.53	-112.088	-50.69	10.259	7.68	-43.01 **		-50.673		7.684	7.684		-42.99
6	0 + 198.73	2237.6	-113.825	-51.08	9.511	7.12	-43.96 **		-51.061		7.093	7.093		-43.97
6	0 + 303.82	2242.3	-115.084	-52.21	10.630	7.96	-44.25 **		-52.188		7.964	7.964		-44.22
6	0 + 405.11	2223.24	-116.054	-53.72	13.250	9.93	-43.79 **		-53.693		9.925	9.925		-43.77
6	0 + 488.99	2288.97	-117.197	-53.02	11.282	8.45	-44.56 **		-52.993		8.379	8.379		-44.61
6	0 + 602.34	2342.58	-118.271	-52.59	11.806	8.84	-43.74 **		-52.561		8.815	8.815		-43.75
7	0 + 462.60	2268.37	-112.959	-49.36	10.872	8.14	-41.21 **		-49.331		8.143	8.143		-41.19
7	0 + 290.00	2235.93	-111.179	-48.48	10.130	7.59	-40.90 **		-48.462		7.588	7.588		-40.87
7	0 + 145.70	2271.2	-111.575	-47.89	9.709	7.27	-40.62 **		-47.868		7.271	7.271		-40.60
7	0 + 080.00	2259.46	-111.672	-48.32	9.338	6.99	-41.32 **		-48.293		6.968	6.968		-41.33
7	0 + 655.00	2234.38	-111.374	-48.72	9.253	6.93	-41.79 **		-48.699		6.942	6.942		-41.76
7	0 + 120.00	2247.7	-111.885	-48.86	9.789	7.33	-41.53 **		-48.837		7.333	7.333		-41.50
7	0 + 320.00	2303.88	-114.44	-49.84	9.568	7.17	-42.67 **		-49.815		7.178	7.178		-42.64
7	0 + 540.00	2355.97	-116.706	-50.65	11.199	8.39	-42.26 **		-50.637		8.389	8.389		-42.25
7	0 + 598.00	2374.57	-117.499	-50.92	11.250	8.43	-42.49 **		-50.892		8.413	8.413		-42.48
8	0 + 394.80	2503.02	-121.109	-50.93	15.797	11.83	-39.09 **		-50.9		11.831	11.831		-39.07
8	0 + 144.00	2464.35	-117.37	-48.27	11.375	8.52	-39.75 **		-48.244		8.523	8.523		-39.72
8	0 + 268.00	2493.16	-120.678	-50.77	13.386	10.03	-40.74 **		-50.744		10.026	10.026		-40.72
8	0 + 400.80	2520.91	-122.384	-51.70	13.558	10.16	-41.54 **		-51.673		10.17	10.170		-41.50
8	0 + 737.60	2578.17	-123.735	-51.44	12.009	9.00	-42.45 **		-51.416		8.763	8.763		-42.65
8	0 + 804.30	2590.43	-124.18	-51.55			**		-51.52		8.247	8.247		-43.27
8	0 + 919.20	2590.40	-125.508	-52.87			**		-52.104		8.009	8.009		-44.10
8	1 + 000.00	2607.79	-124.019	-50.90			**		-50.871		5.996	5.996		-44.88
8	1 + 144.45	2587.72	-122.082	-49.52			**		-49.514		4.629	4.629		-44.89
8	1 + 219.50	2617.00	-123.263	-49.88			**		-49.856		4.787	4.787		-45.07
8	1 + 276.00	2633.68	-123.607	-49.76			**		-49.645		4.763	4.763		-44.88
8	1 + 371.90	2652.09	-124.111	-49.75			**		-49.719		5.136	5.136		-44.58
8	1 + 472.70	2651.13	-123.963	-49.63			**		-49.5		4.686	4.686		-44.81

DENSITY =

2

check 1

LINE #	STATION #	ELEVATION	G boug (dens. = 2.67) #gals	G boug (new dens.) #gals	TOPO CORR. (orig.)	TOPO CORR. (new)	G boug (with topo corr)	** #gals	G boug (dens. = 2.00) #gals	G boug (new dens.) #gals	TOPO CORR. (orig.)	TOPO CORR. (new)	G boug (with topo corr)	** #gals
8	1 + 554.60	2651.86	-124.489	-50.13				**	-50.104	-50.10	5.403	5.403	-44.70	
8	1 + 777.40	2640.08	-124.336	-50.31				**	-50.481	-50.48	5.076	5.076	-45.41	

DENSITY = 2.2

check 1

LINE #	STATION #	ELEVATION	6 boug (dens. = 2.67) agals	6 boug (new dens.) agals	TOPO CORR. (orig.)	TOPO CORR. (new)	6 boug (with topo corr)	** (dens. = 2.00) agals	6 boug (with topo corr) **	G boug (new dens.) agals	TOPO CORR. (orig.)	TOPO CORR. (new)	G boug (with topo corr) **
1	1 + 297.70	2031.93	-112.297	-72.33	6.668	5.49	-66.84 **	-55.302		-72.31	4.986	5.485	-66.82
1	1 + 200.00	2036.75	-112.238	-72.18	6.836	5.63	-66.54 **	-55.106		-72.15	5.052	5.557	-66.60
1	1 + 211.91	2049.28	-112.642	-71.94	6.396	5.27	-66.67 **	-54.601		-71.92	4.791	5.270	-66.65
1	1 + 000.00	2084.36	-112.763	-71.76	6.432	5.30	-66.46 **	-54.296		-71.74	4.745	5.220	-66.52
1	0 + 900.00	2090.32	-113.772	-72.66	6.07	5.00	-67.65 **	-54.588		-72.08	4.546	5.001	-67.08
1	0 + 800.00	2086.59	-113.772	-72.73	6.342	5.23	-67.50 **	-55.243		-72.71	4.751	5.226	-67.48
1	0 + 706.80	2097.98	-114.693	-73.43	7.256	5.98	-67.45 **	-55.847		-73.41	5.435	5.979	-67.43
1	0 + 600.00	2111.87	-116.174	-74.63	8.376	6.90	-67.73 **	-56.935		-74.61	6.274	6.901	-67.71
1	0 + 493.00	2136.12	-117.200	-75.18	9.158	7.55	-67.64 **	-57.283		-75.16	6.87	7.557	-67.61
1	0 + 408.00	2146.18	-118.000	-75.79	10.362	8.54	-67.25 **	-57.802		-75.77	7.762	8.538	-67.23
1	0 + 302.00	2201.37	-120.309	-77.01	10.907	8.99	-68.02 **	-58.560		-76.99	8.17	8.987	-68.00
1	0 + 197.00	2249.83	-122.055	-77.80	10.672	8.79	-69.01 **	-58.945		-77.78	7.994	8.793	-68.98
2	0 + 928.67	2014.73	-108.622	-68.99	8.871	7.31	-61.68 **	-52.110		-68.97	6.645	7.310	-61.66
2	0 + 820.69	2041.99	-109.779	-69.61	7.460	6.15	-63.47 **	-52.504		-69.60	5.605	6.166	-63.43
2	0 + 741.68	2060.72	-112.292	-71.37	9.100	7.50	-63.87 **	-53.948		-71.36	6.817	7.499	-63.86
2	0 + 637.72	1984.49	-111.141	-72.11	10.074	8.30	-63.81 **	-55.476		-72.09	7.546	8.301	-63.79
2	0 + 525.00	1890.87	-112.058	-74.87	14.385	11.85	-63.01 **	-59.018		-74.84	10.776	11.854	-62.99
2	0 + 412.10	1953.69	-110.882	-72.45	10.655	8.78	-63.67 **	-56.081		-72.43	7.981	8.779	-63.65
2	0 + 330.31	1953.90	-110.844	-72.41	10.369	8.54	-63.87 **	-56.037		-72.39	7.768	8.545	-63.85
2	0 + 240.78	1992.83	-111.478	-72.28	8.519	7.02	-65.26 **	-55.581		-72.26	6.381	7.019	-65.24
2	0 + 130.02	2018.32	-112.739	-73.04	8.298	6.84	-66.20 **	-56.126		-73.02	6.216	6.838	-66.18
2	0 + 850.00	2042.36	-112.551	-72.38	8.079	6.66	-65.72 **	-55.262		-72.36	6.052	6.657	-65.70
2	0 + 071.51	2032.90	-113.394	-73.41	8.449	6.96	-66.45 **	-56.371		-73.39	6.329	6.962	-66.42
2	0 + 168.49	2017.82	-113.929	-74.24	9.956	8.20	-66.04 **	-57.330		-74.22	7.455	8.201	-66.02
2	0 + 274.86	2031.34	-114.128	-74.17	10.623	8.75	-65.42 **	-57.782		-74.78	7.952	8.747	-66.04
2	0 + 372.00	2042.06	-116.608	-76.44	12.448	10.26	-66.18 **	-59.330		-76.42	9.325	10.258	-66.16
2	0 + 470.47	2082.97	-117.840	-76.87	12.968	10.69	-66.18 **	-59.410		-76.84	9.714	10.685	-66.16
2	0 + 570.63	2152.43	-119.222	-76.88	12.144	10.01	-66.88 **	-58.847		-76.86	9.096	10.006	-66.86
2	0 + 661.85	2226.04	-121.260	-77.47	11.240	9.26	-68.21 **	-58.840		-77.47	8.445	9.290	-68.18
2	0 + 736.44	2195.00	-121.067	-77.89			**	-59.497		-77.87	10.414	11.455	-66.41
2	0 + 856.91	2311.17	-123.162	-77.70			**	-58.333		-77.68	8.985	9.884	-67.79
2	0 + 971.53	2404.37	-125.977	-78.68			**	-58.534		-78.66	8.836	9.720	-68.94
2	1 + 189.12	2544.88	-128.044	-77.99			**	-58.231		-79.53	7.893	8.682	-70.85
2	1 + 271.49	2591.70	-131.244	-80.27			**	-58.541		-80.23	7.152	7.867	-72.37
2	1 + 334.09	2639.12	-134.219	-82.31			**	-60.398		-82.49	7.246	7.971	-74.52
2	1 + 371.32	2644.36	-134.219	-82.21			**	-60.043		-82.18	6.586	7.245	-74.93
2	1 + 493.42	2625.38	-131.438	-79.80			**	-57.796		-79.77	4.857	5.343	-74.43
2	1 + 567.60	2625.47	-131.566	-79.92			**	-57.911		-79.89	4.644	5.108	-74.78
2	1 + 676.35	2644.44	-132.5	-80.49			**	-58.325		-80.46	4.507	4.958	-75.50
2	1 + 792.31	2672.99	-134.199	-81.62			**	-59.224		-81.60	4.807	5.288	-76.31
2	1 + 880.57	2676.17	-133.436	-80.80			**	-58.369		-80.77	4.673	5.140	-75.63
2	1 + 986.21	2707.54	-133.24	-79.98			**	-57.295		-79.96	4.729	5.202	-74.76
2	2 + 095.22	2745.62	-134.608	-80.60			**	-57.597		-80.58	4.927	5.420	-75.16
2	2 + 189.42	2799.47	-136.706	-81.64			**	-58.18		-81.61	5.185	5.784	-75.91

DENSITY = 2.2

check I

LINE #	STATION #	ELEVATION	6 boug (dens. = 2.67) mgals	6 boug (new dens.) mgals	TOPO CORR. (orig.)	TOPO CORR. (new)	6 boug (with topo corr)	**	6 boug (dens. = 2.00) mgals	6 boug (new dens.) mgals	TOPO CORR. (orig.)	TOPO CORR. (new)	6 boug (with topo corr)	**
3	1 + 000.00	2006.50	-110.341	-70.87	8.549	7.04	-63.83	**	-54.058	-70.85	6.404	7.044	-63.81	**
3	0 + 871.00	1908.13	-109.093	-71.56	10.948	9.02	-62.54	**	-55.571	-71.54	8.2	9.020	-62.52	**
3	0 + 800.00	1881.82	-109.031	-72.02	12.340	10.17	-61.85	**	-56.247	-72.00	9.234	10.157	-61.84	**
3	0 + 718.20	1877.49	-109.455	-72.53	12.694	10.46	-62.07	**	-56.791	-72.51	9.48	10.428	-62.08	**
3	0 + 593.20	1904.29	-109.897	-72.44	12.102	9.97	-62.47	**	-56.484	-72.42	9.065	9.972	-62.45	**
3	0 + 510.20	1916.59	-110.605	-72.91	12.25	10.09	-62.81	**	-56.845	-72.89	9.176	10.094	-62.79	**
3	0 + 434.00	1948.15	-110.514	-72.19	11.764	9.69	-62.50	**	-55.867	-72.17	8.693	9.562	-62.61	**
3	0 + 285.00	2010.22	-111.651	-72.11	8.139	6.71	-65.40	**	-55.265	-72.09	6.097	6.707	-65.38	**
3	0 + 203.00	2018.54	-111.628	-71.92	8.532	7.03	-64.89	**	-55.010	-71.91	6.391	7.030	-64.88	**
3	0 + 100.00	2027.70	-112.087	-72.20	8.992	7.41	-64.79	**	-55.210	-72.18	6.737	7.411	-64.77	**
3	0 + 364.98	2038.92	-112.944	-72.84	9.869	8.13	-64.71	**	-55.747	-72.81	7.392	8.131	-64.68	**
3	0 + 101.70	2060.05	-113.700	-73.18	11.12	9.16	-64.02	**	-55.914	-73.16	8.364	9.200	-63.96	**
3	0 + 200.00	2069.17	-114.741	-73.65	12.136	10.00	-63.65	**	-56.139	-73.63	9.09	9.999	-63.63	**
3	0 + 300.00	2117.23	-116.884	-75.24	13.913	11.46	-63.78	**	-57.497	-75.22	10.42	11.462	-63.76	**
3	0 + 491.00	2253.21	-120.846	-76.53	13.635	11.23	-65.29	**	-57.644	-76.50	10.22	11.242	-65.26	**
4	1 + 221.70	1858.08	-108.227	-71.68	12.64	10.41	-61.26	**	-56.107	-71.66	9.498	10.448	-61.21	**
4	1 + 125.50	1878.11	-108.470	-71.53	12.517	10.31	-61.21	**	-55.789	-71.51	9.396	10.336	-61.17	**
4	1 + 034.70	1902.97	-108.775	-71.34	12.239	10.08	-61.26	**	-55.399	-71.33	9.167	10.084	-61.24	**
4	0 + 922.70	1977.20	-109.691	-70.80	10.24	8.44	-62.36	**	-54.231	-70.78	7.671	8.438	-62.34	**
4	0 + 825.00	1998.27	-109.355	-70.05	9.242	7.62	-62.43	**	-53.303	-70.03	6.949	7.644	-62.38	**
4	0 + 725.00	2010.85	-109.314	-69.76	8.963	7.39	-62.38	**	-52.909	-69.74	6.714	7.385	-62.35	**
4	0 + 625.00	2026.27	-107.78	-67.92	8.637	7.12	-60.81	**	-52.942	-69.90	6.53	7.183	-62.72	**
4	0 + 518.00	2035.44	-110.248	-70.21	8.503	7.01	-63.21	**	-53.156	-70.19	6.367	7.004	-63.19	**
4	0 + 425.00	2050.85	-110.305	-69.97	8.557	7.05	-62.92	**	-52.777	-69.94	6.409	7.050	-62.89	**
4	0 + 325.00	2057.29	-110.886	-70.42	8.989	7.41	-63.01	**	-53.179	-70.40	6.733	7.406	-62.99	**
4	0 + 225.00	2067.44	-111.467	-70.80	9.828	8.10	-62.70	**	-53.477	-70.78	7.362	8.098	-62.68	**
4	0 + 125.00	2072.36	-112.449	-71.69	10.779	8.88	-62.81	**	-54.318	-71.66	8.074	8.881	-62.78	**
4	0 + 100.30	2070.24	-113.833	-73.11	12.877	10.61	-62.50	**	-55.764	-73.09	9.646	10.611	-62.48	**
4	0 + 071.40	2089.03	-114.122	-73.03	13.327	10.98	-62.05	**	-55.626	-73.11	9.983	10.981	-62.13	**
4	0 + 175.00	2127.05	-115.567	-73.73	13.576	11.19	-62.54	**	-55.902	-73.71	10.17	11.187	-62.52	**
4	0 + 249.80	2182.34	-116.79	-73.86	12.589	10.37	-63.49	**	-55.577	-73.84	9.426	10.369	-63.47	**
4	0 + 375.00	2249.97	-118.668	-74.41	13.094	10.79	-63.62	**	-55.558	-74.39	9.81	10.791	-63.60	**
4	0 + 474.00	2328.34	-120.579	-74.78	13.051	10.75	-64.03	**	-55.27	-74.76	9.776	10.754	-64.00	**
4	0 + 575.80	2402.01	-121.989	-74.74	12.892	10.62	-64.12	**	-54.613	-74.72	9.657	10.623	-64.10	**
4	0 + 680.56	2496.02	-122.212	-73.12			-54.354	**	-54.354	-75.25	9.582	10.540	-64.71	**
4	0 + 795.45	2596.56	-124.102	-73.03			-53.637	**	-53.637	-75.37	8.382	9.220	-66.15	**
4	0 + 896.43	2633.69	-127.081	-75.28			-54.05	**	-54.05	-76.09	7.374	8.111	-67.98	**
4	1 + 011.56	2697.38	-127.419	-74.36			-53.818	**	-53.818	-76.40	6.424	7.066	-69.33	**
4	1 + 094.36	2721.44	-130.354	-76.82			-54.05	**	-54.05	-76.83	8.501	9.351	-67.48	**
4	1 + 100.10	2720.89	-129.76	-76.24			-53.439	**	-53.439	-76.21	8.392	9.231	-66.98	**
4	1 + 225.46	2731.6	-128.373	-74.64			-51.895	**	-51.895	-74.76	6.639	7.303	-67.46	**
4	1 + 300.00	2785.83	-131.89	-77.09			-53.748	**	-53.748	-77.07	7.459	8.206	-68.86	**
4	1 + 408.64	2806.87	-131.891	-76.68			-53.157	**	-53.157	-76.65	7.65	8.415	-68.24	**
4	1 + 500.00	2841.41	-133.341	-77.45			-53.64	**	-53.64	-77.42	6.706	7.379	-70.04	**

DENSITY = 2.2

check 1

LINE #	STATION #	ELEVATION #	G boug		TOPO CORR.		G boug		G boug		TOPO CORR.		G boug	
			(dens. = 2.67) #gals	(new dens.) #gals	(orig.)	(new)	(with topo corr)	** #	(dens. = 2.00) #gals	(new dens.) #gals	(orig.)	(new)	(with topo corr)	** #gals
4	1 + 600.62	2849.29	-133.199	-77.15										
4	1 + 674.64	2835.67	-132.702	-76.93										
5	1 + 400.09	1864.17	-106.235	-69.57	12.306	10.14								
5	1 + 200.07	1899.91	-107.573	-70.22	12.424	10.24	-59.43 **	-53.944						
5	1 + 000.23	1937.96	-108.573	-70.45	12.381	10.20	-59.98 **	-54.306						
5	1 + 797.32	1981.4	-110.109	-71.14	11.817	9.74	-60.25 **	-54.236						
5	0 + 600.02	2049.13	-109.91	-69.60	8.833	7.28	-61.40 **	-54.531						
5	0 + 399.81	2083.37	-110.741	-69.76	8.21	6.76	-62.33 **	-52.433						
5	0 + 200.22	2104.22	-111.303	-69.91	8.448	6.96	-63.00 **	-52.302						
5	0 + 290.04	2116.74	-112.465	-70.83	10.431	8.59	-62.95 **	-52.28						
5	0 + 199.99	2131.44	-114.332	-72.41	12.364	10.19	-62.23 **	-53.091						
5	0 + 399.84	2234.86	-117.537	-73.58	11.943	9.84	-62.22 **	-54.546						
6	0 + 311.58	2167.96	-111.145	-68.50	9.255	7.63	-63.74 **	-54.848						
6	0 + 200.30	2167.47	-111.218	-68.58	8.992	7.41	-60.88 **	-50.335						
6	0 + 117.63	2192.56	-111.37	-68.24	8.548	7.04	-61.18 **	-50.42						
6	0 + 510.00	2171.03	-111.059	-68.36	9.738	8.02	-61.20 **	-49.818						
6	0 + 105.69	2189.53	-112.088	-69.02	10.259	8.45	-60.33 **	-50.163						
6	0 + 198.73	2237.6	-113.825	-69.81	9.511	7.84	-60.57 **	-50.673						
6	0 + 303.82	2242.3	-115.084	-70.98	10.630	8.76	-61.98 **	-51.061						
6	0 + 405.11	2223.24	-116.054	-72.32	13.250	10.92	-62.22 **	-52.188						
6	0 + 488.99	2288.97	-117.197	-72.17	11.282	9.30	-61.41 **	-53.693						
6	0 + 602.34	2342.58	-118.271	-72.19	11.806	9.73	-62.88 **	-52.993						
7	0 + 462.60	2268.37	-112.959	-68.34	10.872	8.96	-62.47 **	-52.561						
7	0 + 280.00	2235.93	-111.179	-67.20	10.130	8.35	-59.38 **	-49.331						
7	0 + 145.70	2271.2	-111.575	-66.90	9.709	8.00	-58.85 **	-48.462						
7	0 + 080.00	2259.46	-111.672	-67.23	9.338	7.69	-58.90 **	-47.868						
7	0 + 655.00	2234.38	-111.374	-67.42	9.253	7.62	-59.54 **	-48.293						
7	0 + 120.00	2247.7	-111.885	-67.67	9.789	8.07	-59.80 **	-48.699						
7	0 + 320.00	2303.88	-114.44	-69.12	9.568	7.88	-59.61 **	-48.837						
7	0 + 540.00	2355.97	-116.706	-70.37	11.199	9.23	-61.24 **	-49.815						
7	0 + 598.00	2374.57	-117.499	-70.79	11.250	9.27	-61.14 **	-50.637						
8	0 + 394.80	2503.02	-121.109	-71.88	15.797	13.02	-61.52 **	-50.892						
8	0 + 144.00	2464.35	-117.37	-68.90	11.375	9.37	-58.86 **	-50.9						
8	0 + 268.00	2493.16	-120.678	-71.64	13.386	11.03	-59.52 **	-48.244						
8	0 + 400.80	2520.91	-122.384	-72.80	13.558	11.17	-60.61 **	-50.744						
8	0 + 737.60	2578.17	-123.735	-73.02	12.609	9.90	-61.63 **	-51.673						
8	0 + 804.30	2590.43	-124.18	-73.23			-63.13 **	-51.416						
8	0 + 919.20	2590.40	-125.508	-74.56			**	-51.52						
8	1 + 000.00	2607.79	-124.019	-72.73			**	-52.104						
8	1 + 144.45	2587.72	-122.082	-71.18			**	-50.871						
8	1 + 219.50	2617.00	-123.263	-71.79			**	-72.70						
8	1 + 276.00	2633.68	-123.607	-71.80			**	-71.17						
8	1 + 371.90	2652.09	-124.111	-71.95			**	-71.76						
8	1 + 472.70	2651.13	-123.963	-71.82			**	-49.856						
							**	-49.545						
							**	-49.719						
							**	-49.5						
							**	-77.13	6.547	7.202				-69.92
							**	-76.90	5.662	6.228				-70.67
							**	-69.55	9.222	10.144				-59.40
							**	-70.20	9.234	10.157				-60.04
							**	-70.46	9.277	10.205				-60.25
							**	-71.12	8.712	9.583				-61.53
							**	-69.58	6.617	7.279				-62.31
							**	-69.74	6.149	6.754				-62.98
							**	-69.89	6.328	6.961				-62.93
							**	-70.81	7.814	8.595				-62.21
							**	-72.39	9.263	10.189				-62.20
							**	-73.55	8.946	9.841				-63.71
							**	-68.48	6.933	7.626				-60.85
							**	-68.17	6.403	7.043				-61.13
							**	-68.56	6.733	7.406				-61.16
							**	-68.33	7.267	7.994				-60.34
							**	-69.00	7.684	8.452				-60.55
							**	-69.79	7.093	7.802				-61.99
							**	-70.96	7.964	8.760				-62.20
							**	-72.30	9.925	10.918				-61.38
							**	-72.15	8.379	9.217				-62.93
							**	-72.17	8.815	9.697				-62.47
							**	-68.32	8.143	8.957				-59.36
							**	-67.18	7.588	8.347				-58.83
							**	-66.88	7.271	7.998				-58.88
							**	-67.20	6.968	7.665				-59.54
							**	-67.40	6.942	7.636				-59.76
							**	-67.65	7.333	8.066				-59.58
							**	-69.10	7.178	7.896				-61.20
							**	-70.36	8.389	9.228				-61.13
							**	-70.77	8.413	9.254				-61.51
							**	-71.85	11.831	13.014				-58.84
							**	-68.87	8.523	9.375				-59.50
							**	-71.61	10.026	11.029				-60.58
							**	-72.77	10.17	11.187				-61.59
							**	-73.00	8.763	9.639				-63.36
							**	-73.20	8.247	9.072				-64.13
							**	-73.79	8.009	8.810				-64.98
							**	-72.70	5.996	6.596				-66.10
							**	-71.17	4.629	5.092				-66.06
							**	-71.76	4.787	5.266				-66.49
							**	-71.69	4.763	5.239				-66.45
							**	-71.92	5.136	5.650				-66.27
							**	-71.69	4.686	5.155				-66.54

DENSITY = 2.2

check 1

LINE #	STATION #	ELEVATION	G boug	G boug	TOPO CORR.	TOPO CORR.	G boug	**	G boug	G boug	TOPO CORR.	TOPO CORR.	G boug	**	
			(dens. = 2.67)	(new dens.)	(orig.)	(new)	(with topo corr)	(dens. = 2.00)	(new dens.)	(orig.)	(new)	(with topo corr)	(new dens.)	(orig.)	(new)
			mgals	mgals						mgals					
8	1 + 554.60	2651.86	-124.489	-72.33						-50.104	-72.30	5.403	5.943	-66.36	
8	1 + 777.40	2640.08	-124.336	-72.41						-50.481	-72.58	5.076	5.584	-66.99	

DENSITY = 2.3

check 1

LINE #	STATION #	ELEVATION	G boug (dens. = 2.67) # #gals	G boug (new dens.) (new dens.) #gals	TOPO CORR. (orig.)	TOPO CORR. (new)	G boug (with topo corr) #	** #	G boug (dens. = 2.00) # #gals	G boug (new dens.) #gals	TOPO CORR. (orig.)	TOPO CORR. (new)	G boug (with topo corr) #	** #
1	1 + 297.70	2031.93	-112.297	-80.83	6.668	5.74	-75.09	**	-55.302	-80.81	4.986	5.734	-75.08	**
1	1 + 200.00	2036.75	-112.238	-80.70	6.836	5.89	-74.81	**	-55.106	-80.68	5.052	5.810	-74.87	**
1	1 + 211.91	2069.28	-112.642	-80.60	6.396	5.51	-75.09	**	-54.601	-80.58	4.791	5.510	-75.07	**
1	1 + 000.00	2084.36	-112.763	-80.49	6.432	5.54	-74.95	**	-54.296	-80.47	4.745	5.457	-75.01	**
1	0 + 900.00	2090.32	-113.772	-81.40	6.07	5.23	-76.18	**	-54.588	-80.83	4.546	5.228	-75.60	**
1	0 + 800.00	2086.59	-113.772	-81.46	6.342	5.46	-76.00	**	-55.243	-81.44	4.751	5.464	-75.98	**
1	0 + 706.80	2097.98	-114.693	-82.21	7.256	6.25	-75.96	**	-55.847	-82.19	5.435	6.250	-75.94	**
1	0 + 600.00	2111.87	-116.174	-83.47	8.376	7.22	-76.26	**	-56.935	-83.45	6.274	7.215	-76.23	**
1	0 + 493.00	2136.12	-117.200	-84.12	9.158	7.89	-76.23	**	-57.283	-84.10	6.87	7.900	-76.20	**
1	0 + 408.00	2146.18	-118.000	-84.77	10.362	8.93	-75.84	**	-57.802	-84.75	7.762	8.926	-75.82	**
1	0 + 302.00	2201.57	-120.309	-86.22	10.907	9.40	-76.83	**	-58.560	-86.20	8.17	9.395	-76.80	**
1	0 + 197.00	2249.83	-122.055	-87.22	10.672	9.19	-78.02	**	-58.945	-87.19	7.994	9.193	-78.00	**
2	0 + 928.67	2014.73	-108.622	-77.42	8.871	7.64	-69.78	**	-52.110	-77.40	6.645	7.642	-69.76	**
2	0 + 820.69	2041.99	-109.779	-78.16	7.460	6.43	-71.73	**	-52.504	-78.14	5.605	6.446	-71.70	**
2	0 + 741.68	2080.72	-112.292	-80.07	9.100	7.84	-72.23	**	-53.948	-80.07	6.817	7.840	-72.23	**
2	0 + 637.72	1984.49	-111.141	-80.41	10.074	8.68	-71.73	**	-55.476	-80.39	7.546	8.678	-71.71	**
2	0 + 525.00	1890.87	-112.058	-82.78	14.385	12.39	-70.39	**	-59.018	-82.76	10.776	12.392	-70.37	**
2	0 + 412.10	1953.69	-110.882	-80.63	10.655	9.18	-71.45	**	-56.081	-80.61	7.981	9.178	-71.43	**
2	0 + 330.31	1953.90	-110.844	-80.59	10.369	8.93	-71.66	**	-56.037	-80.57	7.768	8.933	-71.64	**
2	0 + 240.78	1992.83	-111.478	-80.62	8.519	7.34	-73.28	**	-55.581	-80.60	6.381	7.338	-73.26	**
2	0 + 130.02	2018.32	-112.739	-81.49	8.298	7.15	-74.34	**	-56.126	-81.47	6.216	7.148	-74.32	**
2	0 + 850.00	2042.36	-112.551	-80.93	8.079	6.96	-73.97	**	-55.262	-80.90	6.052	6.960	-73.94	**
2	0 + 071.51	2032.90	-113.394	-81.92	8.449	7.28	-74.64	**	-56.371	-81.89	6.329	7.278	-74.62	**
2	0 + 168.49	2017.82	-113.929	-82.68	9.956	8.58	-74.11	**	-57.330	-82.66	7.455	8.573	-74.09	**
2	0 + 274.86	2031.34	-114.128	-82.67	10.623	9.15	-73.52	**	-57.782	-83.29	7.952	9.145	-74.14	**
2	0 + 372.00	2042.06	-116.608	-84.99	12.448	10.72	-74.26	**	-59.330	-84.97	9.325	10.724	-74.24	**
2	0 + 470.47	2082.97	-117.840	-85.59	12.968	11.17	-74.42	**	-59.410	-85.56	9.714	11.171	-74.39	**
2	0 + 570.63	2152.43	-119.222	-85.89	12.144	10.46	-75.43	**	-58.847	-85.87	9.096	10.460	-75.41	**
2	0 + 661.85	2226.04	-121.260	-86.79	11.240	9.68	-77.11	**	-58.840	-86.79	8.445	9.712	-77.08	**
2	0 + 736.44	2195.00	-121.067	-87.06			**	**	-59.497	-87.06	10.414	11.976	-75.08	**
2	0 + 856.91	2311.17	-123.162	-87.37			**	**	-58.333	-87.35	8.985	10.333	-77.02	**
2	0 + 971.53	2404.37	-125.977	-88.75			**	**	-58.534	-88.72	8.836	10.161	-78.56	**
2	1 + 189.12	2544.88	-128.044	-88.64			**	**	-58.231	-90.18	7.893	9.077	-81.11	**
2	1 + 271.49	2591.70	-131.244	-91.11			**	**	-58.541	-91.08	7.152	8.225	-82.85	**
2	1 + 334.09	2639.12	-134.219	-93.35			**	**	-60.398	-93.53	7.246	8.333	-85.20	**
2	1 + 371.32	2644.36	-134.219	-93.27			**	**	-60.043	-93.24	6.586	7.574	-85.67	**
2	1 + 493.42	2625.38	-131.438	-90.79			**	**	-57.796	-90.76	4.857	5.586	-85.17	**
2	1 + 567.60	2625.47	-131.566	-90.91			**	**	-57.911	-90.87	4.644	5.341	-85.53	**
2	1 + 676.35	2644.44	-132.5	-91.55			**	**	-58.325	-91.53	4.507	5.183	-86.34	**
2	1 + 792.31	2672.99	-134.199	-92.81			**	**	-59.224	-92.78	4.807	5.529	-87.26	**
2	1 + 880.57	2676.17	-133.436	-92.00			**	**	-58.369	-91.97	4.673	5.374	-86.59	**
2	1 + 986.21	2707.54	-133.24	-91.32			**	**	-57.295	-91.29	4.729	5.436	-85.85	**
2	2 + 095.22	2745.62	-134.608	-92.09			**	**	-57.597	-92.07	4.927	5.666	-86.40	**
2	2 + 189.42	2799.47	-136.706	-93.36			**	**	-58.18	-93.33	5.135	5.963	-87.36	**

DENSITY = 2.3

check I

LINE #	STATION #	ELEVATION	G boug (dens. = 2.67) mgals	G boug (new dens.) mgals	TOPO CORR. (orig.)	TOPO CORR. (new)	G boug (with topo corr) **	** (dens. = 2.00) mgals	G boug (new dens.) mgals	TOPO CORR. (orig.)	TOPO CORR. (new)	G boug (with topo corr) **	** mgals
3	1 + 000.00	2006.50	-110.341	-79.27	8.549	7.36	-71.91 **	-54.058	-79.25	6.404	7.365	-71.89	
3	0 + 871.00	1908.13	-109.093	-79.55	10.948	9.43	-70.12 **	-55.571	-79.53	8.2	9.430	-70.10	
3	0 + 800.00	1881.82	-109.031	-79.89	12.340	10.63	-69.26 **	-56.247	-79.87	9.234	10.619	-69.25	
3	0 + 718.20	1877.49	-109.455	-80.38	12.694	10.93	-69.45 **	-56.791	-80.36	9.48	10.902	-69.46	
3	0 + 593.20	1904.29	-109.897	-80.41	12.102	10.42	-69.99 **	-56.484	-80.39	9.065	10.425	-69.97	
3	0 + 510.20	1916.59	-110.605	-80.93	12.25	10.55	-70.38 **	-56.845	-80.91	9.176	10.552	-70.36	
3	0 + 434.00	1948.15	-110.514	-80.35	11.764	10.13	-70.21 **	-55.867	-80.33	8.693	9.997	-70.33	
3	0 + 285.00	2010.22	-111.651	-80.52	8.139	7.01	-73.51 **	-55.265	-80.50	6.097	7.012	-73.49	
3	0 + 203.00	2018.54	-111.628	-80.37	8.532	7.35	-73.02 **	-55.010	-80.35	6.391	7.350	-73.00	
3	0 + 100.00	2027.70	-112.087	-80.69	8.992	7.75	-72.94 **	-55.210	-80.67	6.737	7.748	-72.92	
3	0 + 364.98	2038.92	-112.944	-81.37	9.869	8.50	-72.87 **	-55.747	-81.35	7.392	8.501	-72.84	
3	0 + 101.70	2060.05	-113.700	-81.80	11.12	9.58	-72.22 **	-55.914	-81.78	8.364	9.619	-72.16	
3	0 + 200.00	2089.17	-114.741	-82.39	12.136	10.45	-71.94 **	-56.139	-82.37	9.09	10.453	-71.92	
3	0 + 300.00	2117.23	-116.884	-84.10	13.913	11.98	-72.11 **	-57.497	-84.06	10.42	11.983	-72.10	
3	0 + 491.00	2253.21	-120.846	-85.96	13.635	11.75	-74.21 **	-57.644	-85.93	10.22	11.753	-74.18	
4	1 + 221.70	1858.08	-108.227	-79.46	12.64	10.89	-68.57 **	-56.107	-79.44	9.498	10.923	-68.51	
4	1 + 125.50	1878.11	-108.470	-79.39	12.517	10.78	-68.61 **	-55.789	-79.37	9.396	10.805	-68.56	
4	1 + 034.70	1902.97	-108.775	-79.31	12.239	10.54	-68.77 **	-55.399	-79.29	9.167	10.542	-68.75	
4	0 + 922.70	1977.20	-109.691	-79.08	10.24	8.82	-70.25 **	-54.231	-79.05	7.671	8.822	-70.23	
4	0 + 825.00	1998.27	-109.355	-78.41	9.242	7.96	-70.45 **	-53.303	-78.39	6.949	7.991	-70.40	
4	0 + 725.00	2010.85	-109.314	-78.18	8.963	7.72	-70.46 **	-52.909	-78.16	6.714	7.721	-70.43	
4	0 + 625.00	2026.27	-107.78	-76.40	8.637	7.44	-68.96 **	-52.942	-78.38	6.53	7.510	-70.87	
4	0 + 518.00	2035.44	-110.248	-78.73	8.503	7.32	-71.41 **	-53.156	-78.71	6.367	7.322	-71.39	
4	0 + 425.00	2050.85	-110.305	-78.55	8.557	7.37	-71.18 **	-52.777	-78.53	6.409	7.370	-71.16	
4	0 + 325.00	2057.29	-110.886	-79.03	8.989	7.74	-71.29 **	-53.179	-79.01	6.733	7.743	-71.27	
4	0 + 225.00	2067.44	-111.467	-79.45	9.828	8.47	-70.99 **	-53.477	-79.43	7.362	8.466	-70.97	
4	0 + 125.00	2072.36	-112.449	-80.36	10.779	9.29	-71.07 **	-54.318	-80.34	8.074	9.285	-71.05	
4	0 + 100.30	2070.24	-113.833	-81.78	12.877	11.09	-70.68 **	-55.764	-81.76	9.646	11.093	-70.66	
4	0 + 071.40	2089.03	-114.122	-81.77	13.327	11.48	-70.29 **	-55.626	-81.85	9.983	11.480	-70.37	
4	0 + 175.00	2127.05	-115.567	-82.63	13.576	11.69	-70.94 **	-55.902	-82.61	10.17	11.696	-70.91	
4	0 + 249.80	2182.34	-116.79	-83.00	12.589	10.84	-72.15 **	-55.577	-82.98	9.426	10.840	-72.14	
4	0 + 375.00	2249.97	-118.668	-83.83	13.094	11.28	-72.55 **	-55.558	-83.81	9.81	11.282	-72.52	
4	0 + 474.00	2328.34	-120.579	-84.53	13.051	11.24	-73.28 **	-55.27	-84.50	9.776	11.242	-73.26	
4	0 + 575.80	2402.01	-121.989	-84.80	12.892	11.11	-73.69 **	-54.613	-84.77	9.657	11.106	-73.66	
4	0 + 680.56	2496.02	-122.212	-83.56				-54.354	-85.69	9.582	11.019	-74.67	
4	0 + 795.45	2596.56	-124.102	-83.90				-53.637	-86.24	8.382	9.639	-76.60	
4	0 + 896.43	2633.69	-127.081	-86.30				-54.05	-87.12	7.374	8.480	-76.64	
4	1 + 011.56	2697.38	-127.419	-85.65				-53.818	-87.68	6.424	7.388	-80.20	
4	1 + 094.36	2721.44	-130.354	-88.21				-54.05	-88.22	8.501	9.776	-78.44	
4	1 + 100.10	2720.89	-129.76	-87.63				-53.439	-87.60	8.392	9.651	-77.95	
4	1 + 225.46	2731.6	-128.373	-86.08				-51.895	-86.19	6.639	7.635	-78.56	
4	1 + 300.00	2785.83	-131.89	-88.75				-53.748	-88.72	7.459	8.578	-80.15	
4	1 + 408.64	2806.87	-131.891	-88.43				-53.157	-88.40	7.65	8.798	-79.60	
4	1 + 500.00	2841.41	-133.341	-89.34				-53.64	-89.31	6.708	7.714	-81.60	

DENSITY = 2.3

check 1

LINE #	STATION #	ELEVATION	G boug (dens. = 2.67) agals	G boug (new dens.) agals	TOPO CORR. (orig.)	TOPO CORR. (new)	G boug ** (with topo corr) **	G boug (dens. = 2.00) agals	G boug (new dens.) agals	TOPO CORR. (orig.)	TOPO CORR. (new)	G boug (with topo corr) **	G boug (dens. = 2.00) agals
4	1 + 600.62	2849.29	-133.199	-89.08				-53.277					-89.05
4	1 + 674.64	2835.67	-132.702	-88.79				-53.161					-88.76
5	1 + 400.09	1864.17	-106.235	-77.37	12.306	10.60	-66.77 **	-53.944					-77.35
5	1 + 200.07	1899.01	-107.573	-78.17	12.424	10.70	-67.47 **	-54.306					-78.15
5	1 + 000.23	1937.96	-108.573	-78.56	12.381	10.67	-67.90 **	-54.236					-78.57
5	1 + 797.32	1981.4	-110.109	-79.43	11.817	10.18	-69.25 **	-54.531					-79.41
5	0 + 600.02	2049.13	-109.91	-78.18	8.833	7.61	-70.57 **	-52.433					-78.16
5	0 + 399.81	2083.37	-110.741	-78.48	8.21	7.07	-71.41 **	-52.302					-78.46
5	0 + 200.22	2104.22	-111.303	-78.72	8.448	7.28	-71.44 **	-52.28					-78.70
5	0 + 290.04	2116.74	-112.465	-79.69	10.431	8.99	-70.70 **	-53.091					-79.67
5	0 + 199.99	2131.44	-114.332	-81.33	12.364	10.65	-70.68 **	-54.546					-81.31
5	0 + 399.84	2234.86	-117.537	-82.93	11.943	10.29	-72.64 **	-54.848					-82.91
6	0 + 311.58	2167.96	-111.145	-77.58	9.255	7.97	-69.60 **	-50.335					-77.55
6	0 + 200.30	2167.47	-111.218	-77.66	8.992	7.75	-69.91 **	-50.42					-77.63
6	0 + 117.63	2192.56	-111.37	-77.42	8.548	7.36	-70.06 **	-49.818					-77.35
6	0 + 510.00	2171.03	-111.059	-77.44	9.738	8.39	-69.05 **	-50.163					-77.42
6	0 + 105.69	2189.53	-112.088	-78.18	10.259	8.84	-69.35 **	-50.673					-78.16
6	0 + 198.73	2237.6	-113.825	-79.18	9.511	8.19	-70.98 **	-51.061					-79.15
6	0 + 303.82	2242.3	-115.084	-80.36	10.630	9.16	-71.21 **	-52.188					-80.34
6	0 + 405.11	2223.24	-116.054	-81.63	13.250	11.41	-70.21 **	-53.693					-81.61
6	0 + 488.99	2288.97	-117.197	-81.75	11.282	9.72	-72.03 **	-52.993					-81.73
6	0 + 602.34	2342.58	-118.271	-82.00	11.806	10.17	-71.83 **	-52.561					-81.97
7	0 + 462.60	2268.37	-112.959	-77.83	10.872	9.37	-68.47 **	-49.331					-77.81
7	0 + 280.00	2235.93	-111.179	-76.56	10.130	8.73	-67.83 **	-48.462					-76.53
7	0 + 145.70	2271.2	-111.575	-76.41	9.709	8.36	-68.04 **	-47.868					-76.38
7	0 + 080.00	2259.46	-111.672	-76.69	9.338	8.04	-68.64 **	-48.293					-76.66
7	0 + 655.00	2234.38	-111.374	-76.78	9.253	7.97	-68.80 **	-48.699					-76.75
7	0 + 120.00	2247.7	-111.885	-77.08	9.789	8.43	-68.65 **	-48.837					-77.06
7	0 + 320.00	2303.88	-114.44	-78.77	9.568	8.24	-70.52 **	-49.815					-78.74
7	0 + 540.00	2355.97	-116.706	-80.22	11.199	9.65	-70.58 **	-50.637					-80.22
7	0 + 598.00	2374.57	-117.499	-80.73	11.250	9.69	-71.04 **	-50.892					-80.70
8	0 + 394.80	2503.02	-121.109	-82.35	15.797	13.61	-68.74 **	-50.9					-82.33
8	0 + 144.00	2464.35	-117.37	-79.21	11.375	9.80	-69.41 **	-48.244					-79.18
8	0 + 268.00	2493.16	-120.678	-82.07	13.386	11.53	-70.54 **	-50.744					-82.05
8	0 + 400.80	2520.91	-122.384	-83.35	13.558	11.66	-71.67 **	-51.673					-83.32
8	0 + 737.60	2578.17	-123.735	-83.81	12.009	10.34	-73.47 **	-51.416					-83.78
8	0 + 804.30	2590.43	-124.18	-84.07			**	-51.52					-84.04
8	0 + 919.20	2590.40	-125.508	-85.40			**	-52.104					-84.63
8	1 + 000.00	2607.79	-124.019	-83.64			**	-50.871					-83.61
8	1 + 144.45	2587.72	-122.082	-82.01			**	-49.514					-82.00
8	1 + 219.50	2617.00	-123.263	-82.74			**	-49.856					-82.71
8	1 + 276.00	2633.68	-123.607	-82.83			**	-49.845					-82.71
8	1 + 371.90	2652.09	-124.111	-83.04			**	-49.719					-83.02
8	1 + 472.70	2651.13	-123.963	-82.91			**	-49.5					-82.78

DENSITY = 2.3

check 1

LINE #	STATION #	ELEVATION	G boug (dens. = 2.67) #gals	G boug (new dens.) #gals	TOPO CORR. (orig.)	TOPO CORR. (new)	G boug (with topo corr)	** (dens. = 2.00) ** #gals	G boug ** #gals	G boug (new dens.) #gals	TOPO CORR. (orig.)	TOPO CORR. (new)	G boug (with topo corr)	** #gals
8	1 + 554.60	2651.86	-124.489	-83.43				**	-50.104	-83.40	5.403	6.213	-77.18	
8	1 + 777.40	2640.06	-124.336	-83.46				**	-50.481	-83.63	5.076	5.837	-77.79	

DENSITY = 2.67

check 1

LINE #	STATION #	ELEVATION #	G boug (dens. = 2.67) #gals	G boug (new dens.) #gals	TOPO CORR. (orig.)	TOPO CORR. (new)	G boug (with topo corr) #gals	** (dens. = 2.00) #gals	G boug (new dens.) #gals	TOPO CORR. (orig.)	TOPO CORR. (new)	G boug (with topo corr) #gals	**
1	1 + 297.70	2031.93	-112.297	-112.30	6.668	6.67	-105.63	**	-55.302	-112.28	4.986	6.656	-105.62
1	1 + 200.00	2036.75	-112.238	-112.24	6.836	6.84	-105.40	**	-55.106	-112.22	5.052	6.744	-105.47
1	1 + 211.91	2069.28	-112.642	-112.64	6.396	6.40	-106.25	**	-54.601	-112.62	4.791	6.396	-106.23
1	1 + 000.00	2084.36	-112.763	-112.76	6.432	6.43	-106.33	**	-54.296	-112.74	4.745	6.335	-106.41
1	0 + 900.00	2090.32	-113.772	-113.77	6.07	6.07	-107.70	**	-54.588	-113.20	4.546	6.069	-107.13
1	0 + 800.00	2086.59	-113.772	-113.77	6.342	6.34	-107.43	**	-55.243	-113.75	4.751	6.343	-107.41
1	0 + 706.80	2097.98	-114.693	-114.69	7.256	7.26	-107.44	**	-55.847	-114.67	5.435	7.256	-107.42
1	0 + 600.00	2111.87	-116.174	-116.17	8.376	8.38	-107.80	**	-56.935	-116.15	6.274	8.376	-107.77
1	0 + 493.00	2136.12	-117.200	-117.20	9.158	9.16	-108.04	**	-57.283	-117.18	6.87	9.171	-108.01
1	0 + 408.00	2146.18	-118.000	-118.00	10.362	10.36	-107.64	**	-57.802	-117.98	7.762	10.362	-107.62
1	0 + 302.00	2201.37	-120.309	-120.31	10.907	10.91	-109.40	**	-58.560	-120.29	8.17	10.907	-109.38
1	0 + 197.00	2249.83	-122.055	-122.06	10.672	10.67	-111.38	**	-58.945	-122.03	7.994	10.672	-111.36
2	0 + 928.67	2014.73	-108.622	-108.62	8.871	8.87	-99.75	**	-52.110	-108.60	6.645	8.871	-99.73
2	0 + 820.69	2041.99	-109.779	-109.78	7.460	7.46	-102.32	**	-52.504	-109.76	5.605	7.483	-102.28
2	0 + 741.68	2080.72	-112.292	-112.29	9.100	9.10	-103.19	**	-53.948	-112.29	6.817	9.101	-103.19
2	0 + 637.72	1984.49	-111.141	-111.14	10.074	10.07	-101.07	**	-55.476	-111.12	7.546	10.074	-101.05
2	0 + 525.00	1890.87	-112.058	-112.06	14.385	14.39	-97.67	**	-59.018	-112.04	10.776	14.386	-97.65
2	0 + 412.10	1953.69	-110.882	-110.88	10.655	10.66	-100.23	**	-56.081	-110.86	7.981	10.655	-100.21
2	0 + 330.31	1953.90	-110.844	-110.84	10.369	10.37	-100.48	**	-56.037	-110.82	7.768	10.370	-100.45
2	0 + 240.78	1992.83	-111.478	-111.48	8.519	8.52	-102.96	**	-55.581	-111.46	6.381	8.519	-102.94
2	0 + 130.02	2018.32	-112.739	-112.74	8.298	8.30	-104.44	**	-56.126	-112.72	6.216	8.298	-104.42
2	0 + 850.00	2042.36	-112.551	-112.55	8.079	8.08	-104.47	**	-55.262	-112.53	6.052	8.079	-104.45
2	0 + 071.51	2032.90	-113.394	-113.39	8.449	8.45	-104.95	**	-56.371	-113.37	6.329	8.449	-104.92
2	0 + 168.49	2017.82	-113.929	-113.93	9.956	9.96	-103.97	**	-57.330	-113.91	7.455	9.952	-103.96
2	0 + 274.86	2031.34	-114.128	-114.13	10.623	10.62	-103.51	**	-57.782	-114.74	7.952	10.616	-104.12
2	0 + 372.00	2042.06	-116.608	-116.61	12.448	12.45	-104.16	**	-59.330	-116.59	9.325	12.449	-104.14
2	0 + 470.47	2082.97	-117.840	-117.84	12.968	12.97	-104.87	**	-59.410	-117.82	9.714	12.968	-104.85
2	0 + 570.63	2152.43	-119.222	-119.22	12.144	12.14	-107.08	**	-58.847	-119.20	9.096	12.143	-107.06
2	0 + 661.85	2226.04	-121.260	-121.26	11.240	11.24	-110.02	**	-58.840	-121.26	8.445	11.274	-109.98
2	0 + 736.44	2195.00	-121.067	-121.07	**	**	**	**	-59.497	-121.04	10.414	13.903	-107.14
2	0 + 856.91	2311.17	-123.162	-123.16	**	**	**	**	-58.333	-123.14	8.985	11.995	-111.14
2	0 + 971.53	2404.37	-125.977	-125.98	**	**	**	**	-58.534	-125.95	8.836	11.796	-114.16
2	1 + 189.12	2544.88	-128.044	-128.04	**	**	**	**	-58.231	-129.59	7.893	10.537	-119.05
2	1 + 271.49	2591.70	-131.244	-131.24	**	**	**	**	-58.541	-131.21	7.152	9.548	-121.66
2	1 + 334.09	2639.12	-134.219	-134.22	**	**	**	**	-60.398	-134.40	7.246	9.673	-124.72
2	1 + 371.32	2644.36	-134.219	-134.22	**	**	**	**	-60.043	-134.19	6.586	8.792	-125.40
2	1 + 493.42	2625.38	-131.438	-131.44	**	**	**	**	-57.796	-131.41	4.857	6.484	-124.93
2	1 + 567.60	2625.47	-131.566	-131.57	**	**	**	**	-57.911	-131.53	4.644	6.200	-125.33
2	1 + 676.35	2644.44	-132.5	-132.50	**	**	**	**	-58.325	-132.47	4.507	6.017	-126.46
2	1 + 792.31	2672.99	-134.199	-134.20	**	**	**	**	-59.224	-134.17	4.807	6.417	-127.76
2	1 + 890.57	2676.17	-133.436	-133.44	**	**	**	**	-58.369	-133.41	4.673	6.238	-127.17
2	1 + 986.21	2707.54	-133.24	-133.24	**	**	**	**	-57.295	-133.21	4.729	6.313	-126.90
2	2 + 095.22	2745.62	-134.608	-134.61	**	**	**	**	-57.597	-134.58	4.927	6.578	-128.01
2	2 + 169.42	2799.47	-136.706	-136.71	**	**	**	**	-58.18	-136.68	5.185	6.922	-129.75

DENSITY = 2.67

check 1

LINE #	STATION #	ELEVATION	G boug (dens. = 2.67) #gals	G boug (new dens.) #gals	TOPO CORR. (orig.)	TOPO CORR. (new)	G boug (with topo corr) #gals	** #gals	G boug (dens. = 2.00) #gals	G boug (new dens.) #gals	TOPO CORR. (orig.)	TOPO CORR. (new)	G boug (with topo corr) #gals	** #gals
3	1 + 000.00	2006.50	-110.341	-110.34	8.549	8.55	-101.79 **	-54.058		-110.32	6.404	8.549	-101.77	
3	0 + 871.00	1908.13	-109.093	-109.09	10.948	10.95	-98.15 **	-55.571		-109.07	8.2	10.947	-98.13	
3	0 + 800.00	1891.82	-109.031	-109.03	12.340	12.34	-96.69 **	-56.247		-109.01	9.234	12.327	-96.68	
3	0 + 718.20	1877.49	-109.455	-109.46	12.694	12.69	-96.76 **	-56.791		-109.43	9.48	12.656	-96.78	
3	0 + 593.20	1904.29	-109.897	-109.90	12.102	12.10	-97.80 **	-56.484		-109.88	9.065	12.102	-97.78	
3	0 + 510.20	1916.59	-110.605	-110.61	12.25	12.25	-98.36 **	-56.845		-110.59	9.176	12.250	-98.34	
3	0 + 434.00	1948.15	-110.514	-110.51	11.764	11.76	-98.75 **	-55.867		-110.49	8.693	11.605	-98.89	
3	0 + 285.00	2010.22	-111.651	-111.65	8.139	8.14	-103.51 **	-55.265		-111.63	6.097	8.139	-103.49	
3	0 + 203.00	2018.54	-111.628	-111.63	8.532	8.53	-103.10 **	-55.010		-111.61	6.391	8.532	-103.08	
3	0 + 100.00	2027.70	-112.087	-112.09	8.992	8.99	-103.10 **	-55.210		-112.07	6.737	8.994	-103.07	
3	0 + 364.98	2038.92	-112.944	-112.94	9.869	9.87	-103.08 **	-55.747		-112.92	7.392	9.868	-103.05	
3	0 + 101.70	2060.05	-113.700	-113.70	11.12	11.12	-102.58 **	-55.914		-113.68	8.364	11.166	-102.51	
3	0 + 200.00	2089.17	-114.741	-114.74	12.136	12.14	-102.61 **	-56.139		-114.72	9.09	12.135	-102.58	
3	0 + 300.00	2117.23	-116.884	-116.88	13.913	13.91	-102.97 **	-57.497		-116.86	10.42	13.911	-102.95	
3	0 + 491.00	2253.21	-120.846	-120.85	13.635	13.64	-107.21 **	-57.644		-120.82	10.22	13.644	-107.18	
4	1 + 221.70	1858.08	-108.227	-108.23	12.64	12.64	-95.59 **	-56.107		-108.21	9.498	12.680	-95.53	
4	1 + 125.50	1878.11	-108.470	-108.47	12.517	12.52	-95.95 **	-55.789		-108.45	9.396	12.544	-95.91	
4	1 + 034.70	1902.97	-108.775	-108.78	12.239	12.24	-96.54 **	-55.399		-108.76	9.167	12.238	-96.52	
4	0 + 922.70	1977.20	-109.691	-109.69	10.24	10.24	-99.45 **	-54.231		-109.67	7.671	10.241	-99.43	
4	0 + 825.00	1998.27	-109.355	-109.36	9.242	9.24	-100.11 **	-53.303		-109.33	6.949	9.277	-100.06	
4	0 + 725.00	2010.85	-109.314	-109.31	8.963	8.96	-100.35 **	-52.909		-109.29	6.714	8.963	-100.33	
4	0 + 625.00	2026.27	-107.78	-107.78	8.637	8.64	-99.14 **	-52.942		-109.76	6.53	8.718	-101.04	
4	0 + 518.00	2035.44	-110.248	-110.25	8.503	8.50	-101.75 **	-53.156		-110.23	6.367	8.500	-101.73	
4	0 + 425.00	2050.85	-110.305	-110.31	8.557	8.56	-101.75 **	-52.777		-110.28	6.409	8.556	-101.73	
4	0 + 325.00	2057.29	-110.886	-110.89	8.989	8.99	-101.90 **	-53.179		-110.86	6.733	8.989	-101.88	
4	0 + 225.00	2067.44	-111.467	-111.47	9.828	9.83	-101.64 **	-53.477		-111.45	7.362	9.828	-101.62	
4	0 + 125.00	2072.36	-112.449	-112.45	10.779	10.78	-101.67 **	-54.318		-112.43	8.074	10.779	-101.65	
4	0 + 100.30	2070.24	-113.833	-113.83	12.877	12.88	-100.96 **	-55.764		-113.81	9.646	12.877	-100.94	
4	0 + 071.40	2089.03	-114.122	-114.12	13.327	13.33	-100.80 **	-55.626		-114.20	9.983	13.327	-100.87	
4	0 + 175.00	2127.05	-115.567	-115.57	13.576	13.58	-101.99 **	-55.902		-115.54	10.17	13.577	-101.97	
4	0 + 249.80	2182.34	-116.79	-116.79	12.589	12.59	-104.20 **	-55.577		-116.77	9.426	12.584	-104.19	
4	0 + 375.00	2249.97	-118.668	-118.67	13.094	13.09	-105.57 **	-55.558		-118.65	9.81	13.096	-105.55	
4	0 + 474.00	2328.34	-120.579	-120.58	13.051	13.05	-107.53 **	-55.27		-120.56	9.776	13.051	-107.50	
4	0 + 575.80	2402.01	-121.989	-121.99	12.892	12.89	-109.10 **	-54.613		-121.96	9.657	12.892	-109.07	
4	0 + 680.56	2496.02	-122.212	-122.21				-54.354		-124.34	9.582	12.792	-111.55	
4	0 + 795.45	2596.56	-124.102	-124.10				-53.637		-126.44	8.382	11.190	-115.25	
4	0 + 896.43	2633.69	-127.081	-127.08				-54.05		-127.90	7.374	9.844	-118.05	
4	1 + 011.56	2697.38	-127.419	-127.42				-53.818		-129.45	6.424	8.576	-120.88	
4	1 + 094.36	2721.44	-130.354	-130.35				-54.05		-130.36	8.501	11.349	-119.01	
4	1 + 100.10	2720.89	-129.76	-129.76				-53.439		-129.73	8.392	11.203	-118.53	
4	1 + 225.46	2731.6	-128.373	-128.37				-51.895		-128.49	6.639	8.853	-119.62	
4	1 + 300.00	2785.83	-131.89	-131.89				-53.748		-131.86	7.459	9.956	-121.90	
4	1 + 408.64	2806.87	-131.891	-131.89				-53.157		-131.86	7.65	10.213	-121.65	
4	1 + 500.00	2841.41	-133.341	-133.34				-53.64		-133.31	6.708	8.955	-124.36	

DEENSITY = 2.67

check I

LINE #	STATION #	ELEVATION A	G boug (dens. = 2.67) #gals	G boug (new dens.) #gals	TOPO CORR. (orig.)	TOPO CORR. (new)	G boug (with topo corr) #gals	** #gals	G boug (dens. = 2.00) #gals	G boug (new dens.) #gals	TOPO CORR. (orig.)	TOPO CORR. (new)	G boug (with topo corr) #gals	** #gals		
4	1 + 600.62	2849.29	-133.199	-133.20					-53.277				-133.17	6.547	8.740	-124.43
4	1 + 674.64	2835.67	-132.702	-132.70					-53.161				-132.67	5.662	7.559	-125.11
5	1 + 400.09	1864.17	-106.235	-106.24	12.306	12.31	-93.93 **		-53.944				-106.21	9.222	12.311	-93.90
5	1 + 200.07	1899.01	-107.573	-107.57	12.424	12.42	-95.15 **		-54.306				-107.55	9.234	12.327	-95.23
5	1 + 000.23	1937.96	-108.573	-108.57	12.381	12.38	-96.19 **		-54.236				-108.58	9.277	12.385	-96.19
5	1 + 797.32	1981.4	-110.109	-110.11	11.817	11.82	-98.29 **		-54.531				-110.09	8.712	11.631	-98.46
5	0 + 600.02	2049.13	-109.91	-109.91	8.833	8.83	-101.08 **		-52.433				-109.89	6.617	8.834	-101.06
5	0 + 399.81	2083.37	-110.741	-110.74	8.21	8.21	-102.53 **		-52.302				-110.72	6.149	8.209	-102.51
5	0 + 200.22	2104.22	-111.303	-111.30	8.448	8.45	-102.86 **		-52.28				-111.28	6.328	8.448	-102.83
5	0 + 290.04	2116.74	-112.465	-112.47	10.431	10.43	-102.03 **		-53.091				-112.44	7.814	10.432	-102.01
5	0 + 199.99	2131.44	-114.332	-114.33	12.364	12.36	-101.97 **		-54.546				-114.31	9.263	12.366	-101.94
5	0 + 399.84	2234.86	-117.537	-117.54	11.943	11.94	-105.59 **		-54.848				-117.51	8.946	11.943	-105.57
6	0 + 311.58	2167.96	-111.145	-111.15	9.255	9.26	-101.89 **		-50.335				-111.12	6.933	9.256	-101.87
6	0 + 200.30	2167.47	-111.218	-111.22	8.992	8.99	-102.23 **		-50.42				-111.19	6.733	8.989	-102.21
6	0 + 117.63	2192.56	-111.37	-111.37	8.548	8.55	-102.82 **		-49.818				-111.30	6.403	8.548	-102.75
6	0 + 510.00	2171.03	-111.059	-111.06	9.738	9.74	-101.32 **		-50.163				-111.04	7.267	9.701	-101.34
6	0 + 105.69	2189.53	-112.088	-112.09	10.259	10.26	-101.83 **		-50.673				-112.07	7.684	10.258	-101.81
6	0 + 198.73	2237.6	-113.825	-113.83	9.511	9.51	-104.31 **		-51.061				-113.80	7.093	9.469	-104.33
6	0 + 303.82	2242.3	-115.084	-115.08	10.630	10.63	-104.45 **		-52.188				-115.06	7.964	10.632	-104.43
6	0 + 405.11	2223.24	-116.054	-116.05	13.250	13.25	-102.80 **		-53.693				-116.03	9.925	13.250	-102.78
6	0 + 488.99	2288.97	-117.197	-117.20	11.282	11.28	-105.92 **		-52.993				-117.17	8.379	11.186	-105.99
6	0 + 602.34	2342.58	-118.271	-118.27	11.806	11.81	-106.47 **		-52.561				-118.25	8.815	11.768	-106.48
7	0 + 462.60	2288.37	-112.959	-112.96	10.872	10.87	-102.09 **		-49.331				-112.93	8.142	10.871	-102.06
7	0 + 280.00	2235.93	-111.179	-111.18	10.130	10.13	-101.05 **		-48.462				-111.16	7.588	10.130	-101.03
7	0 + 145.70	2271.2	-111.575	-111.58	9.709	9.71	-101.87 **		-47.868				-111.55	7.271	9.707	-101.84
7	0 + 080.00	2259.46	-111.672	-111.67	9.338	9.34	-102.33 **		-48.293				-111.65	6.968	9.302	-102.34
7	0 + 655.00	2234.38	-111.374	-111.37	9.253	9.25	-102.12 **		-46.699				-111.35	6.942	9.268	-102.08
7	0 + 120.00	2247.7	-111.885	-111.89	9.789	9.79	-102.10 **		-48.837				-111.86	7.333	9.790	-102.07
7	0 + 320.00	2303.88	-114.44	-114.44	9.568	9.57	-104.87 **		-49.815				-114.41	7.178	9.563	-104.83
7	0 + 540.00	2355.97	-116.706	-116.71	11.199	11.20	-105.51 **		-50.637				-116.70	8.389	11.199	-105.50
7	0 + 598.00	2374.57	-117.499	-117.50	11.250	11.25	-106.25 **		-50.892				-117.47	8.412	11.231	-106.24
8	0 + 394.80	2503.02	-121.109	-121.11	15.797	15.80	-105.31 **		-50.9				-121.08	11.831	15.794	-105.29
8	0 + 144.00	2464.35	-117.37	-117.37	11.375	11.38	-106.00 **		-48.244				-117.34	8.523	11.378	-105.96
8	0 + 268.00	2493.16	-120.678	-120.68	13.386	13.39	-107.29 **		-50.744				-120.65	10.026	13.385	-107.27
8	0 + 400.80	2520.91	-122.384	-122.38	13.558	13.56	-108.83 **		-51.673				-122.36	10.17	13.577	-108.76
8	0 + 737.60	2578.17	-123.735	-123.74	12.609	12.61	-111.73 **		-51.416				-123.71	8.762	11.699	-112.01
8	0 + 804.30	2590.43	-124.16	-124.18			**		-51.52				-124.15	8.247	11.610	-113.14
8	0 + 919.20	2590.40	-125.508	-125.51			**		-52.104				-124.74	8.009	10.692	-114.05
8	1 + 000.00	2607.79	-124.019	-124.02			**		-50.871				-123.99	5.996	8.005	-115.99
8	1 + 144.45	2587.72	-122.082	-122.08			**		-49.514				-122.07	4.629	6.190	-115.89
8	1 + 219.50	2617.00	-123.263	-123.26			**		-49.856				-123.24	4.787	6.391	-116.84
8	1 + 276.00	2633.68	-123.607	-123.61			**		-49.645				-123.49	4.763	6.359	-117.13
8	1 + 371.90	2652.09	-124.111	-124.11			**		-49.719				-124.08	5.136	6.857	-117.23
9	1 + 472.70	2651.13	-123.963	-123.96			**		-49.5				-123.84	4.686	6.256	-117.58

DENSITY = 2.67

check I

LINE #	STATION #	ELEVATION	G boug (dens. = 2.67) #gals	G boug (new dens.) #gals	TOPO CORR. (orig.)	TOPO CORR. (new)	G boug (with topo corr)	** **	G boug (dens. = 2.00) #gals	G boug (new dens.) #gals	TOPO CORR. (orig.)	TOPO CORR. (new)	G boug (with topo corr)	** **
8	1 + 554.60	2651.86	-124.489	-124.49				**	-50.104	-124.46	5.403	7.213	-117.25	**
8	1 + 777.40	2640.08	-124.336	-124.34				**	-50.481	-124.51	5.076	6.776	-117.73	**

APPENDIX 3

NUMERICAL MODEL PARAMETERS FOR GRAVITY MODELS

Input parameters to the Program GM3 for the computation of gravity anomalies due to multiple 3-dimensional right-rectangular prisms.

Explanation:

Prism: body number, shown in lower left corner.

X1, X2: west and east side of the body (distance from grid center, in m)

Y1, Y2: south and north side of the body (distance from grid center, in m)

D1, D2: depth to top and bottom of body (m).

DC: density contrast, g/cm^3 . Background assigned to 2.20 g/cm^3 for Zunil I.

Appendix 3.1

Model input parameters for Zunil Model 1, Iteration 2 which is shown as Figure 2. The model simulates a variable depth to the top of the granodiorite with a density of 2.67 g/cm^3 (21 bodies) and volcanics with a density of 2.00 g/cm^3 to the west (2 bodies). The background density used for the volcanic rocks is 2.20 g/cm^3 .

Project name: ZUNIL
 MODEL 1, Iter #2
 Model: MODEL 1

Units in Meters

MAGNETIC PARAMETERS

Earth's field: 0. gammas.

Inclination = 0. degrees

Declination = 0. degrees.

PRISM	X1	X2	Y1	Y2	D1	D2	DC	SC
1	0.	370.	840.	2000.	780.	4000.	0.47	0.
2	-170.	275.	560.	840.	850.	4000.	0.47	0.
3	-420.	-320.	0.	360.	950.	4000.	0.47	0.
4	-320.	140.	0.	560.	980.	4000.	0.47	0.
5	730.	2000.	560.	840.	700.	4000.	0.47	0.
6	550.	1000.	200.	560.	700.	4000.	0.47	0.
7	-670.	-470.	-410.	-170.	1200.	4000.	0.47	0.
8	-470.	-390.	-410.	0.	1100.	4000.	0.47	0.
9	-230.	0.	-460.	0.	1035.	4000.	0.47	0.
10	0.	375.	-600.	-370.	1000.	4000.	0.47	0.
11	370.	1100.	840.	2000.	1200.	4000.	0.47	0.
12	275.	730.	560.	840.	1200.	4000.	0.47	0.
13	140.	550.	200.	560.	1500.	4000.	0.47	0.
14	140.	2000.	0.	200.	1500.	4000.	0.47	0.
15	-390.	-230.	-460.	0.	1530.	4000.	0.47	0.
16	0.	800.	-370.	0.	2000.	4000.	0.47	0.
17	375.	2000.	-600.	-370.	2000.	4000.	0.47	0.
18	0.	2000.	-2000.	-600.	2000.	4000.	0.47	0.
19	1100.	2000.	560.	2000.	1000.	4000.	0.47	0.
20	1000.	2000.	200.	560.	1000.	4000.	0.47	0.
21	800.	2000.	-370.	0.	1000.	4000.	0.47	0.
22	-1200.	-320.	0.	2000.	0.	600.	-0.20	0.
23	-1200.	-350.	-2000.	0.	0.	600.	-0.20	0.

Appendix 3.2

Model input parameters for Zunil Model 1, Iteration 4 which is shown as Figure 3. The model simulates a variable depth to the top of the granodiorite with a density of 2.67 g/cm^3 (21 bodies), volcanics with a density of 2.00 g/cm^3 to the west (2 bodies). This model also includes the presence of volcanics with a density of 2.00 g/cm^3 (7 bodies) above the granodiorite. The background density used for the volcanic rocks is 2.20 g/cm^3 .

Project name: ZUNIL
MODEL 1, Iter # 4
Model: MODEL 1

Units in Meters

MAGNETIC PARAMETERS

Earth's field: 0. gammas.
Inclination = 0. degrees

Declination = 0. degrees.

PRISM	X1	X2	Y1	Y2	D1	D2	DC	SC
1	0.	370.	840.	2000.	780.	4000.	0.47	0.
2	-170.	275.	560.	840.	850.	4000.	0.47	0.
3	-420.	-320.	0.	360.	950.	4000.	0.47	0.
4	-320.	140.	0.	560.	980.	4000.	0.47	0.
5	730.	2000.	560.	840.	700.	4000.	0.47	0.
6	550.	1000.	200.	560.	700.	4000.	0.47	0.
7	-670.	-470.	-410.	-170.	1200.	4000.	0.47	0.
8	-470.	-390.	-410.	0.	1100.	4000.	0.47	0.
9	-230.	0.	-460.	0.	1035.	4000.	0.47	0.
10	0.	375.	-600.	-370.	1000.	4000.	0.47	0.
11	370.	1100.	840.	2000.	1200.	4000.	0.47	0.
12	275.	730.	560.	840.	1200.	4000.	0.47	0.
13	140.	550.	200.	560.	1500.	4000.	0.47	0.
14	140.	2000.	0.	200.	1500.	4000.	0.47	0.
15	-390.	-230.	-460.	0.	1530.	4000.	0.47	0.
16	0.	800.	-370.	0.	2000.	4000.	0.47	0.
17	375.	2000.	-600.	-370.	2000.	4000.	0.47	0.
18	0.	2000.	-2000.	-600.	2000.	4000.	0.47	0.
19	1100.	2000.	560.	2000.	1000.	4000.	0.47	0.
20	1000.	2000.	200.	560.	1000.	4000.	0.47	0.
21	800.	2000.	-370.	0.	1000.	4000.	0.47	0.
22	-1200.	-320.	0.	2000.	0.	600.	-0.20	0.
23	-1200.	-350.	-2000.	0.	0.	600.	-0.20	0.

Appendix 3.3

Model input parameters for a deep granodiorite body with a density of 2.67g/cm^3 simulating the effects of vertical displacement by faults. The depths to the top of the granodiorite vary from 500 to 3000 m. The background density used for the volcanic rocks is 2.20g/cm^3 . The results of the model are shown as Figure 4.

Project name: ZUNIL
DEEP GRANITE STRUCTURE
Model: DEEP GRANITE STRUCTURE

Units in Meters

MAGNETIC PARAMETERS

Earth's field: 0. gammas.

Inclination = 0. degrees

Declination = 0. degrees.

PRISM	X1	X2	Y1	Y2	D1	D2	DC	SC
1	-300.	200.	-100.	1500.	800.	4000.	0.47	0.
2	200.	700.	-100.	1500.	1200.	4000.	0.47	0.
3	700.	1200.	-100.	1500.	500.	4000.	0.47	0.
4	-300.	200.	-1200.	-100.	1000.	4000.	0.47	0.
5	200.	700.	-1200.	-100.	1400.	4000.	0.47	0.
6	700.	1200.	-1200.	-100.	700.	4000.	0.47	0.
7	-800.	-300.	-1200.	1500.	3000.	4000.	0.47	0.

Appendix 3.4

Model input parameters simulating the effects of varying the density of the near surface volcanics. The background volcanics have a density of 2.20 g/cm³. Density contrasts of -0.3, -0.20, -0.10, +0.10 g/cm³ were used for bodies extending from the surface to a depth of 500 m.

Project name: ZUNIL
SURFACE VOLCANICS
Model: SURFACE VOLCANICS

Units in Meters

MAGNETIC PARAMETERS

Earth's field: 0. gammas.

Inclination = 0. degrees

Declination = 0. degrees.

PRISM	X1	X2	Y1	Y2	D1	D2	DC	SC
1	-900.	-400.	-1200.	1200.	0.	500.	-0.20	0.
2	100.	400.	-100.	1200.	0.	500.	-0.20	0.
3	700.	100.	200.	800.	0.	500.	0.10	0.
4	500.	900.	-500.	-100.	0.	500.	0.10	0.
5	-300.	200.	-1200.	-800.	0.	500.	-0.30	0.

ALL

PLATES

ARE

WITH

Howard Ross

Joe Moore

or

Davy

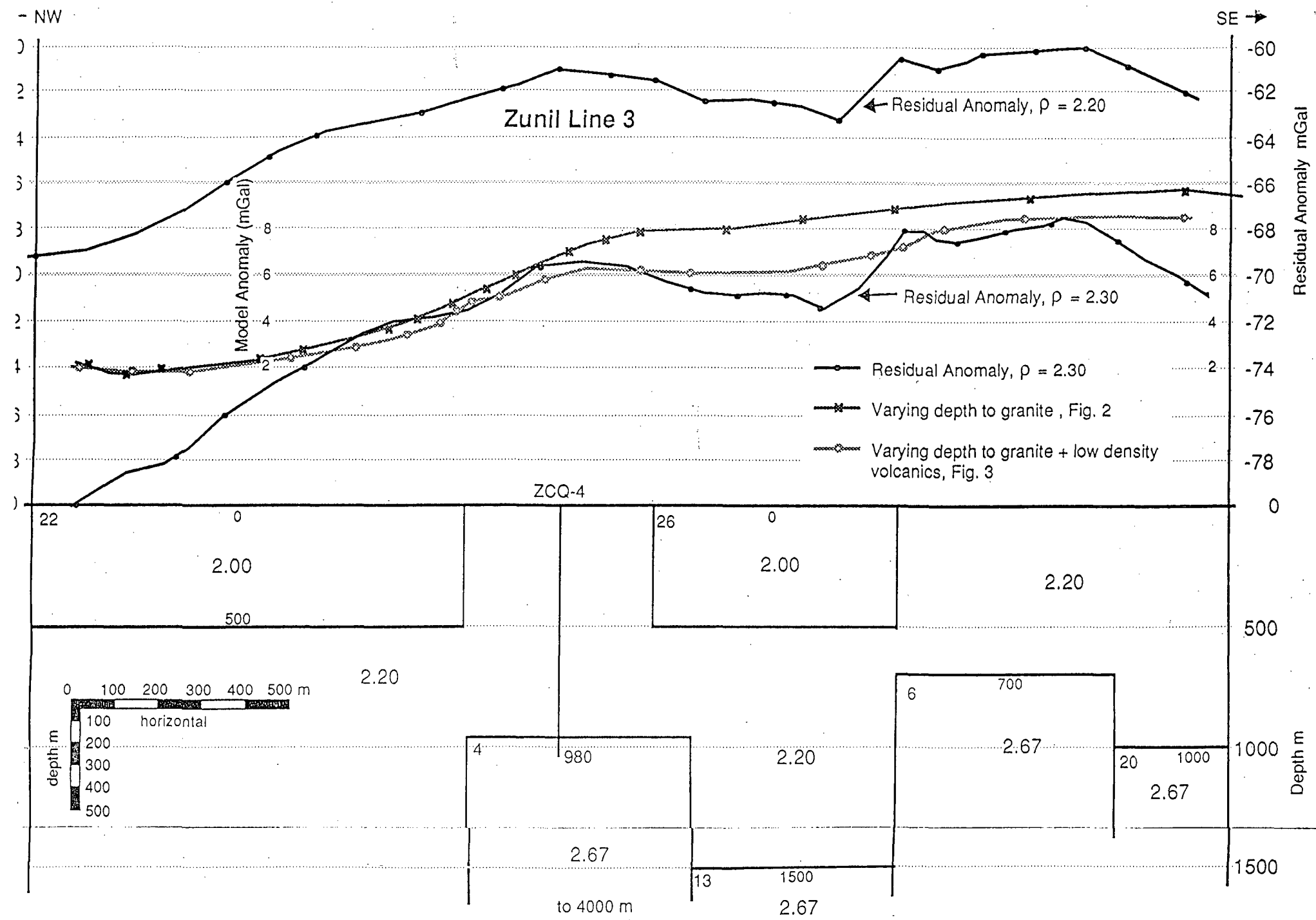


Figure 6

FLUID INCLUSION SYSTEMATICS OF
THE ZUNIL GEOTHERMAL SYSTEM

SUMMARY

Microthermometric measurements on 525 fluid inclusions from the Zunil I geothermal system have been used to characterize the chemistry of the reservoir as well as the processes occurring within it. Three distinct fluid types have been identified in the reservoir. These are: high-temperature, low salinity fluids with low gas contents; low salinity steam-heated waters with variable gas contents; and near surface, low-temperature, steam-heated water with low gas contents. The high-temperature fluids are most similar to the deep reservoir fluids.

The steam-heated waters form a CO₂-enriched cap over the geothermal system that thickens from the west to east. The geometry of this cap suggests that the deep upwelling center of the system originates near the western side of Zunil I. As the high-temperature fluids migrate from west to east, they are progressively diluted by downward incursions of CO₂-enriched steam-heated waters.

INTRODUCTION

Fluid inclusions can be used to characterize the chemistry of a geothermal reservoir and the processes occurring within it, particularly in regions that are not directly sampled by the production or gradient wells (Hedenquist and Henley, 1985; Moore and others, 1989). Fluid inclusions are micron-sized cavities filled with the fluid trapped during mineral precipitation or during subsequent fracturing. Information on the temperature of trapping and on the composition of the inclusion fluids they contain are derived from phase changes occurring in the inclusions during heating and freezing. At room temperature, fluid inclusions from geothermal systems typically contain a single liquid and vapor phase. If the inclusion trapped a single phase, either liquid or vapor (steam), then the trapping temperature can be determined from the temperature at which the liquid and vapor phases homogenize (homogenization temperature).

Figure 2 shows examples of two-phase inclusions.

Types I and II differ only in the amount of CO₂ present in the inclusion fluids. Concentrations of CO₂ greater than approximately 3.8 weight percent (Type II) will produce CO₂ clathrate upon freezing that melts at temperatures greater than 0.0°C. If the CO₂ content is less than 3.8 weight percent (Type I), the last solid phase to melt will be ice, which will melt at temperatures less than or equal to 0.0°C.

The presence of planes of vapor-rich inclusions (Type III) in the vein minerals studied is significant because these inclusions provide evidence of boiling within the reservoir. Unfortunately, it was not possible to make reliable microthermometric measurements on the vapor-rich inclusions because of their small size (less than 10μ). Vapor-rich inclusions were found at depths of 200 - 300 m in ZCQ-5 and ZCQ-6, and at a depth of 1015 m in ZCQ-4.

All of the inclusions measured in this study were liquid-rich and contained a small vapor bubble that occupied about 15% of the inclusion volume at room temperature. The majority of the inclusions studied had maximum dimensions of 2 to 15μ. Fluid inclusion heating and freezing measurements were made using a Fluid Inc. heating/freezing system. All measurements were made in duplicate. Replicate measurements were within ± 0.2°C. We estimate a temperature uncertainty of ± 0.1°C for freezing measurements and ± 2.0°C for heating measurements. The results of the fluid inclusion measurements are listed in Appendix I, and illustrated in Figures 3 through 20.

FLUID INCLUSION DATA

ZCQ-6

Vein minerals containing fluid inclusions are common in the upper 800 m of ZCQ-6. At greater depths, the small size of the drill cuttings limited the amount of vein material suitable for study. The maximum

homogenization temperature recorded in this well was 263°C.

Figure 3 compares the measured homogenization temperatures to the downhole temperature log. Most depth intervals display a relatively narrow range of homogenization temperatures. In several samples, the homogenization temperature varied by approximately 40°C. However, within an individual primary growth zone or secondary plane the temperatures were consistent; the variation was between different areas of the same crystals. At depths shallower than 400 m, the homogenization temperatures are higher than the downhole measured temperatures. In contrast, homogenization temperatures from depths greater than 400 m plot below the present day temperatures. Figure 3 also compares the inclusion temperatures to the boiling point curve for a fluid with a chlorinity of 1800 ppm, which is estimated to be the reservoir fluid composition. Since the exact elevation of the piezometric surface at the time of inclusion formation is unknown, we have assumed that the boiling point curve intersected the surface at the time of trapping. This assumption is consistent with evidence of boiling found in primary inclusions from a depth of 200 m.

Figure 4 shows the variations with depth in the ice-melting temperatures of Type I inclusions. The ice-melting temperatures of Type I inclusions in the upper 200 m defined a narrow range; 0.0° to -0.2°C. Type II inclusions with clathrate-melting temperatures that ranged from +0.4° to +0.6°C were found at 200 m. From approximately 300 to 700 m, individual samples showed a broad range of ice-melting temperatures. For example, several crystals recorded ice-melting temperatures that ranged from 0.0° to -0.7°C. In contrast, the deepest sample measured in ZCQ-6 (790 m) had ice-melting temperatures that were consistently -0.2°C.

ZCQ-5

Figure 5 shows homogenization temperatures of samples from ZCQ-5, which ranged from 152° to 282°C. In contrast to ZCQ-6, the present day temperatures are most similar to the lower homogenization temperatures. However, the upper limits of the data plot close to the boiling point to depth

curve for a fluid with a chlorinity of 1800 ppm. Extensive evidence of boiling was also found in inclusions from 200 to 300 m in ZCQ-5 .

Variations in ice-melting temperatures of Type I inclusions with respect to depth are illustrated in Figure 6. Ice-melting temperatures ranged from 0.0° to -0.7°C between depths of 400 and 900 m. In contrast the inclusions at 940 m had ice-melting temperatures ranging from 0.0° to -0.2°C. Type II inclusions were found in the shallow portions of the well, between depths of 200 and 400 m. The CO₂ clathrate-melting temperatures of the Type II inclusions ranged from +0.1° to +0.3°C. The vertical extent of Type II inclusions appears to be greater in ZCQ-5 than in ZCQ-6.

ZCQ-3

Figure 7 depicts the homogenization temperatures for ZCQ-3. Inclusion temperatures in this well ranged from 152° to 300°C. There are some subtle differences between this data set and the data from ZCQ-5 and ZCQ-6. The homogenization temperatures from ZCQ-3 follow the present day temperature profile closely, while the downhole measured temperatures from ZCQ-5 and ZCQ-6 plot on upper and lower limits of the inclusion data, respectively. In addition, homogenization temperatures from ZCQ-3 plot below the boiling point curve to a depth of approximately 600 m. At greater depths the inclusion temperatures follow the boiling point curve closely. In ZCQ-5 and ZCQ-6, the homogenization temperatures plot close to the boiling point curve even at shallow depths.

Figure 8 illustrates the ice-melting temperatures of Type I inclusions in ZCQ-3. The general trends displayed by inclusions in ZCQ-5 and 6 are also observed in ZCQ-3. Ice-melting temperatures close to 0.0°C were found near the surface. Below 400 m there is an increase in the range of ice-melting temperatures with depth (0.0° to -1.1°C). However, the low apparent salinity fluids that were found at the bottom of ZCQ-5 and ZCQ-6 were not observed in ZCQ-3. Type II inclusions were found between depths of 200 and 400 m. CO₂ clathrate-melting temperatures of these inclusions ranged from +0.1° to +0.3°C.

Z-11

Although considerably less data was available for Z-11, the fluid inclusion measurements were similar to those found in ZCQ-3. This was expected since the two wells are located adjacent to each other. As in ZCQ-3, homogenization temperatures plot below the boiling point curve to a depth of 600 m. Below this depth, the data plot close to the boiling point curve (Fig. 9). Figure 10 shows that the same trends in freezing data found in ZCQ-3, -5 and -6 were also found in Z-11. Ice-melting temperatures of Type I inclusions ranged from 0.0 to -0.4°C below a depth of 200 m. Type II inclusions occurred at a depth of 200 m and have CO_2 clathrate-melting temperatures that ranged from $+0.3^{\circ}$ to $+0.6^{\circ}\text{C}$.

ZCQ-4

Fluid inclusion measurements were conducted on core samples taken at depths of 776 m and 1015 m. The upper core consists of andesite containing veins of calcite. The deeper core sample was taken in granodiorite that is cut by veins of quartz-chlorite-epidote-pyrite. The veins in these samples contained inclusions that recorded some of the highest homogenization temperatures found in any of the wells at Zunil I (252° to 342°C). Figure 11 shows that the homogenization temperatures plot close to the boiling point curve, which is consistent with the presence of vapor-rich inclusions found in samples from 1015 m (refer to Figure 2c). The measured downhole temperatures plot significantly below these homogenization measurements. Figure 12 illustrates the ice-melting temperatures of inclusions in the two samples. Only Type I inclusions were found.

ZCQ-1

Figure 13 shows the homogenization temperatures for inclusions from ZCQ-1. These temperatures ranged from 145° to 248°C . The homogenization temperatures displayed little variation with depth and

within each individual sample the range of homogenization temperatures was approximately the same as the overall range. With the exception of inclusions from a depth of 200 m, where both the homogenization and measured temperatures are similar, the present day temperatures fall closest to the maximum homogenization temperatures of the inclusions. The sample from 200 m is also the only sample which plots on the boiling point curve.

Figure 14 shows that the ice-melting temperatures of Type I inclusions from ZCQ-1 are similar to those of the other wells. From 800 m to 1100 m, the range in ice-melting temperatures increases (-0.2° to -1.6°C). Similar large variations were found in sections of ZCQ-6, -5, -4, -3. At the base of ZCQ-1, the range of ice-melting temperatures narrows to 0.0° to -0.2°C . The same range of freezing point depressions were also found at the base of ZCQ-5, -6, and -2.

Type II inclusions, however, are found over a much greater vertical extent in ZCQ-1 than they are in the other wells studied. In ZCQ-1 Type II inclusions occur between depths of approximately 200 to 800 m. In contrast, Type II inclusions are restricted to a zone that is 100 m thick in ZCQ-6, 200 m thick in ZCQ-5, and 300 m thick in ZCQ-3. The CO_2 clathrate-melting temperatures range from 0.0° to $+0.6^{\circ}\text{C}$.

Z-2

Homogenization and ice-melting temperatures of fluid inclusions from depths of 500 to 600 m in Z-2 are illustrated in figures 15 and 16 respectively. The homogenization temperatures fall below both the present day temperature profile and the boiling point curve. Ice-melting temperatures (Type I inclusions) ranged from 0.0° to -0.4°C .

ZCQ-2 and Z-7

Only one sample was obtained from each well. These data are presented in figures 17 to 20. In both cases the samples were from shallow

intervals above a depth of 200 m. Homogenization temperatures ranged from 132° to 209°C. The ice-melting temperatures of these inclusions are consistent with values found at similar depths in ZCQ-5 and -6, and ranged from 0.0° to -0.2°C.

DISCUSSION

Thermal history of Zunil I

The temperatures of homogenization indicate that both minor heating and cooling are occurring in Zunil I. The overall homogenization temperatures vary slightly from the downhole measured temperatures in most cases. Temperature variations are also indicated within a single individual crystal. The homogenization temperatures are consistent within each secondary plane or growth zone. However, other secondary planes in the same crystal will differ in temperature. Thus, the crystal must have been exposed to fluids with different temperatures. However, the salinities are approximately the same, which implies that the fluids have not changed composition. These variations in temperature appear to be caused by two factors as discussed below: self sealing of fractures resulting in a permeability decrease; and local downward incursions of cool steam-heated waters.

In ZCQ-6, present-day measured temperatures display a conductive gradient down to 480 m, followed by a convective gradient. In contrast, the fluid inclusion data (Fig. 3) indicate that temperatures in well ZCQ-6 followed the boiling point curve to depths of approximately 520 m. These data demonstrate the development of a shallow low-permeability zone, possibly due to mineral precipitation. The present day temperature profile below 520 m is higher than the homogenization temperatures indicating heating has occurred since inclusion formation. This heating could be due to the shallow low-permeability zone having cut off the downward percolation of low-temperature fluid, preventing mixing between the high-

and low-temperature fluids.

A comparison of homogenization temperatures with downhole measured temperatures indicates that ZCQ-5 is cooling down. The downhole logs record temperatures that follow the lower measured homogenization temperatures. In addition, primary growth zones and secondary planes in the same crystals also record temperature decreases. The cooling in ZCQ-5 could have been caused by a combination of local self-sealing and downward incursions of steam-heated waters.

The fluid inclusion and measured temperature curves are nearly identical in well ZCQ-3 (Fig. 7). The slight downward shift of fluid inclusion temperatures with respect to the boiling point curve in the upper 500 m suggests that the permeability in the shallow 500 m of ZCQ-3 may be low, or that fluid in the upper portions of the well boiled at lower temperatures due to high gas contents. There appears to be a temperature reversal at the base of ZCQ-3 that is apparent in both the fluid inclusion data and in the measured temperatures. This reversal is likely due to a downward incursion of cooler steam-heated waters.

The fluid inclusion temperatures and downhole measured temperatures in well ZCQ-1 increase with depth until approximately 700 m (Fig. 13). Then both the homogenization temperatures and measured temperatures decrease slightly and stay relatively constant to depths of approximately 1100 to 1200 m. At the bottom of the hole, both data sets indicate that the well heats up again. This observation implies that there is a downward incursion of cooler waters that is intersecting ZCQ-1 at depths of approximately 700 to 1100 m.

Estimation of Salinities and Gas Contents

Consistent variations in the apparent salinities were found in all of the wells studied. Samples from the upper 200 m recorded ice-melting temperatures that ranged from 0.0° to -0.2°C. Underlying this zone is a 200 to 500 m thick interval where most of the samples contained Type II

inclusions with clathrate-melting temperatures that ranged from 0.0° to +0.6°C. Beneath this interval inclusions typically displayed large ranges of ice-melting temperatures (0.0° to -1.6°C). Finally, in the deepest portions of the wells, the inclusions recorded ice-melting temperatures that ranged from 0.0° to -0.2°C. A few crystals from the intermediate interval with the large range of ice-melting temperatures in ZCQ-6 and -3 had relatively small ice-melting temperatures ranging from 0.0° to -0.4°C. As discussed below, these are more similar to the inclusions from the deeper portions of the wells.

The systematic differences in the ranges of ice-melting temperatures and the presence of Type II inclusions implies that there has been extensive gas flux through the reservoir. Inclusions can become gas-enriched by trapping gas that is released during boiling within the reservoir (Moore et al., 1989). Since CO₂ is typically the dominant non-condensable gas in geothermal reservoir fluids, it is likely that most of the gas flux was CO₂. At least 3.8 weight percent CO₂ must have been present in the fluids in order for Type II inclusions to form. The large differences in ice-melting temperatures of the Type I inclusions that are found at intermediate depths in the reservoir also suggest large variations in their CO₂ contents. For example, an inclusion containing fluid with a salinity of 3500 ppm NaCl would have an ice-melting temperature of -0.2°C (Potter et al., 1978). The freezing point depression would be due entirely to the salts in the fluid. However, if the same inclusion contained one weight percent CO₂, the ice-melting temperature would be -0.6°C. In this case the freezing point depression would be caused by the combination of salts and CO₂. Thus, calculations based on the ice-melting temperatures of the fluid inclusions can yield information not only on the salinities of the fluids, but on their CO₂ contents as well.

The narrow range of ice-melting temperatures of inclusions from the upper 150 m indicates they have low salinities and low gas contents, as evidenced by the narrow range in ice-melting temperature and the lack of

Type II inclusions. These inclusions can be differentiated from deeper fluids by their lower temperatures.

The Type II inclusions from depths of 200 to 500 m contain considerable CO₂ and have low salinities. Although the both the CO₂ contents and the salinity of the fluid determines the melting temperatures of the CO₂ clathrate, the contribution made by salinity cannot be determined in Type II inclusions unless the CO₂ occurs in both a liquid and vapor phase. None of the CO₂-enriched inclusions in Zunil I contained sufficient CO₂ to produce a liquid phase. However, crystals which contained the Type II inclusions typically contained a few low salinity Type I inclusions as well. The presence of these low salinity inclusions indicates that the salt content in the Type II inclusions is also low. Because of the low salinity, the CO₂ contents of the Type II inclusions can be calculated by combining the decomposition curve of CO₂ clathrate in pure water (Bozzo, et al., 1975), with Henry's law relationships and the homogenization temperatures of the inclusions (Moore et al., 1989). Using this approach, the calculated CO₂ contents of the Type II inclusions in Zunil I range from 3.8 to 4.3 weight percent.

The salinity and CO₂ contents of inclusions that displayed large variations in ice-melting temperatures can be calculated from the minimum and maximum ice-melting temperatures and the average homogenization temperatures of an individual crystal. For example, the inclusions from 890 m in ZCQ-3 have ice-melting temperatures that range from 0.0° to -1.1°C, and homogenization temperatures that average 270°C. Assuming that the variation in the ice-melting temperatures is due to gas, the maximum CO₂ content of these inclusions is calculated to be 2.79 weight percent, or 27,900 ppm. The salinity of these fluids can be calculated by using the average minimum freezing point depression of samples in this zone, which is -0.1°C. This corresponds to a salinity of 0.2 equivalent weight percent NaCl or 2000 ppm.

Fluid inclusions from the deepest samples in ZCQ-6, -5 and -1 are

characterized by high homogenization temperatures and low freezing point depressions (0.0° to -0.2°C). This indicates that these fluids have a low salinity and also contain a low CO₂ content. These fluids appear to represent the production fluid which is found at similar depths. The production fluid is estimated to have a salinity of 3500 ppm, which corresponds to a freezing point depression of -0.2°C. This value is similar to the ice-melting temperatures that we measured in the deep samples from ZCQ-6, -5, and 1. A few similar inclusions that also appear to be related to the production fluid were found shallower depths in ZCQ-6 and -3. These inclusions have a slightly greater range of ice-melting temperatures (0.0° to -0.4°C). The greater range is likely due to a slightly higher CO₂ content.

Well ZCQ-4 is of particular interest since it is the only well where a core sample of the granodiorite could be obtained. There appears to be no variation between the salinities of inclusions in quartz veins from the granodiorite at 1015 m and inclusions in calcite veins from the shallower volcanics. This suggests that the geothermal system is not limited to the volcanic rocks, but exists in the granodiorite basement as well.

Conceptual Model of the Reservoir

A conceptual model of the Zunil I geothermal system is shown in Figure 21a and b. The main feature of this model is the compositional zonation of the reservoir. The reservoir can be divided into three distinct regions: a deep high temperature reservoir fluid; a region of steam-heated, CO₂-enriched waters that forms a cap over the geothermal system; and shallow, gas poor, steam-heated groundwaters.

The gas poor steam-heated groundwaters are characterized by moderate temperatures and low salinities. These shallow waters extend to a depth of approximately 150 m and typically have temperatures less than 200°C.

The region of CO₂-enriched steam-heated waters can be divided into two zones based on the amount of CO₂ present. In the upper portion, the

fluids contain at least 3.8 weight percent CO₂ as indicated by the presence of Type II inclusions. The lower portion has insufficient CO₂ to form Type II inclusions. However, there is still significant CO₂ present in the fluids.

The high CO₂ contents of inclusions could only have formed at pressures above hydrostatic since all of the inclusions were trapped as a single liquid phase. Thus, the fluids must have been trapped in zones of low permeability where gas pressures could have exceeded hydrostatic. Low permeabilities could have been developed locally by boiling and self-sealing of fractures.

The deep reservoir fluid is characterized by high temperatures, low salinities and low gas contents. Where the reservoir fluid has reached shallow depths, as in ZCQ-6 and 3, the fluids appear to be slightly gas-enriched relative to the deeper fluids. The reservoir fluids are located in both the granodiorite and the volcanics.

The CO₂-enriched fluids extend to greater depths in the eastern portion of Zunil I, and appear to form a "cap" over the system. The geometry of the CO₂-rich cap suggests that both upwelling of the deep reservoir fluid and downwelling of the cooler CO₂-enriched fluids is occurring. The upflow zones are represented by high temperature inclusions with a narrow range of freezing point depressions. These zones occur principally in ZCQ-6 and 3. However, fluid inclusion data shows that well ZCQ-4 was a major upwelling zone in the past. The main downwelling zones occur in the eastern portion of the field. The upwelling and downwelling suggested by the fluid inclusion data is also similar to flow patterns indicated by present day isotherms (Figure 21 a and b).

CONCLUSIONS

Fluid inclusions from nine wells in Zunil I have been studied to better characterize the reservoir and develop a fluid flow model. Microthermometric measurements indicate that the fluids have low

salinities and contain variable but significant CO₂ contents. Fluids from the upper 150 m of the reservoir have homogenization temperatures less than 200°C and low gas contents. These low-temperature fluids overlie a region of the reservoir that is enriched in CO₂. The upper part of this region is characterized by CO₂ contents in excess of 3.8 weight percent. The low salinities and low to moderate temperatures of both the CO₂-enriched fluids and the overlying gas poor fluids indicate that they represent steam-heated groundwaters. These steam-heated waters overlie a deep high temperature gas poor fluid.

Zones of upwelling of the deeper fluids are represented by inclusions with low gas contents, low salinities and temperatures above 200°C. The distribution of these inclusions correspond closely with location of upwelling zones defined by downhole measured temperatures.

The steam-heated waters form a cap over the geothermal system that becomes progressively thicker to the east. The geometry of the cap suggests that the thermal fluids originate near the western edge of Zunil I. The thermal fluids are progressively diluted by downward incursions of CO₂-enriched steam-heated waters as they move laterally away from the upwelling center.

REFERENCES

Bozzo, A. T., Chen, H-S., Kass, J. R., and Barduhn, A. J., 1975, The properties of the hydrates of chlorine and carbon dioxide: *Desalination*, v. 16, p. 303-320.

Hedenquist, J., W., and Henley, R. W., 1985, The importance of CO₂ on the freezing point depression of fluid inclusions: evidence from active geothermal systems and implications for epithermal ore deposition: *Economic Geology*, v. 80, p. 1379-1406.

Mink, L., Merida, L., and Caicedo, A., 1988, Zunil, Guatemala geothermal project (overview and update): *Transactions geothermal Resource Council*, v. 12, p. 185 -192.

Potter, R. W., II, Clynne, M. A., and Brown, D. L., 1978, Freezing point depression of aqueous sodium chloride solutions: *Economic Geology*, v. 73, p. 284 - 285.

Moore, J. N., Adams, M. C., Bishop, B. P., and Hirtz, P., 1989, A fluid flow model of the Coso geothermal system: data from production fluids and fluid inclusions: *Proceedings, Fourteenth Workshop on Geothermal Reservoir Engineering*, Stanford University, Stanford California, in press.

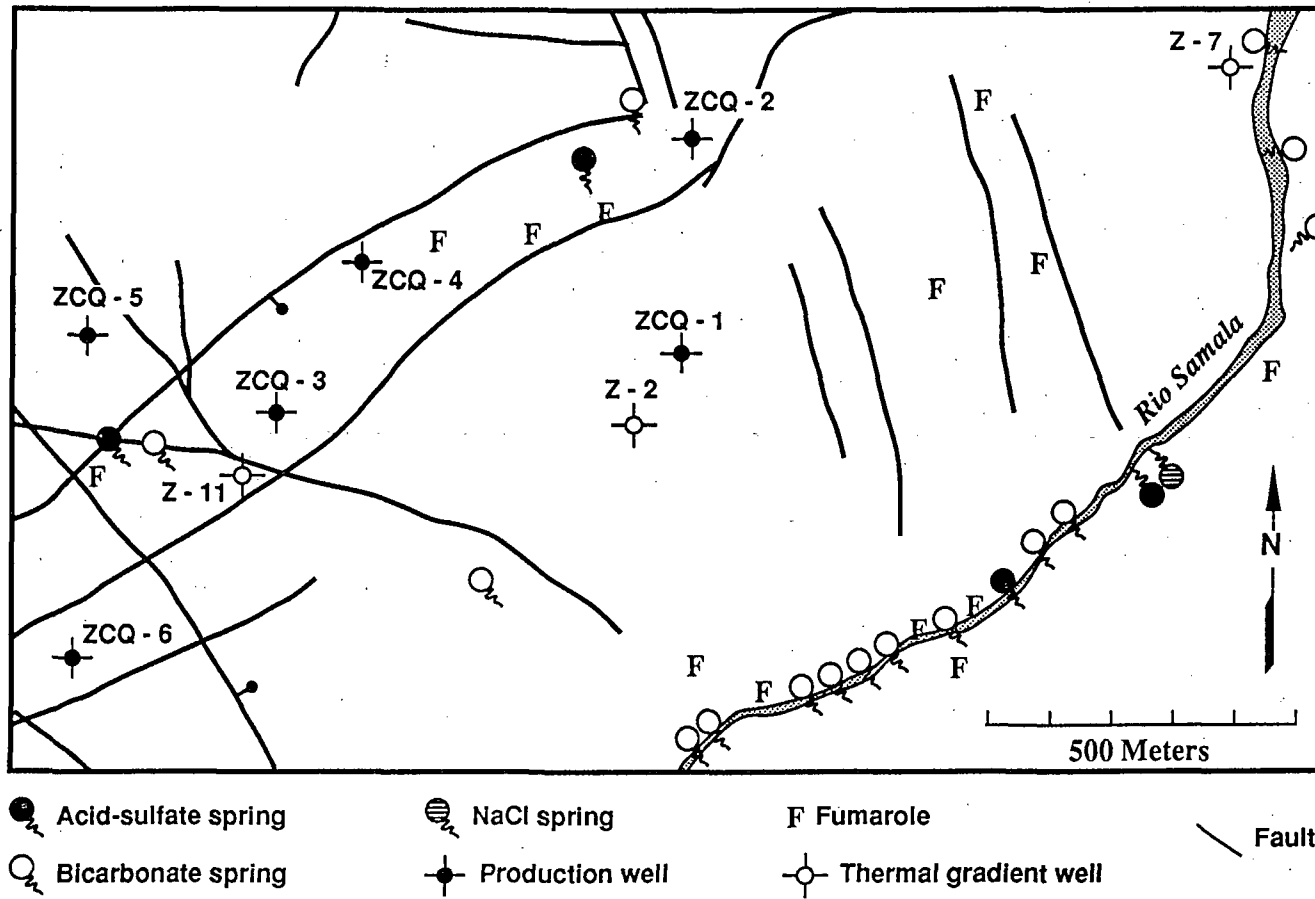


Figure 1. Location of wells studied.

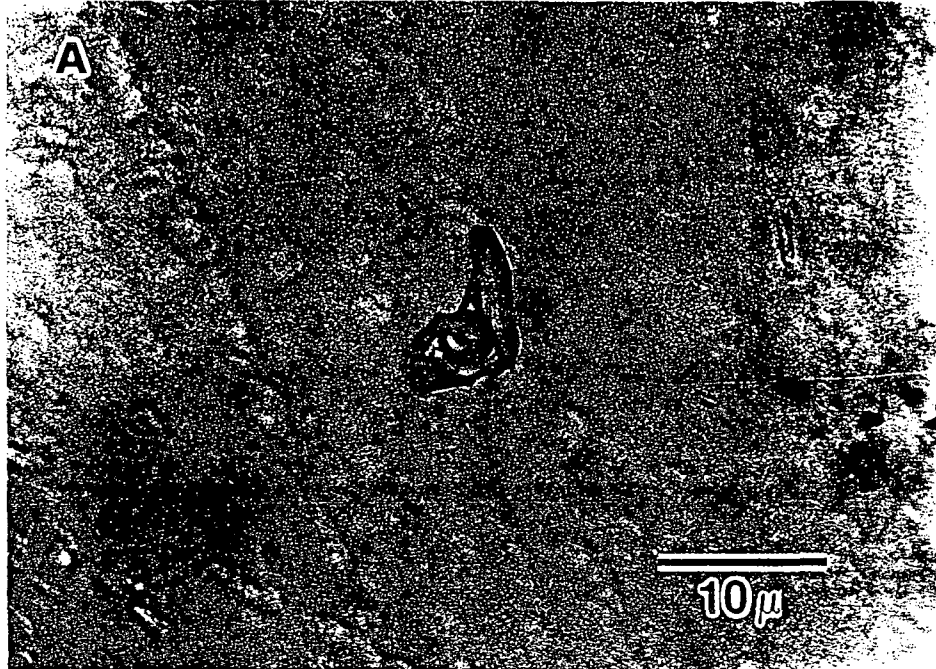


Figure 2a. Two-phase liquid-rich inclusions in Quartz from 1015 m in ZCQ-4.

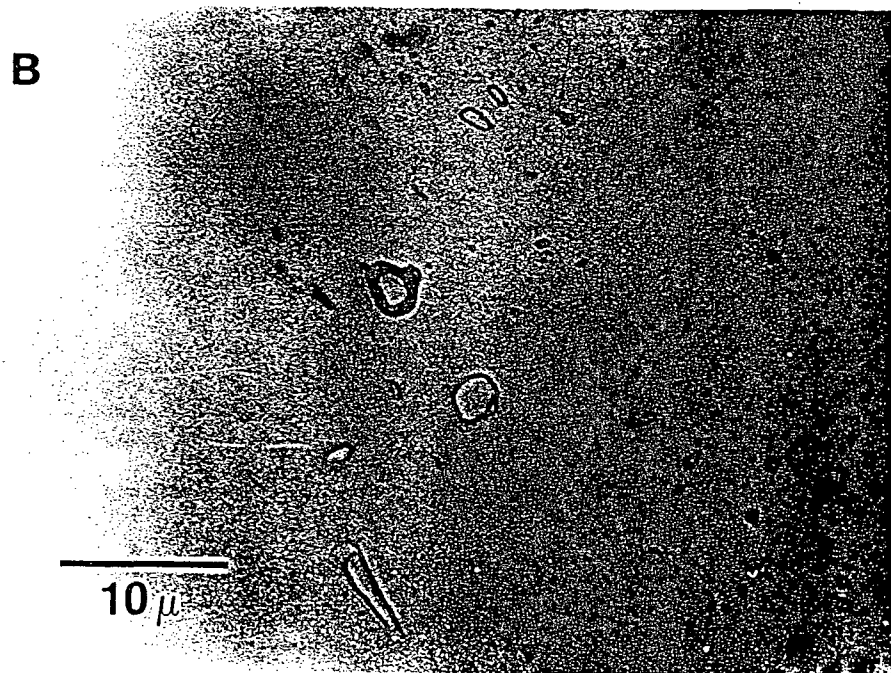


Figure 2b. Two-phase vapor-rich inclusions in Quartz from 1015 m in ZCQ-4.

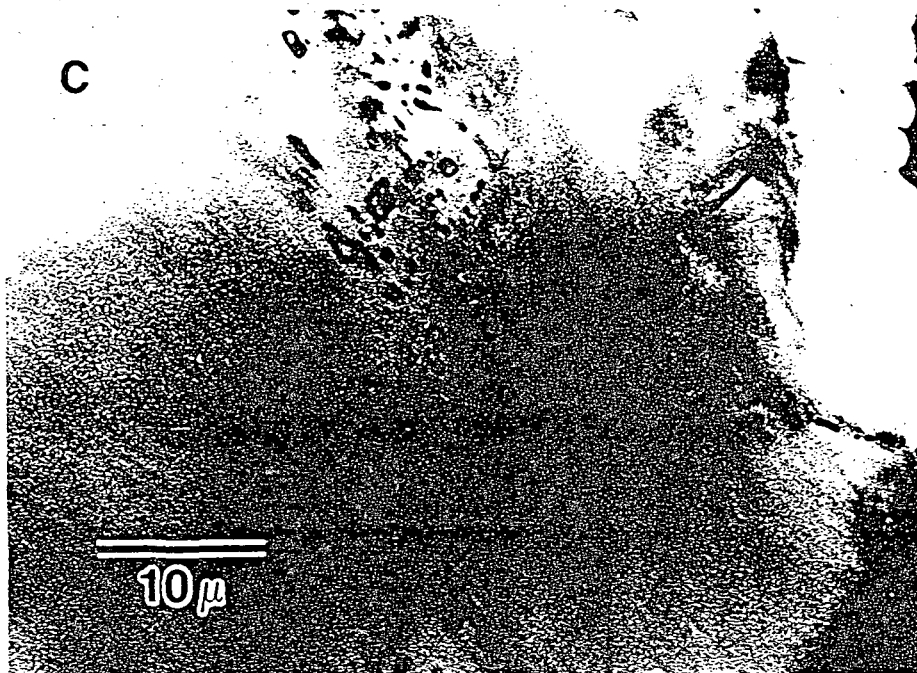


Figure 2c. Two-phase liquid-rich inclusions in Calcite occurring on two cross-cutting secondary planes. Sample is from 455 m in ZCQ-1.

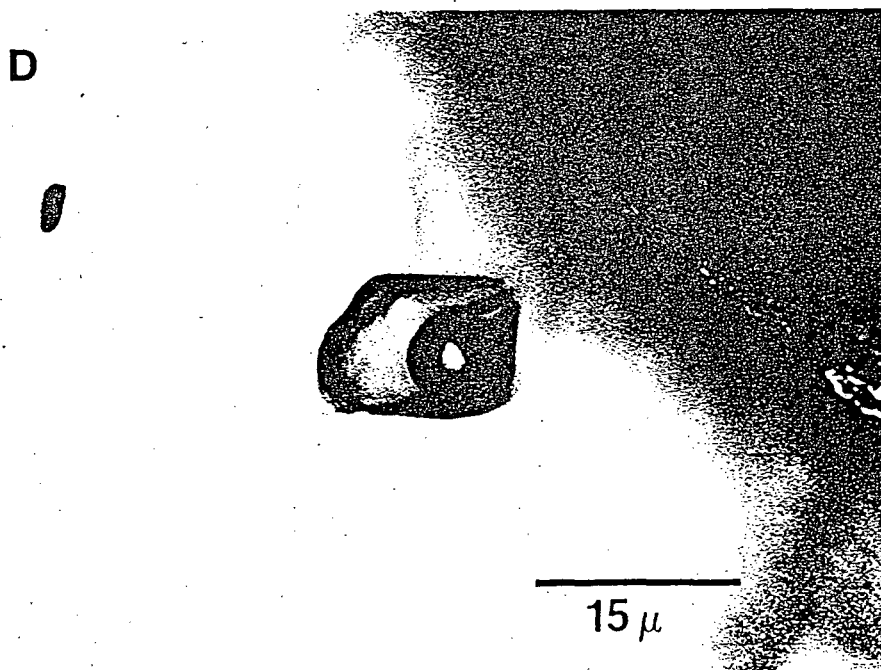


Figure 2d. Two-phase liquid-rich inclusion in Quartz from 200 m in ZCQ-6.

ZCQ-6

Th (C)

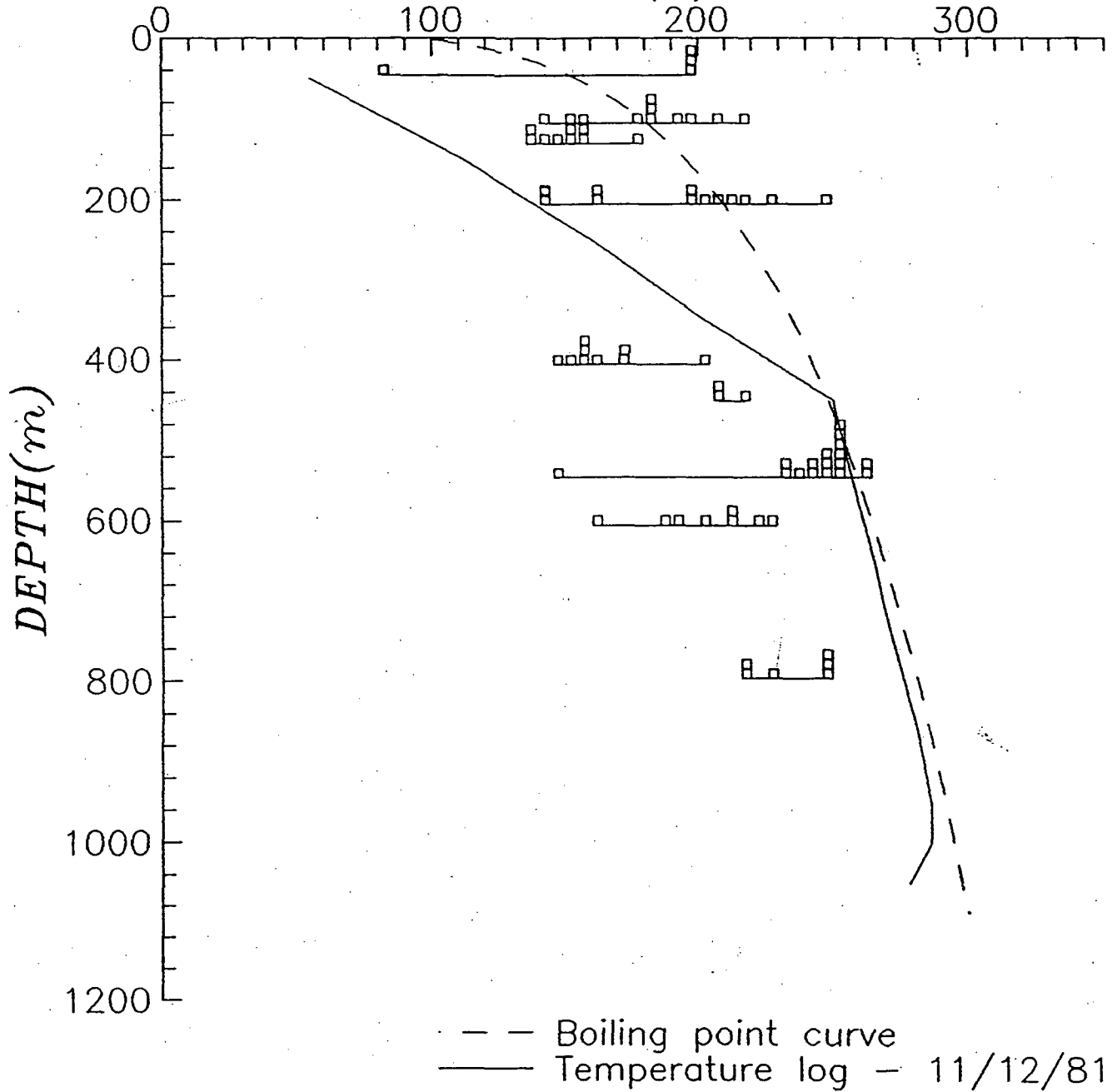


Fig. 3. Temperatures of homogenization (Th) versus depth for ZCQ-6.

ZCQ-6

T_{m-ice} (C)

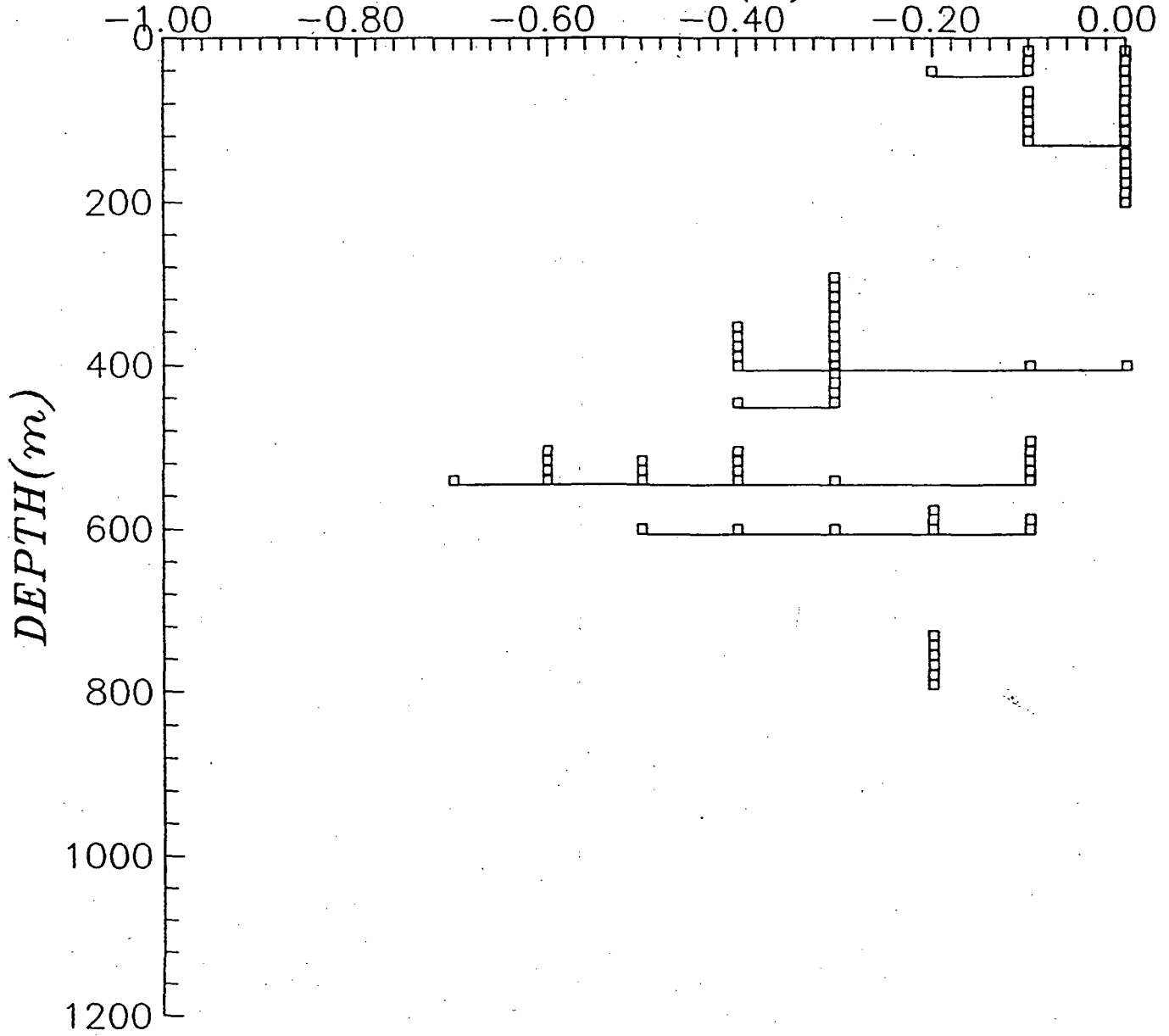


Fig. 4. Temperatures of ice-melting (T_{m-ice}) versus depth for ZCQ-6.

ZCQ-5

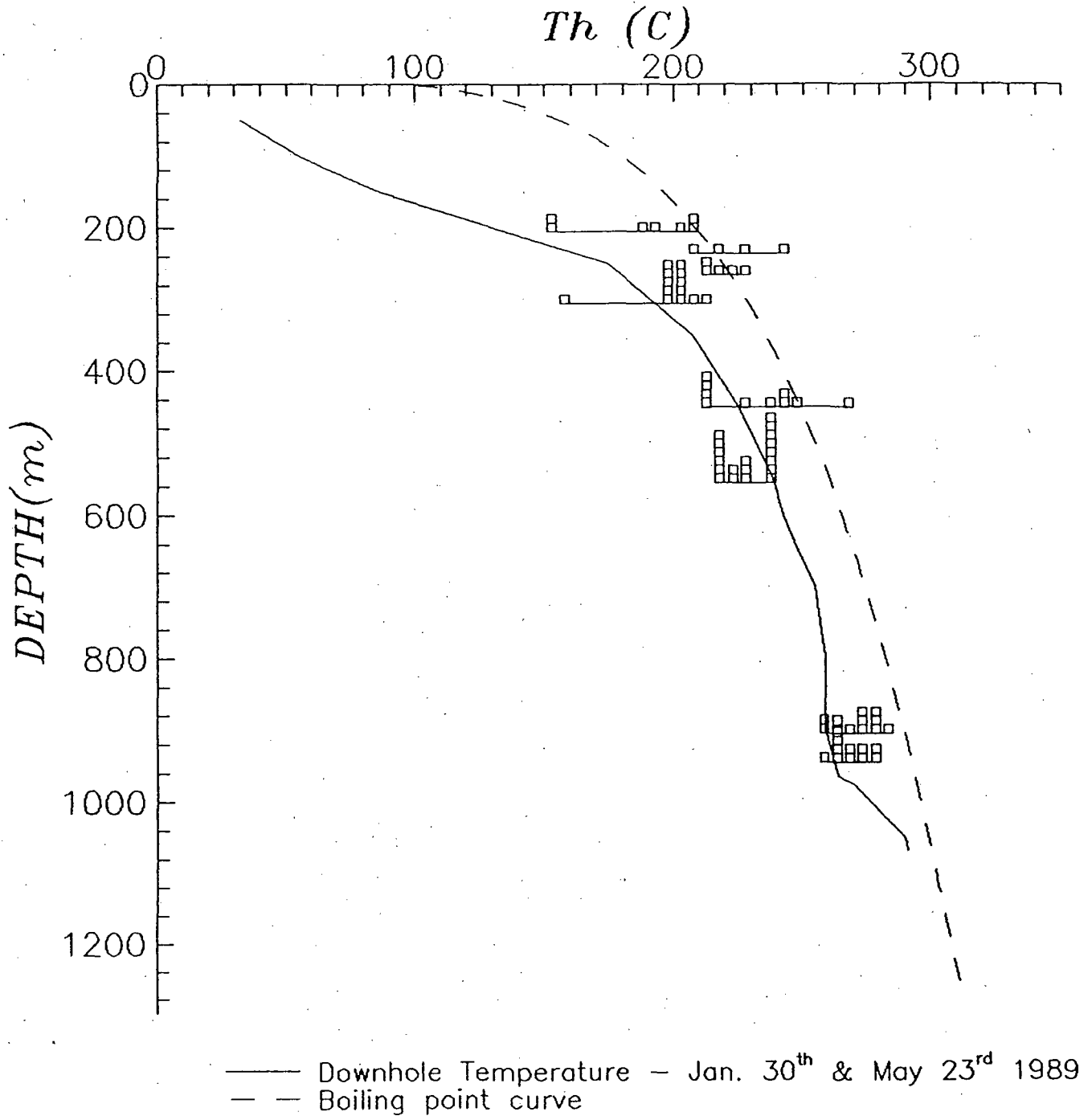


Fig. 5. Temperatures of homogenization (Th) versus depth for ZCQ-5.

ZCQ-5

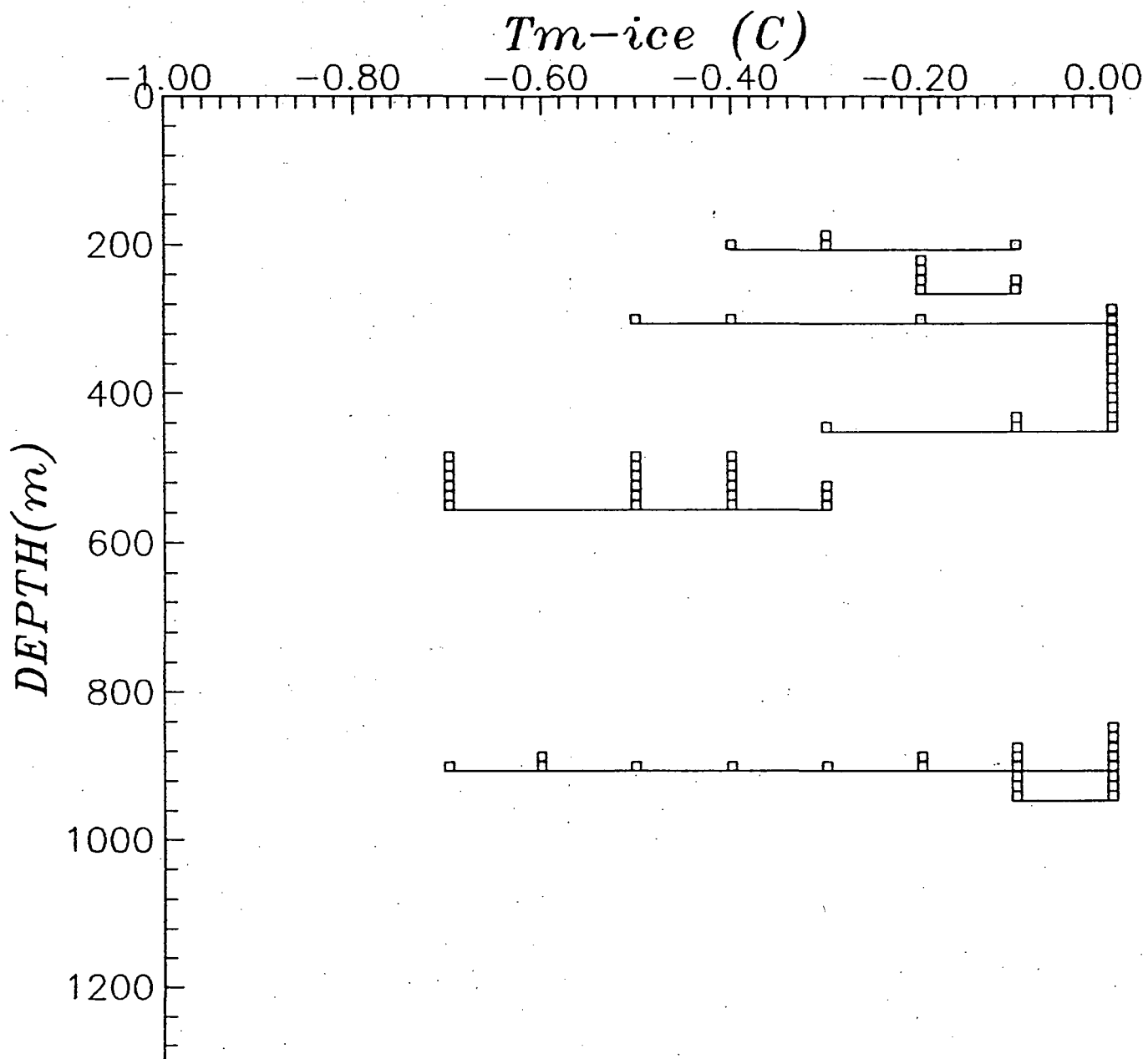


Fig. 6. Temperatures of ice-melting (T_{m-ice}) versus depth for ZCQ-5.

ZCQ-3

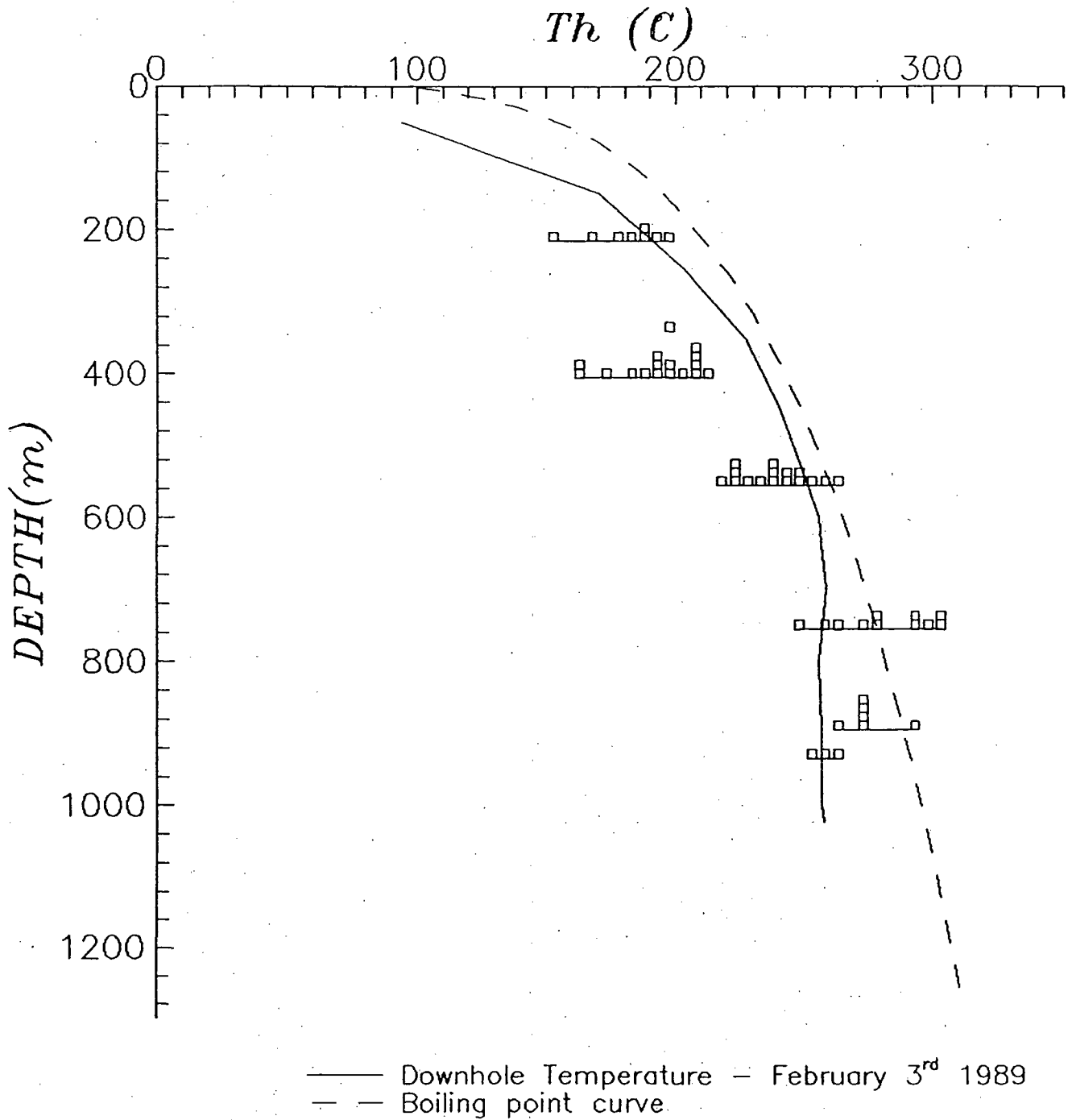


Fig. 7. Temperatures of homogenization (Th) versus depth for ZCQ-3.

ZCQ-3

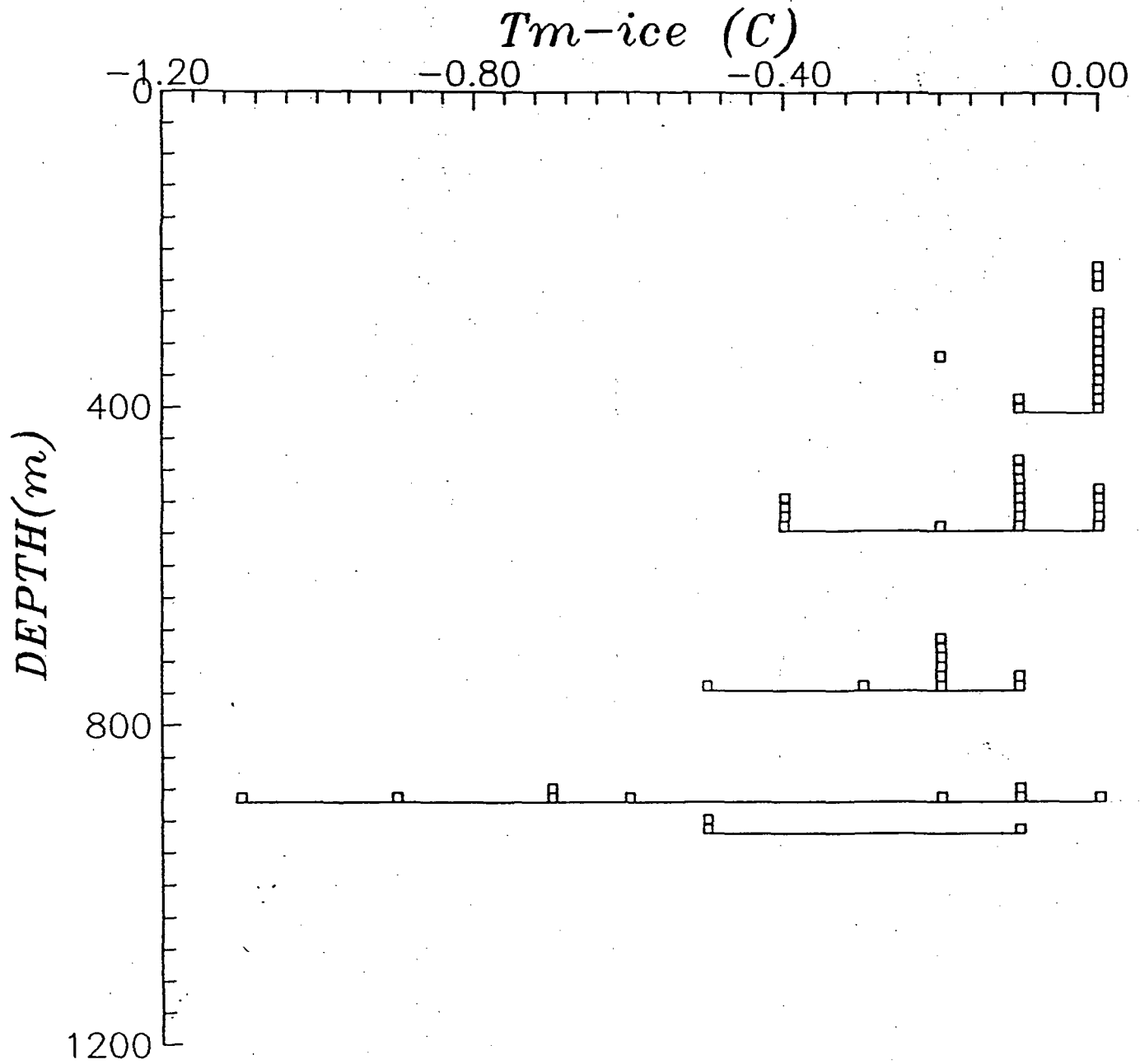


Fig. 8. Temperatures of ice-melting (T_{m-ice}) versus depth for ZCQ-3.

Z-11

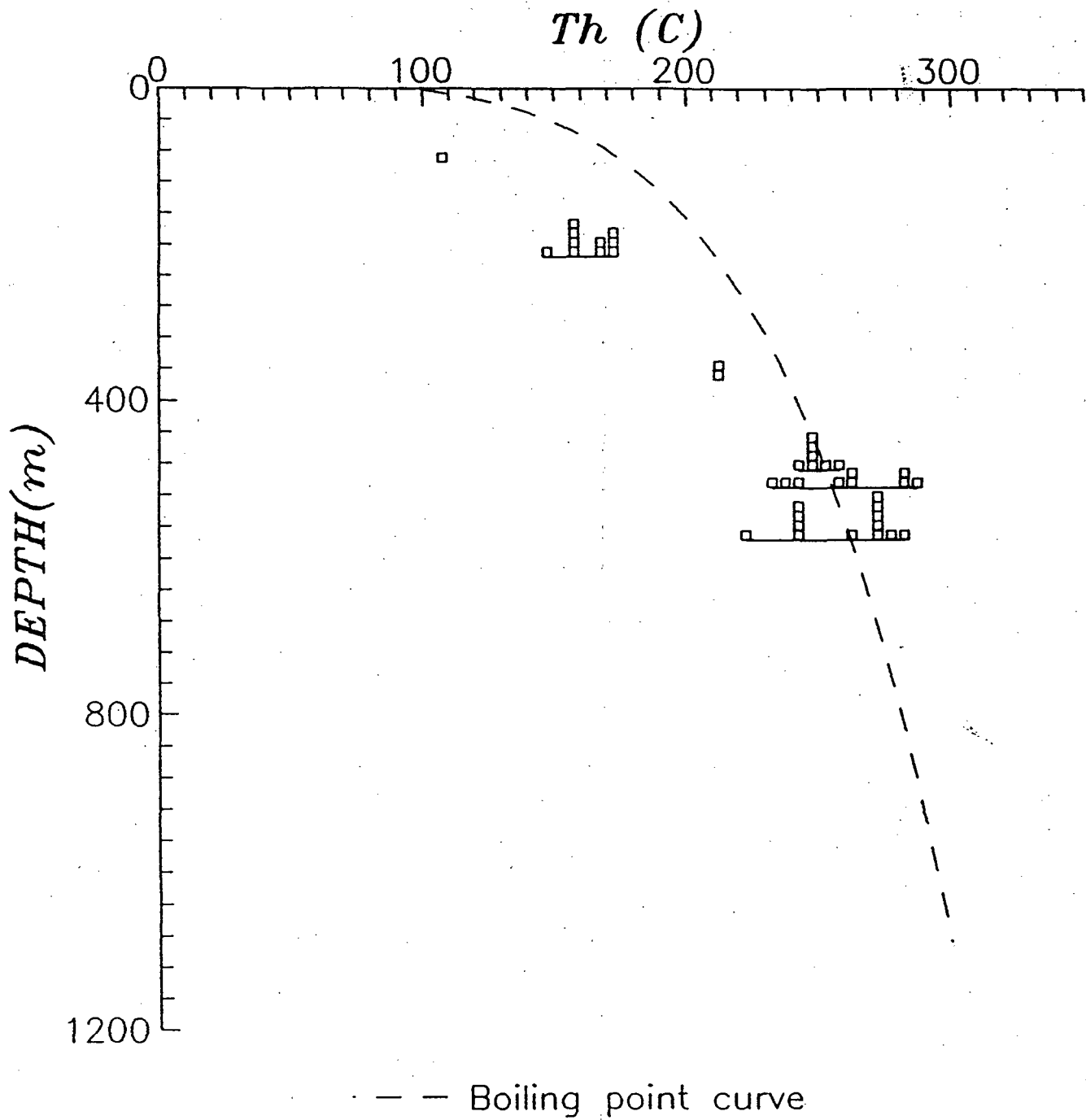


Fig. 9. Temperatures of homogenization (Th) versus depth for Z-11.

Z-11

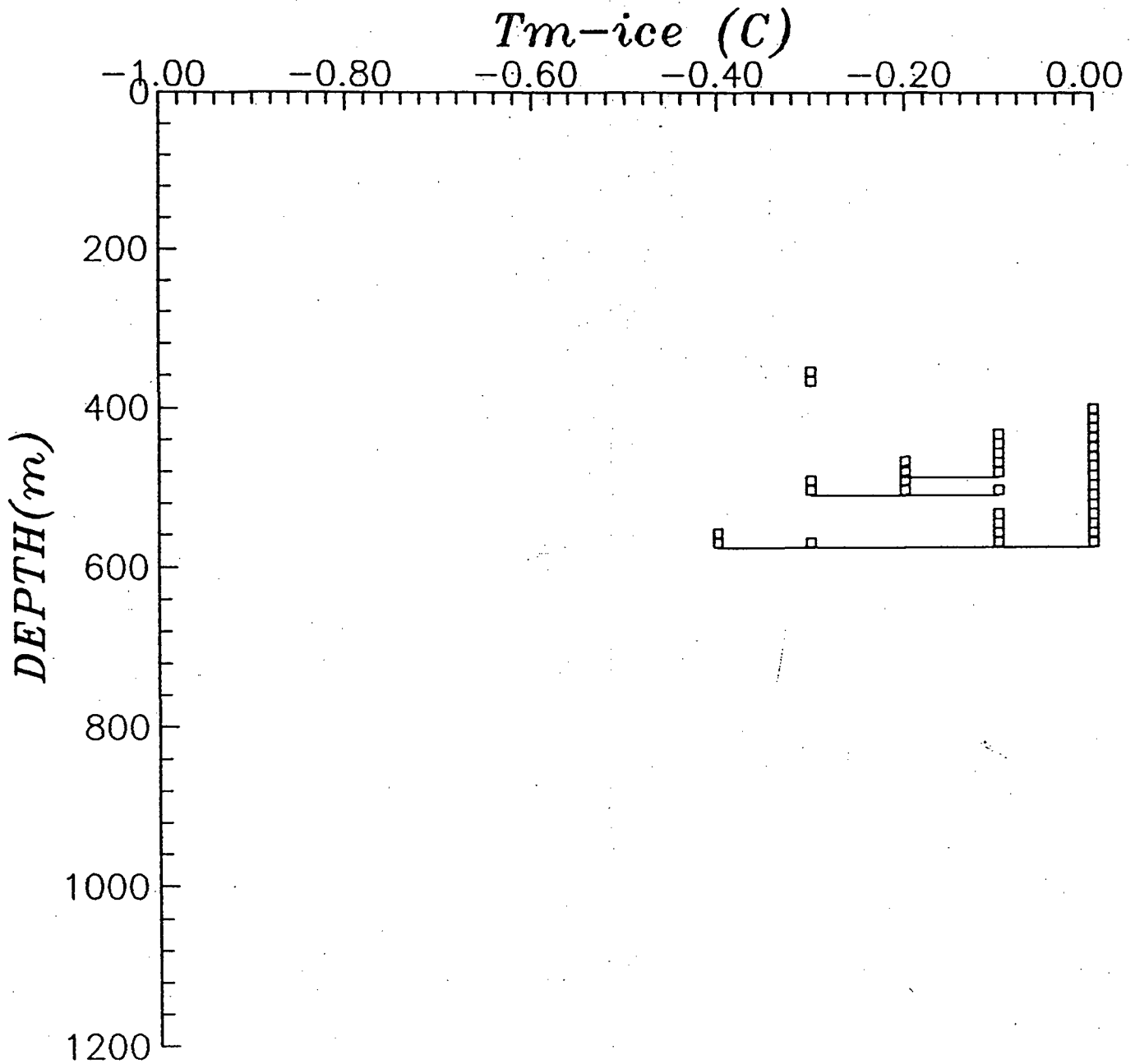


Fig. 10. Temperatures of ice-melting (T_{m-ice}) versus depth for Z-11.

ZCQ-4

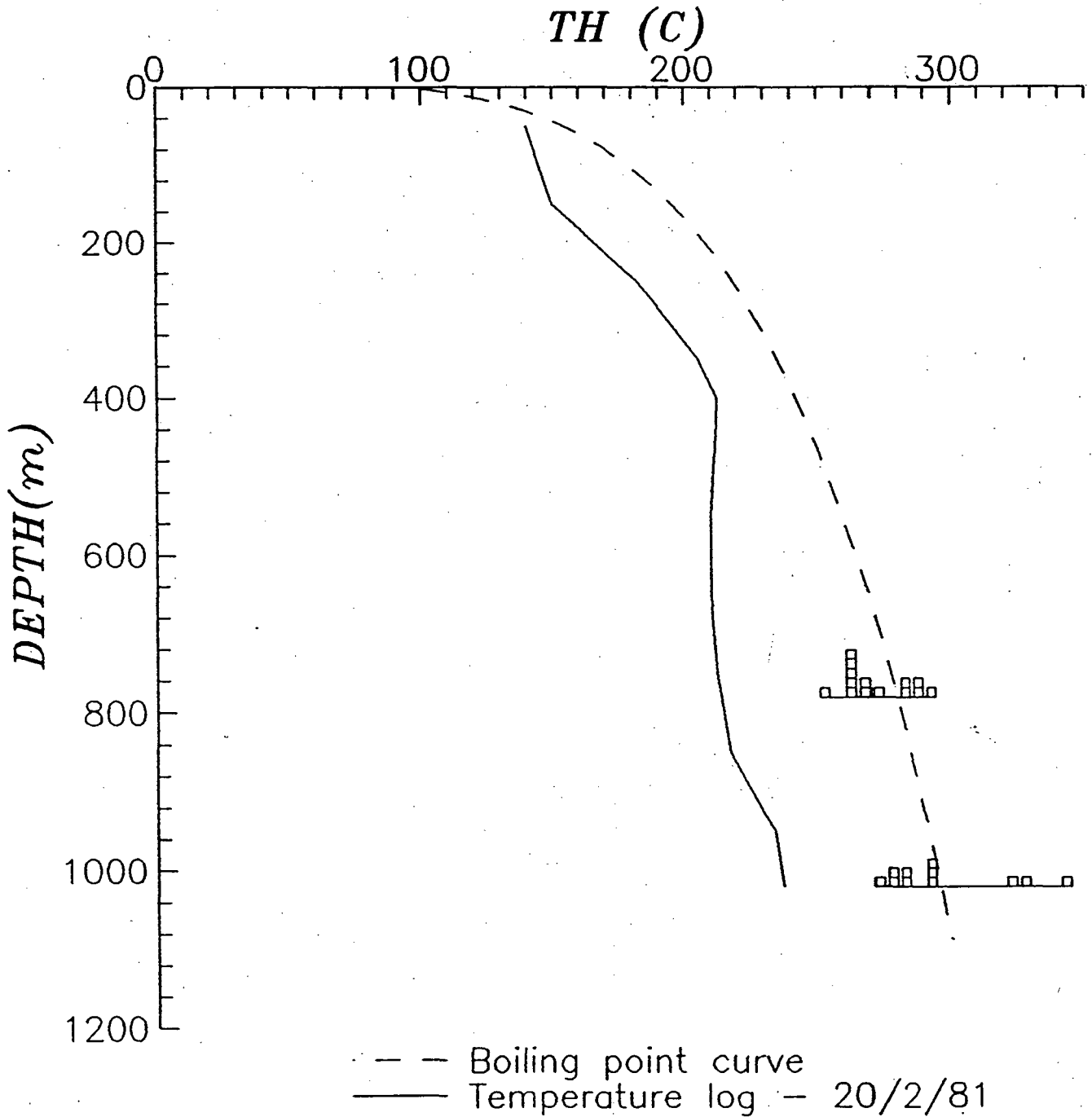


Fig. 11 Temperatures of homogenization (Th) versus depth for ZCQ-4.

ZCQ-4

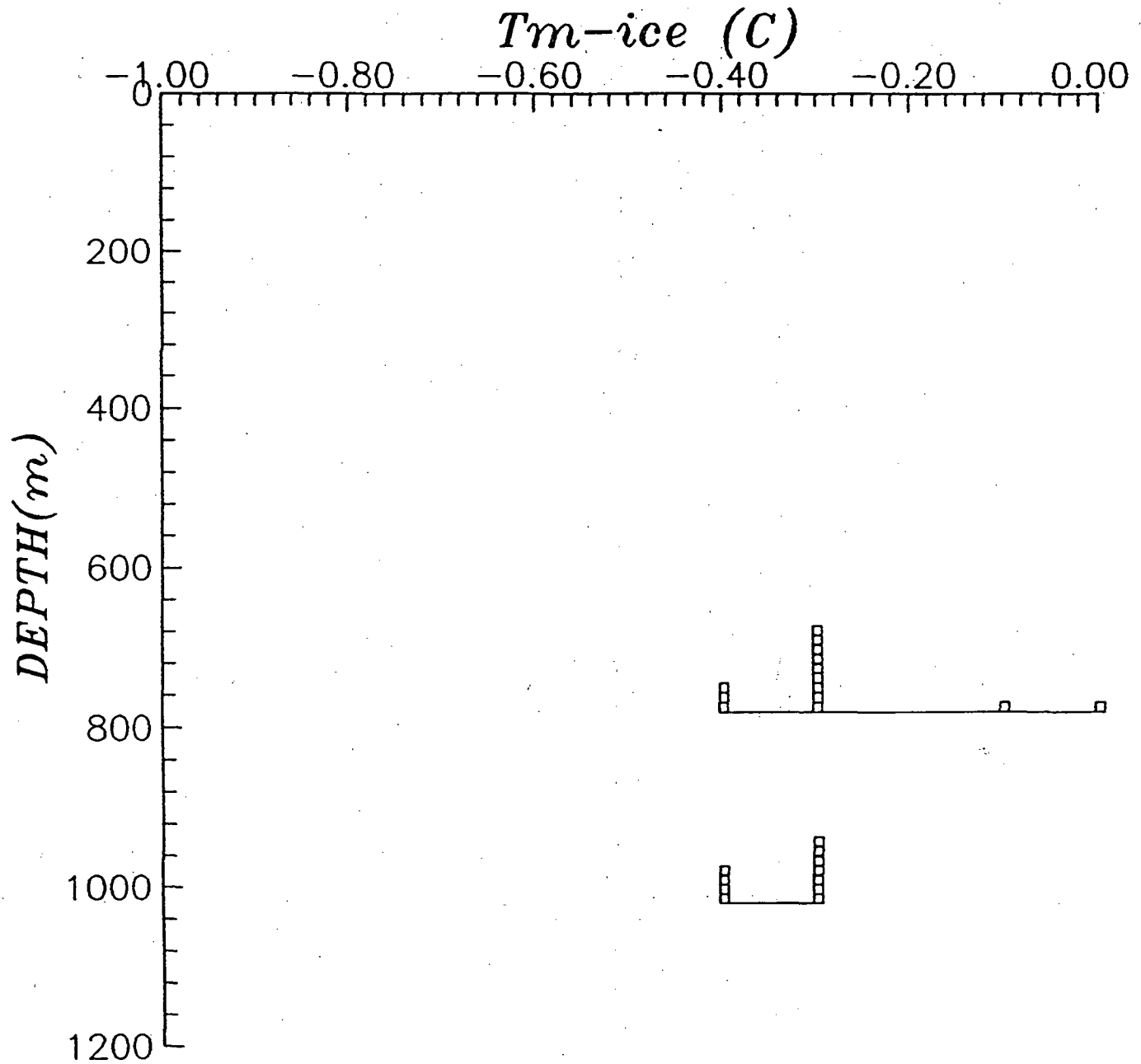


Fig. 12. Temperatures of ice-melting (T_{m-ice}) versus depth for ZCQ-4.

ZCQ-1

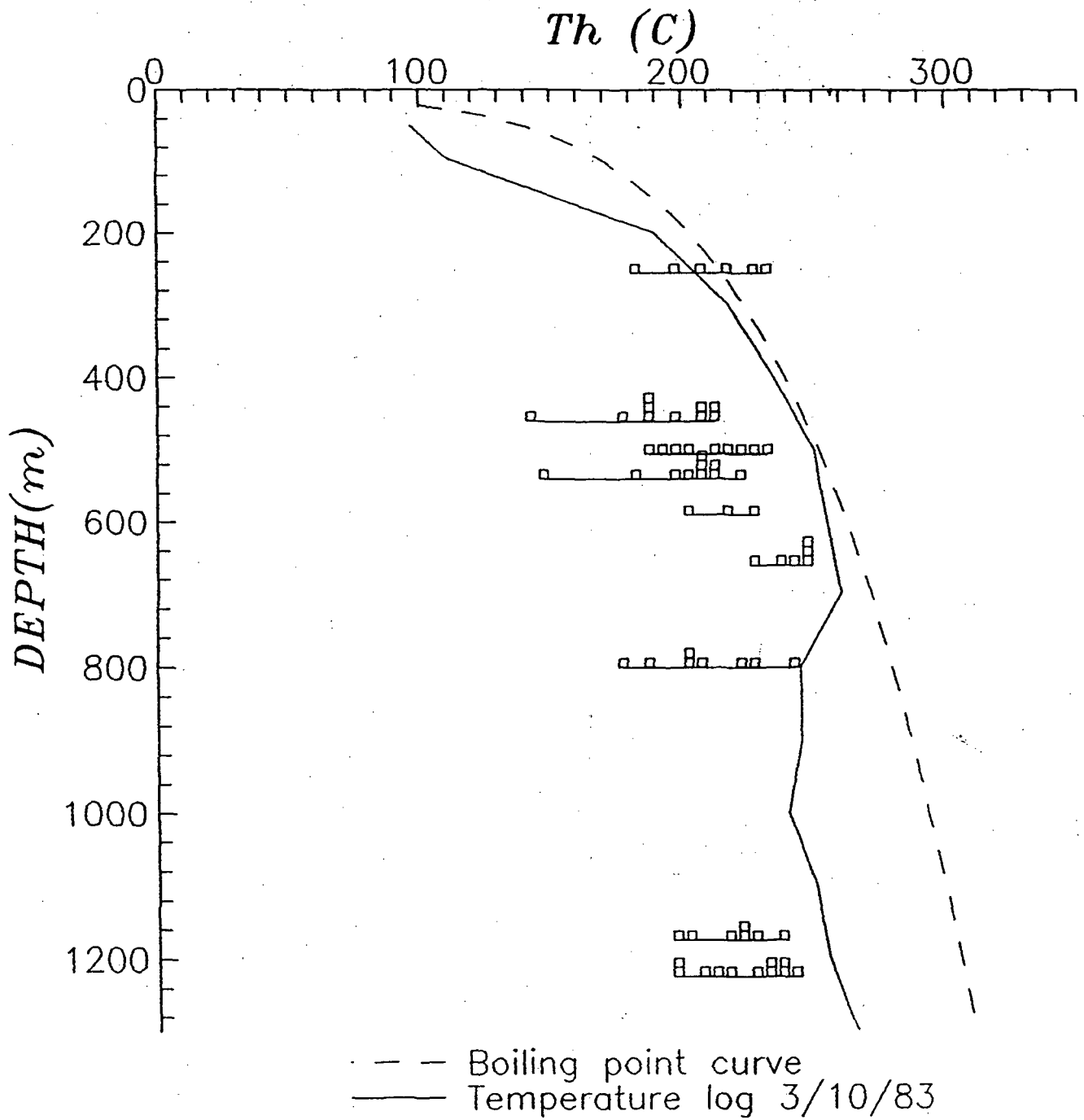


Fig. 13. Temperatures of homogenization (Th) versus depth for ZCQ-1.

ZCQ-1

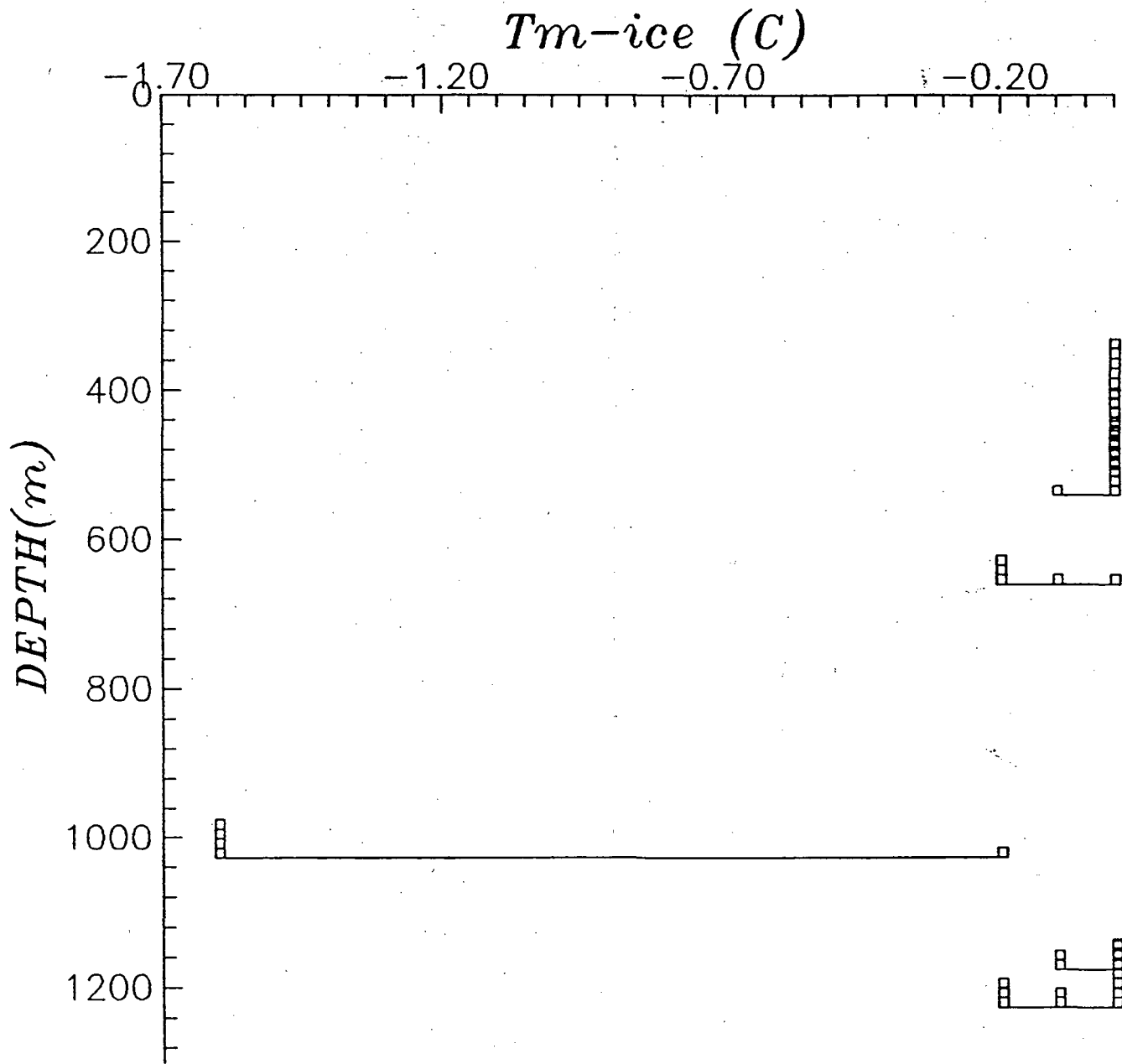


Fig. 14. Temperatures of ice-melting (T_{m-ice}) versus depth for ZCQ-1.

Z-2

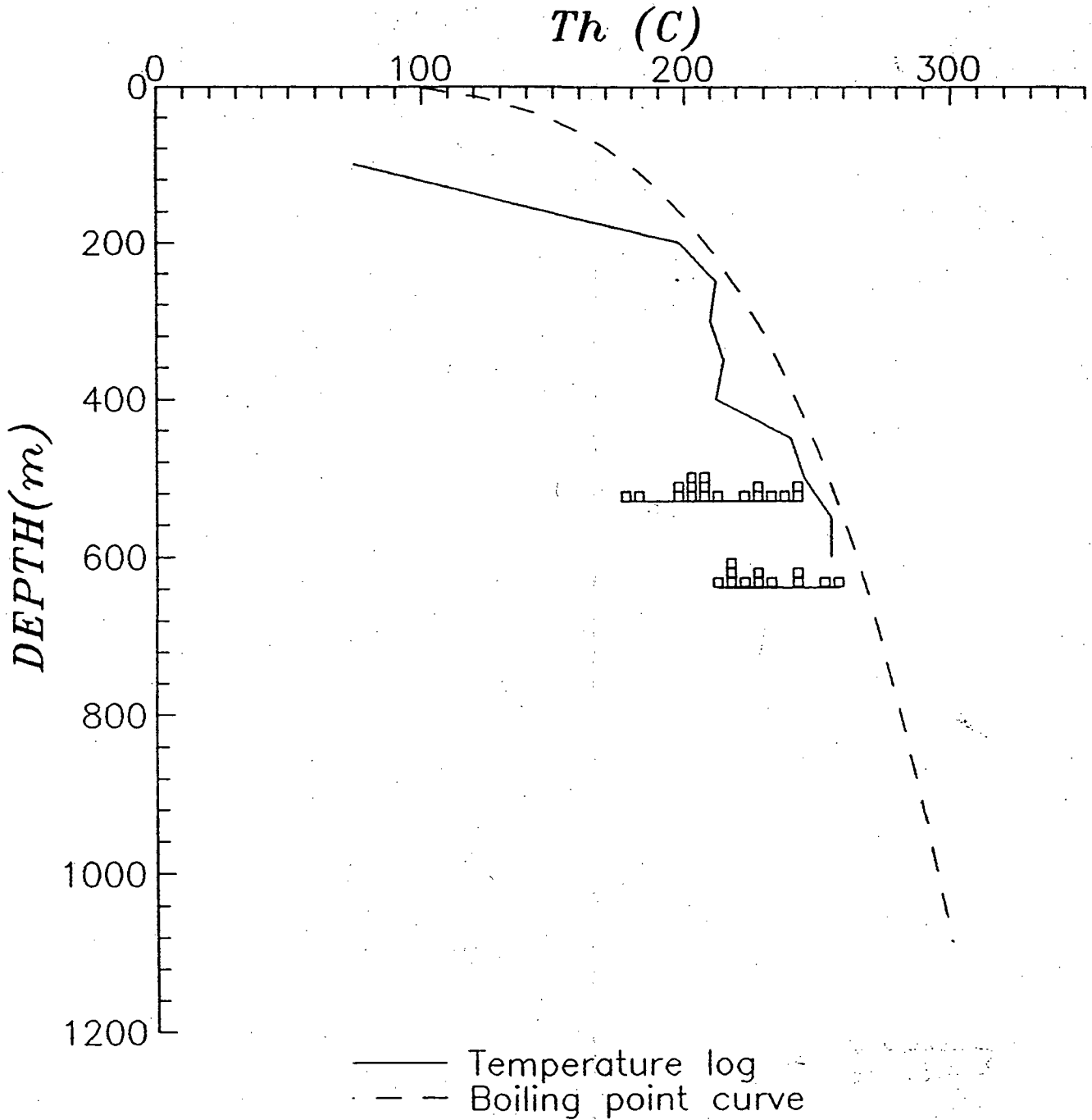


Fig. 15. Temperatures of homogenization (T_h) versus depth for Z-2.

Z-2

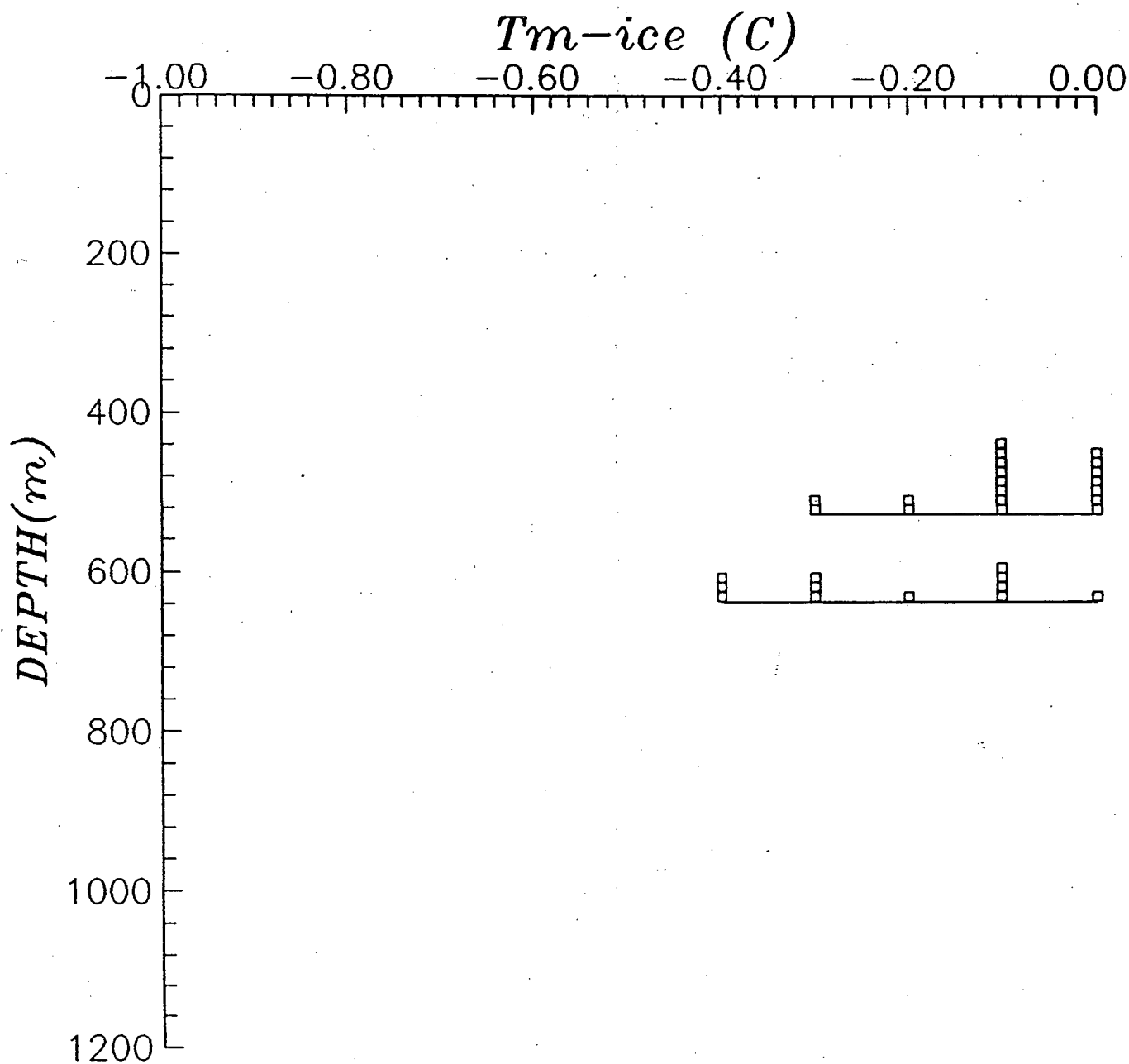


Fig. 16. Temperatures of ice-melting (T_{m-ice}) versus depth for Z-2.

ZCQ-2

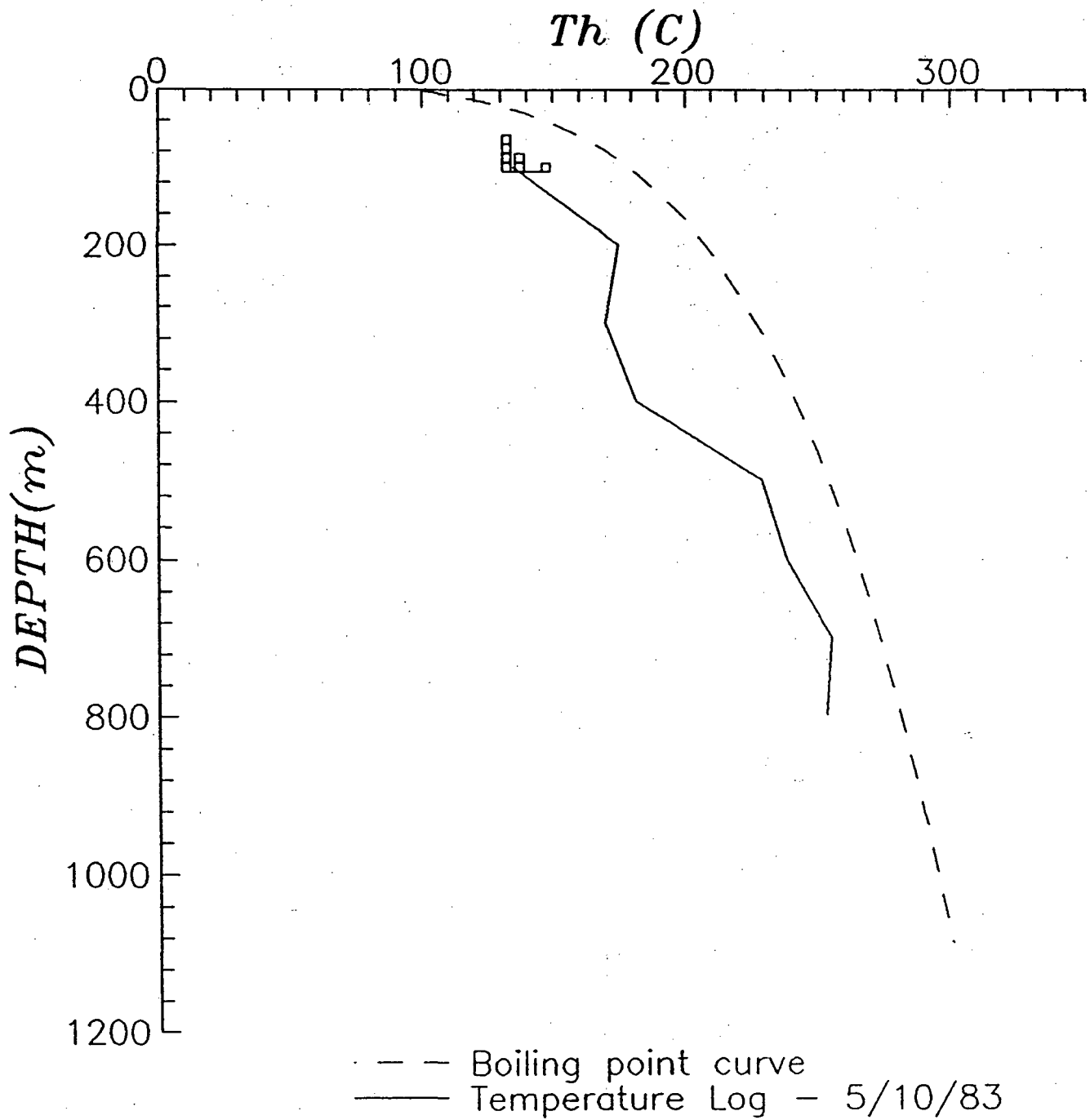


Fig. 17. Temperatures of homogenization (Th) versus depth for ZCQ-2.

ZCQ-2

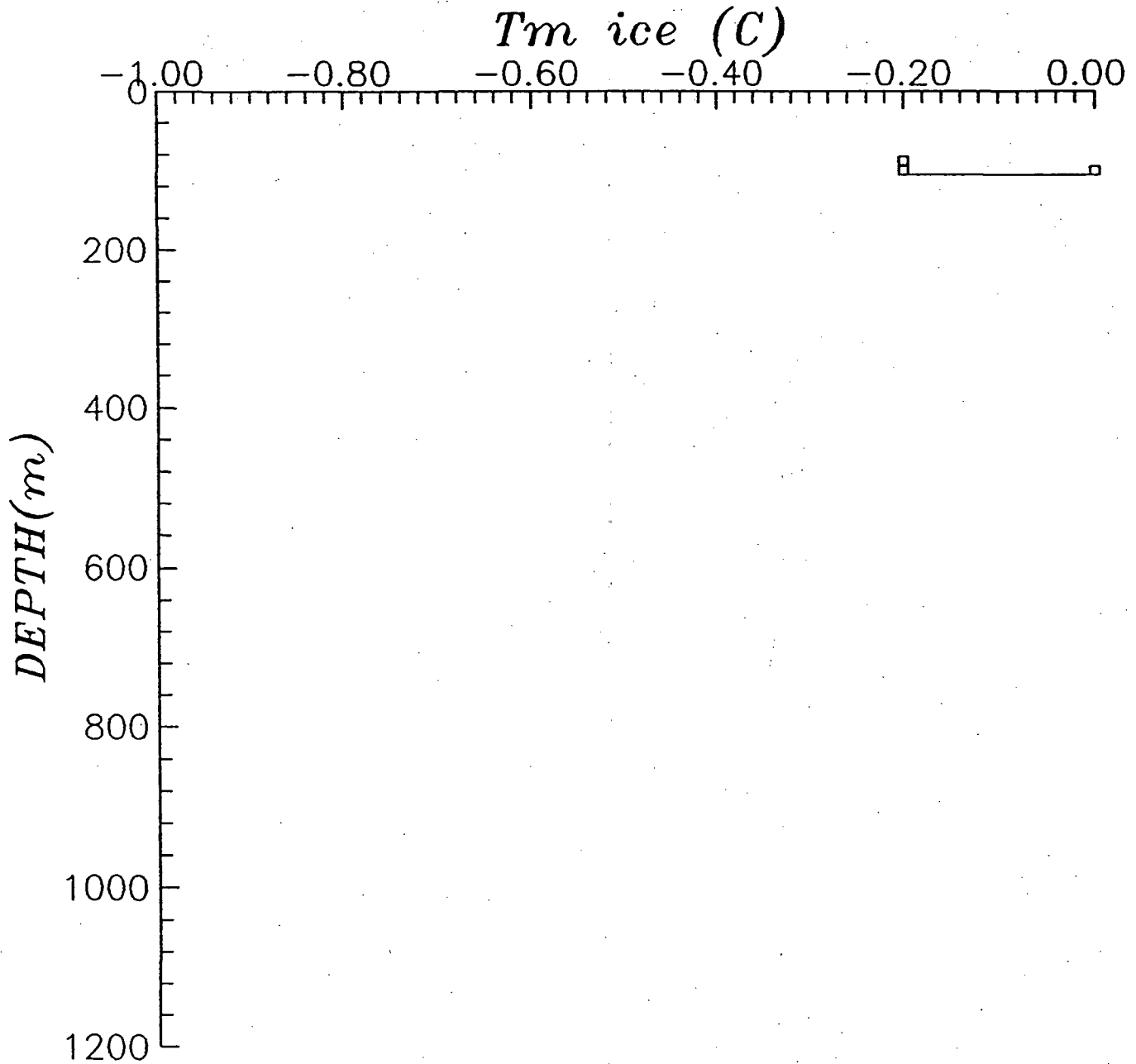


Fig. 18. Temperatures of ice-melting (T_m -ice) versus depth for ZCQ-2.

Z-7

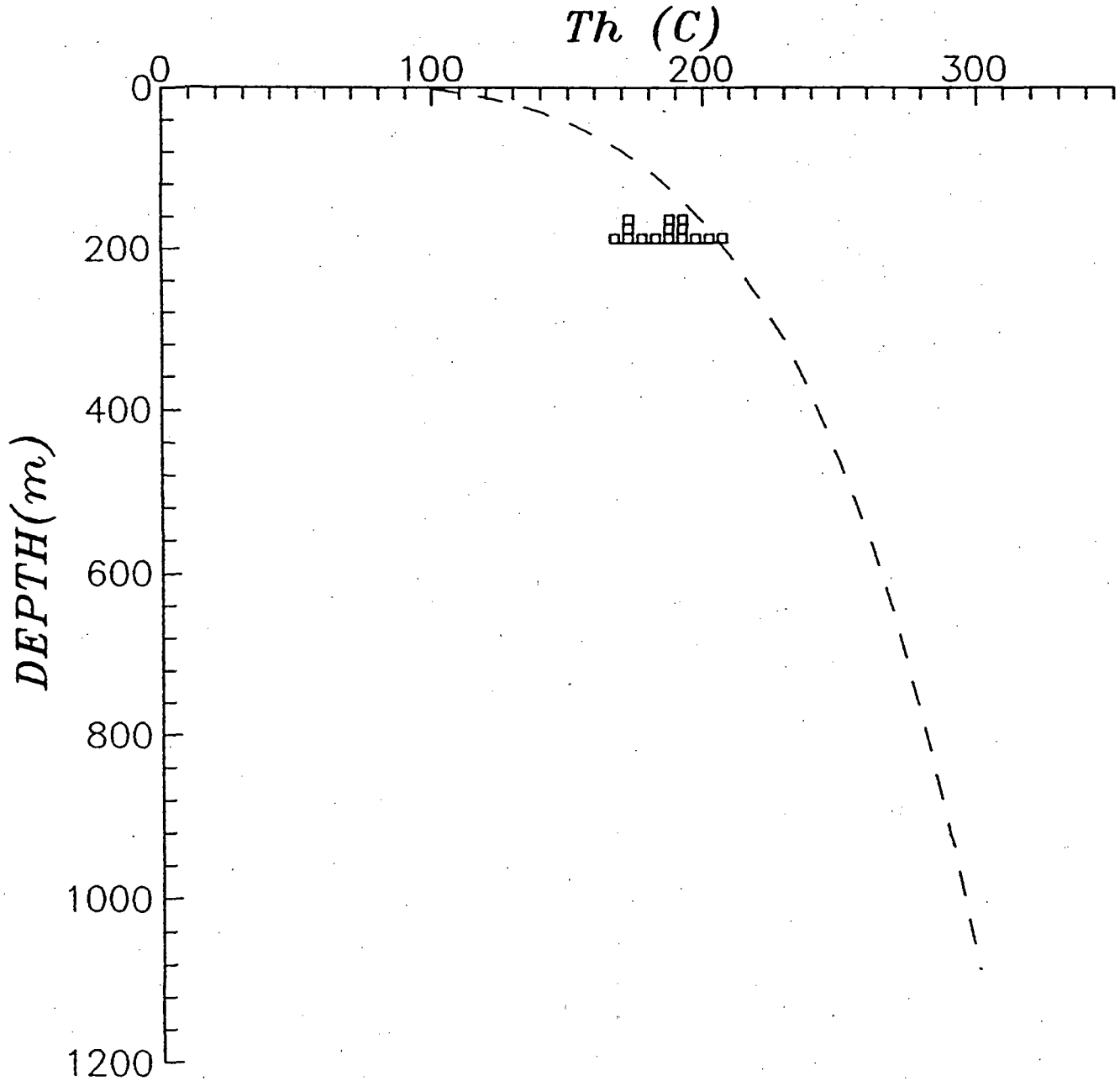


Fig. 19. Temperatures of homogenization (Th) versus depth for Z-7.

Z-7

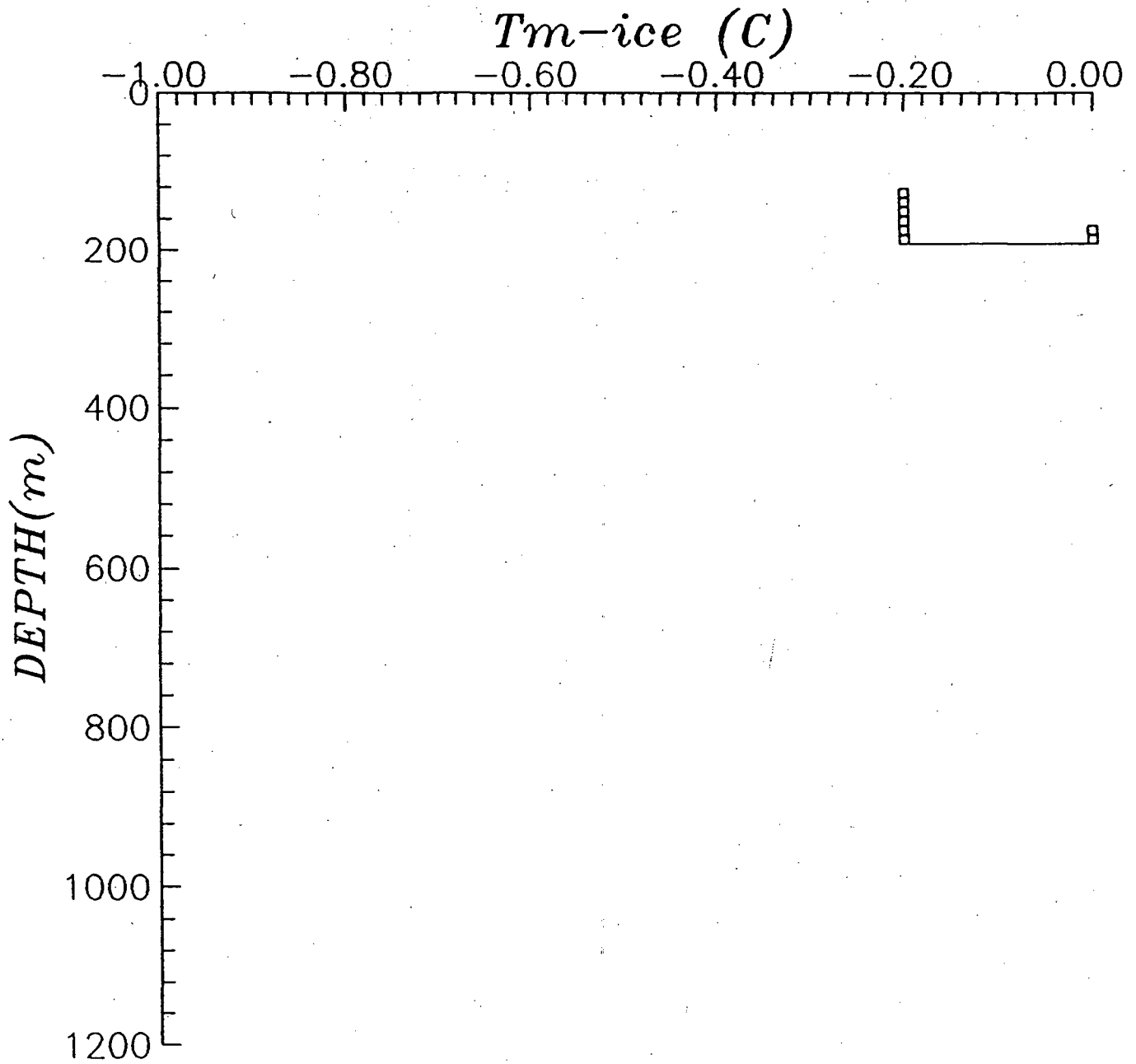


Fig. 20. Temperatures of ice-melting (T_m -ice) versus depth for Z-7.

Figure 21. Conceptual model of the Zunil I geothermal field. a) Cross-section orientated approximately west to east; wells ZCQ-5, -3, -1. b) Cross-section orientated approximately southwest to northeast; wells ZCQ-6, -3, -4, -2. Arrows indicate upwelling and downwelling fluids. See Figure 21a for legend.

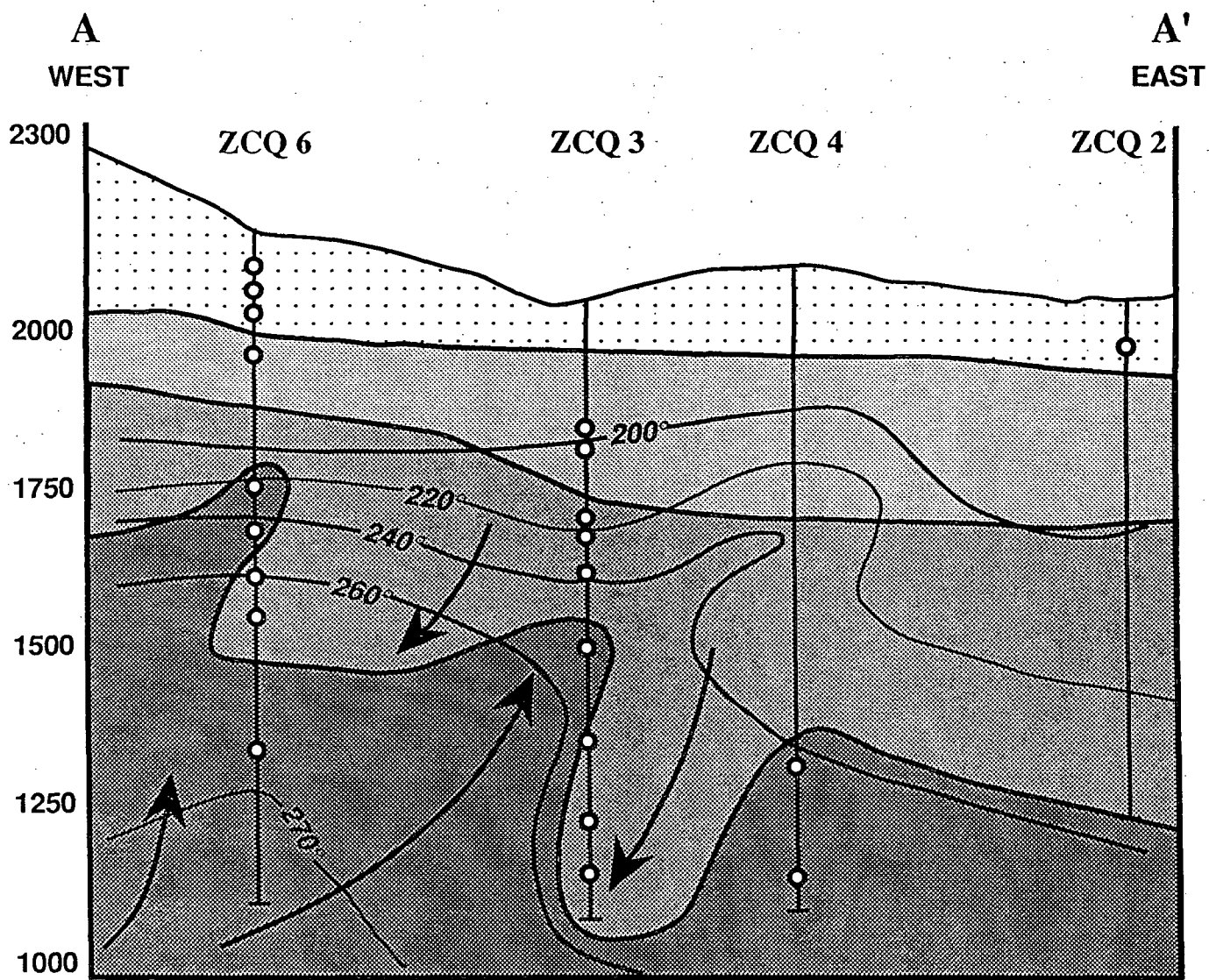


Figure 21b

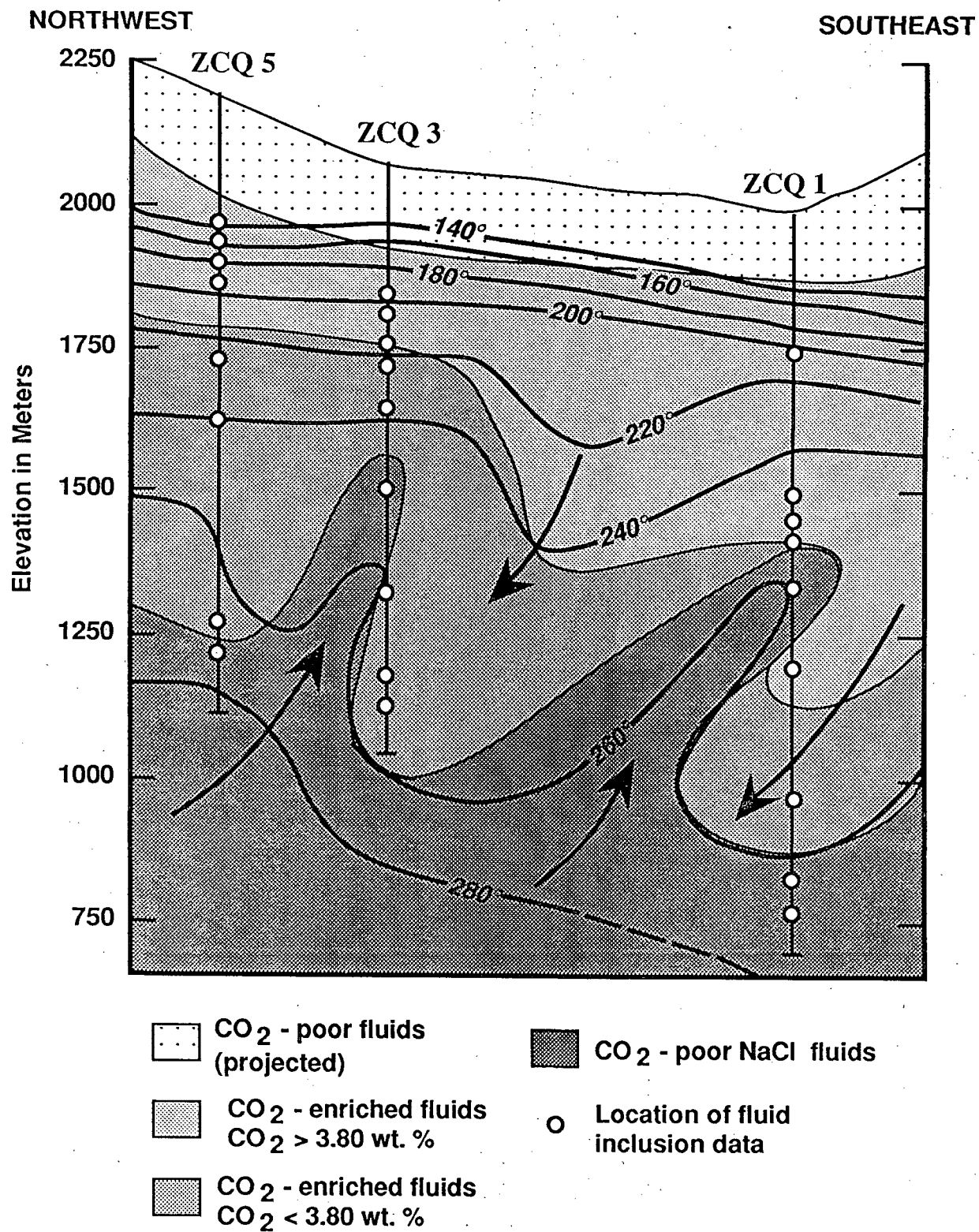


Figure 21a

APPENDIX

Key Abbreviations: Th = temperatures of homogenization
Tm = temperatures of melting
 Tm < or = 0.0°C ice-melting temperature
 Tm > 0.0°C CO₂ clathrate-melting temperature
NaCl wt % = Equivalent weight percent
 sodium chloride
p = primary inclusions
s = secondary inclusions
? = origin of inclusion unknown
Cc = Calcite
Qtz = Quartz
Ep = Epidote

ZCQ-6

DEPTH(m)	Th	Tm	NaCl wt%	Density (g/cc)	prim.(p) or sec.(s)	mineral
40	196	-0.1	0.2	0.87	s	Qtz
40	197	-0.1	0.2	0.87	s	Qtz
40	84				p	Qtz
40	196	-0.1	0.2	0.87	s	Qtz
40					?p	Qtz
40	197	-0.2	0.4	0.87	s	Qtz
100	206	0.0	0.0	0.86	s	Cc
100	141				?	Qtz
100	193	0.0	0.0	0.88	s	Cc
100	216				s	Cc
100	215	0.0	0.0	0.85	s	Cc
100	198	0.0	0.0	0.87	s	Cc
100	184				s	Cc
100	175	0.0	0.0	0.90	s	Cc
100	183				s	Cc
100	182	0.0	0.0	0.89	s	Cc
100	190	0.0	0.0	0.88	s	Cc
100	152	0.0	0.0	0.92	?	Qtz
125	139	-0.1	0.2	0.93	s	Cc
125	135	-0.1	0.2	0.94	s	Cc
125	150				s	Cc
125	151	0.0	0.0	0.92	s	Cc
125	141	-0.1	0.2	0.93	s	Cc
125	156	0.0	0.0	0.92	s	Cc
125	156	-0.1	0.2	0.92	s	Cc
125	147				s	Cc
125	179	-0.1	0.2	0.89	s	Cc
125		-0.1	0.2		s	Cc
125	157				s	Cc
190	140				?	Cc
200	219	+0.1			s?	Qtz
200	227	0.0	0.0	0.83	p	Qtz
200	143				p	Qtz
200	208	0.0	0.0	0.86	p	Qtz
200		+0.4			p	Qtz
200	144	+0.6			p	Qtz
200		+0.4			p	Qtz
200	160	0.0	0.0	0.91	p	Qtz
200		+0.4			p	Qtz
200	198				p	Qtz
200	198				p	Qtz
200	195	0.0	0.0	0.87	p	Qtz
200	203				p	Qtz
200	212	0.0	0.0	0.85	p	Qtz
200		+0.1			s?	Qtz
200	217				p	Qtz
200	197	+0.3			s	Qtz
200		+0.4			p	Qtz
200	215				p	Qtz

ZCQ-6

DEPTH(m)	Th	Tm	NaCl wt%	Density (g/cc)	prim. (p) or sec. (s)	mineral
200	160	0.0	0.0	0.91	p	Qtz
200	246	+0.6			p	Qtz
400		-0.4	0.7		s	Cc
400		0.0	0.0		s	Cc
400	147				s	Cc
400		-0.3	0.5		s	Cc
400	157	-0.3	0.5	0.92	s	Cc
400	156	-0.3	0.5	0.92	s	Cc
400	200	-0.3	0.5	0.87	s	Cc
400	164	-0.3	0.5	0.91	s	Cc
400		-0.3	0.5		s	Cc
400	156	-0.3	0.5	0.92	s	Cc
400		-0.1	0.2		s	Cc
400		-0.4	0.7		s	Cc
400		-0.4	0.7		s	Cc
400	152	-0.3	0.5	0.92	s	Cc
400	150	-0.4	0.7	0.93	s	Cc
400	174	-0.4	0.7	0.90	s	Cc
400	171	-0.3	0.5	0.90	s	Cc
400	155	-0.3	0.5	0.92	s	Cc
445	209	-0.3	0.5	0.86	p	Cc
445	218	-0.4	0.7	0.85	p	Cc
445	216	-0.3	0.5	0.85	p	Cc
445	215	-0.3	0.5	0.85	p	Cc
445	209	-0.3	0.5	0.86	p	Cc
540	242	-0.6	1.0	0.82	p	Cc
540	252	-0.4	0.7	0.80	s	Cc
540	254	-0.1	0.2	0.79	?p	Cc
540	146	-0.5	0.9	0.93	p	Cc
540	252	-0.5	0.9	0.80	p	Cc
540		-0.7	1.2		p	Cc
540	232	-0.3	0.5	0.83	p	Cc
540	248	-0.6	1.0	0.81	p	Cc
540	249				p	Cc
540	251	-0.6	1.0	0.80	?p	Cc
540	240	-0.4	0.7	0.82	s	Cc
540	239	-0.4	0.7	0.82	?p	Cc
540	231	-0.1	0.2	0.82	s	Cc
540	263	-0.1	0.2	0.77	?p	Cc
540	252				p	Cc
540	263	-0.5	0.9	0.78	p	Cc
540	247	-0.1	0.2	0.80	p	Cc
540	246	-0.6	1.0	0.81	p	Cc
540	252	-0.4	0.7	0.80	p	Cc
540	246	-0.1	0.2	0.80	p	Cc
600	163	-0.2	0.4	0.91	s	Cc
600		-0.2	0.4		?	Cc
600	189	-0.1	0.2	0.88	?	Cc
600	222	-0.3	0.5	0.84	p	Cc

ZCQ-6

DEPTH(m)	Th	Tm	NaCl wt%	Density (g/cc)	prim. (p)	
					or sec. (s)	mineral
600	202				?	Cc
600		-0.4	0.7		?	Cc
600	213	-0.2	0.4	0.85	s	Cc
600	228				?	Cc
600	212	-0.5	0.9	0.86	s	Cc
600	193	-0.1	0.2	0.88	?	Cc
790	245	-0.2	0.4	0.80	s	Cc
790	227	-0.2	0.4	0.83	s	Cc
790	245	-0.2	0.4	0.80	s	Cc
790	219	-0.2	0.4	0.84	s	Cc
790	245	-0.2	0.4	0.80	?	Cc
790	219	-0.2	0.4	0.84	s	Cc

ZCQ-5

DEPTH(m)	Th	Tm	NaCl wt%	Density (g/cc)	prim. (p) or sec. (s)	mineral
200	204	-0.1	0.2	0.86	s	Cc
200	206	-0.4	0.7	0.86	s	Cc
200	152	-0.3	0.5	0.92	s	Cc
200	190				s	Cc
200	188				s	Cc
200	206	-0.3	0.5	0.86	s	Cc
200	151				s	Cc
230	228	+0.3			s	Qtz
230	209	+0.3			p	Qtz
230	216	+0.2			?	Qtz
230	225	+0.1			s	Qtz
230	241	+0.2			?	Qtz
260	217	-0.1	0.2	0.85	p	Cc with Ep
260	215	-0.2	0.4	0.85	p	Cc with Ep
260	213	-0.2	0.4	0.85	p	Cc with Ep
260	216				p	Cc with Ep
260	213	-0.2	0.4	0.85	p	Cc with Ep
260	227	-0.1	0.2	0.83	p	Cc with Ep
260	226	-0.2	0.4	0.83	p	Cc with Ep
260	221				p	Cc with Ep
300	204	0.0	0.0	0.86	s	Qtz
300	204	+0.3			s	Qtz
300	204	0.0	0.0	0.86	s	Qtz
300	206				?	Qtz
300	196	-0.4	0.7	0.88	?	Qtz
300	198	-0.5	0.9	0.88	?	Qtz
300		-0.2	0.4		p	Qtz
300	198				?	Qtz
300	204	+0.3			s	Qtz
300	204	+0.3			s	Qtz
300	157				?	Qtz
300	195				?	Qtz
300	211	+0.3			s	Qtz
300	196				p	Qtz
300	204	+0.3			s	Qtz
445	213	0.0	0.0	0.85	s	Qtz
445	211	0.0	0.0	0.85	s	Qtz
445	210	0.0	0.0	0.85	s	Qtz
445	211	0.0	0.0	0.85	s	Qtz
445	211	0.0	0.0	0.85	s	Qtz
445	242	-0.1	0.2	0.81	s	Qtz
445	210	0.0	0.0	0.85	s	Qtz
445	229	-0.3	0.5	0.83	?	Qtz
445		0.0	0.0		s	Qtz
445	240	0.0	0.0	0.81	?	Qtz
445	249	0.0	0.0	0.79	s	Qtz
445	236	-0.1	0.2	0.82	s	Qtz
445	211	0.0	0.0	0.85	s	Qtz
445	265	0.0	0.0	0.77	?	Qtz

ZCQ-5

DEPTH(m)	Th	Tm	NaCl wt%	Density (g/cc)	prim. (p) or sec. (s)	mineral
445	243	0.0	0.0	0.80	s	Qtz
550	217	-0.4	0.7	0.85	s	Cc
550	223	-0.3	0.5	0.84	s	Cc
550		-0.5	0.9		s	Cc
550	236	-0.7	1.2	0.83	s	Cc
550	237	-0.5	0.9	0.82	s	Cc
550	216	-0.5	0.9	0.85	s	Cc
550	226	-0.4	0.7	0.84	s	Cc
550	236	-0.7	1.2	0.83	s	Cc
550	226				s	Cc
550	236	-0.7	1.2	0.83	s	Cc
550	216	-0.4	0.7	0.85	s	Cc
550	224	-0.3	0.5	0.84	s	Cc
550	237	-0.5	0.9	0.82	s	Cc
550	217	-0.4	0.7	0.85	s	Cc
550	236	-0.7	1.2	0.83	s	Cc
550	217	-0.3	0.5	0.85	s	Cc
550	236	-0.7	1.2	0.83	s	Cc
550	226				s	Cc
550	236	-0.7	1.2	0.83	s	Cc
550		-0.5	0.9		s	Cc
550	216	-0.5	0.9	0.85	s	Cc
550	229				s	Cc
550	216	-0.4	0.7	0.85	s	Cc
550	225	-0.4	0.7	0.84	s	Cc
900	282	-0.2	0.4	0.74	?	Cc
900	274	-0.2	0.4	0.76	?	Cc
900	258	0.0	0.0	0.78	s	Cc
900	267	-0.6	1.0	0.77	s	Cc
900	260	0.0	0.0	0.78	s	Cc
900	276	-0.1	0.2	0.75	s	Cc
900	273	-0.1	0.2	0.75	s	Cc
900	277	-0.3	0.5	0.75	s	Cc
900	274	-0.4	0.7	0.76	s	Cc
900	258	0.0	0.0	0.78	s	Cc
900	279	-0.5	0.9	0.75	s	Cc
900	268	-0.6	1.0	0.77	?	Cc
900		-0.7	1.2		s	Cc
900	258	0.0	0.0	0.78	s	Cc
900	260	0.0	0.0	0.78	s	Cc
900	278				s	Cc
940	276				p	Cc
940	275				p	Cc
940	272				p	Cc
940	262	0.0	0.0	0.77	p	Cc
940	262	-0.1	0.2	0.78	p	Cc
940		-0.1	0.2		p	Cc
940	264	0.0	0.0	0.77	p	Cc
940	268	-0.1	0.2	0.76	?	Cc

ZCQ-5

DEPTH(m)	Th	Tm	NaCl wt%	Density (g/cc)	prim. (p) or sec. (s)	mineral
940	267	0.0	0.0	0.76	?	Cc
940	258	-0.1	0.2	0.78	p	Cc
940	265	-0.1	0.2	0.77	p	Cc
940	273	0.0	0.0	0.75	?p	Cc
940	276				?	Cc
940	266	0.0	0.0	0.77	?	Cc
940	268	-0.1	0.2	0.76	p	Cc
940	263	0.0	0.0	0.77	p	Cc

ZCQ-3

DEPTH(m)	Th	Tm	NaCl wt%	Density (g/cc)	prim. (p) or sec. (s)	mineral
210	190	+0.3			p	Cc
210	183	+0.3			p	Cc
210	188	+0.3			p	Cc
210	152	+0.3			p	Cc
210	181	+0.3			p	Cc
210	199				p	Cc
210	188				p	Cc
210	169	+0.3			p	Cc
210	177				p	Cc
245		0.0	0.0		s	Cc
245		0.0	0.0		s	Cc
245		0.0	0.0		s	Cc
310		+0.3			p?	Cc
335	198	-0.2	0.4	0.87	p?	Cc
400	195	0.0	0.0	0.87	p	Cc
400	172	0.0	0.0	0.90	p	Cc
400	195	0.0	0.0	0.87	p	Cc
400	205				p	Cc
400	205				p	Cc
400	192				p	Cc
400	181	0.0	0.0	0.89	p	Cc
400	201	0.0	0.0	0.87	p?	Cc
400	164	0.0	0.0	0.91	p	Cc
400	194	0.0	0.0	0.87	p	Cc
400	185	0.0	0.0	0.89	p	Cc
400	160	0.0	0.0	0.91	s	Cc
400	214	+0.1			p	Cc
400	192	+0.1			p	Cc
400	199	-0.1	0.2	0.87	s	Cc
400	206	-0.1	0.2	0.86	p	Cc
400	199	0.0	0.0	0.87	p	Cc
400	209	0.0	0.0	0.85	p	Cc
550	253	-0.1	0.2	0.79	s	Cc
550	260	0.0	0.0	0.78	?	Cc
550	233	-0.2	0.4	0.82	s	Qtz
550	240	-0.1	0.2	0.81	s	Qtz
550	222				?	Cc
550	216	0.0	0.0	0.84	?	Cc
550	220				?	Cc
550	249	-0.1	0.2	0.80	s	Qtz
550	259	-0.1	0.2	0.78	p	Cc
550	264	0.0	0.0	0.77	p	Cc
550	244	-0.1	0.2	0.80	s	Qtz
550	236	-0.1	0.2	0.82	s	Qtz
550		0.0	0.0		s	Cc
550	227	-0.4	0.7	0.84	s	Qtz
550	237	-0.4	0.7	0.82	s	Qtz
550	246	-0.1	0.2	0.80	s	Qtz
550	249	-0.4	0.7	0.80	s	Qtz

ZCQ-3

DEPTH(m)	Th	Tm	NaCl wt%	Density (g/cc)	prim. (p) or sec. (s)	mineral
550	254	-0.1	0.2	0.79	p	Cc
550	223	0.0	0.0	0.84	s	Qtz
550	237	-0.4	0.7	0.82	s	Qtz
750	278	-0.2	0.4	0.75	s	Cc
750	291	-0.1	0.2	0.72	s	Cc
750	256				?	Cc
750	277	-0.2	0.4	0.75	s	Cc
750	263	-0.1	0.2	0.77	s	Cc
750	299	-0.2	0.4	0.71	s	Cc
750	300	-0.3	0.5	0.71	s	Cc
750	300	-0.5	0.9	0.71	s	Cc
750	270	-0.2	0.4	0.76	s	Cc
750	291	-0.2	0.4	0.72	s	Cc
750	274	-0.2	0.4	0.76	s	Cc
750	248				s	Cc
890		-0.7	1.2		s	Cc
890	271	-0.7	1.2	0.77	s	Cc
890	273	-0.1	0.2	0.75	s	Cc
890	290				s	Cc
890	271	0.0	0.0	0.76	s	Cc
890		-0.6	1.0		s	Cc
890	260	-0.2	0.4	0.78	s	Cc
890	263	-0.1	0.2	0.77	s	Cc
890		-0.9	1.6		s	Cc
890	272	-1.1	1.9	0.78	s	Cc
930	256	-0.5	0.9	0.79	p?	Cc
930	254	-0.1	0.2	0.79	p?	Cc
930	262	-0.5	0.9	0.78	p?	Cc

ZUNIL Z-11

DEPTH(M)	Th	Tm	NaCl wt%	Density (g/cc)	prim. (p) or sec. (s)	mineral
89	109				s	Cc
210	145	+0.3			s	Cc
210	174	+0.6			?	Cc
210	168				?	Cc
210	174	+0.3			s	Cc
210	158	+0.4			s	Cc
210	158				s	Cc
210	157	+0.4			s	Cc
210	158				s	Cc
210	169				?	Cc
210	174	+0.6			?	Cc
368	211	-0.3	0.5	0.86	p?	Cc
368	210	-0.3	0.5	0.86	p?	Cc
483	245	-0.1	0.2	0.80	s	Cc
483	242	-0.1	0.2	0.81	s	Cc
483	245				s	Cc
483	254	-0.1	0.2	0.79	s	Cc
483	242	-0.1	0.2	0.81	s	Cc
483	259	-0.1	0.2	0.78	s	Cc
483	245	-0.2	0.4	0.80	s	Cc
483	249				s	Cc
505	244	-0.2	0.4	0.81	s	Cc
505	283				s	Cc
505	235	-0.1	0.2	0.82	s	Cc
505	262	-0.3	0.5	0.78	s	Cc
505	283	-0.2	0.4	0.74	s	Cc
505	287	-0.3	0.5	0.73	s	Cc
505	259	-0.2	0.4	0.78	s	Cc
505	262	-0.2	0.4	0.78	s	Cc
505	231				s	Cc
571	242	-0.1	0.2	0.81	s	Cc
571	272	0.0	0.0	0.75	s	Cc
571	282	0.0	0.0	0.74	s	Cc
571	272	0.0	0.0	0.75	s	Cc
571	241	-0.1	0.2	0.81	s	Cc
571	275	-0.4	0.7	0.76	s	Cc
571	241	-0.1	0.2	0.81	s	Cc
571	263	0.0	0.0	0.77	s	Cc
571	242	0.0	0.0	0.81	s	Cc
571		0.0	0.0		s	Cc
571	241	0.0	0.0	0.81	s	Cc
571		-0.1	0.2		s	Cc
571	242	0.0	0.0	0.81	s	Cc
571	270	-0.4	0.7	0.77	s	Cc
571	241	0.0	0.0	0.81	s	Cc
571	242	0.0	0.0	0.81	s	Cc
571	244	0.0	0.0	0.80	s	Cc
571	284	0.0	0.0	0.73	s	Cc
571		-0.3	0.5		s	Cc

ZUNIL Z-11

DEPTH(M)	Th	Tm	NaCl wt%	Density (g/cc)	prim. (p) or sec. (s)	mineral
571	220	0.0	0.0	0.84	s	Cc
571	270	0.0	0.0	0.76	s	Cc
571	270	0.0	0.0	0.76	s	Cc

ZCQ-4

DEPTH(M)	Th	Tm	NaCl wt%	Density (g/cc)	prim. (p) or sec. (s)	mineral
775	269	-0.1	0.2	0.76	p?	Cc
775	288	-0.3	0.5	0.73	s	Cc w/ epid.
775	291	-0.3	0.5	0.73	s	Cc w/ epid.
775	261	-0.3	0.5	0.78	s	Cc w/ epid.
775	283	-0.3	0.5	0.74	s	Cc w/ epid.
775	252	-0.4	0.7	0.80	s	Cc w/ epid.
775	288	-0.3	0.5	0.73	s	Cc w/ epid.
775	260	-0.4	0.7	0.78	s	Cc w/ epid.
775	284	-0.3	0.5	0.74	s	Cc w/ epid.
775	264	0.0	0.0	0.77	p?	Cc
775	268	-0.3	0.5	0.77	p?	Cc
775	260	-0.4	0.7	0.78	s	Cc w/ epid.
775	293				s	Cc w/ epid.
775	273	-0.3	0.5	0.76	s	Cc w/ epid.
775	264	-0.3	0.5	0.77	p?	Cc
1015	274	-0.4	0.7	0.76	p	Qtz
1015	282	-0.3	0.5	0.74	p	Qtz
1015	277	-0.4	0.7	0.75	p	Qtz
1015	292	-0.3	0.5	0.72	p	Qtz
1015	342				p	Qtz
1015	292	-0.3	0.5	0.72	p	Qtz
1015	293	-0.3	0.5	0.72	p	Qtz
1015	292	-0.3	0.5	0.72	p	Qtz
1015	326				p	Qtz
1015	282	-0.3	0.5	0.74	p	Qtz
1015	321	-0.4	0.7	0.67	p	Qtz
1015	293	-0.3	0.5	0.72	p	Qtz
1015	279	-0.4	0.7	0.75	p	Qtz

ZCQ-1

DEPTH(M)	Th	Tm	NaCl wt%	Density (g/cc)	prim. (p) or sec. (s)	mineral
250	184				p	Cc
250	205	+0.6			p	Cc
250	195				s	Cc
250	233				s	Cc
250	227				?	Cc
250	215				p	Cc
250	198	+0.2			p	Cc
455	188	0.0	0.0	0.88	s	Cc
455	177				s	Cc
455	186	0.0	0.0	0.88	s	Cc
455	196	0.0	0.0	0.87	s	Cc
455	198	0.0	0.0	0.87	s	Cc
455	209	0.0	0.0	0.86	s	Cc
455	213	0.0	0.0	0.85	s	Cc
455	209	0.0	0.0	0.86	s	Cc
455	210	0.0	0.0	0.85	s	Cc
455	186	0.0	0.0	0.88	s	Cc
455	140				s	Cc
455	210	0.0	0.0	0.85	s	Cc
500	191	0.0	0.0	0.88	s	Cc
500	216	0.0	0.0	0.85	s	Cc
500	221	+0.3			s	Cc
500	204	+0.3			s	Cc
500	195				s	Cc
500	224	0.0	0.0	0.83	s	Cc
500	226	0.0	0.0	0.83	s	Cc
500	185	+0.3			s	Cc
500	231	+0.3			s	Cc
500	211	0.0	0.0	0.85	s	Cc
535	196	0.0	0.0	0.87	s	Cc
535	205	0.0	0.0	0.86	s	Cc
535	224	0.0	0.0	0.83	s	Cc
535	212	0.0	0.0	0.85	s	Cc
535	207	0.0	0.0	0.86	s	Cc
535	221				s	Cc
535	203	0.0	0.0	0.86	s	Cc
535	182	0.0	0.0	0.89	s	Cc
535	208	0.0	0.0	0.86	s	Cc
535	206	0.0	0.0	0.86	s	Cc
535	209				s	Cc
535	145	-0.1	0.2	0.93	s	Cc
535	212	0.0	0.0	0.85	s	Cc
585	218	+0.3			s	Cc
585	229	+0.3			s	Cc
585	204	+0.3			s	Cc
655	244	0.0	0.0	0.80	s	Cc
655	229				s	Cc
655	235	-0.2	0.4	0.82	s	Cc
655	248	-0.2	0.4	0.80	s	Cc

ZCQ-1

DEPTH(M)	Th	Tm	NaCl wt%	Density (g/cc)	prim. (p) or sec. (s)	mineral
655	246	-0.1	0.2	0.80	s	Cc
655	248	-0.2	0.4	0.80	s	Cc
795	178	+0.5			s	Cc
795	200				s	Cc
795	200	+0.5			s	Cc
795	223	+0.5			s	Cc
795	243	+0.1			s	Cc
795	185	+0.5			s	Cc
795		+0.1			s	Cc
795	205	+0.1			s	Cc
795		+0.5			s	Cc
795	244	+0.5			s	Cc
795	225	+0.4			s	Cc
795		+0.3			s	Cc
795		+0.1			s	Cc
1020		-1.6	2.7		s	Cc
1020		-1.6	2.7		s	Cc
1020		-1.6	2.7		s	Cc
1020		-1.6	2.7		s	Cc
1020		-0.2	0.4		s	Cc
1170	221	0.0	0.0	0.84	p	Cc
1170	221				p	Cc
1170	195				p	Cc
1170	227	-0.1	0.2	0.83	p	Cc
1170	218	0.0	0.0	0.84	p	Cc
1170	235	-0.1	0.2	0.82	p	Cc
1170	200	0.0	0.0	0.87	p	Cc
1220	227	-0.2	0.4	0.83	s	Cc
1220	230				s	Cc
1220	237	0.0	0.0	0.81	s	Cc
1220	215				s	Cc
1220	233	-0.2	0.4	0.82	s	Cc
1220	235	-0.1	0.2	0.82	s	Cc
1220	196	0.0	0.0	0.87	s	Cc
1220	213	-0.1	0.2	0.85	s	Cc
1220	237	0.0	0.0	0.81	s	Cc
1220	208	0.0	0.0	0.86	s	Cc
1220	235	0.0	0.0	0.82	s	Cc
1220	196	0.0	0.0	0.87	s	Cc
1220	241	-0.2	0.4	0.81	s	Cc
1220	234	0.0	0.0	0.82	s	Cc

ZUNIL Z-2

DEPTH(M)	(Th)	Tm	NaCl wt%	Density (g/cc)	prim.(p) or sec.(s)	mineral
524	234	0.0	0.0	0.82	?	Cc
524	203	-0.1	0.2	0.86	s	Cc
524	205	-0.3	0.5	0.86	?	Cc
524	223	-0.1	0.2	0.84	s	Cc
524	208	0.0	0.0	0.86	s	Cc
524	228	-0.2	0.4	0.83	s	Cc
524	207	-0.1	0.2	0.86	s	Cc
524	242	-0.1	0.2	0.81	s	Cc
524	204	-0.2	0.4	0.86	s	Cc
524	225	-0.1	0.2	0.83	s	Cc
524	197	0.0	0.0	0.87	s	Cc
524	225	0.0	0.0	0.83	?	Cc
524	228	-0.1	0.2	0.83	s	Cc
524	231	-0.1	0.2	0.82	s	Cc
524	182	0.0	0.0	0.89	s	Cc
524	214	-0.3	0.5	0.85	s	Cc
524	198				s	Cc
524	200	0.0	0.0	0.87	s	Cc
524	239				s	Cc
524	241	0.0	0.0	0.81	s	Cc
524	177	-0.1	0.2	0.90	s	Cc
633	216	-0.4	0.7	0.85	s	Cc
633	256	-0.1	0.2	0.79	?	Cc
633	225	-0.2	0.4	0.84	s	Cc
633	252				?	Cc
633	243	-0.3	0.5	0.81	s	Cc
633	222	-0.1	0.2	0.84	s	Cc
633	244	0.0	0.0	0.80	?	Cc
633	227	-0.1	0.2	0.83	s	Cc
633	218	-0.3	0.5	0.85	s	Cc
633	216	-0.4	0.7	0.85	s	Cc
633	211	-0.3	0.5	0.86	?	Cc
633	233	-0.4	0.7	0.83	s	Cc
633	226	-0.1	0.2	0.83	s	Cc

ZCQ-2

WELL/DEPTH(M)	Th	Tm	NaCl wt%	Density (g/cc)	prim. (p) or sec. (s)	mineral
100	138				s	Qtz
100	132	-0.2	0.4	0.94	s	Qtz
100	147	-0.2	0.4	0.93	s	Qtz
100	134				s	Qtz
100	134				s	Qtz
100	138				s	Qtz
100	132	0.0	0.0	0.94	s	Qtz

ZUNIL Z-7

DEPTH(M)	Th	Tm	NaCl wt%	Density (g/cc)	prim. (p) or sec. (s)	mineral
188	165				s	Cc
188	185	-0.2	0.4	0.89	s	Cc
188	201	-0.2	0.4	0.87	s	Cc
188	182				s	Cc
188	173				s	Cc
188	171				s	Cc
188	199				s	Cc
188	192	-0.2	0.4	0.88	s	Cc
188	194	0.0	0.0	0.87	s	Cc
188	171	0.0	0.0	0.90	s	Cc
188	177	-0.2	0.4	0.90	s	Cc
188	209				s	Cc
188	190				s	Cc
188	188	-0.2	0.4	0.88	s	Cc
188	189	-0.2	0.4	0.88	s	Cc

**HYDROTHERMAL ALTERATION AND STRATIGRAPHY
OF THE ZUNIL I GEOTHERMAL AREA**

SUMMARY

Mineralogic and petrographic studies of cores and cuttings from Zunil I suggest that the well field is located within the high-temperature portion of a fracture-controlled geothermal reservoir. Hydrothermal alteration is widespread within the reservoir rocks and generally increases in intensity with depth. Temperatures inferred from mineral relationships are consistent with measured downhole temperatures, and suggest that no significant cooling has occurred within the explored portions of the reservoir.

Veining in the lower portions of wells ZCQ-3, 5 and 6 is associated with fault zones that offset the volcanic rocks and underlying granodiorite. Hydrothermal breccias and the mineral assemblages in these wells show that boiling occurred primarily in the volcanic rocks as the fluids moved upward from the granodiorite. Veins within the volcanic rocks consist of calcite + quartz \pm epidote \pm wairakite. In contrast, veins near the top of the granodiorite are filled with quartz + epidote, suggesting that mineralization occurred in response to cooling. Veins and textures within well ZCQ-1 indicate that boiling has occurred throughout both the volcanic section and granodiorite in this well.

The condensation of steam and CO₂ in the shallow groundwaters has produced a steam-heated cap over the thermal system. These steam-heated waters have resulted in pervasive but locally intense illitization and the deposition of veins containing illite or plagioclase. Petrographic relationships demonstrate that these veins postdate the propylitic alteration present in the reservoir rocks.

Illite veins and zones of intense illitization are most common in ZCQ-1, where they are present in both the volcanic rocks and the granodiorite. Plagioclase-bearing veins occur in the western part of the well field in wells ZCQ-3, 5 and 6 and Z-11. The distribution of vein plagioclase and illite suggests that the steam-heated reservoir is thickest in the vicinity of ZCQ-1 and thins to the west. These relationships imply that wells ZCQ-3, 5 and 6

are closer to the upwelling center of the geothermal system than well ZCQ-1.

INTRODUCTION

Detailed geologic models of geothermal systems are needed to site exploration and development wells. These models must provide information on the size, geometry and temperature of the resource, the geologic factors controlling the location of permeable zones, and the composition of the thermal fluids. The secondary minerals occurring in drill chips and core are an important source of information since their distributions are strongly dependant on the physical and chemical conditions within the reservoir. Consequently, petrologic studies have proven to be an essential part of most exploration and development programs.

In this paper we document the results of petrographic and mineralogic studies of core and cuttings samples from production wells ZCQ-1, 3, 4, 5, and 6, and thermal gradient wells Z-2 and 11 (Figure 1). The data are used to better characterize the size and shape of the geothermal reservoir and the geologic controls on reservoir permeability at Zunil I.

ANALYTICAL METHODS AND PROCEDURES

Mineral assemblages in approximately 100 samples were studied using petrographic and X-ray diffraction techniques (Tables 1 and 2). Thin sections were prepared of each of the major lithologies encountered in the wells. Particular emphasis was placed on samples containing veins in order to better characterize fracture permeabilities. Mineral identifications and abundances in 25 samples were confirmed by X-ray diffraction analysis. Bulk rock samples were prepared for analysis by grinding in acetone to <325 mesh. The clay minerals (less than 5 μ fraction) were separated from the bulk samples by sonic disaggregation in deionized water, Stokes's law settling and centrifugation. The resulting slurries were smeared on glass

slides and irradiated after each of the following processes: air drying, vapor glycolation at 60°C for 24 hours, heating to 250°C for 1 hour, and heating to 550°C for one hour. Approximate weight percentages were determined by referring to appropriate calibration curves prepared using standard phases mixed in different proportions.

STRATIGRAPHIC RELATIONSHIPS

The lithologies encountered in the thermal gradient and production wells at Zunil I consist of a thick sequence of lava flows and ash-flow tuffs that unconformably overlie a basement of granodiorite (ELC-Electroconsult, 1980; Tobias, 1978, unpub. lithologic logs). Throughout most of the area, the volcanic rocks are covered by a thin veneer of alluvium, pumiceous deposits, and recent landslide debris.

The volcanic rocks range in composition from basaltic andesite to rhyodacite. Hydrothermal alteration related to geothermal activity has converted the glassy matrix and primary mineral assemblages of these rocks to mixtures of clays, calcite, iron oxides, quartz and epidote. However, even in the intensely altered rocks, the primary textures and proportions of ferromagnesian minerals and phenocrysts can frequently be determined.

Stratigraphic relationships within the deep production wells are illustrated in Figures 2A and 2B and shown in detail in Figures 3 through 7. According to Tobias (1978), the volcanic rocks can be assigned to four volcanic sequences that range in age from Pleistocene to Tertiary. These include the Galapago Andesite (Pleistocene), Almolonga Volcanics (Pleistocene), Green Tuff (Pliocene), and the Old Zunil Lavas (Pliocene). However, the absolute ages of the rocks have not yet been well established.

The Galapago Andesite consists of a sequence of lava flows that reach a maximum thickness of 200 m in ZCQ-5 and 6. The flows thin to the east, suggesting that they were erupted from a vent located to the west of Zunil I. In thin section, the andesite flows were found to contain phenocrysts of plagioclase and rare clinopyroxene in a matrix of variably altered glass,

plagioclase microlites, and disseminated magnetite. The microlites commonly exhibit well developed flow-banding.

The andesite flows are underlain by a thick succession of dacite lava flows, minor ash-flow tuffs and andesite flows of the Almolonga Volcanics. The Almolonga Volcanics have a maximum thickness of 800 m in well ZCQ-3. The dacite lava flows are porphyritic and mostly crystal-poor, containing 10-20% percent phenocrysts of plagioclase and rare hornblende and biotite in a matrix of altered and devitrified glass. Granophyric and spherulitic devitrification textures are common. Hydrothermal alteration has replaced the devitrified matrix with fine-grained quartz that is accompanied in places by sericite. The plagioclase phenocrysts have been replaced by calcite, illite-smectite and rare epidote. The ferromagnesian minerals have been altered to chlorite-smectite.

Some ash-flow tuffs are interbedded with the dacite lava flows in the upper half of the flow sequence, especially in ZCQ-3. The ash-flow tuffs contain a few percent broken plagioclase phenocrysts in a matrix of ash and rare shards. Lithic fragments of andesite are also present.

In wells ZCQ-1, 5 and 6 and Z-11, thin (25-50 m thick) andesite lava flows separate the Almolonga Volcanics into upper and lower dacite flow sequences. The andesite flows vary in texture and mineralogy. Most of the flows in the production wells are porphyritic and contain phenocrysts of clinopyroxene and orthopyroxene, plagioclase, and magnetite. Aphyric andesite flows occur in well Z-11 and are distinguished from the porphyritic varieties by a lack of pyroxene phenocrysts, abundant fine-grained matrix magnetite, and elongated amygdules. The amygdules are filled with quartz, chlorite-smectite, and calcite.

Spherulitic and granophyric textures are common in the upper part of the lower flow sequence beneath the andesite flows. These textures probably represent the rapidly cooled upper portion of a thick dacite flow. The lower part of the sequence may be locally tuffaceous. Unfortunately, the primary textures of these rocks have been obscured by silicification.

The contact between the Almolonga Volcanics and the underlying Green Tuff is marked by a lithic-rich ash-flow tuff in wells ZCQ-1, 5 and 6. The Green Tuff is composed of two major units, an upper lithic-rich tuff and a lower welded dacite ash-flow tuff. Both units are highly variable in thickness. In well ZCQ-6, only the lithic-rich unit is present. It is about 100 m thick. In well ZCQ-5, the Green Tuff is predominantly poorly to moderately welded tuff and nearly 200 m thick. Farther to the east, in wells ZCQ-3 and 1, the Green Tuff is thin or absent.

The Green Tuff can be distinguished from all other volcanic units by the presence of quartz phenocrysts that are commonly resorbed. In addition, the Green Tuff is characterized by a few percent phenocrysts of plagioclase and rare biotite in a devitrified and altered matrix of variably welded ash and shards. Lithic fragments of andesite are common and constitute up to 30% of some samples. The Green Tuff is silicified in the production wells. Veins of hematite are especially common in the more poorly welded units.

The lithic-rich unit at the top of the Green Tuff has previously been interpreted as an intraformational conglomerate (Conglomerate A; CyM/MKE, 1988). However, the presence of poorly welded shards, pumice fragments, and quartz phenocrysts suggest that the rock is an ash-flow tuff.

The oldest volcanic unit encountered in the wells consists of up to 200 m of thinly interbedded andesite and dacite flows. The sequence has been variously assigned to the Old Zunil Lavas by Tobias (1978) and to the undifferentiated Tertiary Volcanics of CyM/MKE (1988). The andesite lava flows are porphyritic and contain phenocrysts of clinopyroxene, plagioclase, and magnetite. The dacite flows are also porphyritic. Granophyric textures are well-developed around some of the plagioclase phenocrysts. Hydrothermal alteration varies from moderate to strong.

The contact between the volcanic rocks and the underlying granodiorite is marked by a paleosol that is up to about 10 m thick in exposures south and east of Zunil I. There is no evidence for the development of a thick paleosol in the production wells at Zunil I. However,

some of the cuttings from the base of the volcanic rocks in ZCQ-1 and 3 may represent altered soil. Petrographically, these cuttings consist of hematite-stained clay containing angular quartz, plagioclase, and biotite grains. The grain size and mineralogy of these crystals are similar to that of the underlying granodiorite. The absence of a thick paleosol in ZCQ-1 and 3, in contrast to areas outside of Zunil I, suggests that these wells may have been drilled on basement highs.

The base of the volcanic section in ZCQ-3 and 6 is associated with intense veining and lost circulation. In ZCQ-5, the granodiorite displays evidence of brecciation. These relationships indicate that the permeable zones located near the base of these wells are associated with faults.

The granodiorite encountered in the wells is equigranular and coarse-grained. The essential minerals are quartz, plagioclase, biotite, potassium feldspar, and apatite. The age of the granodiorite has not been established. However, based on its texture and grain size, the granodiorite must be significantly older and, must have been deeply eroded prior to deposition of the volcanics.

ALTERATION

The hydrothermal alteration in Zunil I can be broadly characterized as argillic, phyllic, or propylitic. The secondary minerals are found as both pervasive alteration that has affected the groundmass and phenocrysts of the volcanic rocks, and as vein fillings. Detailed distributions of the alteration minerals are shown in Figures 3 through 7. A generalized cross-section of the alteration zoning is illustrated in Figure 8.

Argillic Zone

Argillic alteration is restricted to the upper 100-200 m of the wells. This zone is characterized by the assemblage smectite, kaolin, quartz, chalcedony, calcite, interlayered chlorite-smectite, zeolites, and minor

hematite. The clay minerals occur principally as an alteration product of the groundmass of the volcanic rocks. Quartz, zeolites, and smectite fill amygdules. Calcite is found primarily as a replacement of plagioclase and clinopyroxene phenocrysts.

Veins within the argillic zone are most common in wells ZCQ-3 and Z-11. These veins consist of calcite \pm barite, quartz + calcite, and calcite + hematite.

Upper Propylitic Zone

The rocks underlying the argillic zone can be divided into an upper and a lower propylitic zone. The upper propylitic zone is characterized by traces of epidote as a replacement of plagioclase phenocrysts. In contrast, the lower propylitic zone contains abundant epidote-bearing veins.

Propylitic alteration is at least weakly established in all of the wells below 200 to 300 m. The top of the propylitic zone consists of a hydrothermal breccia that is developed in lava flows of the Galapago Andesite in wells ZCQ-5 and 6 and in dacite flows occurring at the top of the Almolonga Volcanics in well ZCQ-3. In thin section, the breccia consists of rounded clasts in a matrix of quartz and finely comminuted country rock. Veins of intergrown calcite and quartz are common in the lower portion of the breccia. The breccia occurs at depths of 175-250 m and reaches a maximum thickness of about 100 m in ZCQ-6.

The hydrothermal breccias appear to be closely associated with fault zones. Chip and core samples from the base of the breccias are characterized by jigsaw fracturing, abundant veining, and gouge material.

Epidote occurs as a trace constituent in the upper propylitic zone below the hydrothermal breccia in wells ZCQ-3 and Z-11. In this zone, it is associated with calcite as a replacement of plagioclase phenocrysts.

With the exception of veins related to the shallow hydrothermal breccia, little veining has been recognized within the upper propylitic zone.

Minor amounts of chlorite or chlorite-smectite are present in the

upper propylitic zone. These minerals compose up to 20% of the clay fraction. Some of the chlorite in the dacite flow rocks may represent alteration of biotite phenocrysts; chlorite or chlorite-smectite is also common as a replacement of the matrix of the andesitic rocks.

Weak propylitic alteration is overprinted by phyllic alteration throughout the upper propylitic zone. These rocks are pervasively but weakly altered to mixtures of interlayered illite-smectite, illite and quartz to depths of 600 m. Phyllic alteration is best developed in the upper dacite lava flows of the Almolonga Volcanics.

The illite-smectite minerals display systematic changes in composition and structure with respect to depth. The results of X-ray diffraction analyses of the clay minerals in ZCQ-5 and 6 are illustrated in Figures 9 and 10 respectively. The upper propylitic zone in ZCQ-5 extends from 250 to 585 m (Figure 9) and from 250 to 640 m in ZCQ-6 (Figure 10). Illite and illite-smectite, comprise up to 15 to 20% of the bulk samples and about 85% of the clay fraction of the rocks. The X-ray data indicate that the illite content of the interlayered illite-smectite is about 90% in ZCQ-5 and ranges from 70 to 90% in ZCQ-6. Reconnaissance X-ray studies of the clay minerals at the base of the upper propylitic zone in ZCQ-1 and 3 indicate that the illite lacks expandable (smectite) interlayers.

Lower Propylitic Zone

The lower propylitic zone is characterized by veins containing plagioclase, chlorite, wairakite, epidote, calcite, and quartz. Illite, pyrite, magnetite, and hematite are also present. In general, the intensity of the propylitic alteration and veining increases with depth.

The top of the lower propylitic zone is marked by veins consisting of plagioclase + epidote + chlorite. These veins occur at depths of 500 to 600 m in wells ZCQ-5 and 6, and Z-11. At greater depths, the most common hydrothermal vein assemblage is quartz + epidote ± calcite. These veins are

most abundant near the granodiorite contact, in both the overlying volcanics and within the granodiorite.

Veins containing wairakite occur in the upper part of this zone and near the granodiorite contact in wells ZCQ-3 and 5. Wairakite in these veins is associated with calcite, epidote, and quartz.

Hydrothermal rutile and leucoxene become gradually more common with depth within the lower propylitic zone of wells ZCQ-6 and 5. Rutile and leucoxene occur in veins with quartz, and as disseminated granular aggregates intergrown with illite or interlayered illite-smectite. These aggregates represent an alteration product of magnetite and ilmenite originally present in the groundmass of the andesite.

Quartz veins containing abundant hematite and traces of pyrite and magnetite are found in the poorly welded dacite ash-flow tuff adjacent to the granodiorite contact in all of the wells but are best developed in ZCQ-5 where these ash-flow tuffs are thickest. In places the hematite clearly replaces preexisting pyrite or magnetite. However, the hematite may also be a primary phase in some of the veins. Quartz + pyrite veins are also present in the granodiorite samples from 1015 m in ZCQ-4 and at 755 m in ZCQ-1.

Veins of calcite and illite are found sporadically in the volcanic rocks and in the granodiorite in ZCQ-1 (Figure 8). Illite and calcite commonly occur in separate veins. Where found together, calcite is always present in the center of the vein having precipitated after the illite.

Thin zones of intensely sericitized dacite flows are found in the upper part of the lower propylitic zone. Fragments of dacite altered to illite were ejected from wells ZCQ-1 and 5 during the flow tests conducted in 1989. X-ray diffraction and petrographic analyses of the sample from well ZCQ-5 indicate that it consists dominantly of illite with minor pyrite (4 wt.%). This assemblage closely matches the mineralogy from a depth of about 770 m. The sample from well ZCQ-1 is mostly illite with some plagioclase and epidote. This assemblage matches the mineralogy at about 625 m depth.

Interlayered illite-smectite occurs within the lower propylitic zone in well ZCQ-6. X-ray diffraction analysis indicates that the mixed-layer clay in the volcanic rocks is more than 90% illite whereas the illite content of illite-smectite in the granodiorite ranges from about 85 to 90%. In contrast, illite from the lower propylitic zone of the other deep production wells is devoid of expandable interlayers.

Chlorite is found as a replacement of the groundmass in the andesite lava flows and as an alteration product of biotite and hornblende in the granodiorite. Calcite and epidote are common replacement products of plagioclase.

DISCUSSION

The distribution of secondary mineral assemblages observed in samples from Zunil I provides a unique record of the physical and chemical conditions within the reservoir. Browne (1978) has shown that six factors are of particular importance in controlling the distribution of alteration minerals in geothermal systems. These factors are temperature, fluid chemistry, permeability, rock type, and time. Although it is difficult to separate the importance of each factor, the results of the present petrologic studies suggest that the distribution of secondary minerals at Zunil I has been controlled primarily by permeability, temperature, and fluid chemistry.

Variations in the permeabilities of the reservoir rocks are reflected in the abundance of the secondary minerals occurring within the drill holes. Petrographic studies suggest that the intensity of pervasive alteration in the reservoir rocks is closely related to the distribution of veins and that in general, there is an increase in both the abundance of alteration minerals and veining with depth.

Several major zones of veining and alteration were encountered in the wells. The highly altered volcanic rocks in the lower portions of ZCQ-3, 5, and 6 are located above zones of lost circulation (ZCQ-3, 6) or microbreccia (ZCQ-5). These relationships suggest that the deep alteration is developed

in highly fractured fault zones. Zones of strong alteration at shallower depths in these wells suggest that either the faults are steeply dipping or multiple faults are present. Figure 8 shows the locations of the fault zones inferred from the distribution of veins and pervasive alteration. Despite the strong structural control on the distribution of alteration and vein assemblages, Figure 8 shows that the zones are nearly horizontal. This pattern of zoning implies that the wells in Zunil 1 are located within the central region of the geothermal field rather than on the margins where isotherms dip steeply.

Variations in temperature with depth are also reflected in the distribution of clay minerals. A comparison of many geothermal systems indicates that Ca-smectite is stable to temperatures of 140°C, interlayered illite-smectite to 220°C, and illite above 220°C (Moore and Adams, 1989). With the exception of ZCQ-6, temperatures defined by the clay minerals are consistent with present downhole measured temperatures.

In well ZCQ-6, interlayered illite-smectite is present to depths where the well temperatures are 280°C. Such temperatures are significantly higher than the commonly observed upper stability limit of this mineral. In contrast, illite at the bottom of well ZCQ-5 (where present temperatures are similar to those of ZCQ-6) lacks smectite interlayers. These relationships suggest that either some of the fractured zones in ZCQ-6 have been sealed by mineral deposition, or the rocks in this portion of the geothermal area may have recently undergone heating. Both of these cases would result in the persistence of lower temperature illite-smectite.

With few exceptions, epidote and wairakite occur in the reservoir rocks at Zunil I where measured temperatures exceed 200°C. This temperature range is consistent with the lower stability limit of epidote in other high-temperature systems (Henley and Ellis, 1983). Traces of epidote in rocks with slightly lower temperatures were observed in the upper portions of ZCQ-3. Here, epidote occurs in plagioclase at depths of 355 m where measured temperatures are 190°C. The matrix of these rocks is altered to interlayered illite-smectite, indicating that peak temperatures are

not likely to have exceeded 220°C at these depths. Thus, temperatures at this depth may have been several tens of degrees hotter in the past. This cooling may be due to sealing of the shallow fracture zones around this well. Alternatively, the cooling trend may be due to the downward circulation of cooler steam-heated fluids as discussed below.

Veins of epidote (or wairakite) + quartz are abundant in the lower portions of production wells ZCQ-3, 5, and 6. These veins are indicative of high-temperature, near-neutral reservoir fluids.

Boiling is a common and important process in many high-temperature geothermal systems. Textures and mineral assemblages indicative of boiling are found in all of the wells. Veins indicative of boiling are found in the propylitically altered volcanic rocks in ZCQ-3, 5, and 6 and in both the granodiorite and volcanic rocks in ZCQ-1. These veins consist of quartz + calcite ± epidote ± wairakite. Their distribution indicates that boiling has been widespread.

Hydrothermal breccias that formed as a result of violent boiling occur in the upper portions of many of the wells at a depth of about 200 m. These breccias also occur at a depth of 600 m in ZCQ-3 and Z-11. Core from Z-11 shows that the breccias form steeply dipping veins that crosscut the host rocks.

Hydrothermal brecciation in the upper part of ZCQ-5 and 6 is associated with the base of the andesite lava flows. The zone of brecciation is about 100 m thick in both wells. The association of the breccias with the basal portion of the andesite suggests that boiling may have occurred where the upwelling hydrothermal fluids encountered highly permeable flow breccias. Calcite + quartz veins are common in these breccias.

Differences in the permeabilities between the granodiorite and the volcanic rocks appear to have resulted in local boiling above the contact in wells ZCQ-3, 5 and 6. Veins within the volcanic rocks adjacent to the contact contain quartz + calcite ± epidote ± wairakite. In contrast, veins within the granodiorite in wells ZCQ-3, 5, and 6 consist mainly of quartz + epidote. This assemblage suggests that mineral deposition in the

granodiorite occurred as a result of cooling. Boiling within the volcanic rocks may have been promoted by increased fracture permeability in the hanging walls of the faults encountered near the base of these wells.

Veins containing plagioclase or illite rather than potassium feldspar (which is common in the reservoir rocks) suggest that boiling of the geothermal fluids has led to the development of a shallow steam-heated reservoir. These minerals will precipitate in response to heating and/or a lowering of the fluid's pH (Browne and Ellis, 1970). These conditions can result from the condensation of steam and CO₂ released from a boiling fluid.

Veins containing plagioclase + epidote + chlorite are present at intermediate depths (500-600 m) in wells ZCQ-3, 5 and 6. Illite-bearing veins crosscut the silicified matrix of the hydrothermal breccia in Z-11 and occur in the upper and lower portions of ZCQ-1. In Z-11, the vein paragenesis is illite followed by calcite + epidote ± anhydrite. This paragenesis suggests that the illite was deposited first as a result of mixing between the acidic steam-heated waters and the neutral upwelling fluids. Sealing of the vein walls by illite may have prohibited further mixing, resulting in the deposition of calcite + epidote ± anhydrite by boiling.

Illite-bearing veins formed from steam-heated waters are common in ZCQ-1. Illite and calcite veins crosscut epidotized rock in this well. The superposition of these veins on earlier propylitically altered rocks is indicative of the more recent downward migration of steam-heated water in this portion of the field. Such steam-heated water appears to be an important feature of high-temperature geothermal systems (Henley and Ellis, 1983; Lemieux et al., 1988).

Because of its reverse solubility with respect to temperature, calcite will deposit as a result of heating. The presence of calcite ± hematite veins further suggest that ZCQ-1 is located in an area of downwelling. These veins are common below 700 m in the granodiorite in ZCQ-1. Aumento et al., 1982, observed similar veins at Ahuachapan, El Salvador. They attributed these veins to the deep influx of oxidized groundwaters.

Fracture zones associated with fluid entries in ZCQ-1, 3, and 6 are characterized by veins containing quartz + hematite \pm pyrite \pm magnetite. Petrographic observations indicate that the hematite postdates the pyrite and magnetite. Thus, the present fluids may be more oxidizing than the fluids that precipitated the quartz veins. These entries probably represent reactivation of older structures. In contrast, production intervals in ZCQ-5 and Z-11 appear to be associated with highly illitized rock. The low permeabilities of ZCQ-5 may be due to the deposition of illite by steam-heated waters in the producing fractures.

REFERENCES

- Aumento, F., Viale, P., Choussy, M., Santana, A., 1982, Alteration mineralogy of the Ahuachapan geothermal field: Geothermal Resources Council Transactions, v. 6, p. 7-10.
- Browne, P. R. L., 1978, Hydrothermal alteration in active geothermal fields: Annual Review of Earth and Planetary Sciences, v. 6, p. 229-250.
- Browne, P. R. L. and Ellis, A. J., 1970, The Ohaki-Broadlands hydrothermal area, New Zealand: Mineralogy and related geochemistry: American Journal of Science, v. 269, p. 97-131.
- CyM/MKE, 1988; Neotectonic study: Report submitted to INDE, 24 p.
- ELC-Electroconsult, 1980, Proyecto Zunil, Evaluacion del potencial del campo; Petrografia ignea y mineralogia de alteracion: report submitted to INDE, ZUN-D-5110, 11 p.
- Henley, R. W., and Ellis, A. J., 1983, Geothermal systems: ancient and modern: Earth Sciences Reviews, v. 19, p. 1-50.
- Lemieux, M. M., Moore, J. N., Gonzales P., E., Izquierdo, G., and Huitron E., R., 1988, Chemistry of Los Azufres Reservoir Fluids: data from fluid inclusions: Preliminary proceedings, Final Symposium Agreement Between U. S. Department of Energy and Comision Federal de Electricidad de Mexico in the Field of Geothermal Energy, in press.

Moore, J. N. and Adams, M. C., 1989, Mineral and rock geochemistry in geothermal exploration in Proceedings of Exploration '87: Third Decennial International Conference on Geophysical and Geochemical Exploration for Minerals and Groundwater: Ontario Geological Survey, Special Volume 3, p. 645-654.

Tobias G., E., 1978, Zunil project: prefactibility study. Geologic inform: exploratory boreholes of small diameter.

TABLE 2

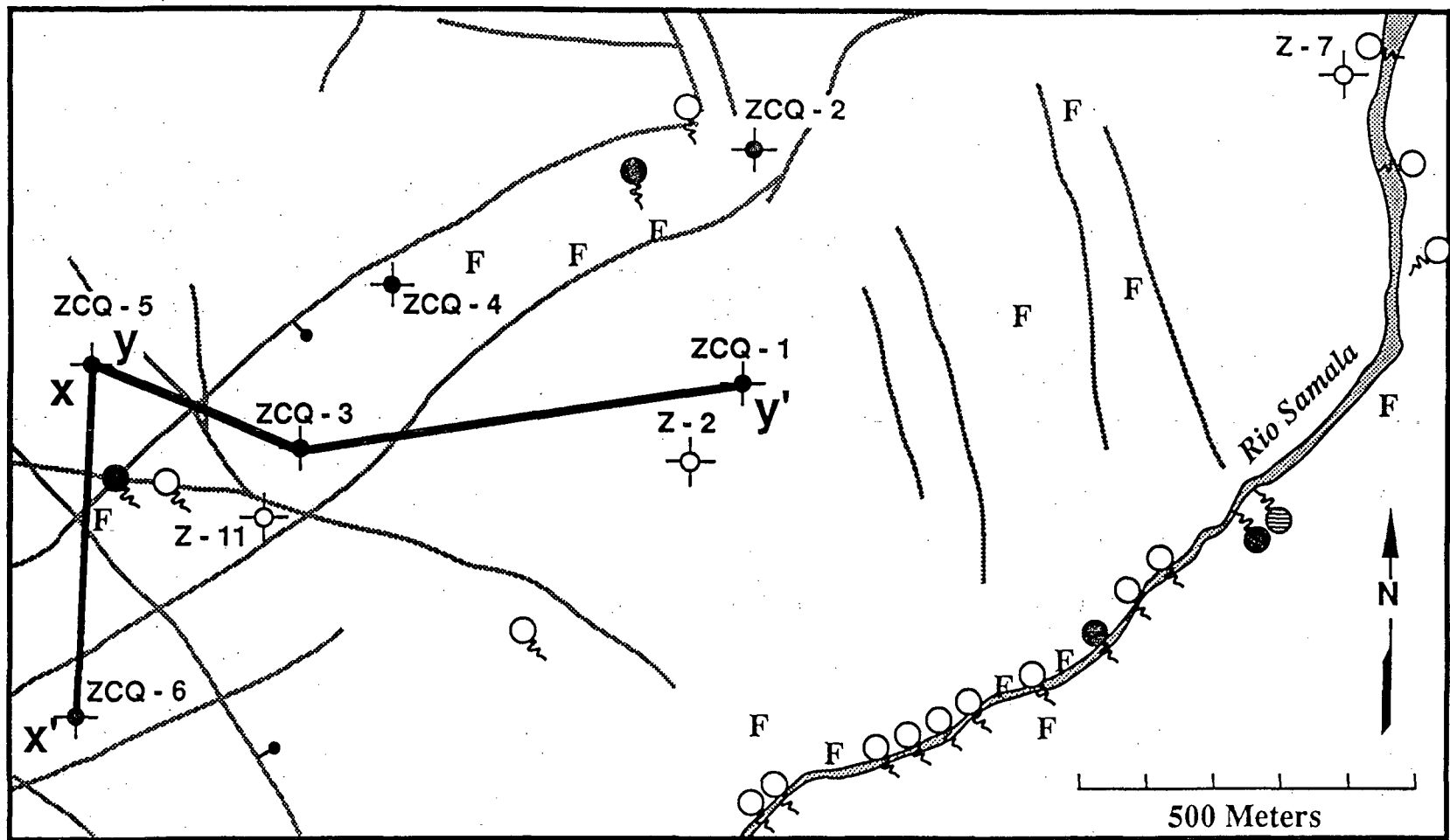
DEPTHS OF SAMPLES SELECTED FOR
X-RAY DIFFRACTION ANALYSIS (in m)

<u>ZCO-6</u>	<u>ZCO-5</u>	<u>ZCO-3</u>	<u>ZCO-1</u>
100			
	140		
250	250		
	350		
	450		
550			
640		620	655
	750		
840	840		
955	940		
	975		
1035	1070	120	
			1310

TABLE 2

DEPTHS OF SAMPLES SELECTED FOR
X-RAY DIFFRACTION ANALYSIS (in m)

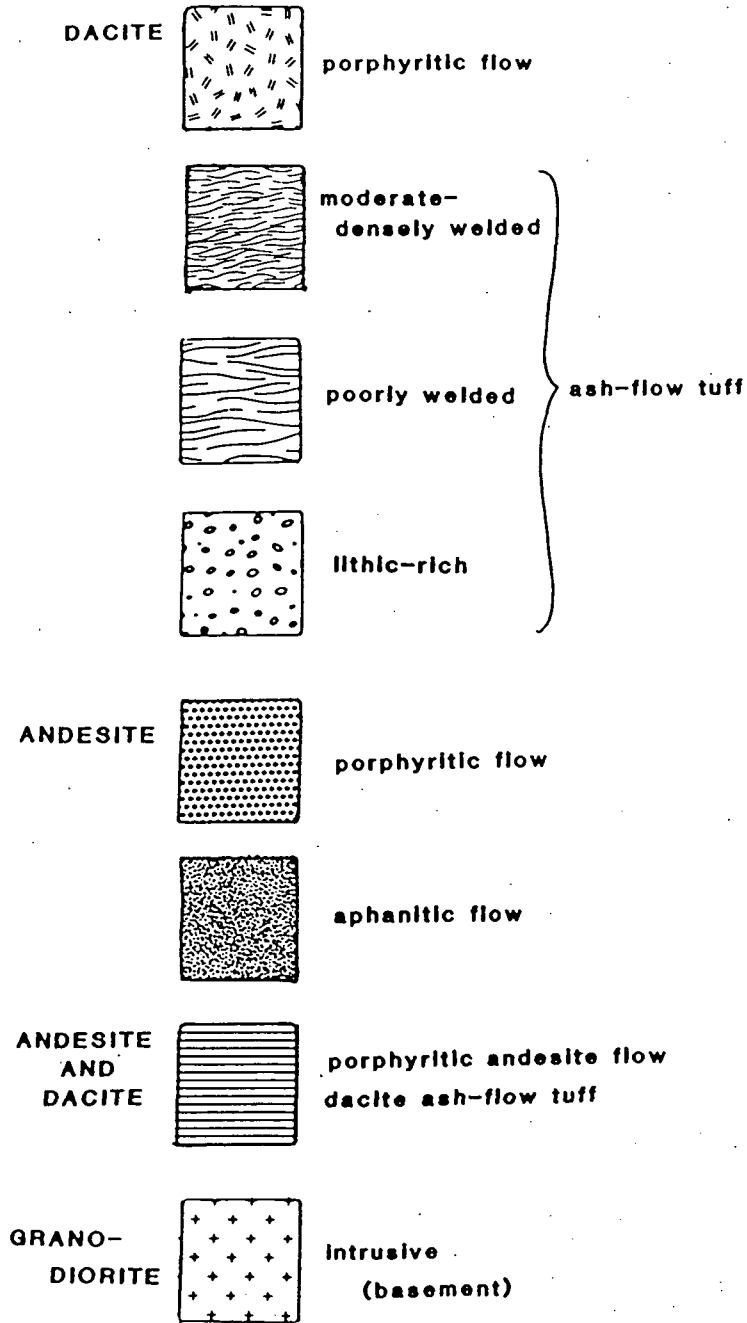
<u>ZCO-6</u>	<u>ZCO-5</u>	<u>ZCO-3</u>	<u>ZCO-1</u>
100			
	140		
250	250		
	350		
	450		
550			
640		620	655
	750		
840	840		
955	940		
	975		
1035	1070	120	
			1310



- | | | | |
|---------------------|-----------------|-----------------------|-------|
| Acid-sulfate spring | NaCl spring | F Fumarole | Fault |
| Bicarbonate spring | Production well | Thermal gradient well | |

Figure 1: Well and cross-section locations, Zunil geothermal field, Guatemala.

LITHOLOGY:



MINERALOGY

- QTZ Quartz
- CC Calcite
- EP Epidote
- WAI Wairakite
- PL Plagioclase
- KF Potassium Feldspar
- ANH Anhydrite
- CHL Chlorite
- HEM Hematite
- IL Illite
- SM Smectite
- IL/SM Mixed-layer Illite-smectite
- CH/SM Mixed-layer Chlorite-smectite

STRATIGRAPHY

- GA Galapogo Andesite
- AV Almolonga Volcanics
- GT Green Tuffs
- OZL Old Zunil Lavas
- Gr Granodiorite



Legend for Figures

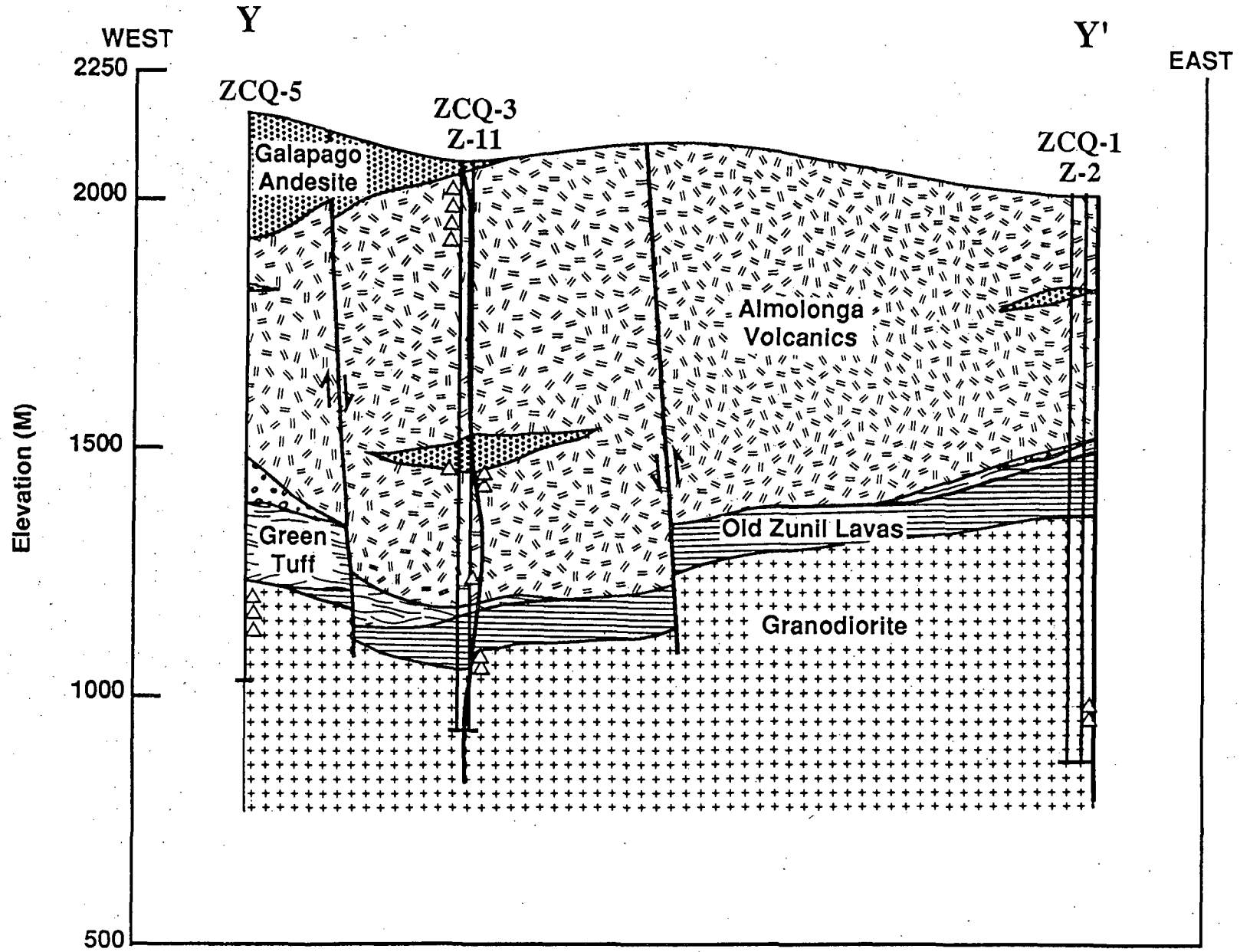


Figure 2A. Generalized stratigraphy and structure of wells ZCQ-5, Z-11, ZCQ-3 and ZCQ-1.

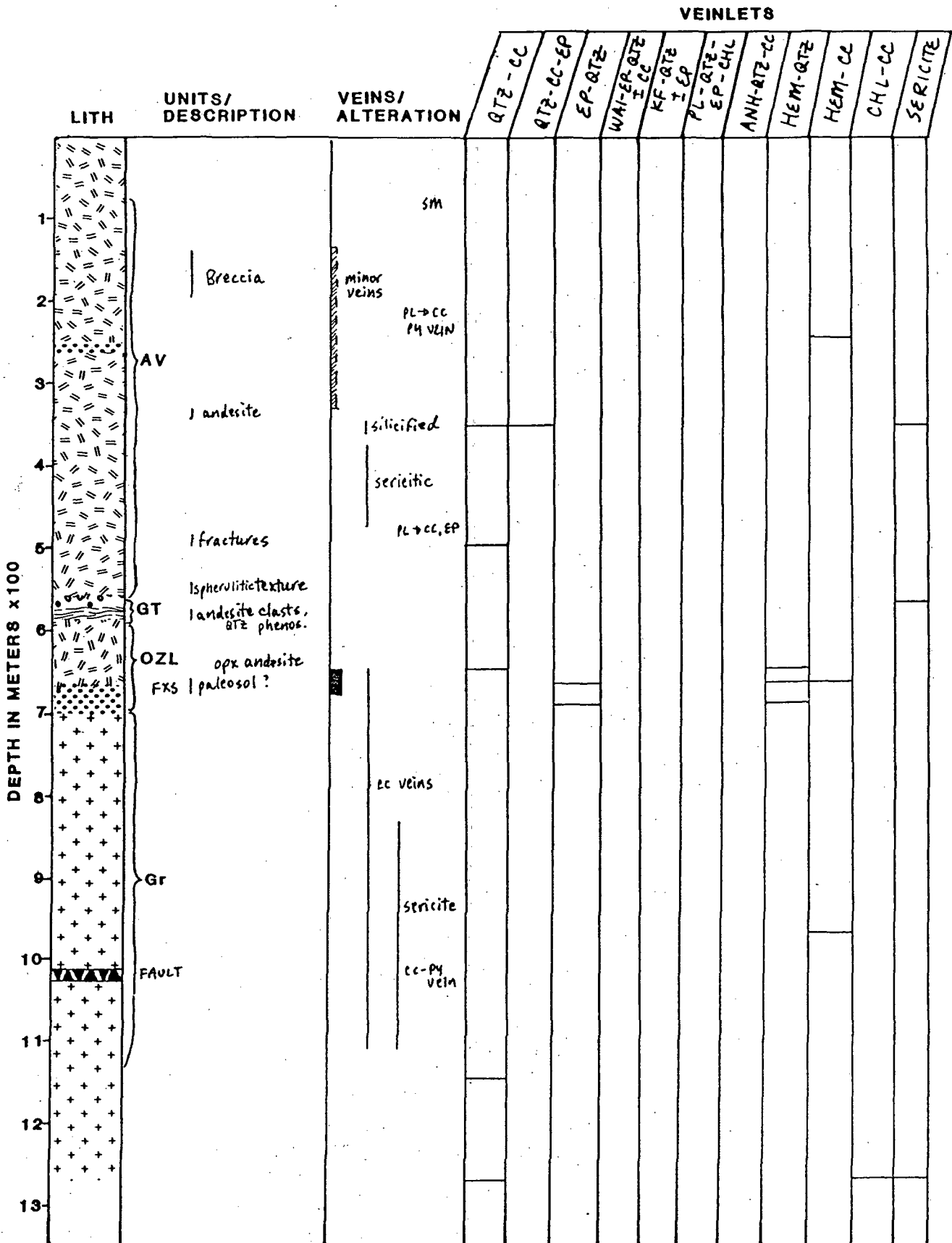


Figure 3. Summary of volcanic stratigraphy and hydrothermal alteration mineralogy in well ZCQ-1. Refer to legend for abbreviations.

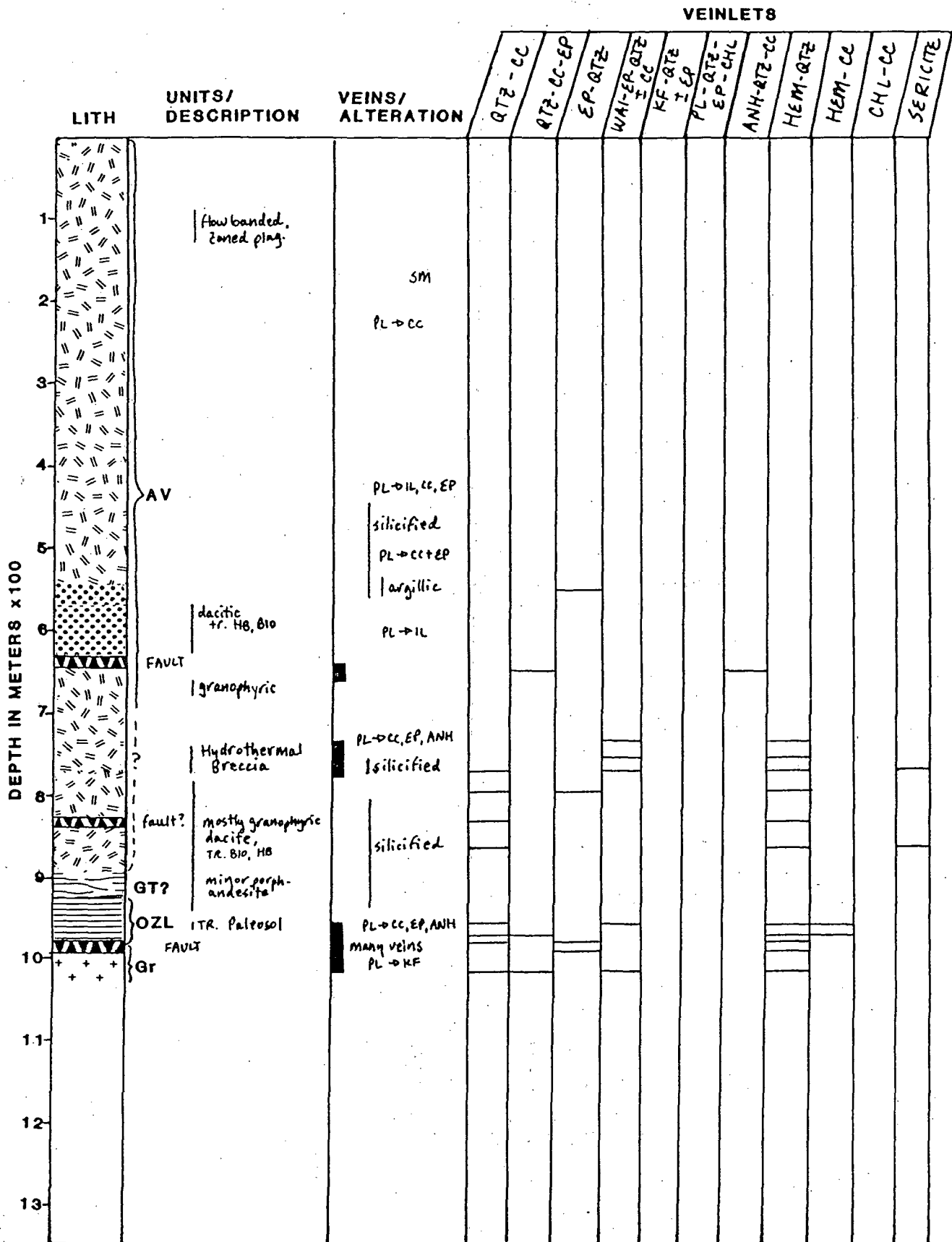


Figure 4. Summary of volcanic stratigraphy and hydrothermal alteration mineralogy in well ZCQ-3. Refer to legend for abbreviations.

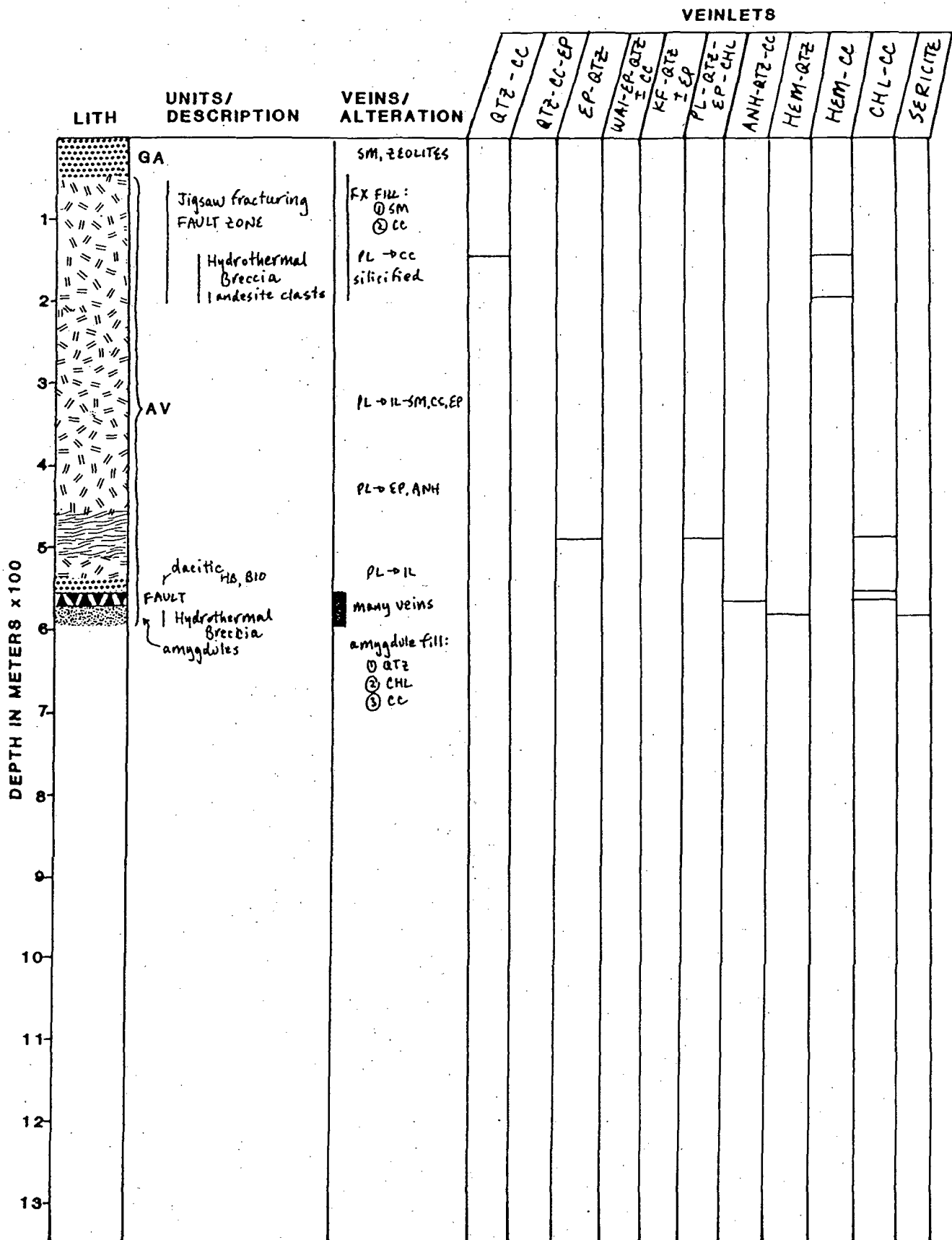


Figure 5. Summary of volcanic stratigraphy and hydrothermal alteration mineralogy in well Z-11. Refer to legend for abbreviations.

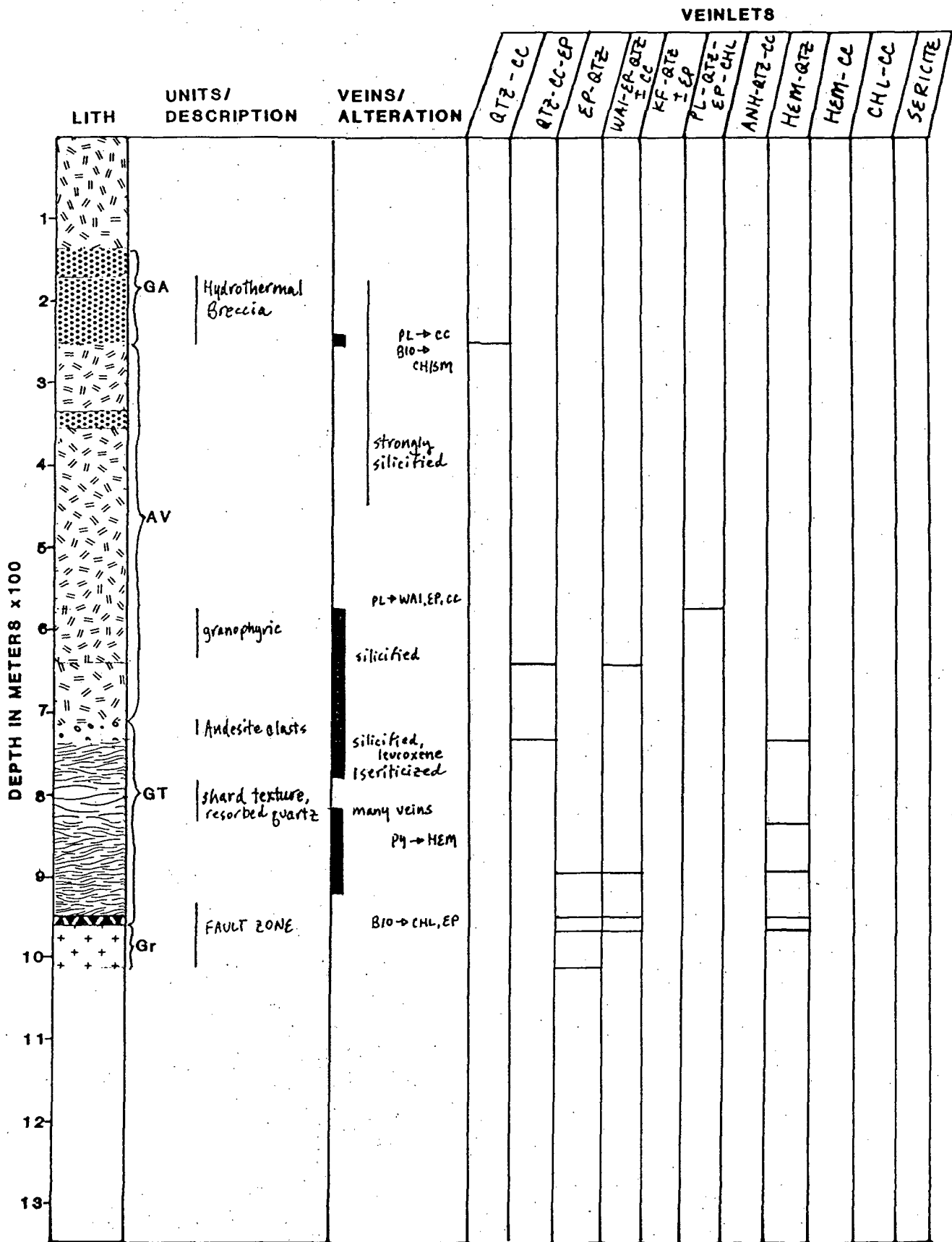


Figure 6. Summary of volcanic stratigraphy and hydrothermal alteration mineralogy in well ZCQ-5. Refer to legend for abbreviations.

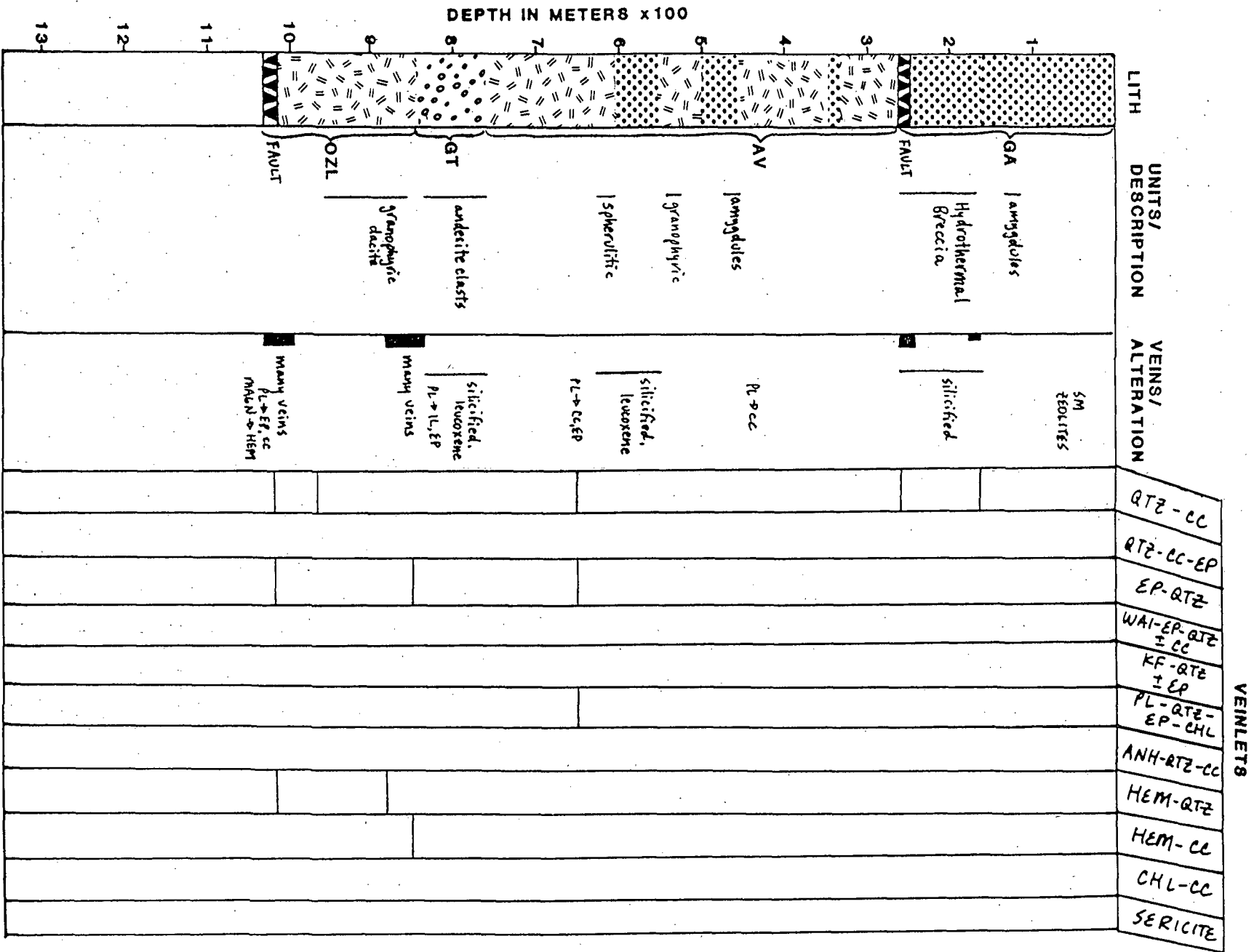


Figure 7. Summary of volcanic stratigraphy and hydrothermal alteration mineralogy in well ZCQ-6. Refer to legend for abbreviations.

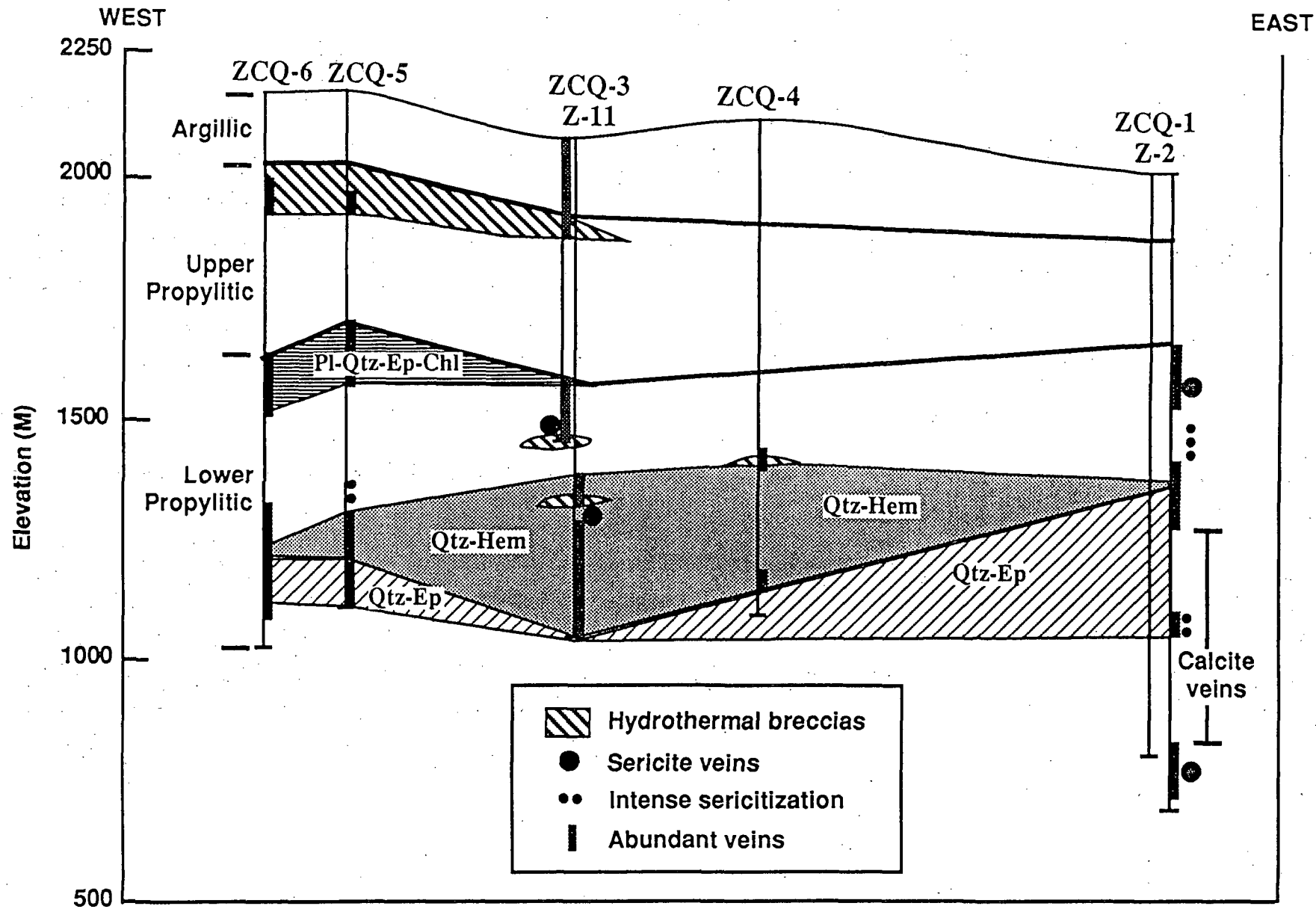


Figure 8. Generalized distribution of alteration zones, hydrothermal breccias and veined intervals. The locations of faults based on the distribution of veins and breccias are shown in Figures 2A and 2B.

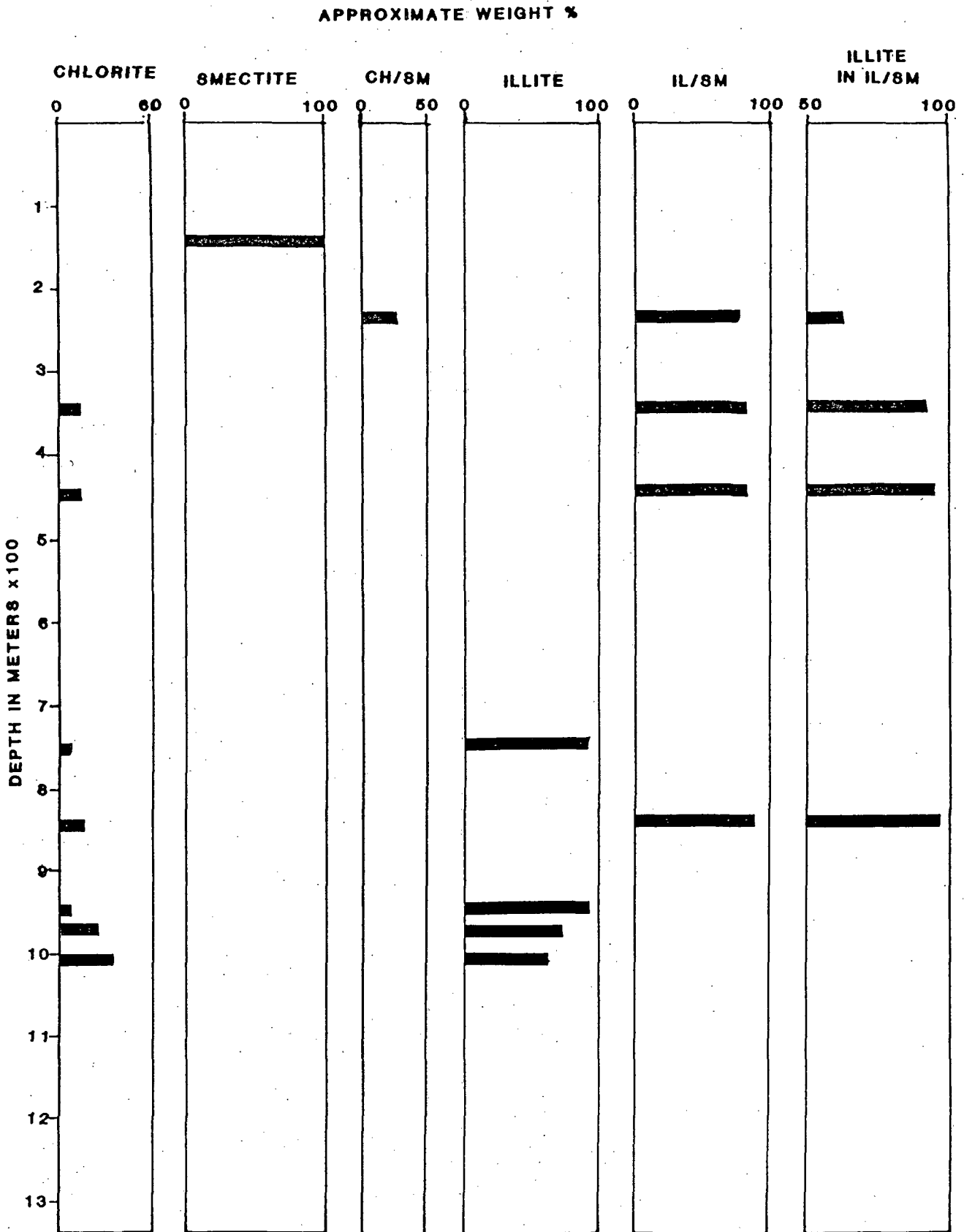


Figure 9. Distributions of hydrothermal layer silicates in clay (< 5 μm) fractions of cuttings samples from well ZCQ-5. Column at right shows increasing amount of illite in mixed-layer illite-smectite with a complete loss of expandable layers at the bottom of the well.

APPROXIMATE WEIGHT %

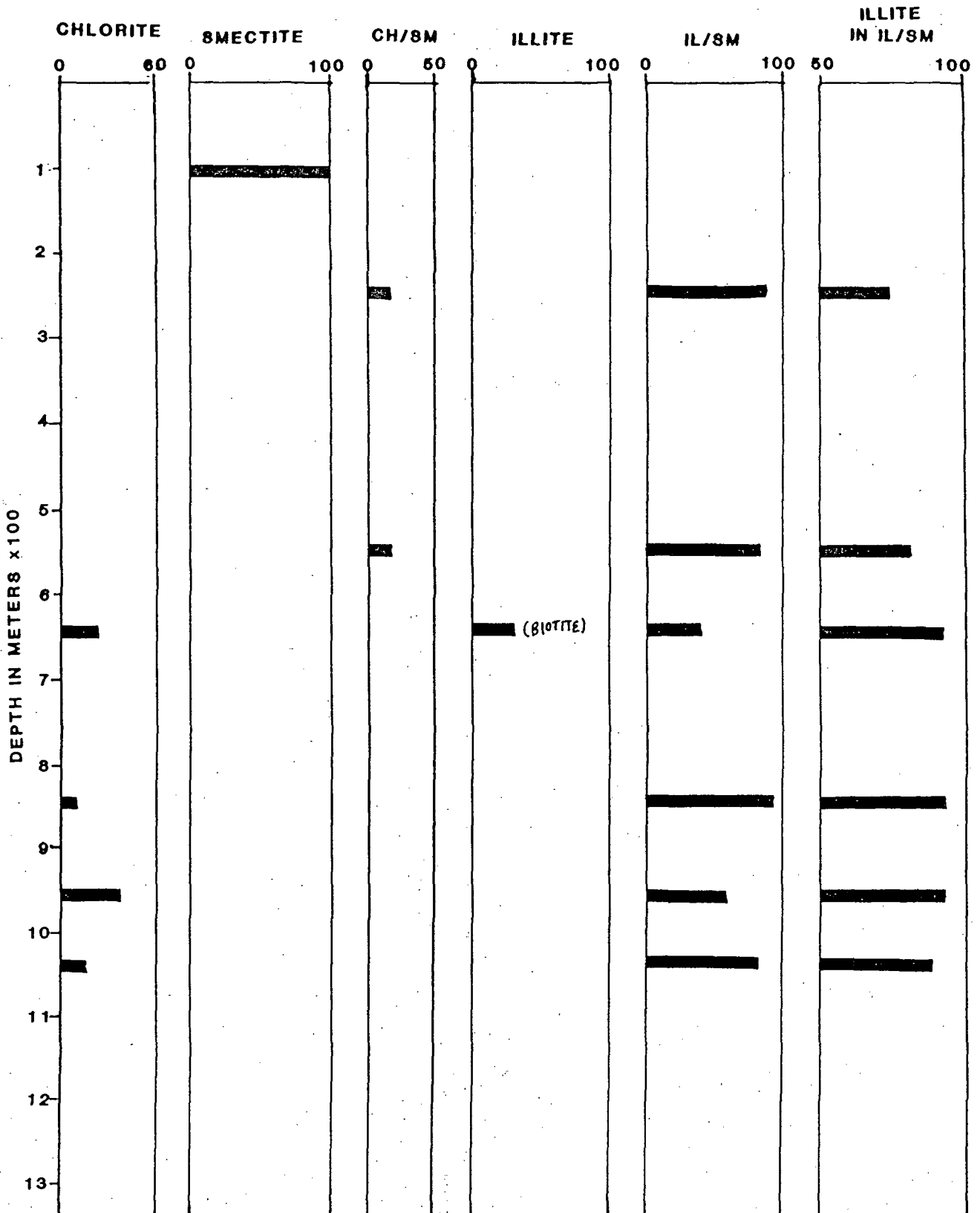


Figure 10. Distributions of hydrothermal layer silicates in clay ($< 5 \mu\text{m}$) fractions of cuttings samples from well ZCQ-6. Column on right shows downward increasing amount of illite in mixed-layer illite-smectite, without complete loss of expandible layers at the bottom of the well.

GEOCHEMISTRY OF THE ZUNIL GEOTHERMAL FLUIDS

SUMMARY

The chemical and isotopic relationships of fluids from wells and springs in the region of the Zunil I geothermal field follow a clear and consistent pattern with respect to their location. The chemical data indicate that a shallow upflow zone lies near wells ZCQ-3, 5, and 6, and that the parent fluid may have a temperature as high as 335°C and a chlorinity of up to 1550 ppm. As this high-temperature fluid travels south and east throughout the Zunil I area, it boils and mixes with shallow waters. The steam produced by the boiling geothermal fluid interacts with groundwater to produce sulfate- and bicarbonate-rich thermal springs. Some of the high-temperature fluid that does not mix significantly with groundwater forms a relatively pristine outflow plume southeast of wells ZCQ-6.

INTRODUCTION

More than 700 chemical analyses of spring and well fluids have been collected from the Zunil geothermal area during the past ten years. In this report, we describe the chemical and isotopic relationships among these fluids and then use these data to develop a hydrogeochemical model of the geothermal system at Zunil I. Our evaluation of the fluid geochemistry is based on chemical analyses of springs sampled by JICA (1977); chemical data on springs, production wells and thermal gradient wells collected by INDE and compiled by Michels (1988); and isotopic and chemical analyses of springs and production wells collected by CyM/MKF (this study), Fournier and Handshaw (1981), and Giggenbach (1986). These data are listed in Tables 1 to 5. The locations of the wells and springs discussed in this section can be found in the hydrogeology section of this report.

DISTRIBUTION OF FLUID TYPES

The thermal fluids that have been sampled in the region encompassing the Zunil I geothermal area show an obvious division into Na

Cl, Na HCO₃-SO₄, and Na SO₄ fluid types (Fig. 1 and 2). These designations indicate the dominant anions and cations in the fluid. Fluids produced by the wells are Na Cl in character whereas the springs discharge fluids that are dominantly Na HCO₃-SO₄ and Na SO₄. One exception is spring z-20, which is clearly a Na Cl fluid similar to that of well ZCQ-2.

Na Cl waters are generally recognized as primary reservoir fluids in geothermal systems (Henley et al., 1984). Fluids that are Na HCO₃-SO₄ or Na SO₄ may form secondary reservoirs over and around the deep Na Cl fluids. These reservoirs develop through the heating of shallow groundwaters by steam containing H₂S and CO₂ (Mahon et al., 1980). The oxidation of H₂S, particularly in highly oxidized groundwaters, and the formation of carbonic acid from CO₂, can result in high acidities and disequilibrium with the enclosing rocks as the fluids react with them. Consequently the chemistries of steam-heated waters are frequently difficult or impossible to interpret in terms of equilibrium reservoir parameters. The chemical data shown on the Piper plot in Figure 1 indicate that most of the springs are indeed steam-heated waters with significant HCO₃ and CO₃ contents. Because of the difficulties inherent in the interpretation of chemical data from steam-heated springs, we have not used the analyses of hot springs at Zunil to obtain quantitative information on parameters of the primary geothermal reservoir.

Giggenbach (1988) has attempted to quantify the degree of chemical equilibrium reached by thermal waters through the application of geothermometers based on Na-, K-, and Mg-bearing minerals. He suggests that a chemically mature fluid, that is a fluid which is in equilibrium with the reservoir rocks, will have identical temperatures predicted by the K/Mg and K/Na geothermometers. When these predicted temperatures differ widely, the fluid is defined as immature. The most immature fluid will be one produced by the acidification and heating of a groundwater by steam. Because acid fluids will quantitatively dissolve rock, transferring the

elemental ratios of the rock to the fluid, the compositions of these fluids will produce spurious geothermometer temperatures.

The maturity relationships for the Zunil fluids are summarized in a ternary plot of Na, K, and Mg, shown in Figure 3. Points that plot below the lowermost curved line are immature fluids. Most of the springs from the Zunil area plot in this region. The indicated immaturity of these fluids is in agreement with the high acidity and sulfate contents found in some of these fluids. Fluids that plot between the lower and upper curved line have intermediate maturities, and those that plot on the upper curved line are fully mature, with concordant K/Na and K/Mg geothermometer temperatures. The predicted temperatures of the geothermometers that Giggenbach (1988) uses for this method are marked on the upper curve. These geothermometers have not yet been extensively tested, and therefore the discussion of chemical geothermometry presented below relies on more established geothermometers.

GEOOTHERMOMETRY

Chemical geothermometers based on fluid-mineral equilibria can be used to predict the subsurface temperature of a geothermal fluid. The most commonly used and extensively tested of these are the Na-K-Ca (Fournier and Truesdell, 1973), Na/K (Fournier, 1981), and quartz (Fournier, 1981) geothermometers. The geothermometer temperatures and chemical analyses of fluids from wells ZCQ-3 and 6, which were sampled and analyzed by CyM/MKF and UURI, are listed in Tables 1 and 2. Fluids from the other wells in the field, which were sampled prior to 1989 and analyzed by a variety of laboratories, are summarized in Table 5. The quartz geothermometer temperatures are not listed in Table 3 because the samples were not preserved for silica.

The geothermometer temperatures listed in Tables 1, 2, and 5 indicate maximum reservoir temperatures of approximately 290°C (Na/K) to 307°C (K/Na). Production of fluids with these temperatures through deeper

drilling is considered reasonable because the maximum measured temperatures in ZCQ-6 reached 288°C.

Enthalpies derived from geothermometer temperatures can also be used in conjunction with the concentrations of Cl in the fluids to predict maximum reservoir temperatures and to define areas of mixing and boiling. Because enthalpy and Cl are both conserved when a fluid undergoes mixing, boiling, or conductive cooling, these processes yield characteristic trends on an enthalpy-Cl diagram.

Enthalpy-Cl plots have been prepared for the Zunil fluids using both the Na/K and the Na-K-Ca geothermometers (Fig. 4 and 5) from the data in Tables 1, 2, and 5. The trends expected for boiling, mixing, and conductive cooling are also shown in these figures. It is apparent from these figures that the fluids from different wells in Zunil I can all be related to a single parent fluid that has undergone varying degrees of boiling, mixing with heated groundwaters, and conductive cooling. The enthalpy-Cl plot shows that fluids from ZCQ-3 and 6 are nearly identical. The position of ZCQ-3 and 6 indicates that these fluids could be derived from the parent fluid by mixing with a cooler groundwater. Based on the diagram, the cooler endmember of the mixing trend would have a temperature of about 170°C. Fluids from ZCQ-2 and Z-4 are similar to each other and could be produced by further dilution of ZCQ-3 and 6. The composition of ZCQ-4 lies along a boiling trend that extends through the parental fluid to the enthalpy of pure steam. Finally, fluid from thermal gradient wells Z-2 and 6 can be derived by conductive cooling of a fluid that was slightly more concentrated than that from wells ZCQ-3 and 6. As shown in Figures 4 and 5, the parent fluid is predicted to have a temperature of approximately 335°C and a chlorinity of 1550 ppm.

Several significant points can be drawn from the discussion above. The fluids that are most closely related to the parent fluid are found in wells ZCQ-3 and 6. Fluids that have conductively cooled and represent outflow have been sampled from gradient wells Z-6 and Z-2. These wells are located south and southeast of wells ZCQ-3 and 6 (Fig. 2). Diluted fluids flow from

wells ZCQ-2, Z-4, northeast of wells ZCQ-3 and 6. Dilute fluid similar to that of well ZCQ-2 also flows from spring z-20, which lies on the southeast bank of the River Samala (Fig. 2). Spring z-20 is the only spring that is significantly Na Cl in character. Well ZCQ-4, located northeast of wells ZCQ-3 and 6, produces fluid that can be related to the parent fluid by boiling.

EXCESS ENTHALPY IN THE PRODUCTION WELLS

The measured enthalpies of production wells ZCQ-3, 5, and 6 imply temperatures that are higher than the geothermometer temperatures if it is assumed that only a liquid phase is present in the reservoir around the wells. These temperature differences indicate that these wells are "excess enthalpy" wells, and that the geothermal fluids are either boiling around the wellbore, absorbing heat in the process, or that both liquid and steam phases are present throughout the reservoir. Our analysis of the chemical data implies that the reservoir fluid near wells ZCQ-3 and 6 is dominantly in the liquid phase, and that the excess enthalpies are due to production-induced boiling. The evidence for this is that: 1) the reconstructed fluids have low gas contents, which would not be the case if reservoir steam were present; 2) the reconstructed analyses of ZCQ-3 and 6 are similar to one another, which would be unlikely if variable amounts of reservoir steam were feeding each wellbore; and 3) the temperature of the quartz geothermometer is less than that calculated using the cation geothermometers by a reasonable amount only if rock heat is assumed. If it is assumed that the excess enthalpy is due only to reservoir steam, the quartz geothermometer yields higher temperatures than the cation geothermometers, which is inconsistent with the expected relationship among the geothermometers. The measured enthalpies of wells ZCQ-3 and 6 were 1423 J/g and 1507 J/g, respectively. Based on a pre-production enthalpy of 1180 J/g, which corresponds to the average Na-K-Ca geothermometer temperature, wells ZCQ-3 and 6 have excess enthalpies of

243 and 327 J/g, respectively. This reconstruction procedure assumes that all of the excess enthalpy is due to local boiling. The higher gas contents of ZCQ-6 may indicate that there is a small component of reservoir steam in the discharge of ZCQ-6. However, the Na, HCO₃ and SO₄ contents of ZCQ-6 are also high, suggesting that the fluid contains a component of steam-heated water. The steam-heated water, and not a separate reservoir steam phase, may be the source of the extra gas.

Well ZCQ-5 produced a two-phase mixture of steam and liquid that was dominantly steam. Use of the measured enthalpy in the reconstruction of the fluid indicates that the wellbore feed was not a single liquid phase, but instead consisted of at least one liquid and one steam feed zone. This situation makes reconstruction of the reservoir fluid unreliable. Thus, the reconstructed data are not listed in this report. However, the ion ratios and approximate concentrations of the fluid feed into ZCQ-5 were similar to those of wells ZCQ-3 and 6. Although the composition of the fluids feeding these wells are similar, the geothermometer temperatures calculated from the approximately reconstructed reservoir composition of ZCQ-5 are 20° to 30°C cooler than wells ZCQ-3 and 6. The gas in steam concentrations, which were similar to those from wells ZCQ-3 and 6, indicate that the steam was formed from production-induced boiling.

STABLE ISOTOPES

Fluids from wells ZCQ-3 and 6 and several hot and cold springs and cold wells were sampled by CyM/MKF and analyzed for their concentrations of oxygen and hydrogen isotopes. The results of these analyses are plotted on Figure 6a and listed in Table 3. These data are also plotted on Figure 6b, along with isotopic analyses of hot and cold springs and the thermal gradient wells Z-2 and 4 taken from the literature. The literature data and sources are listed in Table 6. Also plotted on these figures are the Western Guatemala local (Fournier and Hanshaw, 1981) and the global (Craig, 1961) meteoric water line.

Rain- and groundwater from any given region will usually plot near the global meteoric water line. Small deviations from the global meteoric water line result from local variations in storm paths and elevation. These deviations result in a local water line.

It has been shown that geothermal water is derived from meteoric water, and subsequent reactions with rock alter the oxygen isotopic composition but do not generally alter the hydrogen composition of the fluid (Craig, 1963). This relationship is called the geothermal oxygen shift. Thus, geothermal fluids will generally plot to the right of the meteoric fluids on a graph of oxygen-18 vs. deuterium fluid concentrations.

The isotopic compositions of the geothermal fluids from Zunil show a 5 part per mil oxygen shift. This is comparable to high-temperature productive geothermal systems throughout the world. The compositional range of the hot spring fluids is similar to that of the cold groundwaters, implying a significant component of groundwater in the hot spring fluids. Although the geothermal and groundwaters define a clear linear relationship suggestive of mixing (Figs. 6a and b), the source of recharge for the deep geothermal fluids is not clear. Because the groundwater compositions are significantly lighter in deuterium than the geothermal well fluids, these groundwaters do not appear to represent the source of recharge for the geothermal system. However, analyses of water from the Samala River taken by Fournier (1981) indicates deuterium values of -71.5 and -68 parts per mil, which are similar to the deuterium composition to the geothermal fluids. The Samala River samples were taken at gauging station no. 4, and at the bridge located between Zunil and Quezaltenango on the main road. Thus, the regions drained by the Samala River, which are northeast of the geothermal system, may be the source of recharge. This conclusion is tentative because it is based on just two data points. It has been shown (Craig, 1961) that the isotopic compositions of meteoric water can vary seasonally as well as over a several year time span.

TRITIUM

Tritium has been analyzed in samples from the Samala River, hot and cold springs, and thermal wells. Concentrations of tritium in the thermal well waters are greater than or equal to those in the hot springs (Fig.7). Tritium in the cold springs and the Samala River are 5 to 25 times greater than the thermal well waters. The concentrations in the thermal waters are sufficiently low that precision is ± 10 to 50%.

Natural tritium is produced by the impact of cosmic neutrons on nitrogen nuclei in the upper atmosphere, resulting in steady-state concentration of approximately 5 tritium units in North American meteoric water. However, this natural background has been swamped since 1952 by enormous amounts of man-made tritium from open air thermonuclear tests. At its maximum level, which occurred in 1963, the contribution of artificial tritium to precipitation reached 2 to 3 orders of magnitude above that of natural tritium. Levels of artificial tritium also vary from year to year due to atmospheric destorage and radioactive decay, so that there is no longer a steady-state concentration in groundwater.

The residence time of the thermal fluids can be calculated by the method of Pearson and Truesdell (1978) if it is assumed that the fluids contain no component of tritium-enriched groundwater. This method takes into account the hydrodynamic-dispersive mixing that may occur within the geothermal system as well as the possibility of multiple sources of fluid recharge. The ratio of system volume to input or output is taken to be the turnover time, or residence time, of the system. This has been shown to be identical to the average transit time or average age of particles leaving the reservoir.

Data on the tritium levels in precipitation in Central America are required in order to apply the differential equation of Pearson and Truesdell (1978) to the Zunil tritium data. This data has been compiled by C. O. Grigsby and is published in Goff et al. (1987). The results of the integration are shown in Figure 7. It can be seen on this figure that the tritium

contents of the Zunil thermal waters, which average 1.3 T.U., imply a residence time of approximately 200 years.

The tritium concentrations in the hot springs are generally consistent with steam-enriched groundwaters, as shown in Figure 8. Tritium and oxygen-18 concentrations in the hot springs are less than or equal to those in the well waters. Isotopic depletion of heavy isotopes in steam applies to tritium as well as oxygen and deuterium. Thus, the steam-enriched hot springs show less tritium and oxygen-18 than either groundwaters or deep thermal waters.

REFERENCES

- Craig, H., 1961, Isotopic variations in meteoric waters: *Science*, v. 133, p. 1702.
- Craig, H., 1963, The isotopic geochemistry of water and carbon in geothermal areas, in E. Tongiorgi, ed., *Nuclear Geology on Geothermal Areas*, Spoleto, Consiglio Nazionale delle Ricerche, Laboratorio di Geologia Nucleare, Pisa, p. 17-53.
- D'Amore, F., and Panichi, C., 1980, Evaluation of deep temperatures of hydrothermal systems by a new gas geothermometer: *Geochimica et Cosmochimica Acta*, pp. 549-556.
- Fournier, R. O., 1981, Application of water geochemistry to geothermal exploration and reservoir engineering, in Rybach, L., and Muffler, L. J. P., eds., *Geothermal Systems: Principles and Case Histories*: New York, John Wiley & Sons, p. 109-143.
- Fournier, R. O., and Hansaw, B., 1981, Oxygen and hydrogen isotopes in thermal waters at Zunil, Guatemala: Report Submitted to the INDE, U.S. Geological Survey, Menlo Park, CA, 16 p.
- Fournier, R. O., and Potter, R. W., II, 1982, A revised and expanded silica (quartz) geothermometer: *Geothermal Resources Council Bulletin*, Nov., pp. 3-12.
- Fournier, R. O., and Truesdell, A. H., 1973, An empirical Na-K-Ca geothermometer for natural waters: *Geochimica et Cosmochimica Acta*, v. 37, p. 1255-1275.

Giggenbach, W. F., 1988, Geothermal solute equilibria. Derivation of Na-K-MG-Ca geoindicators: *Geochimica et Cosmochimica Acta*, v. 52, p. 2749-2765.

Giggenbach, W. F., 1986, The isotope and chemical composition of water and steam discharges from the Lago de Amatitlán, San Marcos and Zunil geothermal fields, Guatemala: IAEA Coordinated Research Programme On The Application Of Isotopic And Chemical Techniques To Geothermal Exploration In Latin America, Mission To Guatemala, 1985, 39 pp.

Goff, F. E., Truesdell, A. H., Grigsby, C. O., Janik, C. J., Shevenell, L. A., Paredes, J. R., Gutierrez, J. W., Trujillo E., Jr., and Counce, D. A., 1987, Hydrogeochemical investigations of six geothermal sites in Honduras, Central America: Los Alamos National Laboratory report LA-10785-MS, 170 pp.

Henley, R. W., Truesdell, A. H., Barton, P. B., Jr., and Whitney, J. A., 1984, Fluid mineral equilibria in hydrothermal systems: *Reviews in Economic Geology*, v. 1, 267 p.

JICA, 1977, Proyecto Zunil, Estudio de factibilidad preliminar: Informe Geoquimico.

Mahon, W. A. J., Klyen, L.E., and Rhode, M., 1980, Neutral sodium/bicarbonate/sulphate hot waters in geothermal systems: *Chinetsu (Journal of the Japan Geothermal Energy Association)*, v. 17, p. 11-24.

Michels, D. E., 1988, Evaluation of chemical data: Zunil I Quezaltenango, Mision de Enfoque Report, Submitted to CyM/MKF, 32 p.

Pearson, F. J., and Truesdell, A. H., 1978, Tritium in the waters of Yellowstone National Park: U. S. Geological Survey Open-file Report 78-701.

Table 1. Chemical analyses of ZCQ-3 fluid restored to reservoir composition using measured enthalpy (steam fraction = .377). ND = not detected, NA = not analyzed. Geothermometer temperatures; Tqtz = quartz (Fournier and Potter, 1982), Tnkc = Na-K-Ca (Fournier and Truesdell, 1973), Tnk = Na/K (Fournier, 1981), Tkn = K/Na (Giggenbach, 1988), Tgs = gas geothermometer (D'Amore and Panichi, 1980).

Date	2/7/89	2/8/89	2/9/89	2/10/89	2/11/89	2/12/89
Na	518	525	512	518	522	519
K	107	111	108	111	112	112
Ca	7	7	7	7	7	7
Mg	ND	ND	ND	ND	ND	ND
SiO ₂	470	484	478	484	489	485
B	21.6	21.8	21.3	21.5	21.8	21.3
Li	4.73	4.92	4.75	4.89	4.96	4.91
SO ₄	17.8	17.8	17.2	17.8	17.8	14.5
HCO ₃	47.5	47.5	47.5	46.9	46.9	46.9
Cl	909	900	895	906	909	900
F	2.3	2.3	2.6	2.6	2.4	2.6
TDS	2109	2128	2100	2125	2140	2120
Tqtz	251	254	253	254	255	254
Tnkc	262	264	264	265	265	266
Tnk	288	290	291	292	292	293
Tkn	298	300	300	301	302	302
Tgs	256	258				
CO ₂	1709	1867				
H ₂ S	46.9	51.3				
N ₂	8.25	8.57				
NH ₃	1.36	1.35				
H ₂	0.0762	0.0925				
CH ₄	0.0597	0.0976				
Ar	0.0293	0.0320				

Table 2. Chemical analyses of ZCQ-6 fluid restored to reservoir composition using measured enthalpy (steam fraction = 0.34). ND = not detected, NA = not analyzed, and C = air contamination. Geothermometer temperatures; Tqtz = quartz (Fournier and Potter, 1982), Tnkc = Na-K-Ca (Fournier and Truesdell, 1973), Tnk = Na/K (Fournier, 1981), Tkn = K/Na (Giggenbach, 1988), Tgs = gas geothermometer (D'Amore and Panichi, 1980).

Dates	1/22/89	1/22/89	1/23/89	1/24/89	1/25/89	1/26/89	1/27/89
Na	598	578	577	564	545	548	556
K	135	110	110	108	106	103	106
Ca	6	3	3	3	4	4	5
Mg	ND	ND	ND	ND	ND	ND	ND
SiO ₂	561	466	461	458	451	449	456
B	26.5	24.4	24.1	23.8	22.8	22.6	22.9
Li	5.55	4.65	4.64	4.58	4.47	4.38	4.50
SO ₄	18.6	NA	27.3	27.3	28.5	29.1	22.9
HCO ₃	53.9	NA	82.5	84.9	83.7	86.8	87.4
Cl	997	NA	915	888	897	888	897
F	3.0	NA	2.2	2.1	2.2	2.2	2.2
TDS	2387	NA	2172	2127	2108	2101	2124
Tqtz	272	250	249	248	246	246	248
Tnkc	275	268	268	268	267	264	263
Tnk	298	280	279	280	281	278	279
Tkn	307	290	289	290	292	289	290
Tgs					251		
CO ₂	2098				2905		3069
H ₂ S	34.1				40.2		41.3
N ₂	C				11.7		12.1
NH ₃	1.59				1.81		1.8
H ₂	0.0629				0.0757		0.0815
CH ₄	ND				0.0706		ND
Ar	C				0.0258		0.027

Table 3. Isotopic analyses of samples collected by CyM/MKF. NA = not analyzed. Locations of wells and springs are shown in the hydrogeology section of this report.

Sample	Type	Deuterium (Delta)	Oxygen (Delta)	Tritium (TU)	Source
ZCQ-6	well,liquid	-72	-7.6	NA	CyM/MKF
ZCQ-6	well,liquid	-70	-7.2	NA	CyM/MKF
ZCQ-6	wellsteam	-77	-10.1	<2.0	CyM/MKF
ZCQ-6	well,steam	-74	-10.0	NA	CyM/MKF
ZCQ-5	wellsteam	-75	-9.4	NA	CyM/MKF
ZCQ-5	well,liquid	-70	-6.4	NA	CyM/MKF
ZCQ-3	well,steam	-83	-10.5	NA	CyM/MKF
ZCQ-3	wellsteam	-79	-10.2	NA	CyM/MKF
ZCQ-3	wellsteam	-79	-10.6	NA	CyM/MKF
ZCQ-3	well,liquid	-74	-7.7	NA	CyM/MKF
ZCQ-3	well,liquid	-76	-7.8	<2.0	CyM/MKF
z-60	hotspring	-87	-12.8	NA	CyM/MKF
z-47B	hotspring	-83	-11.5	NA	CyM/MKF
z-47	hotspring	-80	-11	NA	CyM/MKF
z-37	hotspring	-80	-11.9	NA	CyM/MKF
z-20A	hotspring	-81	-11.4	NA	CyM/MKF
z-20	hotspring	-75	-8.5	NA	CyM/MKF
z-15	hotspring	-82	-11.2	NA	CyM/MKF
z-13	hotspring	-89	-11.2	NA	CyM/MKF
Wtrfall	coldspring	-85	-12.2	NA	CyM/MKF
none	hotspring	-86	-12.2	NA	CyM/MKF
LM-1	coldspring	-83	-11.8	NA	CyM/MKF
LDP-5	coldwell	-84	-11.7	NA	CyM/MKF
LDP-1	coldwell	-85	-11.8	NA	CyM/MKF
CH-2	coldspring	-88	-12	NA	CyM/MKF
CH-1	coldspring	-86	-12.2	NA	CyM/MKF
AS-1	coldspring	-87	-12.1	NA	CyM/MKF
z-58	hotspring	-86	-12.5	NA	CyM/MKF
z-47	hotspring	-79	-11.5	<2.0	CyM/MKF
z-46	hotspring	-83	-12.0	NA	CyM/MKF
z-37	hotspring	-87	-12.1	NA	CyM/MKF
z-15	hotspring	-71	-6.8	NA	CyM/MKF
z-13	hotspring	-83	-11.1	<2.0	CyM/MKF

Table 4. Chemical analyses of hot springs, cold springs, and cold wells sampled by CyM/MKF. Concentrations in ppm. ND = not detected, NA = not available.

	z-20	z-20up	z-20down	z-17	LDP-1
Na	545	110	133	305	8
K	45.8	24.7	24.0	35.1	3.8
Ca	14.8	43.7	55.2	42.9	17.7
Mg	0.46	17.72	21.78	39.56	5.69
SiO ₂	358	195	184	205	59
B	21.7	0.6	1.8	5.3	ND
Li	2.75	0.08	0.21	0.55	ND
HCO ₃	44	ND	19	653	60
CO ₃	44	ND	ND	ND	6
Cl	663	10	46	183	12
F	8.0	0.2	0.6	0.6	0.1
SO ₄	183	523	471	213	15
TDS	1938	880	950	1335	164
Temp(°C)	boiling	52	57	75	NA

	CH-2	AS-1	CH-1	z-13A	z-60
Na	8	12	9	240	26
K	4.3	4.3	4.0	32.9	4.6
Ca	11.4	14.2	16.7	38.4	21.9
Mg	6.64	5.19	9.73	44.03	19.80
SiO ₂	63	105	66	193	104
B	ND	ND	ND	4.2	0.1
Li	ND	ND	ND	0.49	0.04
HCO ₃	66	45	105	607	190
CO ₃	ND	2	ND	ND	ND
Cl	4	5	7	100	8
F	0.2	0.1	0.1	0.5	0.2
SO ₄	15	54	11	186	20
TDS	164	230	180	1194	298
Temp (°C)	NA	NA	NA	NA	NA

	LDP-5	LM-1	z-47A	WTRFALL	z-15
Na	7	15	15	47	140
K	2.4	5.3	4.7	13.6	15.6
Ca	11.6	16.8	25.3	43.9	87.6
Mg	4.46	15.03	17.08	28.71	31.13
SiO ₂	60	56	92	130	136
B	ND	ND	ND	0.5	2.3
Li	ND	ND	ND	0.10	0.77
HCO ₃	70	119	160	298	464
CO ₃	ND	8	ND	ND	ND

TABLE 4. Continued

Cl	6	8	6	32	70
F	0.1	0.1	0.2	0.2	0.1
SO ₄	10	27	46	75	236
TDS	134	210	312	508	930
Temp (°C)	NA	NA	NA	NA	NA

Near

	z-58	z-15	z-47C	z-11	z-37
Na	17	49	11	19	141
K	4.3	14.8	3.8	6.9	18.7
Ca	20.2	47.6	19.5	34.2	39.3
Mg	17.06	30.69	13.40	20.23	55.81
SiO ₂	107	146	102	177	145
B	ND	0.5	ND	ND	2.3
Li	ND	0.11	ND	ND	0.30
HCO ₃	163	294	122	ND	547
CO ₃	ND	ND	ND	ND	ND
Cl	4	20	6	5	84
F	0.2	0.2	0.2	ND	0.4
SO ₄	16	77	18	312	102
TDS	266	531	235	597	859
Temp (°C)	NA	NA	NA	NA	NA

Table 5. Summary of average chloride contents (in ppm) and geothermometer temperatures (in °C) of wells not sampled in this study. Geothermometer temperatures; Tqtz = quartz (Fournier and Potter, 1982), Tnkc = Na-K-Ca (Fournier and Truesdell, 1973), Tnk = Na/K (Fournier, 1981), Tkn = K/Na (Giggenbach, 1988).

	Cl	Tnk	Tnkc	Tkn
ZCQ-2	625	246	235	259
ZCQ-4	2299	259	244	270
Z-2	1154	246	221	259
Z-4	694	219	211	234
Z-6	1077	231	208	221
Z-11	2020	225	224	240

Table 6. Isotopic analyses of Zunil fluids collected prior to this study. NA = not analyzed. F = Fournier and Handshaw (1981), G = Giggenbach (1986).

	Sample Type (Delta)	Deuterium (Delta)	Oxygen	Tritium (TU)	Source
ZCQ-6	well, total	-75.9	-8.36	1.3	G
ZCQ-5	well, steam	-75	-8.66	0.5	G
ZCQ-3	well, total	-79.3	-8.74	1.3	G
Z-4	well, steam	-94	-12.95	NA	F
Z-4	well, liquid	-70	-8.5	0.7	F
Z-2	well, liquid	-68	-7.3	1.1	F
Z-2	well, steam	-86.5	-11.45	NA	F
Rio Samala ¹		-71.5	-10.25	5.9	F
Rio Samala ²		-68.0	-9.9	7.3	F
none ³	cold spring	-79.5	-11.95	3.8	F
none ⁴	cold spring	-79	-12.25	24.7	F
none ⁵	cold spring	-86.5	-12.25	NA	F
none ⁶	cold spring	-73	-11.15	NA	F
z-59	hot spring	-81	-12.05	0.8	F
z-41	hot spring	-80	-11.1	1.1	F
z-29	hot spring	-75	-10.8	0.7	F
z-23	hot spring	-79	-11.4	.5	F
z-20	hot spring	NA	-8.2	1.1	F
z-17	hot spring	-77	-11.05	0.1	F
z-15	hot spring	-80.5	-10.9	3.4	F
z-13	hot spring	-80.5	-11.35	0.8	F
z-10	hot spring	-80.5	-11.2	NA	F

1. Rio Samala at gaging station no. 4.
2. Rio Samala at bridge between Zunil and Quetzaltenango on the main road.
3. Cold spring on side of hill about 12 m above Rio Pachamiyo, above and west of town of Zunil.
4. Cold spring at Finca del Parador on eastern slope of hillside west of Santiaquito Volcano.
5. Cold well water at Llanos del Pinal near Quezaltenango.
6. Cold spring near San Amargas Spa.

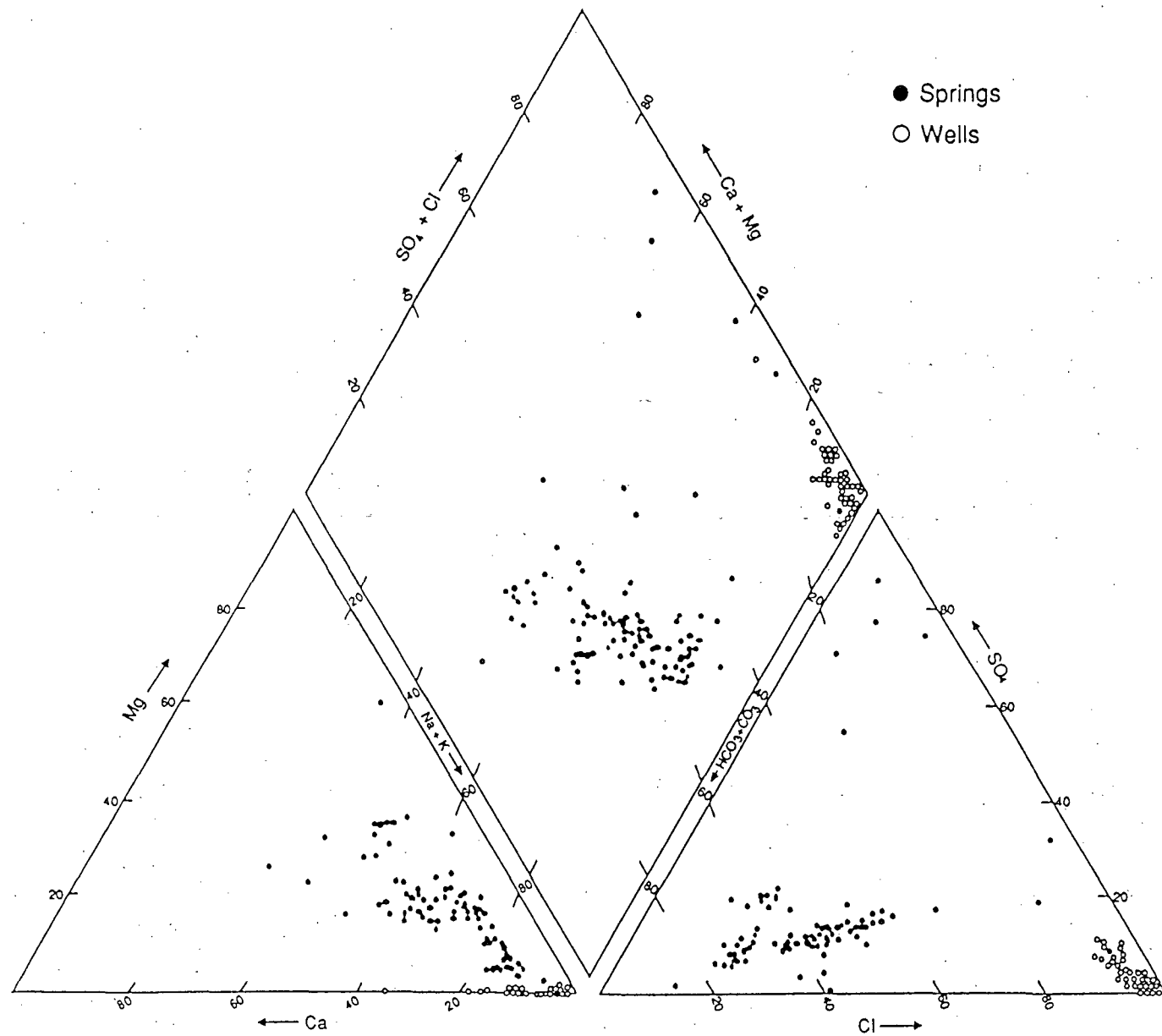
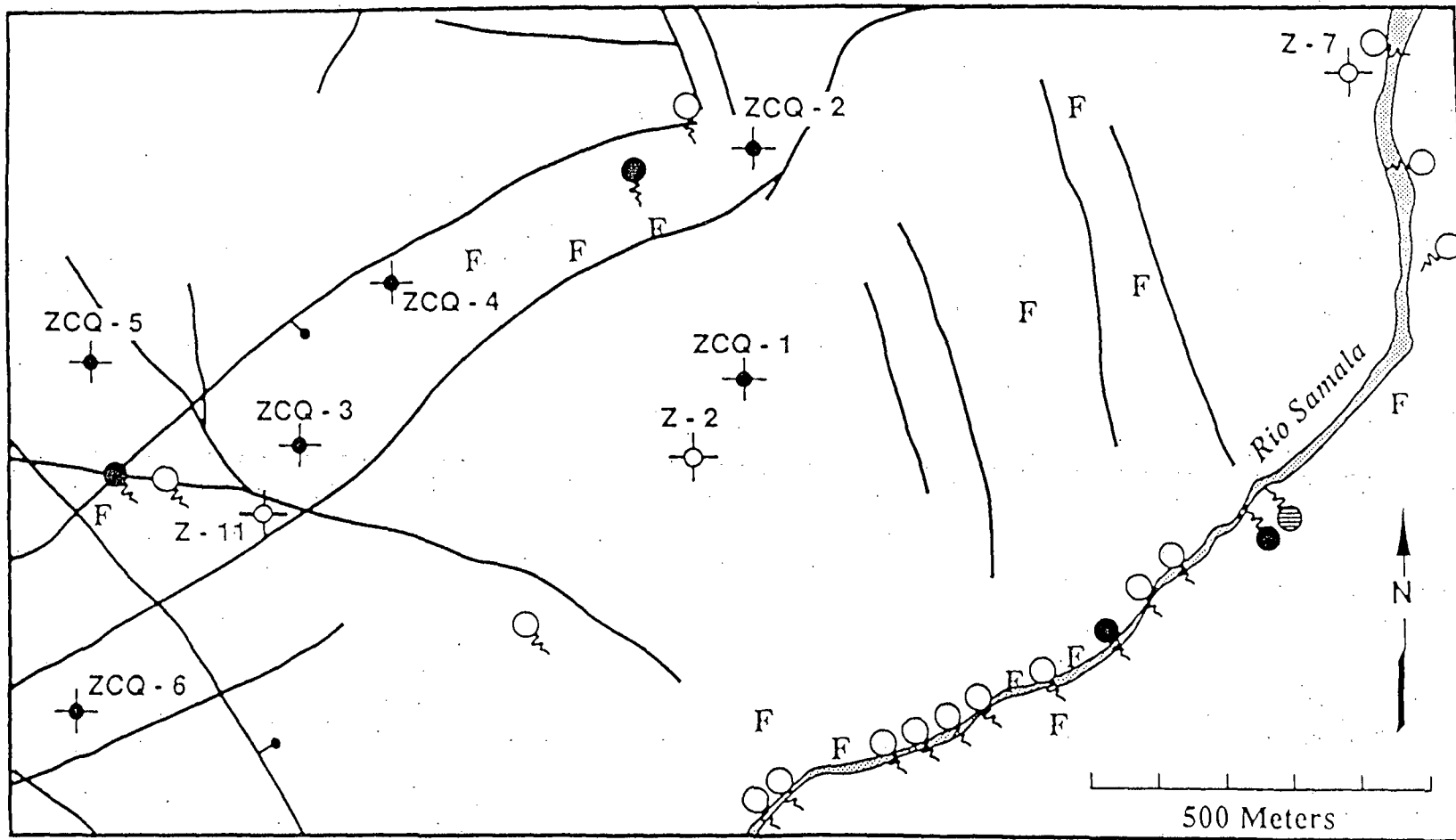


Figure 1. Piper plot of hot springs and thermal well fluids from the Zunil geothermal system.



- Acid-sulfate spring
- NaCl spring
- Bicarbonate spring
- Production well
- Thermal gradient well
- F Fumarole
- Fault

Figure 2. Location of thermal fluid types in the Zunil geothermal system. Fluid produced by thermal wells are Na Cl in character.

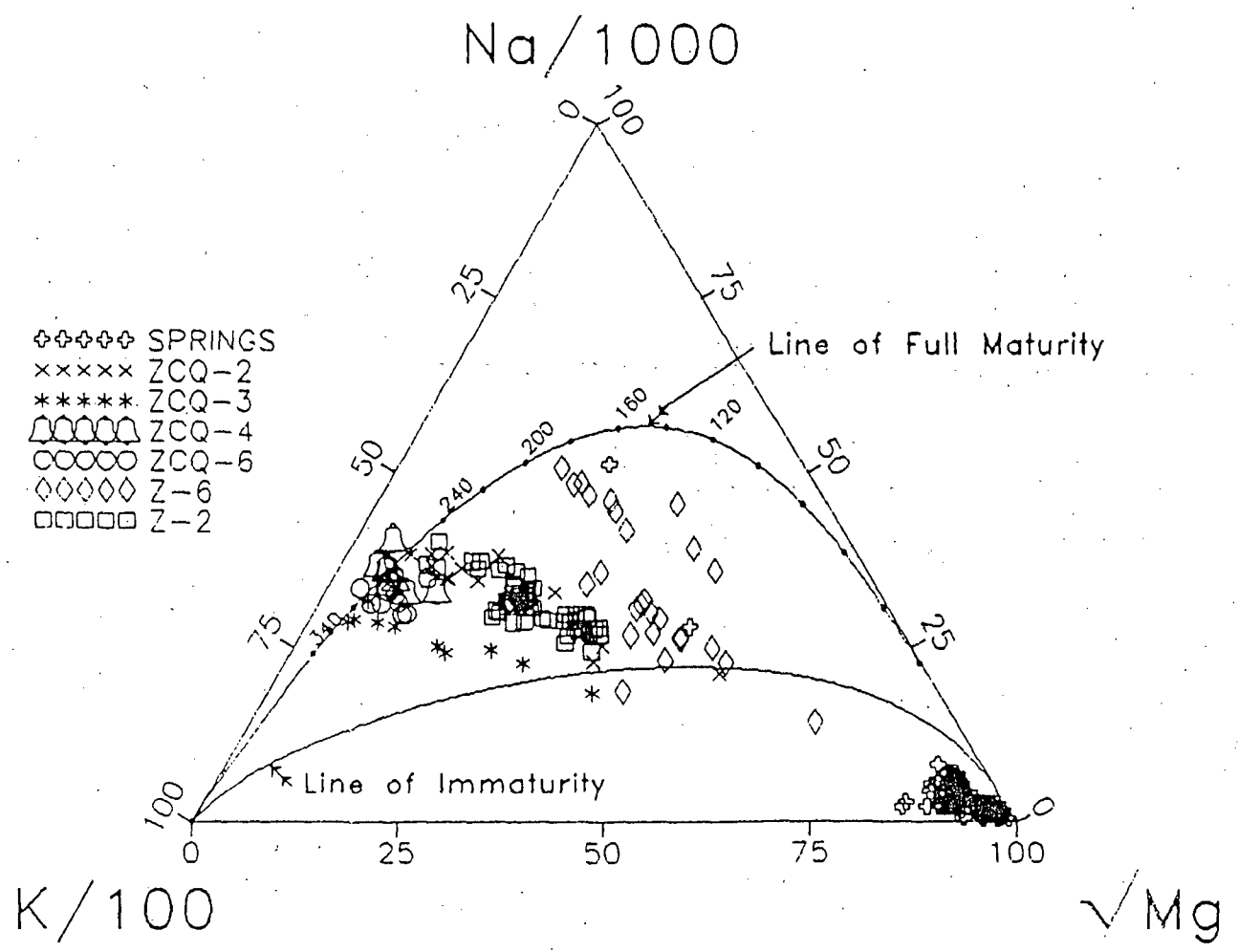


Figure 3. Maturity indices of thermal fluids from the Zuni geothermal system.

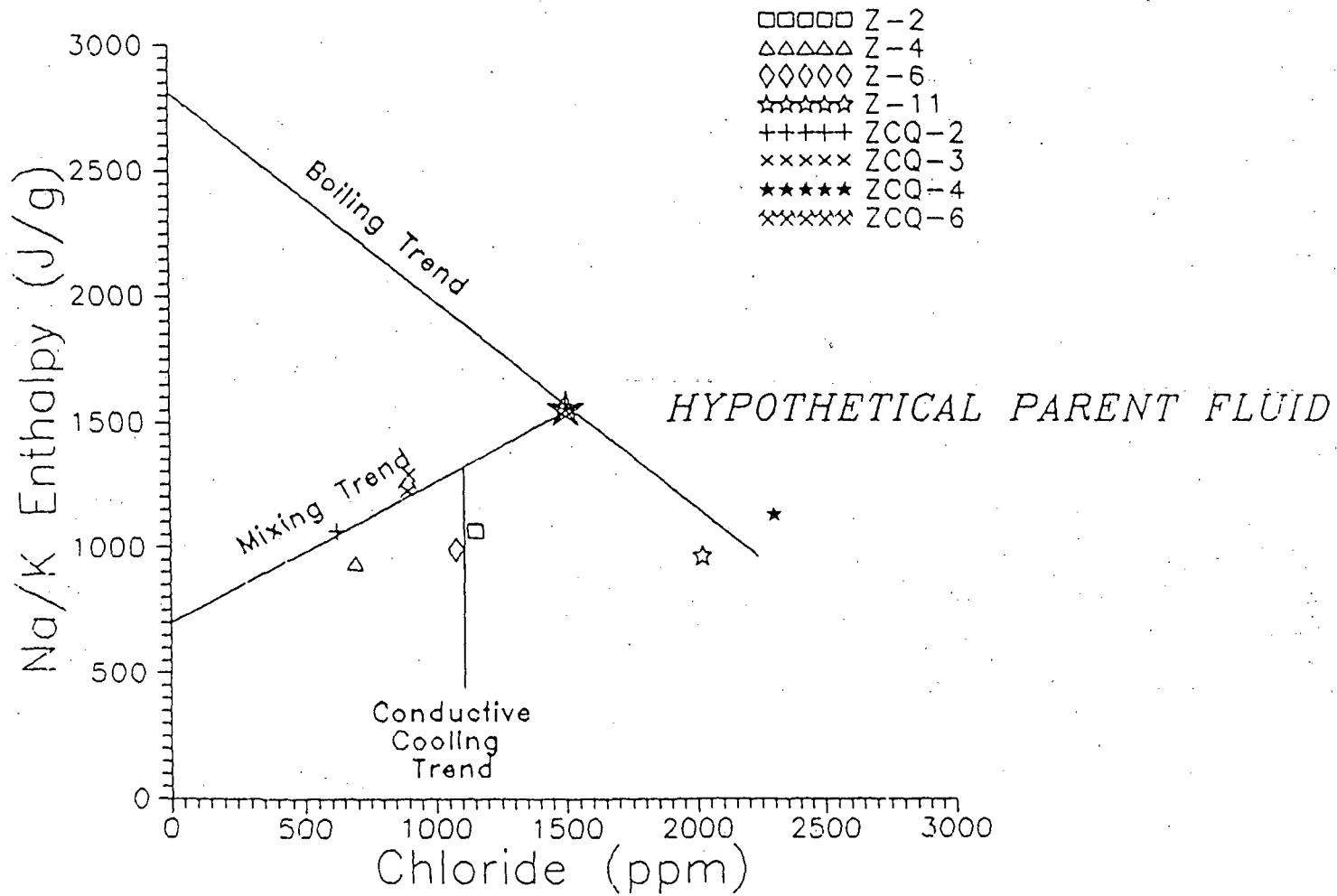


Figure 4. Chloride-enthalpy diagram for the Zunil thermal fluids. Enthalpies are derived from the Na/K (Fournier, 1981) geothermometer.

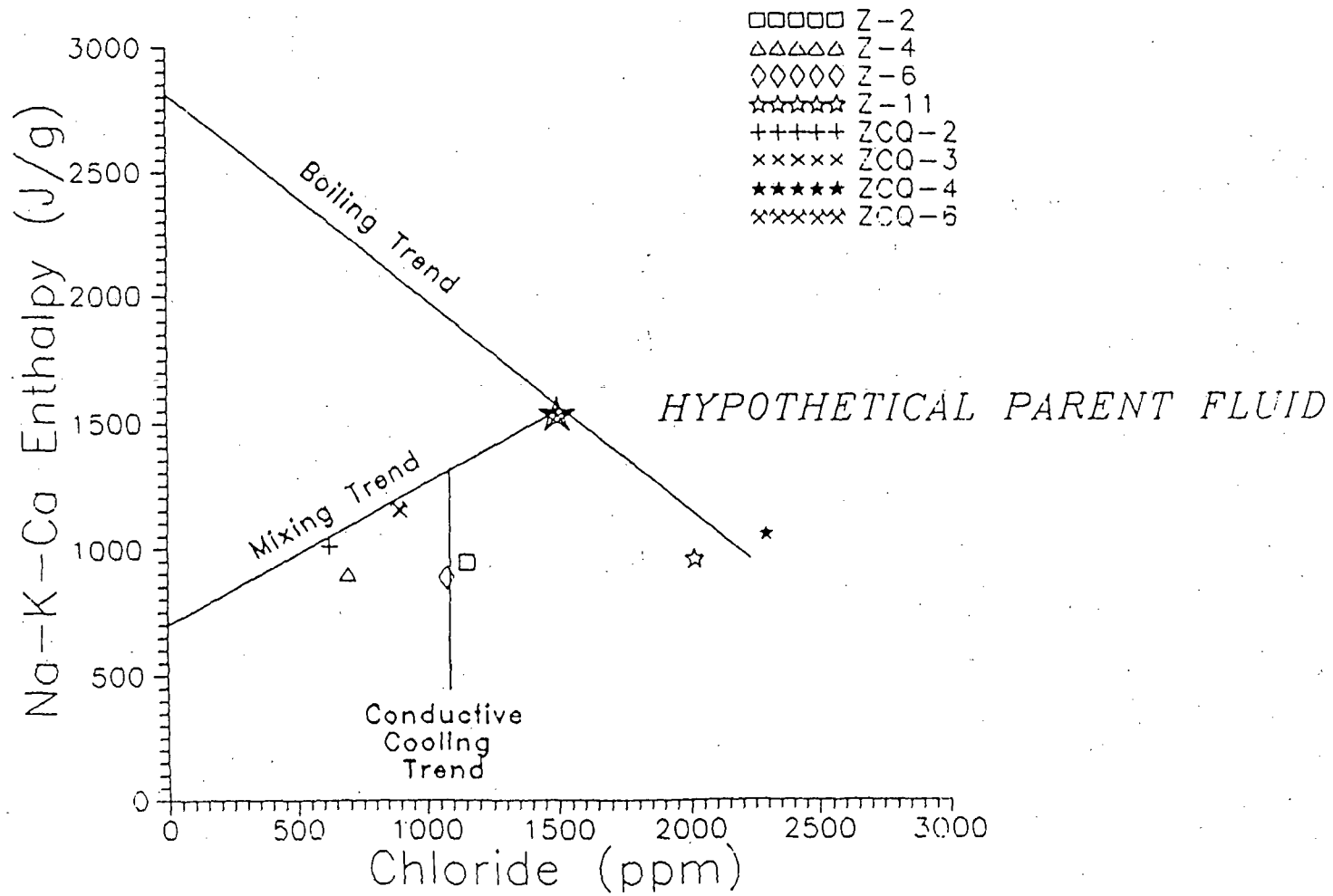


Figure 5. Chloride-enthalpy diagram for the Zunil thermal fluids. Enthalpies are derived from the Na-K-Ca (Fournier and Truesdell, 1973) geothermometer.

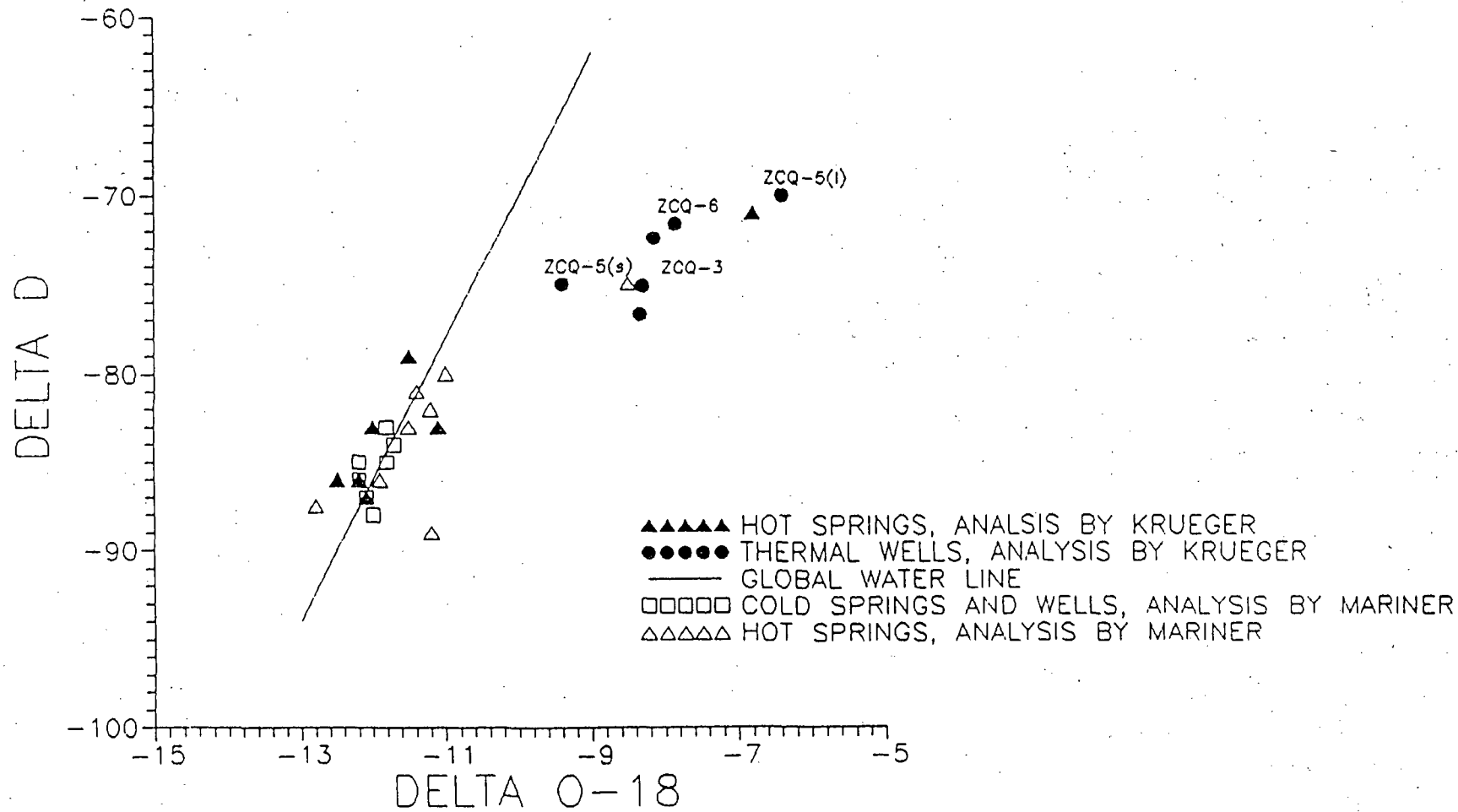


Figure 6a. Isotopic composition of Zunil fluids. Data from this study. l = liquid fraction, s = steam fraction.

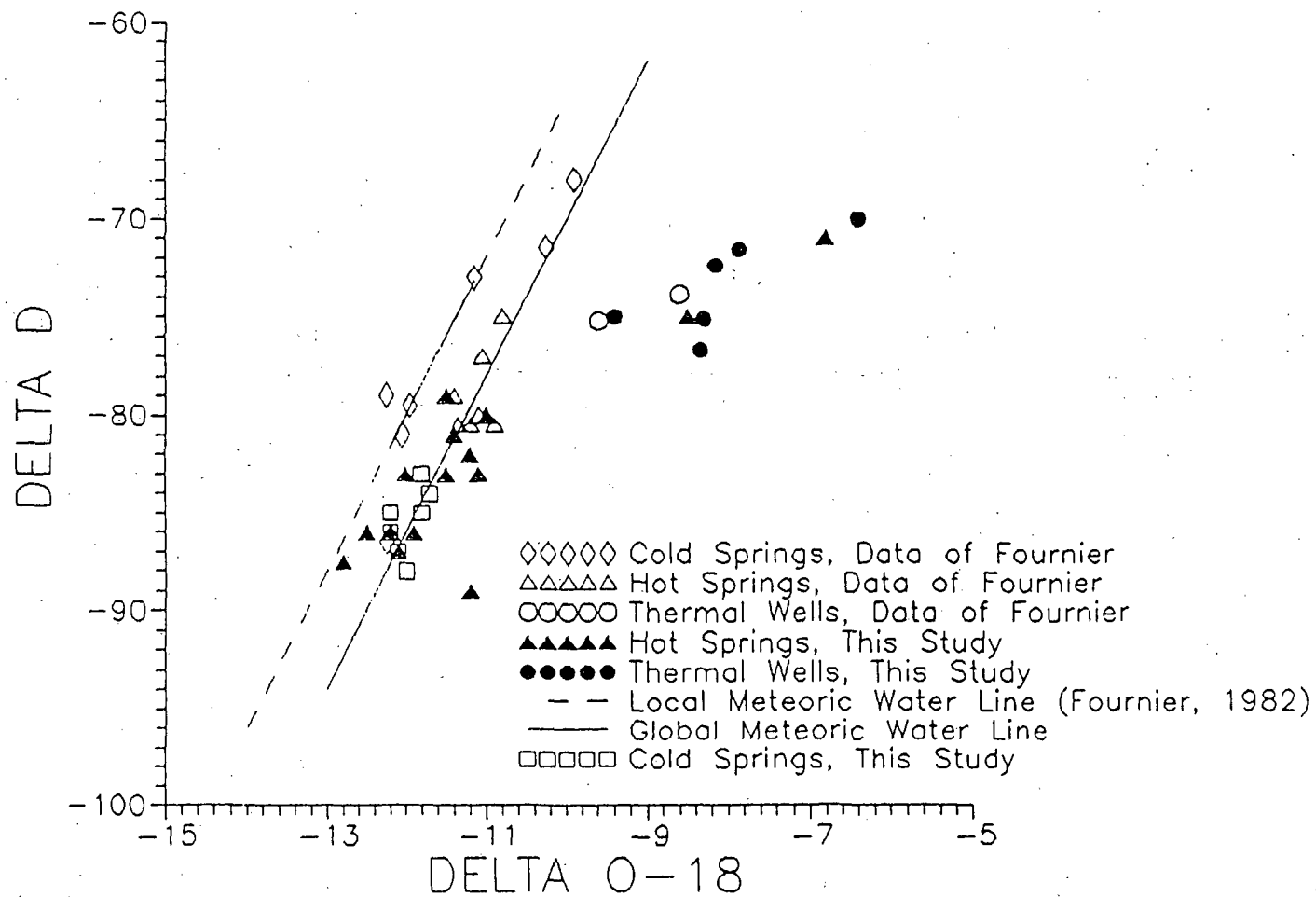


Figure 6b. Isotopic composition of Zunil fluids. Data from this and previous studies.

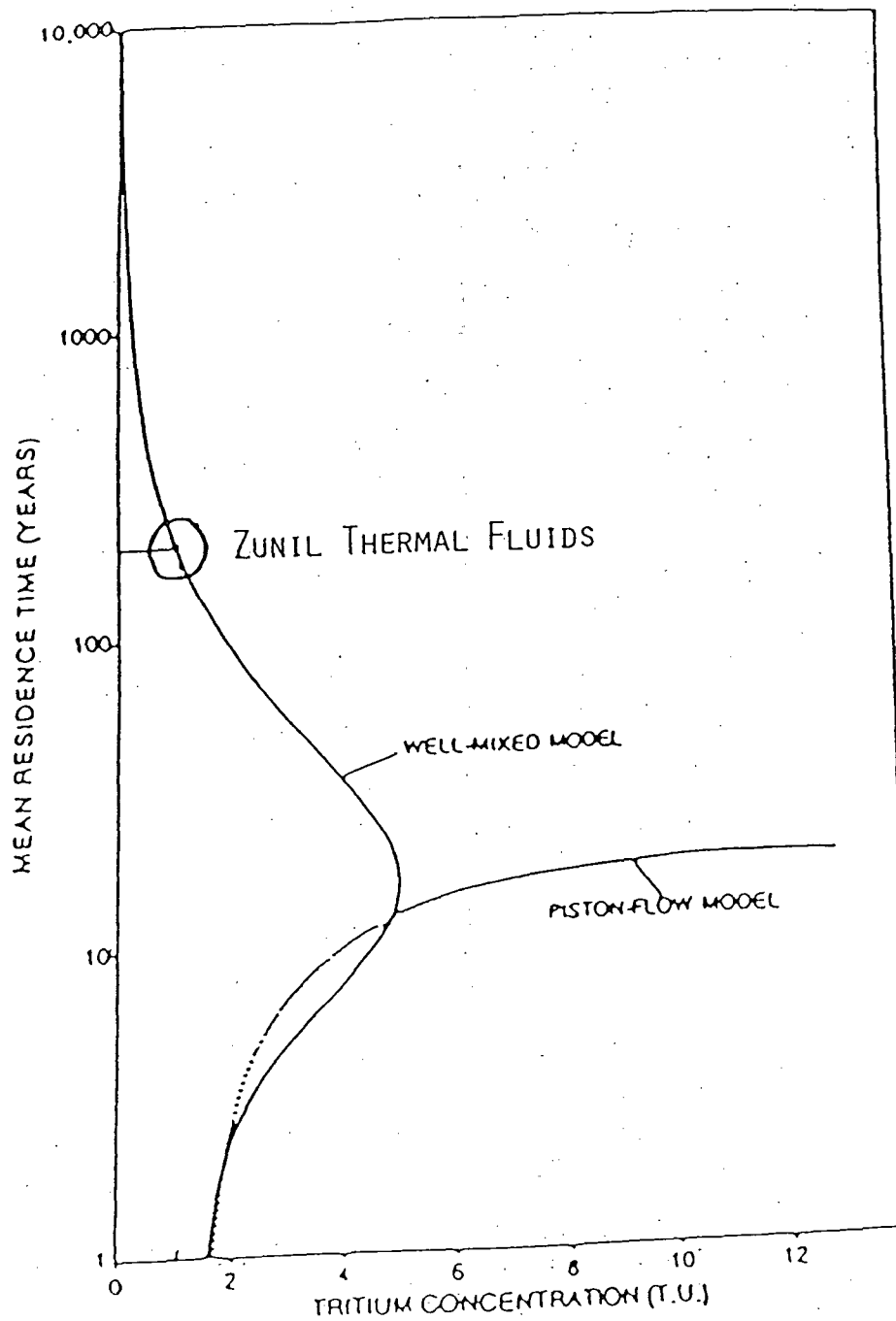


Figure 7. Plot of mean residence time versus tritium concentration with curves representing the well-mixed and piston-flow models for Central America (from Goff et al., 1987).

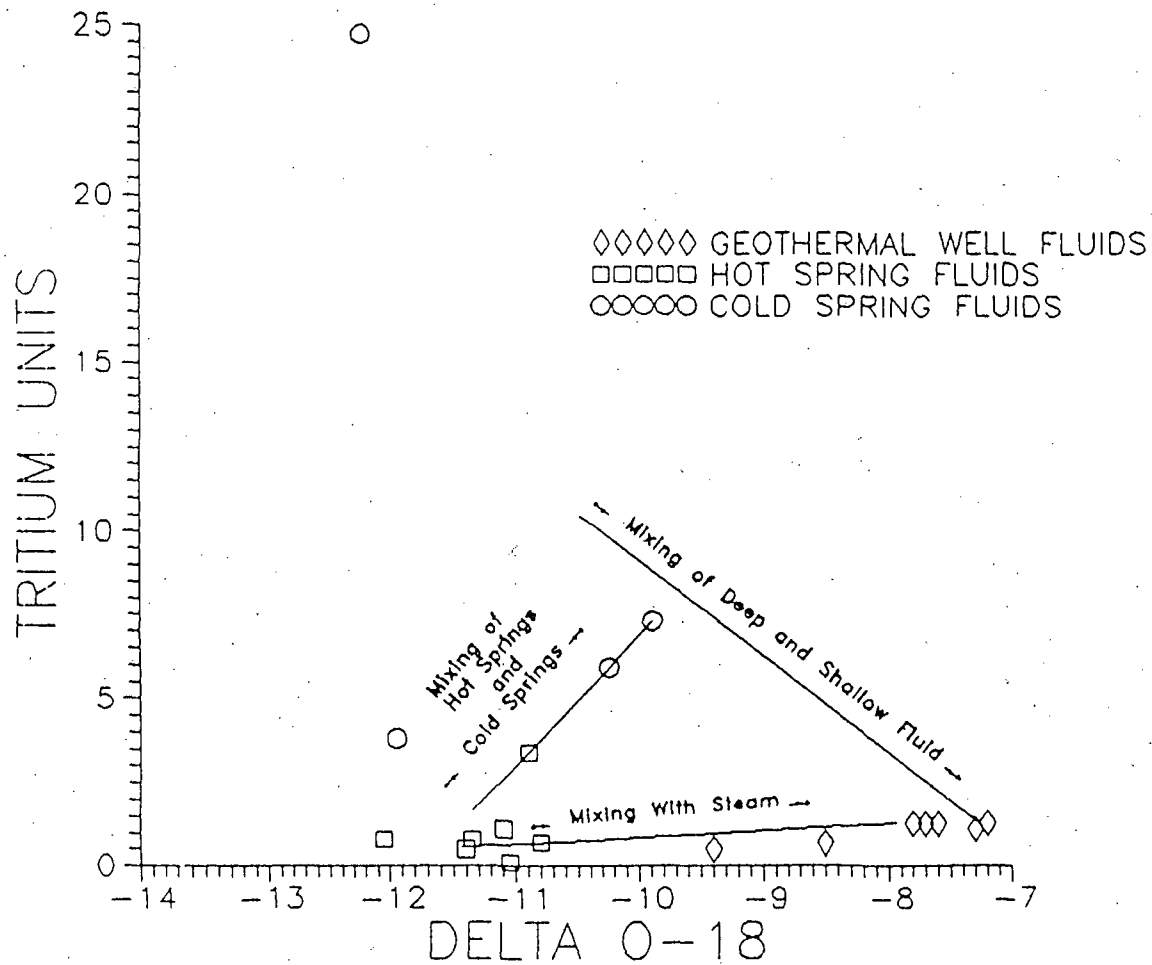


Figure 8. Tritium-oxygen isotopic relationships for Zunil fluids.